BLEJSKE DELAVNICE IZ FIZIKE LETNIK 26, ŠT. 1
BLED WORKSHOPS IN PHYSICS VOL. 26, NO. 1

ISSN 1580-4992

Proceedings to the 28th Workshop

What Comes Beyond the Standard Models

Bled, July 6–17, 2025

Edited by

Norma Susana Mankoč Borštnik
Holger Bech Nielsen
Maxim Yu. Khlopov
Astri Kleppe

UNIVERZA V LJUBLJANI
Fakulteta za matematiko in fiziko

LJUBLJANA, DECEMBER 2025

The 28th Workshop *What Comes Beyond the Standard Models*, 6.– 17. July 2025, Bled

Was organized by
Society of Mathematicians, Physicists and Astronomers of Slovenia

And sponsored by
Department of Physics, Faculty of Mathematics and Physics, University of Ljubljana

Society of Mathematicians, Physicists and Astronomers of Slovenia

Beyond Semiconductor (Matjaž Breskvar)

VIA (Virtual Institute of Astroparticle Physics), Paris

MDPI journal "Symmetry", Basel

MDPI journal "Physics", Basel

MDPI journal "Universe"", Basel

MDPI journal "Particles"", Basel

MDPI journal "Encyclopedia"", Basel

Scientific Committee

Organizing Committee

The Members of the Organizing Committee of the International Workshop "What Comes Beyond the Standard Models", Bled, Slovenia, state that the articles published in the Proceedings to the 28th Workshop "What Comes Beyond the Standard Models", Bled, Slovenia are refereed at the Workshop in intense in-depth discussions.

Workshops organized at Bled

- *What Comes Beyond the Standard Models*
  (June 29–July 9, 1998), Vol. **0** (1999) No. 1
  (July 22–31, 1999)
  (July 17–31, 2000)
  (July 16–28, 2001), Vol. **2** (2001) No. 2
  (July 14–25, 2002), Vol. **3** (2002) No. 4
  (July 18–28, 2003) Vol. **4** (2003) Nos. 2-3
  (July 19–31, 2004), Vol. **5** (2004) No. 2
  (July 19–29, 2005) , Vol. **6** (2005) No. 2
  (September 16–26, 2006), Vol. **7** (2006) No. 2
  (July 17–27, 2007), Vol. **8** (2007) No. 2
  (July 15–25, 2008), Vol. **9** (2008) No. 2
  (July 14–24, 2009), Vol. **10** (2009) No. 2
  (July 12–22, 2010), Vol. **11** (2010) No. 2
  (July 11–21, 2011), Vol. **12** (2011) No. 2
  (July 9–19, 2012), Vol. **13** (2012) No. 2
  (July 14–21, 2013), Vol. **14** (2013) No. 2
  (July 20–28, 2014), Vol. **15** (2014) No. 2
  (July 11–19, 2015), Vol. **16** (2015) No. 2
  (July 11–19, 2016), Vol. **17** (2016) No. 2
  (July 9–17, 2017), Vol. **18** (2017) No. 2
  (June 23–July 1, 2018), Vol. **19** (2018) No. 2
  (July 6–14, 2019), Vol. **20** (2019) No. 2
  (July 4–12, 2020), Vol. **21** (2020) No. 1
  (July 4–12, 2020), Vol. **21** (2020) No. 2
  (July 1–12, 2021), Vol. **22** (2021) No. 1
  (July 4–12, 2022), Vol. **23** (2022) No. 1
  (July 10–18, 2023), Vol. **24** (2023) No. 1
  (July 8–17, 2024), Vol. **25** (2024) No. 1
  (July 6–17, 2025), Vol. **26** (2025) No. 1
- *Hadrons as Solitons* (July 6–17, 1999)
- *Few-Quark Problems* (July 8–15, 2000), Vol. **1** (2000) No. 1
- *Selected Few-Body Problems in Hadronic and Atomic Physics* (July 7–14, 2001), Vol. **2** (2001) No. 1
- *Quarks and Hadrons* (July 6–13, 2002), Vol. **3** (2002) No. 3
- *Effective Quark-Quark Interaction* (July 7–14, 2003), Vol. **4** (2003) No. 1
- *Quark Dynamics* (July 12–19, 2004), Vol. **5** (2004) No. 1
- *Exciting Hadrons* (July 11–18, 2005), Vol. **6** (2005) No. 1
- *Progress in Quark Models* (July 10–17, 2006), Vol. **7** (2006) No. 1
- *Hadron Structure and Lattice QCD* (July 9–16, 2007), Vol. **8** (2007) No. 1
- *Few-Quark States and the Continuum* (September 15–22, 2008), Vol. **9** (2008) No. 1
- *Problems in Multi-Quark States* (June 29–July 6, 2009), Vol. **10** (2009) No. 1
- *Dressing Hadrons* (July 4–11, 2010), Vol. **11** (2010) No. 1
- *Understanding hadronic spectra* (July 3–10, 2011), Vol. **12** (2011) No. 1

- *Hadronic Resonances* (July 1–8, 2012), Vol. **13** (2012) No. 1
- *Looking into Hadrons* (July 7–14, 2013), Vol. **14** (2013) No. 1
- *Quark Masses and Hadron Spectra* (July 6–13, 2014), Vol. **15** (2014) No. 1
- *Exploring Hadron Resonances* (July 5–11, 2015), Vol. **16** (2015) No. 1
- *Quarks, Hadrons, Matter* (July 3–10, 2016), Vol. **17** (2016) No. 1
- *Advances in Hadronic Resonances* (July 2–9, 2017), Vol. **18** (2017) No. 1
- *Double-charm Baryons and Dimesons* (June 17–23, 2018), Vol. **19** (2018) No. 1
- *Electroweak Processes of Hadrons* (July 15–19, 2019), Vol. **20** (2019) No. 1
-
  - *Statistical Mechanics of Complex Systems* (August 27–September 2, 2000)
  - *Studies of Elementary Steps of Radical Reactions in Atmospheric Chemistry* (August 25–28, 2001)

.

Preface in English and Slovenian Language

Let us shortly overview the history of our workshops "What Comes Beyond the Standard Models?":

This year was 28^{th} *time that our series of workshops on "What Comes Beyond the Standard Models?" took place. The series started in 1998 with the idea of organising a workshop where participants would spend most of the time in discussions, confronting different approaches and ideas. The picturesque town of Bled by the lake of the same name, surrounded by beautiful mountains and offering pleasant walks, was chosen to stimulate the discussions.*

The idea was successful and has developed into an annual workshop, which is taking place every year since 1998. Very open-minded and fruitful discussions have become the trademark of our workshops, producing several published works. It took place in the house of Plemelj, which belongs to the Society of Mathematicians, Physicists and Astronomers of Slovenia.

We have been trying, and we are still trying to understand whether the laws of nature, the laws of our universe (of all the universes if there are many universes) are complicated and need many assumptions when we try to make predictions and comment on the experiments and observations, and whether we really have so many different constituents, or whether the law is simple, and there are only two kinds of the elementary constituents: anti-commuting fermions and commuting bosons, and all the anti-commuting fermions can be treated equivalently, and all the commuting bosons can be treated equivalently, while even these two elementary kinds of fields can be treated equivalently.

It is only when many interacting constituents are involved, that the approximate laws start to be needed when we look for the confirmation with the experiments and cosmological observations. And we will be forced also in future, even if we succeed in proving that the laws of nature are simple and the elementary fields are simple, even if the computers will be much more capable, to invent approximate constituents and approximate laws to be able to make predictions.

We will have to show that all the basic fermionic and bosonic fields, as we recognise them today, follow from simple equivalent building blocks of two types of fields. Although these two type of fields are so different, their mutual relation is very simple.

Although in these twenty-eight years, the technology of experiments, as well as astronomical observations, has advanced incredibly, it is still true that we are only guessing how our universe started and why it is expanding exponentially, and then reheated. Why do we experience only three space dimensions and one time, why most of the matter is almost unobservable in direct measurements, what forces our universe to expand faster than expected; many other open questions remain unanswered.

We improve our knowledge in small steps. But there were also large steps like the special theory of relativity, the general theory of gravity, the quantum theory of groups of constituents (in the first quantisation models), the second quantisation of bosons and fermions, the electroweak *standard model*, the *cosmological models*.

What seems trustworthy this year is that there are two kinds of the second quantised fields, commuting and anti-commuting, and that all the fields, fermions and bosons are second-quantised fields. At least some of the members of the organising committee, we are sure. Why the law of nature would make a difference between gravity and the rest of the boson fields.

In the Bled workshops "What comes beyond the standard models", the laws of nature among elementary second quantized fermion and boson fields, which should explain the born and the history of our universe, has been discussed and developed from the very beginning.

This year almost half of the contributions discuss the gravity in the content of the unification with the gauge boson fields.

The two contributions treating fermion and boson second quantized fields in a comparable way, use to describe the internal spaces of fermion and boson fields, the "basis vectors" which are products of nilpotents and projectors, and are the eigenvectors of the Cartan subalgebra members. The "basis vectors" with the odd number of nilpotents, appear in families, and offer in even-dimensional spaces, as it is d = (13 + 1), the unique description of all the properties of the observed fermion fields (with quarks and leptons and antiquarks and antileptons appearing in the same family). The "basis vectors" with the even number of nilpotents offer the description of the observed boson fields (gravitons have two nilpotents in the part $SO(3,1)$, photons (have only projectors), weak bosons (have two nilpotents in the part $SO(4)$), gluons (have two nilpotents in the part $SO(6)$) and scalars), providing that all the fields have non zero momenta only in $d = (3+1)$ of the ordinary space-time. Bosons have the space index α (which is for tensors and vectors $\mu = (0,1,2,3)$ and for scalars $\sigma \geq 5$). The two papers overviews the theory, presents new achievements, discuss the open problems of this theory, the second one with respect to the Feynman diagrams.

One contribution discusses the possibility that the gravitational field in $d = (3+1)$, as well as the quantum gravity emerges from the spontaneus break of the de Sitter $SO(1,4)$or anti-de Sitter $SO(3,2)$ group, formulated on a manifold without a metric structure. The author constructs t he Lagrangian densities using the Levi-Civita symbol. The spontaneus break of the starting symmetry reduces to the Lorentz group $SO(1,3)$ and dynamically generates a space-time metric. The analyse brings the observed Planck mass and the small cosmological constant, the massless graviton and massive scalar.

The author analyses the new anomalies arising from the attempt to develop an extension of the *standard model* with a general theory of gravity, and attempts to eliminate them. Fermions, which have the opposite chirality (chirality) in the left sector than the fermions of the right sector, interact with their own gauge fields with the symmetry $SU(3)$ and $U(1)$. The vector field $SU(2)$ and the metric are common to both sectors. The author assumes that the left sector describes the *standard model* coupled to gravity, and that the right sector describes dark matter consisting of quantum fermions and bosons that interact weakly with gravity and the weak force, and that interact with the bosons and fermions of the Standard Model.

One of the authors observes that the spectral action principle within the noncommutative geometry offers the derivation of the actions of the *standard model* and the *the general relativity* and discusses their phenomenological aspects.
One of the papers analyzes the usefulness of extended phase space for quantizing gravity.
There is an excellent pioneer DAMA project, which measured the presence of the dark matter by annual modulation of signals deep underground in Gran Sasso. It was decommissioned by the end of September 2024. Experiments have been running since 1990, developing several very low background measurement methods for measuring dark matter, as well as for many other rare events. The team presents an overview of the development of the DAMA experiment over the past 30 years.

There are papers which study the early universe.

One paper proposes that the $T \to 0$ vacuum naturally organizes into proton-scale. Suggesting the model, the author derives the Planck surface, the minimal coherent length, the density of the vacuum and the maximal velocity c.
One contribution investigates numerically spontaneous particle production by a pseudo-Nambu-Goldstone boson for small angles.
Another contribution study baryogenesis and the problem of matter-antimatter asymmetry in the early universe. They assume the existence of isolated antimatter domains that survive until the era of first star formation (Z approximately 20).
The author investigate how primordial black holes can catalyze the first-order phase transitions in the early universe, modifying the resulting gravitational wave signals.
The authors attempt to explain the excess of positrons measured by the Pamela experiment by measuring gamma rays. They hypothesize that the cause of this excess is dark matter with a large mass.
The dark atom hypothesis XHe offers with a neutral, atom-like configuration, an explanation for the dark matter. They try to show that their model can explain the existence of dark matter in the universe, anomalies in DAMA/LIBRA measurements.
The authors study the possible Lorentz invariance breaking in the unexplored weak sector. They propose experiments to measure this breaking at the LHC.
The author presents a very precise calculation of the fine structure constants, which is based on the connection between various physical phenomena and their associated logarithms of energy scales and an imagined lattice associated with the quantum oscillations of the phenomena under consideration. This connection provides him with a linear relationship from which he deduces, in the limit of unification, incredibly precise values of the energy scales.
The author discusses the geometric special relativity and its new Lie group in real space.
The author studies the properties of almost democratic matrices by considering the CP-violation, in particular the Jarlskog invariant-strains and finds the interdependence of quark masses.

The relativistic equations with The negative-energy and tachyonic solutions of the relativistic equations for higher spins are studied, bringing the paradoxical conclusions.
The author presents recent results of all-loop renormalization for supersymmetric theories. For some supersymmetric theories $\mathcal{N} = 1$ he shows how to construct expressions that have no quantum corrections at all orders. For the minimal supersymmetric extension of the *Standard Model*, the author checks the dependence of the results on the chosen scheme using three loops.
Maybe next year, we shall report on physically realistic cellular automaton used to offer several illustrations in elementary particle physics. This year, we only received the a short overview.

The workshops at Bled changed a lot after the COVID pandemic: For three years, the workshop became almost virtual and correspondingly less open-minded. The discussions, which asked the speaker to explain and prove each step, can not be done so easily virtually. However, many questions still interrupt the presentations, so the speakers must often continue their talks several times in the following days. Also, this year, the talks were presented virtually.

This year, the organisers are again asking the University of Ljubljana for the help in arranging the DOI number.
Although the *Society of Mathematicians, Physicists and Astronomers of Slovenia* remain our organiser, for which we are very grateful, yet the Faculty of Mathematics and Physics starts to be our publisher together with the University of Ljubljana. The technical procedure is now different, and the possibility that the participants send the contributions "the last moment" is less available.
Several participants have not managed to submit their contributions in time. We have several suggestions for solving the open problems, which have not succeeded to be prepared in time for the discussion section.
The organisers are grateful to all the participants for the lively presentations and discussions and an excellent working atmosphere, although most participants appeared virtually, led by Maxim Khlopov.
The reader can find all the talks and soon also the whole Proceedings on the official website of the Workshop: http://bsm.fmf.uni-lj.si/bled2025bsm/presentations.html, and on the Cosmovia Forum https://bit.ly/bled2025bsm ..

Norma Mankoč Borštnik, Holger Bech Nielsen,
Maxim Khlopov, Astri Kleppe *Ljubljana, December 2025*

1 Predgovor (Preface in Slovenian Language)

Letos je stekla že 28. delavnica na temo "Kako preseči oba standardna modela?". Serija se je začela leta 1998 v Kopenhagenu z željo organizirati delavnice, kjer bi udeleženci večino časa preživeli v razpravah, v soočanju z različnimi pristopi in idejami. Za kraj delavnic je bilo izbrano slikovito mesto Bled ob istoimenskem jezeru, obdano s čudovitimi gorami in s prijetnimi sprehodi.

Ideja je bila uspešna: Delavnica poteka vsako leto od leta 1998. Zelo odprte in plodne razprave so postale zaščitni znak naših delavnic. Zbornicnim objavam so sledila v znanstvenih revijah objavljena dela. Ne vedno, marsikatero se je urednikom zazdelo preveč inovativno, ali pa niso uspeli najti recenzentov. Delavnice domujejo v Plemeljevi hiši, ki pripada Društvu matematikov, fizikov in astronomov Slovenije.

Poskušali smo in še vedno poskušamo razumeti, ali so zakoni narave, zakoni našega vesolja (vseh vesolj, če jih je veliko) zapleteni in potrebujejo veliko predpostavk, ko poskušamo napovedovati in komentirati poskuse in opazovanja, in ali imamo res toliko različnih fermionov in bozonov, ali pa je zakon narave preprost in obstajata le dve vrsti elementarnih polj; antikomutirajoči fermioni in komutirajoči bozoni, in je vse antikomutirajoče fermione mogoče obravnavati enakovredno, in je tudi vse komutirajoče bozone mogoče obravnavati enakovredno, medtem ko je celo ti dve osnovni vrsti polj mogoče obravnavati enakovredno.

Šele ko je vključenih veliko osnovnih fermionskih in bozonskih polj, postanejo približni zakoni potrebni, ko iščemo potrditev s poskusi in kozmološkimi opazovanji. In tudi v prihodnje bomo prisiljeni, celo če nam uspe dokazati, da so zakoni narave preprosti in da so elementarni gradniki preprosti, definirati skupke gradnikov in približne zakone zanje, ne glede na zmožnosi računalnikov, da bomo lahko napovedovali.

Pokazati bomo morali, da vsa osnovna fermionska in bozonska polja kot jih poznamo danes, sledijo iz preprostih gradnikov dveh vrst polj, ki imata zelo rezlične lastosti in vendar je med njima zelo preprosta zveza.

Čeprav se je v teh osemindvajsetih letih tehnologija eksperimentov, pa tudi astronomskih opazovanj, neverjetno razvila, še vedno drži, da le ugibamo, kako se je naše vesolje začelo in zakaj se eksponentno širi, nato pa se ponovno segreje. Zakaj opazimo le tri prostorske razsežnosti in eno časovno, zakaj je večina snovi skoraj neopazna pri neposrednih meritvah, kaj sili naše vesolje, da se širi hitreje, kot je bilo pričakovano; mnoga druga odprta vprašanja ostajajo neodgovorjena.

Znanje izboljšujemo z majhnimi koraki. Vendar so bili v preteklosti tudi veliki koraki, kot so posebna teorija relativnosti, splošna teorija gravitacije, kvantna teorija gruč osnovnih delcev (v modelih prve kvantizacije), druga kvantizacija bozonov in fermionov, elektrošibki in barvni *standardni model*, *kozmološki modeli*.

Kar se letos zdi zanesljivo, je, da obstajata dve polji v drugi kvantizacij, komutirajoča in antikomutirajoča, in da so vsi fermioni in bozoni polja v drugi kvantizaciji. Vsaj nekateri člani organizacijskega odbora smo prepričani. Zakaj bi zakon narave razlikoval med gravitacijo in ostalimi bozonskimi polji?

Vsa leta teče na Blejskih delavnicah diskusija o tem, kaj so osnovni gradniki snovi in kakšne so sile med njimi, ki določajo rojstvo in zgodovino našega vesolja.
Skoraj polovica letošnjh prispevkov poizkuša razumeti gravitacijo kot eno od bozonskih polj v drugi kvantizaciji.
Prispevka, ki obravnavata fermionska in bozonska polja v drugi kvantizaciji, uporabljata za opis notranjih prostorov (spinov in nabojev) "bazne vektorje", ki so superpozicija produktov lihega (za fermione), in sodega (za bozone) števila operatorjev γ^{a}'s, ki so kot nilpotenti in projektorji urejeni v lastne vektorje vseh članov Cartanove podalgebre. Lihi "bazni vektorji", ki se pojavljajo v družinah, ponujajo v sodorazsežnih prostorih, kot je $d = (13 + 1)$, opis kvarkov in leptonov in antikvarkov in antileptonov, ki so vsi v vsaki od družin. Sodi "bazni vektorji" ponudijo opis bozonskih polj; fotonov (ki nimajo nilpotentov), gravitonov, šibkih bozonov gluonov in skalarjev (ki imajo vsi po dva impotenta, vsak v svoji podgrupi grupe $SO(13, 1)$), pod pogojem, da imajo vsa polja, fermionska in bozonska, neničelne gibalne količine samo v $d = (3 + 1)$ običajnega prostora-časa. Bozoni nosijo prostorski indeks α (ki je za tenzorje in vektorje $\mu = (0, 1, 2, 3)$ in za skalarje $\sigma \geq 5$).
Članka predstavita teorijo in njene dosežke, obravnavata še nerešena vprašanja te teorije, eden od člankov pa predstavi razliko med Feynmanovi diagrami običajnih teorij in te teorije in diskutira vzroke in posledice.
Eden od prispevkov pokaže, da gravitacijsko polje v $d = (3 + 1)$ in kvantna gravitacija sledita po spontanem zlomu de Sitterjeve grupe $SO(1, 4)$ ali anti-de Sitterjeve grupe $SO(3, 2)$, formulirani na mnogoterosti brez metrične strukture. Avtor konstruira Lagrangejevo gostoto z uporabo simbola Levi-Civita. Spontani zlom zmanjša začetno simetrijo na Lorentzovo $SO(1, 3)$ in dinamično generira prostorsko-časovno metriko. Ugotavlja, da v tej obravnavi Planckova masa in kozmološka konstanta ustrezata meritvam; graviton je brez mase, skalar, ki sproži spontano zlomitev, pa je masiven.
Avtor enega prispevka analizira nove anomalije, ki jih prinese poskus razširitve *standardnega modela* s splošno teorijo gravitacije, in jih poskuša odpraviti. Fermioni, ki imajo v levem sektorju nasprotno ročnost (kiralnost) kot fermioni desnega sektorja, interagirajo vsak s svojimi umeritvenimi polji s simetrijo $SU(3)$ in $U(1)$. Vektorsko polje $SU(2)$ in metrika pa sta skupna obema sektorjema.
Avtor predvideva, da opiše levi sektor standardni model, sklopljen z gravitacijo, desni sektor pa temno snov kvantnih fermionov in bozonov, ki šibko interagirajo z gravicijo in s šibko silo z bozoni in fermioni standardnega modela.
Eden od avtorjev ugotavlja, da ponudi nekomutativna geometrija akcijo za *standardni model* in za splošno teorijo relativnosti, kar poskuša uporabiti za fenomenološke napovedi.
Eden od prispevkov analizira uporabnost razširjenega faznega prostora za kvantizacijo gravitacije.
Odličen pionirski projekt DAMA, ki je meril prisotnost temne snovi z letno modulacijo signalov globoko pod zemljo v Gran Sassu, so do konca septembra 2024 razgradili. Za poskuse, ki so tekli od leta 1990, je ekipa raziskovalcev razvila nekaj metod merjenja temne snovi z zelo nizkim ozadjem, ki so jih uporabili tudi za študij številnih drugih redkih dogodkov. Ekipa pregledno predstavi razvoj experimanta DAMA v tridesetih letih.

Nekaj člankov diskutira stanje v zgodnjem vesolju.
Avtor enega od člankov domneva, da se vesolje, ko se ohlaja proti absolutni ničli, $T \to 0$, uredi v atome protonske skale. Predlaga model in oceni Plankovo površino, koherenčno dolžino prostora-časa, numerično vrednost za gostoto vakuuma in svetlobno hitrost.
Avtorji preučujejo spontani nastanek fermionov, ki ga sproži pseudo-Nambu-Goldstone bozon pri majhnih kotih.
Prispevek, ki preučuje bariogenezo in problem asimetrije snovi in antisnovi v zgodnjem vesolju, predpostavlja, da izolirane domene antisnovi preživijo do obdobja nastajanja prvih zvezd ($Z \approx 20$).
Avtor raziskuje, kako prvobitne črne luknje katalizirajo fazne prehode prvega reda v zgodnjem vesolju in vplivajo na signale gravitacijskih valov.
Avtorji poskušajo pojasniti presežek pozitronov, ki so ga izmerili z eksperimentom Pamela z merjenjem žarkov gama. Postavijo domnevo, da je vzrok za ta presežek temna snov z veliko maso.
Hipoteza o temnih atomih XHe ponuja z nevtralno, atomom podobno konfiguracijo, razlago za temno snov. Avtorji poskušajo pokazati, da njihov model lahko razloži obstoj temne snovi v vesolju in anomalije pri meritvah z DAMA/LIBRAo.
Avtorja študirata morebitno zlomitev Lorentzove simetrije v še neraziskanem območju šibke sile. Predlagata poskuse za meritev te zlomitve na pospeševalniku v Cernu.
Avtor predstavi zelo natančen izračun konstant fine strukture, ki sloni na povezavi med različnimi fizikalnimi pojavi in z njimi povezanimi logaritmi energijskih skal in namišljeno mrežo, povezano s kvantnim nihanjem obravnavanih pojavov. Ta povezava mu ponudi linearno zvezo, iz katere razbere v limiti poenotenja neverjetno natančne vrednosti energijskih skal.
Prispevek razpravlja o posebni teoriji relativnosti in njeni novi Liejevi grupi v realnem prostoru.
Avtorica proučuje lastnosti skoraj demokratičnih matrik z upoštevanjem kršitve CP, posebej kršitve invariante Jarlskogove. Ugotavlja medsebojno odvisnost mas kvarkov,
Avtor obravnava relativistične enačbe z višjimi spini, ki imajo negativne energijske in tahionske rešitve. Pripeljejo ga do paradoksalnih zaključkov.
Avtor predstavi nedavne rezultate renormalizacije z upoštevanjem vseh zank za supersimetrične teorije. Za nekatere supersimetrične teorije $\mathcal{N} = 1$ pokaže, kako konstruirati izraze, ki nimajo kvantnih popravkov. Za minimalno supersimetrično razširitev *Standardnega modela* avtor preveri odvisnost rezultatov od izbrane sheme, pri kateri upošteva tri zanke.
Morda bomo prihodnje leto poročali o realističnem celičnem avtomatu, ki bo ponudil ilustracijo osnovnih delcev. Letos smo prejeli le povzetke, ki jih objavlamo v posebnem oddelku.
Delavnice na Bledu so se po pandemiji covida zelo spremenile: Tri leta je delavnica postala skoraj virtualna in posledično manj odprta za nova vprašanja. Razprav, kjer je govornik moral vsak korak razložiti in dokazati, ni mogoče tako enostavno izvesti virtualno. Vendar pa številna vprašanja še vedno prekinjajo predavanja,

zato morajo govorniki pogosto nadaljevati svoja predavanja večkrat v naslednjih dneh. Tudi letos so bila predavanja predstavljena virtualno.

Letos organizatorji ponovno prosimo Univerzo v Ljubljani za pomoč pri urejanju DOI.
Čeprav Društvo matematikov, fizikov in astronomov Slovenije ostaja naš organizator, za kar smo zelo hvaležni, pa je Fakulteta za matematiko in fiziko že tretje leto naš založnik skupaj z Univerzo v Ljubljani. Tehnični postopek je zdaj drugačen in možnost, da udeleženci pošljejo prispevke "v zadnjem trenutku", manjša.
Več udeležencev ni pravočasno oddalo svojih prispevkov. Več predlogov za rešitev odprtih vprašanj, največ o zgodovini vesolja, nismo uspeli pravočasno pripraviti za razpravo.
Organizatorji se vsem udeležencem zahvaljujejo za živahne predstavitve in razprave ter odlično delovno vzdušje, četudi virtualno, pod vodstvom Maksima Khlopova.
Bralec lahko najde vse predstavitve in kmalu tudi celoten zbornik na uradni spletni strani delavnice: http://bsm.fmf.uni-lj.si/bled2025bsm/presentations.html,
in na forumu Cosmovia https://bit.ly/bled2025bsm .

Norma Mankoč Borštnik, Holger Bech Nielsen,
Maxim Khlopov, Astri Kleppe *Ljubljana, december 2025*

Contents

1 Counting Vacuum: *SU(3) Atoms, the Cosmological Constant, and Nature's Constants*
Ahmed Farag Ali 1

2 Emergent Gravity from a Spontaneously Broken Gauge Symmetry: a Pre-geometric Prospective
Andrea Addazi 10

3 Unified Pati–Salam from Noncommutative Geometry: Overview and Phenomenological Remarks
Ufuk Aydemir 19

4 Anomalous Isotopes In Dark Atoms models
M.I. Baliño, J.Mwilima, D.O.Sopin, M.Yu.Khlopov 31

5 Research of dark matter particle decays into positrons with suppression of FSR to explain positron anomaly
Y.A. Basov 38

6 The DAMA project legacy
R. Bernabei for DAMA activities 44

7 The bound state of dark atom with the nucleus of substance
T.E. Bikbaev, M.Yu. Khlopov, A.G. Mayorov 59

8 Anomaly footprints in SM+Gravity
L. Bonora 73

9 Chemical evolution of antimatter domains in early Universe
A.I.Dembitskaia, Stephane Weiss, M. Yu. Khlopov, M.A.Krasnov 101

10 Propagators for Negative-energy and Tachyonic Solutions in Relativistic Equations
Valeriy V. Dvoeglazov 114

11 Dark Matter as Screened ordinary Matter
C. D. Froggatt, H.B.Nielsen 121

12 Probing Lorentz Invariance Violation at High-Energy Colliders via Intermediate Massive Boson Mass Measurements: Z Boson Example
Z. Kepuladze, J. Jejelava 142

13 Simulation of the Propagation and Diffusion of Dark Atoms in the Earth's Crust
A. Kharakhashyan 158

14 On CP-violation and quark masses: reducing the number of parameters
A. Kleppe 167

15 Spontaneous baryosynthesis with large initial phase
M.A. Krasnov, M.Yu. Khlopov, U. Aydemir 175

16 Describing the internal spaces of fermion and boson fields with the superposition of odd (for fermions) and even (for bosons) products of operators γ^a, enables understanding of all the second quantised fields (fermion fields, appearing in families, and boson fields, tensor, vector, scalar) in an equivalent way
N.S. Mankoč Borštnik 185

17 How to present and interpret the Feynman diagrams in this theory describing fermion and boson fields in a unique way, in comparison with the Feynman diagrams so far presented and interpreted?
N.S. Mankoč Borštnik, H.B. Nielsen 216

18 How Should We Interpret Space Dimension? – Trial for a Mathematical Foundation in Higher Dimensional Physics
Euich Miztani 238

19 Erratum to the Proceedings of 27^{th} Workshop What Comes Beyond the Standard Models (2024), pp. 156-175
Euich Miztani 268

20 Ontological Fluctuating Lattice Cut Off
Holger Bech Nielsen 269

21 Multimessenger probes of fundamental physics: Gravitational Waves, Dark Matter and Quantum Gravity
S. Ray et al. 303

22 The extended phase space approach to quantization of gravity and its perspective
T. P. Shestakova 323

23 The renormalization group invariants and exact results for various supersymmetric theories
K.V. Stepanyantz 333

24 Formation and Evolution of Antimatter Objects
Sattvik Yadav 344

25 PBH-Catalyzed Phase Transitions and Gravitational Waves: Insights from PTA Data
Jiahang Zhong 354

26 DISCUSSIONS
Elia Dmitrieff, Euich Mitzani,.. 364

27 VIA: *Discussion of BSM research on the platform of Virtual Institute of Astroparticle physics*
Maxim Yu. Khlopov 368

28 A poem
Astri Kleppe 382

BLED WORKSHOPS
IN PHYSICS
VOL. 26, NO. 1

Proceedings of the 28th Workshop
What Comes Beyond . . . *(p. 1)*
Bled, Slovenia, July 6–17, 2025

1 Counting Vacuum: *SU(3) Atoms, the Cosmological Constant, and Nature's Constants*

Ahmed Farag Ali†

Essex County College, 303 University Ave, Newark, NJ 07102, USA
Department of Physics, Benha University, Benha 13518, Egypt

Abstract. We propose that the $T \to 0$ vacuum naturally organizes into proton-scale *SU(3) vacuum atoms* by the combined weight of color confinement, Meissner-like suppression of U(1), the Third Law of thermodynamics, and horizon holography. Two independent counts—a bulk volume ratio $N \simeq (R_u/R_p)^3$ and a boundary tiling with per-atom area $A_{\rm atom} = 4\pi R_u^2/N$—converge to $N \sim 10^{123}$ and $A_{\rm atom} \simeq \ell_{\rm Pl}^2$, fixing the Planck area without being postulated. A cosmological uniform force–area law on the horizon then yields an exact $1/N$ dilution of the bare SU(3) zero-point density to the observed ρ_Λ, with no fine-tuned counterterms. Matching to a Snyder/GUP-regularized vacuum energy fixes a minimal *spacetime coherence length* $\ell_S = \ell_{\rm Pl} N^{1/4} = (\ell_{\rm conf}^3 R_u)^{1/4} \sim 10^{-5}$ m, testable in opto-mechanics and cold-atom interferometry. Modeling each atom as a radial cylinder of base $\ell_{\rm Pl}^2$ and height R_u produces a Planck-volume overlap carrying $\sim M_{\rm Pl}$ rest energy, geometrically tying confinement to $(\hbar, G, c)$. Quantization about this vacuum satisfies OS/Wightman axioms and yields a strictly positive vacuum-sector spectral gap. This proceedings article synthesizes [1,2].

Povzetek: Avtor domneva, da se vesolje, ko se ohlaja proti absolutni ničli $T \to 0$, uredi v atome protonske skale, ki jo določajo barvna sila, Meisnerjev efekt, tretji zakon termodinamike in holografski princip. Dve neodvisni oceni ponudita vrednost 10^{123}, ki določi Plankovo površino. Oceni tudi koherenčno dolžino prostora-časa, numerične vrednosti za gostoto vakuuma in svetlobno hitrost. Članek povzema članka: M. Ali and A. F. Ali, "Deriving the cosmological constant and nature's constants from SU(3) confinement volume", EPL 151 (2025) 39002 in A. F. Ali, Unbreakable SU(3) Atoms of Vacuum Energy: A Solution to the Cosmological Constant Problem, Symmetry 17 (2025) 888.

1.1 Motivation and synopsis

We begin by framing the problem and the organizing *counting* perspective we will use throughout. Zero-point estimates of vacuum energy density, $\rho_{\rm vac} \sim E_{\rm Pl}^4/(\hbar c)^3$, overshoot observations by $\sim 10^{123}$ [1,3,4]. Rather than cancel energies, we *count* degrees of freedom in a late-time vacuum that retains an unbroken, gapped $SU(3)_c$ sector and fragments into stable, proton-scale *SU(3) vacuum atoms*. The thermal history to low temperatures leaves $SU(3)_c$ confining while $U(1)_{\rm em}$ is effectively expelled in a Meissner-like vacuum (consistent with bounds on a *vacuum* photon mass, $m_\gamma \lesssim 10^{-18}$ eV [6]), suggesting that only a non-Abelian, gapped sector is compatible with Nernst's postulate at $T \to 0$ [7–16]. Holography then encodes

†email: aali29@essex.edu

these atoms on the horizon with a fixed per-atom patch; equating the bulk count and the boundary tiling enforces a Planck area per atom and a global $1/N$ factor that appears both in the action density (via lattice blocking) and in a macroscopic force–area law on the horizon. Identifying the bare vacuum density with the SU(3) massless zero-point value and dividing by N reproduces ρ_Λ without introducing new sectors or tunable counterterms. Matching to a Snyder/GUP-regularized density fixes a minimal *spacetime coherence length* $\ell_S \sim 10^{-5}$ m [17, 18, 20–25]. The geometry of N radial cylinders has a Planck-volume overlap carrying $\sim M_{Pl}$ rest energy, tying $(\hbar, G, c)$ to confinement. Quantization about this vacuum satisfies OS/Wightman axioms and yields a positive vacuum-sector spectral gap via a Hardy–Poincaré bound. The construction is conceptually economical, consistent with cosmology, and testable near ℓ_S [26–30]. We summarize [1, 2]. *With this motivation in place, we next justify why the late-time remnant must be* $SU(3)$ *and not* $U(1)$*, and then quantify the vacuum by two complementary counts.*

1.2 Why only SU(3) survives at $T \to 0$

Below the electroweak scale, the gauge symmetry breaks to $SU(3)_c \times U(1)_{em}$ [7–11]. Lattice thermodynamics confirms an area law and a gapped spectrum for $SU(3)$ as $T \to 0$ [12–14, 50, 51]. In contrast, Meissner-type expulsion of $U(1)$ flux in condensed backgrounds motivates effective suppression of long-range $U(1)$ modes in the dark-energy vacuum [15, 16]. A gapless Abelian vacuum would leave $s(T \to 0) > 0$, in tension with the Third Law (Nernst–Planck). Thus, an unbroken, confining $SU(3)$ sector is the minimal, robust assumption at $T \to 0$. Homogeneity beyond ~ 100 Mpc justifies coarse-graining on cosmic scales [1]. *Having identified the surviving sector, we now turn to counting how many vacuum atoms this implies.*

1.3 Two independent counts fix N and the Planck patch

Bulk (volume) count

Connected correlators at $T = 0$ decay with a finite correlation length set by the lightest gapped excitation. Lattice screening lengths place this at the hadronic scale; taking the proton radius $R_p \simeq 0.84$ fm [6, 31] as the coarse-graining radius and tiling $V_u = \frac{4\pi}{3} R_u^3$ by non-overlapping balls of $V_{atom} = \frac{4\pi}{3} R_p^3$ gives

$$N = \frac{V_u}{V_{atom}} = \left(\frac{R_u}{R_p}\right)^3 \simeq 10^{123}. \tag{1.1}$$

Equivalently, $N = (R_u/\ell_{conf})^3$ with the RG-invariant confinement length $\ell_{conf} = \sigma^{-1/2}$, $\sigma \simeq (440\,\mathrm{MeV})^2$.

Boundary (area) count

Holography encodes bulk information on the apparent horizon $S^2(R_u)$ [32–34]. If the horizon is tiled by N equal patches, the per-atom area is

$$A_{atom} = \frac{4\pi R_u^2}{N}. \tag{1.2}$$

Combining (1.1) and (1.2) yields

$$A_{\text{atom}} \simeq \ell_{\text{Pl}}^2, \qquad V_{\text{atom}} = A_{\text{atom}} R_u \simeq \ell_{\text{Pl}}^2 R_u, \tag{1.3}$$

so each SU(3) vacuum atom projects to a *Planck-area* patch and occupies a radial volume $\sim \ell_{\text{Pl}}^2 R_u$. (Order-unity geometric factors in the spherical vs. cylindrical idealization do not affect the leading $N \sim 10^{123}$ scaling and can be fixed by the variational argument below.) *These bulk and boundary counts set the stage for how the coarse-grained dynamics encodes an overall* $1/N$ *factor.*

1.4 Lattice echo: global $1/N$ in the coarse-grained action

Wilson blocking L^3 elementary cubes into one coarse atom and normalizing $A_\mu^{(b)} = A_\mu/\sqrt{L^3}$ preserves the Wilson action and yields

$$S_{\text{eff}} = -\frac{1}{4L^3}\int d^4x\, G^a_{\mu\nu} G^{a\mu\nu}.$$

Identifying the cosmological block with the Hubble volume sets $L^3 = N$. Thermodynamically, the free-energy density factorizes as $f(T) = f_{\text{local}}(T)/N + \mathcal{O}(e^{-\ell_{\text{conf}} T})$. The same global $1/N$ thus arises independently of the area/volume argument [1,2]. *We now translate this counting into an observable dilution law on the horizon.*

1.5 Uniform force–area law and the $1/N$ dilution

Each atom obeys $P_{su(3)} = -\rho_{su(3)}$ and exerts a mechanical force $F_{su(3)} = |P_{su(3)}|\, A_{\text{atom}} = \rho_{su(3)} A_{\text{atom}}$ on its patch. FLRW isotropy and the near-uniform CMB imply vanishing tangential shear of the Brown–York quasi-local tensor on the horizon [35,36], enforcing a *uniform* outward force per patch: $F_{su(3)} = F_u$. Hence $A_{\text{atom}} = F_u/\rho_{su(3)}$, and the total area is $A_u = N F_u/\rho_{su(3)}$. A coarse-grained observer, unable to resolve atoms, writes $F_u = \rho_u A_u$. Eliminating F_u and A_u gives the exact identity

$$\rho_u = \frac{\rho_{su(3)}}{N}. \tag{1.4}$$

Parallel-circuit intuition. Treat F_u as a common "voltage," A_{atom} as branch "current," and $\rho_{su(3)}$ as branch "resistance." N identical branches in parallel reduce the effective resistance (hence the effective energy density) by N. *With the dilution law in hand, we now check numbers and then connect to a GUP regularization that fixes a testable scale.*

1.6 Numerics: from Planck to ρ_Λ

The bare massless zero-point density up to P_{Pl} is $\rho_{su(3)} \sim E_{\text{Pl}}^4/[(2\pi)^2(\hbar c)^3] \sim 10^{76}\,\text{GeV}^4$ [3]. Dividing by $N \sim 10^{123}$ via (1.4) yields $\rho_u \sim 10^{-47}\,\text{GeV}^4$, consistent with ρ_Λ inferred from supernovae, BAO, and CMB [1,37,38]. The smallness of Λ thus emerges as a *count*, not a cancellation. *To anchor this count in a microscopic modification of the density of states, we match it to a Snyder/GUP regularization that fixes a testable scale.*

1.7 Snyder/GUP match and a minimal spacetime coherence length

In Snyder's Lorentz-covariant noncommutative spacetime and in GUP realizations, the density of states is modified so the vacuum integral

$$\rho_{\mathrm{vac}}^{\mathrm{GUP}} c^2 \;=\; \frac{1}{(2\pi\hbar)^3}\int \frac{d^3p}{(1+\beta p^2)^3}\,\frac{\hbar c\, p}{2}$$

converges to $\propto \hbar c/\ell_S^4$, with $\ell_S = \hbar\sqrt{\beta}$ a *minimal spacetime coherence length* [17, 18, 20–25]. Equating $\rho_{\mathrm{vac}}^{\mathrm{GUP}}$ to ρ_u gives

$$\ell_S \;=\; \ell_{\mathrm{Pl}}\, N^{1/4} \;=\; (\ell_{\mathrm{conf}}^3 R_u)^{1/4} \;\simeq\; \sqrt{\ell_{\mathrm{Pl}}\, R_u} \;\sim\; 10^{-5}\,\mathrm{m}, \tag{1.5}$$

and fixes β as $\beta = \sqrt{N}\, c^2/E_{\mathrm{Pl}}^2$. This scale aligns with macroscopic quantum coherence in cold-atom condensates and nano-opto-mechanics [26–29] and with recent tabletop gravity verifications at sub-centimeter scales [30]. The phrase "spacetime coherence length" is therefore both conceptually precise and experimentally grounded. *Geometrically, the same picture is captured by a cylinder model, to which we now turn.*

1.8 Cylinder geometry and a Planck-mass overlap

Representing each atom by a radial cylinder of base ℓ_{Pl}^2 and height R_u is consistent with both bulk and boundary constraints. A variational argument shows that among interfaces enclosing $V = \ell_{\mathrm{Pl}}^2 R_u$ and cutting a disk of area ℓ_{Pl}^2 on $S^2(R_u)$, a right cylinder of base ℓ_{Pl}^2 orthogonal to the sphere minimizes area (constant-mean-curvature surface), dynamically selected as $T \to 0$. Superposing n such cylinders with axes uniformly distributed in azimuth, the common overlap near the origin has volume [39]

$$V_n(r) \;=\; \frac{8n}{3}\,\tan\!\Big(\frac{\pi}{2n}\Big)\, r^3 \;\underset{n\to\infty}{\to}\; \frac{4\pi}{3}\, r^3,$$

so for $n = N$ and $r = \ell_{\mathrm{Pl}}$ the overlap tends to a ball of volume $\frac{4\pi}{3}\ell_{\mathrm{Pl}}^3$. Filled with $\rho_{su(3)}$, this core encloses rest mass $\sim M_{\mathrm{Pl}}$, tying $(\hbar, G, c)$ geometrically to confinement, with no exotic sectors. *Having established the geometry, we now connect to thermodynamics and the existence of a gap.*

1.9 Thermodynamics and a positive vacuum-sector gap

Pure-glue lattice thermodynamics finds $s(T)/T^3 \to 0$ as $T \to 0$ [14, 50, 51], indicating a unique ground state and a gapped spectrum. A gapless $U(1)$ vacuum would violate Nernst's theorem. In our picture, the impossibility of subdividing atoms at $T = 0$ and the strictly positive coarse-grained density supply a physical basis for a nonzero *vacuum-sector* mass gap. *We next place this on a rigorous footing via OS/Wightman quantization and coercivity bounds.*

1.10 Quantization and a coercive lower bound

Quantization about the cylinder–forest vacuum fits the OS/Wightman scheme [40–42]. Reflection positivity with uniform radial vortex footprints implies a positive transfer matrix and a self-adjoint Hamiltonian. Balaban's multiscale renormalization and convergent SU(3) cluster expansions control the continuum limit [43–46]. Expanding $A = A_{\mathrm{bg}} + a$ in background-covariant gauge, the quadratic fluctuation operator obeys Hardy–Poincaré coercivity outside atom cores and a Dirichlet–Poincaré bound on the cosmological domain, yielding a strictly positive lower bound to the nonzero spectrum and thus a vacuum-sector mass gap. Using $R_u \simeq 1.30 \times 10^{26}\,\mathrm{m}$ gives $\lambda_1 = \pi^2/R_u^2 \simeq 5.35 \times 10^{-52}\,\mathrm{m}^{-2}$ and

$$m_{\mathrm{gap}} \gtrsim \sqrt{0.654\,\lambda_1} \simeq 3.7 \times 10^{-33}\,\mathrm{eV},$$

far below GeV glueballs (the latter pertain to localized hadronic excitations). See [1,2] for the topological sector summary (center vortex Z_3 sectors [47], bundle classification [48]) and detailed coercivity estimates [49]. *With consistency established, we now discuss cosmological evolution and observational robustness.*

1.11 Cosmic evolution and robustness

Two scenarios are natural. If atoms keep a fixed physical volume (consistent with the RG invariance of ℓ_{conf}), expansion adds atoms at constant per-atom volume and maintains ρ_Λ strictly constant, consistent with ΛCDM [1]. Alternatively, if atoms comove and stretch, N is fixed and ρ would slowly evolve; DESI's recent analyses probe such possibilities [52–54]. Our framework prefers the fixed-volume scenario on thermodynamic and RG grounds, while keeping the evolving case empirically testable. *Either way, the framework yields near-term empirical handles, which we summarize next.*

1.12 Phenomenology and tests

The central, falsifiable prediction is a *spacetime coherence length* $\ell_S \simeq 10^{-5}$ m. Quantum opto-mechanical platforms and cold-atom interferometers can probe GUP-like corrections in this window [26–29]. Gravitational tests at millimeter scales can bound residual departures from Newtonianity [30]. A secondary implication is a glueball-like dark-matter window in the ∼GeV range [55,56]. Cosmologically, precise tests of the redshift independence of ρ_Λ can discriminate the fixed-volume-atom scenario from evolving alternatives. *Finally, we situate the proposal within broader approaches to the cosmological constant.*

1.13 Context within other proposals

Our account differs by relying solely on established QCD confinement, thermodynamics, and holography. Landscape/anthropic approaches [57], extra-dimensional

dilution [58, 59], QFT-in-curved-spacetime renormalizations [60, 61], sequestering [62], SUSY cancellations [63], and holographic dark-energy scalings [64] each rest on unverified assumptions. Here the smallness of Λ follows from a bulk–boundary *count*, a lattice echo, and a force–area law at the horizon, with a concrete experimental target at ℓ_S.

Conclusion

Confinement, Meissner-like U(1) suppression, the Third Law, and horizon holography suffice to organize the late-time vacuum into *SU(3) vacuum atoms*. The integer $N \simeq (R_u/R_p)^3$ simultaneously fixes a Planck-sized horizon patch and, via a uniform force–area law, enforces $\rho_\Lambda = \rho_{su(3)}/N$ without fine tuning. Matching to Snyder/GUP fixes a *spacetime coherence length* $\ell_S \simeq 10^{-5}$ m, squarely in reach of current quantum technologies. Quantization about the resulting cylinder–forest background satisfies OS/Wightman axioms and yields a positive vacuum-sector spectral gap. Counting and geometry, not cancellation, connect SU(3) confinement to the smallness of Λ and the numerical values of $(\hbar, G, c)$.

Acknowledgments. We thank colleagues for helpful discussions and the organizers of the 28th Bled Workshop for the invitation.

Appendix: Snyder/GUP vacuum integral

With density-of-states factor $(1+\beta p^2)^{-3}$,

$$\rho_{\rm vac}^{\rm GUP} c^2 = \frac{1}{(2\pi\hbar)^3}\int \frac{d^3p}{(1+\beta p^2)^3}\,\frac{\hbar c\, p}{2} = \frac{2\pi\hbar c}{(2\pi\hbar)^3}\int_0^\infty \frac{p^3\,dp}{(1+\beta p^2)^3}.$$

Let $u = 1+\beta p^2$. Then $p^2 = (u-1)/\beta$ and $2p\,dp = du/\beta$, so

$$\int_0^\infty \frac{p^3\,dp}{(1+\beta p^2)^3} = \frac{1}{2\beta^2}\int_1^\infty \frac{u-1}{u^3}\,du = \frac{1}{2\beta^2}\left[\ln u + \frac{1}{u} - \frac{1}{2u^2}\right]_1^\infty = \frac{1}{2\beta^2}.$$

Thus $\rho_{\rm vac}^{\rm GUP} c^2 \propto (\hbar c)/\beta^2 \equiv \hbar c/\ell_S^4$ with $\ell_S = \hbar\sqrt{\beta}$.

References

1. M. Ali and A. F. Ali, Deriving the cosmological constant and nature's constants from SU(3) confinement volume, EPL **151** (2025) 39002.
2. A. F. Ali, Unbreakable SU(3) Atoms of Vacuum Energy: A Solution to the Cosmological Constant Problem, Symmetry **17** (2025) 888.
3. S. Weinberg, The Cosmological Constant Problem, Rev. Mod. Phys. **61** (1989) 1–23.
4. P. J. E. Peebles and B. Ratra, The Cosmological Constant and Dark Energy, Rev. Mod. Phys. **75** (2003) 559–606.
5. N. Aghanim et al. (Planck Collaboration), Planck 2018 results. VI. Cosmological parameters, Astron. Astrophys. **641** (2020) A6.
6. Particle Data Group, Review of Particle Physics, Phys. Rev. D **98** (2018) 030001.

7. S. L. Glashow, Partial-symmetries of Weak Interactions, Nucl. Phys. **22** (1961) 579–588.
8. S. Weinberg, A Model of Leptons, Phys. Rev. Lett. **19** (1967) 1264–1266.
9. A. Salam, Weak and Electromagnetic Interactions, in: *Elementary Particle Theory*, Nobel Symposium 8 (1968) 367–377.
10. G. Aad et al. (ATLAS Collaboration), Observation of a new particle with the ATLAS detector at the LHC, Phys. Lett. B **716** (2012) 1–29.
11. S. Chatrchyan et al. (CMS Collaboration), Observation of a New Boson at a Mass of 125 GeV, Phys. Lett. B **716** (2012) 30–61.
12. M. Creutz, Confinement and the Critical Dimensionality of Space-Time, Phys. Rev. Lett. **43** (1979) 553–556.
13. M. Creutz, Monte Carlo Study of Quantized SU(2) Gauge Theory, Phys. Rev. D **21** (1980) 2308–2315.
14. A. Bazavov et al. (HotQCD Collaboration), Meson screening masses in (2+1)-flavor QCD, Phys. Rev. D **100** (2019) 094510.
15. S. D. Liang and T. Harko, Superconducting Dark Energy, Phys. Rev. D **91** (2015) 085042.
16. N. Inan, A. F. Ali, K. Jusufi, A. F. Yasser, Graviton Mass due to Dark Energy as a Superconducting Medium, JCAP **08** (2024) 012.
17. H. S. Snyder, Quantized space-time, Phys. Rev. **71** (1947) 38–41.
18. A. Kempf, On quantum group symmetric minimal uncertainty relations, J. Math. Phys. **35** (1994) 4483–4496.
19. A. Kempf and G. Mangano, Minimal length uncertainty relation and ultraviolet regularization, Phys. Rev. D **55** (1997) 7909–7920.
20. S. Hossenfelder, Minimal Length Scale Scenarios for Quantum Gravity, Living Rev. Relativity **16** (2013) 2.
21. A. F. Ali, S. Das, E. C. Vagenas, Discreteness of Space from the GUP, Phys. Lett. B **678** (2009) 497–499.
22. A. F. Ali, S. Das, E. C. Vagenas, Proposal for testing quantum gravity in the lab, Phys. Rev. D **84** (2011) 044013.
23. L. N. Chang, D. Minic, N. Okamura, T. Takeuchi, Effect of the minimal length uncertainty relation on the density of states, Phys. Rev. D **65** (2002) 125027.
24. L. N. Chang, Z. Lewis, D. Minic, T. Takeuchi, On the minimal length uncertainty relation, Adv. High Energy Phys. **2011** (2011) 493514.
25. M. A. Gorji, Minimal length and quantum gravitational corrections, Int. J. Mod. Phys. D **25** (2016) 1650078.
26. M. R. Andrews et al., Observation of interference between two Bose–Einstein condensates, Science **275** (1997) 637–641.
27. A. D. O'Connell et al., Quantum ground state and single-phonon control of a mechanical resonator, Nature **464** (2010) 697–703.
28. M. Bawaj et al., Probing deformed commutators with macroscopic harmonic oscillators, Nat. Commun. **6** (2015) 7503.
29. I. Pikovski, M. R. Vanner, M. Aspelmeyer, M. S. Kim, C. Brukner, Probing Planck-scale physics with quantum optics, Nat. Phys. **8** (2012) 393–397.
30. J. G. Lee et al., New test of gravity at millimeter scales, Phys. Rev. Lett. **124** (2020) 101101.
31. R. Pohl et al., The Size of the Proton, Nature **466** (2010) 213–216.
32. J. D. Bekenstein, Black holes and entropy, Phys. Rev. D **7** (1973) 2333–2346.
33. S. W. Hawking, Particle Creation by Black Holes, Commun. Math. Phys. **43** (1975) 199–220.
34. G. W. Gibbons and S. W. Hawking, Cosmological event horizons, thermodynamics, and particle creation, Phys. Rev. D **15** (1977) 2738–2751.

35. J. D. Brown and J. W. York Jr., Quasilocal energy and conserved charges derived from the gravitational action, Phys. Rev. D **47** (1993) 1407–1419.
36. J. D. Brown and J. W. York Jr., Microcanonical functional integral for the gravitational field, Phys. Rev. D **47** (1993) 1420–1431.
37. A. G. Riess et al., Observational Evidence for an Accelerating Universe, Astron. J. **116** (1998) 1009–1038.
38. S. Perlmutter et al., Measurements of Ω and Λ from 42 High-Redshift Supernovae, Astrophys. J. **517** (1999) 565–586.
39. D. Hilbert and S. Cohn-Vossen, *Geometry and the Imagination*, AMS Chelsea (2021).
40. K. Osterwalder and R. Schrader, Axioms for Euclidean Green's Functions, Commun. Math. Phys. **31** (1973) 83–112.
41. K. Osterwalder and R. Schrader, Axioms for Euclidean Green's functions II, Commun. Math. Phys. **42** (1975) 281–305.
42. J. Glimm and A. Jaffe, *Quantum Physics: A Functional Integral Point of View*, 2nd ed., Springer (2012).
43. T. Balaban, Propagators and renormalization transformations for lattice gauge theories. I, Commun. Math. Phys. **95** (1984) 17–40.
44. T. Balaban, Ultraviolet stability of 3D lattice pure gauge theories, Commun. Math. Phys. **102** (1985) 255–275.
45. T. Balaban, Renormalization group approach to lattice gauge fields. I, Commun. Math. Phys. **109** (1987) 249–301.
46. E. Seiler, *Gauge Theories as a Problem of Constructive QFT and Statistical Mechanics*, Lecture Notes in Physics **159** (1982).
47. J. Greensite, *An Introduction to the Confinement Problem*, Springer LNP **821** (2011).
48. A. Hatcher, *Algebraic Topology*, Cambridge Univ. Press (2002).
49. E. Hebey, *Nonlinear Analysis on Manifolds: Sobolev Spaces and Inequalities*, AMS (2000).
50. G. Boyd et al., Thermodynamics of SU(3) lattice gauge theory, Nucl. Phys. B **469** (1996) 419–444.
51. S. Borsanyi et al., Fluctuations of conserved charges at finite temperature from lattice QCD, JHEP **01** (2012) 138.
52. DESI Collaboration, DESI 2024 results I: BAO measurements (2024), arXiv:2404.xxxxx.
53. DESI Collaboration, DESI 2024 results II: Cosmological constraints (2024), arXiv:2404.xxxxx.
54. DESI Collaboration, DESI 2024 results III: Hubble tension implications (2024), arXiv:2404.xxxxx.
55. P. Carenza et al., Glueball dark matter: constraints and prospects (2022).
56. B. S. Acharya, M. Fairbairn, E. Hardy, Glueball Dark Matter in Non-standard Cosmologies, JHEP **07** (2017) 100.
57. L. Susskind, The anthropic landscape of string theory, in: *Universe or Multiverse?* (2003).
58. N. Arkani-Hamed, S. Dimopoulos, G. R. Dvali, The hierarchy problem and new dimensions at a millimeter, Phys. Lett. B **429** (1998) 263–272.
59. L. Randall and R. Sundrum, An alternative to compactification, Phys. Rev. Lett. **83** (1999) 4690–4693.
60. N. D. Birrell and P. C. W. Davies, *Quantum Fields in Curved Space*, Cambridge Univ. Press (1982).
61. L. Parker and D. Toms, *Quantum Field Theory in Curved Spacetime*, Cambridge Univ. Press (2009).
62. N. Kaloper and A. Padilla, Sequestering the Standard Model Vacuum Energy, Phys. Rev. Lett. **112** (2014) 091304.
63. L. Girardello and M. T. Grisaru, Soft Breaking of Supersymmetry, Nucl. Phys. B **194** (1982) 65.

64. A. G. Cohen, D. B. Kaplan, A. E. Nelson, Effective field theory, black holes, and the cosmological constant, Phys. Rev. Lett. **82** (1999) 4971–4974.

BLED WORKSHOPS
IN PHYSICS
VOL. 26, NO. 1

Proceedings of the 28th Workshop
What Comes Beyond . . . *(p. 10)*
Bled, Slovenia, July 6–17, 2025

2 Emergent Gravity from a Spontaneously Broken Gauge Symmetry: a Pre-geometric Prospective

Andrea Addazi†

Center for Theoretical Physics, College of Physics Science and Technology, Sichuan University, 610065 Chengdu, China; Laboratori Nazionali di Frascati INFN, Frascati (Rome), Italy, EU

Abstract. We explore the paradigm of pre-geometric gravity, where spacetime geometry and the gravitational field are not fundamental but emerge from the spontaneous symmetry breaking (SSB) of a larger gauge symmetry. Specifically, we consider a gauge theory based on the de Sitter $SO(1,4)$ or anti-de Sitter $SO(3,2)$ group, formulated on a manifold without a prior metric structure. General covariance is maintained by constructing Lagrangian densities using the Levi-Civita symbol. The SSB is triggered by an internal vector field ϕ^A, which reduces the symmetry to the Lorentz group $SO(1,3)$ and dynamically generates a spacetime metric. We analyze two specific models: the MacDowell-Mansouri formulation, which yields the Einstein-Hilbert action plus a cosmological constant and a Gauss-Bonnet term, and the Wilczek model, which produces a pure Einstein-Hilbert action with a cosmological constant. In both cases, the observed Planck mass and the small cosmological constant emerge from a see-saw mechanism dependent on the symmetry-breaking scale. We then present the Hamiltonian formulation of this pre-geometric theory, demonstrating that it possesses three number of physical degrees of freedom, corresponding to a massless graviton and a massive scalar. Integrating out the massive scalar, the Arnowitt-Deser-Misner Hamiltonian of General Relativity is obtained after SSB. This establishes a foundational bridge between pre-geometric theories and canonical quantum gravity approaches like Loop Quantum Gravity, and allows for the formulation of a pre-geometric Wheeler-DeWitt equation.

Povzetek: Avtor predstavi svoj predlog za umeritveno de Sitterjevo $SO(1,4)$ ali anti-de Sitterjevo $SO(3,2)$ teorijo, brez metrične strukture v prostoru-času. Gravitacijsko polje in geometrija prostora-časa se pojavita po spontani zlomitvi teh dveh simetrij. Izbere Levi-Civitajevo Lagrangeovo gostoto tako, da vektorsko polje ϕ^A zlomi začetno simetrijo na Lorentzovo simetrijo $SO(1,3)$ in generira metriko prostora-časa. Analizira dva modela: MacDowell-Mansourijevo formulacijo, ki ponudi Einstein-Hilbertovo akcijo, kozmološko konstanto in Gauss-Bonnetov člen, in Wilczekov model, ki ponudi Einstein-Hilbertovo akcijo in kozmološko konstanto. Oba primera ponudita razlago za izmerjeno Planckovo maso in majhno kozmološko konstanto. Hamiltonova formulacija problema ponudi graviton brez mase in skalar z maso. Sledi Arnowitt-Deser-Misnerjeva Hamiltonova funkcija splošne teorije relativnosti. Avtor tako poveže teorijo kvantne gravitacije brez metrične strukture v prostoru-času s splošno teorijo relativnosti.

†addazi@scu.edu.cn

2.1 Introduction

The quest for a theory of quantum gravity remains one of the most profound challenges in theoretical physics. Traditional approaches, such as string theory and loop quantum gravity, often quantize the gravitational field as described by General Relativity (GR), treating the metric $g_{\mu\nu}$ as the fundamental dynamical variable. An alternative and radical perspective posits that spacetime itself, along with its geometric properties, is not fundamental but is an emergent, low-energy phenomenon arising from more primitive, pre-geometric degrees of freedom. This emergent gravity paradigm suggests that the Einstein equivalence principle, the Diffeomorphism invariance and the dynamics of Riemannian geometry are effective consequences of the dynamics of underlying structures. A compelling realization of this idea is to derive gravity from a gauge principle, where the metric and the spin connection emerge as components of a gauge field for a larger symmetry group, which is then spontaneously broken.
In this work, we review the results from recent investigations following this pre-geometric prospective [1–3], by starting from a gauge theory of the de Sitter $SO(1,4)$ or anti-de Sitter $SO(3,2)$ groups on a four-dimensional manifold. Crucially, this manifold is initially devoid of any metric structure; the only geometric object available is the Levi-Civita symbol $\epsilon^{\mu\nu\rho\sigma}$, which is used to construct generally covariant actions. The mechanism for emergence is the spontaneous breaking of the full gauge group down to the Lorentz group $SO(1,3)$, achieved through a Higgs field ϕ^A transforming in the vector representation of the internal group.
We focus on two pivotal pre-geometric Lagrangians: the MacDowell-Mansouri action [4] and the Wilczek action [5]. We show how, upon symmetry breaking, they successfully reproduce the Einstein-Hilbert action and generate a cosmological constant whose small observed value can be naturally explained via a see-saw mechanism with a large vacuum expectation value. Furthermore, we transition to the Hamiltonian formulation of this theory, as a basis of a detailed constraint analysis following Dirac's procedure [6]. This analysis shows the correct number of physical degrees of freedom of the theory revealing its deep connection to the canonical formulation of GR, opening a new pathway to explore quantum gravity from a pre-geometric standpoint.

2.2 Emergent Gravity from a Spontaneously Broken Phase

Let us consider a gauge field theory defined on a pre-geometric four-dimensional spacetime manifold. The gauge group is taken to be either the de Sitter group $SO(1,4)$ or the anti-de Sitter group $SO(3,2)$. The associated gauge potentials are denoted by A_μ^{AB}, and the corresponding field strengths by $F_{\mu\nu}^{AB}$, with antisymmetry in both the Latin and Greek indices. The objective of this construction is to dynamically generate a Riemannian metric structure and consequently the Einstein-Hilbert action—thereby recovering the Einstein Equivalence Principle—without presupposing the existence of a spacetime metric or tetrads, while still adhering to the principle of general covariance. Only an internal metric with signature $(-,+,+,+,+)$ or $(+,+,+,-,-)$, generalizing the Minkowski metric η,

is assumed for each tangent space. This can be achieved via the Higgs mechanism, utilizing a spacetime scalar field ϕ^A which is a vector in the internal space. A spontaneous symmetry breaking (SSB) of its ground state can reduce the original gauge symmetry down to the Lorentz group $SO(1,3)$ [5]. In this broken phase, the curvature of spacetime and its dynamics emerge effectively from the interactions of the pre-geometric fields A_μ^{AB} and ϕ^A below a specific energy scale.
Adherence to general covariance mandates that Lagrangian densities must be scalar densities of weight -1. Since A_μ^{AB} and $F_{\mu\nu}^{AB}$ are covariant tensors in their spacetime indices, the formation of scalar densities requires contravariant objects to contract these indices. In the absence of an inverse metric, the only intrinsically defined four-dimensional contravariant object on the manifold is the constant Levi-Civita symbol $\epsilon^{\mu\nu\rho\sigma}$, which is a tensor density of weight -1. The term 'intrinsically' here implies that no structure beyond the differential properties of the manifold is necessary; in particular, a metric is not required. The density character itself is defined solely through the Jacobian determinant of coordinate transformations. Consequently, the Levi-Civita symbol, used to its first power, is the fundamental object for constructing generally covariant Lagrangian densities, as it contracts exactly four covariant indices and already possesses the correct weight.
Utilizing the Levi-Civita symbol, two distinct gravitational Lagrangian densities can be formulated for the unbroken phase. The first, introduced by MacDowell and Mansouri [4], is given by

$$\mathcal{L}_{MM} = k_{MM}\epsilon_{ABCDE}\epsilon^{\mu\nu\rho\sigma}F_{\mu\nu}^{AB}F_{\rho\sigma}^{CD}\phi^E, \tag{2.1}$$

while the second, proposed by Wilczek [5], takes the form

$$\mathcal{L}_W = k_W\epsilon_{ABCDE}\epsilon^{\mu\nu\rho\sigma}F_{\mu\nu}^{AB}\nabla_\rho\phi^C\nabla_\sigma\phi^D\phi^E. \tag{2.2}$$

Here, ∇_μ signifies the gauge covariant derivative acting on internal vectors as

$$\nabla_\mu\phi^A = \partial_\mu\phi^A + A_{B\mu}^A\phi^B = (\delta_B^A\partial_\mu + A_{B\mu}^A)\phi^B, \tag{2.3}$$

where $A_{B\mu}^A \equiv \eta_{BC}A_\mu^{AC}$. Uppercase Latin indices range from 1 to 5, and Greek indices from 1 to 4. The mass dimensions of the coupling constants are $[k_{MM}] = [\phi]^{-1}$ and $[k_W] = [\phi]^{-3}$, with the dimension of the field ϕ^A left unspecified for now.
Before examining the SSB mechanism itself, this section will analyze the effective theory after the symmetry breaking from $SO(1,4)$ or $SO(3,2)$ to $SO(1,3)$ has occurred. This allows us to first understand the classical physical implications of these theories before venturing into the pre-geometric regime.

2.2.1 The MacDowell-Mansouri Model

The SSB mechanism singles out a preferential direction in the internal space, characterized by a fixed vacuum expectation value $\phi^A = v\delta_5^A$, where v is a non-zero constant. This breaking allows for a classification of the gauge potentials: for each spacetime index μ, four potentials are of the type $A_\mu^{A5} \equiv A_\mu^{a5}$ (where the

index 5 is fixed), and the remaining six are $A_\mu^{AB} \equiv A_\mu^{ab}$ (with $A, B \neq 5$). Lowercase Latin indices (1 to 4) are used to describe the broken phase.
Let us first compute the form of $\mathcal{L}_{MM}$ after SSB. Upon making the identifications

$$e_\mu^a \equiv m^{-1} A_\mu^{a5}, \qquad \omega_\mu^{ab} \equiv A_\mu^{ab}, \tag{2.4}$$

where e, ω are tetrads and spin connections, where a mass parameter m is introduced for dimensional consistency, the Lagrangian density decomposes into three distinct terms:

$$\mathcal{L}_{MM} \overset{SSB}{\rightarrow} \pm 16 k_{MM} \nu m^2 e e_a^\mu e_b^\nu R_{\mu\nu}^{ab} - 96 k_{MM} \nu m^4 e - 4 k_{MM} \nu e \mathcal{G}, \tag{2.5}$$

which correspond to the EH plus the Cosmological Constant plus the Gauss-Bonnet terms. For consistency with established physics, the reduced Planck mass must be identified as

$$M_P^2 \equiv \pm 32 k_{MM} \nu m^2. \tag{2.6}$$

This indicates the emergent nature of the Planck scale, as it arises from a specific combination of the fundamental parameters k_{MM}, ν, and m. Consequently, the cosmological constant is also emergent, given by

$$\Lambda \equiv \pm 3 m^2 = \frac{3 M_P^2}{32 k_{MM} \nu}. \tag{2.7}$$

This expression for Λ reveals a natura see-saw suppression mechanism. Assuming the experimentally measured value $M_P^2 \sim 10^{37}$ GeV^2 and a coupling constant of order unity ($k_{MM} \sim \pm 1\,[\phi]^{-1}$), the observed small value $\Lambda \sim 10^{-84}$ GeV^2 can be generated from a large vacuum expectation value $\nu \sim 10^{119}\,[\phi]$. Within this framework, the cosmological constant is set by the mass scale m of the symmetry breaking.

2.2.2 The Wilczek Model

The analysis of the SSB for $\mathcal{L}_W$ follows a parallel path to that of $\mathcal{L}_{MM}$. One additional element is required: the action of the covariant derivative on the internal vector ϕ^A after its vacuum value is fixed. From Eq. (2.3), we find

$$\nabla_\mu \phi^A \overset{SSB}{\rightarrow} \nu \nabla_\mu \delta_5^A = \nu(\cancel{\partial_\mu \delta_5^A} + A_{B\mu}^A \delta_5^B) = \nu A_{5\mu}^A = \pm \nu A_\mu^{a5}. \tag{2.8}$$

Utilizing the identifications (2.4) and following a computation analogous to the previous case, we arrive at the result:

$$\mathcal{L}_W \overset{SSB}{\rightarrow} -4 k_W \nu^3 m^2 e e_a^\mu e_b^\nu R_{\mu\nu}^{ab} \pm 48 k_W \nu^3 m^4 e. \tag{2.9}$$

This theory yields precisely the Einstein-Hilbert Lagrangian plus a cosmological constant term, with no Gauss-Bonnet contribution. The reduced Planck mass and cosmological constant are identified as

$$M_P^2 \equiv -8 k_W \nu^3 m^2, \qquad \Lambda \equiv \pm 6 m^2 = \mp \frac{3 M_P^2}{4 k_W \nu^3}. \tag{2.10}$$

Again, assuming a coupling of order unity ($k_W \sim -1\,[\phi]^{-3}$), the observed value $\Lambda \sim 10^{-84}$ GeV^2 emerges from a large VEV $\nu \sim 10^{40}\,[\phi]$.

2.2.3 Spontaneous Symmetry Breaking Mechanism

The process of spontaneous symmetry breaking (SSB), which reduces the gauge symmetry from $SO(1,4)$ or $SO(3,2)$ to the Lorentz group $SO(1,3)$ via the field ϕ^A, is responsible for the dynamical emergence of a classical spacetime metric. This mechanism can be implemented by introducing a simple symmetry-breaking potential term into the Lagrangian density:

$$\mathcal{L}_{SB} = -k_{SB}\nu^{-4}|J|(\eta_{AB}\phi^A\phi^B \mp \nu^2)^2, \tag{2.11}$$

where k_{SB} is a positive dimensionless constant. The mass dimension of the coupling is $[k_{SB}] = [\phi]^{-5}$. The potential $-\mathcal{L}_{SB}$ is minimized, and this term is stationarized, for field configurations satisfying $\eta_{AB}\phi^A\phi^B = \pm\nu^2$. A specific solution, such as $\phi^A = \nu\delta^A_5$, can be chosen; any other vacuum expectation value (v.e.v.) related to this by a gauge transformation is physically equivalent [5]. The factor of $|J|$ ensures that $\mathcal{L}_{SB}$ transforms as a scalar density, thus preserving general covariance. It is noteworthy that if one imposes a unimodular condition, as done by Wilczek [5], the $|J|$ factor can be omitted. In that case, the coupling constant k_{SB} assumes a fixed mass dimension of $[M]^4$, independent of the chosen dimensions for the field ϕ^A. The field ϕ^A is quantized by expanding it around its v.e.v. as $\phi^A = (\nu + \rho)\delta^A_5$, which defines the unitary gauge. In this gauge, the four would-be Goldstone bosons associated with the broken generators are absorbed, leaving a single scalar degree of freedom ρ.

An alternative mechanism for achieving spontaneous symmetry breaking, which circumvents the introduction of an explicit potential, was explored in Ref. [3]. This approach posits that the field ϕ^A can dynamically evolve towards a fixed expectation value through a gradient descent process. This relaxation is mathematically governed by a set of Langevin equations, situating the mechanism within the broader context of stochastic quantization.

2.3 The Hamiltonian Formulation of Pre-geometric Gravity

The total Lagrangian density introduced above exhibits degeneracy due to its structure as a summation of terms that are linear in the temporal derivatives (velocities) of the pre-geometric fields. Consequently, to finalize the Hamiltonian analysis, it is necessary to implement Dirac's systematic procedure for handling constrained systems or gauge theories [6].

In case of Wilczek model, the complete Hamiltonian density [2] is given by

$$\begin{aligned}\mathcal{H} = -A_0^{AB}\Big[&\partial_i\Pi^i_{AB}(\phi,A) + 2\Pi^i_{BC}(\phi,A)A^C_{Ai} \\ &+ \eta_{BC}\Pi_A(\phi,A)\phi^C\Big] + \lambda^A Z_A + \lambda_i^{AB}Z^i_{AB} + \lambda_0^{AB}Z^0_{AB},\end{aligned}$$

with λ^A, λ_i^{AB}, and λ_0^{AB} representing arbitrary Lagrange multipliers, where the conjugate momenta on the constraint surface in phase space are

$$\begin{aligned}\Pi_A(\phi,A) &\equiv 2\epsilon_{ABCDE}\epsilon^{0ijk}\nabla_k\phi^D\phi^E[k_W F^{BC}_{ij} \\ &\quad - 2(J)k_{SSB}\nu^{-4}\nabla_i\phi^B\nabla_j\phi^C(\phi^2 \mp \nu^2)^2], \\ \Pi^\lambda_{AB}(\phi,A) &\equiv 2k_W\epsilon_{ABCDE}\epsilon^{0\lambda jk}\nabla_j\phi^C\nabla_k\phi^D\phi^E;\end{aligned} \tag{2.12}$$

in particular,

$$\Pi^{i}_{AB}(\phi, A) = 2k_W \epsilon_{ABCDE} \epsilon^{0ijk} \nabla_j \phi^C \nabla_k \phi^D \phi^E, \tag{2.13a}$$

$$\Pi^{0}_{AB}(\phi, A) = 0. \tag{2.13b}$$

The three primary constraints of the theory are then

$$Z_A \equiv \Pi_A - \Pi_A(\phi, A) \approx 0, \tag{2.14a}$$

$$Z^{i}_{AB} \equiv \Pi^{i}_{AB} - \Pi^{i}_{AB}(\phi, A) \approx 0, \tag{2.14b}$$

$$Z^{0}_{AB} \equiv \Pi^{0}_{AB} \approx 0, \tag{2.14c}$$

where the symbol $\approx$ denotes a weak equality on the constraint surface.
Imposing the time preservation of the primary constraint Z^0_{AB} leads to the secondary constraint:

$$\begin{aligned} \dot{Z}^{0}_{AB} = \{Z^{0}_{AB}, H\} &= \partial_i \Pi^{i}_{AB}(\phi, A) \\ &\quad + 2\Pi^{i}_{BC}(\phi, A) A^{C}_{Ai} + \eta_{BC} \Pi_A(\phi, A) \phi^C \approx 0. \end{aligned} \tag{2.15}$$

Consequently, the total Hamiltonian density simplifies to

$$\begin{aligned} \mathcal{H} &= -A^{AB}_0 \dot{Z}^{0}_{AB} + \lambda^A Z_A + \lambda^{AB}_i Z^{i}_{AB} + \lambda^{AB}_0 Z^{0}_{AB} + \tilde{\lambda}^{AB}_0 \dot{Z}^{0}_{AB} \\ &\equiv \lambda^A Z_A + \lambda^{AB}_i Z^{i}_{AB} + \lambda^{AB}_0 Z^{0}_{AB} + \tilde{\lambda}^{AB}_0 \dot{Z}^{0}_{AB}, \end{aligned} \tag{2.16}$$

where in the final expression the terms proportional to $\dot{Z}^0_{AB}$ have been consolidated through a redefinition of the multiplier $\tilde{\lambda}^{AB}_0$. It is noteworthy that the field A^{AB}_0 no longer appears in the total Hamiltonian density, confirming its status as a gauge degree of freedom. As a result, the multiplier λ^{AB}_0 associated with its corresponding primary constraint Z^0_{AB} remains arbitrary.
As shown in Ref. [2] , the phase space of the theory is described by 90 dynamical variables, comprised of the fields and their conjugate momenta: 10 components of A^{AB}_0, 30 of A^{AB}_i, 5 of ϕ^A, 10 of Π^0_{AB}, 30 of Π^i_{AB}, and 5 of Π_A. The gauge freedom of the system is characterized by 20 gauge-fixing conditions, which remove the unphysical degrees of freedom associated with A^{AB}_0 and Π^0_{AB}. The constraint structure consists of 10 independent first-class constraints (Z^0_{AB}) generating gauge transformations, and 44 independent second-class constraints (30 Z^i_{AB}, 5 Z_A, 10 $\dot{Z}^0_{AB}$, minus one combination fixing the Hamiltonian H).
The number of physical degrees of freedom is consequently determined by the formula:

$$2 \times \#(\text{degrees of freedom}) = \#(\text{dynamical variables}) - \#(\text{gauge choices})$$

$$-2 \times \#(\text{first-class constraints}) - \#(\text{second-class constraints}) = 6\,.$$

This result implies the theory possesses 3 physical degrees of freedom. This count is consistent with the particle content of a massless spin-2 graviton (2 degrees of freedom) and a massive scalar field, identified as $\phi^5 \equiv \rho$, contributing one additional degree of freedom, analogous to the field content of a scalar-tensor

theory formulated in a metric framework. Note that, such counting of d.o.f. is a general background independent result.
As shown in Ref. [2] , after the SSB, the Hamiltonian of pre-geometric gravity reduces exactly to the EH Hamiltonian in ADM formalism, while the heavy scalar ρ as frozen in IR limit. Consequently, the theoretical framework presented here exhibits full compatibility with the formalism of Loop Quantum Gravity. Notably, a compelling connection arises as the pre-geometric theory naturally gives rise to variables analogous to Ashtekar's electric fields obtained from the pre-geometric Π^{i}_{A0} after SSB.
It is noteworthy that, having derived an explicit form for the pre-geometric Hamiltonian, one can consequently formulate a pre-geometric analogue of the Wheeler–DeWitt equation:

$$\mathcal{H}|\Psi\rangle = 0, \tag{2.17}$$

where $|\Psi\rangle$ represents the quantum state encompassing configurations of both the gauge and Higgs fields. This formulation provides a novel framework to re-examine the foundational issue of time in quantum gravity [2].

2.4 Conclusions

In this work, we have elaborated on a robust framework for emergent gravity from a spontaneously broken gauge symmetry, operating within a pre-geometric setting where no prior metric exists. The core findings of our analysis can be summarized as follows:

1. **Successful Emergence of Geometry:** We demonstrated that both the MacDowell-Mansouri and Wilczek Lagrangian densities, constructed solely from the gauge field A_{μ}^{AB}, the Higgs field ϕ^{A}, and the Levi-Civita symbol, dynamically generate the Einstein-Hilbert action and a cosmological constant upon spontaneous symmetry breaking of $SO(1,4), SO(3,2)$ to $SO(1,3)$. The resulting Planck mass M_P is emergent, arising from a combination of the fundamental parameters of the pre-geometric theory.
2. **A Natural See-Saw for the Cosmological Constant:** A particularly attractive feature of this mechanism is the natural explanation for the smallness of the observed cosmological constant Λ. In both models, Λ is proportional to the square of the symmetry-breaking mass scale m. A large vacuum expectation value v for the Higgs field ϕ^{A} suppresses Λ, leading to a see-saw relation. For couplings of order unity, the measured value of Λ requires v to be very large, while m is of the order of the Hubble scale, an intriguing and potentially significant outcome.
3. **Consistent Hamiltonian Structure:** The Hamiltonian analysis of the pre-geometric theory reveals a constrained system with a consistent number of physical degrees of freedom. The count confirms the presence of a massless spin-2 graviton (2 dof) and a massive scalar mode (1 dof), aligning with the field content of a scalar-tensor theory. After symmetry breaking, the Hamiltonian reduces to the well-known ADM Hamiltonian of General Relativity, with the scalar mode freezing in the infrared limit.

4. **Bridge to Quantum Gravity:** The formulation of a pre-geometric Hamiltonian and the associated constraints provides a direct link to canonical quantization approaches. The structure naturally gives rise to variables analogous to Ashtekar's electric fields, suggesting a deep connection to Loop Quantum Gravity. Furthermore, it allows for the definition of a pre-geometric analogue of the Wheeler-DeWitt equation, $\mathcal{H}|\Psi\rangle = 0$, offering a novel perspective to address the problem of time in quantum gravity by considering quantum states of the pre-geometric fields.

Looking forward, several intriguing questions remain open. The quantization of this pre-geometric theory appears promising but non-trivial, with issues of operator ordering still to be tackled. An alternative pathway via stochastic quantization suggests the theory may interpolate between a topological BF theory in the ultraviolet and General Relativity in the infrared. Finally, the robustness of the see-saw mechanism for the cosmological constant against quantum corrections must be investigated; it may necessitate supplementary mechanisms like virtual black-hole screening [7] or generalized holographic principles [8–10] to ensure naturalness. The pre-geometric approach presented here offers a fertile and compelling framework to explore these fundamental questions at the intersection of gravity, particle physics, and quantum theory.

Acknowledgements

I would like to thank my main collaborators on these subjects: Salvatore Capozziello, Giuseppe Meluccio and Antonino Marciano. My work is supported by the National Science Foundation of China (NSFC) through the grant No. 12350410358; the Talent Scientific Research Program of College of Physics, Sichuan University, Grant No. 1082204112427; the Fostering Program in Disciplines Possessing Novel Features for Natural Science of Sichuan University, Grant No.2020SCUNL209 and 1000 Talent program of Sichuan province 2021.

References

1. A. Addazi, S. Capozziello, A. Marciano and G. Meluccio, Class. Quant. Grav. **42** (2025) no.4, 045012 doi:10.1088/1361-6382/ada767 [arXiv:2409.02200 [hep-th]].
2. A. Addazi, S. Capozziello, A. Marcianò and G. Meluccio, [arXiv:2505.01272 [gr-qc]].
3. A. Addazi, S. Capozziello, J. Liu, A. Marciano, G. Meluccio and X. L. Su, [arXiv:2505.17014 [gr-qc]].
4. S. MacDowell, F. Mansouri, Unified Geometric Theory of Gravity and Supergravity, Phys. Rev. Lett. **38**, 739 (1977).
5. F. Wilczek, Riemann-Einstein Structure from Volume and Gauge Symmetry, Phys. Rev. Lett. **80**, 4851–4854 (1998).
6. P. A. M. Dirac, Generalized Hamiltonian Dynamics, Can. J. Math. **2**, 129–148 (1950).
7. A. Addazi, EPL **116** (2016) no.2, 20003 doi:10.1209/0295-5075/116/20003 [arXiv:1607.08107 [hep-th]].
8. A. Addazi, Int. J. Mod. Phys. D **29** (2020) no.14, 2050084 doi:10.1142/S0218271820500844 [arXiv:2004.08372 [hep-th]].

9. A. Addazi, Eur. Phys. J. Plus **135** (2020) no.11, 940 doi:10.1140/epjp/s13360-020-00933-4
10. A. Addazi, P. Chen, F. Fabrocini, C. Fields, E. Greco, M. Lulli, A. Marciano and R. Pasechnik, Front. Astron. Space Sci. **8** (2021), 1 doi:10.3389/fspas.2021.563450 [arXiv:2004.13751 [gr-qc]].

BLED WORKSHOPS
IN PHYSICS
VOL. 26, NO. 1

Proceedings of the 28th Workshop
What Comes Beyond . . . *(p. 19)*
Bled, Slovenia, July 6–17, 2025

3 Unified Pati–Salam from Noncommutative Geometry: Overview and Phenomenological Remarks

Ufuk Aydemir[†]

Department of Physics, Middle East Technical University, Ankara 06800, Türkiye

Abstract. The lack of clear new-physics signals at the LHC searches motivates models that can guide current and future collider searches. The spectral action principle within the noncommutative geometry (NCG) framework yields such models with distinctive phenomenology. This formalism derives the actions of the Standard Model, General Relativity, and beyond from the underlying algebra, putting them on a common geometric footing. Certain versions of Pati-Salam (PS) models with *gauge coupling unification* and limited scalar content can be derived from an appropriate noncommutative algebra. In this paper, I review these gauge-coupling-unified Pati-Salam models and discuss their phenomenological aspects, focusing on the S_1 scalar leptoquark.

Povzetek: Meritve na pospeševalniku LHC v Cernu doslej ne kažejo signalov, ki bi pomagali ugotoviti kako razložiti privzetke *standardnega modela*. Avtor uporabi nekomutativno algebro, ki mu omogoči izpeljati akcijo. Ta poveže *standardni model* in splošno teorijo relativnosti. Uporabi model Patija in Salama, ki poenoti sklopitvene konstante umeritvenih polj. Pregleda napovedi različic tega modela, posebej predstavi napovedi za skalarni leptokvark S_1.

Keywords: Noncommutative Geometry, Spectral Action, Pati-Salam, $R_{D^{(*)}}$ anomaly, scalar leptoquarks

3.1 Introduction

Since the discovery of the Higgs boson, a relentless effort has been put into the search for new physics beyond the Standard Model (SM). Contrary to high expectations stemming from the paradigms that contributed to the outstanding success of the SM, there has been no discovery of new physics at the LHC yet. In these difficult times, we should leave no stone unturned and explore all promising models that can help guide the experimental searches. In particular, models based on paradigms toward a deeper understanding of nature are specifically important. This is where Noncommutative Geometry (NCG) [1, 2] comes in. In analogy with quantum mechanics, NCG, by redefining notions of geometry, describes nature in terms of operator algebras instead of point sets of ordinary geometry. In the modern version of the framework, one can derive the SM, General Relativity (GR), and beyond by utilizing an appropriate action based on the Spectral Action

[†]uaydemir@metu.edu.tr

principle [3–5]. Reconciling the SM and gravity in a geometric setting, NCG offers a unifying picture of their origin.

The main object in NCG is the *spectral triple* $(\mathcal{A}, \mathcal{H}, \mathcal{D})$, where $\mathcal{A}$ is an involutive algebra, $\mathcal{H}$ is a Hilbert space on which the algebra acts as bounded operators, and the (generalized) Dirac operator $\mathcal{D}$, a (possibly) unbounded self-adjoint operator. The spectral triple is augmented by extra structures [3] such as a $\mathbb{Z}_2$ grading through the chirality operator Γ (generalized γ_5) and an antilinear unitary operator $\mathcal{J}$ (generalized charged conjugation) on $\mathcal{H}$. This structure encodes the information on the geometry; the ordinary points are now replaced by the spectrum of the Dirac operator, the inverse of which acts as a metric. On the other hand, the information on the manifold is recovered by the algebra $\mathcal{A}$.

The spectral data $(\mathcal{A}, \mathcal{H}, \mathcal{D}, \Gamma, \mathcal{J})$ is given as the product of the ordinary part, corresponding to four-dimensional manifold M, with a finite space with noncommutative geometry. This corresponds to two sheeted spacetime with $M \times \mathbb{Z}_2$. One can obtain physical models, depending on the choice of the finite part, and using the spectral action given by $\mathcal{S} = \mathcal{S}_F + \mathcal{S}_B = (J\psi, \mathcal{D}_A\psi) + \mathrm{Tr}\,[\chi(\mathcal{D}_A/\Lambda)]$, where the former term corresponds to the fermionic sector (which also yields the Yukawa terms due to the Higgs embedded in the Dirac operator) and the latter is for purely bosonic part [3,4]. "Tr" is the trace over the Hilbert space $\mathcal{H}$. The cutoff function χ acts as a regulator that selects the eigenvalues of the covariant Dirac operator, $\mathcal{D}_A$, smaller than the cutoff Λ.

In the basic construction [3,4], the algebra is chosen as $\mathcal{A} = C^\infty(M) \otimes \mathcal{A}_F$ such that the finite part of the algebra is given as $\mathcal{A}_F = \mathbb{C} \oplus \mathbb{H} \oplus M_3(\mathbb{C})$, where $\mathbb{H} \subset M_2(\mathbb{C})$ is the algebra of quaternions, and $M_3(\mathbb{C})$ is the algebra of 3×3 matrices with elements in $\mathbb{C}$. Then, the spectral action yields the SM action and the action of a modified gravity model, the latter of which consists of the Einstein-Hilbert and the cosmological constant terms, a non-minimal coupling term between the Higgs boson and the curvature, the Gauss-Bonnet term, and the Weyl (or the conformal gravity) term. The SM parameters are included in the Dirac operator, and the Higgs boson arises as the connection in the extra discrete dimension. The gauge transformations emerge from the unitary inner automorphisms of the algebra $\mathcal{A}$ while diffeomorphisms arise from the outer automorphisms. In Refs. [6,7], by utilizing the algebra $\mathcal{A}_F = \mathbb{H}_R \oplus \mathbb{H}_L \oplus M_4(\mathbb{C})$, constructed models with Pati-Salam (PS) gauge structure $G_{422} = SU(4) \times SU(2)_L \times SU(2)_R$. Depending on whether the so-called order-one condition is satisfied, three versions of these models are obtained with different scalar content and with/without left-right symmetry.

PS models based on noncommutative geometry (NCG-PS) come with a number of appealing features compared to the ordinary counterparts, heavily studied in the literature [9–11]. First, NCG-PS models require *gauge coupling unification*, which is a feature that is not mandatory in ordinary PS models unless they are embedded in a larger group such as $SO(10)$ [12–16]. Furthermore, as opposed to the ordinary PS models, NCG-PS models come with a restricted content of scalar fields with enough number and quality required for certain symmetry-breaking patterns and mass generation; not all interaction terms are allowed in the Lagrangian. These features increase the predictivity of these models. Finally, the proton stability due to the light leptoquarks S_1 (which is our interest in our work, as will be discussed

below) is not generally guaranteed; in NCG-PS, on the other hand, the diquark couplings of some of these leptoquarks are missing, and them being light does not cause an issue of concern, as pointed out in Ref. [8]. I also note that the fermion content in the NCG-PS models is the same as the Standard Model (SM) plus the right-handed neutrinos of each generation, similar to the GUT models.
In this presentation, I briefly review NCG-based Pati-Salam (NCG-PS) models, with gauge coupling unification, and discuss certain differences from the ordinary Pati-Salam models. Regarding the low-energy phenomenology, I focus on the new physics scenario of TeV-scale leptoquark(s) of S_1 type.

3.2 Minimal NCG framework; Spectral Standard Model (with gravity)

As mentioned above, the algebra chosen for the construction that accommodates the SM is given as [3–5]

$$\mathcal{A} = C^\infty(M) \otimes \mathcal{A}_F \,, \quad \text{where} \quad \mathcal{A}_F = \mathbb{C} \oplus \mathbb{H} \oplus M_3(\mathbb{C}) \,, \tag{3.1}$$

$\mathbb{H} \subset M_2(\mathbb{C})$ is the algebra of quaternions, and $M_3(\mathbb{C})$ is the algebra of 3×3 matrices with elements in $\mathbb{C}$. One can easily recognize the correspondence between the elements of the finite algebra $\mathcal{A}_F$ and the SM gauge groups $U(1)$, $SU(2)$, and $S(3)$. The action, called the *spectral action*, is constructed as

$$\mathcal{S} = \mathcal{S}_F + \mathcal{S}_B = (J\psi, \mathcal{D}_A\psi) + \mathrm{Tr}\left[\chi\left(\frac{\mathcal{D}_A}{\Lambda}\right)\right] \,. \tag{3.2}$$

The second term corresponds to the purely bosonic part of the action, whereas the first term is the fermionic part, including the Yukawa sector. Note that the Dirac operator includes the Higgs field as the gauge connection between the two sides of the finite part of the spacetime (two points, at each of which a 4d manifold is located) connecting the left and right sectors. χ is the cutoff function that selects the eigenvalues of the covariant Dirac operator $\mathcal{D}_A$ smaller than the cutoff scale Λ. J is the generalized charge conjugation to account for the antiparticles and manages the real structure on $\mathcal{H}$ [3, 4]; it is an antiunitary operator acting on the Hilbert space $\mathcal{H}$. Finally; the covariant Dirac operator, $\mathcal{D}_A$, in terms of the unperturbed Dirac operator $\mathcal{D}$, real structure operator J, and a Hermitian one-form potential A, is given as

$$\mathcal{D}_A = \mathcal{D} + A + JAJ^\dagger, \quad \text{where} \quad A = \sum a_i\,[\mathcal{D}, b_i]\,, \quad a_i, b_i \in \mathcal{A}, \quad \text{and} \quad A = A^* \,. \tag{3.3}$$

The first equation accounts for the inner fluctuations of the line element (inverse D). There is also the so-called first-order condition [17], given as

$$\left[[\mathcal{D}, a], JbJ^{-1}\right] = 0, \quad \forall a, b \in \mathcal{A} \,, \tag{3.4}$$

which is specifically important beyond the standard framework, as will be mentioned in the next section.

The generalized Dirac operator is chosen accordingly to yield the fermionic sector of the SM, including the Yukawa terms. The construction predicts certain relations among the Yukawa couplings to be satisfied at the energy scale at which the spectral action is assumed to emerge [3,4]. Note also that this construction requires gauge coupling unification with the same field content as the SM. At this point, we need to look at the bosonic part of the action, given in Eq. (3.2). Since the details are not important for this talk (and the interested reader can check Refs. [3–5] for more details), I just give the final action here. The bosonic part of the spectral SM action is given as

$$\begin{aligned}\mathcal{S}_B = \int \Bigg(& \frac{1}{2\kappa_0^2} R + \alpha_0 C_{\mu\nu\rho\sigma} C^{\mu\nu\rho\sigma} + \gamma_0 + \tau_0 R^* R^* \\ & + \frac{f_0}{2\pi^2} \left[g_3^2 G^i_{\mu\nu} G^{\mu\nu i} + g_2^2 F^m_{\mu\nu} F^{\mu\nu m} + \frac{5}{3} g_1^2 B_{\mu\nu} B^{\mu\nu} \right] \\ & + |D_\mu H|^2 - \mu_0^2 |H|^2 - \xi_0 R |H|^2 + \lambda_0 |H|^4 + O\left(\frac{1}{\Lambda^2}\right) \Bigg) \sqrt{|g|}\, d^4x \,, \end{aligned} \tag{3.5}$$

where R is the usual Ricci scalar, $C_{\mu\nu\rho\sigma}$ is the Weyl tensor, R^*R^* denotes the topological Gauss-Bonnet term, and $(\kappa_0, \alpha_0, \gamma_0, \tau_0, \mu_0, \xi_0, \lambda_0)$ are constants defined in terms of original parameters in the theory. The theory is truncated in the lowest relevant order in the energy scale Λ and is clearly not UV-complete in the common sense, which can be viewed as a shortcoming of the framework. Another issue is that a QFT formalism that is faithful to the NCG structure has not been completely established (see Ref. [18] for a recent study to this end.) Therefore, it is conceivable to consider that the action emerges as a geometric structure at a certain high energy scale, much lower than the cutoff scale Λ. On top of that geometric structure, we assume that the usual QFT framework is valid as an initial approximation. Note that the model based on Lagrangian (3.5) leads to the wrong Higgs mass. In Ref. [19], the authors argue that there is an extra singlet field in the theory that can correct the Higgs mass.

One can see in the bosonic action, given in Eq. (3.5), the requirement of gauge coupling unification. Sticking to the canonical normalization of the kinetic terms, one obtains the condition

$$g_3^2 = g_2^2 = \frac{5}{3} g_1^2 \,, \tag{3.6}$$

assumed to satisfy at a certain unification scale M_U. One may have an immediate tendency to identify M_U with the cutoff scale Λ ($M_U \sim \Lambda$), but for the truncation of the action in (3.5) to be acceptable, it is more reasonable to require $M_U \ll \Lambda$. Since in this minimal construction, we only have the SM field content, the gauge coupling unification is not achievable with the usual perturbative RG running. Ref. [20] examined a modification of the minimal construction that yields several additional scalar fields; however, Ref. [21] demonstrated that gauge coupling unification cannot be realized within this modified framework, regardless of the mass hierarchy of the extra fields. Therefore, it is necessary to extend the spectral formalism beyond the minimal framework.

3.3 Pati-Salam models from NCG with gauge coupling unification

3.3.1 Basics

In Refs. [6,7], the formalism was extended by changing the the algebra, given in Eq. (3.1), to

$$\mathcal{A} = C^\infty(M) \otimes \mathcal{A}_F \ , \quad \text{where} \quad \mathcal{A}_F = \mathbb{H}_R \oplus \mathbb{H}_L \oplus M_4(\mathbb{C}) \ , \tag{3.7}$$

and selecting the rest of the spectral data appropriately. The framework yields three models with different scalar contents and initial gauge symmetries, depending on whether the order-one condition is fully satisfied. The scalar contents of the models are listed in Table 3.1, with the notation $G_{422D} = SU(4)_C \otimes SU(2)_L \otimes SU(2)_R \otimes D$, where the D symbol refers to the left-right symmetry, a Z_2 symmetry which keeps the left and the right sectors equivalent. The symbol G_{422} is used for the case where the Pati-Salam gauge group appears without the D symmetry. For the full spectral Pati-Salam action, including gravitational terms, see Ref. [6].

Table 3.1: The scalar content of the three NCG-based Pati-Salam models.

Model	Symmetry	Scalar Content
A	G_{422}	$\phi(1,2,2)_{422}$, $\Sigma(15,1,1)_{422}$, $\widetilde{\Delta}_R(4,1,2)_{422}$
B	G_{422}	$\phi(1,2,2)_{422}$, $\widetilde{\Sigma}(15,2,2)_{422}$, $\Delta_R(10,1,3)_{422}$, $H_R(6,1,1)_{422}$
C	G_{422D}	$\phi(1,2,2)_{422}$, $\widetilde{\Sigma}(15,2,2)_{422}$, $\Delta_R(10,1,3)_{422}$, $H_R(6,1,1)_{422}$, $\Delta_L(10,3,1)_{422}$, $H_L(6,1,1)_{422}$

A common way to break the PS symmetry into the SM can be schematically shown as [8]

$$\text{NCG} \xRightarrow{M_U} G_{422D} \xrightarrow[\langle \Delta_R \rangle]{M_C} G_{321} \ , \tag{3.8}$$

where the double arrow denotes the symmetry emerging from the underlying NCG at the unification scale M_U (or above), while the single arrow denotes the spontaneous symmetry breaking in the usual way. Breaking of the Pati-Salam symmetry into the SM proceeds through the SM singlet within $\Delta_R(10,1,3)_{422}$, acquiring a VEV. Depending on whether the selected model (i.e. A, B, or C) contains the necessary fields, intermediate symmetry-breaking stages can be included [22, 23].

As in the case of ordinary PS models, the fermions are in $(4,2,1)_{422}$ and $(4,1,2)_{422}$ representations, which can be put in the following form.

$$\psi_{aI} = (\psi_{a0}, \psi_{ai}) \ = \ \begin{pmatrix} \psi_{10}, \psi_{1i} \\ \psi_{20}, \psi_{2i} \end{pmatrix} \ = \ (L_L, Q_L) \ = \ \begin{pmatrix} \nu_L, u_L \\ e_L, d_L \end{pmatrix} \ ,$$

$$\psi_{\dot{a}I} = (\psi_{\dot{a}0}, \psi_{\dot{a}i}) \;=\; \begin{pmatrix} \psi_{\dot{\imath}0}, \psi_{\dot{\imath}i} \\ \psi_{\dot{\jmath}0}, \psi_{\dot{\jmath}i} \end{pmatrix} \;=\; (L_R, Q_R) \;=\; \begin{pmatrix} \nu_R, u_R \\ e_R, d_R \end{pmatrix} , \qquad (3.9)$$

which is the SM fermion content with the right-handed neutrinos for each generation. The dotted and undotted lower-case Latin letters toward the beginning of the alphabet denote $SU(2)_R$ and $SU(2)_L$ indices in the fundamental representation, respectively: e.g. $\dot{a} = 1, 2$ and $a = 1, 2$. The $SU(4)$ index in the fundamental representation is denoted with upper-case Latin letters toward the middle of the alphabet: e.g. $I = 0, 1, 2, 3$, where $I = 0$ is the lepton index and $I = i = 1, 2, 3$ are the quark-color indices. The spinor and generation indices are omitted. Complex (hermitian, Dirac) conjugation raises or lowers both indices, e.g.

$$\overline{\psi}^{aI} \;=\; \overline{\psi_{aI}} , \qquad \overline{\psi}^{\dot{a}I} \;=\; \overline{\psi_{\dot{a}I}} . \qquad (3.10)$$

In the case of the $SU(2)$'s, the index can be lowered or raised using

$$(\epsilon)_{ab} , \qquad (\epsilon^\dagger)^{ab} , \qquad (\epsilon)_{\dot{a}\dot{b}} , \qquad (\epsilon^\dagger)^{\dot{a}\dot{b}} , \qquad (3.11)$$

where $\epsilon = i\sigma_2$.
The complex scalar fields in this framework are given as

$$\begin{aligned} \Sigma^{bJ}_{\dot{a}I} &= (1,2,2)_{422} + (15,2,2)_{422} , \\ H_{aIbJ} &= (6,1,1)_{422} + (10,3,1)_{422} , \\ H_{\dot{a}I\dot{b}J} &= (6,1,1)_{422} + (10,1,3)_{422} . \end{aligned} \qquad (3.12)$$

In model C, we have all of these fields, whereas in model B, which is, unlike model C, is not let-right symmetric, H_{aIbJ} is turned off. Finally, in model A, which is referred to as the *composite* model in Refs. [6,7], the $H_{\dot{a}I\dot{b}J}$ and $\Sigma^{bJ}_{\dot{a}I}$ fields are not fundamental and composed of the fields $\phi(1,2,2)_{422}$, $\Sigma(15,1,1)_{422}$, and $\widetilde{\Delta}_R(4,1,2)_{422}$.

3.3.2 Remarks on the low energy phenomenology

For the sake of this presentation, I will continue with the most general model, model C. I will only focus on the Yukawa sector, leaving out the scalar sector since the latter is not relevant for our discussion. The G_{422D} invariant Yukawa terms for each family of fermions can be written schematically as [6,8]

$$\mathcal{L}_Y \;=\; \left(\overline{\psi}^{\dot{a}I} \gamma_5 \Sigma^{bJ}_{\dot{a}I} \psi_{bJ} + \overline{\psi^C}_{aI} \gamma_5 H^{aIbJ} \psi_{bJ} + \overline{\psi^C}_{\dot{a}I} \gamma_5 H^{\dot{a}I\dot{b}J} \psi_{\dot{b}J} \right) \;+\; \text{h.c.} , \qquad (3.13)$$

where $\psi^C = C\overline{\psi}^T$. The Yukawa coupling constants are embedded in the complex scalar fields $\Sigma^{bJ}_{\dot{a}I}$, H^{aIbJ}, and $H^{\dot{a}I\dot{b}J}$. The γ_5 that appears in this expression is due to the grading of the geometry. Actually, the "grading" in the product space $M \times F$, where M is the continuous 4D manifold and F is the finite part, is realized by the generalized chirality operator $\Gamma = \gamma_5 \otimes \gamma_F$; here, γ_5 is the usual chirality operator for the continuous manifold and γ_F introduces a Z_2 grading and responsible for the algebra of quaternionic matrices $M_2(\mathbb{H})$ into $\mathbb{H}_R \oplus \mathbb{H}_L$ [24]. The first

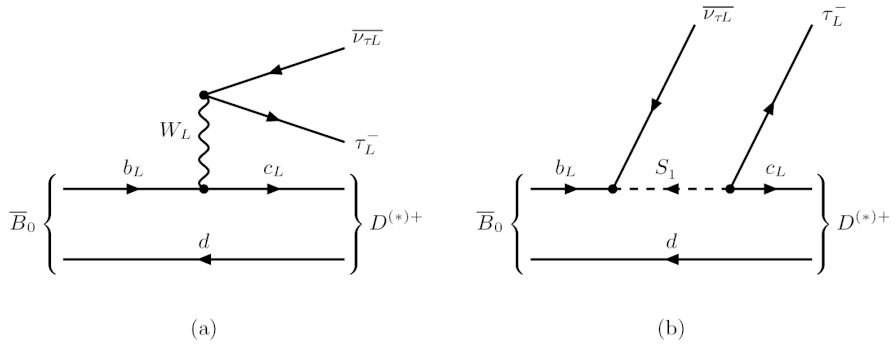

Fig. 3.1: (a) SM and (b) S_1 leptoquark contribution to $\overline{B}_0 \to D^{(*)+}\tau^-\overline{\nu_\tau}$. Adapted from Ref. [8].

term in Eq. (3.13) yields terms containing fermions with opposite chiralities (LR) through the 'connection' $\Sigma^{bJ}_{\dot{a}I}$. The LL and RR terms arise from the second and third terms due to fields H^{aIbJ} and $H^{\dot{a}I\dot{b}J}$, respectively, which connect fermions and antifermions with the same chirality.

After spontaneous symmetry breaking to the SM, the terms in Eq. (3.13) yield all the SM terms in addition to interaction terms between the SM sector and new fields. This is similar to the ordinary Pati-Salam models. However, in addition to gauge coupling unification and the restricted scalar content, the NCG-based Pati–Salam (NCG–PS) models differ further from the ordinary ones in terms of the allowed Lagrangian terms. Some of the terms that would be expected in the ordinary case (unless some extra ad-hoc symmetries are imposed) do not appear in the NCG-PS models automatically due to the underlying noncommutative geometry. These differences lead to advantages/predictions that could help to probe these models.

Consider the anomalies in the charged-current B decays that have been around for over a decade [25–27][1], notably in the $R_{D^{(*)}}$ observables, defined as

$$R_{D^{(*)}} = \frac{\mathrm{BR}\left(B \to D^{(*)}\tau\nu\right)}{\mathrm{BR}\left(B \to D^{(*)}\ell\nu\right)}\,, \tag{3.14}$$

where $\ell = \{e, \mu\}$ and BR denotes branching ratio. The latest averaged experimental values of these observables deviate from the SM values by more than 3σ, as estimated by the Heavy Flavor Averaging Group [29]. The leptoquark $S_1(\overline{3}, 1, 1/3)_{321}$ is a popular minimal option, providing a tree-level solution [8, 15, 16, 30–32] (see Fig. 3.1).[2]

[1] See Ref. [28] for a recent review of current anomalies in high energy physics.

[2] The leptoquark $S_3\left(\overline{3}, 3, \frac{1}{3}\right)_{321}$ can also provide a solution [31] through its component with electric charge 1/3. While it provides a safe option regarding the proton stability, it comes in rather larger multiplets compared to $S_1(\overline{3}, 1, 1/3)_{321}$, which might be more appealing for a compact explanation.

The existence of such a scalar leptoquark at the TeV scale would prompt important questions. The immediate one is its UV origin. Leptoquarks [33,34] appear in supersymmetric extensions of the SM, composite (strongly-coupled) models, grand unified theories, and Pati-Salam-type partially unified models, and finally our NCG-PS models with complete gauge coupling unification. NCG-PS models have an appealing feature over the other. As previously mentioned, due to the underlying noncommutative structure, the scalar sector of each of the three models is quite restrictive, thus predictive. Another important point would be the mechanism that prevents diquark couplings of S_1 type leptoquark, since such couplings would mediate proton decay [35]. In fact, proton stability is the reason why, in grand unified theories, S_1 type leptoquarks are assumed to be heavy near the unification scale. Particularly in $SO(5)$ and $SO(10)$ theories, as well as in supersymmetric theories in general, the SM Higgs doublet is accompanied by a leptoquark in a larger multiplet. Keeping the leptoquark heavy while having the SM doublet light is known as the infamous double-triplet splitting problem.
In NCG-PS models, even though there are several S_1 type leptoquarks, only one of them can appropriately provide a solution to the $R_{D^{(*)}}$ anomaly, reflecting the restricted and predictive aspect of this framework. The S_1 leptoquarks in models A and B couple either only to right-handed fermions or only to diquarks [8]; hence, they are not useful for the $R_{D^{(*)}}$ anomaly. On the other hand, in model C, one of the leptoquarks in the (complexified) $H(6,1,1)_{422}$ possesses the required couplings to left-handed fermions, while lacking the diquark couplings. Therefore, it can provide a solution and does not mediate proton decay. Namely, in model C, we have the object

$$H_{aIbJ} = \Delta_{(ab)(IJ)} + H_{[ab][IJ]} = \Delta_L(10,3,1)_{422} + H_L(6,1,1)_{422}\ . \tag{3.15}$$

The sextet is decomposed into the SM components as

$$H_L(6,1,1)_{422} = H_{3L}\left(3,1,-\frac{1}{3}\right)_{321} + H_{\bar{3}L}\left(\bar{3},1,\frac{1}{3}\right)_{321}\ , \tag{3.16}$$

which, for the complexified sextet, corresponds to two different leptoquarks. Then, the second term (with its h.c.) in Eq. (3.13) yields, for each family, the terms [8]

$$\begin{aligned}&\bar{\psi}^C_{aI}\gamma_5 H^{[ab][IJ]}\psi_{bJ} + \text{h.c.}\\ &= 2\left[\left(\overline{d^C_{Lj}}\nu_L - \overline{u^C_{Lj}}e_L\right)H^{*j}_{3L} + \varepsilon^{ijk}\overline{u^C_{Li}}d_{Lj}H^*_{\bar{3}Lk}\right] + \text{h.c.}\ ,\end{aligned} \tag{3.17}$$

where H^*_{3L} can be identified as the "good" leptoquark that has left-handed couplings while lacking diquark couplings. On the other hand, $H^*_{\bar{3}L}$ couples to diquarks, thus mediating proton decay, and should be taken heavy.[3] The exclusive

[3] In the ordinary, non-unified, PS framework, the scalar sector is generally constructed with $\Delta_R(10,1,3)_{422}$, $\Delta_L(10,3,1)_{422}$, and the bidoublet $\phi(1,2,2)_{422}$. Due to the totally symmetric nature of the scalar sector, there exists a symmetry that prevents these couplings [36]. However, if one includes the multiplet $(6,1,1)_{422}$, as is the case in NCG-PS models, which transforms antisymmetrically under $SU(4)$, then the symmetry no longer naturally exists.

left-handed couplings of S_1 should not impede $R_{D^{(*)}}$ solutions; however, they reduce the available parameter space compared with regular models. One possible significance of the absence of the right-handed couplings could be in the context of the magnetic moment of the muon, $g-2$ (a_μ). The S_1 contribution to a_μ (see Fig. 3.2) with only left-handed couplings is suppressed and comes with a negative sign. This would have been a problem for the a_μ discrepancy between theory and experiment that persisted for several decades. However, recent developments on both sides suggest that such a discrepancy may be absent.

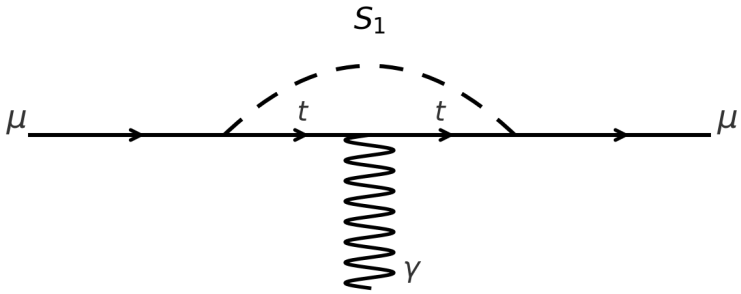

Fig. 3.2: Leading order contribution to a_μ from a S_1 leptoquark.

Note that I have selected the above model just as a sample. I have aimed to address the $R_{D^{(*)}}$ anomaly with a single S_1 that does not cause proton decay. The only one at our disposal was H^*_{3L}, contained in $H_L(6,1,1)_{422}$ in model C. If the right-handed couplings of S_1 are also needed to address a measurement of a particular observable, one can include the one in $H_R(6,1,1)_{422}$ (see Table 3.1), whose decomposition is the counterpart of Eq. (3.16) with the components denoted as H_{3R} and $H_{\bar{3}R}$. The corresponding Yukawa terms, in addition to the ones in Eq. (3.17), come from the third term (with its h.c) in Eq. (3.13) given for each family as [8]

$$\begin{aligned}&\overline{\psi^C}_{\dot{a}I}\gamma_5 H^{[\dot{a}\dot{b}][IJ]}\psi_{\dot{b}J} \;+\; \text{h.c.}\\ &= 2\left[\left(\overline{d^C_{Rj}}\nu_R - \overline{u^C_{Rj}}e_R\right)H^{*j}_{3R} \;+\; \varepsilon^{ijk}\overline{u^C_{Ri}}d_{Rj}H^*_{\bar{3}Rk}\right] \;+\; \text{h.c.}\,, \end{aligned} \tag{3.18}$$

with H^{*j}_{3R} being the "good" leptoquark with no diquark couplings.
Besides a_μ and $R_{D^{(*)}}$, one can analyze

In our case, the proton-decay–mediating diquark couplings of our leptoquark are automatically absent due to the geometric construction. Compared to the regular PS models, NCG-PS may not seem to have an advantage regarding this issue, since in both cases, the proton is safe. Yet, considering other advantages of the latter, such as gauge coupling unification, restricted scalar content, and an underlying geometric explanation for the theory that reconciles also gravity on the same footing, one can argue in favor of the appeal of NCG-PS models.

$$R_{K^{(*)}} \equiv \frac{BR\left(B \to K^{(*)}\mu^+\mu^-\right)}{BR\left(B \to K^{(*)}e^+e^-\right)} \quad \text{and} \quad R_K^{\nu} \equiv \frac{BR(B \to K\nu\nu)}{BR(B \to K\nu\nu)_{SM}} ,$$

along with observables, such as $BR(\tau \to \mu\gamma)$, $BR(\tau \to 3\mu)$, $BR\left(B_c \to \tau\nu\right)$, among others [16,37], for specific candidate particle(s) (e.g. S_1). Given the restricted and predictive structure of NCG–PS models, such a global analysis can yield stringent, model-discriminating information on physics beyond the SM.

3.4 Summary and Outlook

By analogy with quantum mechanics, noncommutative geometry (NCG) reformulates geometry in terms of operator algebras rather than point sets. In its modern formulation, an action based on the spectral action principle [3–5] can be used to accommodate the SM, GR, and beyond. By placing the particle physics theories and gravity on the same geometric footing, this framework offers a unified perspective on their origin and may be viewed as a step toward quantum gravity. Using an appropriate algebra, one can construct models with the Pati–Salam (PS) gauge group $SU(4) \times SU(2)_L \times SU(2)_R$ with the condition of gauge-coupling unification [6,7]. Depending on an underlying geometric condition, referred to as the order-one condition, three versions of these models are obtained with different scalar content and with/without left-right symmetry.

The NCG–based Pati–Salam framework, with its restricted scalar content and Yukawa structure, yields a characteristic setup. As an illustration, I focused on a TeV-scale S_1 leptoquark. In Model C, the required couplings to address current flavor anomalies are present, whereas proton-decay–mediating diquark couplings of this leptoquark are automatically absent due to the geometric construction, rather than by ad hoc assumptions.

The absence of clear new-physics signals at the LHC motivates models that can guide current and future searches. The spectral action formalism in the NCG framework provides distinctive Pati-Salam models with gauge coupling unification that deserve attention.

Acknowledgements

This work was supported by The Scientific and Technological Research Council of Türkiye (TÜBİTAK) BİDEB 2232-A program under project No. 121C067.

References

1. A. Connes, *Noncommutative geometry*. 1994.
2. A. Connes and M. Marcolli, *Noncommutative Geometry, Quantum Fields and Motives*. American Mathematical Society, 2007.
3. A. H. Chamseddine and A. Connes, *Universal formula for noncommutative geometry actions: Unification of gravity and the standard model*, *Phys. Rev. Lett.* **77** (1996) 4868–4871, [hep-th/9606056].

4. A. H. Chamseddine and A. Connes, *The Spectral action principle*, *Commun. Math. Phys.* **186** (1997) 731–750, [hep-th/9606001].
5. W. D. van Suijlekom, *Noncommutative Geometry and Particle Physics*. Springer, 12, 2024, 10.1007/978-3-031-59120-4.
6. A. H. Chamseddine, A. Connes and W. D. van Suijlekom, *Beyond the Spectral Standard Model: Emergence of Pati-Salam Unification*, *JHEP* **11** (2013) 132, [1304.8050].
7. A. H. Chamseddine, A. Connes and W. D. van Suijlekom, *Grand Unification in the Spectral Pati-Salam Model*, *JHEP* **11** (2015) 011, [1507.08161].
8. U. Aydemir, D. Minic, C. Sun and T. Takeuchi, B*-decay anomalies and scalar leptoquarks in unified Pati-Salam models from noncommutative geometry*, *JHEP* **09** (2018) 117, [1804.05844].
9. J. C. Pati and A. Salam, *Lepton Number as the Fourth Color*, *Phys. Rev.* **D10** (1974) 275–289.
10. R. N. Mohapatra and J. C. Pati, *A Natural Left-Right Symmetry*, *Phys. Rev.* **D11** (1975) 2558.
11. R. N. Mohapatra and J. C. Pati, *Left-Right Gauge Symmetry and an Isoconjugate Model of CP Violation*, *Phys. Rev.* **D11** (1975) 566–571.
12. D. Chang, R. N. Mohapatra, J. Gipson, R. E. Marshak and M. K. Parida, *Experimental Tests of New SO(10) Grand Unification*, *Phys. Rev. D* **31** (1985) 1718.
13. S. Bertolini, L. Di Luzio and M. Malinsky, *Intermediate mass scales in the non-supersymmetric SO(10) grand unification: A Reappraisal*, *Phys. Rev. D* **80** (2009) 015013, [0903.4049].
14. U. Aydemir and T. Mandal, *LHC probes of TeV-scale scalars in* SO(10) *grand unification*, *Adv. High Energy Phys.* **2017** (2017) 7498795, [1601.06761].
15. U. Aydemir, T. Mandal and S. Mitra, *Addressing the* $R_{D^{(*)}}$ *anomalies with an* S_1 *leptoquark from* SO(10) *grand unification*, *Phys. Rev. D* **101** (2020) 015011, [1902.08108].
16. U. Aydemir, T. Mandal, S. Mitra and S. Munir, *An economical model for* B*-flavour and* a_μ *anomalies from SO(10) grand unification*, 2209.04705.
17. A. H. Chamseddine, A. Connes and W. D. van Suijlekom, *Inner Fluctuations in Noncommutative Geometry without the first order condition*, *J. Geom. Phys.* **73** (2013) 222–234, [1304.7583].
18. T. D. H. van Nuland and W. D. van Suijlekom, *One-loop corrections to the spectral action*, *JHEP* **05** (2022) 078, [2107.08485].
19. A. H. Chamseddine and A. Connes, *Resilience of the Spectral Standard Model*, *JHEP* **09** (2012) 104, [1208.1030].
20. M. A. Kurkov and F. Lizzi, *Clifford Structures in Noncommutative Geometry and the Extended Scalar Sector*, *Phys. Rev.* **D97** (2018) 085024, [1801.00260].
21. U. Aydemir, *Clifford-based spectral action and renormalization group analysis of the gauge couplings*, *Eur. Phys. J. C* **79** (2019) 325, [1902.08090].
22. U. Aydemir, D. Minic, C. Sun and T. Takeuchi, *Pati-Salam unification from noncommutative geometry and the TeV-scale* W_R *boson*, *Int. J. Mod. Phys.* **A31** (2016) 1550223, [1509.01606].
23. U. Aydemir, D. Minic, C. Sun and T. Takeuchi, *The 750 GeV diphoton excess in unified* $SU(2)_L \times SU(2)_R \times SU(4)$ *models from noncommutative geometry*, *Mod. Phys. Lett. A* **31** (2016) 1650101, [1603.01756].
24. A. H. Chamseddine and W. D. Van Suijlekom, *A survey of spectral models of gravity coupled to matter*. 1904.12392.
25. BaBar collaboration, J. P. Lees et al., *Evidence for an excess of* $\bar{B} \to D^{(*)}\tau^-\bar{\nu}_\tau$ *decays*, *Phys. Rev. Lett.* **109** (2012) 101802, [1205.5442].
26. LHCb collaboration, R. Aaij et al., *Measurement of the ratio of branching fractions* $\mathcal{B}(\bar{B}^0 \to D^{*+}\tau^-\bar{\nu}_\tau)/\mathcal{B}(\bar{B}^0 \to D^{*+}\mu^-\bar{\nu}_\mu)$, *Phys. Rev. Lett.* **115** (2015) 111803, [1506.08614].

27. Belle collaboration, S. Hirose et al., *Measurement of the τ lepton polarization and $R(D^*)$ in the decay $\bar{B} \to D^* \tau^- \bar{\nu}_\tau$ with one-prong hadronic τ decays at Belle*, *Phys. Rev. D* **97** (2018) 012004, [1709.00129].
28. A. Crivellin and B. Mellado, *Anomalies in Particle Physcis*, *PoS* **DIS2024** (2025) 007.
29. Heavy Flavor Averaging Group (HFLAV) collaboration, S. Banerjee et al., *Averages of b-hadron, c-hadron, and τ-lepton properties as of 2023*, 2411.18639.
30. M. Bauer and M. Neubert, *Minimal Leptoquark Explanation for the $R_{D^{(*)}}$, R_K, and $(g-2)_\mu$ Anomalies*, *Phys. Rev. Lett.* **116** (2016) 141802, [1511.01900].
31. A. Angelescu, D. Be?irevi?, D. A. Faroughy and O. Sumensari, *Closing the window on single leptoquark solutions to the B-physics anomalies*, *JHEP* **10** (2018) 183, [1808.08179].
32. U. Aydemir, *B-flavour and a_μ anomalies with S_1 leptoquark in SO(10) Grand Unification*, in *Beyond Standard Model: From Theory to Experiment*, 2023, DOI.
33. W. Buchmuller, R. Ruckl and D. Wyler, *Leptoquarks in Lepton - Quark Collisions*, *Phys. Lett. B* **191** (1987) 442–448.
34. I. Doršner, S. Fajfer, A. Greljo, J. F. Kamenik and N. Košnik, *Physics of leptoquarks in precision experiments and at particle colliders*, *Phys. Rept.* **641** (2016) 1–68, [1603.04993].
35. P. Nath and P. Fileviez Perez, *Proton stability in grand unified theories, in strings and in branes*, *Phys. Rept.* **441** (2007) 191–317, [hep-ph/0601023].
36. R. N. Mohapatra and R. E. Marshak, *Local B-L Symmetry of Electroweak Interactions, Majorana Neutrinos and Neutron Oscillations*, *Phys. Rev. Lett.* **44** (1980) 1316–1319.
37. A. Bhaskar, A. A. Madathil, T. Mandal and S. Mitra, *Combined explanation of W-mass, muon g-2, RK(*) and RD(*) anomalies in a singlet-triplet scalar leptoquark model*, *Phys. Rev. D* **106** (2022) 115009, [2204.09031].

BLED WORKSHOPS
IN PHYSICS
VOL. 26, NO. 1

Proceedings of the 28th Workshop
What Comes Beyond . . . *(p. 31)*
Bled, Slovenia, July 6–17, 2025

4 Anomalous Isotopes In Dark Atoms models

M.I. Baliño[1¶], J.Mwilima[1‖], D. O. Sopin[1,2**], M. Yu. Khlopov[3††]

[1] National Research Nuclear University MEPhI 115409 Moscow, Russia
[2] Research Institute of Physics, Southern Federal University 344090, Rostov on Don, Russia
[3] Virtual Institute of Astroparticle physics 75018 Paris, France

Abstract. In this work, we study some aspects of the dark atom model. We consider a finite-size nucleus to find the wave functions of the bound state of a stable particle with a charge of $-2n$ and helium-4 $^4He^{++}$. Then we address the problem of calculating the abundance of anomalous isotopes arising from the capture of helium nuclei by dark atoms during Big Bang nucleosynthesis. We use an analogy with the proton–neutron capture process to calculate the reaction cross section and thus determine the concentration of OBe nuclei.

4.1 Introduction

Dark matter constitutes about 26% of the total energy density of the Universe, while its nature remains one of the key unsolved problems in modern cosmology [1]. Convincing evidence for its existence is manifested in the behavior of galaxies, gravitational lensing, and the anisotropy of the cosmic microwave background radiation. These observations indicate that dark matter is non-baryonic in nature. Various candidates for its composition are discussed, including weakly interacting massive particles (WIMPs), supersymmetric particles (SUSY), and other similar possibilities. The absence of positive detection results for WIMPs and supersymmetric particles at the Large Hadron Collider (LHC) makes it interesting to consider alternative candidates for dark matter.

A promising explanation is provided by the concept of *dark atoms*. In this scenario, a new heavy stable particle X with electric charge $-Z_X = -2n$ (where n is a natural number) binds with n helium nuclei (^{4}He) through the electromagnetic Coulomb interaction, forming neutral bound states. These composite systems, often referred to as XHe, represent a viable candidate for dark matter [2, 3]. The model can explain the paradoxes arising in the search for dark matter particles in underground experiments.

In the simplest case $n = 1$ ($Z_X = 2$), the system forms an OHe atom consisting of one heavy particle X with charge -2 (denoted O^{--}), and one ^{4}He nucleus with charge $+2$. The properties of such bound states are determined by their internal structure, the analysis of which is one of the main objectives of this study.

¶balinomagela@gmail.com
‖joshuamwilima02@gmail.com
**sopin@sfedu.ru
††7khlopov@apc.univ-paris7.fr

OHe atoms, created during Big Bang Nucleosynthesis in reaction

$$O^{--} + {}^4He^{++} \quad \searrow \quad OHe,$$

may interact with ordinary nuclei and thereby influence the chemical and cosmological evolution of the early Universe. In particular, the capture of ^{4}He nuclei by OHe can lead to the formation of anomalous isotopes such as OBe, whose abundance and physical consequences are the subject of this work.
This paper is organised as follows: in section 4.2 the Schrodinger equation is solved to find the wave functions of dark atoms. Then, in section 4.3, the probability and cosmological consequences of helium capture by dark atoms are estimated. We analyse the corresponding cross-sections estimated by analogy with the radiative capture of neutrons by protons and evaluate the resulting abundance of anomalous isotopes. The obtained results are briefly discussed in section 4.4 and in the Conclusion.

4.2 Solution of the Schrodinger equation

The inner structure of the dark atom should be similar to that assumed in Thomson's plum pudding model. Indeed, in most cases, the Bohr radius (in natural units: $\hbar = c = 1$) $r_B = (Z_N Z_X \alpha m_N)^{-1}$ of the nucleus N in the shell of such bound states is smaller than the nuclear charge radius r_N. Therefore, to describe the structure of the dark atom, it is necessary to consider the eigenvalue problem for the Schrodinger equation with a piecewise potential. The inner part should describe the charge distribution inside the nucleus, while the external part must coincide with the Coulomb potential.
The simplest choice is to consider a nucleus as a uniformly charged sphere. This assumption leads to an oscillatory potential

$$V(\rho) = \begin{cases} \dfrac{1}{a}\left(3 - \dfrac{\rho^2}{a^2}\right), \rho < a; \\ \dfrac{2}{\rho}, \rho > a, \end{cases} \tag{4.1}$$

where $\rho = r/r_B$, $a = r_N/r_B$. It describes the intersection of the heavy multicharged particle X^{-2n} and an ordinary, relatively light isotope N in the center of mass system. Other charge distributions require additional parameters, the values of which are determined by experiments. On the one hand, a more accurate spherically symmetric potential should provide only an insignificant correction for most combinations of particles. On the other hand, the deformation of the nuclei caused by the presence of a multicharged core eliminates the expected gain in accuracy. However, in several special cases, the use of spherically symmetric potentials may lead to unreliable predictions. In particular, to describe the structure of the anomalous isotope OBe^{++}, it is necessary to make more accurate calculations.
The radial Schrodinger equation in considered unites is

$$\partial_\rho^2 P(\rho) + \left(\varepsilon - \frac{l(l+1)}{\rho^2} + V(\rho)\right) P(\rho) = 0, \tag{4.2}$$

n	1	2	3	4	5
r_N, Fm	1.678 [4,5]				
$r_B, 10^{-3}$ MeV^{-1}	9.19	4.60	3.06	2.30	1.84
a	0.913	1.826	2.739	3.652	4.566
$E_{XN}^{Coulomb}$, MeV	1.588	6.352	14.291	25.406	39.698
$E_{XN}^{Piecewise}$, MeV	1.256	3.891	7.130	10.708	14.506

Table 4.1: Properties of X^{-2n}–^{4}He bound states

where $\varepsilon = 2m_N r_B^2 E_{XN}$, $P(r) = rR(r)$. This eigenvalue problem solution for different charges of the heavy core X is presented in Table 4.1. The obtained values of the ground state binding energy are significantly smaller than the Bohr-like estimate $E_{XN}^{Coulomb} = (2m_N r_B^2)^{-1}$ predicts. The corresponding eigenfunctions in the form of the physical radial functions $R(\rho) = P(\rho)/\rho$ for ^{4}He nucleus are shown in the left panel of Figure 4.1. Although the value at the origin decreases with increasing core charges, the probability of finding the heavy particle X inside the nucleus grows due to the change of the Bohr radius. The similar dependence may be found for the neutral states (see the right panel of Figure 4.1).

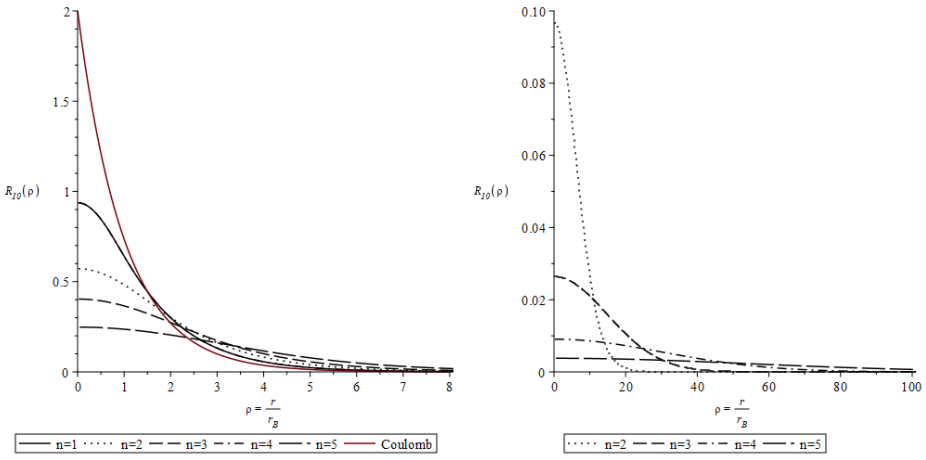

Fig. 4.1: The physical radial functions $R(\rho) = P(\rho)/\rho$ for X^{-2n}–^{4}He (left panel) and electrically neutral X – N bound states.

4.3 Interaction with nuclei

4.3.1 Rates of reactions

To produce the correct estimation of anomalous isotope concentration, it is necessary to consider at least two new reactions: dark atom recombination (radiative capture of the first helium) and the capturing of additional light nucleus. The

ratio of the first of them can be found with the analogy of ordinary hydrogen recombination. The rescaled semiclassical Kramer's formula [12] was used:

$$\langle \sigma v \rangle_{rec} = \frac{32}{3}\sqrt{\frac{\pi}{3}}\frac{Z_N}{Z_X}\frac{1}{m_N^4 r_B^2}\left(\frac{E_{X-N}}{T}\right)^{\frac{1}{2}}\left(\ln\left(\frac{E_{X-N}}{T}\right)+\gamma\right), \tag{4.3}$$

where $\gamma = 0.5772$ is an Euler constant. It approximately takes into account the transitions on excited states and therefore the estimation should be more accurate than with Stobbe formula. In case of ordinary recombination, the exact rate is 3.2% less than calculated with (4.3). However, in the processes that involve the dark atoms, the structure of the finite-size nucleus should be significant. It leads to a higher error and makes it possible only to get a quite accurate estimation.
The rate of the OHe atom interaction with light nuclei such as ^{4}He can be estimated by analogy with the radiative capture of neutrons by protons, taking into account:

- the absence of M1 transition (orbital angular momentum conservation),
- suppression of the E1 transition for the OHe system.

Since OHe is isoscalar, the isovector E1 transition is only possible due to isospin violation, parameterised by $f \sim 10^{-3}$. The resulting capture rate is given by [6]:

$$\langle \sigma v \rangle = \frac{f\alpha}{m_p^2}\cdot\sqrt{\frac{3}{2}}\left(\frac{Z}{A}\right)^2\cdot\frac{T}{\sqrt{A m_p E}}\,. \tag{4.4}$$

where A and Z are the atomic mass and charge numbers, E is the binding energy of the state, and T is the plasma temperature. For ^{4}He ($A = 4$, $Z = 2$), $E_{X-N} \approx 1.6$ MeV. At $T \sim 100$ keV the cross-section is of order $\sim 10^{-36}$ cm^2.
The rate of OHe photodestruction can be found with detailed equilibrium:

$$\frac{\langle \sigma v \rangle_{rec}}{\langle \sigma v \rangle_{\gamma}} = \left\langle \frac{2E_\gamma^2}{p_N^2} \right\rangle \approx \frac{2E_{X-N}^2}{m_N^2}\sqrt{\frac{2m_N}{\pi T}}, \tag{4.5}$$

where the approximation $E_\gamma \approx E_{X-N}$ was used. The right side of the equation is averaged over the Maxwellian distribution.

4.3.2 Numerical Estimation of OBe Abundance with LINX

To estimate the abundance of anomalous isotopes produced after the interaction of OHe with ordinary nuclei, we employed the nucleosynthesis code `LINX` [7], which uses methods and tables from [8–11]. This numerical framework is designed for modeling nuclear reactions under the conditions of Big Bang Nucleosynthesis (BBN). For the purposes of this study, we have introduced additional particle species (OHe and OBe) and implementing new reaction channels describing the radiative capture of two ^{4}He by new charged particle O^{--}.
The reaction cross-sections, described in Section 20.1, were incorporated into the network of reactions, allowing us to evolve the abundances consistently with cosmological parameters. However, the program requires to include the relative

concentration of photons with high enough energy $Y_\gamma(T) = n_\gamma/n_b$ by hands in case of radiative reactions. Therefore, it is necessary to find

$$Y_\gamma \frac{\langle\sigma v\rangle_\gamma}{\langle\sigma v\rangle_{rec}} = \frac{\delta\pi^{3/2}}{2\eta\zeta(3)} m_N^{3/2} E_{X-N}^{\xi-2} T^{-\xi+1/2} \exp\left(\frac{(\kappa-1)E_{X-N}}{T}\right), \tag{4.6}$$

where δ, ξ and κ is obtained by approximation of

$$Y_\gamma = \frac{1}{\eta}\frac{\pi^2}{2\,\zeta(3)\,T^3}\int_{E_{X-N}}^{\infty}\frac{E^2}{\exp\left(\frac{E}{T}\right)-1}dE, \tag{4.7}$$

$\eta = 6.04\cdot 10^{-10}$ is the baryon-to-photon ratio and $\zeta(3) \approx 1.202$ is the value of zeta function. The photodestruction $OBe + \gamma \to OHe + He$ becomes possible only at low energies, when the excess of XHe is generated. Also it requires at least the same energy of photon. Therefore, we can neglect it: $\langle\sigma v\rangle_\gamma / \langle\sigma v\rangle_{rec} \approx 0$.
Finally, with the assumption that initially all of the dark matter density is provided by O^{--} ($\frac{\rho_{DM}}{\rho_B} \approx 5.36$) the Fig. 4.2 can be calculated. The relative concentrations of dark matter particles at the end of nucleosynthesis ($T_{end} \approx 5$ keV) are

$$Y_{O--} \approx 1.2\cdot 10^{-18}, \qquad Y_{OHe} \approx 2.5\cdot 10^{-3}, \qquad Y_{OBe} \approx 8.5\cdot 10^{-9} \tag{4.8}$$

Almost all charged lepton-like particles recombine with helium. Moreover, there is the significant overproduction of anomalous isotopes OBe^{++}. The process of its formation freezes out shortly after the dark atom neutralization.

4.4 Discussion

The obtained result is only a preliminary estimation. To find the realistic concentrations of anomalous isotopes in the dark atom model, a more comprehensive treatment of nuclear processes is necessary.
Proton capture is expected to be strongly suppressed due to the excess of high-energy photons. Using the Saha-like formula, it is possible to estimate the temperature at which dark recombination with isotopes of hydrogen becomes possible. It is a few keV. At this time the concentration of free negatively charged particles should be negligible and, therefore, there is no production of OH bound states. Nevertheless, late proton capture is dangerous. Although ^{5}Li cannot be stabilized in a dark atom shell solely by the suppression of Coulomb repulsion, the synthesis of other lithium isotopes may be catalyzed [13]. The overproduction of primordial metals and anomalous isotopes is constitutes the central challenge for dark atom nucleosynthesis scenarios.
A potential resolution of this problem for the case of doubly charged particles ($n = 1$) may be found by considering the reactions $XN_1 + N_2 \to XN_3 + N_4 + ...$ The Fig. 4.2 shows that anomalous isotope production freezes out at relatively high temperatures. The interaction with primordial plasma may lead to the destruction of anomalous bound states at late nucleosynthesis stages. However, this requires much more careful analysis.
Generally, the same problems arise for all values of heavy core charges. However, there are several qualitative changes. First of all, the increased binding energy of

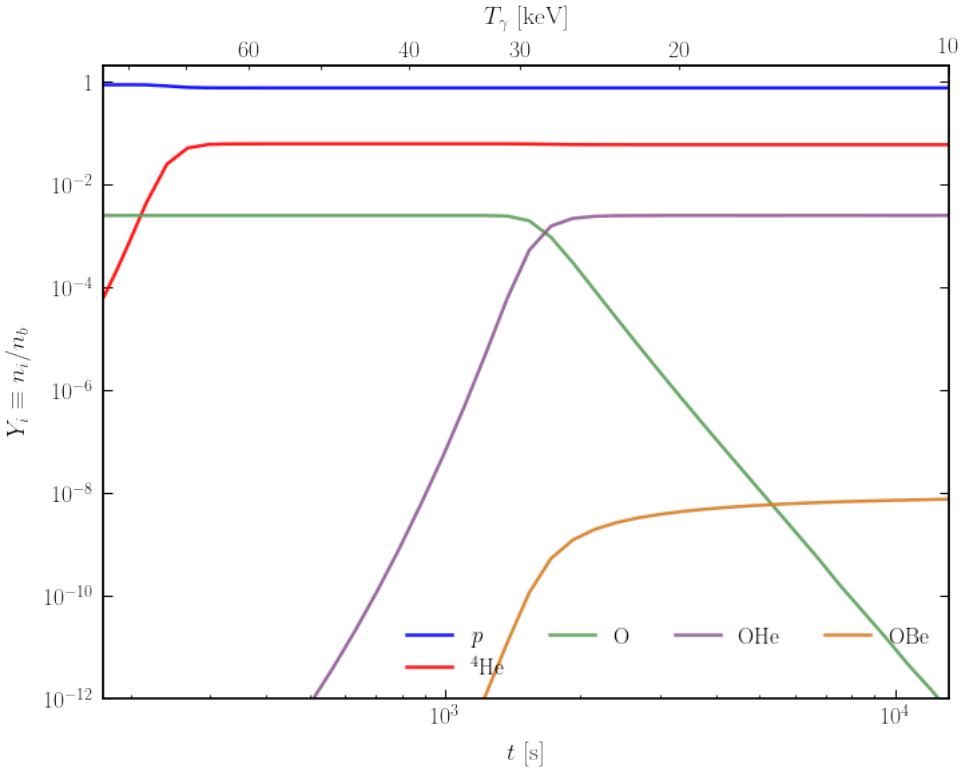

Fig. 4.2: Concentrations of bound states during nucleosynthesis

dark ions prevents the destruction of the nuclear shell. Moreover, the Coulomb repulsion should be significantly suppressed. It allows for the consideration of nuclei that are unstable in the free state. The lifetime of the proton-rich isotopes of beryllium, boron and carbon may be extended due to the suppression of proton emission in the shell of the dark atom. This also should catalyze the formation of XC bound states in a 3-α process, analogous to the one occurring during stellar nucleosynthesis.

For higher-charge heavy cores, dark atom recombination becomes a multi-stage process. Therefore, the probability of hydrogen capture should increase. This may open new channels of dark atom recombination. In particular, for $n \geq 5$, the capture of protons at the initial stage of this process should be a dominant process. Therefore, the enhanced overproduction of odd-charged dark ions is expected. On the other hand, numerical estimation of binding energies shows that for $n \geq 4$, the formation of the intermediate bound state $(XHe)p$ becomes possible. The main feature of this configuration is the absence of nuclear fusion within the shell of dark ion, which could significantly alter the subsequent nucleosynthetic pathway.. Finally, the large number of stages leads to the prolongation of the overall dark atom recombination timescale. Consequently, a sufficient concentration of neutral

states may only be formed at low temperatures, when the production of anomalous isotopes should freeze out.

4.5 Conclusion

Heavy, stable, multicharged particles X^{-2n}, predicted in several extensions of the Standard Model, should bind with light primordial nuclei during Big Bang nucleosynthesis to form the neutral dark atoms. However, a more careful consideration of this process reveals some problems of the dark atom scenario. In particular, the simple estimation of particle abundances indicates a significant overproduction of anomalous isotopes. To provide the realistic estimation of ordinary and dark matter particle concentrations, it is necessary to include the additional reactions.

Acknowledgements

The work of D.O.S. was performed in Southern Federal University with financial support of grant of Russian Science Foundation № 25-07-IF.

References

1. Planck Collaboration: Planck 2018 results. VI. Cosmological parameters, Astronomy & Astrophysics **641** (2020).
2. M. Khlopov, "What comes after the Standard Model?," *Progress in Particle and Nuclear Physics* **116** (2021) 103824.
3. V.A. Beylin, M.Yu. Khlopov, D.O. Sopin: Problems of Dark Atom Cosmology, Bled Workshops Physics **27** (2024) arXiv:2410.13424 [hep-ph].
4. A. Antognini, F. Kottmann, R. Pohl: Laser spectroscopy of light muonic atoms and the nuclear charge radii, SciPost Phys. Proc. **5** (2021) 021
5. J.J. Krauth, K. Schuhmann, M.A. Ahmed, et al.: Measuring the alpha-particle charge radius with muonic helium-4 ions, Nature **589** (2021) 527-531
6. M.Yu. Khlopov, A.G. Mayorov, E.Yu. Soldatov: Composite Dark Matter and Puzzles of Dark Matter Searches, Int. J. Mod. Phys. D **19** (2010), arXiv:1003.1144 [astro-ph.CO].
7. C. Giovanetti, M. Lisanti, H. Liu, S. Mishra-Sharma, J. T. Ruderman: LINX: A Fast, Differentiable, and Extensible Big Bang Nucleosynthesis Package, arXiv:2408.14538 [astro-ph.CO] (2024)
8. M. Escudero: Neutrino decoupling beyond the Standard Model: CMB constraints on the Dark Matter mass with a fast and precise Neff evaluation, Journal of Cosmology and Astroparticle Physics **2019(02)** (2019), 007.
9. M. E. Abenza: Precision early universe thermodynamics made simple:Neff and neutrino decoupling in the Standard Model and beyond, Journal of Cosmology and Astroparticle Physics **2020(05)** (2020), 048.
10. C. Pitrou, A. Coc, J-Ph. Uzan, E. Vangioni: Precision big bang nucleosynthesis with improved Helium-4 predictions, Physics Reports **754** (2018), 1–66.
11. A.-K. Burns, T. M. Tait, M. Valli: PRyMordial: the first three minutes, within and beyond the Standard Model, Eur. Phys. J. C **84(1)** (2024), 86.
12. I. A. Kotelnikov, A. I. Milstein: Electron radiative recombination with a hydrogen-like ion, Phys. Scripta **94(5)** (2019), 055403.
13. E. Akhmedov, M. Pospelov: BBN catalysis by doubly charged particles, JCAP **2024(08)**, (2024), 028

BLED WORKSHOPS
IN PHYSICS
VOL. 26, NO. 1

Proceedings of the 28th Workshop
What Comes Beyond . . . *(p. 38)*
Bled, Slovenia, July 6–17, 2025

5 Research of dark matter particle decays into positrons with suppression of FSR to explain positron anomaly

Y.A. Basov†

National Research Nuclear University MEPhI (Moscow Engineering Physics Institute),115409, Kashirskoe shosse 31, Moscow, Russia

Abstract. The PAMELA experiment detected a positron anomaly that remains unresolved to date due to problems with associated gamma radiation. This study explores potential explanation of the positron anomaly by examining gamma-ray suppression in various dark matter particle decay models. We hypothesize the existence of dark matter particles whose decay could serve as a source of the observed positron excess. As our test particle X, we consider a 1000 GeV mass particle with charge 0, +1, or +2, capable of decaying into positrons and other particles. There are models with less production of final state radiation (FSR). Through comparative model analysis, we have derived energy spectra for both positrons and photons to model cosmic ray propagation throughout the Galaxy.
Povzetek: Avtorji poskušajo pojasniti presežek pozitronov, ki so ga izmerili z eksperimentom Pamela z merjenjem žarkov gama. Postavijo domnevo, da je vzrok za ta presežek temna snov z maso 1000 GeV in elektromagnetnimi naboji 0,1 ali 2, ki razpada v pozitrone in druge nabite delce. Določijo energijske spektre pozitronov in fotonov za predpostavljene lastnosti temne snovi različnih lastnosti. Izračunajo, kakšno bi bilo sevanje po vsej galaksiji, če je vzrok sevanju pri Pamelini meritvi njihova izbira temne snovi.

Introduction

The positron excess in cosmic rays, first detected by the PAMELA experiment [1] and subsequently confirmed by data from the AMS-02 and Fermi-LAT experiments [2, 3], still lacks a universally accepted explanation. The most promising hypothesis regarding the nature of the so-called positron anomaly is the existence of previously unknown sources of primary positrons, with the most popular candidates being pulsars and dark matter. However, existing models of dark matter face a significant challenge with the production of accompanying gamma-ray emission. This work aims to find a potential solution to the positron anomaly problem by considering the suppression of gamma-ray emission in models with decay modes of boson and fermion dark matter particles. We investigate the influence of spin and Coulomb interaction effects, particle identity, and the number of positrons in the final state. Also, the Pauli exclusion principle can lead the suppression of gamma-ray emission [4]. The following possible cases of massive dark matter

†yabasov@mephi.ru

particles are considered in this work: scalar and vector bosons X (charge 0, +1, +2) paired with fermions (charge -1, 0, +1); fermions X (charge +1) paired with scalar and vector bosons Y (charge 0). Also, we plan to verify the results of the study of the two-positron decay mode of a particle with a charge of +2 [5]. Dark matter with (single, double) charged particles are considered in the models of dark atomic matter [6–8].

Physical Model

In this work, the following possible cases of massive hidden mass particles were considered. In case of a decay $X \to e^+ + e^{\pm}$:

- A scalar boson X (charge 0, +2).
- A vector boson X (charge 0, +2).

In case of a decay $X \to e^+ + Y$:

- A scalar boson X (charge 0, +1, +2) and a fermion Y (charge -1, 0, +1).
- A vector boson X (charge 0, +1, +2) and a fermion Y (charge -1, 0, +1).
- A fermion X (charge +1) and a scalar boson Y (charge 0).
- A fermion X (charge +1) and a vector boson Y (charge 0).

For these cases, taking into account spin states, [1] corresponding Lagrangians were written, including terms describing the decay mode of the X particle:

$$\mathcal{L}_{X^0 scalar} = \frac{1}{2}\partial_\mu X \partial^\mu X - \frac{1}{2}M_X^2 X^2 - \lambda\overline{\psi}X\psi, \tag{5.1}$$

$$\mathcal{L}_{X^{++} scalar} = D_\mu X^+ D^\mu X - M_X^2 X^+ X - \lambda\overline{\psi}X^+\psi^C - \lambda\overline{\psi}^C X\psi, \tag{5.2}$$

$$\mathcal{L}_{X^0 vector} = -\frac{1}{4}F_{\mu\nu}F^{\mu\nu} + \frac{1}{2}M_X^2 X_\mu X^\mu - \lambda\overline{\psi}\gamma^\mu X_\mu\psi, \tag{5.3}$$

$$\mathcal{L}_{X^{++} vector} = -\frac{1}{2}F^+_{\mu\nu}F^{\mu\nu} + M_X^2 X^+_\mu X^\mu - \lambda\overline{\psi}\gamma^\mu X^+_\mu\psi^C - \lambda\overline{\psi}^C\gamma^\mu X_\mu\psi, \tag{5.4}$$

$$\mathcal{L}_{X^0 scalar, Y^- fermion} = \frac{1}{2}\partial_\mu X\partial^\mu X - \frac{1}{2}M_X^2 X^2 + i\overline{Y}\gamma^\mu D_\mu Y - \\ -M_Y\overline{Y}Y - \lambda X\overline{\psi}Y - \lambda X\psi\overline{Y}, \tag{5.5}$$

$$\mathcal{L}_{X^+ scalar, Y^0 fermion} = D_\mu X^+ D^\mu X - M_X^2 X^+ X + iY\gamma^\mu\partial_\mu Y - \\ -M_Y Y^2 - \lambda X\psi Y - \lambda X^+\overline{\psi}Y, \tag{5.6}$$

$$\mathcal{L}_{X^{++} scalar, Y^+ fermion} = D_\mu X^+ D^\mu X - M_X^2 X^+ X + i\overline{Y}\gamma^\mu D_\mu Y - \\ -M_Y\overline{Y}Y - \lambda X\psi\overline{Y} - \lambda X^+\overline{\psi}Y, \tag{5.7}$$

$$\mathcal{L}_{X^0 vector, Y^- fermion} = -\frac{1}{4}F_{\mu\nu}F^{\mu\nu} + \frac{1}{2}M_X^2 X_\mu X^\mu + i\overline{Y}\gamma^\mu D_\mu Y - \\ -M_Y\overline{Y}Y - \lambda Y\gamma^\mu X_\mu\psi - \lambda\overline{Y}\gamma^\mu X_\mu\overline{\psi}, \tag{5.8}$$

$$\mathcal{L}_{X^+vector,Y^0fermion} = -\frac{1}{2}F^+_{\mu\nu}F^{\mu\nu} + M^2_X X^+_\mu X^\mu + iY\gamma^\mu\partial_\mu Y - \\ -M_Y Y^2 - \lambda\overline{\psi}\gamma^\mu X^+_\mu Y - \lambda Y\gamma^\mu X_\mu\psi, \tag{5.9}$$

$$\mathcal{L}_{X^{++}vector,Y^+fermion} = -\frac{1}{2}F^+_{\mu\nu}F^{\mu\nu} + M^2_X X^+_\mu X^\mu + i\overline{Y}\gamma^\mu D_\mu Y - \\ -M_Y\overline{Y}Y - \lambda\overline{\psi}\gamma^\mu X^+_\mu Y - \lambda\overline{Y}\gamma^\mu X_\mu\psi, \tag{5.10}$$

$$\mathcal{L}_{X^+fermion,Y^0scalar} = \frac{1}{2}\partial_\mu Y\partial^\mu Y - \frac{1}{2}M^2_Y Y^2 + i\overline{X}\gamma^\mu D_\mu X - \\ -M_X\overline{X}X - \lambda\overline{X}\psi Y - \lambda X\overline{\psi}Y, \tag{5.11}$$

$$\mathcal{L}_{X^+fermion,Y^0vector} = -\frac{1}{4}F_{\mu\nu}F^{\mu\nu} + \frac{1}{2}M^2_Y Y_\mu Y^\mu + i\overline{X}\gamma^\mu D_\mu X - \\ -M_X\overline{X}X - \lambda\psi\gamma^\mu Y_\mu X - \lambda\overline{\psi}\overline{X}\gamma^\mu Y_\mu, \tag{5.12}$$

where λ is the interaction constant, taken to be equal to the elementary charge $e \approx 0.313$, M_Y is the mass of particle Y, equal to 0.1 GeV, M_X is the mass of particle X, equal to 1000 GeV and ψ is the wave function of the leptons (electrons and positrons).

Extensions of the Standard Model, which assume the existence of the considered particles, were implemented using the FeynRules package, the Standard Model in FeynRules was used as a basis. The input data consisted of the corresponding Lagrangians for the dark matter particles X and Y and their interactions, given by Eqs. (1-12), the mass of particle X (1000 GeV), and the mass of particle Y (0.1 GeV).

Modeling

The decay of particle X into electrons, positrons, Y particles, and photons was modeled using the CompHEP [9] and MadGraph 5 [10] programs, which utilize model files created in FeynRules [11]. The following decay modes were considered:

$$X \to e^+ + Y + \gamma, \quad X \to e^+ + e^\pm + \gamma,$$

Both programs are Monte Carlo event generators, which allows for more reliable results as the number of generated events increases. The simulation results were processed using the Savitzky–Golay filter and the least squares method.

Modeling of 12 types of particle decays, both with and without a photon in the final state, were performed. In the second case, the decay width was calculated analytically in CompHEP and numerically in MadGraph 5. The obtained values are presented in Table 5.1. These values agree with the theoretical calculation for $X \to e + e$ using Eq. (5.13, 5.14).

$$\Gamma_{scalar} = \frac{\lambda^2 M_X}{8\pi}\left(1 - \frac{4M_e^2}{M_X^2}\right)^{\frac{3}{2}}, \tag{5.13}$$

$$\Gamma_{vector} = \frac{\lambda^2 M_X}{12\pi}\left(1 - \frac{4M_e^2}{M_X^2}\right)^{\frac{3}{2}}, \tag{5.14}$$

where λ is the interaction constant, taken to be equal to the elementary charge $e \approx 0.313$. If the particles in the final state are identical, the value is additionally halved.

Table 5.1: Decay widths for $X \to e + e$

Particle Type	Scalar, 0	Scalar, +2	Vector, 0	Vector, +2
Decay Width Γ, GeV	3.909	1.955	2.606	1.303

To estimate the amount of gamma-ray emission, the corresponding dependencies of the branching ratio R on the photon energy in the final state were plotted, compared to the most common decay mode $X^0_{\text{scalar}} \to e^- e^+$:

$$Br = \frac{\Gamma(X \to eY\gamma)}{\Gamma(X \to eY)}, \quad \frac{dBr}{dE} = \frac{1}{\Gamma(X \to eY)} \frac{d\Gamma(X \to eY\gamma)}{dE}, \tag{5.15}$$

$$R = \frac{dBr(\text{decay})}{dE} \Big/ \frac{dBr(X^0_{\text{scalar}} \to e^- e^+)}{dE} \tag{5.16}$$

Plots of the branching ratio of the energy spectra for various modes were constructed using CompHEP data (Fig. 5.1 for photon energies). It was observed that in the case of X^{++}, suppression of high-energy photon emission occurs due to the Coulomb effect. For X^+, a low photon yield compared to the two-positron decay mode is observed, due to the absence of Coulomb interaction between particles in the final state. In the case of X^0_{vector}, weak suppression of high-energy photons is observed due to spin interaction of particles in the final state.
Furthermore, the obtained results exhibit discrepancies with the results reported in [5] and require further verification.

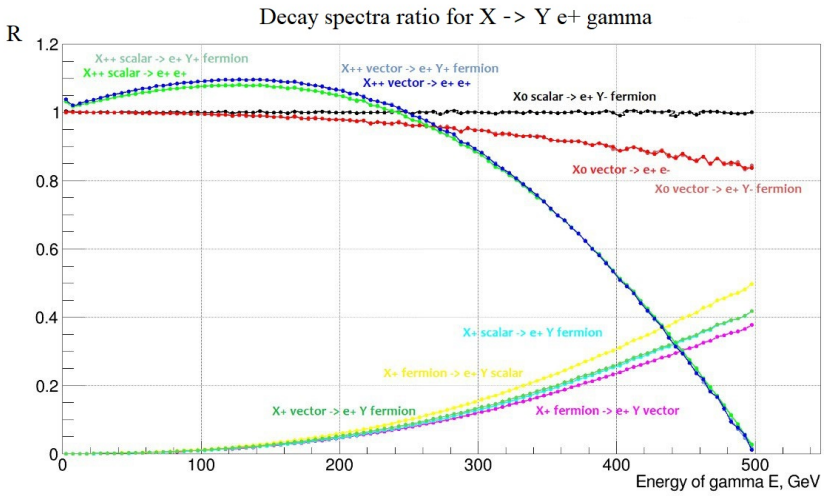

Fig. 5.1: Dependence of the branching ratio of the energy spectra of decay modes on the photon energy in the final state.

Conclusion

This work investigated possible decay modes of boson and fermion dark matter particles. Twelve models for the existence of charged and uncharged dark matter particles and their decay modes, both with and without high-energy photon emission, were considered. Particle decay processes were modeled, and energy spectra were obtained.

As a result, it was observed that in the case of a +1 charged particle, the smallest amount of gamma-ray emission (yield) is produced, which allows for further consideration of this model to explain the positron anomaly. Other decay modes can be refined and used to explain other experimentally observed effects.

A continuation of this work could involve searching for an analytical solution and physical approximations to assess the influence of subtle effects.

Acknowledgements

We would like to thank K. Belotsky for coordinating the work and M. Solovyov for the help and providing relevant reference.

This work was supported by the Russian Science Foundation grant no. 24-22-00325 "Search for an explanation of the positron anomaly in cosmic rays by means of dark matter".

References

1. O. Adriani et al.: An anomalous positron abundance in cosmic rays with energies 1.5–100 GeV, Nature **458** (2009) 607—609.

2. M. Aguilar et al.: First Result from the Alpha Magnetic Spectrometer on the International Space Station: Precision Measurement of the Positron Fraction in Primary Cosmic Rays of 0.5–350 GeV, Phys. Rev. Lett. **110** (2013) 141102.
3. M. Ackermann et al.: Measurement of Separate Cosmic-Ray Electron and Positron Spectra with the Fermi Large Area Telescope, Phys. Rev. Lett. **108** (2012) 011103.
4. K. M. Belotsky et al.: Indirect effects of dark matter, Int. J. Mod. Phys. D **28** (2019) 1941011.
5. R. Barak, K. Belotsky, E. Shlepkina: Proposition of FSR Photon Suppression Employing a Two-Positron Decay Dark Matter Model to Explain Positron Anomaly in Cosmic Rays, Universe **9** (2023) 370.
6. M. Khlopov, C. Kouvaris: Strong Interactive Massive Particles from a Strong Coupled Theory, Phys. Rev. D **77** (2008) 065002.
7. K. Belotsky, M. Khlopov, C. Kouvaris, M. Laletin: High Energy Positrons and Gamma Radiation from Decaying Constituents of a two-component Dark Atom Model, Int. J. Mod. Phys. D 24 (2015) 1545004.
8. K. Belotsky, M. Khlopov, C. Kouvaris, M. Laletin: Decaying Dark Atom Constituents and Cosmic Positron Excess, Adv. High Energy Phys. 2014 (2014) 214258.
9. E. Boos et al.: CompHEP 4.4: Automatic computations from Lagrangians to events, Nucl. Instrum. Meth. A **534** (2004) 250–259.
10. J. Alwall et al.: The automated computation of tree-level and next-to-leading order differential cross sections, and their matching to parton shower simulations, J. High Energ. Phys. **2014** (2014) 79.
11. A. Alloul et al.: FeynRules 2.0 – A complete toolbox for tree-level phenomenology, Comput. Phys. Commun. **185** (2014) 2250–2300.
12. M. E. Peskin, D. V. Schroeder: *An Introduction to Quantum Field Theory*, Westview Press, Boulder, CO, 1995.

BLED WORKSHOPS
IN PHYSICS
VOL. 26, NO. 1

Proceedings of the 28th Workshop
What Comes Beyond . . . *(p. 44)*
Bled, Slovenia, July 6–17, 2025

6 The DAMA project legacy

R. Bernabei for DAMA activities †

[1]Dip. Fisica, Università di Roma "Tor Vergata", INFN sezione di Roma, "Tor Vergata", I-00133 Rome, Italy

Abstract. The DAMA project, a long-standing pioneer in the field of Dark Matter (DM) research, has been conducting experiments deep underground at Gran Sasso National Laboratory (LNGS) since 1990 developing several very low background set-ups and measurements both on DM and on many other rare processes.
As of end of September 2024, all active DAMA experimental setups have been decommissioned, though data analyses on various rare processes continues. This paper provides a short summary of main DAMA activities, highlighting their evolution over time. Contributions from both Italian and International Institutions, as well as individual members, have played a pivotal role in achieving the project's significant results; in particular, the Chinese collaborators have been part of the efforts on highly radio-pure NaI(Tl) set-ups, while the Ukrainian colleagues have been instrumental to set many measurements on rare processes.
Povzetek: Experiment DAMA je dolgoletni pionir raziskav temne snovi. Poskusi tečejo v Nacionalnem laboratoriju Gran Sasso globoko pod zemljo že od leta 1990. Razvil je nekaj metod meritev z zelo nizkim ozadjem, za merjenje temne snovi, pa tudi za številne druge redke dogodke. Do konca septembra 2024 so eksperiment DAMA razgradili, analize podatkov različnih redkih procesov pa se nadaljujejo. Prispevek povzema dejavnosti eksperimenta DAMA in njihov razvoj v teh tridesetih letih. Poleg italijanskih so k uspehu prispevale tudi mednarodne institucije. Avtorji se posebej zahvaljujejo kitajskim sodelavcem za sodelovanje pri skrbi za visoko radioaktivno čiste nastavitve NaI(Tl) in ukrajinskim sodelavcem za pomoč pri izvedbi številnih meritev redkih procesov.

6.1 Introduction

In 1990 the DAMA project [26] has been proposed to the INFN Scientific Committee II (CSN2) as a pioneer activity through the realization of large mass highly radiopure NaI(Tl) and liquid Xenon set-ups, primarily dedicated to the direct detection of DM particles in the galactic halo exploiting the DM model-independent annual modulation signature (originally suggested in the mid-1980s by Ref. [27,28]).
Many other set-ups and measurements on various rare processes have also been developed and carried out along the living time of the DAMA project [4] until end of September 2024 when the DAMA set-ups have been dismounted; data analyses on various topics have been and are continuing. In particular, DAMA was the first experiment proposed and funded specifically for DM direct detection deep underground with ULB NaI(Tl) and with LXe exploiting also the DM annual modulation signature.
Fig. 6.1 summarizes the main DAMA set-ups located deep underground at LNGS.

†e-mail: rita.bernabei@roma2.infn.it

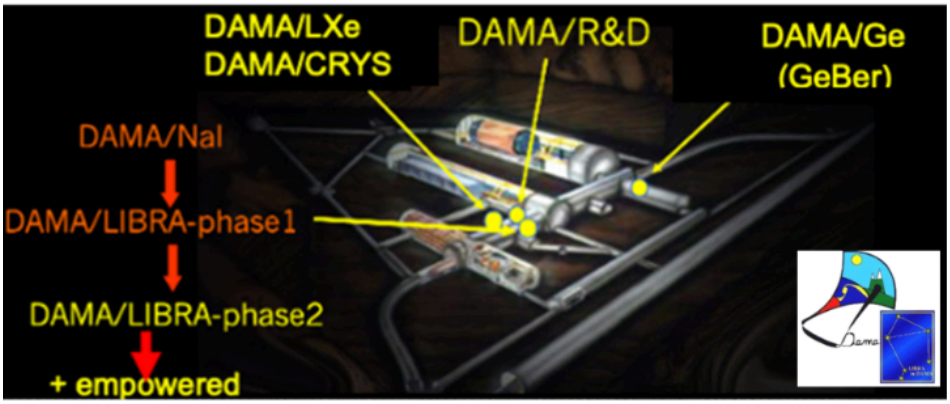

Fig. 6.1: Schematic view of the experimental sites of the main DAMA installations deep underground at LNGS. In each set-up many different investigations on various rare processes have been realized [4].

In numbers, as on April 2025, DAMA's activity can be summarized as follows: i) approximately 350 publications (41 in the last five years); ii) approximately 436 presentations at conferences and seminars (66 in the last five years); iii) approximately 30 theses at various levels; iv) DAMA's H-index = 63.
In the following the time-line of the set-ups shown in Fig. 6.1 and main results are summarized.

6.2 The DAMA/LXe set-up

Following the initial experimental work on the development of liquid xenon (LXe) detectors – carried out within the Italian Xelidon experiment funded by the INFN Scientific Committee V (CSN5) from the late 1980s to 1990 – the Italian DAMA group was approved and funded by CSN2 to develop and operate a pure high-purity LXe scintillator as part of the broader DAMA project. Its main aim was the direct detection of DM deep underground using several experimental approaches; in addition, the group later investigated other rare processes, mainly employing krypton-free xenon enriched in ^{129}Xe or ^{136}Xe, and ^{134}Xe.
During the period 1990 – 1994 several prototypes for low background (LB) were realized up to the creation and installation deep underground of the final LB set-up. Preliminarily measurements were carried out filling the detector with ^{nat}Xe. As a result we pointed out to the CSN2 the intrinsic limitations of this detector medium (see e.g. some arguments in more recent monographs [5, 6]) and agreed to pursue the activity by using $\simeq$ 6.5 kg Kr-free Xenon enriched either in ^{129}Xe at 99.5% or in ^{136}Xe at 68.8% and in ^{134}Xe at 17.1% (the largest LXe detector underground at that time). The inner LXe vessel was excavated from a full block of OFHC Copper (see Fig. 6.2-*Right*); MgF_2 optical windows were used. Fig. 6.2-*Left* shows part of the purification/filling/recovery system; the multi-component shield housing the target can be seen at the bottom.

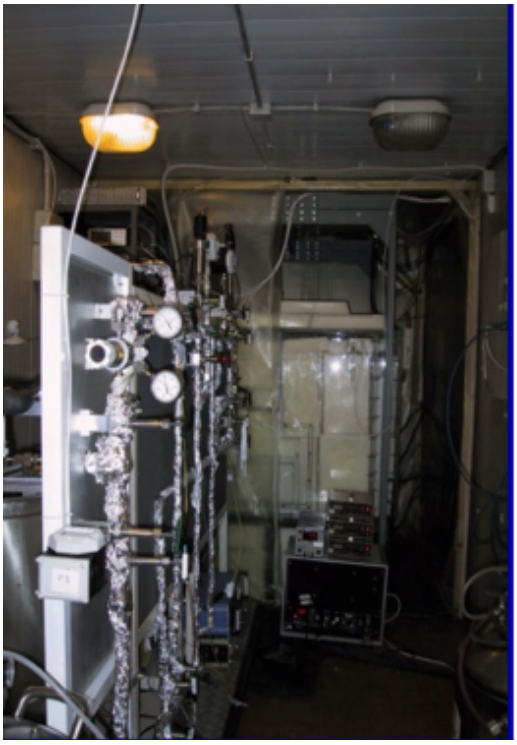

Fig. 6.2: *Left* - Photo of the purification/filling/recovery system of the DAMA/LXe set-up; in the bottom the multi-component shield housing the target vessel. *Right* - the LXe vessel excavated in a full OFHC Copper block with MgF_2 windows.

Several upgrades occurred with time; moreover, a period of stopping occurred at time of the Borexino accident that caused a period of interruption in using liquids deep underground.
In the time period 1996-2018, many results have been achieved and published on the response of a similar pure LXe scintillator to recoil nuclei as well as its pulse shape discrimination capability, on DM elastic- and inelastic-scattering with various approaches, on possible charge non-conserving processes in ^{136}Xe, on nucleon and di-nucleon and tri-nucleon stability, on $\beta\beta$ decay modes in ^{136}Xe and ^{134}Xe as well as on detector details and performances (see DAMA/LXe citations e.g. in [4,6] and related refs. therein).
In 2018 as in the time schedule of the experiment, DAMA/LXe was put out of operation having reached its goals.

6.3 The highly radiopure NaI(Tl) DAMA set-ups

As mentioned, from end of '80s to beginning of 1990 underground tests with some commercial NaI(Tl) detectors were carried out. On April 24, 1990 the Italian groups from INFN and University of Roma Tor Vergata and Roma La Sapienza,

submitted the DAMA proposal to INFN on large mass NaI(Tl) and liquid Xenon experiments mainly for Dark Matter search, and were firstly funded. Initially a search for the more promising manufacture for a joint effort towards very highly radiopure NaI(Tl) was carried out.
Chinese colleagues joined DAMA at LNGS in 1992.
Then, up to end of 1995 several R&Ds were carried out in the framework of a joint collaboration between DAMA members and Crismatec company in order to develop suitable low background NaI(Tl) detectors. Another dedicated R&D with the EMI-Thorn for producing the B53 photomultipliers (PMT) was performed too. In particular, DAMA mainly contributed to materials selections, to protocols definition, and to prototypes tests and qualifications.
From end 1995/beginning 1996 up to July 2002 the setup installation and the running procedures of the $\simeq$ 100 kg DAMA/NaI experiment were realized at LNGS. In particular, in 1998 a minimal upgrade was performed, while in July 2000 new DAQ and new electronic chain were installed.
In fall 1996 DAMA Italian members proposed to INFN (for insertion in the "Piano Triennale") DAMA/1ton, and the about 250 kg DAMA/LIBRA–phase1 was approved and funded as intermediate step. Thus, while running DAMA/NaI – during 1996/97 to 2003 – new R&Ds for more radiopure Nal(TI) were performed by exploiting also new chemical/physical radiopurification techniques, realizing new DAMA/LIBRA detectors with Quartz & Silice co. (former Crismatec). A new low background setup DAMA/R&D was also realized (see later) for related tests, and then for various small scale experiments.
After a renewal of the whole experimental site and of the overall installation, the $\simeq$ 250 kg DAMA/LIBRA–phase1 was put in operation deep underground on September 2003. This apparatus was upgraded on September/October 2008 replacing in particular all the PMTs with new ones having higher quantum efficiency, giving rise to DAMA/LIBRA–phase2. In fall 2012 the preamplifiers system was also upgraded.
DAMA/LIBRA–phase2 (see Fig. 6.3) has started operation on December 2010; while running it – after some new R&Ds – the DAMA/1ton idea was abandoned because of new problems for supplying and purifying high quality NaI and, mainly, TlI powders, and for the new absence of large platinum crucible for Kyropoulos growth. However, the focus to increase the sensitivity was instead maintained by acting on other experimental aspects such as the lowering of the software energy threshold[1].
Thus, following this strategy, in the period 2019 - 2021 new R&Ds towards DAMA/LIBRA–phase2–empowered were carried out with the aim to further lower the software energy threshold below 1 keV. At completion of these R&Ds, a significant upgrade occurred starting this new phase thanks e.g. to: i) the equipment of all the PMTs with new low-background voltage dividers with pre-

[1] In fact, the sensitivity of the DM annual modulation signature, mainly exploited by the DAMA NaI(Tl) setups, depends – apart from the counting rate – on the product: $\epsilon \times \Delta E \times M \times T \times (\alpha - \beta^2)$, thus increasing ϵ and/or T and/or enlarging ΔE is in practice equivalent to increase the exposed mass M. There ϵ is the detection efficiency; ΔE is the energy interval where the modulation signal is studied; T is the live-time.

Fig. 6.3: Photos during installation in HP–N_2 atmosphere of the NaI(Tl) detectors in the inner high purity copper box which is surrounded by the multi-tons multi-materials passive shield.

amplifiers on the same board; ii) the use of new Transient Digitizers with higher vertical resolution (14 bits).
At fall 2021 DAMA/LIBRA–phase2–empowered started operation, and collected data – as planned – up to fall 2024; data analyses are in progress.

6.3.1 Reminding results on the DM annual modulation signature

The pioneer DAMA/Nal, $\simeq$ 100 kg highly radiopure Nal(TI), and its performances profited of dedicated developments as described in Ref. [7] and refs therein. It also produced interesting results on the investigation of various rare processes on: i) possible Pauli exclusion principle violation; ii) possible charge-non-conserving (CNC) processes; iii) electron stability and non-paulian transitions in lodine atoms (by L-shell); iv) search for solar axions; v) possible exotic matter; vi) possible superdense nuclear matter; vii) heavy clusters decays [4].
However, its main aim was the investigation of DM particles in the galactic halo mainly by exploiting the model-independent DM annual modulation signature although some other approaches were also investigated as well: i) by applying the Pulse Shape discrimination; ii) by investigating diurnal effects; iii) by searching for exotic DM [4]. As regards the investigation on the DM annual modulation signature, DAMA/NaI was a pioneer investigating both the experimental model independent signature and various corollary model scenarios [4]. In particular, a

model independent evidence – on the basis of the exploited signature – for a DM particle component in the galactic halo was firstly pointed out at 6.3 σ C.L. with a total exposure of 0.29 ton×yr over 7 annual cycle, which was orders of magnitude larger than those exposures typically available at that time.
The radiopurity, performances, and procedures of the second generation DAMA/LIBRA–phase1 set-up, $\simeq$ 250 kg with new highly radiopure NaI(TI), were discussed in [8]. Also in this case, several other rare processes were investigated e.g.: i) possible processes violating the Pauli exclusion principle; ii) possible CNC processes; iii) internal pair production in ^{241}Am [4]. The DM model independent annual modulation signature and related aspects were extensively further investigated. In particular, DAMA/LIBRA–phase1 over 7 annual cycles with an exposure of 1.04 ton×yr confirmed the model-independent evidence for DM in the galactic halo, reaching 9.3 σ C.L. (see e.g. [4, 9] and refs therein). DAMA/LIBRA–phase2 –

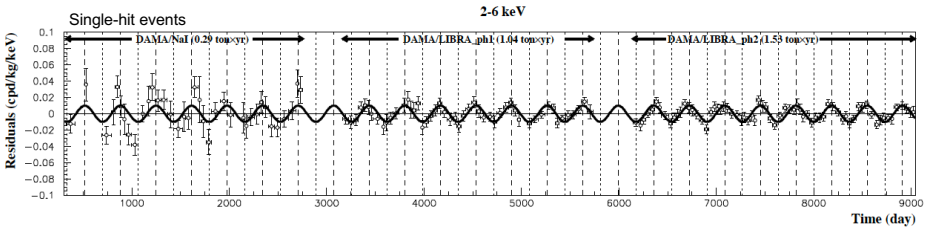

Fig. 6.4: Experimental residual rate of the *single-hit* scintillation events measured by DAMA/NaI, DAMA/LIBRA–phase1 and DAMA/LIBRA–phase2 (total exposure 2.86 ton × yr) in the (2 – 6) keV energy intervals as a function of the time. The superimposed curve is the cosinusoidal functional forms A cos ω(t - t_0) with period T = $\frac{2\pi}{\omega}$ = 1 yr, phase t_0 = 152.5 day (June 2nd) and modulation amplitude, A, equal to the central value obtained by best fit. Vertical dashed lines indicate the expected maximum rate, while the dotted lines represent the expected minimum rate.

with lower software energy threshold – has further confirmed the effect observed by DAMA/NaI and DAMA/LIBRA–phase1, over 8 annual cycles, reaching a cumulative exposure of 2.86 ton×yr [4, 9, 10] and a CL for observing the effect satisfying all the requirements of the exploited DM annual modulation signature of more than 13 σ.
In particular, Fig. 6.4 shows the *single-hit* (i.e. when each detector has all the others in anti-coincidence since the probability that a DM particle would interact in more than one detector is negligible) residual rate in the energy interval (2 – 6) keV in DAMA/NaI, DAMA/LIBRA–phase1 and DAMA/LIBRA–phase2 as a function of the time. A clear annual modulation satisfying all the requirements of the signature is present at high C.L., while the probability of absence of modulation is 2.3×10^{-12}.
Multiple different and independent analyses of the data give completely consistent results: in particular, i) all the many peculiarities of the DM annual modulation signature are satisfied; ii) no competing systematics or side reactions able to mimic

the exploited signature are available; iii) the achieved model independent result is compatible with many different phenomenological scenarios.
The increase of the exposure and the lowering of the energy software threshold has increased with time the sensitivity allowing a more precise determination of the parameters to more precisely investigate: i) the nature of Dark Matter particles; ii) possible diurnal effects with sidereal time; iii) implications of various astrophysical, particle and nuclear models. For details and many information, comparisons and results see the DAMA literature [4].
As mentioned, in Fall 2021 DAMA/LIBRA–phase2 was heavily upgraded: i) equipping all the PMTs with new low-background voltage divider and pre-amplifier systems on the same board; ii) using new Transient Digitizers with higher vertical resolution (14 bits). The aim was to further lower the software energy threshold of the experiment below 1 keV with suitable efficiency. This has been assured, depending on the detector thanks to: i) an improvement of the signal/noise ratio: S/N≃3.0-9.0; ii) a discrimination of the single photoelectron from electronic noise at level of 3 - 8; iii) a peak/valley ratio: 4.7 - 11.6; iv) a residual radioactivity in that system lower than the one of a single PMT. This configuration is named DAMA/LIBRA–phase2–empowered [4]. The data taking has been continued without interruptions, with regular calibration runs: i) $\simeq 7.75\times 10^7$ evts were collected from sources for energy calibration; ii) $\simeq 4.35\times 10^7$ evts ($\simeq 1.74\times 10^6$ evts/keV) have been collected for determination of the acceptance window efficiency near software energy threshold for all the crystals. The collected exposure of DAMA/LIBRA–phase2–empowered up to July 24 is: 0.558 ton $\times$ yr with a parameter $(\alpha - \beta^2) \simeq 0.501$. See Fig. 6.5.

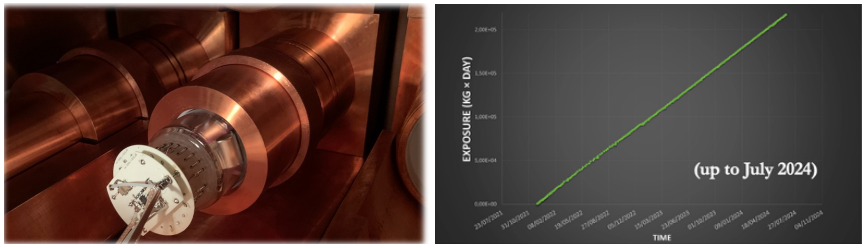

Fig. 6.5: *Left* - Photo of the low-background voltage divider and pre-amplifier system mounted on the same board in DAMA/LIBRA–phase2–empowered; *Right* - exposure versus time, collected by DAMA/LIBRA–phase2–empowered; there the data taking has been continued up to July 2024 without interruptions, with regular calibration runs in the same conditions as the production runs.

Moreover, the operational features of the upgraded system have proven to be very stable, as demonstrated in the examples of Fig. 6.6.
Finally, soon the results from the data collected with this last configuration will be released.

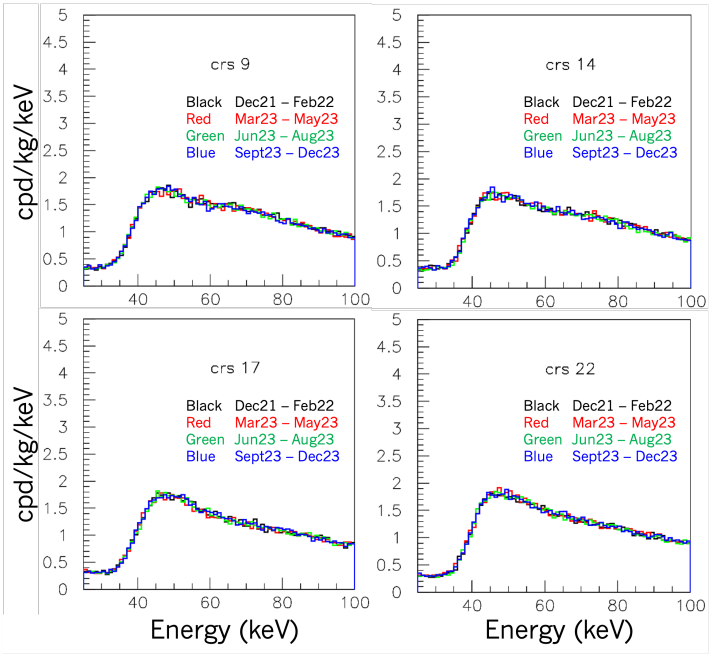

Fig. 6.6: Examples of the stability of the counting rate and energy scale of four detectors in the energy region where the ^{210}Pb and ^{129}I contaminations contribute and are dominant. The data collected in almost one year are grouped in four time-intervals.

6.4 Other DAMA experimental set-ups: DAMA/R&D, DAMA/CRYS, DAMA/Ge

6.4.1 Time-line of DAMA/R&D set-up

The low-background DAMA/R&D set-up (see Fig. 6.7) was realized in 1996-1997 as a setup for testing the prototypes of new R&Ds. At their completion, over several decades many small scale experiments were carried out in this set-up, mainly on various $\beta\beta$ decay modes in several isotopes. In fact, many measurements on various rare processes in this and other DAMA set-ups have also been realized, several within signed collaboration agreements between INFN and INR-Kiev, a collaboration effective from middle '90s to end of DAMA project. Moreover, several other foreigner collaborators have also contributed to some of the many specific measurements carried out [4]. Thus, the DAMA/R&D installation has mainly operated as a DAMA general-purpose low background set-up.
In the measurements on 2β decay modes in various isotopes both the active and the passive source techniques as well as the coincidence technique have been exploited in this and the other set-ups mentioned in this section. Attention has also been dedicated to the isotopes allowing the investigation of the $2\beta^+$ processes and, in particular, to the resonant two electron capture (2ϵ) decay channels. The investigation of neutrino-less $2\beta^+$, and $\epsilon\beta^+$ processes can refine the understanding of the contribution of right-handed currents to neutrino-less $2\beta^-$ decay; therefore,

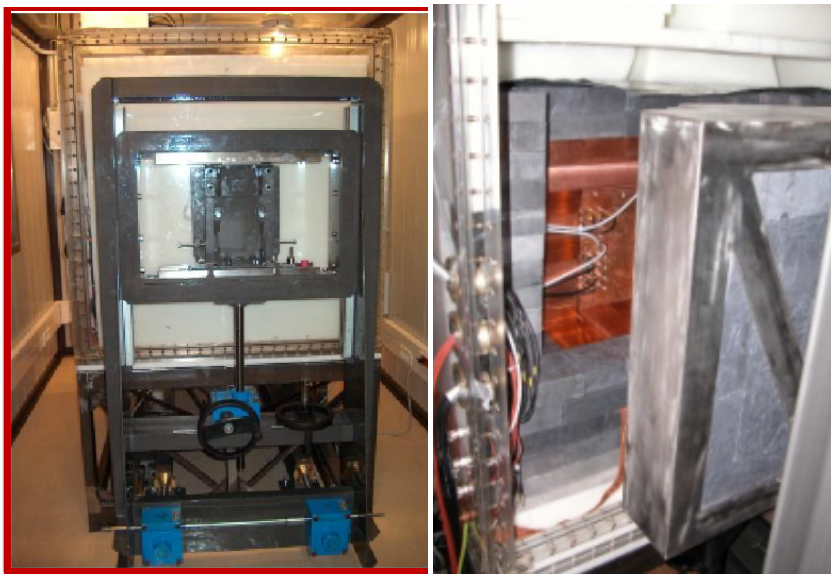

Fig. 6.7: Photos of the DAMA/R&D set-up: *Left* - the multi-component closed shield, which surrounded the inner OFHC Copper box housing the detector(s) in HP-N_2 atmosphere; *Right* - partially open shield, showing the inner OFHC Copper box.

the developments of the experimental technique to search for 2ϵ, $\epsilon\beta^+$, and $2\beta^+$ processes are strongly required. Even more important motivation to search for 2ϵ mode appears from the possibility of a resonant process thanks to the energy degeneracy between the initial and the final state of the parent and daughter nuclei. Therefore, investigations on various kinds of new scintillators and various results have also been progressed within the DAMA activities. In particular, significant efforts were performed investigating the case of the ^{106}Cd nuclide with a $^{106}CdWO_4$ made of Cadmium enriched in ^{106}Cd to 66% in various experimental configuration and DAMA set-ups, see [11] and refs therein.
This set-up has concluded its activity in fall 2024 and has been dismounted.

6.4.2 Time-line of DAMA/CRYS set-up

At the end of 2012 the DAMA/CRYS set-up was proposed to perform further small scale experiments and qualification of various new detectors. At beginning this set-up was installed in another site, while on March 2020 it was moved to the inner part of the ground floor level of the dismounted DAMA/LXe, and the previous DAMA/CRYS site was returned to LNGS.
The passive shield of this set-up was made of high purity copper, lead, cadmium, and polyethylene. Also this set-up was sealed and continuously flushed by HP-N_2 gas to prevent the detector and other materials to be in contact with the environmental air. See Fig. 6.8.

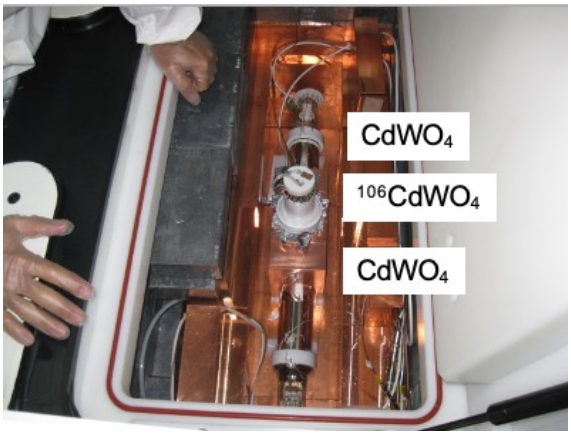

Fig. 6.8: Photo of the DAMA/CRYS shield: the multi-component shield is shown; it housed the inner OFHC box containing the detector(s).

During its operative time in DAMA/CRYS several measurements on various rare processes and detectors characterization were carried out as relatively small scale experiments [4]; here among the many results achieved, just the recent new investigation of the β decay of ^{113}Cd and of ^{113m}Cd allowing to estimate the axial-vector coupling constant g_A is reminded [12].
Also this set-up was in operation up to fall 2024 and then dismounted.

6.4.3 Time-line of DAMA/Ge set-up

This low background HP-Ge detector was located deep underground in the Stella Laboratory of LNGS (headed by Dr. M. Laubenstein) where several other HP-Ge setups are allocated.
In particular, at end '80s - beginning '90 the low-Z-window low-background HP-Ge was realized by company with exchanges with R. Bernabei (useful suggestions also from C. Arpesella and G. Heusser) thanks to funding from Tor Vergata INFN section before/near setting the DAMA project, of which it became then part for testing/selecting/qualifying detectors' materials and detectors themselves. Thus, its original name, GeBer, was changed to DAMA/Ge.
On 2003-2004 a significant upgrade of shielding and protocols occurred, mainly coordinated by Roma La Sapienza members. See Fig. 6.9.
Thus, measurements for qualifications of powders and samples, for materials and prototypes of the DAMA R&Ds mentioned above, for other scintillator materials and for some of the R&Ds on PMTs were pursued. Thus setup was also dedicated to small scale experiments on various rare processes. Other HP-Ge detectors of the Stella Laboratory have also been used when better features for some specific measurement were possible as e.g. the Ge-Multi detector (4 HP-Ge in a single cryostat) [4]. Among the many results achieved, just the recent new investigation of the double beta decay of ^{150}Nd to the excited levels of ^{150}Sm using the Ge-Multi spectrometer and a highly purified neodymium-containing sample over 5.845 yr of

Fig. 6.9: Photos of some of the parts of the DAMA/Ge (GeBer) setup.

running time, is reminded [13]. The two-neutrino double beta transition of ^{150}Nd to the first 740.5 keV 0^+ level of ^{150}Sm was detected in both one-dimensional and coincidence spectra; moreover, a first preliminary indication of the $2\nu2\beta$ decay of ^{150}Nd to the 334.0 keV 2^+ excited level of ^{150}Sm was suggested.

6.4.4 Many achieved results by DAMA/R&D, DAMA/CRYS and DAMA/Ge

These setups have allowed to develop and qualify several kind of new/improved scintillators to investigate rare processes. In Fig. 6.10 main measured detectors, creation site, and citation of related DAMA publications are summarized.
Among the main results obtained by DAMA in the search for rare processes in DAMA/R&D, DAMA/CRYS and DAMA/Ge or other Stella HP-Ge, we remind improved results in the investigation of 2β decay modes in $\simeq 30$ candidate isotopes as: ^{40}Ca, ^{46}Ca, ^{48}Ca, ^{64}Zn, ^{70}Zn, ^{100}Mo, ^{96}Ru, ^{104}Ru, ^{106}Cd, ^{108}Cd, ^{114}Cd, ^{116}Cd, ^{112}Sn, ^{124}Sn, ^{130}Ba, ^{136}Ce, ^{138}Ce, ^{142}Ce, ^{144}Sm, ^{154}Sm, ^{150}Nd, ^{156}Dy, ^{158}Dy, ^{162}Er, ^{168}Yb, ^{180}W, ^{186}W, ^{184}Os, ^{192}Os, ^{190}Pt and ^{198}Pt, in addition to ^{134}Xe and ^{136}Xe in DAMA/LXe setup. In particular, one of the best experimental sensitivities in the field for 2β decays with positron emission (in ^{106}Cd) was achieved and three two neutrinos double beta decay modes were observed: i) $^{100}\text{Mo} \rightarrow {}^{100}\text{Ru}(0^+_1)$; ii)

^{116}Cd $\rightarrow$ ^{116}Sn; iii) ^{150}Nd $\rightarrow$ ^{150}Sm(0^+_1), with a preliminary indication for ^{150}Nd $\rightarrow$ ^{150}Sm(2^+_1) [4].

Detector	site of creation	DAMA results
$ZnWO_4$	Ukraine	NIMA1029(2022)166400, J. of Lumin. 249 (2022) 119028, EPJA56(2020)83, NIMA935(2019)89, NIMA833(2016)77, PS90(2015)085301, EPJC73(2013)2276, JPG:NPP38(2011)115107, NIMA626-627(2011)31, NPA826(2009)256, PLB658(2008)193
$CdWO_4$	Ukraine	EPJA36(2008)167, PRC76(2007)064603
$^{106}CdWO_4$	Ukraine	Universe 11 (2025) 123 , NPAE24(2023)193, Univ.6(2020)182, PRC93(2016)045502, PRC85(2012)044610, NIMA615(2010)301, AstroPhys10(1999)115
$^{116}CdWO_4$	Ukraine	Phys.Scr.97(2022)085302, PRD98(2018)092007, NIMA833(2016)77, JINST6(2011)08011
Cs_2HfCl_6	Canada (by S. Nagorny)	NPA1053(2025)122976, NPA1002(2020)121941
Cs_2ZrCl_6	Canada (by S. Nagorny)	JINST19(2024)P05037, EPJA59(2023)176
SrI_2	Ukraine, USA	NIMA670(2012)10, analysis in progress
CaF_2(Eu)	Bicron/Crismatec(Saint Gobain)	NPA789(2007)15, NPA705(2002)29, NPB563(1999)97, AstroPhys7 (1997)73
CeF_3	Crystal Clear coll. or China	NIMA498(2003)352, NCIM 110A (1997) 189
BaF_2	China or Bicron/Saint Gobain	EPJA50(2014) 134, NIMA525(2004)535
LiF(W)	Ukraine	NPA806(2008)388
^{7}LiI(Eu)	Ukraine	NIM704(2013)40
$LaCl_3$(Ce)	Saint Gobain	Ukr. J. of Phys.51(2006)1037, NIMA555(2005)270
$CeCl_3$	Iltis/Saint Gobain	JPG:NPP38(2011)015103, NPA824 (2009)101
Li_2MoO_4	Ukraine	NIMA607(2009)573
$Li_6Eu(BO_3)_3$	Ukraine	NIMA572(2007)734
$BaWO_4$	Canada (by S. Nagorny)	NIMA901(2018)150
Rb_2ZrCl_6	Canada (by S. Nagorny)	paper in preparation
GAGG:Ce	Epic-crystal	submitted
and polycrystalline powder:	ZnS(Ag)	Saint-Gobain MPLA27, No. 8 (2012)1250031

Fig. 6.10: List of main measured detectors (other than NaI(Tl) and LXe) operating in the framework of these DAMA set-ups with creation site, and citation of related DAMA publications.

Moreover, among other investigated rare processes we remind here e.g.: i) first observation of α decays of ^{151}Eu with a CaF_2(Eu) scintillator; ii) first observation of α decay of ^{190}Pt to the first excited level (E_{exc} = 137.2 keV) of ^{186}Os; iii) first observation of α decays of ^{174}Hf with the measured half-life is in good agreement with theoretical predictions; iv) investigations of rare β decays of ^{113}Cd and ^{113m}Cd with $CdWO_4$ scintillators and of ^{48}Ca with a CaF_2(Eu) detector; v) observation of correlated e^+e^- pairs emission in α decay of ^{241}Am ($A_{e^+e^-}/A_\alpha \simeq 5\times 10^{-9}$); vi) search for cluster decays of ^{138}La and ^{139}La (in addition to the ^{127}I case investigated with NaI(Tl) detectors); vii) search for ^{7}Li solar axions using resonant absorption in LiF crystal (in addition to the search for solar axions by Primakoff effect performed with NaI(Tl) setup); viii) CNC processes in ^{100}Mo and ^{139}La (in addition to the cases investigated in ^{127}I, ^{136}Xe, where the NaI(Tl) and

the LXe set-ups have instead been used); ix) search for long-lived super-heavy eka-tungsten with $ZnWO_4$ and $CdWO_4$; x) best sensitive measurement of 2β decays of ^{150}Nd to 0^+ level and first indication of 2^+ level [4].

6.5 Main ideas and legacy of DAMA

The pioneer DAMA project during its 35 years of operation has developed many low-background setups and measurements. In particular, we remind: i) the first use of new low-background scintillators (NaI, LXe, and others) for DM experimental investigations exploiting several approaches and mainly the DM annual modulation signature; ii) pioneer activity developing very low background setups and dedicated methodology since 1990; iii) the first idea on the use of anisotropic scintillators for DM directionality and related detectors developments and measurements. In particular, first measurements of anisotropic response to nuclear recoils in anisotropic scintillators ($ZnWO_4$) have been realized; iv) firstly addressing the role of the Migdal effect in DM field; v) firstly addressing the role of the channeling effect in DM field; vi) accounting also for electromagnetic signals from DM interactions; vii) investigating several kinds of DM candidates and scenarios; viii) investigating the impact of Galactic and SagDEG streams; ix) investigating DM diurnal modulation; ix) investigating DM Shadow effects; x) performing R&Ds for many low background scintillators for rare processes investigations; xi) axions investigations in underground experiments.
All these topics have given rise to many competing results and to a detailed wide DAMA literature (for most production after 1996 see e.g. [4]), sometime acting – at some extent – as a flywheel for the field.
In particular, as mentioned, the result obtained so far over 22 independent annual cycles for the presence of a DM particle component in the galactic halo by exploiting the model independent DM annual modulation signature contemporaneously satisfies all the several requirements of that signature; in fact: 1) the *single-hit* events show a clear cosine-like modulation as expected for the DM signal; 2) the measured period is well compatible with the 1 yr period as expected for the DM signal; 3) the measured phase is compatible with the roughly $\simeq 152.5$ days expected for the DM signal; 4) the modulation is present only in the low energy (1–6) keV interval and not in other higher energy regions, consistently with expectation for the DM signal; 5) the modulation is present only in the *single-hit* events, while it is absent in the *multiple-hit* ones as expected for the DM signal; 6) the measured modulation amplitude in NaI(Tl) target of the *single-hit* scintillation events in the (2–6) keV energy interval, for which data are also available by DAMA/NaI and DAMA/LIBRA–phase1, is: (0.01014 ± 0.00074) cpd/kg/keV (13.7 σ C.L.). Moreover, no systematic or side processes able to mimic the signature, i.e. able to simultaneously satisfy all the many peculiarities of the signature and to account for the whole measured modulation amplitude, has been found or suggested by anyone throughout some decades thus far (see e.g. [4,9,10] and refs therein)
Many theoretical and experimental parameters and models are possible and many hypotheses must also be considered when corollary model dependent interpretations are carried out. In particular, the DAMA model-independent evidence is

compatible with a wide set of astrophysical, nuclear and particle physics scenarios for high and low mass candidates inducing nuclear recoil and/or electromagnetic radiation as also shown at some extent in a wide literature. It is worthy to note that in complete model-dependent corollary analyses, the estimate of the upper limit on the signal component in the measured rate has to be considered as a prior as well as - at possible extent - the existing uncertainties in the various possible astrophysical, nuclear and particle physics considered scenarios and related parameters have to be included (see e.g. in Ref. [4,9,10] and refs therein).

6.6 Conclusions

Several radiopure DAMA set-ups and many low background measurements have been realized by the DAMA collaboration over several decades, achieving many new/improved results both on Dark Matter and on many other rare processes. Many low background detectors have been developed sometimes with challenging performances.
After 35 years the DAMA project has been concluded as planned, and DAMA set-ups have been dismounted at fall 2024, while the GeBer (DAMA/Ge) detector is still in operation in the Stella Laboratory.
In conclusion, the experimental activities of the DAMA project have been concluded at fall 2024, while model independent and model dependent analyses on several rare processes are continuing within the collaboration, and several other results and papers are in preparation.

6.7 Acknowledgements

Thanks are due to those who were inspiring at setting the DAMA activities and passed away: 1) Prof. L. Paoluzi, Director of the INFN-Roma Tor Vergata section and INFN vice president at beginning this project; 2) Prof. D. Prosperi, one of the main proponents of the DAMA project; 3) Prof. S. d'Angelo, later in some DAMA measurements; 4) Prof. E. Bellotti, first Director of LNGS at that time. Thanks are also due to: i) the INFN Scientific Committee II in the various periods; ii) the Tor Vergata Physics department; iii) the INFN sections of Roma Tor Vergata and Roma on whose annual budgets the DAMA set-ups were mainly realized. Thanks are also due to all the technical staffs and companies who supported the collaborative efforts along the time. Finally, DAMA works and results would have not been possible without the dedicated and effective works of all the Italian and Foreigner Institutions, and collaborators.

References

1. P. Belli, R. Bernabei, C. Bacci, A. Incicchitti, R. Marcovaldi, D. Prosperi, DAMA proposal to INFN Scientific Committee II, April 24th, 1990.
2. A.K. Drukier, K. Freese, D.N. Spergel, Detecting cold dark-matter candidate, Phys. Rev. D **33** (1986) 3495 – 3508.

3. K. Freese, J.A. Frieman, A. Gould, Signal modulation in cold-dark-matter detection, Phys. Rev. D **37** (1988) 3388 – 3405.
4. see publication list in dama.web.roma2.infn.it
5. R Bernabei et al., Liquid Noble gases for Dark Matter searches: a synoptic survey, pagg. 1-53, Exorma ed. (2009) ISBN: 978-88-95688-12-1
6. R. Bernabei et al., Liquid noble gases for dark matter searches: an updated survey, Int. J Mod. Phys. A **30** (2015) 26, 1530053 (pagg.1-76).
7. R. Bernabei et al., N. Cim. A **112** (1999) 545; Riv. N. Cim. **26** n. 1 (2003) 1-73, Int. J. Modern Phys. D **13** (2004) 2127.
8. R. Bernabei et al., Nucl. Instr. and Meth. A **592** (2008) 297; J. of Instr. **7** (2012) 03009.
9. R. Bernabei et al., The DAMA project: achievements, implications and perspectives, Progress in Particle and Nuclear Physics **114** (2020) 103810.
10. R. Bernabei et al., Further results from DAMA/LIBRA–phase2 and perspectives, Nucl. Phys. At. Energy **22** (2021) 329.
11. P Belli et al., New Results of the Experiment to Search for Double Beta Decay of ^{106}Cd with Enriched $^{106}CdWO_4$ Scintillator, Universe **11** (2025) 123.
12. P. Belli et al., Spectroscopy of ^{113m}Cd, Phys. Rev. C **112** (2025) 045503.
13. A S Barabash, P Belli, et al., Double-beta decay of ^{150}Nd to excited levels of ^{150}Sm, Eur. Phys. J. C **85** (2025) 174.

Bled Workshops
in Physics
Vol. 26, No. 1

Proceedings of the 28th Workshop
What Comes Beyond . . . *(p. 59)*
Bled, Slovenia, July 6–17, 2025

7 The bound state of dark atom with the nucleus of substance

T.E. Bikbaev[1,2‡], M.Yu. Khlopov[3§], A.G. Mayorov[1]

[1] National Research Nuclear University MEPhI
115409 Moscow, Russia;
[2] Institute of Physics, Southern Federal University
Stachki 194 Rostov on Don 344090, Russia;
[3] Virtual Institute of Astroparticle physics,
75018 Paris, France

Abstract. The hypothesis of composite XHe dark atoms offers a compelling framework to address the challenges in direct dark matter particles detection, as their neutral, atom-like configuration evades conventional experimental signatures. A critical issue may arise in interaction between XHe and atomic nuclei due to the unshielded nuclear attraction, which could destabilize the dark atom's bound state. To resolve this, we propose a novel numerical quantum mechanical approach that accounts for self-consistent electromagnetic-nuclear couplings. This method addresses to eliminate the inherent complexity of the XHe-nucleus three-body system, where analytical solutions are intractable. By reconstructing the effective interaction potential — including dipole Coulomb barrier and shallow potential well — we demonstrate how these features lead to the formation of XHe-nucleus bound states and modulate low-energy capture processes. Our model enables validation of the dark atom hypothesis, particularly in interpreting experimental anomalies like annual modulation signals observed in DAMA/LIBRA. These findings advance the theoretical foundation for dark matter interactions and provide a robust framework for future experimental design.
Povzetek: Hipoteza o temnih atomih XHe ponuja z nevtralno, atomom podobno konfiguracijo, razlago za temno snov. Avtorji preverjajo interakcijo med XHe in atomskimi jedri, ki bi lahko destabilizirala vezano stanje temnega atoma. Rešujejo tedaj problem, ki vodi do nastanka vezanih stanj jedra XHe in interakcije jedra z atomi z nizko energijo. Poskušajo pokazati, da njihov model lahko razloži obstoj temne snovi v vesolju, anomalije pri meritvah z DAMA/LIBRAo in pomaga načrtovati nove eksperimente

Keywords: Dark atoms; XHe; X-helium; composite dark matter; stable charged particles; bound state; cross section of radiation capture; effective interaction potential

7.1 Dark atoms of X-helium

The non-baryonic nature of dark matter necessitates the existence of novel, stable forms of non-relativistic matter. A particle-based origin for dark matter implies

‡bikbaev.98@bk.ru
§khlopov@apc.univ-paris7.fr

physics beyond the Standard Model, requiring new, stable fundamental particles. Among the candidates put forth are stable particles bearing electric charge [1–5]. This work examines the nuclear-interacting dark atom scenario, which reveals the composite essence of dark matter [6–9]. While the specific electric charge of new stable, multicharged particles is not predetermined a priori, rigorous experimental bounds significantly restrict the viable configurations, permitting solely stable, negatively charged states with a charge multiplicity of $-2n$ [10, 11], where n is a natural number. Herein, these particles are designated as X, with the particular instance of a doubly charged particle, X with charge of -2, being referred to as O^{--}.

Thus, this work investigates composite dark matter model wherein hypothetical, stable, heavy, multicharged X^{-2n} particles, possessing leptonic-like properties (absence or significant suppression of QCD interactions), combine with n primary helium-4 nuclei to form electrically neutral, atom-like states through standard Coulomb attraction. These composite systems are designated as XHe dark atoms. The X^{-2n} particles may either be lepton-like in nature or arise from exotic, novel heavy quark families, characterized by weak-scale interaction cross-sections with standard model hadrons [1].

The structural properties of bound dark atom system are governed by key parameter defined as $a \approx Z_\alpha Z_X \alpha A_{nHe} m_p R_{nHe}$. In this expression, α is the fine-structure constant, Z_X and Z_α correspond to the charge numbers of the X particle and the nHe nucleus, m_p denotes the proton mass, A_{nHe} signifies the mass number of the nHe nucleus, and R_{nHe} represents its radius. Physically, the parameter a quantifies the ratio of the dark atom's Bohr radius to the radius of the n-helium nucleus. The value of this ratio dictates the transition between two distinct structural regimes: Thomson-like configuration is realized when the Bohr radius of the XHe atom is less than the n-helium nucleus radius, whereas Bohr-like atomic structure is adopted in the opposite case.

Within the parameter range $0 < a < 1$, the XHe system conforms to the Bohr atom picture. In this regime, the helium nucleus can be treated as a point-like particle executing an orbital motion around a central, massive X particle with negative charge. In the complementary domain $1 < a < \infty$, the system's structure is more accurately described by Thomson's atomic model. Here, the helium nucleus, which can no longer be considered point-like, undergoes oscillatory motion around the heavier, negatively charged X particle, resulting in a more diffuse and distributed atomic configuration.

The distinct properties of dark atoms lead to a scenario of "warmer-than-cold dark matter" during the formation of large-scale cosmic structure. While this model necessitates further detailed study, its predictions are consistent with the precision cosmological data [1]. The timeliness and significance of this research are driven by the necessity to deepen the investigation into the nuclear interaction characteristics of dark atoms and to evaluate the potential influence of X-helium on processes of nuclear transformations. A comprehensive understanding of these interactions is paramount for accurately assessing the contribution of dark atoms to primordial nucleosynthesis, the evolution of stars, and a spectrum of other physical, astrophysical, and cosmological phenomena in the early Universe [13].

7.2 Low energy binding of dark atoms to nuclei

Direct dark matter detection experiments is characterized by a diversity of outcomes, underscoring the complex nature of potential interactions between dark matter candidates and subterranean detector materials. The X-helium model offers a potential resolution to the apparent conflicts among different direct dark matter detection experiments, which may stem from the unique mechanisms through which dark atoms engage with ordinary matter. Instances of this contradiction include the positive signals registered by the DAMA/NaI and DAMA/LIBRA experiments, which appear inconsistent with the null results reported by experiments including XENON100, LUX, and CDMS, among others [14].
The slowing down of cosmic XHe within the terrestrial crust precludes the application of conventional direct detection techniques, which rely on identifying nuclear recoil signatures from Weakly Interacting Massive Particles (WIMPs) colliding with target nuclei. Nevertheless, the collisions of slow-moving X-helium atoms with these nuclei can result in the formation of low-energy bound states, a process described by the reaction:

$$A + ({}^4He^{++}X^{--}) \rightarrow [A({}^4He^{++}X^{--})] + \gamma. \tag{7.1}$$

It is assumed that within the uncertainties inherent to nuclear parameters, a certain range exists where the binding energy for the XHe–Na system falls within the 2–4 keV range [1], representing a comparatively subtle energy scale. The capturing of dark atoms into such a bound state results in the deposition of an equivalent energy quantum, detectable as an ionization signal in NaI(Tl) crystal detectors like those used in the DAMA experiment. The resultant concentration of XHe within the materials of underground detectors is governed by a balance between the falling cosmic flux of dark atoms and their diffusive transport towards the Earth's center. The availability of X-helium in the terrestrial subsurface is rapidly regulated by the kinematics of dark atom interactions with ordinary matter; it closely tracks variations in the incoming cosmic XHe flux. Consequently, the capture rate of dark atoms is expected to exhibit annual modulation, which should be directly reflected as a corresponding periodic variation in the ionization signal originating from these capture events.
A direct result of the proposed model is the emergence of anomalous superheavy isotopes of sodium within the NaI(Tl) detector material of the DAMA experiment. The mass of these anomalous isotopes exceeds that of standard sodium isotopes by approximately the mass of the X particle [13]. In contrast, the formation of analogous superheavy isotopes of iodine and thallium is improbable, as the formation of bound states between dark atoms and these nuclei is unfavorable [13]. Should these anomalous sodium atoms remain in a non-fully ionized state, their transport properties are governed by atomic cross-sections, resulting in a mobility reduced by approximately nine orders of magnitude compared to that of OHe [13]. This reduction in mobility effectively leads to their accumulation and retention within the detector material. Consequently, mass spectroscopic examination of this substance could offer a crucial independent test for verifying the X-helium origin of the DAMA signal. Any methodology employed for such an analysis

must account for the fragile nature of the XHe-Nα bound systems, characterized by binding energies of merely several keV [15].
The anticipated energy release in detector materials alternative to NαI is predicted to occupy a spectral range predominantly above 2–6 keV [13]. Furthermore, such a signal may be entirely absent in detectors utilizing heavy target nuclei, such as xenon [13].
The unscreened nuclear charge of the dark atom introduces the possibility of a strong interaction between XHe and terrestrial nuclei. This interaction can dissociate the dark atom's bound system, potentially giving rise to anomalous isotopes whose abundance in the environment is stringently constrained by existing experimental data [10]. To resolve this challenge, the XHe hypothesis postulates the existence of potential well in conjunction with a repulsive potential barrier within the effective interaction potential (see Figure 7.1). This potential structure inhibits the merger of the dark atom's constituents — namely, the n–He nucleus and the X particle — with nuclei of ordinary matter. This specific feature of the interaction potential constitutes a critical prerequisite for the phenomenological viability of the X-helium hypothesis.

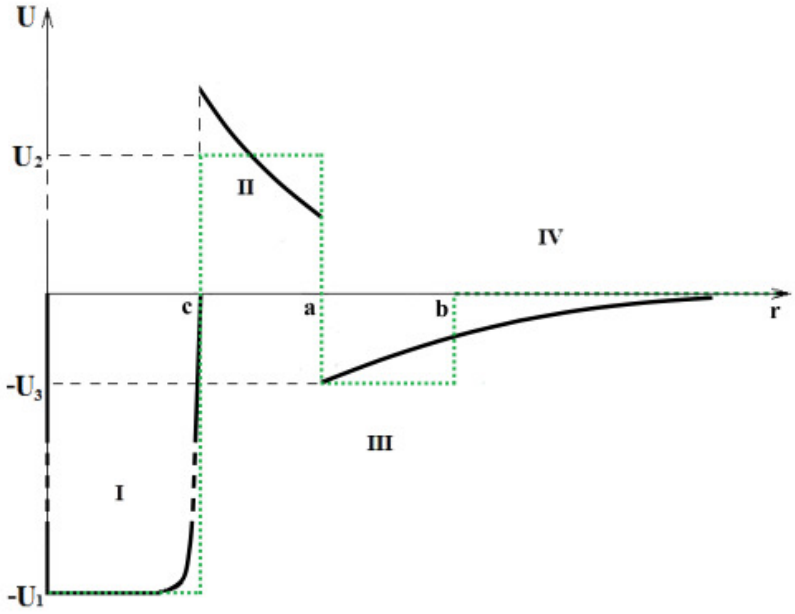

Fig. 7.1: Hypothetical qualitative image of the shape of the effective interaction potential of XHe dark atom with the nucleus of atom of matter [13].

The specific profile of this effective potential (see Figure 7.1) arises principally from the rivalry between the electromagnetic repulsion and the attractive nuclear force originating from the nuclear shell of the dark atom and the target nucleus.

The total effective interaction potential of the XHe–nucleus system is defined as the aggregate potential experienced by the nucleus of matter under the influence of the various forces emanating from the dark atom. This description holds within a coordinate system centered on the dark atom, when the nucleus undergoes a slow approach towards the dark atom from an initial distance much large compared to the characteristic sizes of the particles.

Eventually, the capture mechanism proceeds as follows: nucleus, moving with slow, thermal velocities relative to the dark atom in the detector, interacts with the XHe. The dark atom becomes polarized via the Stark effect induced by the electric field of the approaching nucleus itself, effectively forming a dipole. This interaction enables the nucleus to transition into a low-energy bound state within the potential well of the XHe-nucleus system's effective potential. The energy released in this capture process corresponds to a photon whose energy equals the sum of the nucleus's initial kinetic energy and the binding energy in the potential well. This energy release mechanism is ultimately registered as the ionization signal observed in the NaI(Tl) detectors of the DAMA experiment.

The theoretical description of interactions between dark atoms and ordinary nuclei constitutes a three-body problem, which is not amenable to an exact analytical solution. To elucidate the physical consequences of this scenario, characterized by its specific effective interaction potential, a precise quantum mechanical numerical model for this three-body system has been constructed. In article [16], a quantum mechanical numerical model describes the OHe-Nα system, representing it as three particles interacting via electromagnetic, nuclear, and centrifugal forces. The computational approach involves solving the Schrödinger equation for the helium in the OHe-Nα system at different fixed positions of the sodium nucleus, $\vec{R}_{OA}$, relative to the dark atom. This methodology, which incorporates both nuclear and electromagnetic interaction characteristics, enables precise determination of dark atom polarization through calculated dipole moments of the OHe atoms. These distance-dependent dipole moments, varying with separation between the sodium nucleus and dark atom, facilitate reconstruction of the Stark potential - a crucial component in constructing the total effective interaction potential for the OHe-Nα system. The total effective interaction potential is formulated as the sum of multiple contributions (see Figure 7.2): the Stark potential, centrifugal potential, nuclear potential, and the electric interaction potential U^{e}_{XHe} of an unpolarized dark atom with the nucleus. The latter two potentials exhibit short-range character, diminishing exponentially with increasing particle separation. Thus, the model presented in [16] therefore represents advancement toward a self-consistent quantum mechanical description of dark atoms with unshielded nuclear attraction interacting with usual matter nuclei.

Building upon the results presented in [16], we construct the total effective interaction potential for the OHe–Nα system. This enables the determination of energy level for low-energy bound state between the OHe dark atom and sodium nucleus, and facilitates computation of the corresponding capture reaction cross-section (see Figure 7.2). The form of this potential is influenced by the spin of the O^{--} particle, as the centrifugal component of the OHe-nucleus total effective interaction potential depends on this spin magnitude. The specific value of the

O^{--} spin represents a model-dependent quantity that varies with the underlying particle physics framework [1]. For the scenario depicted in Figure 7.2, the spin is taken as $I_{O^{--}} = 1$. The illustrated potential profile demonstrates consistency with theoretical expectations, exhibiting a potential well of approximately 136 keV depth preceded by a repulsive potential barrier. The height of this barrier significantly exceeds the thermal energy of sodium nuclei at room temperature (approximately 10^{-2} eV). This potential barrier plays a crucial role in maintaining dark atom integrity by preventing the merger of either constituent (helium or O^{--}) with nucleus.

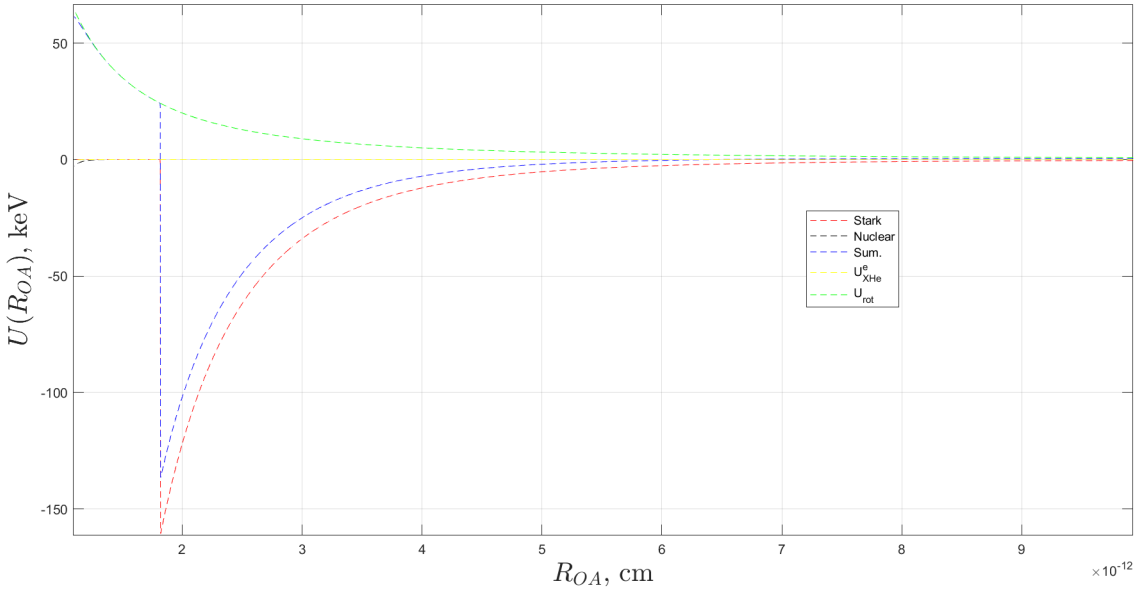

Fig. 7.2: Interaction potentials within the OHe–Na system, presented as functions of the distance between the OHe dark atom and nucleus of Na, R_{OA}: the Stark potential (red dotted curve), the centrifugal potential (green dotted curve), nuclear potential (black dotted curve), the electric interaction potential U^e_{XHe} of unpolarized dark atom with the nucleus (yellow dotted curve) and the total effective interaction potential (blue dotted curve). This particular configuration corresponds to a total angular momentum quantum number for the OHe-sodium nucleus interaction of $\vec{J}_{OHe-Na} = \overrightarrow{5/2}$. The calculations were performed utilizing the results of the [16] paper.

The bound states of sodium nucleus within the total effective interaction potential of the OHe–Na system (depicted by the blue dotted curve in Figure 7.2) are obtained by solving one-dimensional stationary Schrödinger equation for free sodium nucleus in the corresponding potential. This procedure yields the discrete energy spectrum of bound states localized in the potential well, along with their associated normalized wave functions.

The solution to this quantum mechanical problem is presented in Figure 7.3. Analysis reveals that the potential well contains only a single bound state, corresponding to the ground state of the system with energy $E_{1_{Na}} \approx -2.4$ keV. The Figure 7.3 displays the total effective interaction potential (solid blue curve) alongside the squared modulus of the wave function (solid red curve) for this single bound state within the OHe–Na potential.

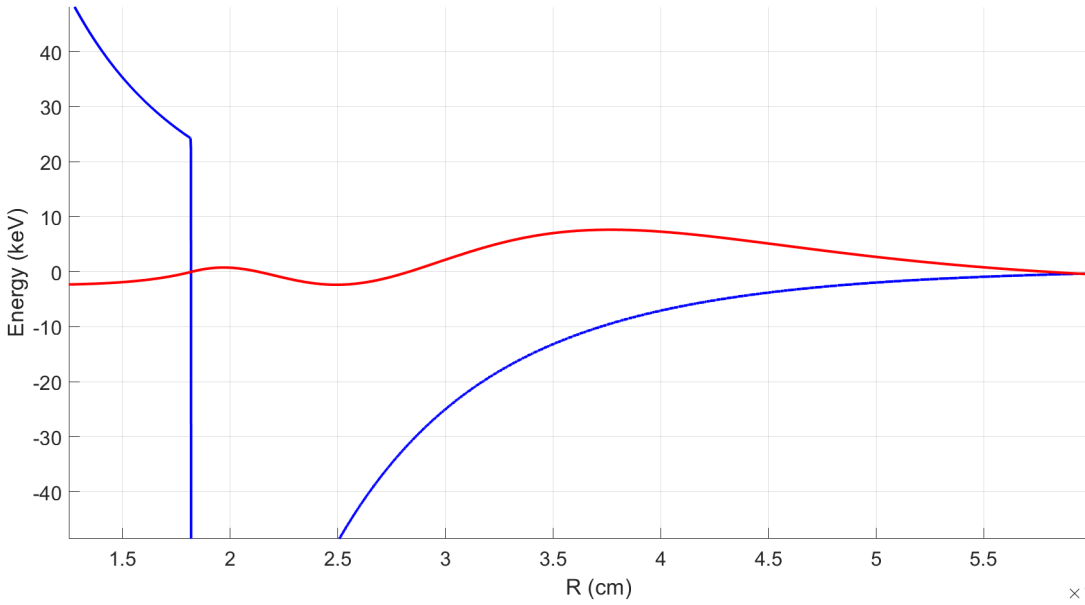

Fig. 7.3: The figure illustrates the dependence of the total effective interaction potential between the OHe dark atom and the sodium nucleus (solid blue curve) and the probability density given by the squared modulus of the wave function (solid red curve) from the radius vector of sodium nucleus. Squared modulus of the wave function correspond to the ground state energy level of $E_{1_{Na}} \approx -2.4$ keV for sodium within the OHe–Na system's effective potential.

7.3 Calculation of the cross-section of radiative capture in the OHe-nucleus system

We now proceed to compute the radiative capture cross-section for sodium nucleus into the bound state of the OHe–Na system. This calculation employs the previously derived unit-normalized wavefunction $\Psi_{f_{Na}}$, which describes the sodium nucleus in its ground bound state and will be consider as the final quantum state in the capture process.

In the initial configuration, the sodium nucleus exists as an unbound free particle represented by its wave function $\Psi_{i_{Na}}(r)$. This eigenfunction satisfies the

Schrödinger equation governing the thermal relative motion of the nucleus of matter in the total effective interaction potential $V_{eff}(r)$ characterizing the OHe–Na system:

$$\left[-\frac{\hbar^2}{2\mu}\nabla^2 + V_{eff}(r) - E\right]\Psi_{i_{Na}}(r) = 0, \tag{7.2}$$

where μ is the reduced mass of the OHe-Na system, $E = \frac{3}{2}k_bT$ is the energy of relative thermal motion in the center of mass system.

Owing to the spherical symmetry of the potential $V_{eff}(r)$, the wave function $\Psi_{i_{Na}}(r)$, which is modified by its influence, can be expressed as an expansion in partial waves corresponding to the angular momentum eigenfunctions:

$$\Psi_{i_{Na}}(r) = \sum_{l=0}^{\infty}\sum_{m=-l}^{l}\frac{u_l(r)}{r}Y_{lm}(\theta,\varphi), \tag{7.3}$$

where $u_l(r)$ is the radial wave function, and $Y_{lm}(\theta,\varphi)$ these are spherical harmonics.

Inserting the partial wave expansion (7.3) into the Schrödinger equation (7.2) and applying the orthogonality relations of spherical harmonics yields the radial equation for individual partial waves:

$$\left[-\frac{\hbar^2}{2\mu}\frac{d^2}{dr^2} + V_{eff}(r) + \frac{\hbar^2 l(l+1)}{2\mu r^2} - E\right]u_l(r) = 0, \tag{7.4}$$

where the term $\frac{\hbar^2 l(l+1)}{2\mu r^2}$ represents the centrifugal potential arising naturally from the separation of variables in spherical coordinates.

Thus, throughout the spatial domain where the effective interaction potential possesses non-zero values, the initial state wave function admits the following expansion:

$$\Psi_{i_{Na}}(r) = \sum_{l=0}^{\infty}(2l+1)i^l R_l^{norm}(r)P_l(\cos\theta), \tag{7.5}$$

where $R_l^{norm}(r) = N_l \cdot u_l(r)/r = N_l \cdot R_l(r)$ is the normalized radial component of wave function, N_l is the normalization factor, and $P_l(\cos\theta)$ denotes the Legendre polynomials.

The normalization of the radial wave function $R_l^{norm}(r)$ is chosen such that in the asymptotic limit ($r \to \infty$) it satisfies the condition:

$$R_l^{norm}(r) = e^{i\delta_l}\left[\cos\delta_l\, j_l(k_{Na}r) - \sin\delta_l\, n_l(k_{Na}r)\right], \tag{7.6}$$

where $k_{Na} = \frac{p_{Na}}{\hbar} = \frac{m_{Na}v}{\hbar}$ represents the wave number of the sodium nucleus, p_{Na} and m_{Na} denote its momentum and mass respectively, and v is the relative velocity between interacting particles in the OHe–Na system. Here $j_l(kr)$ and $n_l(kr)$ correspond to spherical Bessel and Neumann functions, while δ_l represents

the scattering phases determined by the effective potential $V_{eff}(r)$, which fully characterize the scattering behavior for each partial wave with orbital angular momentum l.

The scattering phases δ_l are determined through numerical integration of the radial Schrodinger equation (7.4) to obtain the wavefunction $R_l(r)$, which is subsequently matched to its asymptotic form given by equation (7.6). The phase shift computation employs the logarithmic derivative method, evaluating the quantity $L = R_l'(r_0)/R_l(r_0)$ at a sufficiently large radial coordinate r_0 where the effective potential $V_{eff}(r)$ becomes negligible:

$$\tan \delta_l = \frac{k_{Na} j_l'(k_{Na} r_0) - j_l(k_{Na} r_0) \cdot L}{k_{Na} n_l'(k_{Na} r_0) - n_l(k_{Na} r_0) \cdot L}, \tag{7.7}$$

where j_l' and n_l' represent the derivatives of the spherical Bessel and Neumann functions, respectively.

The effective interaction potential supports only one bound state for the sodium nucleus within the 1–6 keV energy range, restricting possible quantum transitions to an electric dipole (E1) process from an initial $l_i = 1$ partial wave to the final $l_f = 0$ bound state. Although thermal-energy nuclei predominantly occupy s-wave states ($l = 0$), the initial state wavefunction contains a minor p-wave ($l = 1$) admixture. We therefore employ a partial wave decomposition of the unbound free nuclear wavefunction, where each radial component satisfies the Schrödinger equation for the relative thermal energy $E = \frac{3}{2} k_B T$ in the OHe–Na center-of-mass system. Selecting the $l_i = 1$ component from this expansion enables computation of the transition amplitude from this initial p-wave state to the final bound state. The reaction rate is significantly attenuated owing to the negligible population of p-wave states compared to the dominant s-wave component at thermal energies. In accordance with Fermi's Golden Rule, the probability of transition per unit of time from an initial quantum state $|i\rangle$ to a specific final state $|f\rangle$ is given by:

$$\Gamma_{i \to f} = \frac{2\pi}{\hbar} \left| \langle f | \hat{H}_{int} | i \rangle \right|^2 g(E_f), \tag{7.8}$$

where $\langle f | \hat{H}_{int} | i \rangle$ represents the transition matrix element of the interaction operator, $\hat{H}_{int}$, for the electrical transition between the final and initial states, and $g(E_f)$ denotes the density of final states at energy E_f.

Fermi's golden rule expresses the transition rate between quantum states in terms of the density of available final states. For the capture process of a sodium nucleus by a dark atom accompanied by photon emission, this density of the final states is determined by the emitted photon. In the specific reaction under consideration, the sodium nucleus undergoes a transition from an unbound state to a bound configuration with the dark atom, emitting a photon whose energy is given by:

$$E_\gamma = T_{Na} + I_{OHe-Na} \approx I_{OHe-Na} \approx 2 \text{ keV}, \tag{7.9}$$

where $T_{Na} = \frac{p_{Na}^2}{2m_{Na}} \approx 10^{-2}$ eV represents the thermal kinetic energy of the unbound free sodium nucleus, and I_{OHe-Na} denotes the binding energy of the sodium nucleus in the total effective interaction potential.

The initial configuration of the system consists of unbound sodium nucleus and OHe dark atom, while the final state includes the bound OHe–Na system accompanied by photon emission. The continuum of final states is characterized by the photon parameters, as the initial sodium state exists in the continuous spectrum (free particle) while the final bound state is discrete. The transition becomes physically permissible only through photon emission, where the photon states themselves form a continuous spectrum. Consequently, the total density of final states is governed by the photon, since the OHe–Na bound state represents a fixed discrete configuration, whereas the photon can occupy various momentum and directional states.

The bound OHe–Na system possesses a discrete energy eigenvalue (approximately 2 keV) following the sodium nucleus capture, thus its contribution to the density of final states $g(E_f)$ corresponds to a single quantum state, represented by a Dirac delta function. In contrast, the emitted photon, with energy closely matching the binding energy I_{OHe-Na}, may be emitted in any spatial direction with essentially fixed energy (when neglecting the recoil of the OHe–Na system), which determines the angular distribution of the final state density. Consequently, the number of end states per unit energy interval and unit volume for photon emission into solid angle $d\Omega$, accounting for the two possible polarization states of the electromagnetic wave, in three-dimensional space is given by:

$$g(E_\gamma) = 2\frac{d}{dE_\gamma}\left(\int \frac{d^3\vec{q}_\gamma}{(2\pi)^3}\right) = \frac{E_\gamma^2}{4\pi^3 c^3 \hbar^3} d\Omega, \tag{7.10}$$

where $|\vec{q}_\gamma| = \dfrac{E_\gamma}{c\hbar}$ denotes the photon wave vector.

The radiative capture cross section for sodium nucleus forming bound state with OHe is defined by the relation:

$$\sigma_{OHe-Na} = \frac{\Gamma_{i\to f}}{j}, \tag{7.11}$$

where j represents the incident flux of sodium nuclei.

For the radiative capture process, the initial state corresponds to scattering wave function normalized to unit flux, ensuring the probability flux associated with the incident wave satisfies:

$$j = \frac{\hbar k_{NA}}{\mu} = \upsilon \tag{7.12}$$

where υ represents the relative velocity between the interacting particles. This relative velocity corresponds to the thermal velocity of the sodium nucleus relative to the dark atom in the center-of-mass system. For the specific capture process analyzed here, the substantial mass difference between the dark atom and sodium nucleus results in the center-of-mass system being effectively coincident with the laboratory system where the dark atom rests.

Substituting $\Gamma_{i\to f}$ into the formula for the cross sections, we get:

$$\sigma_{OHe-Na} = \frac{2\pi}{\hbar}\frac{1}{\upsilon}\left|\langle f|\hat{H}_{int}|i\rangle\right|^2 g(E_\gamma) = \frac{2\pi}{\hbar}\frac{1}{\upsilon}\left|\langle f|\hat{H}_{int}|i\rangle\right|^2 \frac{E_\gamma^2}{4\pi^3 c^3 \hbar^3} d\Omega. \tag{7.13}$$

The transition of sodium nucleus into bound state with dark atom is mediated by its interaction with the electromagnetic field. The interaction Hamiltonian $\hat{H}_{int}$ governing the electric multipole transition of order J in the dipole approximation is derived from the multipole expansion of the electromagnetic vector potential into functions with a certain moment and parity. For the long-wavelength approximation, which is fully applicable to the low-energy radiative capture process considered here given that $(q_\gamma \cdot r) \approx 10^{-4} << 1$, the operator for electric multipole transition of order J is given by the expression [17]:

$$\hat{H}_{int} = -A_0 \sqrt{\frac{2\pi(J+1)}{J[(2J+1)!!]^2}} q_\gamma^J \hat{Q}_{Jm}, \tag{7.14}$$

here, $\hat{Q}_{Jm} = eZ_{Na} r^J Y_{Jm}(\theta, \phi)$ represents the static electric multipole moment operator, with Z_{Na} denoting the charge number of the sodium nucleus, while $A_0 = \sqrt{\frac{2\pi c\hbar}{q_\gamma}}$ corresponds to the electromagnetic vector potential amplitude, conventionally normalized to the single-photon per unit volume condition.
Consequently, the matrix element $\langle f|\hat{H}_{int}|i\rangle$ for the transition operator between the initial and final states can be evaluated. Employing the representation of the initial state wave function from Eq. (7.5) as a partial wave with definite orbital angular momentum l_i, this matrix element factorizes into distinct radial and angular components as follows:

$$\langle f|\hat{H}_{int}|i\rangle = -A_0 \sqrt{\frac{2\pi(J+1)}{J[(2J+1)!!]^2}} q_\gamma^J eZ_{Na} \langle l_f|Y_{Jm}(\theta, \phi)|l_i\rangle \cdot I_{radial}, \tag{7.15}$$

where $I_{radial} = \int_0^\infty \Psi^*_{f_{Na}}(r) \cdot r^{J+2} \cdot (2l_i + 1) i^{l_i} \cdot R^{norm}_{l_i}(r) dr$ and $\langle l_f|Y_{Jm}(\theta, \phi)|l_i\rangle$ are the radial and angular parts of the matrix element, respectively.
The angular component of the transition matrix element for the process $l_i = J \to l_f = 0$ is determined through integration over the solid angle:

$$\begin{aligned}\langle 0|Y_{Jm}(\theta, \phi)|J\rangle = \int Y_{00}(\theta, \phi) \cdot Y_{Jm}(\theta, \phi) \cdot P_J(\cos(\theta)) d\Omega = \\ = \frac{1}{\sqrt{(2J+1)}}.\end{aligned} \tag{7.16}$$

Consequently, the squared modulus of the reduced matrix element for the static electric multipole moment operator $\hat{Q}Jm$ takes the form:

$$|\langle 0||\hat{Q}_{Jm}||J\rangle|^2 = \frac{e^2 Z^2_{Na}}{(2J+1)} \left| \int_0^\infty \Psi^*_{f_{Na}}(r) \cdot r^{J+2} \cdot (2J+1) i^J \cdot R^{norm}_1(r) dr \right|^2. \tag{7.17}$$

Incorporating the expression of matrix element $\langle f|\hat{H}_{int}|i\rangle$ into the radiative capture cross-section formula (7.13) for the OHe–Na bound state, and taking into consideration, that $e^2 = \alpha\hbar c$, where α denotes the fine structure constant, we arrive at:

$$\sigma^{J\to 0}_{OHe-Na} = \frac{8\pi q_\gamma^{2J+1}\alpha c Z^2_{Na}}{v}\frac{(J+1)(2J+1)}{J[(2J+1)!!]^2}\left|\int_0^\infty \Psi^*_{f_{Na}}(r)\cdot r^{J+2}\cdot i^J\cdot R_1^{norm}(r)dr\right|^2. \tag{7.18}$$

The resulting formulation for the radiative capture cross section of sodium nucleus transitioning from unbound free state with orbital angular momentum $l_i = 1$ to the ground bound state (with $l_f = 0$) within the total effective interaction potential of the OHe–Na system and the corresponding the rate of radiation capture, is given by:

$$\sigma^{1\to 0}_{OHe-Na} = \frac{16\pi}{3}\frac{\alpha c}{v}\frac{E_\gamma^3}{c^3\hbar^3}Z^2_{Na}\left|\int_0^\infty \Psi^*_{f_{Na}}(r)\cdot r^3\cdot i\cdot R_1^{norm}(r)dr\right|^2, \tag{7.19}$$

$$(\sigma^{1\to 0}_{OHe-Na}\cdot v) = \frac{16\pi}{3}\alpha c\frac{E_\gamma^3}{c^3\hbar^3}Z^2_{Na}\left|\int_0^\infty \Psi^*_{f_{Na}}(r)\cdot r^3\cdot i\cdot R_1^{norm}(r)dr\right|^2. \tag{7.20}$$

Upon numerical evaluation of expressions (7.19) and (7.20) using the relevant physical parameters – including the matrix element squared $\left|\int_0^\infty \Psi^*_{f_{Na}}(r)\cdot r^3\cdot i\cdot R_1^{norm}(r)dr\right|^2 \approx 1.8\cdot 10^{-65}\ cm^5$, velocity ratio $\frac{v}{c} = \sqrt{\frac{3kT}{m_{Na}}} \approx 2\cdot 10^{-6}$, nuclear charge $Z_{Na} = 11$, and energy of the OHe-Na bound state $E_\gamma \approx -2.4\ keV$ – we obtain the following quantitative results for the radiative capture cross-section and corresponding radiative capture rate:

$$\sigma^{1\to 0}_{OHe-Na} \approx 2.8\cdot 10^{-35}\ cm^2 = 2.8\cdot 10^{-11}\ barn. \tag{7.21}$$

$$(\sigma^{1\to 0}_{OHe-Na}\cdot v) \approx 1.6\cdot 10^{-30}\ cm^3/sec. \tag{7.22}$$

The capture rate can be evaluated using the formalism presented in [13]:

$$\begin{aligned} R &= 1\cdot\frac{\rho_O}{M_O}(\langle\sigma v\rangle_{Na} + \langle\sigma v\rangle_I)\cdot N_T,\\ \rho_O &= \frac{M_O\, n_0}{320\cdot S_3\cdot 30^{1/2}}V_h + \frac{M_O\, n_0}{640\cdot S_3\cdot 30^{1/2}}V_E\cos(\omega(t-t_0)), \end{aligned} \tag{7.23}$$

where the scaling parameter $S_3 = M_O/1$ TeV, with the OHe mass equal to $M_O = 2.5$ TeV, the number of targets $N_T = 4.015\cdot 10^{24}$ nuclei per kilogram of NaI(Tl), Solar system velocity $V_h = 220\cdot 10^5$ cm/s, Earth's orbital velocity $V_E = 30\cdot 10^5$ cm/s, and local dark matter concentration $n_0 = 1.5\cdot 10^{-4}\ cm^{-3}$ for the considered particles. The substantial mass of the DAMA/LIBRA detectors (approximately 9.7 kg each) ensures near-complete absorption of the low-energy gamma radiation inside the active detector volume.

Employing the equation (7.23), the capture rate can be computed utilizing the derived value for the rate of sodium radiative capture (7.22), under the assumption that the radiative capture rate for iodine is significantly suppressed:

$$R_{numerical} \approx 0.440 + 2.83\times 10^{-2}\cos(\omega(t-t_0))\ counts/day\ kg, \tag{7.24}$$

this numerical result closely aligns with the experimental data reported by the DAMA/NaI and DAMA/LIBRA experiments.
Specifically, considering the energy interval from 1 keV to 6 keV, experimental analysis yields the following results:

$$\begin{aligned} \Delta R &= (6.95 \pm 0.45) \times 10^{-2}\,\text{counts/(day kg)}, \\ R_0 &< 0.5\,\text{counts/(day kg)}, \end{aligned} \tag{7.25}$$

the modulated signal amplitude ΔR is determined by integrating the annual modulation amplitudes reported by the DAMA/NaI and DAMA/LIBRA collaborations [14, 18, 19] over the energy range from the energy threshold to 6 keV. The upper limit R_0 on the unmodulated component is inferred from the corresponding constraints on the constant signal rate provided in the same references [14, 18, 19].

7.4 Conclusions

The developed quantum mechanical model provides a self-consistent description of the interaction between OHe dark atom and atomic nucleus, addressing the fundamental challenges in direct dark matter detection. Through numerical solution of Schrödinger equations in the three-body system, we have reconstructed the total effective interaction potential for the OHe–Na system, revealing its characteristic form, comprising a shallow potential well and repulsive potential barrier. This potential configuration ensures the stability of dark atoms against nuclear fusion while permitting the formation of low-energy bound states through radiative capture processes. The wave functions of the initial state of the free nucleus of matter, $\Psi_{i_{Na}}(r)$, and the final ground bound state of the nucleus of matter in the OHe-Na system, $\Psi_{f_{Na}}(r)$, are calculated by numerically solving the Schrodinger equation in the restored total effective interaction potential of the considered system of three bodies.
Our calculations demonstrate that the OHe–Na system supports exactly one bound state within the 1–6 keV energy range, corresponding to the ground state with binding energy $E_{1_{Na}} \approx -2.4$ keV. The radiative capture cross-section for the electric dipole transition from the initial $l_i = 1$ partial wave to the final $l_f = 0$ bound state yields $\sigma^{1\to0}_{\text{OHe–Na}} \approx 2.8 \times 10^{-35}$ cm^2, with the corresponding capture rate $\langle\sigma v\rangle \approx 1.6 \times 10^{-30}$ cm^3/s.
The computed count rate of $R_{numerical} \approx 0.440 + 2.83 \times 10^{-2}\cos(\omega(t - t_0))$ counts/(day·kg) exhibits agreement with the annual modulation signal observed by DAMA/NaI and DAMA/LIBRA experiments in the 1–6 keV energy window where $\Delta R = (6.95 \pm 0.45) \times 10^{-2}$ counts/(day·kg). This consistency provides substantial support for the X-helium dark atom hypothesis as a viable explanation for the DAMA results.
The methodology established in this work offers a robust foundation for further investigations into dark atom-nucleus interaction. Future research directions should take into account the not-point-like of interacting particles in the quantum mechanical model and include a detailed study of the dependence of capture rates for other conditions and detector materials.

Acknowledgements

The work of T.B. was performed in Southern Federal University with financial support of grant of Russian Science Foundation № 25-07-IF. The work by A.M. was performed with the financial support provided by the Russian Ministry of Science and Higher Education, project "Fundamental and applied research of cosmic rays", No. FSWU-2023-0068.

References

1. Khlopov, M. Fundamental particle structure in the cosmological dark matter. *International Journal of Modern Physics A* **2013**, *28*, 1330042.
2. Bertone, G.; Hooper, D.; Silk, J. Particle dark matter: evidence, candidates and constraints. *Physics Reports* **2005**, *405*, 279 – 390.
3. Scott, P. Searches for Particle Dark Matter: An Introduction. *arXiv* **2011**, arXiv:1110.2757.
4. Belotsky, K. M.; Khlopov, M.Y.; Shibaev, K. I. Composite Dark Matter and its Charged Constituents. *Grav.Cosmol.* **2006**, *12*, 93-99, arXiv:astro-ph/0604518.
5. Belotsky, K.; Khlopov, M.; Shibaev, K. Stable quarks of the 4th family? *arXiv* **2008**, arXiv:0806.1067.
6. Khlopov, M.Y.; Kouvaris, C. Strong interactive massive particles from a strong coupled theory. *Phys. Rev. D* **2008**, *77*, 065002.
7. Khlopov, M. Yu.; Kouvaris, C. Composite dark matter from a model with composite Higgsboson. *Phys. Rev.* **2008**, *78*, 065040.
8. Fargion, D.; Khlopov, M. Yu. Tera-leptons' shadows over Sinister Universe. *Gravitation Cosmol.* **2013**, *19*, 219.
9. Beylin, V.; Khlopov, M.; Kuksa, V.; Volchanskiy, N. New Physics of Strong Interaction and Dark Universe. *Universe* **2020**, *6*, 196.
10. Cudell, J. R.; Khlopov, M. Y.; Wallemacq, Q. The nuclear physics of OHe. *Bled Workshops in Physics* **2012**, *13*, 10 –27.
11. Bulekov, O. V.; Khlopov, M. Yu.; Romaniouk, A. S.; Smirnov, Yu. S. Search for Double Charged Particles as Direct Test for Dark Atom Constituents. *Bled Workshops in Physics* **2017**, *18*, 11-24.
12. Khlopov, M. What comes after the Standard Model? *Prog. Part. Nucl. Phys.* **2020**, *116*, 103824.
13. Khlopov, M.Y.; Mayorov, A.G.; Soldatov, E.Y. The dark atoms of dark matter. *Prespace J.* **2010**, *1*, 1403–1417.
14. Bernabei, R.; Belli, P.; Bussolotti, A.; Cappella, F.; Caracciolo, V.; Cerulli, R.; Dai, C.J.; d'Angelo, A.; Di Marco, A.; Ferrari, N.; et al. The DAMA project: Achievements, implications and perspectives. *Prog. Part. Nucl. Phys.* **2020**, *114*, 103810.
15. Beylin, V.; Khlopov, M. Y.; Kuksa, V.; Volchanskiy, N. Hadronic and Hadron-Like Physics of Dark Matter. *Symmetry* **2019**, *11(4)*, 587.
16. Bikbaev, T.; Khlopov, M.; Mayorov, A. Quantum Mechanical Numerical Model for Interaction of Dark Atom with Atomic Nucleus of Matter. *Physics* **2025**, *7(1)*, 8.
17. A. S. Davydov, "Theory of the Atomic Nucleus," Nauka, Moscow, 1958 (in Russian).
18. Bernabei, R.; et al. Further results from DAMA/LIBRA-phase2 and perspectives. *Nuclear Physics and Atomic Energy* **2021**, *22*, 329–342.
19. Bernabei, R.; et al. Dark matter investigation with DAMA set-ups. *International Journal of Modern Physics A* **2022**, *37.7*.

BLED WORKSHOPS
IN PHYSICS
VOL. 26, NO. 1

Proceedings of the 28th Workshop
What Comes Beyond . . . *(p. 73)*
Bled, Slovenia, July 6–17, 2025

8 Anomaly footprints in SM+Gravity

L. Bonora[†]

International School for Advanced Studies (SISSA),
Via Bonomea 265, 34136 Trieste, Italy

Abstract. This is a follow-up of [8]. A simplified version of the SM plus gravity, put forward there, is presented here and some of its aspects delved into. The basic structure consists of two sectors, left and right, with chirally mirror fermions and scalars, as well as $SU(3)$ and $U(1)$ gauge fields, while the $SU(2)$ gauge fields as well as the metric are in common to both sectors. This structure is dictated by the request to cancel all dangerous anomalies. The left sector consists of the fermion, gauge and scalar fields of the SM, now minimally coupled to gravity. The right sector is a mirror image of the left, with distinct fields, except the metric and the $SU(2)$ gauge potentials. The first new aspect is the proposed and motivated interpretation of the right sector as the dark matter one. The second new subject covered here is Weyl symmetry and its possible application to cosmology and its theoretical fallout on unitarity and renormalization of the model. A background solution of the Weyl invariant theory is derived, which may apply to the very early stages of the universe. This solution also suggests interesting applications to the cosmological constant problem. On the quantum field theory side the subject of Weyl symmetry and Weyl anomalies is reviewed and, among other things, an application of the WZ terms is illustrated to the problem of one-loop quantization of the model which may avoid negative norm states.
Povzetek: Avtor predstavi nov doprinos k delu, ki ga je objavil v referenci [8] in v katerem poveže *stardandni model* z gravitacijo v minimalni razširitvi. Na kratko predstavi dosedanje ugotovitve, nekatere pa podrobneje razloži. Postavi dva sektorja, v katerih imajo fermioni in skalarji obe kiralnosti in so sklopljeni z ustreznima poljema $SU(3)$ in $U(1)$, Polje $SU(2)$ in metrika pa sta skupna obema sektorjema. Tako mu uspe odpraviti nezaželene anomalije. Avtor interpretira desni sektor kot temno snov v vesolju. Predlaga tudi uporabo Weylove simetrije v kozmologiji v zgodnjih fazah nastanka vesolja, tudi zaradi njene unitarnosti in renormalizabilnosti. Izpelje osnovno rešitev Weylove teorije, ki ponudi pojasnilo za kozmološko konstanto. V kvantni teoriji polja predlaga uporabo WZ členov pri iskanju rešitev z eno zanko, ki morda omogoči, da seavtor izogne stanjem z negativno normo.

8.1 Introduction

Gauge and gravitational anomalies in local field theories come in two species. In [8] these two types were labeled type O (obstructive) and type NO (non-obstructive). The reason of the partition is due to their drastically different nature. The former are a symptom that (chiral fermion) propagators do not exist. For they signal topological obstructions to invert the corresponding Dirac operators, made precise by the family's index theorem of Atiyah and Singer[1]; when present in a theory, they

[†]email:bonora@sissa.it

[1]A full treatment of O-type anomalies can be found in [7].

make impossible its quantization. The NO-type anomalies are simply quantum effect, they signal that a symmetry is violated at the quantum level but have no obstructive effect on propagators and do not endanger quantization. Needless to say chiral theories that contain O-type anomalies must be discarded. The minimal standard model (MSM) is free of the latter. But when we couple it to gravity new anomalies come into play. They mostly cancel out due to the particular algebraic combination of the fields in it. But some residual odd-parity trace anomalies survive. They are generated by their coupling to gravity and are built with the $SU(2)$ gauge fields.

In [8] a theory was tentatively proposed which is free of all O-type anomalies. It consists of mirror right-handed multiplets of fermions added to the left-handed multiplets that define MSM. Altogether it features a sort of two distinct standard models coupled to gravity, which have in common the $SU(2)$ gauge fields, while they have distinct $SU(3)$ and $U(1)$ gauge sectors, as well as two distinct gravity sectors, each one with its own metric, and distinct scalar sectors. It was also shown that this model can be extended with the addition of dilaton fields that guarantees Weyl invariance. This model is type-O anomaly free and has a quality, it answers the question: why does nature use only left-handed particles and right-handed antiparticles to build up our universe while disdaining right-handed particles and left-handed antiparticles? Having to include the latter in the cast is an anomaly footprint.

But once its merits are recognized, how do we interpret the particles that mirror the MSM (the right sector)? One possibility is to use the modeler's privilege and simply imagine a mechanism that assign very large masses and exclude them from any realistic possibility of experimental detection, as was done in part in the last-but-one section of [8]. A more appealing possibility, not altogether disconnected from the previous one, is to interpret them as the dark matter sector. We shall discuss this point later on. But before that we should clarify the nature of the above outlined theory. It is an attempt to assemble a theory starting from different (and non-homogeneous) components, the MSM on one side and general relativity (GR) on the other. They are not homogeneous in the sense that while the MSM is a unitary and renormalizable quantum field theory, GR is a classical theory yet without any known quantum field theory UV completion. In a theory describing the four fundamental forces, there is a stage where the SM, a quantum field theory, live together with GR. This is the stage where the scale of energy is such that life is possible. But it is natural to ask ourselves what happens when the reference energy increases and we trace back the evolution of the universe toward the big-bang beginning with a constantly increasing scale of energy.

The most natural thing to do is to couple the SM fields to gravity in the simplest way, the minimal one, and deal with the resulting theory as a unique theory and quantize it. As a first step in quantization one has to deal with the anomalies. This is what was done in [8], and we reconsider here. The theory complies with the first elementary requirement, absence of O-type anomalies. It contains only renormalizable terms, that is it is a power-counting renormalizable theory, although

this is not enough to secure renormalization and unitarity[2]. On the other hand expecting a unitary and renormalizable field theory with a limited number of fields including gravity would seem to be overly naive. In other words the theory put forward in [8] and studied here is at an initial stage, but this does not mean that we cannot extract from it useful and non-trivial information, such as the doubling of dofs with opposite chiralities required by the anomaly cancelation. This bottom-up approach is not of course the only possible one. There are several top-down approaches, notably the ones based on supergravity field theories or on superstring theories. They rely on the effective field theory (EFT) techniques [11], which goes essentially back to the Wilsonian philosophy. It stems from the idea of integrating out the high energy (momenta and masses, high with respect to a scale parameter) degrees of freedom and retain only the renormalizable terms among those obtained, relying on the expectation that the higher order terms should be suppressed by the inverse power of the scale factor. Although obtained through a different path the result in [8] is similar. For this reason that action is to be viewd in the spirit of the EFT approach.
Another aspect analyzed in [8] as well as below is Weyl (conformal) symmetry. It is often stated in the literature that at very high energy masses and other dimensionful constants become irrelevant. Introducing a dilaton field it is possible to reformulate field theories containing dimensionful constants in a Weyl invariant way, whereby masses and dimensionful constants need not be naively set to zero in a high energy regime, but appear in the action in such a way that their values are irrelevant. This symmetry however is challenged by trace anomalies. The latter are NO-type and do not endanger quantization, but only break conformal symmetry. If our aim is to preserve conformal invariance, there is a way to restore it by means of Wess-Zumino terms, which require introducing an extra field. This amounts to adding them to the action by identifying the extra field with the dilaton. These additional terms are another anomaly footprint.
The purpose of this conference paper is to present a simplified version of the theory put forward in [8], in particular only one metric, instead of two, is considered, and then add a few, although still incomplete, remarks on two particular aspects: the interpretation of the mirror model and conformal invariance. The paper is organized as follows. Section two is a presentation of the theory introduced in [8] in a simplified form. Section 3 is devoted to a comment on the physical interpretation of the right sector of the theory. In section 4 Weyl invariance is presented and discussed, together with a possible application to the description of physics of the early universe. Section 5 is dedicated to the trace anomalies and their cancelation by means of WZ terms, together with their possible implications for unitarity.

8.2 A left-right symmetric model

The following model was introduced in [8] with two metrics. Here we consider a simplified version in which there is only one metric. The fermion matter part

[2]This is due to the presence of zero dimension fields, like the metric, which allow for infinite many interaction terms in the action, [42]

is based on the same multiplet as the MSM with the addition of a right-handed sterile neutrino. In the usual SM notation it is

$$\begin{array}{ccccc} G/fields & SU(3) & SU(2) & U(1) \\ \begin{pmatrix} u \\ d \end{pmatrix}_L & 3 & 2 & \frac{1}{6} \\ (u_R)^c & \bar{3} & 1 & -\frac{2}{3} \\ (d_R)^c & \bar{3} & 1 & \frac{1}{3} \\ \begin{pmatrix} \nu_e \\ e \end{pmatrix}_L & 1 & 2 & -\frac{1}{2} \\ (e_R)^c & 1 & 1 & 1 \\ (\nu_R)^c & 1 & 1 & 0 \end{array} \tag{8.1}$$

where X^c represents the Lorentz conjugate spinor of X, i.e. $X^c = \gamma_0 C X^*$. This multiplet couples to a gravitational metric and connection, and to the $SU(3)_L \times SU(2) \times U(1)_L$ gauge fields. In [8] it was shown that all the anomalies cancel out except for 4 units of the trace anomaly with density $F * F$, due to the gauge field $F \equiv F^{\mathfrak{su}(2)}$, computed in the doublet representation of $\mathfrak{su}(2)$.

The multiplet (8.1) describes left-handed particles and right-handed antiparticles.
The main difference with the MSM is that the spectrum is completed by a right-handed multiplet

$$\begin{array}{ccccc} G/fields & SU(3) & SU(2) & U(1) \\ \begin{pmatrix} u' \\ d' \end{pmatrix}_R & 3 & 2 & \frac{1}{6} \\ (u'_L)^c & \bar{3} & 1 & -\frac{2}{3} \\ (d'_L)^c & \bar{3} & 1 & \frac{1}{3} \\ \begin{pmatrix} \nu'_e \\ e' \end{pmatrix}_R & 1 & 2 & -\frac{1}{2} \\ (e'_L)^c & 1 & 1 & 1 \\ (\nu'_L)^c & 1 & 1 & 0 \end{array} \tag{8.2}$$

coupled to the gravitational metric and connection. It also couples to the $SU(3)_R \times SU(2) \times U(1)_R$ gauge fields. The anomaly analysis of this mirror multiplet[3] is the same as for the left-handed one except for the sign of the trace anomaly due to the gauge field $F \equiv F^{\mathfrak{su}(2)}$, which is opposite. Therefore the overall sum of the anomalies of the system vanishes.
The multiplet (8.2) describes right-handed particles and left-handed antiparticles. Of course we should write three families of left-handed and three families of right-handed fermions. But since the physics that intetwines different families will not be discussed here, one single family will do.
We shall call these two intertwined theories, with field content (8.1) and (8.2), $\mathcal{T}_L$ and $\mathcal{T}_R$, respectively. The overall theory is free of type O anomalies. We denote it

[3] A mirror sector of the SM has been considered earlier in the literature, see [3, 25, 30], with various purposes related to cosmology.

simply by $\mathcal{T} = \mathcal{T}_L \cup \mathcal{T}_R$. The symbol $\cup$ is because the two half theories have the metric and the SU(2) gauge potentials in common.
Important. Both multiplets couple to the same $SU(2)$ gauge fields. Only in this case do all anomalies cancel! We remark that, since, contrary to [8] there is only one metric, the presence of the sterile neutrinos ν_R and ν'_L is not necessary in order to cancel all type O anomalies.

Let us see explicitly in the sequel the various possible pieces of the relevant actions. Let us start with the fermion kinetic actions. We have

$$S_f^{(+)} \equiv S_{fR} = \int d^4x \left(\sqrt{g}\, i\overline{\psi'_R}\gamma^a e_a^\mu \left(\mathcal{D}_\mu^{(+)} + \frac{1}{2}\omega_\mu \right) \psi'_R \right)(\hat{x}) \tag{8.3}$$

where ψ'_R represents the right-handed multiplet (8.2), and

$$\mathcal{D}_\mu^{(+)} = \partial_\mu + g_X^+ X_\mu^{(+)} + g_W W_\mu + g_B^+ B_\mu^{(+)} \tag{8.4}$$

As usual $\omega_\mu = \omega_\mu^{ab}\Sigma_{ab}$ represents the spin connection corresponding to the metric g and Σ_{ab} the anti-hermitean Lorentz generators. For the left sector

$$S_f^{(-)} \equiv S_{fL} = \int d^4x \left(\sqrt{g}\, i\overline{\psi_L}\gamma^a e_a^\mu \left(\mathcal{D}_\mu^{(-)} + \frac{1}{2}\omega_\mu \right) \psi_L \right)(\hat{x}) \tag{8.5}$$

where ψ_L represents the left-handed multiplet (8.1), and

$$\mathcal{D}_\mu^{(-)} = \partial_\mu + X_\mu^{(-)} + W_\mu + B_\mu^{(-)} \tag{8.6}$$

The symbols $X_\mu^{(\pm)}, W_\mu, B_\mu^{(\pm)}$ refer to the $SU(3)_{R/L}, SU(2)$ and $U(1)_{R/L}$ potentials, respectively. Of course each potential has its own distinct coupling to the fermions, which can be made explicit through a redefinition of the potentials.
Let us recall that the symbol such as $(\psi_R)^c$ (for instance $(u_R)^c, (d_R)^c, ...$) can be rewritten as

$$(\psi_R)^c = \gamma^0 C\psi_R^* = \gamma^0 C P_R^* \psi^* = P_L \gamma^0 C\psi^* = P_L \psi^c = (\psi^c)_L. \tag{8.7}$$

Inserted into the kinetic term, this gives

$$\int d^4x \sqrt{g}\, \overline{(\psi^c)_L}\, \gamma^\mu (\partial_\mu + \frac{1}{2}\omega_\mu)(\psi^c)_L = \int d^4x \sqrt{g}\, \overline{\psi_R}\, \gamma^\mu (\partial_\mu + \frac{1}{2}\omega_\mu)\psi_R \tag{8.8}$$

taking account that Σ_{ab} are anti-hermitean, using an overall transposition and a partial integration. Therefore the kinetic term of the multiplet (8.1), coupled only to the metric, splits into 16 independent Weyl fermion kinetic terms, 8 left-handed and 8 right-handed, with opposite contribution to the odd parity trace anomaly.
The SU(2) gauge field action has the usual form

$$S_g^{SU(2)} = -\frac{1}{4g^2} \int d^4x\, \sqrt{g}\, \mathrm{tr} \left(g^{\mu\mu'} g^{\nu\nu'} F_{\mu\nu} F_{\mu'\nu'} \right) \tag{8.9}$$

where $F_{\mu\nu} = dV + \frac{1}{2}[V, V]$ is the curvature of the SU(2) gauge field[4].

[4] In [8] two $SU(2)$ gauge couplings were introduced, one for each sector; however the cancelation of $SU(2)$ gauge-induced odd trace anomalies requires that there be only one coupling.

For the groups $SU(3)_L \times SU(3)_R$ and $U(1)_L \times U(1)_R$ we have instead $S_g^{(+)} + S_g^{(-)}$ with

$$S_g^{(\pm)} = -\frac{1}{4g_\pm^2} \int d^4x \sqrt{g}\, \mathrm{tr}\left(g^{\mu\mu'} g^{\nu\nu'} F_{\mu\nu}^{(\pm)} F_{\mu'\nu'}^{(\pm)}\right) \tag{8.10}$$

where $F_{\mu\nu}^{(\pm)} = dV^{(\pm)} + \frac{1}{2}[V^{(\pm)}, V^{(\pm)}]$ and $F^\pm$ denotes the curvatures of the $SU(3)_R$ and $U(1)_R$, and $SU(3)_L$ and $U(1)_L$ potentials, respectively. $S_g^{(\pm)}$ is supposed to represent the sum of both for $SU(3)$ and $U(1)$ gauge action with distinct couplings, which can be absorbed, as usual, in a redefinition of the respective gauge potentials. The action for the metric is the usual EH action with different cosmological constants in the left and right sector

$$S_{EH}^{(\pm)} = -\frac{1}{2\kappa} \int d^4x \sqrt{g}\, (R + \mathfrak{c}_\pm) \tag{8.11}$$

Here R is the Ricci scalar, κ the gravitational constant and $\mathfrak{c}_\pm$ the left/right cosmological constant.
In the MSM we need also a couple $H_\pm$ of complex scalar fields, which minimally couple to the metric $g_{\mu\nu}$ and are a doublet under $SU(2)$. The corresponding actions in the two sectors are given by

$$S_d^{(\pm)} = \int d^4\hat{x} \sqrt{g} \left[g^{\mu\nu} \mathcal{D}_\mu H_\pm^\dagger \mathcal{D}_\nu H_\pm - M_\pm^2 H_\pm^\dagger H_\pm - \frac{\lambda_\pm}{4} \left(H_\pm^\dagger H_\pm\right)^2\right] \tag{8.12}$$

where $\mathcal{D}_\mu = \partial_\mu - igW_\mu$, and W_μ is the $SU(2)$ gauge field.
So far we have considered pieces of action representing matter minimally coupled to the metric and to gauge potentials. Now we need the interaction among matter fields. This is given by the Yukawa couplings. They split into left and right parts. For instance, for SU(2) doublets we have

$$S_{YdL} = \frac{\bar{y}_{H_d}}{2} \int d^4x \sqrt{g} \left(\overline{\psi_{dL}}\, H_{d-} \chi_{sR}\right) + h.c. \tag{8.13}$$

where ψ_{dL} is a left-handed SU(2) doublet, H_{d-} is also an $SU(2)$ doublet, conjugate to the ψ_{dL} one in the inner product of the $SU(2)$ doublet representation space, while χ_{sR} is a right-handed singlet, all of them belonging to $\mathcal{T}_L$. Similarly, for $\mathcal{T}_R$,

$$S_{YdR} = \frac{y_{H_d}^+}{2} \int d^4\hat{x} \sqrt{g} \left(\overline{\psi'_{dR}}\, H_{d+} \chi'_{sL}\right) + h.c. \tag{8.14}$$

Let us write $S_f = S_f^{(+)} + S_f^{(-)}$, $S_g = S_g^{SU(2)} + S_g^{(+)} + S_g^{(-)}$, $S_{EH} = S_{EH}^{(+)} + S_{EH}^{(-)}$, $S_d = S_d^{(+)} + S_d^{(-)}$ and $S_Y = S_{YdL} + S_{YdR}$. Then for the total action of our model minimally coupled to gravity we can tentatively set

$$S = S_f + S_g + S_{EH} + S_d + S_Y \tag{8.15}$$

This theory is invariant under $SU(2)$, as well as $SU(3)_L \times SU(3)_R$ and $U(1)_L \times U(1)_R$, gauge transformations. It is also invariant under diffeomorphisms and

local Lorentz transformations. Concerning the discrete symmetries, each term of the sum (8.15) is CP and T invariant in the left and right sector separately; but in general it is not P and C invariant. P invariance of the overall S requires that all constants and masses appearing in S with labels + and - be equal, i.e. $\mathfrak{c}_- = \mathfrak{c}_+$, etc. Moreover both left and right parts separately have the same symmetries. We say that $\mathcal{T}$ is left-right or chirally symmetric. For conciseness, we shall call left the matter fields of $\mathcal{T}_L$ and right the matter fields of $\mathcal{T}_R$, of course with the exclusion of the metric and the $SU(2)$ gauge fields.
Eq.(8.15) is likely to be the minimal form of the anomaly-free action including both the MSM and gravity. As was mentioned before and shown in [8], both $\mathcal{T}_L$ and $\mathcal{T}_R$ are separately free of O-type anomalies, except for the trace anomaly whose density is $\sim F*F$. Putting together the two halves has the effect of canceling also this anomaly. In this statement there is no claim of completeness and up to here we do not consider the problem of renormalization and unitarity. S is obtained by putting together the indispensable ingredients. It complies however with the first essential requirement for an effective theory: it is free of obstructive anomalies, so that all the propagators and vertices are well defined and a perturbative quantization can be carried out. The next condition for effectiveness is unitarity. If, in addition, the theory happens to be renormalizable, then it is UV complete.

8.3 Dark matter?

The theory described by S splits into two halves, each with distinct scalar and fermion matter components. Also the gauge groups $SU(3)_L \times SU(3)_R$ and $U(1)_L \times U(1)_R$, respectively, are distinct, while the metric and the $SU(2)$ gauge fields are the same on both sides. The left matter and the right matter interact only via the latter fields and in no other way. For instance the left fermions (left-handed particles and right-handed antiparticles) interact among themselves strongly via the $SU(3)_L$ gauge bosons and electromagnetically via the $U(1)_L$ potential. Thanks to the Yukawa couplings they interact with the left doublet of scalars. They interact also weakly via the $SU(2)$ gauge fields and gravitationally via the metric. However with the mediation of the latter they interact also with the right fermions (right-handed particles and left-handed antiparticles). An example of these types of interaction is the scattering of a left fermion with a right one via the exchange of an $SU(2)$ gauge boson or a graviton as in figure 1 below. In an analogous way the left scalar fields interact among themselves via the scalar potential, then they interact with the metric and the $SU(2)$ gauge fields, and, via the latter, with the right scalars.
For the right-handed fermions and scalars we have of course a mirror description. If we imagine that this is the theory at the basis of the evolution of the universe after what is called the grand-unification era, $10^{-35} sec$ after the beginning, there is certainly something missing, at least one or more fields (which, for simplicity, are not explicitly written down) that can describe the inflationary period and possibly a quintessence field, if the cosmological constants are not enough to describe the present accelerating expansion. But all the rest is there. In particular the left-handed part with the addition of an inflaton field, for instance, can effectively

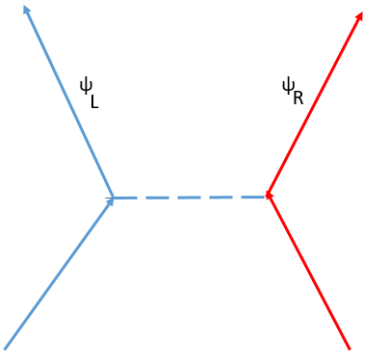

Fig. 8.1: *A scattering between left and right fermions mediated by* $\mathrm{SU}(2)$ *gauge bosons or gravitons (dashed line).*

describe, resting on the background of a LFRW metric, the physics of the universe's evolution (inflation, reheating, particle creation and density perturbations, perhaps even dark energy, for reviews see [4, 10, 17, 18, 23, 26, 27, 31, 38, 39, 50, 53–55] and references therein). Then the question is: if this is the correct picture, what does the right part represent in it? It does not take much imagination to see in it a candidate for the dark matter. This part (the right one) of the total matter+energy evolves in a way parallel to the ordinary matter+energy, although with different coupling constants, masses and cosmological constant. And at the present time energy scale the interaction between the two is limited to the gravitational one, since the common weak force between left and right matter has a too short range to be effective (but of course this is not the case in very high energy scattering phenomena that can involve left and right matter). What makes the difference between the two half theories are the couplings, scalar masses and cosmological constant, beside the handedness of the respective fermions (representing at the massless level left-handed particles and right-handed antiparticles, on the left side, and right-handed particle and left-handed antiparticles on the right one). For instance, the evolution in the right part (supposedly the dark matter) might be sensibly different from the ordinary matter in what concerns inflation, particle creation, density perturbations and so on. Certainly we cannot 'see' the right-handed world, but at most 'feel' it via gravity, and also the weak force if the energy is high enough. This is suggestive, but it remains for us to explain many aspects, of which the most important is why the amount of dark matter is more than five times larger than the visible matter. And figure out experiments that permit to falsify the idea.

This said, can we say on this subject something more than the above rather generic considerations? The answer, somewhat surprisingly, is yes. The literature on dark matter is vast, with a variety of different ideas and proposals. It is classified in

cold, warm and hot dark matter. Focusing on the most popular cold dark matter (CDM), it may be made of baryonic objects, i.e. made of the SM baryons, like MACHOs (massive astrophysical compact halo objects) or primordial black holes. The non-baryonic matter might be made of particles: massive neutrinos, axions, or weakly interacting particles present in supersymmetric models: neutralinos (a mixture of supersymmetric partners), fotinos, Binos,... popularly denoted by the acronim WIMPs (weakly interacting massive particles). WIMPs have been considered as among the most likely candidates for dark matter. They are massive, thus they feel gravity. They belong to the same left sector as the SM particles, and usually are taken from supersymmetric extensions of the SM, or supergravity, or superstring inspired models. But the essential aspect is that they weakly interact with the SM sector. In this sense the right sector, $\mathcal{T}_R$, can well play the same role and one can simply parasitize, at least in a phase of research designing, the WIMP literature, see [1,2,4–6,14] for reviews. In this sense the first striking aspect of it is the so-called 'WIMP miracle': with the freeze-out mechanism, WIMPs achieve the relic density for dark matter appropriate to reproduce the latest experimental data, $\Omega_{matter} \approx 0.25$. Although it is not clear what form the mirror matter will take in this new description, whether macroscopic bodies, gas of neutral particles, like the neutrinos in the left sector, or neutral atoms, or all of them together. This depends very much on the details of the evolution of the mirror world.
No doubt the idea is suggestive and not airy-fairy. It has also the virtue of unveiling a mistery: why does nature use only left-handed particles and right-handed antiparticles to build up our universe while disdaining right-handed particles and left-handed antiparticles? This should not be confused with the problem of baryon asymmetry, which has to do with the fact that our universe is made essentially by matter (as opposed to antimatter), but it is rather an additional puzzle. It is pleasing that several papers in the literature have considered that baryon asymmetry and its solution (baryogenesis) might be interrelated with dark matter, [9,46]. This is an additional motivation to study the two puzzles (baryon asymmetry and left-right asymmetry) in the framework of $\mathcal{T}$.

8.4 Weyl symmetry

It is a common belief that whatever local theory we consider, when the energy regime grows very large, masses and dimensionful constants become irrelevant. A related point of view is that these constants may not be true constants, but vacuum expectation values of suitable fields that condense at low enough energies; so that in a fundamental theory only dimensionless constants and fields will appear. In any case, since in any such theory there is no explicit scale, we expect it to be invariant under a rescaling of the metric. Under general conditions this means that the theory is invariant not only under rigid rescalings of the metric, a property referred to as scale symmetry, but also under local ones, which defines conformal or Weyl symmetry. The full $\mathcal{T}$ theory is not invariant under local Weyl transformations

$$g_{\mu\nu} \to e^{2\omega} g_{\mu\nu} \tag{8.16}$$

where ω is a local parameter, but several pieces thereof are. They are S_f, S_g and S_Y. The remaining pieces are not in general Weyl invariant as they contain dimensionful constants. But it is actually very simple to transform a local theory into a Weyl invariant one by adding a new field, φ, the dilaton. Under the same Weyl rescaling it transforms as $\varphi \to \varphi + \omega$. The procedure is as follows. Let us start from the Christoffel symbols. They transform as

$$\Gamma^\lambda_{\mu\nu} \to \Gamma^\lambda_{\mu\nu} + \delta^\lambda_\mu \, \partial_\nu \omega + \delta^\lambda_\nu \, \partial_\mu \omega - g_{\mu\nu} g^{\lambda\rho} \partial_\rho \omega \tag{8.17}$$

We can construct Weyl-invariant Christoffel symbols as follows

$$\widetilde{\Gamma}^\lambda_{\mu\nu} = \Gamma^\lambda_{\mu\nu} - \left(\delta^\lambda_\mu \, \partial_\nu \varphi + \delta^\lambda_\nu \, \partial_\mu \varphi - g_{\mu\nu} g^{\lambda\rho} \partial_\rho \varphi\right) \tag{8.18}$$

We can use these symbols to build the Riemann and Ricci tensor. The latter is

$$\widetilde{R}_{\mu\nu} = R_{\mu\nu} + 2\partial_\mu \partial_\nu \varphi + g_{\mu\nu} \Box \varphi + 2\partial_\mu \varphi \partial_\nu \varphi - 2 g_{\mu\nu} \partial\varphi \cdot \partial\varphi \tag{8.19}$$

and Ricci scalar is

$$\widetilde{R} = R + 6\left(\Box\varphi - \partial\varphi \cdot \partial\varphi\right), \tag{8.20}$$

$\widetilde{R}_{\mu\nu}$ is Weyl invariant, while $\widetilde{R} \to e^{-2\omega}\widetilde{R}$. For the sequel let us remark that if we write $\widetilde{g}_{\mu\nu} = e^{2\varphi} g_{\mu\nu}$ we can write

$$\widetilde{R}_{\mu\nu}(g) = R_{\mu\nu}(e^{2\varphi} g) \tag{8.21}$$

where the entry g in the round brackets is a shorthand for the metric $g_{\mu\nu}$.
Now the recipe is as follows. In the action we replace R with $\widetilde{R}$. Then we multiply every dimensionful constant of mass dimension s by the factor $e^{-s\varphi}$. When applied to scalar fields we replace the simple derivatives ∂_μ by:

$$D_\mu = \partial_\mu + \partial_\mu \varphi \tag{8.22}$$

The pieces S_f, S_g and S_Y need not be modified because they are already Weyl invariant. In the sequel we introduce two distinct dilatons $\varphi_\pm$, one for each sector. They behave exactly as the just introduced φ.
Specifically, for $\mathcal{T}$ we have the following modifications. The EH part becomes

$$S^{(c\pm)}_{EH} = -\frac{1}{2\kappa} \int d^4x \sqrt{g}\, e^{-2\varphi_\pm} \left(\widetilde{R}_\pm + c_\pm \, e^{-2\,\varphi_\pm}\right) \tag{8.23}$$

where $\widetilde{R}_\pm = R + 6\left(\Box\varphi_\pm - \partial\varphi_\pm \cdot \partial\varphi_\pm\right)$, and the doublet scalar action becomes

$$S^{(c\pm)}_d = \int d^4x \, \sqrt{g} \left[g^{\mu\nu} \mathcal{D}^\pm_\mu H^\dagger_\pm \mathcal{D}^\pm_\nu H_\pm - e^{-2\varphi_\pm} M^2_\pm H^\dagger_\pm H_\pm - \frac{\lambda_\pm}{4}\left(H^\dagger_\pm H_\pm\right)^2\right] \tag{8.24}$$

where $\mathcal{D}^\pm_\mu = \partial_\mu + \partial_\mu \varphi_\pm - igW_\mu = D_\mu - igW_\mu$, W_μ being a gauge field valued in the $SU(2)$ Lie algebra representation to which $H_\pm$ belongs.
The Weyl invariant generalization of $\mathcal{T}$ is therefore

$$S^{(c)} = S_f + S_g + S_Y + S^{(c)}_{EH} + S^{(c)}_d \tag{8.25}$$

where $S_{EH}^{(c)} = S_{EH}^{(c+)} + S_{EH}^{(c-)}$ and $S_d^{(c)} = S_d^{(c+)} + S_d^{(c-)}$.
For later discussion we add also Weyl invariant action terms. One is the higher derivative term $S_C = S_C^{(+)} + S_C^{(-)}$ where

$$S_C = \frac{1}{\eta}\int d^4x\sqrt{g}\, C_{\mu\nu\lambda\rho}C^{\mu\nu\lambda\rho} \tag{8.26}$$

$C_{\mu\nu\lambda\rho}$ is the Weyl tensor (invariant under Weyl transformations). If we disregard total derivatives in the action, (8.26) can be replaced by

$$S'_C = -\frac{2}{\eta}\int d^4x\sqrt{g}\left(-R_{\mu\nu}R^{\mu\nu} + \frac{1}{3}R^2\right) \tag{8.27}$$

The quadratic terms in brackets contain higher derivative kinetic and interaction terms.
Another Weyl invariant action can be constructed for a scalar field Φ.

$$S_\Phi = \frac{1}{2}\int d^4x\,\sqrt{g}\left(\partial_\mu\Phi\partial^\mu\Phi + \frac{1}{6}R\,\Phi^2\right) \tag{8.28}$$

where R is the Ricci scalar.
In the literature the action $S_{EH}^{(c\pm)}$ is sometimes modified with the addition of a non-minimal gravitational coupling, so that it becomes:

$$S_{EH}^{(c'\pm)} = -\frac{1}{2\kappa}\int d^4x\sqrt{g}\,\left(e^{-2\varphi_\pm} + \zeta_{h\pm}H_\pm^\dagger H_\pm\right)\left(\widetilde{R} + c_\pm\, e^{-2\,\varphi_\pm}\right) \tag{8.29}$$

where $\zeta_{h\pm}$ are dimensionless couplings
The theory defined by (8.25), with the possible addition of (8.26), and $S_{EH}^{(c'\pm)}$ instead of $S_{EH}^{(c\pm)}$, has the same symmetries as S, (8.15). In particular it is invariant under the diffeomorphisms spanned by the parameter ξ^μ, with the dilaton transforming as

$$\delta\varphi_\pm = \xi^\mu\partial_\mu\varphi_\pm \tag{8.30}$$

In addition it is conformally invariant. It should be duly appreciated that conformal invariance of the action $S^{(c)}$ precisely embodies the idea that at high energies constants and masses are indefinite. For instance the mass factor $M_\pm e^{-2\varphi_\pm}$, and other similar factors, can take any value, from 0 to ∞, without changing the value of the action. We shall call the new theory $\mathcal{TW}$.

Refs.: [20–22, 29, 47], see also the reviews [45, 48].

8.4.1 Meaning and import of conformal invariance

The theory outlined in the previous section is classical, its quantum aspects will be considered later. But suppose that one such theory is adherent to the physics of fundamental interactions in a certain range of energy and a semiclassical approach makes sense, we face a problem of interpretation: what is the significance of conformal invariance? It was noted above that, although a local symmetry, conformal

invariance has characteristics that differentiate it from ordinary gauge theories. First, the 'gauge field', in the version presented here, is a scalar, and, unlike the usual gauge fields or metrics, its propagator is well defined without any gauge fixing. Second, for this reason the gauge fixing needs not be accompanied by the introduction of ghost fields. In other words, conformal symmetry can be treated like an ordinary rigid symmetry, like $O(N)$, for instance, in models with the same name. This means that it is a physical symmetry. Different configurations of φ are physically distinct, although with the peculiarity that their description differ by a symmetry operation. Different configurations of φ define equivalent solutions of $S^{(c)}$, but considering them from an energy regime where conformal invariance is not anymore a symmetry, they may describe a very different physics.
As a first step let us plug our conformal invariant theory in a cosmological framework. To this end we search for classical solutions of time-dependent, but space-independent, fields. and, to be concrete, we choose for the metric the Friedmann-Robertson one:

$$ds^2 = dt^2 - a^2(t)\left(\frac{dr^2}{1-kr^2} + r^2 d\theta^2 + r^2 \sin^2\theta\, d\phi^2\right) \tag{8.31}$$

Let us recall that with this metric we have

$$\begin{aligned} &g_{tt} = g^t_t = 1, \qquad g^r_r = g^\theta_\theta = g^\phi_\phi = 1 \\ &R_{tt} = R^t_t = -3\frac{\ddot a}{a}, \qquad R^r_r = R^\phi_\phi = R^\theta_\theta = -\left(\frac{\ddot a}{a} + 2\frac{\dot a^2}{a^2} + 2\frac{k}{a^2}\right) \\ &R = -6\left(\frac{\ddot a}{a} + \frac{\dot a^2}{a^2} + \frac{k}{a^2}\right) \end{aligned} \tag{8.32}$$

As usual, dots denote derivative with respect to time. For simplicity let us start with a conformal invariant action for a metric, a dilaton and a scalar field Φ:

$$S_1^{(c)} = -\tfrac{1}{2\kappa}\int d^4x\sqrt{g}\, e^{-2\varphi}\left(\widetilde{R} + c_\pm\, e^{-2\,\varphi}\right) + \tfrac{1}{2}\int d^4x\,\sqrt{g}\,\left[g^{\mu\nu}D_\mu\Phi D_\nu\Phi - e^{-2\varphi}m^2\Phi^2 - \tfrac{\lambda}{4}\Phi^4\right] \tag{8.33}$$

where $D_\mu = \partial_\mu + \partial_\mu\varphi$ and the ζ non-minimal coupling has been dropped. This is clearly a drastically simplified model in which a few action terms and fields are dropped and the part of the action that does not involve φ is disregarded, not to speak of the quantum corrections. But all the ignored terms can be re-introduced in the analysis later on. The equation of motion for φ is

$$\Phi + \Phi\ddot\varphi + \dot\Phi\dot\Phi + \Phi\dot\Phi\dot\varphi = e^{-2\varphi}\left(\tfrac{6}{\kappa}\left(\tfrac{\ddot a}{a} + \tfrac{\dot a^2}{a^2} + \tfrac{k}{a^2}\right) + \tfrac{6}{\kappa}\left(-\ddot\varphi + \dot\varphi\dot\varphi\right) - m^2\Phi^2 - \tfrac{2c}{\kappa}e^{-2\varphi}\right) \tag{8.34}$$

while for Φ is

$$\ddot\Phi + \Phi\ddot\varphi + 2\dot\Phi\dot\varphi + \Phi\dot\varphi\dot\varphi = m^2 e^{-2\varphi}\Phi - \frac{\lambda}{2}\Phi^3 \tag{8.35}$$

Now let us make the ansatz

$$\Phi(t) = \frac{\alpha}{t}, \qquad \varphi(t) = \ln(\beta t), \qquad a(t) = \gamma\, t \tag{8.36}$$

where α, β, γ are coefficients to be determined. We obtain a relation for these coefficients and the constants of the theory by inserting (8.36) into (8.34)

$$\frac{6}{\kappa}\left(3+\frac{k}{\gamma^2}\right)-\frac{2c}{\kappa\beta^2}-2m^2\alpha^2+\alpha^2\beta^2-\frac{\lambda}{2}\alpha^4\beta^2=0 \tag{8.37}$$

Another independent relation is obtained directly from (8.35):

$$2+\alpha=\frac{2m^2\alpha}{\beta^2}-\lambda\alpha^3 \tag{8.38}$$

Nothing changes if we replace in (8.36) t with $t-t_0$, with arbitrary t_0. A new solution can be obtained by replacing t with bt, where b is any positive real number. This residual scale invariance is clearly inherited from the conformal invariance of (8.33). It implies that a physical meaning can be attached only to ratios of different values of t.
Further relations can be gotten by the variation of the metric. The eom is

$$R_{\mu\nu}-\frac{1}{2}g_{\mu\nu}\left(R-ce^{-2\varphi}\right)=2\kappa e^{2\varphi}T^{(m)}_{\mu\nu} \tag{8.39}$$

Let us write the em tensor in the form familiar in cosmology, i.e., that of a perfect fluid

$$T^{(m)}_{\mu\nu}=(\rho+P)u_\mu u_\nu-Pg_{\mu\nu} \tag{8.40}$$

where ρ and P are the energy density and pressure, respectively. In the rest frame $u_\mu=(1,0,0,0)$, from the tt component of (8.39) one gets

$$\rho=\frac{3}{2\kappa\beta^2}\left(1+\frac{k}{\gamma^2}-\frac{c}{6\beta^2}\right)\frac{1}{t^4},\qquad \text{i.e.}\qquad \rho\sim\frac{1}{a^4} \tag{8.41}$$

From the $\begin{smallmatrix} i \\ i \end{smallmatrix}$ component one gets

$$\frac{\ddot{a}}{a}+\frac{\kappa}{3}(\rho+3P)e^{2\varphi}+\frac{c}{6}e^{-2\varphi}=0 \tag{8.42}$$

from which it follows that

$$P\sim\frac{1}{a^4} \tag{8.43}$$

It must be remarked that the continuity equation is different from the familiar one in cosmology

$$\dot{\rho}=-3\frac{\dot{a}}{a}\left(\rho+3P+\frac{c}{6\kappa}e^{-4\varphi}\right)-\left(2\rho-\frac{c}{2\kappa}e^{-4\varphi}\right)\dot{\varphi} \tag{8.44}$$

The previous analysis can be straightforwardly extended to include in the action other fields and terms.
We shall refer to the time profile (8.36,8.41,8.43) as the conformal regime.

8.4.2 The problem of scales

Let us recall that in a matter dominated universe $a \sim t^{\frac{2}{3}}$, in a radiation dominated one $a \sim t^{\frac{1}{2}}$, while in a dS geometry $a \sim e^{\Lambda t}$. Thus the conformal regime is different from the latter three. Now, in the big bang picture the universe crosses several regimes: an initial explosion of pure energy without matter, followed at some time after perhaps $10^{31} sec$ by a period of inflation, during which a expands exponentially like in dS geometry. This is followed by a period of reheating, when the inflaton energy is transferred to the creation of particles, giving rise to a radiation dominated regime. Favored by the cooling due the expansion this is followed by a matter dominated regime where nucleosynthesis, elctroweak symmetry breaking, QCD phase transition, etc., take place in succession. The conformal regime is different from the above mentioned three, and due to its relevance, if any, to very high energy physics, it may be thought appropriate only for the very early stage of the evolution, just after the big bang and before inflation takes place (provided of course that this phase can be described by field theory).
Now let us remark that in $S^{(c)}$ the cosmological constant c is multiplied by the factor $e^{-4\varphi}$. If time increases by a power of 10, for instance from $10^{-43} sec$ to $10^{-33} sec$ the factor $e^{-4\varphi}$ decreases by a factor 10^{40}. That is, the effective cosmological constant evolves by 40 orders of magnitudes or even more while spanning equivalent configurations of the theory due to conformal symmetry. The important thing here is that, while the cosmological constant evolves by this huge amount, the fermion and gauge part of the action is unaffected by this change. This suggests a possible application.
There is a longstanding problem facing any approach which aspires to unify gravity with the SM, due to the relation between the cosmological constant and the energy of the vacuum; more precisely the vacuum energy density due to gravitation is represented by

$$\rho_\Lambda = \frac{c}{2\kappa} \tag{8.45}$$

The observed value is

$$|\rho_\Lambda^{(obs)}| \sim 2 \times 10^{-10} erg/cm^3 \tag{8.46}$$

The trouble is that when we put together in a unique theory, as we have done above, gravity and matter, the matter field theory comes with its own vacuum energy. The latter is always a divergent quantity and can be estimated only using different cutoffs, [12,19,49]. If one uses the QCD scale one finds $\rho_{vac}^{QCD} \sim 1.6 \times 10^{36} erg/cm^3$. If one uses the electroweak scale one finds $\rho_{vac}^{EW} \sim 3 \times 10^{47} erg/cm^3$. Finally if the scale of the cutoff is the Planck mass, one gets $\rho_{vac}^{Pl} \sim 2 \times 10^{110} erg/cm^3$. In any case the gap with (8.46) is gigantic, and one is obliged to imagine another unknown entry in the above calculations to fill in the gap.
This sounds utterly unnatural and constitutes the so-called cosmological constant problem, see [56–58] and references therein. But if we look instead at $S^{(c)}$, (8.25), the problem takes a different turn. First, as just pointed out, the fermion and gauge parts of the action, as well as the Yukawa coupling and the quartic scalar couplings,

are unaffected by Weyl transformations. On the contrary the other terms in $S^{(c)}$, and in particular the cosmological constant term may undergo drastic changes under a Weyl transformation. If we choose, for instance, a 'gauge' $\varphi = 0$ we reproduce the just mentioned unnatural situation, but if we choose a sufficiently negative value for φ, for instance a 'gauge' $\varphi \approx -25$ or a similar one, the effective cosmological constant takes on a value for which the gravitational vacuum energy may be comparable with the value of the vacuum energy of the theory, whatever it may be. As pointed out above what really matters is the ratio between these two times. These two 'gauges' correspond, according to our background solutions to different times along the cosmological evolution.

The previous gauge fixing is not simply a formal manipulation. It means that we can deal in the same theory with very different scales of energy. Now, the point is that we are able to quantize field theories only via a perturbative series. Therefore, for instance, the smallness of the measured cosmological constant disappears compared to the quantum corrections of the SM. Simply it does not make much sense to juxtapose matter and gravity (if the cosmological constant represents its vacuum energy) in the same quantum theory. However, the theory $\mathcal{TW}$ is conformal invariant. Therefore we can quantize it at the scale (i.e. the 'gauge') where the perturbative approach makes sense, and transfer the quantized results (renormalization and unitarity) to the other scales, much as we do in quantum gauge theories where we do quantization in our favorite gauge and then we prove gauge fixing independence. In the present case therefore what we have to do next is to do quantization and show that conformal invariance is preserved.

But before turning to quantization, let us stress the particular flexibility of the just outlined idea. In a cosmological framework the gigantic jump from the electroweak scale to the tiny cosmological constant may not be the only one. We may need other intermediate scales. They can be inserted in the above scheme as follows. With reference to the beginning of section 4, in particular to eq.(8.20), let us introduce two dilaton fields φ_1 and φ_2, which transform like φ above, and pose

$$\widetilde{R}_{12} = R + 6\,(\partial\cdot S - S\cdot S)\,, \tag{8.47}$$

where

$$S_\mu = \epsilon\,\partial_\mu\varphi_1 + (1-\epsilon)\,\partial_\mu\varphi_2 \tag{8.48}$$

and ϵ is a real number. Next consider, as an example, the action

$$\begin{aligned} S_{12}^{(c)} = &-\frac{1}{2\kappa}\int d^4x\sqrt{g}\,e^{-2\varphi_1}\left(\widetilde{R}_{12} + \mathfrak{c}\,e^{-2\,\varphi_1}\right) \\ &+\int d^4x\,\sqrt{g}\left[g^{\mu\nu}D_\mu^{(2)}\Phi^\dagger D_\nu^{(2)}\Phi - e^{-2\varphi_2}M^2\Phi^\dagger\Phi - \frac{\lambda}{4}\left(\Phi^\dagger\Phi\right)^2\right] \end{aligned} \tag{8.49}$$

for a complex scalar field Φ, where the possible subscript $\pm$ has been ignored and $D_\mu^{(2)} = \partial_\mu + \partial_\mu\varphi_2$.

$S_{12}^{(c)}$ is confomal invariant, and with a suitable choice of the two 'gauges' for φ_1 and φ_2, we can prepare the theory in a reasonable form for quantization whatever the intermediate scale for M^2 is.

8.5 The quantum costs

As shown above it is relatively easy to transform a classical local field theory containing matter and gravity into a conformally invariant one. The price is cheap, it is enough to introduce a dilaton field and suitably manipulate with it the terms which are not by themselves confomal invariant, [13] (but we shall see below that there may be limitations). The main question is whether the invariance survives the quantization process. Quantization, at least perturbative quantization, requires that propagators and vertices be unambiguously defined. This is the case for $\mathcal{TW}$ because the theory has been constructed in order to guarantee this requirement, namely absence of O-type anomalies. The next sensible requirement for an effective theory, as was noted above, is unitarity. The icing on the cake would be the proof of renormalizabilty. In [8] these issues were broached in the form of a brief review of the existing literature.

To illustrate them without facing the complex technicalities of a detailed treatment, I will quote one example. In [33] the author focuses on a theory defined by the classical action (8.28). As noted, this theory is Weyl-invariant and is known as Weyl-invariant scalar-tensor gravity. The author fixes both the diffeomorphsms and the Weyl gauge and works out the corresponding BRST symmetries. The quantization is carried out in the canonical way. The author computes the equal time (anti)commutation relations among all the fields and their conjugates. On this basis, he is able to prove the existence of a global symmetry the 'choral' symmetry, which is spontaneously broken at the quantum level. Its Nambu-Goldstone bosons are the graviton and the dilaton, which are consequently massless. The author is also able to analyse the physical S-matrix using the method introduced by Kugo and Ojima, [28] and prove that it is unitary.

This important result, further generalized with more general actions in subsequent papers of the same author and collaborators, meets obstacles when faced with renormalization. For renormalization theory, see for instance [42], requires that we introduce in the action all the terms with the right dimensions and the same symmetry as the original ones in (8.28). This would mean adding to the latter also (8.26) (or (8.27)). This fact triggers the appearance of a new entry. We can get an idea of how this works as follows. If we limit ourselves to the lowest order kinetic operator for the graviton $h_{\mu\nu} = g_{\mu\nu} - \eta_{\mu\nu}$ in (8.28) we find, after a suitable gauge fixing, $\alpha\Box$, where α is a constant with the dimension of a square mass. The addition of the term (8.26) brings in the kinetic operator a quartic derivative, which in the simplest case can be represented as $\beta\Box^2$, where β is a dimensionless constant. Disregarding the tensorial factor the propagator is proportional to the inverse of $\alpha\Box + \beta\Box^2$, i.e. the inverse of $-\alpha p^2 + \beta p^4$, which can be written as follows

$$\frac{1}{-\alpha p^2 + \beta p^4} = \frac{1}{p^2(-\alpha + \beta p^2)} = -\frac{1}{\alpha}\left(\frac{1}{p^2} - \frac{1}{p^2 - \frac{\alpha}{\beta}}\right) \tag{8.50}$$

This inevitably introduces a quadratic pole with negative residue, corresponding to a negative norm state, which is likely to violate unitarity.

The occurrence of physical ghosts in similar gravity or gravity plus matter theories has been confirmed in several papers, [24,35–37,43,44,51,52]. Based on these results one can reasonably expect that the theory $\mathcal{TW}$, defined by the action $S^{(c)}$, eq.(8.25), may present problems both for unitarity and renormalizability. The algebraic renormalization procedure requires the addition of the action term (8.26), which is likely to break unitarity. In an effective approach we must privilege unitarity, but this prevents renormalizability. We therefore take $S^{(c)}$ to be an effective field theory of SM plus gravity, effective in the sense that it is not UV complete, but forms a conformal unitary approximation of a still unknown UV complete theory. In the sequel we put on standby the issue of renormalizability and, while studying the effective action, we rather keep an eye on unitarity.

8.5.1 Weyl invariance and Weyl anomalies

Let us recall that $S^{(c)}$ beside the invariance under the gauge transformations already present in S and under diffeomorphims, possesses conformal (or Weyl) invariance. These three invariances cannot be treated on the same footing, as attested, for instance, by the research of ref. [36]: it is impossible to fix the gauges for all three symmetries in a consistent way, since the usual procedure does not produce compatible corresponding BRST symmetries. Only for two of them (or for two combinations thereof) is this possible. It is obvious that the fundamental symmetries are the gauge symmetry and the diffeomorphism one. In order to proceed with quantization they have to be both gauge fixed with the associate introduction of relevant ghosts, and produce compatible BRST symmetries. This has been done, for instance, in [8] for theories like $\mathcal{T}$ and $\mathcal{TW}$. As for the conformal symmetry, it is rather popular in the literature to introduce a corresponding gauge vector field C_μ, i.e. to treat it like, for instance, the Abelian gauge symmetry in QED. Although this is legitimate, it is not necessary. The point of view expressed in [8] is different: a new gauge field of conformal invariance is not necessary because a 'gauge field' is already there, it is φ. For we have shown above that by its means we can fully implement Weyl symmetry. In geometric language this defines an integrable Weyl structure and comes with a bonus: the propagator of the 'gauge field' φ exists already in the theory with no need to fix a gauge, contrary to what happens for a vector gauge field like C_μ; moreover when 'fixing the gauge' there is no need to introduce corresponding ghosts. Ghosts are necessary when, like in the case of the usual gauge theories, there is a mismatch between the number of dofs of the gauge field, which one needs to introduce in order to implement the gauge invariance, and the number of parameters of the gauge transformations. In such a case a gauge fixing does not cut out precisely the unphysical degrees of freedom, and the ghosts are called on to repair the discrepancy. In the case of Weyl invariance the 'gauge field', φ, has the same dofs as the Weyl parameter ω, a gauge fixing is extremely simple (for instance $\varphi = 0$) and completely determines the physical dofs, i.e. zero; there is no room for ghosts.
Quantizing a theory like $S^{(c)}$ means, as already pointed out, fixing the gauge both for the gauge groups and the diffeomorphisms, inserting them in the action, introducing the corresponding ghosts and writing down their actions. Then one

proceeds by singling out the quadratic kinetic terms for all the fields, in order to identify the corresponding propagators, and, finally, by determining the interaction vertices. Once we have these tools we can start calculating the Feynman diagrams; to start with, the one-loop ones. Some of them will be UV divergent and we suppose that such divergences can be absorbed with a redefinitions of the fields and constants (couplings and masses). Motivated by the above references we suppose that this one-loop renormalization can be carried out possibly at the cost of introducing physical ghosts through the term (8.26). We obtain in this way a one-loop effective action $W^{(1)}$ in terms of renormalized fields and constants, with the same form as the classical action but in terms of redefined fields and renormalized constants. What we want to discuss next is the fate of conformal invariance.

Let us start from the classical definition of the e.m. tensor for free matter fields interacting with a background metric, which is

$$T_{\mu\nu} = \frac{2}{\sqrt{g}} \frac{\delta S}{\delta g^{\mu\nu}} \tag{8.51}$$

S being the classical action. If the latter is Weyl-invariant the e.m. tensor is traceless. This follows from the classical Ward identity

$$\delta_\omega S = \int d^4 \left(\frac{\delta S}{\delta g^{\mu\nu}} \delta_\omega g^{\mu\nu} + \sum_i \frac{\delta S}{\delta f_i} \delta_\omega f_i \right) = 0 \tag{8.52}$$

where f_i denotes generic matter fields. For infinitesimal ω, $\delta_\omega g^{\mu\nu} = -2\omega g^{\mu\nu}$, $\delta_\omega f_i = -2y_i \omega f_i$ (where y_i is 0 for gauge fields, 1 for scalars and $\frac{3}{2}$ for fermions, etc.). If the matter fields are on shell (with the exception of the gauge fields), i.e. $\frac{\delta S}{\delta f_i} = 0$, it follows that $T_{\mu\nu} g^{\mu\nu} = 0$ due to the arbitrariness of ω.

The problem we have to consider in the case of $S^{(c)}$ is however more complicated because the metric is dynamical and there are multiple interaction terms that couple the fields in various ways. Invariance of the classical action $S^{(c)}$ under Weyl transformations is given by $\delta_\omega S^{(c)} = 0$. The procedure is the same as for (8.52) except that the metric is not anymore a spectator, but we have to differentiate also the EH action $S_{EH}^{(c\pm)}$. The equation we obtain is

$$R + 2c\, e^{-2\varphi} = 2\kappa\, e^{2\varphi}\, T^{(m)}, \qquad \text{where} \qquad T^{(m)} = g^{\mu\nu} T^{(m)}_{\mu\nu} \tag{8.53}$$

which is the trace of the eom of $g_{\mu\nu}$, see eq.(8.39). Here $T^{(m)}_{\mu\nu}$ denotes the e.m. tensor of all the matter fields (including the dilaton) coupled to the metric.

For simplicity of notation here we have dropped the $\pm$ suffix, since the rest of this section applies indifferently to both left and right sector. This oversimplification does not affect in an essential way what comes in the sequel. How do we have to interpret the above equation (8.53)? Classically it is a part (the trace) of the equation of motion for $g_{\mu\nu}$. We understand it as an equation that (partly) identifies a background solution over which a quantization will be carried out. We limit ourselves to the subclass of such solutions where a nontrivial background configuration is present only for the metric and possibly for the dilaton and some scalar

field, while all the other fields represent fluctuations about the null configuration. There can be nontrivial solutions of this type, [40], but as an introductory approach we focus on the very simple case where the metric is the flat Minkowski one and the background of φ vanishes. For the same reason we choose $\mathfrak{c}_{\pm} = 0$. Therefore at the background level eq.(8.53) reads: 0=0.
Some comments on nontrivial background solutions can be found in Appendix.
Now let us come to the fluctuating fields. First we split the action $S^{(c)} = S_0^{(c)} + S_{int}^{(c)}$ into its free and the interacting part. $S_0^{(c)}$ contains only the kinetic quadratic terms in each separate field. $S_{int}^{(c)}$ contains all the interaction vertices (which are infinite in number because the metric and the dilaton have dimension 0)[5] . Perturbative quantization is based on the propagators derived from $S_0^{(c)}$ and on the above mentioned vertices. The e.m. tensor of the matter fields is obtained by expanding $S^{(c)}$ in $h_{\mu\nu}$ and selecting the first order in this expansion (the 0-th order is the action of the matter fields coupled to the flat metric). The first order splits into various pieces in which the matter fields are generally entangled, but, if we restrict ourselves to the lowest (non-interacting) order, the entanglement disappears and we find a sum of distinct e.m. tensors, one for each species of matter fields including the dilaton. For instance, the zero-th order e.m. tensor obtained in this way for fermios is

$$T_{\mu\nu}^{(f)} = \frac{i}{4}\overline{\psi}\gamma_\mu \overleftrightarrow{\partial_\nu}\psi + (\mu \leftrightarrow \nu) - \eta_{\mu\nu}\frac{i}{2}\overline{\psi}\gamma^\lambda \overleftrightarrow{\partial_\lambda}\psi, \tag{8.54}$$

and for Abelian gauge fields, after fixing the Lorenz gauge, is

$$T_{\mu\nu}^{(g)} = -\frac{1}{g^2}\left(\partial_\mu A_\lambda \partial_\nu A^\lambda + \partial_\lambda A_\mu \partial^\lambda A_\nu - \frac{1}{2}\eta_{\mu\nu}\partial_\lambda A_\rho \partial^\lambda A^\rho\right) \tag{8.55}$$

For the other fields the expression may be less simple, see [8].
As for the role of R, present in the $S_{EH}^{(c)}$ action, its contribution at this order is null because it is at least quadratic in $h_{\mu\nu}$. Thus at the classical level eq.(8.53) reduces to

$$T^{(m)} = 0 \tag{8.56}$$

on shell. Since the various e.m. tensors are disentangled from one another and the equations of motion without interactions reduce to the free ones for each separate species, the e.m. for each species turns out to be tracelss on shell.
The same things can be repeated also for the one-loop renormalized theory for we assume that the difference consists only in renormalized fields and couplings, instead of the classical ones. But in the quantum case we have to introduce also the ghosts, both for gauge and diffeomorphism symmetry. Therefore in the one-loop quantum case in the right hand side of (8.53) and in (8.56), we will have also the contribution from the ghosts, see [8].
To complete the quantization of $S^{(c)}$ we must verify the one-loop validity of (8.56). This consists in the calculation of the trace of the e.m. tensor of each species

[5] We assume that possible linear terms in φ are renormalized to zero by tadpole diagrams, [41].

separately, thus we can utilize the results found for free fields. We know that the e.m. tensor trace in general does not vanish because of anomalies. Any trace anomaly can be written in the form

$$\mathcal{A}_\omega[g, f] = \int d^4x \sqrt{g}\, \omega\, F[g, f] \tag{8.57}$$

where $g = \{g_{\mu\nu}\}$ is the metric, ω is the Weyl transformation parameter, f denotes any other field and F is a local function of g and f. For instance, the e.m. trace of matter fields contain in general terms where the density F takes the form of the quadratic Weyl density

$$\mathcal{W}^2 = R_{\mu\nu\lambda\rho}R^{\mu\nu\lambda\rho} - 2R_{\mu\nu}R^{\mu\nu} + \frac{1}{3}R^2, \tag{8.58}$$

the Gauss-Bonnet (or Euler) density,

$$E = R_{\mu\nu\lambda\rho}R^{\mu\nu\lambda\rho} - 4R_{\mu\nu}R^{\mu\nu} + R^2, \tag{8.59}$$

and the Pontryagin density,

$$P = \frac{1}{2}\left(\varepsilon^{\mu\nu\mu'\nu'}R_{\mu\nu\lambda\rho}R_{\mu'\nu'}{}^{\lambda\rho}\right). \tag{8.60}$$

Other possible anomalies have densities

$$T_e[V] = F_{\mu\nu}F^{\mu\nu}, \tag{8.61}$$

and

$$T_o[V] = \varepsilon^{\mu\nu\lambda\rho}F_{\mu\nu}F_{\lambda\rho}. \tag{8.62}$$

for an Abelian field V_μ with $F_{\mu\nu} = \partial_\mu V_\nu - \partial_\nu V_\mu$, as well as others, which are listed in [8]. These are all anomalies that do not involve the dilaton field φ. But there are other possible trace anomalies which explicitly involve φ. For instance those with densities

$$\widetilde{R}^2 \qquad \text{and} \qquad \widetilde{R}_{\mu\nu}\widetilde{R}^{\mu\nu} \tag{8.63}$$

are also consistent Weyl cocycles. We do not include the density with squared tilded Riemann tensor, because a suitable sum of the three would boil down to the quadratic Weyl tensor anomaly (8.58).

All the above anomalies appear with a definite coefficient in front, depending on the field species which are integrated over (but not on the regularization used).

We have to mention also other cocycles, the trivial ones, or coboundaries. An example is given by the cocycle with density $\Box R$. It satisfies the consistency conditions, and does appear in many instances, but its coefficient depends on the regularization used to compute it. Thus this coefficient cannot have any physical meaning. There is an easy way to get rid of this anomaly by subtracting from the effective action a suitable local term. For the above case, in particular, this term can be chosen to be, for instance, the integral of R^2 with the appropriate

coefficient. However, for a reason explained further on, this is not going to be a good counterterm.
Concerning the odd parity anomalies, we have constructed the theory $\mathcal{T}$ so as to get rid of them (and they are not modified by introducing φ). But for the even parity trace anomalies the story is different. Let us recall that they do not obstruct the existence of propagators, therefore they are not dangerous from the point of view of quantization. But the even parity trace anomalies have the same sign in both chiral sectors and the coefficients in front of them are so random that it is impossible to cancel them adding up different species, except perhaps in very exotic models. In order to ensure the survival of conformal invariance while preserving locality there remain the Wess-Zumino terms.

8.5.2 Wess-Zumino terms

Assuming that ω is an anticommuting Abelian field, any anomaly (8.57) must satisfy the consistency condition

$$\delta_\omega \mathcal{A}_\omega = 0 \tag{8.64}$$

which expresses simply the fact that two subsequent Weyl transformations made in opposite order yield the same result. This is in fact an integrability condition. It means that, with the help of an auxiliary field σ, which transform as $\delta_\omega \sigma = -\omega$, we can construct a local functional $\mathcal{W}_{WZ}[\sigma, g, f]$, such that

$$\delta_\omega \mathcal{W}_{WZ}[\sigma, g, f] = -\mathcal{A}_\omega[g, f] \tag{8.65}$$

This functional can be explicitly constructed

$$\mathcal{W}_{WZ}[\sigma, g, f] = \int_0^1 dt \int d^4x \sqrt{g(t)} F[g(t), f(t)]\, \sigma \tag{8.66}$$

where

$$g_{\mu\nu}(t) = e^{2\sigma t} g_{\mu\nu}, \qquad \text{so that} \qquad \delta_\omega g_{\mu\nu}(t) = 2(1-t)\,\omega\, g_{\mu\nu}(t), \tag{8.67}$$

and

$$f(t) = e^{-y\,t\,\sigma} f, \qquad \delta_\omega f(t) = -y(1-t)\omega f(t) \tag{8.68}$$

where $y = 0$ for a gauge field, $y = 1$ for a scalar field.
For the field φ we put $f(t) \equiv \varphi(t) = \varphi + \sigma t$, thus

$$\delta_\omega \varphi(t) = \omega(1-t), \qquad \frac{d}{dt}\varphi(t) = \sigma \tag{8.69}$$

It can be easily proved that it satisfies (8.65). For instance, for the anomaly with density (8.61) the WZ term has a particularly simple form

$$\mathcal{W}_{WZ}[\sigma, g, V] \sim \int d^4x \sqrt{g}\, \sigma\, F_{\mu\nu} F^{\mu\nu} \tag{8.70}$$

In conclusion at one-loop we have the possibility to recover conformal invariance for $W^{(1)}$ by adding to the one-loop renormalized action a few suitable WZ terms while identifying σ with $-\varphi$. This addition brings in the effective action new (renormalizable) interaction terms. Let us call the new effective action $W^{(c,1)}$.

8.5.3 On the use of WZ terms and 'gauge fixing'

WZ terms do not simply restore Weyl symmetry, they may be used also to secure unitarity. The renormalization program prescribes that at every order of quantization we add all the counterterms compatible with the underlying symmetry, in the present case gauge invariance, diffeomorphism and Weyl symmetry. The first two are the fundamental symmetries that are guaranteed via the BRST formalism and the Slavnov-Taylor identities. Weyl symmetry is preserved by the corresponding Ward identity we have discussed above. But the theory $S^{(c)}$ contains another symmetry, which we will need for quantization. Let us see it.
To contain the size of formulas let us limit ourselves to the action

$$S_1^{(c)} = -\tfrac{1}{2\kappa}\int d^4x\sqrt{g}\,e^{-2\varphi}\left(\widetilde{R} + c_\pm\, e^{-2\varphi}\right) + \tfrac{1}{2}\int d^4x\,\sqrt{g}\,\left[g^{\mu\nu}\partial_\mu\Phi\partial_\nu\Phi + \tfrac{1}{6}R\Phi^2 - e^{-2\varphi}m^2\Phi^2 - \tfrac{\lambda}{4}\Phi^4\right] \quad (8.71)$$

with the possible addition of (8.26), which contains the essential features for the following discussion. If we express the action in terms of

$$\widetilde{g}_{\mu\nu} = e^{-2\varphi}g_{\mu\nu} \qquad \text{and} \qquad \widetilde{\Phi} = e^{-\varphi}\Phi \quad (8.72)$$

S_C remains the same like the fermionic and gauge part of $S^{(c)}$, while (8.33) becomes

$$S_1 = -\tfrac{1}{2\kappa}\int d^4x\sqrt{\widetilde{g}}\,(R + c_\pm) + \tfrac{1}{2}\int d^4x\,\sqrt{\widetilde{g}}\left[\widetilde{g}^{\mu\nu}\partial_\mu\widetilde{\Phi}\partial_\nu\widetilde{\Phi} + \tfrac{1}{6}R\widetilde{\Phi}^2 - m^2\widetilde{\Phi}^2 - \tfrac{\lambda}{4}\widetilde{\Phi}^4\right] \quad (8.73)$$

where $R = R(\widetilde{g})$. From the path integral point of view what we have done is a field redefinition, with a trivial Jacobian (i.e. a Jacobian that does not contain derivatives), after which we can integrate out φ and make it disappear from the game. Thus one can say that φ is a Stückelberg field.
Returning to the issue of symmetry, let us notice that although the action S_1 is not Weyl invariant, it exhibits this symmetry (i.e. $\widetilde{g} \to e^{2\omega}\widetilde{g}$ and $\widetilde{\Phi} \to e^{-\omega}\widetilde{\Phi}$) in all the terms (which include S_C and all the fermionic and gauge terms) except the soft ones, i.e. those field monomials with dimension less than 4. Let us call this partial symmetry after the redefinition (8.72) Weyl-reduced symmetry. It is an important symmetry because it limits the number of possible counterterms in the quantization process.
The counterterms allowed in the renormalization process are all local integrable terms with the right dimensions, invariant under the three symmetries + the Weyl-reduced one, thus they include in particular all the terms in the action $S^{(c)}$ (excluding the non-minimally coupled ones, i.e. $\zeta_h = 0$). In particular among the action terms given by S_C, eq.(8.26), and

$$S_{C1} = \frac{1}{\eta_1}\int d^4x\sqrt{g}\,\widetilde{R}^2 \qquad \text{and} \qquad S_{C2} = \frac{1}{\eta_2}\int d^4x\sqrt{g}\,\widetilde{R}_{\mu\nu}\widetilde{R}^{\mu\nu}, \quad (8.74)$$

only S_C is allowed, because S_{C1}, S_{C2} do not satisfy the request after the redefinition (8.72).
The problem with these two terms is that they contain quartic derivatives of the metric and the dilaton, that is they introduce physical ghosts in the theory with the annexed risks for unitarity. Therefore it is good news that they are excluded.

The only counterterm that remains is S_C. It contains four derivatives of the metric, therefore it can give rise to the problem illustrated in example (8.50). A WZ term may provide a way out.

We know that there is an anomaly with the same density as S_C, (8.58). But recall that we also have the corresponding WZ term. In this case the WZ term has the same form as the anomaly with ω replaced by $\sigma = -\varphi$. Inserting it in the first quantized action $W^{(1)}$ we restore conformal invariance at one loop and obtain, say, the conformal invariant effective action $W^{(c1)}$. However the latter contain physical ghosts due to the counterterms. This is true for a generic 'gauge' of φ. But suppose that we choose a 'gauge' by fixing φ to a suitable constant value, so that the WZ terms exactly cancels the corresponding counterterm. In this 'gauge' the physical ghosts disappear and a possible violation of unitarity at one loop is removed. Due to Weyl invariance we can assume that if unitarity holds for this gauge it can be extended to all values of φ. Notice that this is similar to [43, 44, 51], where the unwanted negative norm state appears only at the tree level, but not in higher loops, a rather mild and controllable violation of unitarity. Remark that the necessary cancelation would be impossible if in addition there were also the counterterms (8.74), because we have only one gauge fixing at our disposal.

As for the trivial anomaly with density $\Box R$ we have already noticed that it can be canceled by a counterterm with density R^2, but this introduces again physical ghosts. Therefore, in this case, to cancel the anomaly it is more convenient to use the corresponding WZ term, which introduces in the theory only interaction terms. In conclusion it seems to be possible to renormalize $S^{(c)}$, without non-minimal couplings, at one loop, while preserving Weyl invariance and avoiding physical ghosts. Whether this is possible at higher loop order is an open problem.

Let us now return to the issue of 'gauge fixing', i.e. making a specific choice for φ among the infinite many physically realizable ones. As noted before, in a unique theory we can describe radically different physical situations. We can study unitarity and renormalization for a specific choice of the 'gauge' for φ. As long as conformal invariance is preserved the results extends to all configurations of the dilaton. The problem next is to understand why a specific configuration for φ, say $\varphi_0 = const$[6], describes the physics of the universe in the present era. This is sometime called the second cosmological constant problem. The example of a ferromagnetic material in 2d can help intuition. The source of magnetization in such materials is the spin of the electrons in incomplete atomic shells, each electron carrying one unit of magnetic moment. Such spins can be imagined to be attached to lattice points and to interact with the neighboring ones in such a way that the state of lowest energy corresponds to all the spins being aligned. At temperature T = 0 all the spins are aligned. When the temperature increases the thermal motion destroys this order, but not completely if the temperature is low enough; there remains patches where the spins are all aligned, with the result that a finite magnetization survives. As T reaches the critical temperature T_c and goes beyond it, order is completely destroyed and magnetization vanishes (disordered or paramagnetic phase). Of course if we reverse the procedure in the

[6] Due to the residual scale invariance we can always rescale t so that $e^{\varphi_0} c$ corresponds to the measured cosmological constant.

direction of lower temperatures, we are going to see larger and larger patches of oriented spin reappearing. The system is characterized by a correlation length ξ that becomes infinite at $T = T_c$. The correlation length is interpreted as the average size of the polarized spin patches; the fact that at the critical point this becomes infinite, means that we have patches of any size. Therefore the physical picture does not change, not only when we rescale the system rigidly, but also when we rescale it with a varying scale from point to point. But this is precisely conformal symmetry.

We can imagine something similar happening in our $\mathcal{TW}$ theory. At very high energy we expect conformal invariance to hold. In this regime all the configurations of φ are equivalent. When the energy density decreases patches with different solutions for φ start to appear and consolidate. Each patch φ has a precise value depending on the time it broke off from the rest. Time plays the role of spin direction in the above example. Within this picture our present universe is thought to live in one of these patches with φ fixed for ever. This way of figuring out the evolution of the universe in our theory, at least in the very early stage, is a resignation to the anthropic principle. But, in the theory $\mathcal{TW}$, there does not seem to be a viable alternative. The above is a mechanism to 'fix the gauge' for conformal invariance. What are the alternatives? The breaking of conformal symmetry cannot be an explicit one, of course, if one wants this theory to represent a faithful approximation to a fundamental one, in which no explicit breaking is allowed. It cannot be a spontaneous breaking either, because that would require a potential with a minimum. But in a conformal invariant theory also the potential must be conformal invariant and cannot have minima. Perhaps a different mechanism might exist in a UV completion of $\mathcal{TW}$.

8.6 Conclusion

This paper is a continuation of [8]. The model, proposed there, that incorporates both SM and gravity, in a form that avoids all the type-O anomalies, has been presented here in a simplified version including only one metric, instead of two. It preserves however the basic structure of two sectors, left and right, with mirror fermions and scalars, as well as $SU(3)$ and $U(1)$ gauge fields, while the $SU(2)$ gauge fields as well as the metric are in common. Two subjects have been developed. The first is an interpretation of the right sector as dark matter, a rather attractive and reasonable idea, but still at the level of research project. The second concerns Weyl symmetry and its possible connection with cosmology on the applicative side and with unitarity and renormalization on the theoretical field theory side. It has been shown that a background solution of the Weyl invariant theory exists that represents a regime different from the well known DeSitter, radiation dominated and matter dominated ones, a solution that may apply to the very early stages of the universe. This solution also suggests interesting applications to the cosmological constant problem. On the quantum field theory side the subject of Weyl symmetry and Weyl anomalies, already developed in [8] has been reviewed and an application of the WZ terms has been illustrated to the problem of one-loop quantization of the model to show that it may be used to secure unitarity.

Acknowledgements. I woud like to thank the organizers of the workshop *What comes beyond the standard model* 2025, for inviting me to give a talk which has motivated this paper.

8.7 Appendix. Non-trivial background

If we plug the background solution of section 4.1 in the lhs of eq.(8.53) we see that it does not vanish (although R does). Of course the rhs cannot vanish either, which means that some of the energy-momentum matter traces cannot vanish due to the presence of some background value of the involved scalar fields. Therefore the discussion of section 5.1 has to be improved by allowing for the presence of a non-trivial classical background for the metric, the dilaton and possibly other scalar fields.
What should one do in this and similar cases? The first thing is to expand the involved fields into a classical and quantum part

$$g_{\mu\nu} = g_{0\mu\nu} + h_{\mu\nu}, \qquad \varphi = \varphi_0 + \chi, \qquad \Phi = \Phi_0 + \phi, \qquad \text{etc.}$$

In the previous example $g_{0\mu\nu}$ is the FLRW metric and φ_0, Φ_0 are given by eq.(8.36). We assume that the classical background satisfies (8.53) and look for a quantum version thereof. The same solution must of course satisfy (8.39). Then we contract the latter with the inverse background metric $g_0^{\mu\nu}$ and subtract from the result eq.(8.53). In the rhs we obtain

$$2\kappa e^{2\varphi_0}\left(g_0^{\mu\nu}\langle\!\langle T^{(m)}_{\mu\nu}\rangle\!\rangle - \langle\!\langle g_0^{\mu\nu} T^{(m)}_{\mu\nu}\rangle\!\rangle\right) \tag{8.75}$$

where $\langle\!\langle\cdot\rangle\!\rangle$ represent the first order quantization. In the corresponding lhs we can safely assume that $\langle\!\langle h_{\mu\nu}\rangle\!\rangle = 0$, which is the same condition fulfilled in section 5.1 (i.e. absence of first order in $h_{\mu\nu}$), while the term $\langle\!\langle e^{2\varphi}\rangle\!\rangle = 0$ is subtracted away. Thus eq.(8.75) denotes the violation of conformal invariance at the lowest order. The expression

$$g_0^{\mu\nu}\langle\!\langle T^{(m)}_{\mu\nu}\rangle\!\rangle - \langle\!\langle g_0^{\mu\nu} T^{(m)}_{\mu\nu}\rangle\!\rangle \tag{8.76}$$

reproduces the expression of the trace anomaly proposed by Duff, [15, 16]. The first order expressions of these anomalies may in general be different from those analysed before because they may explicitly contain the background fields. When computing perturbative anomalies we have to use the perturbative cohomology in order to verify whether they satisfy the consistency conditions.
The WZ consistency condition $\delta_\omega \Delta_\omega = 0$ for the cocycle Δ_ω is split according to the decomposition

$$\delta_\omega = \sum_{i=0}^{\infty} \delta_\omega^{(i)}, \qquad \Delta_\omega = \sum_{i=1}^{\infty} \Delta_\omega^{(i)} \tag{8.77}$$

In particular

$$\delta_\omega^{(0)}\Delta_\omega^{(0)} = 0, \qquad \delta_\omega^{(0)}\Delta_\omega^{(1)} + \delta_\omega^{(1)}\Delta_\omega^{(0)} = 0, \qquad \delta_\omega^{(1)}\Delta_\omega^{(1)} + \delta_\omega^{(0)}\Delta_\omega^{(2)} + \delta_\omega^{(2)}\Delta_\omega^{(0)} = 0, \tag{8.78}$$

The basic BRST transformations are

$$\delta^{(0)}_\omega h_{\mu\nu} = \omega g_{0\mu\nu}, \quad \delta^{(1)}_\omega h_{\mu\nu} = 2\omega h_{\mu\nu}, \quad \delta^{(2)}_\omega h_{\mu\nu} = 0, \quad ... \tag{8.79}$$

$$\delta^{(0)}_\omega \varphi = -\omega\varphi_0, \quad \delta^{(1)}_\omega \varphi = -\omega\chi, \quad \delta^{(2)}_\omega \phi = 0, \quad \dots \tag{8.80}$$

$$\delta^{(0)}_\omega \phi = -\omega\Phi_0, \quad \delta^{(1)}_\omega \phi = -\omega\phi, \quad \delta^{(2)}_\omega \phi = 0, \quad ... \tag{8.81}$$

An explicit example can be found in Appendix D of [8].

References

1. A. Arbey and F. Mahmoudi, *Dark matter and the early Universe: a review*, ArXiv:2104.11488v1.
2. Chiara Arina, *Review of Dark Matter tools*, PoS, *TOOLS2020*, arXiv:2012.0962v2[hep-th].
3. Y.Bai and P.Schwaller, *Scale of dark QCD*, Phys.Rev. **D89** (2014) 063522-1.
4. C. Bambi and A. D. Dolgov, *Introduction to Particle Cosmology*, Springer Verlag GmbH, Berlin Heidelberg 2021.
5. L. Bergström, *Non-Baryonic Dark Matter: Observational Evidence and Detection Methods*, Rept.Prog.Phys.**63**:793,2000, arXiv:hep-ph/0002126v1.
6. G. Bertone, D. Hopper and J. Silk, *Particle dark matter:evidence, candidates and constraints*, Phys. Rep. **405** (2005), 279.
7. L. Bonora, *Fermions and Anomalies in Quantum Field Theories*, Springer 2023.
8. L. Bonora and S. Giaccari, *Something Anomalies can tell about SM and Gravity* , arXiv:2412.07470 [hep-th], Symmetry 17 (2025), 273.
9. S. M. Boucenna and S. Morisi, *Theories relating baryon asymmetry and dark matter. Mini review*, Front. Physics 1:33, arXiv:1310.1904v3 [hep-th].
10. R. H. Brandenberger, *Lectures on the Theory of Cosmological Perturbations*,Lect. Notes Phys. **646** (2004) 127-167, arXiv:hep-th/0306071v1.
11. C. P. Burgess, *Dark Energy and the Symbiosis between Micro-physics and Cosmology (Naturally)*, arXiv:2509.00688v1[hep-th].
12. S. M. Carrol, *The cosmological constant*, http://www.livingreviewes.org/Articles/index.html.
13. A. Codello, G. D'Odorico, C. Pagani, R. Percacci, *The Renormalization Group and Weyl-invariance*, Class.Quant.Grav. 30 (2013) 115015, e-Print: 1210.3284 [hep-th].
14. M. Drees and G. Gerbier, *Mini-Review of Dark Matter: 2012*, arXiv:1204.2373v1 [hep-ph].
15. M. J. Duff, *Twenty years of the Weyl anomaly*, Class. Quant. Grav. **11** (1994) 1387 [hep-th,9308075].
16. M. J. Duff, *Weyl, Pontryagin, Euler, Eguchi and Freund* , Jour. Phys. A: Mathematical and Theoretical, **53** (2020) 301001 [arXiv:2006.03574].
17. L. H. Ford and L. Parker, *Quantized gravitational wave perturbations In Robertson-Walker universes*, Phys.Rev. **D16** (1977) 1601.
18. L. H. Ford, *Cosmological Particle Production: A Review*, Rep. Prog. Phys. **84** (2021) 116901, arXiv:2112.02444v1.
19. M. Gell-Mann, R. J. Oakex and B. Renner, *Behavior of current divergences under* $SU(3) \times SU(3)$. Phys. Rev. **175** (1968) 2195.
20. D. M. Ghilencea, *Standard model in Weyl conformal geometry,* Eur. Phys. J. C **82** (2022) 23, arXiv:2104.15118 [hep-ph].
21. D. M. Ghilencea, *Non-metric geometry as the origin of mass in gauge theories of scale invariance,* Eur. Phys. J. **C 83** (2023) 176, [arXiv:2203.05381 [hep-th]
22. D. M. Ghilencea, *Quantum gravity from Weyl conformal geometry,*, arXiv:2408.07160v1 [hep-ph].

23. P. B. Greene, L. Kofman, A. Linde and A. A. Starobinsky, *Structure of resonance in preheating after inflation*, Phys.Rev. **D56** (1997) 6175.
24. J. Julve and M. Tonin, *Quamtum Gravity with Higher Derivative Terms*, Il Nuovo Cimento, **46** (1978) 137.
25. H. M. Hodges, *Mirror baryons as the dark matter*, Phys.Rev. **D47** (1993) 456.
26. R. Kallosh and A. Linde, *On the Present Status of Inflationary Cosmology*, arXiv:2505.13646v1[hep-th], Lemaître Conference 2004.
27. L. Kofman, A. Linde and A. A. Starobinsky, |it Towards the theory of reheating after inflation, Phys. Rev. **D56** (1995) 3258.
28. T. Kugo and I. Ojima, *Manifestly Covariant Canonical Formulation of the Yang-Mills Field Theories. I*, Prog. Theor. Phys. **60** (1978) 1869.
29. N. Mohammedi, *A note on Weyl gauge symmetry in gravity*, arXiv:2402.04712 [hep-th].
30. R. N. Mohapatra and V. I. Teplitz, *STRUCTURES IN THE MIRROR UNIVERSE*, The Astrophisical Journal **478** (1997) 29.
31. , V. F. Mukhanov, H. A. Feldman and R. H. Brandenberger, *Theory of Cosmological Perturbations*, Phys. Rep. **215** (19992) 203-233.
32. I. Oda, *Quantum scale invariant gravity with DeDonder gauge*, Phys. Rev. **D 105** (2022) 066001.
33. I. Oda, *Quantum Theory of Weyl-invariant Scalar-tensor Gravity*, Phys. Rev. **D 105** (2022) 120618. http://arxiv.org/abs/2204.11200v1 [hep-th]
34. I. Oda and P. Saake, *BRST Formalism of Weyl Conformal Gravity*, Phys. Rev. **D 106** (2022) 106007. http://arxiv.org/abs/2209.14533v1 [hep-th].
35. I. Oda and M. Ohta, *Quantum Conformal Gravity*, JHEP **02** (2024) 213. http://arxiv.org/abs/2311.09582v1 [hep-th].
36. I. Oda, *Conformal Symmetry in Quantum Gravity*, arXiv:2403.04056v1 [hep-th]
37. I. Oda, *BRST Formalism of f (R) Gravity*, ArXiv:2410.20270 [hep-th].
38. L.Parker, *Quantized Fields and Particle Creation in Expanding Universes. I*, Phys.Rev. **183** (1969) 1057.
39. L.Parker, *Quantized Fields and Particle Creation in Expanding Universes. II*, Phys.Rev. **D3** (1971) 346.
40. L. Parker and D. Toms, *Quantum fields in curved space*, Cambridge University Press, 2009.
41. M. E. Peskin and D. V. Schroeder, *An introduction to quantum field theory*, Westview Press 1995.
42. O. Piguet and S. P. Sorella, *Algebraic Renormalization*, Springer 1995.
43. S. Pottel and K. Sibold. *Perturbative quantization of Einstein-Hilbert gravity embedded in a higher derivative model.* Physical Review **D 104** (2021) 086012. arXiv:2012.11450v3 [hep-th]
44. S. Pottel and K. Sibold. *Perturbative quantization of Einstein-Hilbert gravity embedded in a higher derivative model. II*, arXiv:2308.15824v2 [hep-th] .
45. L. Rachwal, *Introduction to Quantization of Conformal Gravity*, arXiv:2204.13856 [hep-th].
46. J. Racker, *Mini-review on baryogenesis at the TeV scale and possible connection with dark matter*, Contribution to the proceedings of ICHEP 2014, arXiv:410.5482v1 [hep-ph].
47. D. Roumelioti, S. Stefas, G. Zoupanos, *Unification of Conformal Gravity and Internal Interactions*, http://arxiv.org/abs/2403.17511v1.
48. E. Scholz, *The Unexpected Resurgence of Weyl Geometry in late 20th-Century Physics,* Einstein Stud. **14** (2018) 261-360, arXiv:1703.03187 [math.HO].
49. M. A. Shifman, A. I. Vainshtein and V. I. Zhakarov, *QCD and resonance physics, sum rules*, Nucl. Phys. **B 147** (1979) 385.
50. Y. Shtanov, J. Traschen and R. Brandenberger, *Universe reheating after inflation*, Phys.Rev. **D51** (1995) 5438.

51. K. Sibold. *Einstein-Hilbert Gravity, Higher Derivatives And a Scalar Matter Field*, arXiv:2405.00528v1 [hep-th]
52. K. S. Stelle, *Renormalization of higher-derivative quantum gravity*. Phys. Rev. **D 16** (1977) 953.
53. J. H. Traschen and R. H. Brandenbergere, *Particie production during out-of-equilibrium phase transitions*, Phys.Rev. **D42** 2491.
54. S. Tsuchikawa, *Introductory Review of Cosmic Inflation*, lecture notes given at The Second Tah Poe School on Cosmology "Modern Cosmology", Naresuan University, Phitsanulok, Thailand, April 17 -25, 2003, arXiv:hep-ph/0304257v1.
55. J. A. Vasquez, L. E. Padilla and T. Matos, *Inflationary Cosmology: From Theory to Observations*, Rev. Mex. Fis. **E17** (2020) 1, arXiv:1810.09934v3 [astro-ph.CO].
56. A. Vilenkin, *Cosmological constant problems and their solutions*, arXiv:hep-th/0106083.
57. S. Weinberg, *The cosmological constant problem*, Rev.Mod. Phys. **61** (1989) .
58. S. Weinberg, *The cosmological constant problem*, arXiv:astro-phys/0005265.

BLED WORKSHOPS
IN PHYSICS
VOL. 26, NO. 1

Proceedings of the 28th Workshop
What Comes Beyond . . . *(p. 101)*
Bled, Slovenia, July 6–17, 2025

9 Chemical evolution of antimatter domains in early Universe

A. I. Dembitskaia[1§], Stephane Weiss[1¶], M. Yu. Khlopov[2‖], M.A.Krasnov[3]

[1]National Research Nuclear University MEPhI, 115409 Moscow, Russia
[2]Virtual Institute of Astroparticle Physics (VIA), 75018, Paris, France
[3]Institute of Physics, Southern Federal University, 194 Stachki,Rostov-on-Don
and National Research Nuclear University MEPhI, 115409 Moscow, Russia

Abstract. According to modern physics, our Universe is baryon-asymmetric. That phenomenon can not be described in the frameworks of the Standard Model of particle physics. Globally, the Universe consists of baryon matter. However, some scenarios can lead to the existence of local antimatter domains. In the research, the chemical evolution of such an isolated antimatter domain, surrounded by baryonic matter, is studied. The size of the domain is estimated according to the conditions of its survival in baryon surrounding, and the process of annihilation at its border is taken into account.
Povzetek: Naš vesolje se zdi sestavljeno samo iz snovi. Izolirane domene antisnovi bi nesimetričnost vesolja omilila. Avtorica preučuje kemično evolucijo izolirane domene antisnovi, obdane z barionsko snovjo. Ocenjuje velikost take domene v interakciji s barionsko snovjo, ki bi preživela do danes..

9.1 Introduction

Modern concepts of the Universe assume its baryon asymmetry, which means the absence of macroscopic antimatter in an amount comparable to the amount of matter. Nevertheless, due to the the strong nonhomogeniety of baryosynthesis, under certain conditions, local generation of antimatter domains is possible.The standard mechanism of baryosynthesis predicts baryon asymmetry, which might be described by the value, equal to the ratio of density difference between baryons and antibaryons to the density of photons. [1]

$$\eta = \frac{n_b - n_{\bar{b}}}{n_\gamma} \tag{9.1}$$

Globally, the Universe is filled with baryonic matter, but there also may be local regions filled with antibaryonic matter (domains dominated by antimatter).
The laws of the strong and electromagnetic interaction are the same for baryons and antibaryons. According to this, we can assume that the evolution of antimatter can be described similarly to the evolution of matter.

§demanna2004@yandex.ru
¶weiss.stephane62500@gmail.com
‖khlopov@apc.in2p3.fr

Despite this, the formation of astronomical objects that are similar to objects that we know is impossible in the antimatter domain: during the evolution of matter, the products of nucleosynthesis from other stars may enter the region from the outside. Since the products of nucleosynthesis inside the antistars leave the domain and cannot influence its chemical evolution, the objects inside the domain must have a composition similar to the primary chemical composition formed during the Big Bang. It means that the processes happening within the regions of antimatter during its evolution are different from those that happen with matter. However, in the early Universe , primary nucleosynthesis processes would occur in the antimatter domain, leading to the formation of antihelium. The AMS-02 experiment located on the ISS makes it possible to detect antihelium nuclei among the helium nuclei of cosmic rays. If similar results are obtained, it will confirm the possibility of the existence of separate antimatter domains in the universe.

9.2 Size of the surviving domain

Since the domain consists of antimatter, during its evolution, annihilation occurs at the boundary of the domain with the horizon. That is why the domain must have a sufficiently large scale to survive to the modern era. Thus, the minimum mass for the domain should be $10^3 M_\odot$.
It is also necessary that the gamma background should correspond to the observed background [2]. This constraint defines an upper limit for the mass. Thus, the mass range:

$$10^3 M_\odot \leq M \leq 10^5 M_\odot. \tag{9.2}$$

Let's assume that the domain we are considering was formed before the era of primary nucleosynthesis, which means that it does not contain heavy elements. The presence of metals in the domain would imply interaction with matter, which would lead to the observed gamma-ray bursts caused by annihilation. Therefore, the domain must be zero-metallic, which leads to certain restrictions on its density. On the one hand, the domain should consist primarily of antihelium, but it cannot contain elements heavier than lithium.
The main characteristic of the domain density is the antibaryon-photon ratio. This physical value makes it possible to determine the mass fractions of chemical elements within a domain.
To analyze the dependence of the mass fractions of chemical elements on the antibaryon-photon ratio, the AlterBBN program was used.
The graphs show the dependence of the mass fraction of the elements formed on the baryon-photon ratio for the following elements: ^{4}He (9.1), ^{12}C (9.2).
According to the data, the density range of the domain:

$$3 \times 10^{-12} \leq \eta \leq 1 \times 10^{-6} \tag{9.3}$$

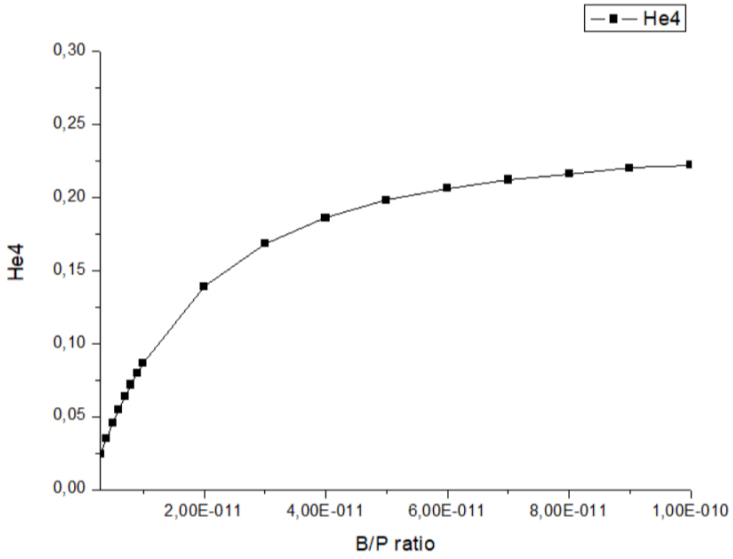

Fig. 9.1: Dependence of the ^{4}He mass fraction on baryon/photon ratio

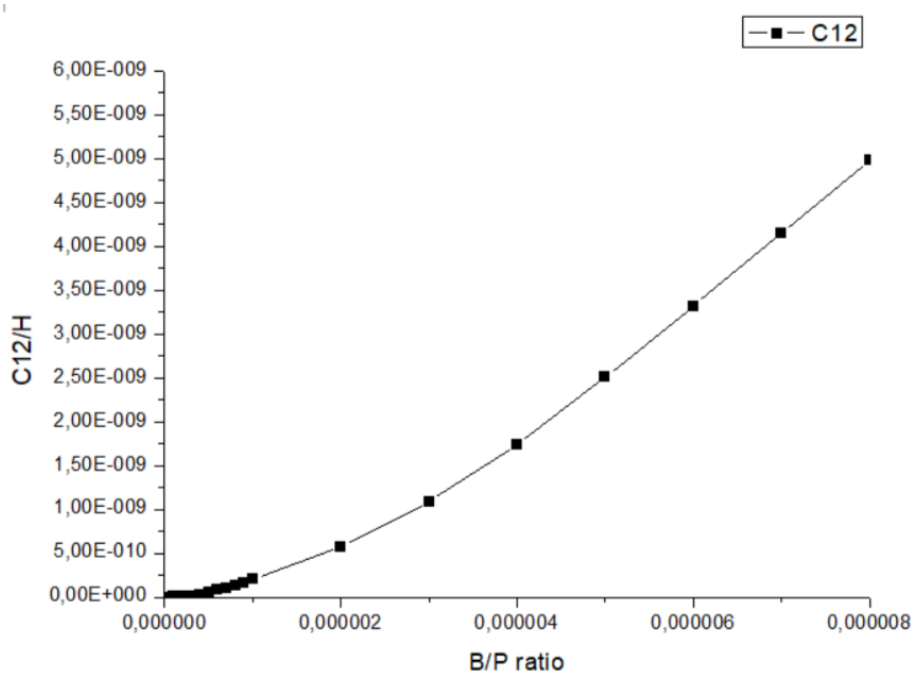

Fig. 9.2: Dependence of the ^{12}C mass fraction on baryon/photon ratio

The size of the domain also might be calculated:

$$R = \left(\frac{N}{n}\right)^{\frac{1}{3}}, \tag{9.4}$$

where $n = \eta n_\gamma$;
n_γ-density of thermal photons in the domain. For the radiation era we have:

$$R = \left(\frac{M}{m_p \eta T^3}\right)^{\frac{1}{3}}. \tag{9.5}$$

Estimated domain size for appropriate temperatures $10^{11} - 10^{19}$ sm. Size of the horizon for the same period is $10^{11} - 10^{21}$ sm.
Therefore, depending on the domain parameters, its size can either exceed the horizon size or be significantly smaller. This will affect the nature of the processes taking place at the domain boundary.
Consider the period of time from which the domain becomes smaller than the horizon:

$$ct \geq R \tag{9.6}$$

Thus, we get time constraints:

$$t \geq \left(\frac{M}{c^3 m_p \eta 10^{30}}\right)^{\frac{2}{3}}. \tag{9.7}$$

The minimal possible time for such constraints is $t_{min} = 1,25 \times 10^3$ c which consider to the radiation era. According to the connection between time and temperature at the radiation era, the maximum temperature is $T = 2,83 \times 10^8$K. In the future, there is a cooling of the domain associated with the cooling of the Universe.

9.3 Antimatter domain in the model of spontaneous baryosynthesis

One possibility to form antimatter domain is the dynamics of pseudo-Nambu-Goldstone boson (PNGB) arising in a simple model of spontaneous baryogenesis. After phase transition the Lagrangian of the model is as follows:

$$\mathcal{L} = \frac{f^2}{2}\partial_\mu\theta\partial^\mu\theta + i\overline{Q}\gamma^\mu\partial_\mu Q + i\overline{L}\gamma^\mu\partial_\mu L - m_Q\overline{Q}Q - m_L\overline{L}L + \\ + \frac{gf}{\sqrt{2}}\left(\overline{Q}Le^{i\theta} + \overline{L}Qe^{-i\theta}\right) - V(\theta). \tag{9.8}$$

In this particular model given by the Lagrangian (13.4) it was found in [6,7] that PNGB rolling from π to 0 produces baryon excess, while rolling from $-\pi$ to 0 would produce antibaryon excess. Since PNGB's potential posses the following symmetry:

$$V(\theta) = V(\theta + 2\pi), \tag{9.9}$$

one can conclude that rolling from π to 2π will produce antibaryon excess. PNGB field would fluctuate during inflation and it could possibly cross π which would lead to the formation of domain walls. In such configuration, there would be a region of antibaryon excess inside the wall and a region of baryon excess around the wall. Size of non-vanishing fluctuations during inflationary stage are determined by Hubble parameter H_{inf} during that stage. If quantum fluctuation takes place at the moment t during inflation, then by the end of cosmological inflation its size is as follows:

$$r_{inf}(t) = H_{inf}^{-1} e^{N_{inf} - H_{inf} t}. \tag{9.10}$$

After inflation ends these fluctuations would be stretched by consequent expansion. When Hubble parameter H would be of order of Λ^2/f, which refers to PNGB's mass, classical motion of the PNGB field would start and formation of closed walls would take place. Mass of the scalar field implies lower limit on size of the antimatter domain, because there are fluctuations which would enter horizon before start of the classical motion of the scalar field. Minimal size is as follows:

$$r_{hor} = H^{-1} = m_{\theta}^{-1} = \frac{f}{\Lambda^2}. \tag{9.11}$$

Then the upper limit on wall's size is determined via its tension. Domain wall with constant surface energy density could start to dominate within Hubble horizon before it could have entered the cosmological horizon if size of this wall is large enough. Following [5, 6], corresponding timescale at which wall would start to dominate and escape into baby universe is as follows:

$$t_{\sigma} = \frac{M_{Pl}^2}{2\pi\sigma}, \tag{9.12}$$

where σ is surface energy density of the wall. In case of considered PNGB it is calculated via model's parameters as follows:

$$\sigma = 4\Lambda^2 f \rightarrow t_{\sigma} = \frac{M_{Pl}^2}{8\pi\Lambda^2 f}. \tag{9.13}$$

Combining expressions above, one can estimate threshold for size of antimatter domain r_{domain} as follows:

$$\frac{f}{\Lambda^2} < r_{domain} < \frac{M_{Pl}^2}{8\pi\Lambda^2 f}. \tag{9.14}$$

Let us now define a threshold for the mass of the antimatter domain M using estimations of its size above. Let m_0 be the mass of a baryon, n_i be the number density of baryons at the moment of wall's crossing the Hubble horizon, then mass of the domain could be estimated as follows:

$$\frac{4}{3}\pi m_0 n_i \left(\frac{f}{\Lambda^2}\right)^3 < M < \frac{4}{3}\pi m_0 n_i \left(\frac{M_{Pl}^2}{8\pi\Lambda^2 f}\right)^3 \tag{9.15}$$

9.4 Diffusion towards the border of domain

The phenomenon of diffusion of baryons and antibaryons towards the boundary is governed by elastic scattering, rather than annihilation. The main distinction is important, first of all the elastic scattering processes, which involves interactions where particles maintain their identity but exchange momentum and energy and they are responsible for randomizing trajectories of particle and make easier macroscopic transport of baryons and antibaryons through the primordial plasma. However, annihilation process is a local process that occurs predominantly at domain boundaries where matter and antimatter and in contact and convert into other particles.
The macroscopic transport is achieved by specific elastic scattering mechanisms
The effective transport of charged anti-baryons in the early Universe is constrained by their coupling to the ambient electron-photon fluid. The Diffusion phenomenon

- Proton Electron Elastic Scattering
  The direct electromagnetic coupling between charged anti-baryons and the ambient plasma electrons $e^{\pm}$. The process is Coulomb Scattering that is mediated by a virtual photon. To preserve the local charge neutrality, any motion of anti-baryons must be following a motion of electrons.
- Electron-Photon Coupling
  The mobility of electrons, that limits the transport of anti-baryons is constrained by by their Elastic Scattering against the dense background of thermal radiation (CMB).The interaction $\gamma + e^{\pm} \rightarrow \gamma + e^{\pm}$ creates radiative friction. This has a consequence that the domination constraint on baryon diffusion comes from the Electron-Photon coupling.
- Direct Proton-Photon Scattering
  Direct Proton-Photon Scattering is negligible due to the extremely low cross-section involved for this interaction.

9.4.1 Time Depend Evolution of the Diffusion Coefficient

The Diffusion Coefficient D quantifies the relation between flux of particles and gradient of density. D is proportional to the mean free path λ and particle velocity v_{th}. The dependence of time of Diffusion Coefficient depend on the cosmological expansion $a(t)$, which determines the dilution of of the scatterer density $n \propto a(t)^{-3}$.
In the Radiation-Dominated era, the scale factor evolves as as $a(t) \propto t^{\frac{1}{2}}$. The medium is a relativistic plasma, the velocity is approximately equal to the speed of light $v_{th} \approx c$. The dilution of the scattered density $n_e \propto t^{-\frac{3}{2}}$ leads to the mean free path $\lambda \propto t^{\frac{3}{2}}$.

$$D_{rad} \propto \lambda \cdot c \propto t^{\frac{3}{2}} \tag{9.16}$$

The consequence is the Diffusion becomes more efficient as the Universe expands and the plasma becomes more transparent. D_{rad} describes the transport lead by the coupling of charged antibaryons with the plasma.

The dynamics change after Radiation-Matter equality when $t > t_{eq}$. Compare to the Radiation-Dominated era, the scale factor becomes $a(t) \propto t^{\frac{2}{3}}$. However, the recombination t_{rec} who has a redshift $z \approx 1100$ hasn't yet occurred, so the charge antibaryons are still interfered with the thermal radiation pressure. The diffusion mechanism remains Radiative Diffusion. The dilution of the scattered density n_e follows a law $n_e \propto a(t)^{-3}$ and because the relation between mean free path and the dilution if scattered density is known

$$\lambda \propto \frac{1}{n_e} \propto a^3 \propto \left(t^{\frac{2}{3}}\right)^3 \propto t^2 \tag{9.17}$$

The Diffusion coefficient is also determined by velocity of electrons moving towards the border. The motion is determined by photon pressure and thermal radiation effect. Because of the thermal equilibrium of electrons with plasma we can assume that the velocity could not be equal to the speed of light anymore. So that value also should be estimated as thermal velocity.

$$v_{th} = \sqrt{\frac{3kT}{m}} \propto t^{-\frac{1}{3}} \tag{9.18}$$

Using the relation between the time and temperature we can estimate the dependence of the Diffusion Coefficient on time as

$$D_{plasma} \propto \lambda \cdot v_{th} \propto t^{\frac{5}{3}} \tag{9.19}$$

The mechanism change fundamentally at t_{rec}. Neutralization of antibaryons into antiatoms occurs. Also the electromagnetic coupling with CMD photons disappears, and radiative friction ceases. The transport is governed now by Atomic Diffusion via kinetic collision between neutral atoms. Th Diffusion Coefficient of kinetic atomic diffusion is given by the fundamental relation of kinetic theory of gases.

$$D_{atoms} \propto \lambda_{coll} \cdot v_{th} \propto t^{\frac{4}{3}} \tag{9.20}$$

The Diffusion process is not static but modulated by feedback mechanism from Annihilation. The products of Annihilation $\pi^0, \pi^\pm$ decay into high-energy photons $\pi^0 \rightarrow 2\gamma$. The total annihilation energy splits into three components

- neutrinos for 50%
- γ-photons for 34%
- $e^\pm$ pairs for 16%

These highly energetic $e^\pm$ pairs deposit energy into the surrounding medium, generating a local, non-uniform Annihilation Pressure P_{ann}

$$P_{ann} \propto \tau_{rad}\, \epsilon \langle \sigma v \rangle n_{\bar{b}}\, n_b \tag{9.21}$$

The gradient of the Annihilation Pressure P_{ann} acts as a drift motion that suppresses the anti-baryon flux towards the interface. The total anti-baryon flux $J_{antibaryons}$ is

modeled through the Generalized Fick's Law, which includes both the standard Diffusion term and the Pressure gradient term

$$J_{\text{antibaryons}} = -D_{\text{rad}} \nabla n_{\bar{b}} - \frac{D_{\text{rad}}}{k_B T n_{\text{eff}}} n_{\bar{b}} \nabla P_{\text{ann}} \tag{9.22}$$

To relate this generalized flux to a simplified form

$$J_{\text{antibaryons}} = -D_{\text{eff}} \nabla n_{\bar{b}} \tag{9.23}$$

the Thin-Boundary Approximation is applied. By substituting the gradients with magnitude ration $\nabla n_{\bar{b}} \approx \frac{n_{\bar{b}}}{\delta}$ and $\nabla P_{\text{ann}} \approx \frac{P_{\text{ann}}}{\delta}$, the effective Diffusion Coefficient for Radiation-Dominated era is obtained

$$D_{\text{eff}} = D_{\text{rad}} \left[1 + \frac{P_{\text{ann}}}{k_B T n_{\text{eff}}} \right] \tag{9.24}$$

In the center of the domain, the Annhilation pressure P_{ann} is vanished, resulting that $D_{\text{center}} \approx D_{\text{rad}}$. This expression is true for Matter Dominated neutral phase.

9.4.2 Processes at the border

Starting from the moment when the size of the horizon exceeds the size of the domain, the annihilation of matter with antimatter will occur at the boundary of the domain, as a result of which high-energy photons will be formed. They will penetrate the domain. Since the domain consists entirely of antimatter, annihilation of baryons with antibaryons will occur at the boundary of the region with the horizon, as a result of which various particles will be formed.
Consider proton-antiproton annihilation. The cross section of the interaction of this reaction can be described using the experimental data obtained [7].

$$\sigma_0 \approx 1,6 \times 10^{-25} \text{cm}^2 \tag{9.25}$$

This reaction passes through various channels. The probability of each of them can be described using the branching coefficient. The most probable channels are those involving the formation of neutral and charged pions [8].
The domain that we are considering consists of antimatter and contains positrons inside. As a result of the processes, it is possible for electrons to enter the domain or to be produced it. Then, positron-electron annihilation inside the domain is possible.
There are 2 sources of electrons inside the domain:
· pair production as a result of interaction between the annihilation and thermal photon;
· formation of an electron after the decay of a negatively charged muon, which is the product of a charged pion decay.
The result of this reaction will be the formation of annihilation photons inside the domain.
After the decay of a neutral pion with an energy of 135MeV, 2 photons are formed, the average energy of each of which is 67,5MeV.

Penetrating inside the domain, a high-energy photon can interact with a thermal photon to form a positron-electron pair.
The distribution of thermal photons obey the Planck distribution. That guarantees the presence of a non-zero concentration of high-energy photons.If the photon energy is greater than 3,9kev, then the pair-production is possible. Required temperature for that is $T = 10^7$K.
The interaction of two photons is described by the Breit-Wheeler formula for high energies:

$$\sigma_{pp} \approx \frac{\pi\alpha^2}{s}\left[2\ln\left(\frac{s}{m_e^2}\right) - 1\right] \tag{9.26}$$

The energy of a thermal photon is significantly less than the energy of an annihilation photon. In this case, an energy asymmetry is observed and the formula describing the reaction cross section will look like this [9]:

$$\sigma_{pp} \approx \frac{2\pi\alpha^2}{s}\left[2\ln\frac{s}{m_e^2} - \frac{3}{2}\right] \approx 2,1 \times 10^{-28}\text{cm}^2, \tag{9.27}$$

where $E_1 >> E_2$.
As a result of the reaction, an electron-positron pair is formed. Moreover, one of the particles will receive almost all the energy of the annihilation photon, while the second will acquire energy comparable to the rest energy of an electron.As the resukt, the annihilation of positrons located in the domain with the resulting high-energy electron is possible.
In addition to the formation of electron-positron pairs within the domain, Compton scattering of a photon by a positron is also possible.This process will be dominant at the temperature $T < 10^7$K.
The relative energy loss after one Compton scattering is described by the following formula:

$$\frac{\Delta E}{E} = \frac{E' - E}{E} = -1 + \frac{1}{1 + \epsilon(1 - \cos\theta)}, \tag{9.28}$$

where $\epsilon = \frac{E}{m_e c^2}$
After a single scattering the photon does not lose all its energy. The evolution of the photon distribution during multiple scattering is described by the Kompaneyets equation [10]:

$$\frac{\partial n}{\partial y} = \frac{1}{x^2}\frac{\partial}{\partial x}\left[x^4\left(\frac{\partial n}{\partial x} + n + n^2\right)\right], \tag{9.29}$$

where
n-the number of photons in a state with dimensionless energy x;
$y = \int \frac{kT_e}{m_e c^2}\sigma_\tau n_p c dt$-Compton parameter.
It follows that the change in photon energy is exponential:

$$E = E_0 e^{-4y} \tag{9.30}$$

The Compton parameter is related to the amount of scattering processes:

$$y = \frac{kT_e}{m_e c^2} N \tag{9.31}$$

For our temperature range the number of scattering processes required to reduce the photon energy from $E_0 = 67.5MeV$ to $E_N = 1MeV$ is $N > 2,5 \times 10^3$. According to the Klein-Nishina formula:

$$\sigma_{KN} = \sigma_\tau f(x), \tag{9.32}$$

where
$\sigma_\tau = \frac{8\pi r_e^2}{3} = 6,7 \times 10^{-25} cm^2$-Thomson cross section,
$f(x)$-correction factor that takes into account relativistic effects,
$x = \frac{E}{m_e c^2}$-the dimensionless energy of a photon.
As the photon energy decreases, the cross-section value will approach the Thompson cross-section.
Taking into account the numerical solutions of the Kompaynets equation [10]:

$$< \sigma >= \sigma_\tau \left[1 - \frac{1}{2}\left(1 - \frac{m_e c^2}{E_0}\right)\right] \approx 0,5\sigma_\tau \approx 3,4 \times 10^{-25} cm^2 \tag{9.33}$$

$$\sigma_{eff} = N < \sigma > \geq 8.4 \times 10^{-22}\ cm^2 \tag{9.34}$$

Since the temperature of the domain decreases over time, it is necessary to consider various scenarios, taking into account all the processes possible under the given conditions:
$T \in [2.83 \times 10^8, 10^7]K$
The following processes are possible during this period:
·pair product during the interaction of annihilation and thermal photons and the further annihilation of an electron with a positron;
·multiple Compton scattering of an annihilation photon on a positron;
The decay of a negatively charged muon and the further annihilation of an electron with a positron.
In this case, the formation of pairs can be considered as the leading process affecting the mean free path of the annihilation photon. Total interaction cross section for an annihilation photon at a given temperature:

$$\sigma \approx \sigma_{pp} \approx 2,1 \times 10^{-28} cm^2. \tag{9.35}$$

$T \leq 10^7 K$. Starting from the moment when the temperature of the domain becomes equal to $T = 10^7 K$ ($t = 10^6 c$), the formation of positron-electron pairs becomes unlikely even taking into account the high-energy tail in the Planck distribution. In this case, two processes will take place inside the domain:
·multiple Compton scattering;
·decay of a negatively charged muon and the further annihilation of an electron with a positron.
At the same time, Compton scattering on a positron should be considered the leading process affecting the mean free path of an annihilation photon. The cross section for the annihilation photon in this case is:

$$\sigma = \sigma_k \approx 8.4 \times 10^{-22} cm^2. \tag{9.36}$$

9.4.3 Penetration depth of photons

The depth of photon penetration into the domain is determined by their mean free path, which can be calculated:

$$\lambda = \frac{1}{n\sigma}, \tag{9.37}$$

where
n-thermal photon/positron density,
σ-cross section.
In case of pair production:

$$\lambda_{pp} = \frac{1}{T^3\sigma_{pp}} \tag{9.38}$$

$$2 \times 10^2 \text{cm} \leq \lambda_{pp} \leq 5 \times 10^6 \text{cm}. \tag{9.39}$$

In case of Compton scattering:

$$n_p = \frac{\rho Z}{m_p}, \tag{9.40}$$

where Z=1-the average number of electrons per nucleon for a domain consisting mainly of antihydrogen and antihelium.
Then, penetration depth for the multiple Compton scattering:

$$\lambda_k = \frac{1}{T^3\eta Z\sigma_{eff}} \tag{9.41}$$

For $T = 10^7$K, $\sigma_{eff} = 8.4 \times 10^{-22}$ cm^2:
$\eta = 3 \times 10^{-12} : \lambda_k = 4 \times 10^{11}$cm;
$\eta = 1 \times 10^{-6} : \lambda_k = 3 \times 10^5$cm.
The obtained photon penetration depth can be compared with the domain size. Assuming spherical symmetry, we write the following inequality:

$$\lambda < R. \tag{9.42}$$

Since the formation of positron-electron pairs is possible only at temperatures of $T \geq 10^7$K, we determine the domain size in the time period $1,25 \times 10^3 \leq t \leq 10^6$c:
$R_{min} \approx 10^{13}$cm;
$R_{max} \approx 10^{17}$cm.
Comparing with the possible range for the path length of $10 \leq \lambda_{pp} \leq 10^5$cm, we can conclude that at any given time in the considered range, the penetration depth of annihilation photons is significantly less than the domain size. Thus, due to the high concentration of thermal photons in the radiation era, the interaction of photons will occur close to the domain boundary. At the same time, there will always be an area within the domain where the formation of pairs will not occur. Since Compton scattering is possible at any temperature, the inequality relating the path length to the domain size will look like this:

$$\frac{1}{T^3\eta Z\sigma_{eff}} < R \tag{9.43}$$

Considering the conditions under which Compton scattering is the dominant process and he expression found for the domain size:

$$\begin{cases} t > 10^6 c \\ t < \frac{Z 10^{20} \sigma_{eff} \eta^{\frac{2}{3}} M^{\frac{1}{3}}}{m_p^{\frac{1}{3}}} \approx \eta^{\frac{2}{3}} M^{\frac{1}{3}} \times 7 \times 10^6 c \end{cases}$$

9.5 Conclusion

In the course of the work, the main processes occurring at the boundary of the antimatter domain and inside it were considered.

The formation of electron-positron pairs during the interaction of a thermal photon with an annihilation photon should be considered a key process affecting the depth of photon penetration because of the concentration of thermal photons inside the domain during the radiation era. The formation of such pairs leads to the annihilation of positrons with electrons inside the domain. In addition, the decay of a negatively charged pion as an electron source should also be taken into account.

At $T \leq 10^7$K, the leading process occurring inside the domain is multiple Compton scattering of annihilation photons by positrons, as a result of which the photon energy will decrease.

For each of the processes described above, the interaction cross-section and the photon penetration depth were estimated. The values obtained were compared with the domain size at the corresponding time. According to the calculated values, it can be concluded that at $T \geq 10^7$K, the depth of photon penetration into the domain is significantly less than its size. In the case of Compton scattering, the path length of the annihilation photons will not exceed the size of the domain only in a limited time range, depending on the mass of the domain and its density.Such an assessment makes it possible to determine an nonhomogeneous region of the antimatter domain, within which various processes will occur that affect its chemical structure.

In the future, a more detailed description of the processes occurring inside the domain is planned, as they will make changes to the chemical structure of the domain. Based on the results obtained, the most accurate assessment of a homogeneous region is possible, which is not subject to changes as a result of processes occurring at the boundary of the domain with the horizon. The main task of further work is to study the evolution of the domain over time.

Acknowledgements

The work of M. K. was performed in Southern Federal University with financial support of grant of Russian Science Foundation № 25-07-IF.

References

1. M.Khlopov: Physics and Cosmology Beyond the Standard Models, Physics of Particles and Nuclei **54** (2023) 896–901.

2. T.Kneiske: Gamma-Ray Background: A Review, Chinese Journal of Astronomy & Astrophysics Supplement **8** (2008) 219–225.
3. A. Dolgov, K. Freese: Calculation of particle production by Nambu-Goldstone bosons with application to inflation reheating and baryogenesis, Physical Review D **51** (1995) 2693–2702.
4. A. Dolgov, K. Freese, R. Rangarajan and M. Srednicki: Baryogenesis during reheating in natural inflation and comments on spontaneous baryogenesis, Physical Review D **56** (1997) 6155–6165.
5. J. Garriga, A. Vilenkin, J. Zhang : Black holes and the multiverse, Journal of Cosmology and Astroparticle Physics **2016** (2016) 064-064.
6. H. Deng, J. Garriga, A. Vilenkin : Primordial black hole and wormhole formation by domain walls, Journal of Cosmology and Astroparticle Physics **2017** (2017) 050–050.
7. Y.Golubkov, M.Khlopov:Antiproton annihilation in the galaxy as a source of diffuse gamma background, Physics of Atomic Nuclei **64** (2001) 1821–1829.
8. L. Adiels, G. Backenstoss: Experimental determination of the branching ratios $p\bar{p} \rightarrow 2\pi^0, \pi^0\gamma$, and 2γ at rest, Z. Phys. C - Particles and Fields **35** (1987) 15–19.
9. V.B.Berestetskii, E.M. Lifshitz , L.P. Pitaevskii: *Quantum Electrodynamics*, Pergamon Press, New York, 1982.
10. G.B.Rybicki,A.P.Lightman: *Radiative Processes in Astrophysics*,Wiley-VCH,Weinheim,1979.
11. G.Cowan: *Statistical Data Analysis*,Clarendon Press,New York, 1998.
12. D.V.Griffiths: *Introduction to elementary particles*,John Wiley&Sons Inc, New York, 1987.
13. M.Khlopov, S.Rubin, A.Sakharov: Possible Origin of Antimatter Regions in the Baryon Dominated Universe, Physical Review D **62** (2003) 083505.
14. D.H. Perkins: *Introduction to High Energy Physics*,Cambridge University Press, Cambridge, 2000.
15. P. Marigo, L. Girardi, C.Chiosi, P.Wood: Zero-metallicity stars, Astronomy and astrophysics **371** (2001) 152–173.
16. O.Lecian, M.Khlopov: Analyses of Specific Aspects of the Evolution of Antimatter Glubular Clusters Domains, Astronomy Reports **65** (2021) 967—972.
17. O.Lecian, M.Khlopov:Baryon-Antibaryon Annihilation in the Evolution of Antimatter Domains in Baryon-Asymmetric Universe, Universe **7** (2021) 347.
18. O.Lecian, M.Khlopov:The Formalism of Milky-Way Antimatter-Domains Evolution, Galaxies **11** (2023) 50.
19. A.Dolgov: Antistars in the Galaxy, Moscow University Physics Bulletin **77** (2022) 89–92.
20. R. Omnès: Possibility of matter-antimatter separation at high temperatures, Physical Review Letters **23** (1969) 38–40.
21. R. Omnès: Matter-antimatter hydrodynamics; the coalescence effect, Astron. Astrophys **15** (1971) 275–284.
22. F.Stecker, D.Morgan, J. Bredekamp: Possible Evidence for the Existence of Antimatter on a Cosmological Scale in the Universe, Phys. Rev. Lett **27** (1971) 1469–1472.
23. F.Stecker: On the Nature of the Baryon Asymmetry,Nucl.Phys.B **252** (1985) 25–36.
24. G. Steigman: Observational tests of antimatter cosmologies, Ann. Rev. Astron. Astrophys **14** (1976) 339–372.
25. V.Chechetkin, M.Khlopov, M.Sapozhnikov, Ya.Zeldovich: Astrophisical aspects of antiproton interaction with He-4 (antimatter in the Universe), Phys.Lett.B **118** (1982) 329-332.
26. V.Chechetkin, M.Khlopov, M.Sapozhnikov: Antiproton interactions with light elements as a test of GUT cosmologies, Rivista Nuovo Cimento **5** (1982) 1–80.
27. A.Cohen, A. De Rujula, S.Glashow: A matter-antimatter universe, Astrophys. J **495** (1998) 539–549.

BLED WORKSHOPS
IN PHYSICS
VOL. 26, NO. 1

Proceedings of the 28th Workshop
What Comes Beyond . . . *(p. 114)*
Bled, Slovenia, July 6–17, 2025

10 Propagators for Negative-energy and Tachyonic Solutions in Relativistic Equations

Valeriy V. Dvoeglazov

UAF, Universidad Autonoma de Zacatecas,
Zacatecas 98061 Zac., Mexico

Abstract. It is well known that the relativistic equations have acausal solutions, which have generally been ignored. This is particularly true for higher spins. We consider spin 1/2 and spin 1 in this talk. We analyze corresponding propagators which may indicate if a theory is local or non-local. Negative-energy and tachyonic solutions are also considered. The conclusions are paradoxical in both spins.
Povzetek: Znano je, da imajo relativistične enačbe akavzalne rešitve, ki pa so prezrte. Še posebej to velja za spine, ki so večji od $\frac{1}{2}$. Avtor obravnava spin 1/2 in spin 1. Analizira ustrezne propagatorje, ki lahko pokažejo, ali je teorija lokalna ali nelokalna. Upošteva tudi rešitve z negativno energijo in tahionske rešitve. Zaključki so paradoksalni pri obeh spinih.

10.1 Introduction

The algebraic characteristic equations of the Dirac equation are $Det(\hat{p} - m) = 0$ and $Det(\hat{p} + m) = 0$, $\hat{p} = p^\mu \gamma_\mu$ for $u-$ and $v-$ 4-spinors of the spin-1/2. They have solutions with $p_0 = \pm E_p = \pm\sqrt{p^2 + m^2}$. The recent problems of superluminal neutrinos, negative-mass squared neutrinos, various schemes of oscillations including sterile neutrinos, require attention. Recently, the concept of the *bi-orthonormality* has been proposed; the (anti) commutation relations and statistics are assumed to be different for *neutral* particles. Next, Sakharov in 1967, Ref. [1], introduced the idea of two universes with opposite arrows of time, born from the same initial singularity (i.e. Big Bang). Next, Debergh et al. constructed (within the framework of the present-day quantum field theory) negative-energy fields for spin-1/2 fermions, Ref. [2]. Currently, the predominating consensus is the existence of dark matter (DM) and dark energy (DE) paradigms. Possible particle candidates have been proposed for the DM, but to date, the search for these candidates has not been successful. This suggests that something was missing in the foundations of relativistic quantum theories. Modifications appear to be necessary in the Dirac sea concept, and in the even more sophisticated Stueckelberg concept of backward propagation in time. The Dirac sea concept is intrinsically related to the Pauli principle. However, the Pauli principle is intrinsically related to the Fermi statistics and the anticommutation relations of fermions. We propose relevant modifications in the basics of relativistic quantum theory below.

The general scheme for construction of the field operator has been presented in [3]. In the case of the $(1/2,0)\oplus(0,1/2)$ representation we have:

$$\Psi(x)=\frac{1}{(2\pi)^3}\int d^4p\,\delta(p^2-m^2)e^{-ip\cdot x}\Psi(p)=$$
$$=\frac{1}{(2\pi)^3}\sum_h\int d^4p\,\delta(p_0^2-E_p^2)e^{-ip\cdot x}u_h(p_0,p)a_h(p_0,p)= \tag{10.1}$$
$$=\frac{1}{(2\pi)^3}\sum_h\int\frac{d^3p}{2E_p}\theta(p_0)$$
$$\left[u_h(p)a_h(p)|_{p_0=E_p}e^{-i(E_pt-p\cdot x)}+u_h(-p)a_h(-p)|_{p_0=E_p}e^{+i(E_pt-p\cdot x)}\right],$$

where $a_h, b_h^\dagger$ are the annihilation/creation operators, and in textbook cases

$$u_h(p)=\begin{pmatrix}\exp(+\boldsymbol{\sigma}\cdot\boldsymbol{\varphi}/2)\phi_R^h(0)\\ \exp(-\boldsymbol{\sigma}\cdot\boldsymbol{\varphi}/2)\phi_L^h(0)\end{pmatrix} \tag{10.2}$$

$\cosh(\varphi)=E_p/m$, $\sinh(\varphi)=|p|/m$. During the calculations above we had to represent $1=\theta(p_0)+\theta(-p_0)$ in order to get positive- and negative-frequency parts [4]. In the Dirac case we should assume the following relation in the field operator:

$$\sum_h v_h(p)b_h^\dagger(p)=\sum_h u_h(-p)a_h(-p)\,. \tag{10.3}$$

We need $\Lambda_{\mu\lambda}(p)=\bar{v}_\mu(p)u_\lambda(-p)$. By direct calculations, we find

$$-mb_\mu^\dagger(p)=\sum_\lambda\Lambda_{\mu\lambda}(p)a_\lambda(-p)\,. \tag{10.4}$$

Hence, $\Lambda_{\mu\lambda}=-im(\boldsymbol{\sigma}\cdot n)_{\mu\lambda}$, $n=p/|p|$. In the $(1,0)\oplus(0,1)$ representation a similar procedure leads to a different situation:

$$a_\mu(p)=[1-2(S\cdot n)^2]_{\mu\lambda}a_\lambda(-p)\,. \tag{10.5}$$

This signifies that in order to construct the Sankaranarayanan-Good field operator [5] to satisfy $[\gamma_{\mu\nu}\partial_\mu\partial_\nu-\frac{(i\partial/\partial t)}{E}m^2]\Psi(x)=0$, we need additional postulates. We have, in fact, $u_h(E_p,p)$ and $u_h(-E_p,p)$ originally, which satisfy the equations:

$$\left[E_p(\pm\gamma^0)-\boldsymbol{\gamma}\cdot p-m\right]u_h(\pm E_p,p)=0$$

. Due to the properties $U^\dagger\gamma^0U=-\gamma^0$, $U^\dagger\gamma^iU=+\gamma^i$ with the unitary matrix $U=\gamma^0\gamma^5$ we have in the negative-energy case: $\left[E_p\gamma^0-\boldsymbol{\gamma}\cdot p-m\right]U^\dagger u_h(-E_p,p)=0$. The explicit forms $\gamma^5\gamma^0u(-E_p,p)$ are different from the textbook "positive-energy" Dirac spinors. After the space inversion operation, we have ($R=(x\to-x,p\to-p)$)

$$PR\tilde{u}(p)=PR\gamma^5\gamma^0u_\uparrow(-E_p,p)=-\tilde{u}(p)\,, \tag{10.6}$$
$$PR\tilde{\tilde{u}}(p)=PR\gamma^5\gamma^0u_\downarrow(-E_p,p)=-\tilde{\tilde{u}}(p)\,. \tag{10.7}$$

Similar formulations have been presented in Refs. [6] and [7]. The group-theoretical basis for such doubling has been given in the papers by Gelfand, Tsetlin and Sokolik [8], who first presented the theory in the 2-dimensional representation of the inversion group in 1956 (later called "the Bargmann-Wightman-Wigner-type quantum field theory" in 1993). Barut and Ziino [7] proposed yet another model. They considered the γ^5 operator to be the operator of charge conjugation. Thus, the charge-conjugated Dirac equation has a different sign compared to the ordinary formulation:

$$[i\gamma^\mu \partial_\mu + m]\Psi^c_{BZ} = 0\,, \tag{10.8}$$

and the charge conjugation so defined applies to the whole system, fermion+electromagnetic field, $e \to -e$ in the covariant derivative. The superpositions of the Ψ_{BZ} and Ψ^c_{BZ} also give us the "doubled Dirac equation", the equations for $\lambda-$ and $\rho-$ self/anti-self charge conjugate spinors. The concept of doubling the Fock space has been developed in the Ziino program (cf. Refs. [8,9]) within the framework of the quantum field theory. In the BZ case the charge conjugate states are simultaneously the eigenstates of the chirality. Here, the relevant paper is Ref. [10]. It is straightforward to merge $u(p)$ and $v(p)$ spinors in one doublet of "positive energy" and $v(p)$ and $u(p)$ spinors, in another doublet of "negative energy" , as Markov and Fabbri did. However, the point of my paper is that both $u(p_0, p)$ and $v(p_0, p)$ contains contributions to both positive- and negative-energies, cf. Ref. [11].

We study the problem of construction of causal propagators in spin $S = 1/2$ and higher-spin theories. The hypothesis is: in order to construct analogues of the Feynman-Dyson propagator we actually need four field operators connected by the dual and parity transformation. We use the standard methods of quantum field theory. Thus, the number of components in the *causal* propagators is enlarged accordingly. The conclusion under discussion is that if we did not expand the number of components in the fields (in the propagator) we would not be able to obtain the causal propagator.

According to the Feynman-Dyson-Stueckelberg conception, the $S = 1/2$ causal propagator S_F has to be constructed on using the formula (*e.g.*, Ref. [12, p.91])

$$S_F(x_2, x_1) = \sum_\sigma \int \frac{d^3p}{(2\pi)^3} \frac{m}{E_p} \left[\theta(t_2 - t_1)\, a\, u^\sigma(p)\overline{u}^\sigma(p) e^{-ip\cdot x} + + \theta(t_1 - t_2)\, b\, v^\sigma(p)\overline{v}^\sigma(p) e^{ip\cdot x}\right], \tag{10.9}$$

where $x = x_2 - x_1$. In the spin $S = 1/2$ Dirac theory, it results in

$$S_F(x) = \int \frac{d^4p}{(2\pi)^4} e^{-ip\cdot x} \frac{\hat{p} + m}{p^2 - m^2 + i\epsilon}\,, \tag{10.10}$$

where $a = -b = 1/i$, ϵ defines the rules of work near the poles.

However, attempts to construct the causal covariant propagator in this way failed in the framework of the Weinberg theory, Ref. [13], which is a generalization of Dirac's ideas to higher spins. The propagator proposed in Ref. [14] is the causal propagator. However, the old problem remains: the Feynman-Dyson propagator is not the Green function of the Weinberg equation. As mentioned, the

covariant propagator proposed by Weinberg propagates kinematically spurious solutions [14]. We construct the propagator in the framework of the model given in Ref. [9]. The concept of the Weinberg field *doubles* has been proposed there. For the functions $\psi_1^{(1)}$ and $\psi_2^{(1)}$, connected with the former by the dual (chiral, $\gamma_5 = diag(1_{3\times3}), -1_{3\times3})$) transformation, the equations are[1]

$$(\gamma_{\mu\nu}p_\mu p_\nu + m^2)\psi_1^{(1)} = 0\,, \tag{10.11}$$

$$(\gamma_{\mu\nu}p_\mu p_\nu - m^2)\psi_2^{(1)} = 0\,, \tag{10.12}$$

with $\mu, \nu = 1, 2, 3, 4$. For the field functions connected with $\psi_1^{(1)}$ and $\psi_2^{(1)}$ by the $\gamma_5\gamma_{44}$ transformations the set of equations is written:

$$\left[\widetilde{\gamma}_{\mu\nu}p_\mu p_\nu - m^2\right]\psi_1^{(2)} = 0\,, \tag{10.13}$$

$$\left[\widetilde{\gamma}_{\mu\nu}p_\mu p_\nu + m^2\right]\psi_2^{(2)} = 0\,, \tag{10.14}$$

where $\widetilde{\gamma}_{\mu\nu} = \gamma_{44}\gamma_{\mu\nu}\gamma_{44}$ is connected with the $S = 1$ Barut-Muzinich-Williams $\gamma_{\mu\nu}$ matrices [16]. In the cited paper I have used the plane-wave expansion. Thus, $u_1^{(2)}(p) = \gamma_5\gamma_{44}u_1^{(1)}(p)$, $\overline{u}_1^{(2)} = \overline{u}_1^{(1)}\gamma_5\gamma_{44}$, $u_2^{(2)}(p) = \gamma_5\gamma_{44}\gamma_5 u_1^{(1)}(p)$ and $\overline{u}_2^{(2)}(p) = -\overline{u}_1^{(1)}\gamma_{44}$. Now we check whether the sum of the four equations

$$\begin{aligned}
&\left[\gamma_{\mu\nu}\partial_\mu\partial_\nu - m^2\right] * \\
&* \int \frac{d^3p}{(2\pi)^3 2E_p}\left[\theta(t_2-t_1)\,a\;u_1^{\sigma\,(1)}(p)\overline{u}_1^{\sigma\,(1)}(p)e^{ip\cdot x} + \theta(t_1-t_2)\,b\;v_1^{\sigma\,(1)}(p)\overline{v}_1^{\sigma\,(1)}(p)e^{-ip\cdot x}\right] + \\
&\left[\gamma_{\mu\nu}\partial_\mu\partial_\nu + m^2\right] * \\
&* \int \frac{d^3p}{(2\pi)^3 2E_p}\left[\theta(t_2-t_1)\,a\;u_2^{\sigma\,(1)}(p)\overline{u}_2^{\sigma\,(1)}(p)e^{ip\cdot x} + \theta(t_1-t_2)\,b\;v_2^{\sigma\,(1)}(p)\overline{v}_2^{\sigma\,(1)}(p)e^{-ip\cdot x}\right] + \\
&\left[\widetilde{\gamma}_{\mu\nu}\partial_\mu\partial_\nu + m^2\right] * \\
&* \int \frac{d^3p}{(2\pi)^3 2E_p}\left[\theta(t_2-t_1)\,a\;u_1^{\sigma\,(2)}(p)\overline{u}_1^{\sigma\,(2)}(p)e^{ip\cdot x} + \theta(t_1-t_2)\,b\;v_1^{\sigma\,(2)}(p)\overline{v}_1^{\sigma\,(2)}(p)e^{-ip\cdot x}\right] + \\
&\left[\widetilde{\gamma}_{\mu\nu}\partial_\mu\partial_\nu - m^2\right] * \\
&* \int \frac{d^3p}{(2\pi)^3 2E_p}\left[\theta(t_2-t_1)\,a\;u_2^{\sigma\,(2)}(p)\overline{u}_2^{\sigma\,(2)}(p)e^{ip\cdot x} + \theta(t_1-t_2)\,bv_2^{\sigma\,(2)}(p)\overline{v}_2^{\sigma\,(2)}(p)e^{-i\cdot px}\right] \\
&\quad = \delta^{(4)}(x_2 - x_1)
\end{aligned} \tag{10.15}$$

can be satisfied by a definite choice of a and b. Simple calculations give

$$\begin{aligned}
&\partial_\mu\partial_\nu\left[a\,\theta(t_2-t_1)\,e^{ip(x_2-x_1)} + b\,\theta(t_1-t_2)\,e^{-ip(x_2-x_1)}\right] = \\
&-\left[a\,p_\mu p_\nu\theta(t_2-t_1)\exp\left[ip(x_2-x_1)\right] + b\,p_\mu p_\nu\theta(t_1-t_2)\exp\left[-ip(x_2-x_1)\right]\right] \\
&+a\left[-\delta_{\mu4}\delta_{\nu4}\delta'(t_2-t_1) + i(p_\mu\delta_{\nu4} + p_\nu\delta_{\mu4})\delta(t_2-t_1)\right] \\
&\exp\left[ip\cdot(x_2-x_1)\right] + b\,\left[\delta_{\mu4}\delta_{\nu4}\delta'(t_2-t_1) + \right. \\
&\left. i(p_\mu\delta_{\nu4} + p_\nu\delta_{\mu4})\delta(t_2-t_1)\right]\exp\left[-ip(x_2-x_1)\right]\,;
\end{aligned} \tag{10.16}$$

We conclude as follows: the generalization of the notion of causal propagators is admitted by the use of the Wick-like formula for the time-ordered particle

[1] I have to use the Euclidean metrics here in order a reader to be able to compare the formalism with the classical cited works.

operators provided that $a = b = 1/4im^2$. It is necessary to consider all four equations, Eqs. (10.11)-(10.14). Obviously, this is related to the 12-component formalism, which I presented in Ref. [9].
Meanwhile, I propose to use the 8-component (or 16-component) spin-1/2 formalism in similarity with the 12-component formalism of this discussion. If we calculate

$$S_F^{(+,-)}(x_2,x_1) = \int \frac{d^3p}{(2\pi)^3}\frac{m}{E_p}\left[\theta(t_2-t_1)\, a\, \Psi_\pm^\sigma(p)\overline{\Psi}_\pm^\sigma(p)e^{-ip\cdot x} + \theta(t_1-t_2)\, b\, \Psi_\mp^\sigma(p)\overline{\Psi}_\mp^\sigma(p)e^{ip\cdot x}\right] =$$

$$= \int \frac{d^4p}{(2\pi)^4} e^{-ip\cdot x}\frac{(\hat{p}\pm m)}{p^2-m^2+i\epsilon},$$

(with Ψ doublets in the field operator) we readily come to the result that the corresponding Feynman-Dyson propagator gives the local theory in the sense:

$$\sum_\pm [i\Gamma_\mu\partial_2^\mu \mp m]S_F^{(+,-)}(x_2-x_1) = \delta^{(4)}(x_2-x_1), \tag{10.17}$$

even in the case of self/anti-self charge conjugate states. [2]
We should use the set of Weinberg propagators obtained in the perturbation calculus of scattering amplitudes. In Ref. [17] the amplitude for the interaction of two $2(2S+1)$ bosons has been obtained on the basis of the use of one field only, and it is obviously incomplete, see also Ref. [16]. But, it is interesting to note that the spin structure was proved there to be the same, whether we consider the two-Dirac-fermion interaction or the two-Weinberg $S = 1$-boson interaction. However, the denominator differs slightly ($1/\vec{\Delta}^2 \to 1/2m(\Delta_0 - m)$) from the fermion-fermion case in the cited papers [17], where $\Delta_0, \vec{\Delta}$ is the momentum-transfer 4-vector in Lobachevsky space. More accurate considerations of the fermion-boson and boson-boson interactions in the framework of the Weinberg theory have been reported elsewhere, Ref. [18]. So, the conclusion is: one can construct analogs of the Feynman-Dyson propagators for the $2(2S+1)$ model and, hence also local theories, provided that the Weinberg states are quadrupled ($S = 1$ case), and the neutral particle states are doubled.
What is the physical sense of the mathematical formalism presented here? In the $S = 1$ Weinberg equation [13] we have 12 solutions.[3] Apart from $p_0 = \pm E_p$ we have tachyonic solutions $p_0 = \pm E_p' = \pm\sqrt{p^2-m^2}$, *i. e.* $m \to im$. This is easily checked by using the algebraic equations and solving them with respect to p_0:

$$Det[\gamma^{\mu\nu}p_\mu p_\nu \pm m^2] = 0\,. \tag{10.18}$$

In constructing the field operator, Ref. [19] we generally need $u(-p) = u(-p_0,-p,m)$ which should be transformed to

[2] The dilemma of the (non)local propagators for the spin $S = 1$ has also been analyzed in Ref. [15] within the Duffin-Kemmer-Petiau (DKP) formalism or the Dirac-Kähler formalism [15].

[3] In Ref. [16] we have causal solutions only for the S=1 Tucker-Hammer equation.

$v(p) = \gamma^5 u(p) = \gamma^5 u(+p_0, +\mathbf{p}, m)$. On the other hand, when we calculate the parity properties we need $\mathbf{p} \to -\mathbf{p}$. The $u(p_0, -\mathbf{p}, m)$ satisfies

$$[\tilde{\gamma}^{\mu\nu} p_\mu p_\nu + m^2] u(p_0, -\mathbf{p}, m) = 0\,. \tag{10.19}$$

The $u(-p_0, \mathbf{p}, m)$ "spinor" satisfies:

$$[\tilde{\gamma}^{\mu\nu} p_\mu p_\nu + m^2] u(-p_0, +\mathbf{p}, m) = 0\,, \tag{10.20}$$

that is the same as above. The tilde signifies $\tilde{\gamma}^{\mu\nu} = \gamma_{00}\gamma^{\mu\nu}\gamma_{00}$ that is analogoues to the $S = 1/2$ case $\tilde{\gamma}^{\mu} = \gamma_0\gamma^{\mu}\gamma_0$. The $u(-p_0, -\mathbf{p}, m)$ satisfies:

$$[\gamma^{\mu\nu} p_\mu p_\nu + m^2] u(-p_0, -\mathbf{p}, m) = 0\,. \tag{10.21}$$

This case is opposite to the spin-1/2 case where the spinor $u(-p_0, \mathbf{p}, m)$ satisfies

$$[\tilde{\gamma}^{\mu} p_\mu + m] u(-p_0, +\mathbf{p}, m) = 0\,, \tag{10.22}$$

and $u(p_0, -\mathbf{p}, m)$,

$$[\tilde{\gamma}^{\mu} p_\mu - m] u(p_0, -\mathbf{p}, m) = 0\,. \tag{10.23}$$

In general we can use $u(-p_0, +\mathbf{p}, m)$ or $u(p_0, -\mathbf{p}, m)$ to construct the causal propagator in the spin-1/2 case. However, we do not need to use both because a) $u(-p_0, +\mathbf{p}, m)$ satisfies a similar equation to $u(+p_0, -\mathbf{p}, m)$ and b) we have an integration over $\mathbf{p}$. This integration is invariant with respect to $\mathbf{p} \to -\mathbf{p}$. The situation is different for spin 1. The tachyonic solutions of the original Weinberg equation

$$[\gamma^{\mu\nu} p_\mu p_\nu + m^2] u(p_0, +\mathbf{p}, m) = 0 \tag{10.24}$$

are just some solutions of the equation with the opposite square of $m \to im$). We cannot transform the propagator of the original equation (10.24) to that solely by a change of variables, as in the spin-1/2 case. The mass squared changes the sign, just as in the case of $v-$ "spinors". When we construct the propagator we have to take this solution into account, as well as the superposition $u(\mathbf{p}, m)$ and $u(\mathbf{p}, im)$, and corresponding equations. The conclusion is paradoxical: in order to construct the causal propagator for spin 1 we have to take acausal (tachyonic) solutions of homogeneous equations into account. It is not surprising that the propagator is not causal for the Tucker-Hammer equation because it does not contain the tachyonic solutions.

Acknowledgements

I acknowledge discussions with Prof. N. Debergh. I am grateful to Zacatecas University for a professorship. I appreciate discussions with participants of several recent Conferences.

References

1. A. D. Sakharov, (1967) *JETP Lett.* **5**, 24.
2. N. Debergh, J-P. Petit and G. D'Agostini, *J. Phys. Comm.* (2018) **2**, 115012.
3. N. N. Bogoliubov and D. V. Shirkov, *Introduction to the Theory of Quantized Fields.* 2nd Edition. (Nauka, Moscow. 1973).
4. V. V. Dvoeglazov, (2011) *J. Phys. Conf. Ser.* **284**, 012024, arXiv:1008.2242.
5. A. Sankaranarayanan and R. H. Good, jr., (1965) *Nuovo Cim.* **36**, 1303.
6. M. Markov, (1937) *ZhETF* **7**, 579; ibid. 603; (1964) *Nucl. Phys.* **55**, 130.
7. A. Barut and G. Ziino, (1993) *Mod. Phys. Lett.* A**8**, 1011; G. Ziino, (1996) *Int. J. Mod. Phys.* A**11**, 2081.
8. I. M. Gelfand and M. L. Tsetlin, (1956) *ZhETF* **31**, 1107; G. A. Sokolik, (1957) *ZhETF* **33**, 1515.
9. V. V. Dvoeglazov, (1998) *Int. J. Theor. Phys.* **37**, 1915.
10. L. Fabbri, (2014) *Int. J. Theor. Phys.* **53**, 1896, arXiv: 1210.1146.
11. G.-J. Ni, in "*Relativity, Gravitation, Cosmology: New Developments*". (Nova Science Pubs., NY, USA, 2010), p. 253.
12. C. Itzykson and J.-B. Zuber, *Quantum Field Theory.* (McGraw-Hill Book Co. New York, 1980).
13. S. Weinberg, (1964) *Phys. Rev.* B**133**, 1318.
14. D. V. Ahluwalia and D. J. Ernst, (1992) *Phys. Rev.* C**45**, 3010.
15. S. I. Kruglov, (2002) *Int. J. Theor. Phys.* **41**, 653, arXiv:hep-th/0110251. S. I. Kruglov, in *"Einstein and Hilbert: Dark Matter".* (Nova Science Pubs, NY, USA, 2012) p. 107, arXiv: 0912.3716.
16. R. H. Tucker and C. L. Hammer, (1971) *Phys. Rev.* D**3**, 2448.
17. V. V. Dvoeglazov, (1996) *Int. J. Theor. Phys.* **35**, 115.
18. V. V. Dvoeglazov, (2008) *J. Phys. Conf. Ser.* **128**, 012002.
19. J. A. Cazares and V. V. Dvoeglazov, (2023) Rev. Mex. Fis. **69**, 050703 1-9.

BLED WORKSHOPS
IN PHYSICS
VOL. 26, NO. 1

Proceedings of the 28th Workshop
What Comes Beyond . . . *(p. 121)*
Bled, Slovenia, July 6–17, 2025

11 Dark Matter as Screened ordinary Matter

C. D. Froggatt[1], H.B.Nielsen[2]

[1]School of Physics and Astronomy, Glasgow Universtity,[2]Niels Bohr Institute, Copenhagen, Denmark

Abstract. We look at our since long studied model for dark matter as being pearls of a speculated new vacuum containing highly compressed ordinary matter, with so much ordinary in it that the content of ordinary matter in the dark matter pearls dominate. Most dark matter models have the dark matter consisting mainly of new-physics-matter such as WIMPs being supersymmetric partners of possibly known particles or, as in Maxim Khlopov's model, a doubly negatively charged new-physics-particle with a helium nucleus attached. But usually the new-physics-matter makes up weightwise the major content. It is only in our model that the ordinary matter content in the dark matter dominates. We here expose some weak phenomenological evidence that, in truth, dark matter should be of the type with a dominant component of ordinary matter (weightwise), thus favouring as the typical example our previously so much studied vacuum type 2 model. The main such evidence is that we manage a fit to data in which the 3.5 keV X-rays, presumed to result from dark matter, come *both* from collisions of dark matter with dark matter and from dark matter with ordinary matter! Both mechanisms are of so similar an order of magnitude that they are both seen, indicating that their similarity is due to a significant similarity between dark with ordinary matter. The fact that the amounts of ordinary and dark matter *only* deviate by a factor 6 points in the same direction. Using the information obtained from this fitting, we develop our speculation that the main content weightwise of dark matter is ordinary matter to the very DAMA experiment. Actually we found three spots on the sky in which we fit the observed production of 3.5 keV X-rays with ordinary + dark scattering.

11.1 Introduction

Most theoretical models on the market for dark matter involve new physics in one form or the other, because seemingly the Standard Model alone cannot explain or even provide an appropriate possibility for a model for the dark matter. However, if the story about the several phases would be right, *we* would only need new physics in explaining that the parameters of the Standard Model were fine tuned to ensure that more than one phase of the vacuum would be competitive and present in Nature. In most models of dark matter, even according to weight, the major constituents of the dark matter are made up from new physics - i.e. speculated new particles such as is the case in typical WIMP models in which the new physics particles could be susy-partners of e.g. gauge bosons. Even in Maxim Khlopov's model in which the main ingredient is a doubly negatively charged particle, this new physics doubly negatively charged particle is expected to be so heavy that its mass dominates over the accompanying ordinary matter helium nucleus. The models that use axion like particles ALP's are of course also having dark matter

dominated by new physics in as far as no axion has as yet been found. But here of course division as to what the dark matter is made from after weight is a bit more delicate, in as far as the genuine constituents are supposed to be extremely light and the "coldness" of the dark matter is only supposed to come in by bose-statistics effects. But, in any case, it is mostly new physics making up the dark matter.

As far as we know it is only in our own model [1–15] that the dark matter is made up after weight dominantly from *ordinary matter*. We have to admit that the utterly important ingredient in our model, that the dark matter consists of bubbles of a new physics vacuum, is of course new physics. However we should keep in mind that if the computer analysis of what is called the Columbia plot should end up telling that there is a phase transition in QCD not hitherto taken so seriously, it could become old physics that we use.

The main attitude of the present article is to consider a slight generalization of our model in the sense of prescribing a class of models. In these models the dark matter is dominantly ordinary matter, only made "dark" in some way, such as e.g. having the nuclei very strongly screened so that they no longer interact with charged particles as strongly as usual atoms. In our model there is actually such a strong screening, because we make the assumption that the vacuum inside the pearls has a lower potential for nucleons than the outside vacuum. This then namely means that a lot of nuclei are pulled into the interior and pressed together by the tension in the domain wall separating the two different vacua - the latter is supposed to have a tension of the order of the third power of a few MeV - and the nuclei pull the electrons with them electrically. Thus we get a high electron density in the pearl and therefore a very strong screening. It is really this screening, which makes the nuclei interact so weakly with electrical objects or atoms, that ensures the dark matter in our model really can be arranged to interact so little that we must call it "dark".

Our model of a dark matter particle or pearl is a cluster of screened nuclei kept inside a skin or domaine wall.

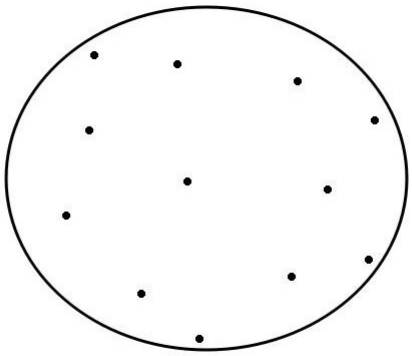

11.2 Interference factor

Let us list and compare some numbers, which we can collect concerning the non-gravitational observations of dark matter, and seek to put them in the form of a ratio $\frac{\text{“}\sigma''}{m}$ of an effective cross section with significant scattering angle “σ” divided by the mass of the particle having this cross section m.
For a given density ρ of a medium in which a particle penetrates, the stopping length is at least crudely given by

$$\text{“stopping length”} \approx \frac{1}{\frac{\text{“}\sigma''}{m} * \rho} \tag{11.1}$$

and so, for a fixed medium, we can consider this ratio $\frac{\text{“}\sigma''}{m}$ a measure for stopping power. We take as our starting point the approximation that the dark matter pearl consists effectively just of a swarm of strongly electrically screened nuclei, which separately scatter independently - so we shall first consider the interference between hitting different constituent nuclei in the next paragraph. In this approximation we shall have this ratio being the same for clusters of the constituents as for the constituent nucleus itself as long, of course, that the m in the denominator is the mass of the cluster.
But now the crucial point is that for elastic scattering of a dark matter pearl there will occur interference between all the cases of a constituent from one of the two colliding pearls meeting a constituent from the other one. Also if an ordinary matter nucleus hits a dark matter pearl we have for the elastic scattering interference between the hitting of all the constituents.
Thus we have interference corrections to this ratio $\frac{\text{“}\sigma''}{m}$:

$$DM + DM \to DM + DM, \text{ correction } \frac{\text{“}\sigma''}{m} \to \frac{\text{“}\sigma''}{m} * \text{“\# nuclei in DM pearl”}^2$$
$$DM + OM \to DM + OM, \text{ correction } \frac{\text{“}\sigma''}{m} \to \frac{\text{“}\sigma''}{m} * \text{“\# nuclei in DM pearl”}$$

How to think on our quantities For the following it may be good to have in mind that given the quantity $\frac{\sigma}{m}$, the stopping power is crudely invariant under splitting up of the particles in the medium into essentially non-interacting constituents, as for example the splitting

$$DM \text{ split into } \; scnu + scnu + ... + scnu \tag{11.2}$$

where $scnu$ stands for screened nuclei.
For seeing this one has to have in mind that a hit particle typically gets a velocity of the order of the velocity of the penetrating particle and thus the momentum loss becomes of the order of $m_{hit}v$. Of course non-relativistically the number n of constituents, $scnu$'s, will equal

$$n = \frac{m_{DM}}{m_{scnu}}. \tag{11.3}$$

where $scnu$ stands for screened nuclei.

So

$$\text{whether } \frac{\sigma}{m} \text{ taken to } \frac{\sigma_{DM+DM}}{m_{DM}} \text{ or } \frac{\sigma_{DM+scnu}}{m_{DM}}$$

$$\text{“stopping f.”} \propto \frac{\sigma_{DM+DM}}{m_{DM}} * \rho_{\#\,DM} * v m_{DM} \text{ or } \frac{\sigma_{DM+scnu}}{m_{DM}} * \rho_{\#\,scnu} * v m_{scnu}$$

$$\text{I.e. “stopping f.”} \propto \frac{\sigma_{DM+DM}}{m_{DM}} \rho_{mass} v \text{ or } \frac{\sigma_{DM+scnu}}{m_{DM}} * \rho_{mass} * v,$$

$$\text{I.e. “stopping f.”} \propto \frac{\sigma}{m_{DM}} \rho_{mass} v \text{ or } \frac{\sigma}{m_{DM}} * \rho_{mass} * v$$

I.e. you get the same stopping force “stopping f.” in a model wherein the DM are genuine particles and $\sigma = \sigma_{DM+DM}$ as in our model in which the dark matter pearls are ideally loosely bound constituents, called $scnu$, provided you put $\sigma = \sigma_{DM+scnu}$ and provided you ignore quantum mechanics, meaning the interference between the scattering on different constituents.
Also the construction of the ratio $\frac{\sigma}{m}$ is invariant under the splitting of the particle into its constituents, say $scnu$'s, by going to the ideally loosely bound cluster, in the sense that

$$\frac{\sigma_{DM+something}}{m_{DM}} = \frac{\sigma_{scnu+something}}{m_{scnu}} \text{(classically)}. \tag{11.4}$$

The above results were only true **classically**, but let us postpone the quantum discussion till we have settled how to interpret the Correa data.

11.2.1 Correa

The self-interaction of the dark matter, as extracted from the dwarf galaxy studies of Camilla Correa [16], are already in the form we go for, in as far as we believe she found

$$\frac{\text{“}\sigma''}{m}_{Correa} = \frac{\text{“}\sigma''_{DM+DM}}{m_{DM}} \tag{11.5}$$

$$\approx \frac{K}{v^2} \tag{11.6}$$

$$\text{where } K = 10^{10} m^4/s^2/kg \tag{11.7}$$

$$\text{With } 1m = 5.07 * 10^{15} GeV^{-1} 1kg = 5.625 * 10^{26} GeV :$$
$$K = 5.08 * 10^{-13} GeV^{-3}/(m^4/s^2/kg) * 10^{10} m^4/s^2/kg$$
$$= 5.08 * 10^{-3} GeV^{-3} \tag{11.8}$$

$$\text{With } v = 3.2 * 10^5 m/s \text{ then } \frac{\text{“}\sigma''}{m}|_{DM+DM} = 0.1 m^2/kg, \tag{11.9}$$

$$= 4.57 * 10^3 GeV^{-3} \tag{11.10}$$

Process

$$DM + DM \to DM + DM(\text{elastic}) \tag{11.11}$$

But now we are in the present article studying the hypothesis, that the dark matter pearls are ideally loosely bound clusters of some screened nuclei $scnu$, so that what really happens in the collisions of dark matter pearls is the collisions of these constituents. The effect of shadowing is supposed small. Now we have to contemplate what Correa by her analysis has really measured, we must expect that she has indeed measured how fast the dark matter particles in the various dwarf galaxies are being stopped by the dark matter density present. That means that, provided our model of loose bound states is right, we can interpret her values for the ratio $\frac{\sigma}{m}$ as

$$\frac{\sigma}{m}|_{Correa} = \frac{\sigma_{DM+scnu}}{m_{DM}} \tag{11.12}$$

$$= \frac{\sigma_{scnu+scnu}}{m_{scnu}}(\text{classically}). \tag{11.13}$$

But now switching on quantum mechanics, so that one has positive interference between all the n^2 possibilities for an $scnu$ in one pearl to interact with an $scnu$ in the other pearl in the collision, the ratio f for the Correa quantity $\frac{\sigma}{m}|_{Correa}$ above gets screwed up by a factor n^2 to

$$\frac{\sigma}{m}|_{Correa} = n^2 * \frac{\sigma_{scnu+scnu}}{m_{scnu}}(\text{quantum mechanically}). \tag{11.14}$$

11.2.2 Cline-Frey

From the Cline-Frey fit [17] we extracted an average for the numbers, which we believed could be fitted with DM+DM scattering, while we left out the items supposedly rather due to mainly DM+OM scattering (here OM means ordinary matter).

$$\left(\frac{N\sigma_{DM+DM\rightarrow---+3.5keV}}{m_{DM}^2}\right)_{exp} = (1.0 \pm 0.2) * 10^{23} cm^2/kg^2 \tag{11.15}$$

$$= (1.0 \pm 0.2) * 10^{19} m^2/kg^2. \tag{11.16}$$

Taking it that the dark matter consists of subparticles - presumably nuclei - with masses Am_N and kinetic energies thus $Am_N v^2/2$ we may, if all the energy goes into the 3.5 keV line, produce per collision of the subparticle get N photons of 3.5 keV, where

$$N \approx Am_n * v^2/(2 * 3.5keV) \tag{11.17}$$

$$\text{and } \frac{\sigma}{M}|_{per\ 3.5keV} = \left(\frac{N\sigma}{M^2}\right) * 3.5keV/v^2 \tag{11.18}$$

$$= 10^{19} m^2/kg^2 * (3.5 * 1.6 * 10^{-19} * 10^3 J/v^2) \tag{11.19}$$

$$= 3500 J m^2/kg^2/v^2. \tag{11.20}$$

For $v = 3.2 * 10^5 m/s$ we then have

$$\frac{\sigma}{M}|_{per\ 3.5keV} = 3.5 * 10^{-7} m^2/kg. \tag{11.21}$$

Process

$$DM + DM \to DM + DM + ph(3.5keV) + ... \tag{11.22}$$

Notice that in (11.18) above the ansatz for the mass $M = Am_n$ dropped out, and so $\frac{\sigma}{M}|_{per\ 3.5keV}$ gives the number 3.5 keV photons produced by penetration of $1kg/m^2$.
Actually we can write the quantity measured by the Cline-Frey analysis in the following three ways **classically**:

$$\left(\frac{N\sigma_{\to...+3.5keV}}{M^2}\right)_{exp} = (1.0 \pm 0.2) * 10^{23} cm^2/kg^2 \tag{11.23}$$

$$= (1.0 \pm 0.2) * 10^{19} m^2/kg^2 \tag{11.24}$$

$$= \frac{\frac{1/2 * m_{DM} * v^2}{3.5keV} * \sigma_{DM+DM\to...3.5keV}}{m_{DM}^2} \tag{11.25}$$

$$= \frac{\frac{1/2 * m_{scnu} * v^2}{3.5keV} * \sigma_{DM+scnu\to...3.5keV}}{m_{DM} m_{scnu}} \tag{11.26}$$

$$= \frac{\frac{1/2 * m_{scnu} * v^2}{3.5keV} * \sigma_{scnu+scnu\to...3.5keV}}{m_{scnu}^2} \tag{11.27}$$

For instance the last version simplifies to

$$\left(\frac{N\sigma_{\to...+3.5keV}}{M^2}\right)_{exp} = \frac{\frac{1/2 * v^2}{3.5keV} * \sigma_{scnu+scnu\to...3.5keV}}{m_{scnu}} \tag{11.28}$$

$$\tag{11.29}$$

This was still **classically**.
When we switch on quantum mechanics we get positive interference between scattering on the different constituents $scnu$ in the same dark matter pearl DM, unless the $scnu$ participating got marked in some way so as to make the interference impossible. We must suppose that, once an excitation of the electron-system has happened by a hole quasi-electron pair having been produced, one of the $scnu$'s hitting each other has been marked so that there remain for these 3.5 keV producing events a positive interference between the $scnu$ particles in just **one** of the two colliding DM's. Thus only one factor n (the number of constituents) will occur as the correction of the classical result to the quantum one:

$$\left(\frac{N\sigma_{\to...+3.5keV}}{M^2}\right)_{exp} = n * \frac{1/2 * v^2}{3.5keV} * \frac{\sigma_{scnu+scnu\to...3.5keV}}{m_{scnu}} \tag{11.30}$$

If $\frac{\sigma_{scnu+scnu\to...+3.5keV}}{m_{scnu}}$ has the inverse square dependence on the velocity which we like to assume

$$\frac{\sigma_{scnu+scnu\to...+3.5keV}}{m_{scnu}} = \frac{K_{scnu+scnu\to...+3.5keV}}{v^2}, \tag{11.31}$$

then

$$\left(\frac{N\sigma_{\to...+3.5keV}}{M^2}\right)_{exp} = \frac{1}{2 * 3.5keV} * n * K_{scnu+scnu\to...+3.5keV}. \tag{11.32}$$

11.2.3 Reaching DAMA

If we assume that the $\frac{\text{“}\sigma''}{M}$ for dark matter on ordinary matter is just so that a dark matter particle gets essentially stopped just in the depth of DAMA of 1400 m, and an estimated stone density of $\rho = 3000\text{kg}/\text{m}^3$, then

$$\frac{\text{“}\sigma''_{DM+OM}}{M} \simeq \frac{1}{1400\text{m} * 3000\text{kg}/\text{m}^3} \tag{11.33}$$

$$= \frac{1}{4.2 * 10^6\text{kg}/\text{m}^2} \tag{11.34}$$

$$= 2.38 * 10^{-7}\text{m}^2/\text{kg}. \tag{11.35}$$

Process

$$DM + OM \rightarrow DM + OM(\text{mainly elastic}) \tag{11.36}$$

Strictly speaking we should not take it that the stopping length just makes the dark matter pearls stop at the depth 1400m of DAMA-LIBRA, since that would be an unlikely coincidence. Rather we should take it that the stopping length is so much smaller than the depth of DAMA that the probability of the particles stopping just at DAMA - and thus giving a seasonal modulated signal at DAMA - could just explain the lack of efficiency (our factor $1/2 * 10^9$ in (11.45) below leaves a factor 10^9 to be explained by the deviation of the DAMA depth from the depth where the highest number of pearls stop).
Let us also remark that we shall see in section 11.3 below that from the sign of the seasonal effect observed in DAMA-LIBRA it is needed that the depth of DAMA is deeper than the dominant stopping depth.
Classically we get the same penetration depth, if we think of m_{OM} as the one divided out i.e. $M = M_{om}$, whether we use,

$$\frac{\text{“}\sigma''_{DM+OM}}{m_{OM}} \text{ or } \frac{\text{“}\sigma''_{scnu+OM}}{m_{OM}}, \tag{11.37}$$

because the higher number of $scnu$ is compensated for by a lower momentum loss by using $m_{scnu}v$ than $m_{DM}v$. Also oppositely if we think of the divided out M as being put m_{DM} or m_{scnu} the difference gets divided away classically. But quantum mechanically we have an interference between the n constituent $scnu$'s in the same pearl, and thus

$$\frac{\text{“}\sigma''_{DM+OM}}{M} \simeq \frac{1}{1400\text{m} * 3000\text{kg}/\text{m}^3} \tag{11.38}$$

$$= \frac{1}{4.2 * 10^6\text{kg}/\text{m}^2} \tag{11.39}$$

$$= 2.38 * 10^{-7}\text{m}^2/\text{kg}. \tag{11.40}$$

$$= n\frac{\text{“}\sigma''_{scnu+OM}}{m_{scnu}}. \tag{11.41}$$

11.2.4 The three exceptional places

In three exceptional places we claim that the 3.5 keV line arises mainly from dark matter colliding with ordinary matter. We speculated then on physical grounds in our rather thinly filled dark matter pearls that, counted after weight, the rate of 3.5 keV line photon production should be the same for $DM + DM$ as for $DM + OM$. We found support for this assumption of approximate equality most simply by believing to have found that in the outskirts of the Perseus Galaxy Cluster, where the ratio of dark to ordinary matter is close to unity, there is a "kink" signalling that the dominant production mechanism for 3.5 keV photons shifts from $DM + DM$ to $DM + OM$. Believing this we assume that dark matter being hit by nuclei inside another dark matter particle or by nuclei just present in the ordinary matter would have the same cross section σ per 3.5 keV photon produced. Interpreting the M in the denominator as the mass of the dark matter particle, that here could either hit an ordinary or a dark-matter-contained nucleus, we should be allowed to use the same $\frac{"\sigma''}{M}$ for the dark matter hitting ordinary matter as it hitting dark matter. Thus

$$\frac{"\sigma''}{M} = 3.5 * 10^{-7} m^2/kg. \tag{11.42}$$

Process

$$DM + OM \rightarrow DM + OM + ph(3.5keV) + ... \tag{11.43}$$

This means we just get the same as we already described under Cline Frey.
Even quantum mechanically we get the same as under Cline-Frey because we suppose that in the Cline Frey case there could anyway only be interference in one of the two colliding dark matter pearls, because of the constituent $scnu$ in one of them was marked by having made a 3.5 keV X-ray or more correctly some hole electron pair.
Thus we have again so to say

$$\left(\frac{N\sigma_{DM+OM\rightarrow...+3.5keV}}{M^2}\right)_{exp} = n * \frac{1/2 * v^2}{3.5keV} * \frac{\sigma_{OM+scnu\rightarrow...3.5keV}}{m_{scnu}} \tag{11.44}$$

11.2.5 The efficiency of getting 3.5 keV line in DAMA

We have estimated how big a fraction of the kinetic energy of the incoming dark matter would be observed as signals in the DAMA-LIBRA experiments and obtained the result that it is about $2 * 10^{-9}$ times the impact kinetic energy of the dark matter coming in. In the philosophy that all the kinetic energy gets converted into the 3.5 keV line - which is of course an overestimate - we would here in the present over-idealized discussion take it that the only other way to dispense with the kinetic energy is by stopping the dark matter by elastic scattering. Then we would have to say that the elastic scattering for $DM + OM$ should be $\frac{1}{2} * 10^9$ times bigger than the inelastic one (by our assumption of only the 3.5 keV line taking the energy meaning $DM + OM \rightarrow DM + OM + ph(3,5keV) + ...$).

So we would conclude in terms of the processes we study

$$\frac{\frac{\text{“}\sigma''}{M}|_{\mathrm{DM+OM(elastic)}}}{\frac{\text{“}\sigma''}{M}|_{\mathrm{DM+OM\ (with\ ph(3.5keV))}}} = \frac{1}{2} * 10^9, \tag{11.45}$$

if all inelastic energy is converted into 3.5 keV X-rays But this is not at all likely for the supposed low energies / low velocities of the dark pearls (see below in section 11.3), because for low velocities the collisions between the lighter nuclei can hardly deliver 3.5 keV at velocities such as 300 km/s. For example:

$$\text{For } 300\,\mathrm{km/s} : \text{thresholds} :$$
$$\text{proton H} : 1/2\,keV \tag{11.46}$$
$$\text{helium He} : 2\,keV \tag{11.47}$$
$$\text{carbon C} : 6\,keV \tag{11.48}$$
$$\text{sodium Na} : 11.5\,keV \tag{11.49}$$
$$\text{iodine I} : 63.5\,keV \tag{11.50}$$
$$\text{Thresholds for } 3.5\,keV$$
$$\text{proton H} : v = 300\,\mathrm{km/s} * \sqrt{7} = 794\,\mathrm{km/s} \tag{11.51}$$
$$\text{helium He} : v = 300\,\mathrm{km/s} * \sqrt{3.5/2} = 397\,\mathrm{km/s} \tag{11.52}$$
$$\text{carbon C} : v = 300\,\mathrm{km/s} * \sqrt{3.5/6} = 229\,\mathrm{km/s} \tag{11.53}$$
$$\text{sodium Na} : v = 300\,\mathrm{km/s} * \sqrt{3.5/11.5} = 166\mathrm{km/s} \tag{11.54}$$
$$\text{iodine I} : v = 400\mathrm{km/s} * \sqrt{3.5/63.5} = 70\mathrm{km/s} \tag{11.55}$$

If the dark matter pearls mainly consist of light nuclei - below carbon say - and we notice that for protection against the cosmic rays the underground experiments have to be of the order of a km down from the earth surface, then all the experiments are under the threshold for easily producing 3.5keV. Thus this production is easily very strongly suppressed even what the non-modulating part of the signal is concerned. If we take it that the modulating velocity of the Earth of the order 30 km/s is about 10% of the typical galactic velocity, the energy at the tails of the dark pearl tracks, which are responsible for the modulation observation have only about 10% of the energy of the incoming dark matter beam and so the typical velocity $300\mathrm{km/s}/\sqrt{10} = 95\mathrm{km/s}$.
Ratio of rates for **low velocity dark matter pearls** :

$$\mathrm{DM} + \mathrm{OM} \rightarrow \mathrm{DM} + \mathrm{OM} \tag{11.56}$$
$$\mathrm{DM} + \mathrm{OM} \rightarrow \mathrm{DM} + \mathrm{OM} + \mathrm{ph}(3.5\mathrm{keV})... \tag{11.57}$$

and for this we have found the $1/2 * 10^9$; but for the **high velocity presumably more relevant for the galactic clusters included by Cline and Frey this ratio could be of order unity.**

Comment on the Efficiency Let us immediately comment that we shall not take this efficiency as seen by DAMA as coming from the whole track with the typical velocity of the dark matter particles being say 300 km/s. In fact we namely show that the part of the track that matters for the seasonal variation to be only the tiny tail, where the velocity is very slow such as to be almost stopping. The point is that we argue in section 11.3 that in the region of a track in which the velocity is high the energy deposited per unit length of the track arising from the stopping is constant independent of the velocity. Then you cannot see the velocity on the track except at the very end, where a fast track extends longer than a slow particle track. This means that the seasonal varying rate observed at DAMA will correspond to very low velocity dark matter and thus likely to be below the threshold in energy for making the 3.5 keV line. Then production of a 3.5 keV photon would only come by statistical fluctuations and might be estimated by some Boltzmann factor, which could give a very low rate.

11.2.6 Discussion

The main idea to seek some regularity in the above values of $\frac{\text{“}\sigma''}{M}$ is to think of the dark matter pearl as effectively being a collection of charged but screened nuclei. The number is really only to be an effective one and probably this effective number of nuclei is much smaller than the true number of nuclei. In fact we shall rather think of the nuclei and their associated electrons forming some electric field and that this electric field around the dark matter pearl is approximated, say, by an effective nucleus with an appropriate number of charges.

We may imagine that the different say nuclei in the effective collection have their interactions interfere maximally constructively.Then the total cross section for a process rate will be increased by the number of effective particles n. In fact, if there is no interference the n constituents will just produce n separate contributions, but if we have interference the total contribution will be n^2 times a single contribution and thus $n^2/n = n$ times what we have without interference.

Now we shall also have in mind, that if we have up to two dark matter pearls involved in the scattering, then we can have interference involving the constituents of both pearls and thus, if each has n effective constituents, get an interference correction up to even n^2,

We expect that, if we have a 3.5 keV photon in the final state, it may have come from one specific nucleus in one af the dark matter pearls colliding and thus prevent the presence of the factor n^2 from interference in both the dark matter particles. The observability of the X-ray might make the emitting nucleus observed and thus prevent the interference in the pearl containing the nucleus. Also of course we can at most get as many factors n as there are dark matter pearls in the collision.

For the presumably elastic scattering, as observed in Correa's dwarf galaxy studies, we should expect to have a factor n^2 compared to having no interference. If we believe that the stopping of the dark matter reaching DAMA just stops after 1400 m, due to elastically dominated DM+OM collisions, we clearly expect the dominant term to have just one factor n from interference going on in the only dark matter pearl in the collision(s).

Similarly we expect that the Cline-Frey value for DM+DM inelasticity giving 3.5 keV radiation will contain an interference enhancement factor n. This is because the presence of the 3.5 keV quantum has prevented - by it potentially being associated with pointing out a specific nucleus in the pearl as the one hit - the interference among the nuclei in one of the two colliding dark matter pearls.
These three items or rather the last two, DAMA versus Cline-Frey, can be considered a success for our hypothesis that the cross section relative to mass $\frac{\text{“}\sigma''}{M}$ should be the same when exchanging OM and DM. Also the quantum interference correction, n in this case, does not distinguish between OM and DM. The values of $\frac{\text{“}\sigma''}{M}$ for DAMA and for Cline-Frey are indeed very close, $(3.5 \text{ and } 2.38) * 10^{-7} m^2/kg$ for respectively Cline Frey and DAMA.
Using the Correa value for $\frac{\text{“}\sigma''}{M}$ we then get $n \simeq \frac{0.1 m^2/kg}{3*10^{-7} m^2/kg} = 3 * 10^5$ or for the ratio of the σ/m for the two supposedly elastic processes (11.9, 11.35),

$$\frac{\frac{\sigma}{m}|_{Correa}}{\frac{\sigma}{m}|_{DAMA}} = \frac{0.1 m^2/kg}{2.38 * 10^{-7} m^2/kg} \tag{11.58}$$

$$= 4.2 * 10^5. \tag{11.59}$$

This ratio should be equal to the number of “atoms” in a dark matter pearl, since we want to explain the difference between the two numbers as due to (positive) interference between n “atoms” in such a pearl.
We should be able to use this “measurement” of the number n of constituent nuclei in the pearl to estimate the size of the pearl, at least if we somehow guess the atomic weight of the constituent nuclei.
By requiring the dark matter pearl to have a homolumo gap of 3.5 keV responsible for the observed X-ray line and thus a Fermi momentum $p_f = 3.3 MeV$ for the electrons inside the pearl, a crude dimensional argument suggests the density of the pearl material is $\rho_B = 5.2 * 10^{11} kg/m^3$. Using this value we obtain estimates for the radius R and the cube root of the surface tension $S^{1/3}$ of the pearl for two different proposals for the atomic weight A of the constituents:

$$\text{And for } A = 12: \; M_{pearl} = A * 1.66 * 10^{-27} kg * 4.2 * 10^5 \tag{11.60}$$

$$= 8.37 * 10^{-21} kg \tag{11.61}$$

$$\text{giving “Volume”} = \frac{8.37 * 10^{-21} kg}{5.2 * 10^{11} kg/m^3} \tag{11.62}$$

$$= 1.61 * 10^{-32} m^3 \tag{11.63}$$

$$\text{so radius } R = \sqrt[3]{1.61 * 10^{-32} m^3 * 3/(4\pi)} \tag{11.64}$$

$$= \sqrt[3]{3.84 * 10^{-33} m^3} \tag{11.65}$$

$$= 1.57 * 10^{-11} m; \tag{11.66}$$

$$\text{Extrapolating from } R = 10^{-10} m \sim S^{1/3} = 8 MeV \tag{11.67}$$

$$S^{1/3} = 8 MeV * \sqrt[3]{\frac{1.57 * 10^{-11} m}{10^{-10} m}} \tag{11.68}$$

$$= 4.3 MeV \tag{11.69}$$

$$\tag{11.70}$$

$$\text{For } A = 100: \; M_{pearl} = A * 1.66 * 10^{-27}\text{kg} * 4.2 * 10^{5} \tag{11.71}$$
$$= 6.97 * 10^{-20}\text{kg} \tag{11.72}$$
$$\text{giving "Volume"} = \frac{6.97 * 10^{-20}\text{kg}}{5.2 * 10^{11}\text{kg/m}^3} \tag{11.73}$$
$$= 1.34 * 10^{-31}\text{m}^3 \tag{11.74}$$
$$\text{so radius R} = \sqrt[3]{1.34 * 10^{-31}\text{m}^3 * 3/(4\pi)} \tag{11.75}$$
$$= \sqrt[3]{3.20 * 10^{-32}\text{m}^3} \tag{11.76}$$
$$= 3.17 * 10^{-11}\text{m}; \tag{11.77}$$
$$S^{1/3} = 8MeV * \sqrt[3]{\frac{3.17 * 10^{-11}\text{m}}{10^{-10}\text{m}}} \tag{11.78}$$
$$= 5.45MeV \tag{11.79}$$

These values of the cube root of the tension $S^{1/3}$ should be compared with the value obtained from the straight line fit in the article ´´Ontological fluctuating Lattice" [18–21] in the same issue as this article of the Bled Workshop Proceedings. In fact since the action for a surface (in Minkowski space a three dimensional track) in the lattice theory is supposed to be related to the third power of the link size a, i.e. the coefficient to the three dimensional surface action is proportional to a^3, we expect in the straight line rule for the energy scales, that the energy scale for the surface tension $S^{1/3}$ shall be three steps, meaning three factors of 220.584, under the "fermion tip" scale, which is at $2.06 * 10^4 GeV$. That is to say we expect from the straight line model the cubic root of the tension to be:

$$S^{1/3} = \frac{\text{"fermion tip"}}{(\text{"step} - \text{factor"})^3} \tag{11.80}$$
$$= \frac{2.06 * 10^4 GeV}{220.584^3} \tag{11.81}$$
$$= 1.92MeV. \tag{11.82}$$

The exact match of this prediction would e.g. be reached with an even lower A than our 12, but one shall consider it a good agreement taking into account the crude calculation.

11.2.7 Suggested Solution

Ignoring at first the efficiency number above, we can understand the numbers above like this:
There are two different electric fields associated with the dark matter pearls

- There is a screened Coulomb potential around each nucleus in the pearl. Because of the high electron density it is quite short range.
- There is Coulomb field very similar to that of huge nucleus sitting in its atom. It is field much like the one in a rather thin spherical condenser. This is caused

by the pull of the pearl skin on the nuclei inside this skin. They are pressed inward towards the center of the pearl by the skin, and for balance there has to be electrons outside driving the nuclei the opposite way.

It is now the idea that in the collisions observed by Correa in the dwarf galaxies it is the field from the electrons just outside the skin and the nuclei just inside the skin that dominates and that the scattering is mainly elastic. The field is built up from many nuclei etc. and from the point of view of these nuclei the scattering becomes the result of strong interference between the different nucleus combinations. This strong interference allows the interaction of just elastic scattering of dark matter on dark matter to become appreciably larger than processes without this interference. It can only be for this elastic scattering of two dark matter pearls that you can expect these fields in the surroundings to work in full interference, because having only one dark matter pearl when we look for DM + OM can at least not have the n^2 interference and also the interference will be spoiled by the excitation of the pearl which would probably carry sign of one or another region in the pearl having been excited.
In fact we shall suggest that the types of scatterings listed above with 3.5 keV photon production or DM+OM scattering shall only have essential interference between screened nuclei inside *one* dark matter pearl, so that the quantum enhancement will only be one factor n, and not n^2 as for the dark + dark elastic scattering (the Correa case). So we should in principle be able to calculate DM+OM scattering with 3.5 keV production as if we had only separate screened nuclei instead of dark matter, except that we should multiply by a single n factor namely only for the interference between the nuclei inside just one of the dark matter pearls.
However, there is a threshold effect that may spoil completely this simple thought when concerning the production of the 3.5 keV line: If the OM nuclei hitting the dark matter are not sufficiently fast, it will be kinematically impossible to reach the kinetic energy threshold with collisions with the velocity v in question. This means that when the velocity is below a threshold, that for say Na nuclei is about 100 km/s formally, 3.5 keV X-rays cannot be produced. The effective threshold is probably a bit higher and the cutting off can be smoothed out. On the other hand iodine would have a bit higher threshold.
Let us now look at the three places on the sky, where we think that the 3.5 keV line comes from dark matter hitting ordinary matter and the situation when the dark matter pearls are about stopping at the DAMA experiment, and especially note the velocity of the collisions

- **PCO** The Perseus Cluster Outskirts:
  In the Perseus Cluster the temperature of the X-ray gas is of the order of 10 keV. This is very high when we are concerned with producing 3.5 keV photons, and we could say it is above threshold.
  So we might expect that for each collision there is an of the order unity chance of getting a large part of the energy of the hit made into electron hole pairs, which in turn becomes hole electron annihilation photons, which are the 3.5

keV line photons to be observed may be on earth or better on a satellite near the earth.
The intensity which we extracted from the data for this outskirts of the Perseus Cluster was

$$\text{Intensity}_{PCO} = 5 * 10^{41} ph * cm^6/s/SNe/GeV. \tag{11.83}$$

- **TSNR** Thyco Super Nova Remnant:
The temperature in supernova remnants - at the time we now see Thyco Brahe's Supernova - is rather only 1 keV, so it already does not immediately guarantee that there is sufficient energy for production of 3.5 keV photons. Rather some sort of good luck is needed, and we would expect that the rate could be appreciably lower.
The rate is

$$\text{Intensity}_{TSNR} = 1.4 * 10^{41} ph * cm^6/s/SNe/GeV \tag{11.84}$$

which is about 3 times lower.
Since the $kT = 1keV$ is lower than the $kT = 10keV$ for the PCO, we could have expected an appreciable lower intensity Intensity_{TSNR} than the Intensity_{PCO} due to some Boltzmann factor, but it seems that the two agree extremely well, since of course a factor 3 is far below our estimation accuracy.
- **MWC** Milky Way Center:
Much gas in the Milky Way Center has very low temperatures like lower than 250 K, although there also is diffuse plasma with 10^6 to 10^7 K. The collision velocity with dark matter will then order of magnitudewise be governed by the velocity of the dark matter which being of the order of 300km/s for hydrogen corresponds to a temperature 1 keV (about 10^7 K).
This means that the rate is expected to be even lower compared to the ideal one - say the one for PCO - than the one for TSNR.
Indeed we have estimated the rate found for the Milky Way Center observed to be

$$\text{Intensity}_{MWC} = 7.3 * 10^{38} ph * cm^6/s/SNe/GeV, \tag{11.85}$$

which is about 200 times smaller than for TSNR. If it - as it seems to - happened that it is in this step -from TSNR to MWC that the threshold for hydrogen and helium collisions being able to produce 3.5 keV, then by this passage a fall in the 3.5 keV production should be by a factor equal to the ratio of hydrogen and helium abundance compared to the metals. This is of the order of 100.
- **DAMA**
We shall see in another section that the modulation part of the signal DAMA-LIBRA sees comes from the very tail of the tracks of the dark matter particles, just before they stop totally. This means that the effective velocity of the particles seen as modulation is very low. If we say that it is the remaining part of the track which is there only in one season, then since the velocity of the Earth around the sun is about 30 km/s, the velocity of this remaining track particles will be of the order of 30 km/s. At so low velocity the effective

temperature in collisions will be for hydrogen 10 eV, and even for iodine with atomic weight $A_{iodine} = 126.905\ amu$ only 1.27 keV. So even for heaviest atoms the velocity is below the threshold and only a very low fraction of the collisions are expected to produce 3.5 keV radiation.
But that is o.k. because we just claimed that of the kinetic energy for incoming dark matter only a fraction of one in half a milliard is turned into 3.5 keV radiation. However this way of explaining away more observations in DAMA has the problem, that it suggests that there are with higher velocities more events that do not vary seasonally. There are, in fact, limits on how much non-modulating background there can be, because it should have been seen as electron recoil background in experiments like LUX-Zeppelin.
LUX Zeppelin claimed that the bit of background spilled over from the electron recoil into the WIMP region was 3.6 mDRU with an expectation 2.6 $\pm$ mDRU. Here a mDRU = $10^{-3} cnts/keV_{ee}/kg/day$. Now we can see on the plot count that there are 20 spilled over events out of a total of 160 background events observed by LUX Zeppelin. This means that the full background essentially of electron recoil events is $\frac{160}{20} * 3.6 mDRU = 28.8 mDRU$.

11.3 Depth and Location Dependence of Underground Dark Matter Signal

We have earlier called attention to the fact that dark matter having significant interaction with the earth, through which it penetrates down to dark matter underground experiments, can cause a significant dependence of the signal on the depth of the experiment. This could potentially explain the fact that DAMA-LIBRA sees a signal while ANAIS and LUX Zeppelin do not see the corresponding signal, which is an impossible situation for simple WIMP models.
Assuming, as we have in the present article, that the main velocity dependence of the ratio $\frac{\text{“}\sigma''}{m}$ is as the inverse square of the velocity and that a major fraction of the stopping energy when the stopping is inelastic goes into the production of 3.5 keV radiation, we can argue in the following way:
We take that the quotation marks around the σ means that a cylinder of the medium being penetrated of cross section “σ” is brought into a velocity of the order of the velocity of the pearl inducing this motion. This means that per unit distance penetration the momentum loss of the pearl or the object considered is “$\sigma'' * \rho * v$. But now since we take the ansatz

$$\frac{\text{“}\sigma''}{m} = K/v^2, \tag{11.86}$$

the loss of momentum comes to behave like

$$\text{“ p-loss per distance unit”} = \rho * m * K/v \tag{11.87}$$

$$\text{“ E-loss per distance unit”} = v/2 * m\rho * K/v = \rho * m * K/2 \tag{11.88}$$

$$\text{i.e.t't'force''} = \rho * K * m/2 \tag{11.89}$$

$$\text{and “acceleration''} = \rho * K/2 \tag{11.90}$$

For such a constant force the energy deposited per unit length becomes the same all along the stopping path, and if the efficiency for making it into the 3.5 keV radiation is constant too, then the stopping track will radiate equally much per length unit whatever the speed of the particle causing this radiation. So whether a dark matter particle enters with low or high velocity will only become visible for instruments observing the 3.5 keV radiation, when the particles stops. Then namely a fast particle still goes on a little longer than the slow one. So in the here sketched approximation the seasonal effect modulation can be calculated as if only the end tip of the stopping track counts.
In the approximation that the motion of the Earth around the sun is small compared to the motion of the solar system in the Milky Way we would just get infinitesimally small pieces of track to count at the end of the track, i.e. where the particles stop. The density of such stopping points in the Earth would just reflect the kinetic energy distribution of the vertical direction, since with our assumption of the force on the particle during the stopping being constant, the length of the track in the vertical direction would just be proportional to the kinetic energy along this direction. (Actually we expect that thinking of a splitting up of the kinetic energy according to coordinate axes is at least crudely o.k.)

11.3.1 Motion of us relative to Dark Matter

The distribution of the dark matter in the galaxy is expected not to follow the rotation of the visible matter, but rather being as a whole at rest in the galaxy and only having a random Maxwellian distribution in velocity

$$f(\vec{v})d^3\vec{v} = \left[\frac{m}{2\pi}\right]^{3/2} \exp(-\frac{mv^2}{2T})d^3\vec{v} \tag{11.91}$$

where the temperature T (with Boltzmann's constant $k = 1$) should be adjusted so as to make the dominant speed of the dark matter particles be around 250 to 280 km/s. I.e. that we should divide the total square of the velocity of the order of $7.02 * 10^4 km^2/s^2 = 7.02 * 10^{10} m^2/s^2$ into three equal portions to the three spatial coordinates. Thus we shall have

$$\frac{2T}{m} = \frac{1}{3} * 7.02 * 10^{10} m^2/s^2 \tag{11.92}$$

$$= 2.34 * 10^{10} m^2/s^2 \tag{11.93}$$

$$\Rightarrow \text{ “typical velocity component ”} = \sqrt{2.34 * 10^{10} m^2/s^2} \tag{11.94}$$

$$= 153 km/s = 1.53 * 10^5 m/s \tag{11.95}$$

The direction of motion of the solar system relative to the Milky Way is close to the direction of Deneb (=α Cygni), which has right ascension $20^h41^m25.9^s$ and declination $+45^0 16' 49''$. Hence the velocity of 232 km/s in this direction will have a component in the direction of the earth rotation axis oriented north

$$\text{“component north”} = 232 km/s * \cos(90^0 - (+45^0 16' 49'')) \tag{11.96}$$

$$= 0.7105 * 232 km/s \tag{11.97}$$

$$= 165 km/s = 1.65 * 10^5 m/s. \tag{11.98}$$

Laboratory on North Pole As an example, we consider first an underground laboratory placed on the North Pole:
The distribution of the velocity component vertically down of the dark matter $D_{N.P.}(v_{vertical})$ would be a displaced Gaussian, though of course one cannot observe up-going dark matter particles in a model wherein the dark matter gets stopped on the km-scale:

$$D_{N.P.}(v_{vertical})dv_{vertical} \propto \exp(-\frac{(v_{vertical} - 165\,km/s)^2}{(153\,km/s)^2})dv_{vertical}$$
$$\text{for } v_{vertical} \in [0\,km/s, \infty] \tag{11.99}$$

One should have in mind that the stopping depth will be rather simply related to this incoming downward speed $v_{vertical}$. Also one should have in mind that the speed of the Earth relative to the Milky Way varies slightly with season, so that what we have put in as the velocity $165\,km/s$ varies with season with a fraction of the earth velocity around the sun, which is $30\,km/s$.
For a detector at the depth corresponding to the stopping point for a vertical velocity smaller than the peak in the distribution, here at the $165\,km/s$, i.e. above where the particles of just this velocity stop, it should see a seasonal variation opposite to that observed by the DAMA-LIBRA experiment. However, for deeper experiments on the northern hemisphere one should get the sign of the seasonal effect which DAMA-LIBRA got. This DAMA-LIBRA experiment actually found that in the season when the Earth moved towards the bulk of the (supposed) dark matter their event rate was higher than when the Earth moved along the dark matter stream, escaping.

Generalized Picture A similar consideration for the South Pole would just change the sign of the velocity $165\,km/s$ and that would lead to that the deeper one goes down with one's experiment, the seasonal effect will remain of opposite sign to that found by DAMA-LIBRA. It would actually correspond to a derivative of the tail of a Gauss distribution.
When one goes to the lower latitudes there should in principle be a variation with the time of the day, but if one just averages that out by not measuring or noting down the time on the day, then the approximate picture for the distribution of the $v_{vertical}$ would be broader as one approaches the equator and the peak velocity will be smaller also. At the equator there would be no seasonal effect at the surface of the earth, the effect just at the surface changes sign when passing the equator.

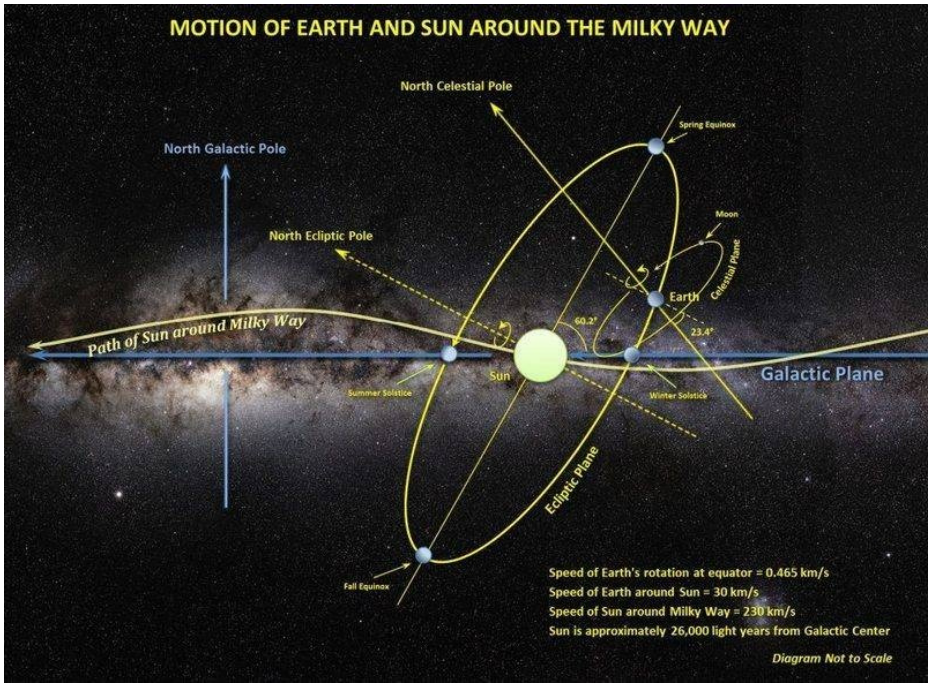

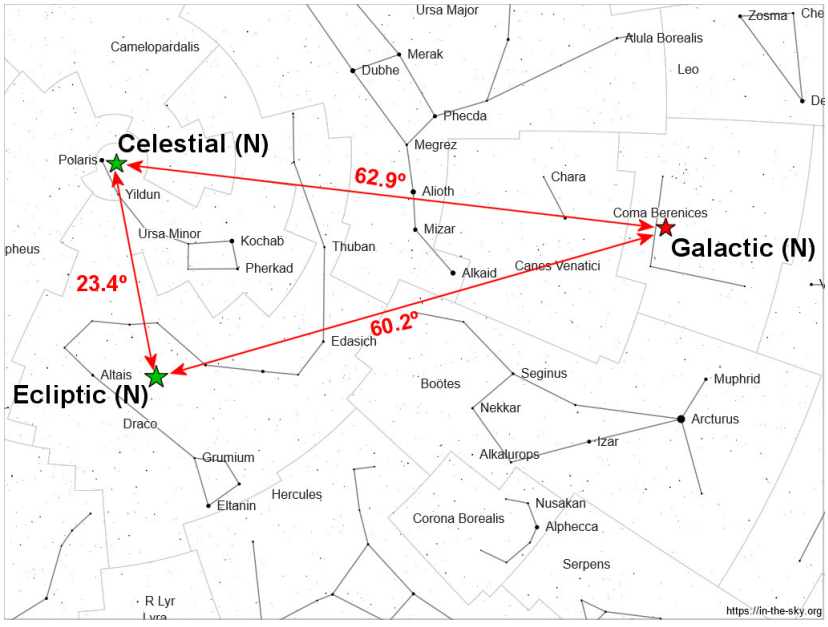

11.4 Conclusion

We have re-looked at our since long announced model for dark matter as being pearls of essentially ordinary matter under very high pressure with correspondingly very strongly screened nuclei in a dense degenerate electron fermi gas,

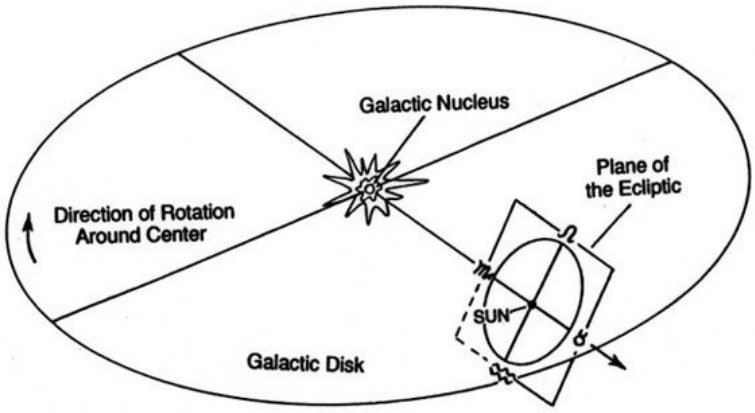

probably surrounded by a vacuum phase separating the surface as suggested by Columbia plots.
Our main new point has been to use how the various nuclei inside such a dark matter pearl interact individuality or strongly interfering respectively in inelastic X-ray producing collisions and elastic events. A major success is that we can treat scattering of dark matter with dark matter and with ordinary matter very similarly. In our crude picture we solve or deliver chance of solving some mysteries about the non-gravitational interactions of dark matter:

- The difficulty of fitting the 3.5 keV observations from the Perseus Cluster we propose to solve by allowing, that the outskirts of this galaxy cluster has its 3.5 keV radiation emitted from collisions of ordinary matter with dark matter processes.
- The mystery that only DAMA-LIBRA so far has seen the dark matter in underground direct detection, while others LUX have upper limits which in WIMP models seem quite contradictory, we solve by:
  The dark matter gets stopped in the earth with a stopping length of the order of the depth of DAMA, and what DAMA sees is really 3.5 keV radiation from dark matter having been excited by its passage through the earth above the experimental hall or in the apparatus.

11.4.1 Main Coincidence

The main coincidence observed in the present article is that the essentially stopping power per (weight per area) quantities $\frac{\rho\sigma''}{m}$ are of similar order of magnitude for three different processes, provided the velocity is higher than where threshold effects would be expected to suppress the 3.5 keV radiation production. These three different processes are:

- The dark matter on dark matter scattering producing 3.5 keV X-rays.
- the dark matter on ordinary matter producing 3.5 keV X-rays.
- and the stopping of dark matter pearls on ordinary matter in the earth assumed to stop them around the depth of the DAMA experiment.

Then we come up with a story of interference that could allow the elastic scattering of dark matter on dark matter being allowed to have much higher cross section per mass than the three processes just mentioned. The Correa interaction of dark matter with dark matter is measured in this way to be about half a million times stronger than the three almost equal values of $\frac{\sigma}{m}$ mentioned above. This number of order $5 * 10^5$ is interpreted as the number of screened nuclei constituents in a dark matter pearl. The size of the dark matter pearls estimated this way fits reasonably well with earlier estimates, as well as with the story about the different energy scales due to a fluctuating lattice by one of us (see the present volume of the Bled Proceedings).

11.4.2 On the Impact on the Earth

We have given a series of predictions for how the chances of finding dark matter in the underground by direct detection should vary between the hemispheres of the Earth and with the depth.

11.5 Appendix Translation of Units

We here list the translations between the two different sets of units, which we use, for the quantities of interest in this article:
Using

$$1\mathrm{m} = 5.07 * 10^{15}\mathrm{GeV}^{-1} \tag{11.100}$$

$$1\mathrm{kg} = 5.625 * 10^{26}\mathrm{GeV} \tag{11.101}$$

we can write:

$$\begin{aligned}
\mathrm{m}^2/\mathrm{kg} &= 4.57 * 10^4\,\mathrm{GeV}^{-3} \\
\mathrm{m}^4/\mathrm{s}^2/\mathrm{kg} &= 5.08 * 10^{-13}\,\mathrm{GeV}^{-3} \\
\mathrm{kg}/\mathrm{m}^3 &= 4.32 * 10^{-21}\,\mathrm{GeV}^4 \\
\text{earth density } 3000\mathrm{kg}/\mathrm{m}^3 &= 1.29 * 10^{-17}\,\mathrm{GeV}^4 \\
\text{DAMA depth } 1400\mathrm{m} &= 7.10 * 10^{18}\,\mathrm{GeV}^{-1} \\
\text{DAMA depth} \times \text{earth density } 4.2 * 10^6\mathrm{kg}/\mathrm{m}^2 &= 91.6\,\mathrm{GeV}^3 \\
\text{inverse of this } 2.38 * 10^{-7}\mathrm{m}^2/\mathrm{kg} &= 1.09 * 10^{-2}\,\mathrm{GeV}^{-3} \\
\text{Typical gal. vel. } 3 * 10^5\mathrm{m}/\mathrm{s} &= 10^{-3}
\end{aligned} \tag{11.102}$$

References

1. C. D. Froggatt and H. B. Nielsen, Phys. Rev. Lett. **95** 231301 (2005) [arXiv:astro-ph/0508513].
2. C.D. Froggatt and H.B. Nielsen, Proceedings of Conference: C05-07-19.3 (Bled 2005); arXiv:astro-ph/0512454.
3. C. D. Froggatt and H. B. Nielsen, Int. J. Mod. Phys. A **30** no.13, 1550066 (2015) [arXiv:1403.7177].

4. C. D. Froggatt and H. B. Nielsen, Mod. Phys. Lett. **A30** no.36, 1550195 (2015) [arXiv:1503.01089].
5. H.B. Nielsen, C.D. Froggatt and D. Jurman, PoS(CORFU2017)075.
6. H.B. Nielsen and C.D. Froggatt, PoS(CORFU2019)049.
7. C. D. Froggatt, H. B. Nielsen, "The 3.5 keV line from non-perturbative Standard Model dark matter balls", arXiv:2003.05018.
8. H. B. Nielsen (speaker) and C.D. Froggatt, "Dark Matter Macroscopic Pearls, 3.5 keV -ray Line, How Big?", 23rd Bled Workshop on What comes beyond the Standard Models (2020), arXiv:2012.00445.
9. C. D. Froggatt and H.B.Nielsen, "Atomic Size Dark Matter Pearls, Electron Signal", 24th Bled Workshop on What comes beyond the Standard Models (2021), arXiv:2111.10879.
10. C. D. Froggatt and H.B. Nielsen, "Atomic Size Pearls being Dark Matter giving Electron Signal", arXiv:2203.02779.
11. H. B. Nielsen (speaker) and C.D. Froggatt, "Dusty Dark Matter Pearls Developed", 25th Bled Workshop on What comes beyond the Standard Models (2022), arXiv:2303.06061.
12. C.D. Froggatt and H.B. Nielsen PoS(CORFU2022)003, arXiv:2305.12291.
13. C.D. Froggatt and H.B. Nielsen PoS(CORFU2022)205, arXiv:2305.18645.
14. H.B. Nielsen (speaker) and C.D. Froggatt, 26th Bled Workshop on What becomes beyond the Standard Models(2023), arXiv:2311.14996.
15. C.D. Froggatt and H.B.Nielsen, PoS(CORFU2023)205, arXiv:2406.07740.
16. C. A. Correa, MNRAS **503**, 920 (2021) [arXiv:2007.02958].
17. J. M. Cline and A. R. Frey, Phys. Rev. **D90**, 123537 (2014) [arXiv:1410.7766].
18. H.B. Nielsen, "Remarkable Scale Relation, Approximate SU(5), Fluctuating Lattice" Universe 11 (2025) 7, 211 [arXiv:2411.03552].
19. H. B. Nielsen, "Fluctuating Lattice, Several Energy Scales" Bled virtual workshop July 2024, arXiv:2502.16369.
20. H.B. Nielsen, "Approximate Minimal SU(5), Several Fundamental Scales, Fluctuating Lattice", arXiv:2505.06716.
21. H.B. Nielsen, "Ontological Fluctuating Lattice Cut Off", Other contribution in this same volume.

BLED WORKSHOPS
IN PHYSICS
VOL. 26, NO. 1

Proceedings of the 28th Workshop
What Comes Beyond . . . *(p. 142)*
Bled, Slovenia, July 6–17, 2025

12 Probing Lorentz Invariance Violation at High-Energy Colliders via Intermediate Massive Boson Mass Measurements: Z Boson Example

Z. Kepuladze[1], J. Jejelava[1]

[1] Andronikashvili Institute of Physics, Tbilisi State University, Ilia State University

Abstract. Lorentz invariance (LI) is a foundational principle of modern physics, yet its possible violation (LIV) remains an intriguing window to physics beyond the Standard Model. While stringent constraints exist in the electromagnetic and hadronic sectors, the weak sector—particularly unstable bosons—remains largely unexplored. In this work, based on our recent studies and conference presentation, we analyze how LIV manifests in high-energy collider experiments, focusing on modifications of Z boson dispersion relations and their impact on resonance measurements in Drell–Yan processes. We argue that precision measurements of resonance masses at colliders provide sensitivity to LIV at the level of 10^{-9}, comparable to bounds derived from cosmic rays. We also discuss the interplay between LIV and gauge invariance, highlighting why only specific operators provide physical effects. The phenomenological implications for both Z and W bosons are outlined, with emphasis on experimental strategies for current and future colliders.

Povzetek: Kršitev Lorentzove invariance ponuja možnost za iskanje teorije, ki razloži privzetke standardnega modela. Iskanje zlomitve Lorentzove invariance v elektromagnetnem in hadronskem sektorju je postavilo stroge omejitve, šibki sektor pa je še neraziskan. Avtorja analizirata morebitno zlomitev pri poskusih z visokoenergijskimi trkalniki, posebej pri disperzijskih relacijah bozonov Z in njihovem vplivu na resonančne meritve v Drell-Yanovih procesih. Menita, da natančne meritve resonančnih mas v trkalnikih omogočijo 10^{-9} večjo občutljivost za merjenje kršitve kot pri meritvah s kozmičnimi žarki. Predstavita operatorje, ki so posebej primerni za ugotavljanje kršitve. Predlagata meritve z bozoni Z in W tudi za nove trkalnike.

12.1 Introduction

Lorentz invariance (LI) underpins the structure of quantum field theory and general relativity. Yet possible violations of this symmetry are theoretically motivated. Spontaneous Lorentz symmetry breaking can give rise to emergent vector or tensor degrees of freedom, which may act as Goldstone modes of spacetime symmetry violation [1]. Alternatively, LIV can appear as a mechanism for ultraviolet completion, rendering theories finite, as in Hořava's construction [2]. At low energies, if present, LIV should be strongly suppressed, but in the ultra–high-energy domain it may have significant phenomenological consequences.

The motivation for studying LIV partly comes from cosmic ray physics. The famous Greisen–Zatsepin–Kuzmin (GZK) cutoff [3] predicts that ultra–high-energy

cosmic rays above $\sim 5 \times 10^{19}$ eV should be strongly attenuated by interactions with the cosmic microwave background. However, experiments such as AGASA and, later, the Pierre Auger Observatory reported excess events beyond the GZK bound, sparking interest in LIV as a possible explanation [4,5]. Such cosmic ray observations thus continue to provide motivation for precise LIV studies.

Another motivation comes from neutrino physics. The possibility of neutrinos traveling at speeds slightly different from light has been considered in multiple contexts. Early hints, such as the controversial OPERA result, suggested superluminal neutrinos, though this was later shown to be an experimental error. Nonetheless, neutrino time-of-flight experiments and supernova neutrino observations (e.g., SN1987A) constrain deviations from the speed of light at the level of 10^{-9} or better [6]. These are directly relevant because they probe LIV in the weak sector, where constraints remain far weaker than in the electromagnetic one.

Thus, cosmic ray and neutrino data both highlight the importance of searching for LIV in controlled environments such as high-energy colliders. While astrophysical observations give very stringent limits in some channels, colliders allow systematic and model-independent tests, especially for unstable weak bosons that cannot be probed astrophysically.

12.2 Constraints and Open Windows

The tightest constraints on LIV arise mostly from astrophysical processes, since cosmic rays may carry energies far beyond those accessible at accelerators or other Earth-based experiments. If we describe these restrictions in the language of possible deviations from the maximal attainable velocity for a given particle species (a particle's "speed of light," so to speak) [7], defined as $\delta = \Delta c/c$, then the following constraints can be quoted. For electrons: $|\delta_e| < 10^{-19}$ [8,9], $|\delta_e - \delta_\gamma| < 5 \cdot 10^{-19}$ [10]. Restrictions on photons and protons fall in approximately the same range [8]. These arise from the non-observation of otherwise expected effects in the presence of LIV, such as photon decay and vacuum Cherenkov radiation (generally derived from threshold-energy arguments), tests of rotating optical cavities, vacuum birefringence, dispersion, Michelson–Morley–type resonators, or time-of-flight measurements. Bounds from these processes are so strong that they effectively rule out LIV in the QED sector at accessible scales.

Neutrinos provide a different picture. Time-of-flight measurements constrain their velocity relative to light. Supernova SN1987A neutrino arrival times imply $|\delta_\nu| < 10^{-9}$ at energies of tens of MeV. At higher energies, IceCube measurements of PeV neutrinos place bounds at the level of 10^{-10}–10^{-11}. Atmospheric neutrino oscillations observed by Super-Kamiokande constrain certain LIV coefficients to 10^{-8} in the GeV range.

In general, unstable particles—among them the weak bosons W and Z, which are both unstable and short-lived—evade such astrophysical probes. Their dispersion relations have never been directly tested outside collider environments. Consequently, the weak sector remains essentially unconstrained with respect to LIV. Whether this is a special feature of the weak sector remains to be determined. At the same time, this gap represents an open experimental window: accelerator

experiments can probe parameter space that astrophysical methods cannot access. Collider studies of massive intermediate boson resonances therefore allow us to test LIV systematically in a sector that has remained hidden from astrophysical scrutiny.
The present contribution builds upon our recent studies [11, 12].

12.3 Testing LIV at Accelerators: Concept

Whatever the origin of LIV might be, the low-energy phenomenology can always be parameterized by possible modifications to particle propagation and interactions. If the preferred direction of LIV is fixed in spacetime by a timelike or spacelike unit vector $n_\mu = (n_0, \mathbf{n})$ [1], one of the simplest renormalizable interactions between the vector field A_μ and fermion field Ψ may take the form

$$e\delta_{\text{int}}(A_\mu n^\mu)\bar{\Psi}(\gamma_\nu n^\nu)\Psi \tag{12.1}$$

To detect such modifications at accelerators, one usually examines their effect on cross sections, which acquire the general form

$$\sigma_{LIV} = \sigma_{LI}(1 + \delta_{\text{int}} f(\Omega, \mathbf{n})) \tag{12.2}$$

where $f(\Omega, \mathbf{n})$ encodes the interplay between the preferred LIV direction n_μ and the orientation of the process in spacetime. Because n_μ picks out a special direction, it introduces anisotropy into the process. Since an accelerator rotates with the Earth, the relative orientation with respect to n_μ also changes with sidereal time. Therefore, daily modulations should emerge in the cross section if LIV is present and the experimental accuracy is sufficient.
Searches for such modulations have been conducted at the Large Hadron Collider (LHC), yielding limits of $|\delta_{\text{int}}| < 10^{-5}$ [13, 14]. While the specific modifications studied in those analyses originated in the quark sector, their functional form is quite general and can be applied to a broad class of LIV operators, including the interaction above. Provided that $f(\Omega, \mathbf{n})$ has no strong energy dependence, these bounds can be generalized accordingly.
A noticeable property of this form of σ_{LIV} is that LIV contributions always enter at the same order in δ_{int}. Detectability therefore depends only on experimental precision, essentially independent of the energy scale. This situation contrasts with modifications of the dispersion relation, which in their simplest form can be written as

$$p^\mu p_\mu = M_{B,eff}^2 = M_B^2 + \delta E^2 \tag{12.3}$$

Here $p_\mu = (E, \mathbf{p})$ is the four-momentum and M_B the given boson mass. We have also introduced notion of the effective mass. In this case the LIV term competes

[1] The preferred direction, fixed by the n_μ vector, transforms as a constant four-vector under Lorentz transformations. The explicit form written in the text corresponds to a particular reference frame; in other frames the components of n_μ change accordingly, while its invariant character as a preferred direction remains.

with the mass term, and the hierarchy between them changes with energy, making LIV effects increasingly accessible at high energies. Scattering processes mediated by a massive intermediate boson therefore become highly sensitive to such modifications in the resonance region.
For the boson with (11.3), one can approximate [15]

$$\Gamma_{LIV} = \frac{M_{B,eff}^2}{M_B^2}\Gamma_{LI} \tag{12.4}$$

so the unstable boson propagator becomes

$$\begin{aligned} D &= \frac{i}{p_\alpha^2 - M_B^2} \to \frac{i}{p_\alpha^2 - (M_{B,eff} - ip_0\Gamma_{LIV}/2M_{B,eff})^2} \\ &= \frac{i}{p_\alpha^2 - M_{B,eff}^2(1 - i\Gamma_{LI}/2M_B)^2} \end{aligned} \tag{12.5}$$

Consequently, the cross section is

$$\sigma_B^{LIV} \sim |D_B|^2 \tag{12.6}$$

and the resonance mass M_{res} now measures the effective mass instead:

$$M_{res}^2 = M_{B,eff}^2(1 - \Gamma_{LIV}^2/4M_B^2) \tag{12.7}$$

Applying this framework to the weak Z boson, and comparing the resonance mass shift with the current precision of M_Z, one finds that at LHC energies of $E = 14$ TeV, the present experimental uncertainty of $\Delta M_Z = |M_Z - M_{Zresonance}| \approx 2$ MeV [16] implies

$$|\delta| \approx \frac{2M_Z\Delta M_Z}{E^2} \approx 2 \cdot 10^{-9} \tag{12.8}$$

This level of sensitivity is comparable to astrophysical constraints for the neutrinos. Such a preliminary result is already convincing enough to justify further investigation. In the next section we turn to the realistic Drell–Yan cross section mediated by the neutral weak boson. When considering Lorentz invariance violation in the weak sector, the Z boson provides the cleanest probe due to its narrow resonance and well-measured leptonic decay modes.

12.4 Modified Dynamics of the Z Boson

To introduce modified dynamics for the neutral weak boson, a natural starting point is to modify the kinetic term of the Z-boson Lagrangian. For a preferred direction fixed in spacetime by the vector n_μ, the kinetic term that introduces LIV, modifies the dispersion relation, and is constrained by two derivatives (i.e. is renormalizable), is

$$\Delta L_{LIV} = \frac{\delta_{LIV}}{2}(\partial_n Z^\mu)(\partial_n Z_\mu), \qquad \partial_n \equiv n_\mu \partial^\mu \tag{12.9}$$

Alongside this term, one can introduce additional LIV operators,

$$\Delta L_{LIV} = \frac{\delta_{LIV}}{2}(\partial_n Z^\mu)(\partial_n Z_\mu) + \frac{\delta_{1LIV}}{2}(\partial_\mu Z_n)(\partial^\mu Z_n) + \delta_{2LIV}(\partial_\mu Z^\mu)(\partial_n Z_n) \tag{12.10}$$

with $Z_n \equiv n_\mu Z^\mu$.

These operators are often introduced because in the literature there is a frequent attempt to enforce a gauge-invariant (GI) form. In that case one sets $\delta_{LIV} = \delta_{1LIV} = -\delta_{2LIV}$. However, neither of the two additional terms influences the dispersion relation. More importantly, LIV and GI do not go hand in hand. One can safely claim that if we want physical LIV in a theory, gauge invariance must be broken at least slightly. In fact, it is possible to obtain GI precisely from the demand that LIV be physically unobservable [1,17].

A simple demonstration is as follows. If we introduce a mass term $m^2(n_\mu A^\mu)^2$ (or any operator for that meter of the form $F(n_\mu A^\mu)$, $F(n_\mu A^\mu)\bar{\Psi}\Psi$, $F(n_\mu A^\mu)\bar{\Psi}n_\lambda\gamma^\lambda\Psi$, etc.) into an otherwise GI theory, then by performing a gauge transformation toward the axial gauge $n_\mu A^\mu = 0$ we can effectively eliminate LIV from the theory. Instead of genuine LIV, we only succeed in fixing a particular gauge. The same is true for any $F(A^\mu)$. If the gauge equation $F(A^\mu + \partial^\mu\omega) = 0$ has a solution for ω for arbitrary A^μ, then $F(A^\mu) = 0$ will become simply a gauge choice. If this gauge equation does not have a solution, gauge invariance is broken and physical LIV necessarily manifests.

A distinct case arises if $F(A^\mu)$ has a manifestly GI form itself, for example $F(A^\mu) \sim \delta n_\mu F^{\mu\lambda} n^\nu F_{\nu\lambda}$, where $F_{\nu\lambda} = \partial_\nu A_\lambda - \partial_\lambda A_\nu$ and δ is the LIV strength. In such a scenario, GI remains exact and gauge can be fixed by our convenience. At first glance everything appears consistent: the massless vector field still describes two propagating degrees of freedom and the Coulomb law is intact. But once U(1) symmetry is broken, a problem emerges: the vector field still carries only two degrees of freedom instead of behaving as a massive vector should. In other words, the theory becomes inconsistent with reality.

Even manifestly GI LIV fermion operators of "mass" type, such as $\bar{\Psi}n_\lambda\gamma^\lambda\Psi$ or $\bar{\Psi}n_\lambda\gamma^\lambda\gamma^5\Psi$, share this issue. The first can be gauged away by a corresponding transformation, while the second explicitly breaks GI. This may seem counter-intuitive, but the problem becomes evident if we calculate the vector-field polarization loop diagram, since this axial mass term is used for radiative generation of Cern-Simons term.

For example, with $S(k) = 1/(\not{k} - \not{b}\gamma^5)$, one finds

$$p_\mu \Pi^{\mu\nu}(p;b) = p_\mu \int \frac{d^4q}{(2\pi)^4} \operatorname{Tr}[\gamma^\mu S(q)\gamma^\nu S(q-p)] \neq 0 \tag{12.11}$$

which explicitly signals a violation of GI [11]. In principle, an easier way to check gauge invariance is by examining the modified Compton scattering matrix element. It is straightforward to see that if the matrix element takes the form $\xi_{1\mu}(k_1)\xi_{2\nu}(k_2)\mathcal{M}^{\mu\nu}$, where $\xi_{1\mu}(k_1)$ and $\xi_{2\nu}(k_2)$ are the photon polarization vectors, then the gauge invariance condition $k_{1\mu}\mathcal{M}^{\mu\nu} = 0$ is not satisfied—even at linear order in b^ν.

In short, we are demotivated from using GI setups for LIV operators. The scheme outlined above justifies focusing on corrections that affect the dispersion relation

directly. Moreover, once LIV operators are introduced, the gauge choice must also be specified, since even a small breaking of GI renders different gauges inequivalent. For concreteness, in what follows we proceed with (11.9) and assume the Standard Model (SM) in the unitary gauge. While it is interesting to speculate about the form of a LIV setup in the unbroken electroweak phase that could lead here, for our purposes this is not essential.
With (11.9) the dispersion relation of the Z boson is modified as

$$Q_\mu Q^\mu = M_{eff}^2 = M_Z^2 + \delta_{LIV} Q_n^2 \tag{12.12}$$

where Q_μ is the four-momentum of the particle, $Q_n \equiv n_\mu Q^\mu$ and M_Z is the Z boson mass. Here we reintroduce the notion of an effective mass.
The corresponding decay width can be written as [12]

$$\Gamma_{eff}(Q) \approx \frac{M_{eff}^2}{M_Z^2}\Gamma_{SM}(Q) = \frac{M_{eff}^2}{Q_0 M_Z}\Gamma_{0SM} \tag{12.13}$$

where Γ_{SM} is SM expression and Γ_{0SM} is its rest frame form.
For the propagator we obtain an expression resembling the massive vector propagator in unitary gauge:

$$\frac{-i}{Q_\lambda^2 - M_{eff}^2}\left(g_{\mu\nu} - \frac{Q_\mu Q_\nu}{M_{eff}^2}\right) \tag{12.14}$$

Usually, unstable massive field propagators are corrected by loop contributions, which acquire an imaginary part near the pole. By the optical theorem this imaginary contribution is proportional to the decay rate of the intermediate particle. Implementing this yields the replacement

$$M_{eff} \to M_{eff} - iQ_0\Gamma_{eff}(Q)/2M_{eff} = M_{eff}(1 - i\Gamma_{0SM}/2M_Z) \tag{12.15}$$

which reduces to the often used complex-mass replacement if Γ_{0SM}^2 is dropped. In the Lorentz-invariant limit this reproduces the well-established propagator [18,19]. Any further corrections in the numerator of the propagator are suppressed by $\alpha_{weak}\delta_{LIV}$, where α_{weak} is the weak fine-structure constant, and are proportional to the $Q_\mu Q_\nu$ term. In the Drell–Yan process mediated by the neutral Z boson, which we will analyze in the later sections, in the limit of massless fermions, all vector and axial currents are conserved. Terms proportional to momentum in the numerator therefore give no contribution. Consequently, the working form of the propagator is

$$D_{\mu\nu} = \frac{ig_{\mu\nu}}{Q_\lambda^2 - M_{eff}^2(1 - i\Gamma_{0SM}/2M_Z)^2} \tag{12.16}$$

12.5 Phenomenology in Drell–Yan Processes

The neutral current Drell-Yan process $pp \to Z/\gamma \to \ell^+\ell^-$ provides the cleanest probe of LIV in the weak sector. This process is carried by the neutral intermediate bosons: photon, Z boson, and Higgs, but the Higgs channel is extremely suppressed and therefore its effects are negligible. In this process, the energy carried by the Z boson is the highest possible during proton–proton collisions. Consequently, the resonance region is particularly sensitive: even a small δ_{LIV} may induce a measurable shift in the fitted Z mass.
When two protons collide at the LHC, they are arranged so they carry the following momenta

$$P_1 = (E, Pr), \quad P_2 = (E, -Pr) \tag{12.17}$$

where r is the unit vector along the collision axis and beam, which is colinear with the detector axis. The high energy of these protons allows us to neglect the proton mass, and within this accuracy we can assume that $E = P$. Partons inside each proton carry an x portion of the energy, with probability $f_{q_f}(x)$. Thus, when protons collide and the process proceeds via the neutral current, the momentum carried by the intermediate boson after parton–antiparton annihilation is:

$$Q = x_1 P_1 + x_2 P_2 = E((x_1 + x_2), (x_1 - x_2)r) \tag{12.18}$$

and the cross section of the process has the form

$$\sigma_P = \sum_f \int dx_1 dx_2 f_{q_f}(x_1) f_{\bar{q}_f}(x_2) \sigma_f \tag{12.19}$$

with index f denoting the flavor of the partons inside the proton, σ_P the cross section of the proton–proton collision, and σ_f the parton–antiparton (quark–antiquark) annihilation cross section. The four–momentum Q_μ is often parametrized by the invariant mass M and rapidity Y:

$$Q_\mu = M(\cosh Y, r \sinh Y), \quad Q_\mu^2 = M^2 \tag{12.20}$$

Here we note that higher rapidity corresponds to higher transferred energy and 3-momentum. If we calculate the Jacobian of this transformation,

$$\frac{\partial(M^2, Y)}{\partial(x_1, x_2)} = 4E^2 \tag{12.21}$$

we can define the differential cross section as

$$\frac{d^2\sigma_p}{dM^2 dY} = \sum_f \frac{f_{qf}(x_1) f_{\bar{q}f}(x_2)}{4E^2} \sigma_f \tag{12.22}$$

We will not go into the details of the direct calculation of σ_f ; instead, we cite it from [12]:

$$\frac{d^2\sigma_p}{dM^2 dY} = \sum_f \frac{f_{qf}(x_1) f_{\bar{q}f}(x_2)}{4E^2} \sigma_{EM} [1 + \frac{g_q g_l \left(M^2 - M_{eff}^2 (1 - \Gamma_{0SM}^2 / 4M_Z^2)\right)}{2|e_f| M^2 \sin^2 2\theta_w} R_s + \frac{(1 + g_q^2)(1 + g_l^2)}{16 e_f^2 \sin^4 2\theta_w} R_s] \tag{12.23}$$

where e_f is the charge of corresponding quark, σ_{EM} the electromagnetic cross section, and R_s resonance factor:

$$\sigma_{EM} = \frac{4\pi\alpha^2}{9M^2} e_f^2, \tag{12.24}$$

$$R_s = \frac{M^4}{\left(M^2 - M_{eff}^2(1 - \Gamma_{0SM}^2/4M_Z^2)\right)^2 + M_{eff}^4\Gamma_{0SM}^2/M_Z^2}$$

From the cross section we see that the resonance value of the invariant mass M_r is now defined as

$$M_r^2 = M_{eff}^2(1 - \Gamma_{0SM}^2/4M_Z^2) \tag{12.25}$$

with

$$M_{eff}^2 = M_Z^2 + \delta_{LIV} M_r^2 (n_0 \cosh Y - (n \cdot r) \sinh Y)^2 \tag{12.26}$$

Thus we can write

$$M_r^2 \approx M_Z^2(1 + \delta_{LIV}(n_0 \cosh Y - (n \cdot r) \sinh Y)^2) - \Gamma_{0SM}^2/4 \tag{12.27}$$

The peak value of the cross section changes in the following manner:

$$\sigma_{f\,max} \approx \sigma_{f\,max}^{LI}(1 - \frac{\delta_{LIV}\,(n \cdot Q_r)^2}{M_Z^2}) \approx \sigma_{f\,max}^{LI}(1 - \delta_{LIV}(n_0 \cosh Y - (n \cdot r) \sinh Y)^2) \tag{12.28}$$

LIV effects depend strongly on the preferred direction n_μ and on rapidity Y. The dependence on rapidity is very strong: effects that are invisible at small rapidities may become glaring at higher rapidities.

We initially postulated n_μ to be a unit vector, but general violation patterns do not exclude the lightlike case either, nor is anything in our assumptions or derivation sensitive to this. Therefore, we can still distinguish three different cases of LIV: timelike, spacelike, and lightlike.

$$\text{Time-like:} \quad n_\mu = (1, \vec{0}), \tag{12.29}$$

$$\text{Space-like:} \quad n_\mu = (0, \vec{n}), \quad \text{with} \quad \vec{n}^2 = 1, \tag{12.30}$$

$$\text{Light-like:} \quad n_\mu = (1, \vec{n}). \tag{12.31}$$

For pure timelike violation we obtain:

$$M_r^2 \approx M_Z^2(1 + \delta_{LIV} \cosh^2 Y) - \Gamma_{0SM}^2/4 \tag{12.32}$$

$$\sigma_{f\,max} \approx \sigma_{f\,max}^{LI}(1 - \delta_{LIV} \cosh^2 Y) \tag{12.33}$$

Here dependence on the orientation does not exist, since in the timelike case no anisotropy appears. The dependence on Y is maximally strong. For timelike violation, separate observation of high-rapidity cases should be the strategy for LIV studies. Probably this is a good idea for any LIV case. If we want to constrain

δ_{LIV} from the accuracy of Z boson mass measurement, using ΔM_Z (Atlas value), we can estimate:

$$\delta_{LIV} \leq \frac{2\Delta M_Z}{M_Z \cosh^2 Y} \tag{12.34}$$

which for $Y = 5, 6$, offers $10^{-8}(10^{-9})$.
For the spacelike violation case, alongside strong rapidity dependence, anisotropy also appears. Since $n \cdot r \equiv \cos\beta$, with β the angle between the preferred direction and the collision axis, the result depends on Earth's orientation in space and consequently on sidereal time:

$$M_r^2 \approx M_Z^2(1 + \delta_{LIV} \sinh^2 Y \cos^2\beta) - \Gamma_{0SM}^2/4 \tag{12.35}$$

$$\sigma_{f\,max} \approx \sigma_{f\,max}^{LI}(1 - \delta_{LIV} \sinh^2 Y \cos^2\beta) \tag{12.36}$$

Unless, by unfortunate combination, $\cos\beta$ is very small, distinct oscillations in the cross section at high rapidity should appear with sidereal time.
For the lightlike case $n_\mu^2 = 0$. If this case is hard to understand separately, we can at least look at it as a limiting case of timelike or spacelike violations. When $n_0 \gg 1$, (11.27) and (11.28) assume a lighlike form:

$$M_r^2 \approx M_Z^2(1 + \delta_{LIV}(\cosh Y - \sinh Y \cos\beta)^2) - \Gamma_{0SM}^2/4 \tag{12.37}$$

$$\sigma_{f\,max} \approx \sigma_{f\,max}^{LI}(1 - \delta_{LIV}(\cosh Y - \sinh Y \cos\beta)^2) \tag{12.38}$$

Similar to the spacelike violation, the lightlike case also exhibits anisotropy, though of a different character. It is different enough to be distinguished from spacelike violation. However, this case is still a kind of hybrid between timelike and spacelike violations.
The conclusion we can quickly draw here is the following: an almost exponential dependence on rapidity and modulations by sidereal time should be the main targets of this kind of LIV study. Dependence on rapidity is the more universal property, while study of sidereal-time signal modulations may be restricted by the experimental statistics.

12.6 Experimental Strategy

As we saw in the earlier section, the driving force behind the LIV effects comes from processes with higher rapidity. While the anisotropy appearing in the spacelike and lightlike cases will leave its mark on experimental data, large rapidities remain a prerequisite for LIV detection. If we look at the standard cross section distribution by rapidity in Drell–Yan processes [20], we can clearly identify that the vast majority of events occur at small rapidity Y, where LIV effects are virtually nonexistent. Thus, the experimentally acquired data in its vast majority will appear almost LI, with only a small fraction of events at higher Y, where LIV can in principle become pronounced.
Therefore, to increase the chance of LIV detection we need to isolate the LIV-sensitive signal by sorting the data according to rapidity and, if anisotropy is present (in the spacelike and lightlike cases), also by sidereal time. This allows

event selection by transferred momentum and spatial orientation. Smaller bin sizes for event selection would naturally give a more accurate picture; however, events with higher rapidities are rare, and there is possibly a practical limit on bin size.

The pure timelike violation case should be easier to analyze, since there is no need for anisotropy searches. In each rapidity bin, statistics will be significantly better, and for the cross section near the Z-boson resonance region we will have slightly different resonance invariant masses and different peak values. Analysis of the peak's shape, size, and location should be sufficient to constrain the LIV parameters δ_{LIV} and n_μ.

Let us analyze the timelike violation case as a demonstration of the above-mentioned strategy. To understand the pure LIV effect, we can plot the relative difference between σ_f and its LI counterpart

Fig. 12.1: $(\sigma_{LIV} - \sigma_{LI})/\sigma_{LI}$

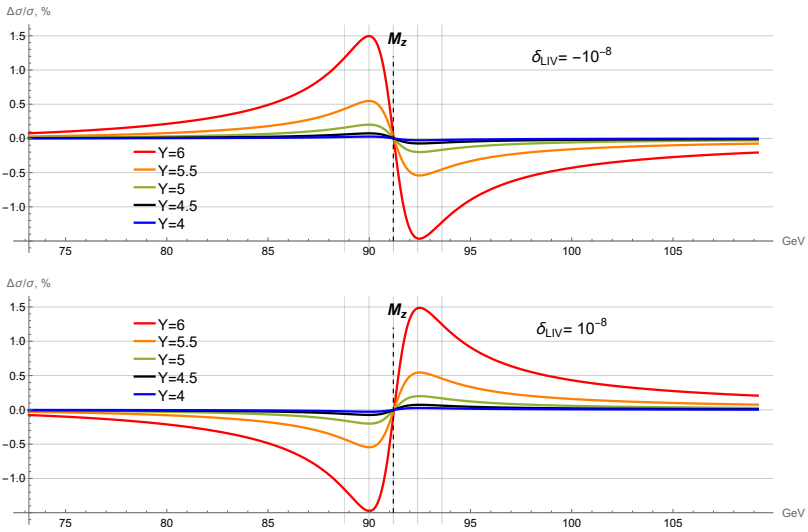

This plot illustrates the behavior of the relative difference between the LIV and LI cross sections at the parton level, thereby isolating the LIV effect for a clearer understanding of its structure. Despite appearances, the LIV effect is not exactly zero at the resonance point. It reaches its maximum value at a point approximately 1.2 GeV away from the true mass ($M_Z = 91.1876$ GeV).

This figure vividly illustrates how the LIV effect is activated near the resonance mass, and how the enhanced effect quickly dies out farther from the resonance, scaling as δ_{LIV} to leading order. Inside the resonance region at $Y = 5$, the effect is of the order of a few tenths of a percent and increases up to about 1.5% at $Y = 6$ for $|\delta_{LIV}| = 10^{-8}$. The sign of the LIV parameter δ_{LIV} determines how the resonance peak shifts, but for both signs the approximate amplitude of the effect remains the

same. This percent-level change is significant but still too subtle for the human eye to discern on the paper's scale. Therefore, next we show an exaggerated plot of the LIV and LI cross sections to better highlight the structure of the LIV effect.

Fig. 12.2: Highly exaggerated comparison of parton's LIV and LI cross-sections.

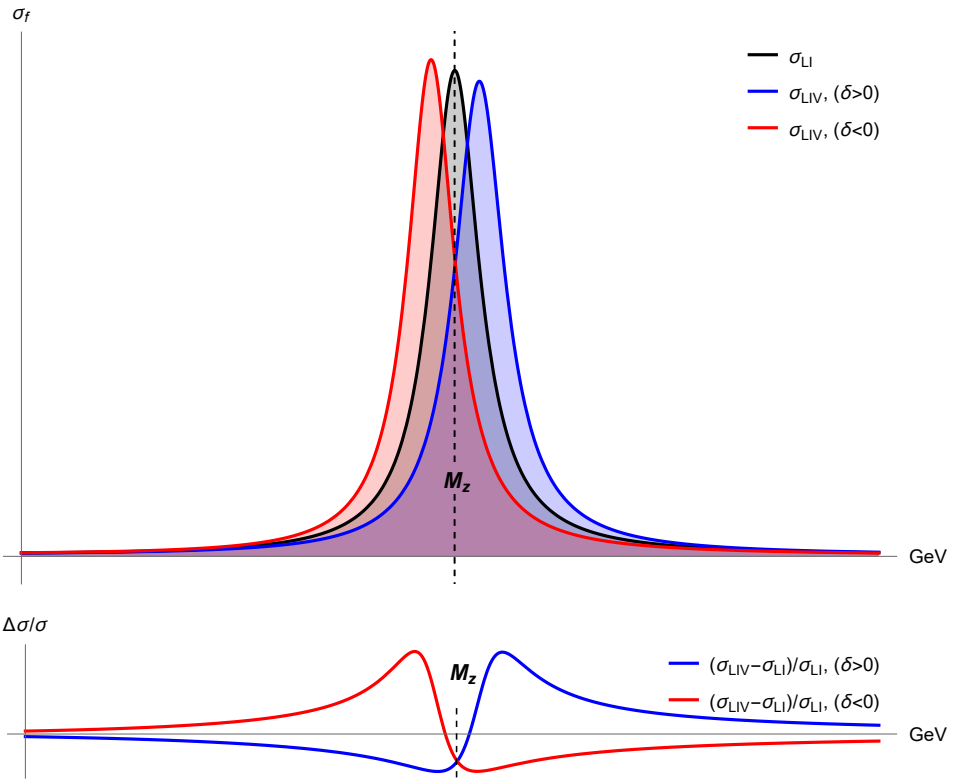

The plot for $Y = 8$ illustrates LIV behavior in contrast to LI. Such an explicit presentation is not feasible for $Y = 4.5$, where the effect amounts to only $\sim 0.1\%$, making it visually indistinguishable.

If LIV is present, the most likely scenario is that all data — both high rapidity (where LIV is pronounced) and low rapidity (where LIV is negligible) — will be combined together. Attempting to fit this LIV-affected cross section into an LI template still yields a result, since the effect is perturbative in nature, but with altered fitting parameters: the extracted boson mass, and to a lesser degree the decay width. To illustrate this behavior, below we provide a table of the fitted mass shift ΔM_Z

Table 12.1: Absolute mass shift $|\Delta M_Z|$ as a function of rapidity Y and the fractional composition of LI and LIV contributions of cross sections in the data.

LI :	100%	90%	80%	70%	60%	50%	40%	30%	20%	10%	0%
LIV :	0%	10%	20%	30%	40%	50%	60%	70%	80%	90%	100%
Y=0.5	0eV	0.1keV	0.1keV	0.2keV	0.2keV	0.3keV	0.3keV	0.4keV	0.5keV	0.5keV	0.6keV
Y=1.0	0eV	0.1keV	0.2keV	0.3keV	0.4keV	0.5keV	0.7keV	0.8keV	0.9keV	1.0keV	1.1keV
Y=1.5	0eV	0.3keV	0.5keV	0.8keV	1.0keV	1.3keV	1.5keV	1.8keV	2.keV	2.3keV	2.5keV
Y=2.0	0eV	0.6keV	1.3keV	1.9keV	2.6keV	3.2keV	3.9keV	4.5keV	5.2keV	5.8keV	6.5keV
Y=2.5	0eV	1.7keV	3.4keV	5.1keV	6.9keV	8.6keV	10.3keV	12.keV	13.7keV	15.4keV	17.1keV
Y=3.0	0eV	4.6keV	9.2keV	13.9keV	18.5keV	23.1keV	27.7keV	32.4keV	37.keV	41.6keV	46.2keV
Y=3.5	0eV	12.5keV	25.1keV	37.6keV	50.1keV	62.6keV	75.2keV	87.7keV	100.2keV	112.7keV	125.3keV
Y=4.0	0eV	34keV	68keV	102keV	136keV	170keV	204keV	238keV	272keV	306keV	340keV
Y=4.5	0eV	92keV	185keV	277keV	370keV	462keV	0.6MeV	0.6MeV	0.7MeV	0.8MeV	0.9MeV
Y=5.0	0eV	251keV	0.5MeV	0.8MeV	1.0MeV	1.3MeV	1.5MeV	1.8MeV	2.0MeV	2.3MeV	2.5MeV
Y=5.5	0eV	0.7MeV	1.4MeV	2.0MeV	2.7MeV	3.4MeV	4.1MeV	4.8MeV	5.5MeV	6.1MeV	6.8MeV
Y=6.0	0eV	1.9MeV	3.7MeV	5.6MeV	7.4MeV	9.3MeV	11.1MeV	13.0MeV	14.8MeV	16.7MeV	18.6MeV
Y=6.5	0eV	5MeV	10MeV	15MeV	20MeV	25MeV	30MeV	35MeV	40MeV	45MeV	51MeV
Y=7.0	0eV	14MeV	27MeV	41MeV	55MeV	69MeV	82MeV	96MeV	110MeV	124MeV	137MeV

This table shows how the resonance mass shifts from the true mass value when an LIV-contaminated cross section is reconstructed as an LI Standard Model fit. The greater the contamination by LIV effects—which corresponds to events at higher rapidities—the larger the mass shift. Although real data would consist of a distribution of events across all possible rapidities, this simplified picture still serves as a clear demonstration. Depending on the event selection process, a different pattern may emerge. In particular, selecting only higher-rapidity events would yield a stronger LIV signal in the form of a mass shift. The sign of δ_{LIV} determines whether the resonance mass is overestimated ($\delta_{LIV} > 0$) or underestimated ($\delta_{LIV} < 0$), but the difference in both cases remains within the displayed accuracy. For this reason, we combine both cases into a single chart.

In the table we see a numerical confirmation of our qualitative expectations. The low-rapidity cases contain virtually no LIV. If the data is a mixture of 90% LI and 10% LIV events at $Y = 5$, the total effect is diluted to $|\Delta M_Z| \approx 0.25$ MeV. By contrast, if 100% of $Y = 5$ data is analyzed, then $|\Delta M_Z| \approx 2.5$ MeV noticeably larger than the quoted experimental uncertainty of 2.1 MeV and therefore impossible to accommodate within the declared accuracy. Clearly, for $Y = 6$ LIV would be even easier to detect, if accelerators could access such high rapidity regimes.
This table is a kind of proxy intended to mimic the realistic effect of PDFs. Even in this simplified approximation, the nature of the LIV effect is very descriptive. Exact calculations using PDFs, or including lower-order processes, cannot alter the general behavior, though they would certainly provide a more quantitatively accurate picture.

12.7 Discussion: Z vs W Bosons

We discussed in detail the case of the Z boson because of its narrow width and clean leptonic channels, properties that make analysis of experimental data and the chance of discovering possible LIV effects more realistic. We understand that the modified dispersion relation affects the resonance region shape in a prominent way, and the effect is more pronounced at higher rapidities. The sign of the LIV parameter determines whether the shift in resonance mass is negative or positive; however, the absolute value of the shift remains approximately the same. Since in all data the pronounced LIV effect will appear only in a small fraction of events,

the total divergence of the fitted parameters from the Lorentz-invariant ones will be less noticeable. This warrants dedicated screening of high-rapidity cases in a separate analysis. In the case of anisotropy, separate binning by sidereal time will be necessary to understand the nature of the effect, although here we may encounter the practical limit imposed by insufficient statistics.

While everything said above holds, we must keep in mind that the Z boson is routinely used for calibration at hadron accelerators (LHC and CDF). This raises the question of whether such a procedure could bias against potential LIV effects, and we are not equipped to answer this question yet.

The Z boson looks like an ideal candidate for such a study in a certain sense, but everything said about the Z boson can in principle be generalized to charged W bosons as well. Interestingly, recent tensions between Tevatron and LHC measurements of M_W, resulting in a discrepancy of about 65 MeV [21], are qualitatively in line with the LIV behavior for negative δ_{LIV}. It is yet unclear whether this discrepancy originates from experimental issues, and it is unlikely that the matter will be resolved soon. Nevertheless, if there is even partial merit to this interpretation, it would warrant serious exploration of LIV in resonance mass measurements.

Taken together, the Z and W boson cases highlight how collider observables provide a unique and complementary window on LIV, one that cannot be accessed through astrophysical probes alone. This motivates the broader conclusions we now turn to.

12.8 Conclusions and Outlook

In this work we have explored how Lorentz invariance violation (LIV) can manifest in the weak sector through modifications of the Z-boson dispersion relation. Starting from a simple but physically motivated Lagrangian deformation, we showed how only a restricted class of operators leads to observable effects, with gauge invariance necessarily compromised to ensure physical LIV. The resulting modifications impact both the propagator and resonance properties of the Z boson in a calculable way.

The Drell–Yan process provides an especially clean testing ground, as the resonance region of the Z boson is both experimentally well measured and theoretically under control. We demonstrated that LIV effects scale almost exponentially with rapidity and, in anisotropic cases, can introduce sidereal modulations. This motivates targeted analyses that separate events by rapidity and, where relevant, by sidereal time. While the majority of experimental data originates at small rapidities where LIV effects are negligible, the high-rapidity bins—though rarer—carry the dominant sensitivity. Our analysis indicates that percent-level modifications of the cross section are possible for $|\delta_{LIV}|$ around 10^{-8}, leading to effective shifts in the fitted Z-boson mass that can exceed current experimental uncertainties.

The timelike violation case offers the clearest starting point, as it avoids anisotropy and maximizes rapidity dependence, but the spacelike and lightlike scenarios remain equally important for a comprehensive picture. Our proxy estimates further show that even after dilution by parton distribution effects, the characteristic signatures of LIV remain robust.

Beyond the Z boson, similar reasoning extends to W bosons. Recent discrepancies in W-mass measurements may be qualitatively consistent with negative δ_{LIV}, although firm conclusions require further scrutiny. Taken together, the Z and W bosons constitute an essentially unexplored sector for LIV searches, one that cannot be constrained astrophysically and is uniquely accessible to collider experiments. In outlook, we emphasize several directions:
1. Dedicated experimental analyses that implement binning in rapidity and, where applicable, sidereal time.
2. Extension of the study to W bosons, especially in light of current experimental tensions.
Altogether, collider studies of unstable bosons provide sensitivity to LIV possibly up the 10^{-9} level, competitive with astrophysical bounds but in a complementary sector. Pursuing this line of research could therefore open a new experimental window on fundamental physics beyond the Standard Model.

Acknowledgments

We thank Jon Chkareuli and the participants of the 25th Workshop 'What Comes Beyond the Standard Models?' (6–17 July, Bled, Slovenia) for valuable and fruitful discussions, and the organizers for providing a productive working environment. This work was supported by SRNSF (grant STEM-22-2604).

References

1. V.A. Kostelecký, S. Samuel. Spontaneous breaking of Lorentz symmetry in string theory. Phys. Rev. D 39, 683 (1989). https://doi.org/10.1103/PhysRevD.39.683
P. Kraus, E.T. Tomboulis. Photons and Gravitons as Goldstone Bosons, and the Cosmological Constant. Phys.Rev. D66 (2002) 045015. https://doi.org/10.48550/arXiv.hep-th/0203221
R. Bluhm, A. Kostelecky. Spontaneous Lorentz Violation, Nambu-Goldstone Modes, and Gravity. Phys.Rev.D71:065008,2005. https://doi.org/10.48550/arXiv.hep-th/0412320
J.L. Chkareuli, Z.R. Kepuladze. Massless and Massive Vector Goldstone Bosons in Nonlinear Quantum Electrodynamics. Contribution to: 14th International Seminar on High Energy Physics: Quarks 2006. https://doi.org/10.48550/arXiv.hep-th/0610277
J.L. Chkareuli, J.G. Jejelava. Spontaneous Lorentz Violation: Non-Abelian Gauge Fields as Pseudo-Goldstone Vector Bosons. Phys.Lett.B659:754-760,2008. https://doi.org/10.48550/arXiv.0704.0553
J.L. Chkareuli, C.D. Froggatt, H.B. Nielsen. Spontaneously Generated Tensor Field Gravity. Nuclear Physics B, V. 848, I. 3. https://doi.org/10.48550/arXiv.1102.5440
J.L. Chkareuli, J.G. Jejelava, G. Tatishvili. Graviton as a Goldstone boson: Nonlinear Sigma Model for Tensor Field Gravity. Phys.Lett.B696:124-130,2011. https://doi.org/10.48550/arXiv.1008.3707
J.L. Chkareuli, J. Jejelava, Z. Kepuladze. Lorentzian Goldstone modes shared among photons and gravitons. Eur.Phys.J.C 78 (2018) 2, 156. https://doi.org/10.48550/arXiv.1709.02736
J.L. Chkareuli, Z. Kepuladze. Gauge Symmetries Emerging from Extra Dimensions. Phys.Rev.D 94 (2016) 6, 065013. https://doi.org/10.48550/arXiv.1607.05919

2. P. Horava. Quantum Gravity at a Lifshitz Point. Phys.Rev.D79:084008,2009. https://doi.org/10.48550/arXiv.0901.3775
3. K.Greisen. End to the Cosmic-Ray Spectrum? Phys. Rev. Lett. 16, (1966) 748. https://doi.org/10.1103/PhysRevLett.16.748
   G.T. Zatsepin and V.A. Kuz'min. Upper limit of the spectrum of cosmic rays. JETP Lett. 41 (1966) 78.
4. AGASA Collab. (M. Takeda et al.). Extension of the Cosmic-Ray Energy Spectrum beyond the Predicted Greisen-Zatsepin-Kuz'min Cutoff. Phys.Rev.Lett. 81 (1998) 1163-1166. https://doi.org/10.48550/arXiv.astro-ph/9807193
   AGASA Collab. (M. Takeda et al.). Energy determination in the Akeno Giant Air Shower Array experiment. Astropart.Phys. 19 (2003) 447-462. https://doi.org/10.48550/arXiv.astro-ph/0209422
5. The Pierre Auger Collaboration. Features of the energy spectrum of cosmic rays above $2.5 * 10^{18}$ eV using the Pierre Auger Observatory. Phys. Rev. Lett. 125, 121106 (2020). https://doi.org/10.48550/arXiv.2008.06488
   The Pierre Auger Collaboration. Measurement of the cosmic-ray energy spectrum above $2.5 * 10^{18}$ eV using the Pierre Auger Observatory. Phys. Rev. D 102, 062005 (2020). https://doi.org/10.48550/arXiv.2008.06486
   The Pierre Auger Collaboration. The energy spectrum of cosmic rays beyond the turn-down around 10^{17} eV as measured with the surface detector of the Pierre Auger Observatory. Eur. Phys. J. C (2021) 81:966. https://doi.org/10.48550/arXiv.2109.13400
6. A. Giarnetti, S. Marciano, D. Meloni. Exploring New Physics with Deep Underground Neutrino Experiment High-Energy Flux: The Case of Lorentz Invariance Violation, Large Extra Dimensions and Long-Range Forces. Universe 10 (2024) 9, 357. https://doi.org/10.48550/arXiv.2407.17247
   K. Hirata et al. [Kamiokande-II Collaboration], Phys. Rev. Lett. 58 (1987) 1490.
7. S. Coleman, S. L. Glashow. High-Energy Tests of Lorentz Invariance. Phys.Rev.D59:116008,1999. https://doi.org/10.48550/arXiv.hep-ph/9812418
8. A. Kostelecky, N. Russell. Data Tables for Lorentz and CPT Violation. Rev.Mod.Phys. 83: 11 (2011). https://doi.org/10.48550/arXiv.0801.0287
9. B. Altschul. Laboratory Bounds on Electron Lorentz Violation. Phys. Rev. D 82, 016002 (2010). https://doi.org/10.48550/arXiv.1005.2994
10. O. Gagnon, G.D. Moore. Limits on Lorentz violation from the highest energy cosmic rays. Phys.Rev. D70 (2004) 065002. https://doi.org/10.48550/arXiv.hep-ph/0404196
    Floyd W. Stecker. Constraining Superluminal Electron and Neutrino Velocities using the 2010 Crab Nebula Flare and the IceCube PeV Neutrino Events. Astroparticle Physics 56 (2014) 16. https://doi.org/10.48550/arXiv.1306.6095
    F. Duenkel, M. Niechciol, M. Risse. Photon decay in UHE air showers: stringent bound on Lorentz violation. Phys. Rev. D 104, 015010 (2021). https://doi.org/10.48550/arXiv.2106.01012
11. Z. Kepuladze. Lorentz Violation: Loop-Induced Effects in QED and Observational Constraints. https://doi.org/10.48550/arXiv.2504.15608
12. J. Jejelava, Z. Kepuladze. Probing Lorentz Invariance Violation in Z Boson Mass Measurements at High-Energy Colliders. https://doi.org/10.48550/arXiv.2504.11248
13. CMS Collaboration. Searches for violation of Lorentz invariance in top quark pair production using dilepton events in 13TeV proton-proton collisions. Phys. Lett. B 857 (2024) 138979. https://doi.org/10.48550/arXiv.2405.14757
14. E. Lunghi, N. Sherrill, A. Szczepaniak, A. Vieira. Quark-sector Lorentz violation in Z-boson production. JHEP 07 (2024) 167 (erratum). https://doi.org/10.48550/arXiv.2011.02632

15. J.L. Chkareuli, Z. Kepuladze. Standard model with partial gauge invariance. Eur. Phys. J. C 72, 1954 (2012). https://doi.org/10.1140/epjc/s10052-012-1954-9
16. ALEPH, DELPHI, L3, OPAL and SLD Collaborations, LEP EW Working Group and SLD EW and Heavy Flavour Groups: S. Schael et al. Precision Electroweak Measurements on the Z Resonance. Phys.Rept.427:257-454, 2006. https://doi.org/10.48550/arXiv.hep-ex/0509008
17. J.L. Chkareuli, C.D. Froggatt, H.B. Nielsen. Deriving Gauge Symmetry and Spontaneous Lorentz Violation. Nucl.Phys.B821:65-73,2009. https://doi.org/10.48550/arXiv.hep-th/0610186
    J.L. Chkareuli, C.D. Froggatt, H.B. Nielsen. Lorentz Invariance and Origin of Symmetries. Phys. Rev. Lett. 87 (2001) 091601. DOI: https://doi.org/10.1103/PhysRevLett.87.091601
    J.L. Chkareuli, C.D. Froggatt, H.B. Nielsen. Spontaneously generated gauge invariance. Nucl. Phys. B 609 (2001) 46. https://doi.org/10.1016/S0550-3213(01)00283-8
18. S. Willenbrock. Mass and width of an unstable particle. Eur.Phys.J.Plus 139 (2024) 6, 523. https://doi.org/10.48550/arXiv.2203.11056.
19. W. Greiner, B. Müller. Gauge Theory of Weak Interactions (fourth edition). Springer-Verlag Berlin Heidelberg, 2009.
20. P. Banerjee, G. Das, P.K. Dhani, V. Ravindran. Threshold resummation of the rapidity distribution for Drell-Yan production at NNLO+NNLL. Phys. Rev. D 98, 054018 (2018). https://doi.org/10.48550/arXiv.1805.01186
21. C. Hays [CDF], High precision measurement of the W-boson mass with the CDF II detector, PoS **ICHEP2022**, 898 (2022) doi:10.22323/1.414.0898
    [CMS], Measurement of the W boson mass in proton-proton collisions at sqrts = 13 TeV, CMS-PAS-SMP-23-002.
    ATLAS Collaboration, Improved W boson Mass Measurement using 7 TeV Proton-Proton Collisions with the ATLAS Detector, ATLAS-CONF-2023-004, CERN, Geneva, 2023.

BLED WORKSHOPS
IN PHYSICS
VOL. 26, NO. 1

Proceedings of the 28th Workshop
What Comes Beyond . . . *(p. 158)*
Bled, Slovenia, July 6–17, 2025

13 Simulation of the Propagation and Diffusion of Dark Atoms in the Earth's Crust

A. Kharakhashyan[1,2†]

[1] Research Institute of Physics, Southern Federal University, Rostov-on-Don, 344090, Russia
[2] Department of Advanced Mathematics, Don State Technical University, Rostov-on-Don, 344000, Russia

Abstract. Over many decades of research, a wide range of robust and theoretically well-founded models of Dark Matter have been proposed. Consequently, experimental verification of the proposed dark matter candidates has become a priority. The obtained results enable, on the one hand, to analyze the expectations for various models, and on the other hand, to explain the observational results themselves, using these models – specifically, in terms of dark atoms having strong interactions with matter. In this paper, we present a framework developed for modeling of the propagation and diffusion processes, and calculating the concentration of dark matter particles within the Earth's surface layers, as well as for performing detection with underground detectors. The developed framework accounts for the Earth's orientation relative to the dark matter halo, the velocities and directions of motion of the Solar System and the Earth relative to the galactic center, the relief of the Earth's surface, the geometry of the detector, and the directions of particle arrival at the Earth's surface. A comparison with the results presented by the DAMA/LIBRA collaboration is made in terms of interpreting the data using the dark atom model. The simulation shows the presence of daily and annual modulations, phase matches DAMA/LIBRA results and qualitative agreement in dynamics is observed.

13.1 Introduction

The detection and investigation of Dark Matter have remained a central and intensively discussed subject within cosmology, astrophysics, and particle physics for many decades [1]. In recent years, significant interest has arisen in the field of detecting dark matter particles using underground detectors. The results obtained and presented by the DAMA team are of particular interest here, because they show that the number of events recorded by the NaI(Tl) detectors exhibits the presence of periodic modulations. The obtained results enable, on the one hand, to analyze the expectations for various models, and on the other hand, try to explain the observational results themselves, using these models. Explanation of DAMA/LIBRA results assumes annual modulation of low energy binding of dark matter particles with nuclei. Such dark matter candidates could not lead to nuclear recoil in underground experiments. Therefore, the particles that exhibit strong interactions with matter are of interest among the possible candidates. The

†aharahashyan@sfedu.ru

assumed bound states could be considered strongly interacting massive particles. These properties are expected within the dark atom model. Dark atoms have strong (nuclear) elastic cross section of interaction with protons and nuclei, however the inelastic process of their radiative capture is strongly suppressed [2]. The properties and behavior expected of dark atoms could potentially lead to effects that might explain the experimental results. The aim of this study was to develop a framework for modeling particle propagation and detection by underground detectors for comparison with the results of the DAMA experiment using the dark atom model. The model assumes that dark atoms are captured by the Earth, leading to an annual modulation of their concentration in the detector material. These dark atoms can then bind to sodium or iodine nuclei at energies of several keV.

13.2 Method for modeling the propagation and detection of particles

To conduct the simulation, it is necessary to determine a number of key characteristics of dark atoms that will have a significant impact on the propagation and detection processes. While the initial estimate of the mass of dark atoms is between 1 TeV and 10 TeV, experiments at the LHC raise the lower limit, so, in this paper, particles with mass $M_O = 2\,\text{TeV}$ are considered. The nuclear interaction cross section is expected to be around $\sigma \sim 10^{-25}\,\text{cm}^2$. The rate of radiative capture of dark atom by nuclei can be estimated with the use of the analogy with the radiative capture of a neutron by a proton [2]:

$$\sigma v = \frac{f\pi\alpha}{m_p^2}\frac{3}{\sqrt{2}}\left(\frac{Z}{A}\right)^2\frac{T}{\sqrt{A m_p E}}. \tag{13.1}$$

Here, $f = 1.4 \cdot 10^{-3}$, m_p is the proton mass, Z and A are charge and mass numbers of captured nucleus of detector matter and E is a binding energy of the bound state. Assuming the detector temperature $T = 300\,\text{K}$, for the fixed binding energy $E = 4\,\text{KeV}$ withing the energy band where the modulations are present in the experiment, we can obtain the following estimates for sodium

$$\langle\sigma v\rangle_{Na} \approx 5.9 \cdot 10^{-31}\,\text{cm}^3/\text{s}, \tag{13.2}$$

and for iodine

$$\langle\sigma v\rangle_{I} \approx 1.9 \cdot 10^{-31}\,\text{cm}^3/\text{s}. \tag{13.3}$$

The thickness of the Earth's crust may be an obstacle to the flow of dark atoms, and since they rapidly thermalize at a depth of about 100 meters and drift toward the center of the Earth via diffusion. Moreover, even a few kilometers of rock could pose a significant obstacle. Another factor is the relative velocities and rotation of the Earth, and the resulting modulation of the flow near the surface (Figure 13.1). In this work, we use the beam approach and consider the particle flow as a beam of given intensity.

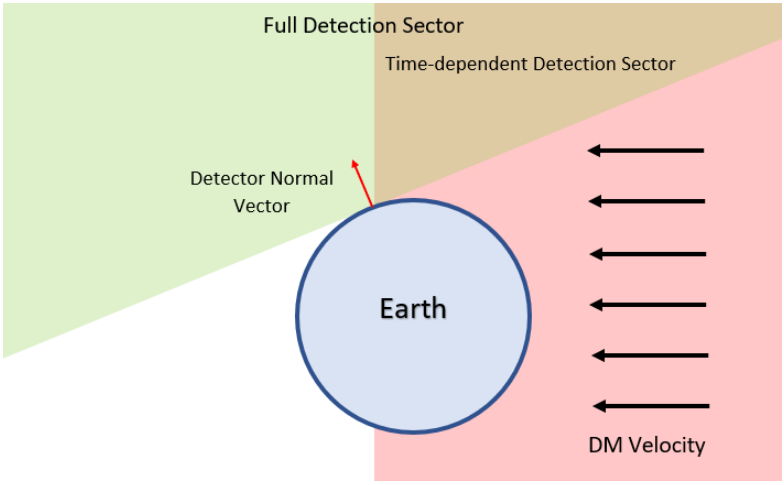

Fig. 13.1: Illustration of the influence of directionality and shadowing on the detection of dark matter particles. Note that since the actual particle velocity distribution is assumed to be Gaussian and particles arrive simultaneously from different directions, the dark matter velocity vectors shown here illustrate only the general direction of motion of the fastest particles relative to Earth, which are moving toward it as Earth orbits the center of the Milky Way.

To take the aforementioned problems into account and assess the effect of terrain roughness on particle dispersion and the resulting impact on particle concentration in the vicinity of the detector (and, consequently, the number of events) over time, it is necessary to determine the path that particles take through the rock and to calculate the velocity vectors of all objects in the system under consideration, with reference to real coordinates and time. The path that a beam takes within the Earth's surface can be estimated using a topographic 3D map, shown in Figure 13.2.

Each beam specifies the potential direction of arrival of the flow of dark atoms from space in the upper region of the half-space, relative to the horizon. The directional vectors $\overline{d}_{beam}$ of the beams are defined in the spherical coordinate system centered on the detector. This coordinate system is then related to the geodetic coordinate system. The azimuthal angle φ is measured counterclockwise from the east direction along the longitude axis of the geodetic coordinate system. The polar angle θ is measured from the normal vector to the Earth's surface. For convenience, the beams are numbered starting from the azimuthal axis; thus, the angle between the azimuthal direction and the beam direction is $\theta_{beam} = \frac{\pi}{2} - \theta$. For each azimuthal angle φ, there is a half-plane passing through the normal vector to the Earth's surface and the direction vector of each beam with the same φ; this half-plane is perpendicular to the azimuthal plane. For each such half-plane, we calculate the intersection points between the two-dimensional interpolated topographic approximation of the Earth's surface and the linear segments defined by the directional vectors $\overline{d}_{beam}$, representing beams (Figure 13.3). The first point

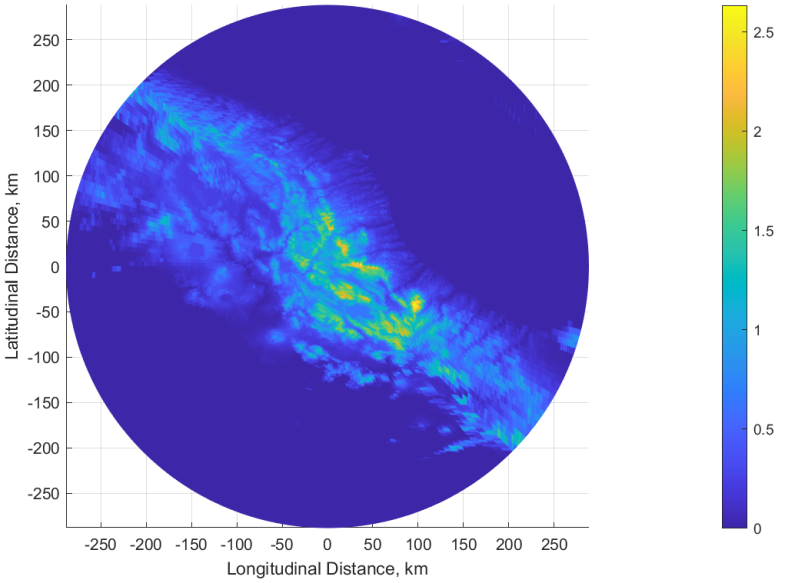

Fig. 13.2: A topographic map showing the relief of the Earth around the detector. Color represents the elevation above the sea level, in kilometers.

of each segment is at the detector, and the second point lies on the surface of a semi-sphere of radius $R = 288$ km, which covers the entire area of interest.
The velocity vector of the detector $\overline{V}_{detector}$, including the rotational component due Earth's rotation, as well as the heliocentric and galactocentric components of the Earth's velocity, can be calculated in Geocentric Celestial Reference System at time t using ephemeris data. The velocity of dark matter particles $\overline{V}_{particle}$ is assumed to have Gaussian distribution [3]:

$$\overline{V}_{full}(t) = \overline{V}_{detector}(t) + \overline{V}_{particle}. \tag{13.4}$$

We can estimate the initial intensity of the beam, as well as their time-dependent intensity as the particles pass through the medium, using the exponential decay law. The flux itself is modulated by the total value of the velocity of the system, as well as by the orientation of the beam in relation to the velocity vector:

$$I_0(\varphi, \theta_{beam}, t) = n_{beam} \cdot V_{beam}(t) \cdot S_{\theta_{beam},\varphi}, \tag{13.5}$$

$$I(\varphi, \theta_{beam}, d, t) = I_0(\varphi, \theta_{beam}, t) \cdot e^{\frac{-d}{l}}, \tag{13.6}$$

$$V_{beam}(t) = \left|\overline{V}_{full}(t)\right| \cdot \cos\left(\overline{d}_{beam}, \overline{V}_{full}(t)\right), \tag{13.7}$$

where I_0 is the initial beam intensity, I is the current beam intensity, d is the distance traveled by beam, and l is the mean free path, V_{beam} is the projection of system's velocity vector onto the directional vector, n_{beam} is the initial concentration.
Using the equation (3) from [2], we can find the approximate particle velocity as $V_{drift} \approx 80 S_3 A^{1/2}$, where $S_3 = M_O/1\ TeV$, gravitational acceleration is

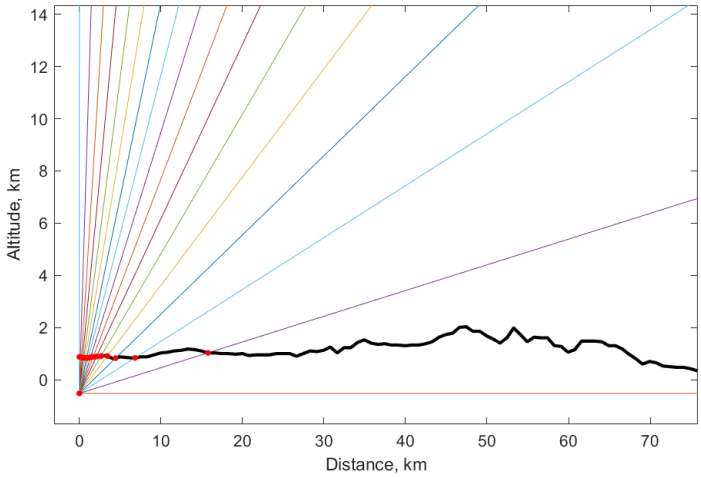

Fig. 13.3: Calculation of coordinates of intersection points of beams with the Earth's surface. The black curve represents Earth's surface; the colored lines represent beams; the red dots represent the points of intersection between the beams and Earth's surface, $\varphi = 0$. The altitude axis is relative to sea level.

$g \approx 980\,\mathrm{cm/s^2}$ and the average atomic weight in terrestrial surface matter $A \sim 30$. The distribution of particle velocities is assumed to be Maxwell–Boltzmann distribution.

The flow of dark atoms is considered as a set of propagating beams, which, upon collision with the Earth's surface, slow down and undergo a thermalization process. To estimate the particle distribution, we use Brownian motion with drift:

$$\boldsymbol{BD}\,(x, y, z, t) = \boldsymbol{BM}\,(x, y, z, t) + \overline{V}_p^T \times \overline{V}_{drift} \cdot t, \tag{13.8}$$

where $\boldsymbol{BM}\,(x, y, z, t)$ represents the standard Brownian motion processes, described as a set of Wiener processes, x, y, z are the beam-specific coordinates of the particles, $\overline{V}_p$ is a row vector of size N_p sampled from Maxwell–Boltzmann distribution, $\overline{V}_{drift} = (0, 0, -1)$ is the drift direction vector. This equation is presented in tensor form and includes equations for both the set of N_p particles, and the beams they originate from. Assuming the particles move in the -Z direction toward the Earth's center, the covariance matrix for the increments of the 3-dimensional normal distribution in the plane perpendicular to the beam velocity vector at a time t can be written as follows:

$$C(t) = \begin{pmatrix} t & 0 & 0 \\ 0 & t & 0 \\ 0 & 0 & \approx 0 \end{pmatrix}. \tag{13.9}$$

The resulting dark atom concentration $\rho_O\,(t)$ can be estimated as the number of particles inside the detector, divided by the volume of the detector:

$$\rho_O\,(t) = \frac{N_p\,(t)}{Vol}. \tag{13.10}$$

The capture rate can be written as:

$$R(t) = \epsilon \frac{\rho_O(t)}{M_O} \left(\langle \nu_{Na} \sigma_{Na} \rangle + \langle \nu_I \sigma_I \rangle \right) N_T, \tag{13.11}$$

where $N_T = 4.015 \times 10^{24}$ nuclei per kg of NaI(Tl), ν is the relative velocity between the dark atom particle and nucleus, σ is the capture cross section of the process, $\epsilon = 1$. Since M_O is much higher than the nuclei masses, ν are mainly the thermal velocities of the sodium and iodine nuclei. Due to the large mass of the DAMA/LIBRA detectors (approximately 9.7 kg each), it is assumed that low-energy γ-rays are fully absorbed within the detector.
The proposed framework allows us to estimate the 3-dimensional spatial distribution of the flow of dark atoms, as well as track its change over time in the Earth's crust. We can observe exactly how a particular direction of arrival of a beam affects the spatial distribution. In addition, the framework also allows to see how the resulting distribution relates to the surface relief above the detector, and what path certain groups of particles took.

13.3 Results and Discussion

In this section, we present qualitative assessments of the simulation results and compare them with the results from the DAMA/LIBRA experiment. At this stage, the initial simulation framework does not allow for an adequate assessment of the absolute number of events, therefore, only qualitative assessments of modulations will be given in terms of the coincidence of the expected positions of maxima, minima, and also the phases and periods of modulations, in relative units.
The figure 13.4 shows the simulation results for the annual modulation of the residual count rate, averaged over 11 years. The expected positions of the maxima, as well as their periods, agree with the estimates and observations of the DAMA/LIBRA experiment [4]. In particular, the annual maximum should be observed around June 2, on day 152.5. For the minimum values, the dynamics are more complex, however, one of the local minima is very close to the experimental minimum expected around December 2.
The Figure 13.5 shows the results of fitting of the simulation results for several years using cosine function approximation. If we compare these results with the Figure 1 from [4], it can be seen that both the modulation phase and the positions of the maxima coincide with the experiment. The period remains consistent throughout all years.
As can be seen from the Figure 13.6, the proposed framework is able to reproduce the expected diurnal modulation, the maximum of which should occur at approximately 20:00 h, and the minimum at approximately 8:00 h. This result is in good agreement with the theoretical model-independent estimates conducted by the DAMA team in the paper [6], which show that the effect of diurnal shielding by Earth is maximal about at 8:00 h and minimal around 20:00 h, as illustrated in Figures 2 and 4 in the original paper. It is important to note that the diurnal modulation is also superimposed by annual modulation, and Greenwich Mean Sidereal Time (GMST) deviates from the solar time, thus, the results averaged over

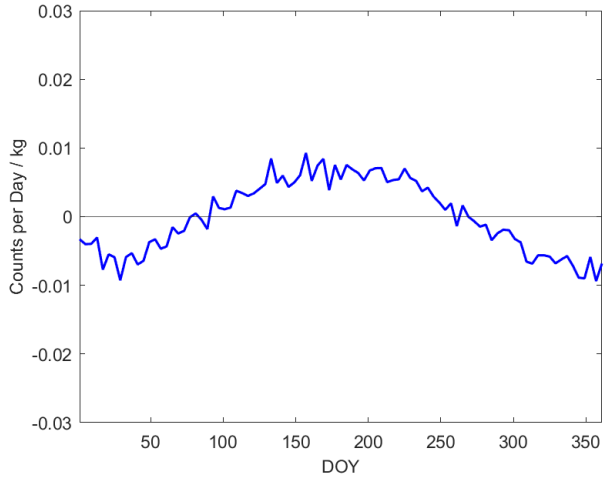

Fig. 13.4: Simulation results for the residual count rate for annual modulation, averaged over 11 years, as a function of day of the year(DOY).

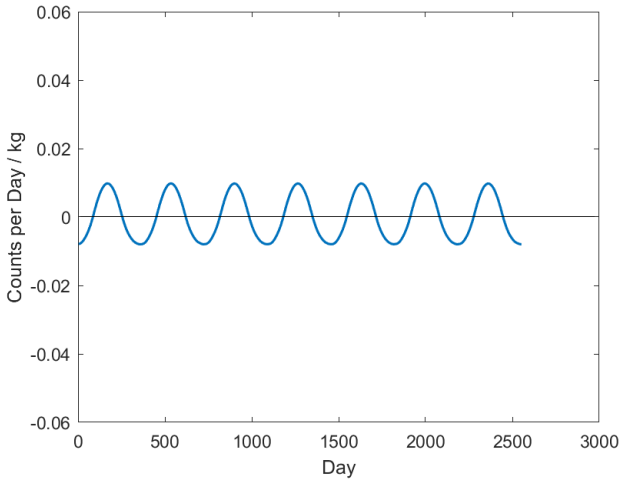

Fig. 13.5: The results of fitting of the simulated residual count rate as $A\cos(\omega(t - t_0))$, day 0 is January 1, 2011.

the entire observation period will be less prominent, and will also depend on the considered energy interval, as shown in [4-6].

13.4 Conclusions

This paper presents the first initial version of the framework for modeling the propagation and detection of dark matter particles within the Earth's crust using underground detectors based on the dark atom model. The framework took into account several key dark atom parameters, such as mass and cross section. The analysis was conducted from a geometric perspective using the beam model with

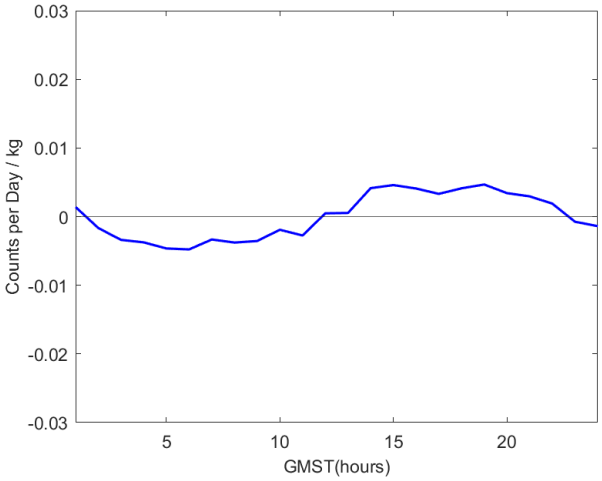

Fig. 13.6: Simulation results for the residual count rate for daily modulation, averaged over one week, as a function of GMST.

an optical analogy involving decay and diffusion. The proposed framework allows to estimate the concentration of dark atoms in underground detectors taking into account their geometry and size, underground depth and effects caused by the unevenness of the terrain above them, and the directions of particle arrival at the Earth's surface. Calculations are carried out with reference to real time, the Earth's orientation relative to the dark matter halo, the velocities and directions of motion of the Solar System and the Earth relative to the galactic center. The simulation shows the presence of daily and annual modulations, phase matches DAMA/LIBRA estimates, and qualitative agreement in dynamics is observed.

Acknowledgements

The research was carried out in the Southern Federal University with financial support from the Ministry of Science and Higher Education of the Russian Federation (State contract GZ0110/23-10-IF)

References

1. M.Khlopov: What comes after the Standard model, Progress in Particle and Nuclear Physics **116** (2021) 103824.
2. M. Y. Khlopov, A. G. Mayorov, and E. Y. Soldatov. Composite dark matter and puzzles of dark matter searches. International Journal of Modern Physics D, **19**:1385–1395, 2010.
3. Warren R. Brown et al. Velocity Dispersion Profile of the Milky Way Halo. AJ, **2010**, 139, 59, arXiv:0910.2242v1 [astro-ph.GA]
4. Bernabei, R., Belli, P., Cappella, F. et al. Dark Matter: DAMA/LIBRA and its perspectives. arXiv:2110.04734 [hep-ph]
5. Bernabei, R., Belli, P., Cappella, F. et al. Model independent result on possible diurnal effect in DAMA/LIBRA-phase1. Eur. Phys. J. C 74, 2827 (2014).

6. Bernabei, R., Belli, P., d'Angelo, S. et al. Investigating Earth shadowing effect with DAMA/LIBRA-phase1. Eur. Phys. J. C 75, **239** (2015). https://doi.org/10.1140/epjc/s10052-015-3473-y

BLED WORKSHOPS
IN PHYSICS
VOL. 26, NO. 1

Proceedings of the 28th Workshop
What Comes Beyond . . . *(p. 167)*
Bled, Slovenia, July 6–17, 2025

14 On CP-violation and quark masses: reducing the number of parameters

A. Kleppe[†]

SACT, Oslo

Abstract. A physically viable ansatz for quark mass matrices must satisfy certain constraints. In this article we study a concrete example, by looking at some generic matrices with a nearly democratic texture, and the implications of the constraint imposed by CP-violation, specifically the Jarlskog invariant. We find that the number of mass parameters is reduced from six to five, implying that the six mass eigenvalues of the up-quarks and the down-quarks are interdependent, which in our approach is explicitly demonstrated.
Povzetek: Avtorica proučuje lastnosti skoraj demokratičnih matrik z upoštevanjem kršitve CP, posebej kršitev invariante Jarlskogove. Ugotavlja, da se število masnih parametrov zmanjša s šest na pet, s čimer dokazuje medsebojno odvisnost mas kvarkov.

14.1 Introduction

A mass matrix ansatz is a suggestion of what form the quark mass matrices may have in the weak (flavour) basis. The hope is to find mass matrices that could shed some light on the enigmatic mass spectra. In this article, we study the constraints imposed by CP-violation on the quark mass matrices, using the mathematical tool provided by the Jarlskog invariant [1].
The usual "mathematical reason" given for CP-violation, is that the 3×3 weak mixing matrix V_{CKM} [2] has a phase that cannot be rotated away, but in the 1980s, Cecilia Jarlskog discovered that a signum of CP-violation is that (determinant of) the commutator of the mass matrices of the up- and down-sectors is nonzero, or $\det[M_u, M_d] \neq 0$, where M_u and M_d are the mass matrices of the up-sector and down-sector, repectively. She subsequently defined a direct measure of weak CP-violation, namely the Jarlskog invariant

$$J_{CP} = -i \det[M_u, M_d]/2P_uP_d$$

where $P_u = (m_u - m_c)(m_c - m_t)(m_t - m_u)$, $P_d = (m_d - m_s)(m_s - m_b)(m_b - m_d)$, and m_j are the mass eigenvalues. Technically speaking, the weak CP-violation is related to the complex elements in the weak mixing matrix, and the connection between the weak mixing matrix and the Jarlskog invariant can be expressed as

$$J_{CP} = \mathrm{Im}(V_{ij}V_{kl}V_{kj}^*V_{il}^*)$$

[†]sactacmk@gmail.com

where V_{ij}, are the matrix elements of the mixing matrix, and $i, j, k, l = 1, 2, 3$. To calculate the Jarlskog invariant J_{CP}, we can use the Wolfenstein parametrization [3] of the weak mixing matrix,

$$V_{Wolf} = \begin{pmatrix} 1-\lambda^2/2 & \lambda & A\lambda^3(\rho - i\eta) \\ -\lambda & 1-\lambda^2/2 & A\lambda^2 \\ A\lambda^3(1-\rho-i\eta) & -A\lambda^2 & 1 \end{pmatrix} \tag{14.1}$$

where $\lambda = 0.2245$, $A = 0.836$, $\rho = 0.122$, $\eta = 0.355$. Inserting the mixing matrix elements for these values in the expression $J_{CP} = Im(V_{ij}V_{kl}V_{kj}^*V_{il}^*)$, we get $J_{CP} = 3.096 \times 10^{-5}$, in agreement with the value given by the Particle Data group [4], $J_{CP} = (3.18 \pm 0.15) \times 10^{-5}$.

14.2 Mass matrices

The Jarlskog invariant implies that in order to be meaningful, an ansatz for the quark mass matrices must provide an explicit matrix ansatz for each of the charge sectors. Only then can we ensure that their commutator satifies the constraint imposed by J_{CP}, and the very first step is obviously to make sure that the commutator has a non-vanishing determinant. For the sake of concreteness, we here study the implications of the Jarlskog invariant for some rather generic matrices. In an earlier article [5], we studied matrices with a certain, nearly democratic structure, with the purpose of investigating the relations between the mass matrices for the two quark sectors. The conclusion was that at least for the proposed matrices, the up- and down-sectors have rather similar textures, which is not so surprising, given that the weak mixing matrix V_{CKM}, being the "bridge" between the two charge sectors, has a structure that is not that far from the 3×3 unit matrix. Our point of departure was the democratic matrix, corresponding to a situation where the mass eigenvalues are degenerate.

14.2.1 Ansatz 1

An ansatz is but an educated guess based on some assumptions, and in our case the assumption is that the fermionic mass matrices have an underlying democratic texture [6] [7], like

$$M_0 = \frac{T}{3}\begin{pmatrix} 1 & 1 & 1 \\ 1 & 1 & 1 \\ 1 & 1 & 1 \end{pmatrix} \tag{14.2}$$

where T has dimension mass. This matrix represents a situation where all the particles within a given charge sector initially have the same Yukawa couplings. The argument for this assumption is that in the Standard Model, all fermions get their masses from the Yukawa couplings via the Higgs mechanism, and since the couplings to the gauge bosons of the strong, weak and electromagnetic interactions are identical for all the fermions in a given charge sector, it seems like a natural assumption that they should also have identical Yukawa couplings. The mass spectrum $(0, 0, T)$ of the democratic matrix (12.2) moreover reflects the experimental

situation with one very heavy and two much lighter fermions. In the weak basis the democratic matrix M_0 is totally flavour symmetric, in the sense that the weak states of a given charge are indistinguishable ("absolute democracy").

14.2.2 Ansatz 2

The spectrum $(0, 0, T)$ is interesting, but we want three non-zero eigenvalues. One natural first step is therefore to modify the diagonal matrix elements,

$$M = \frac{T}{3}\begin{pmatrix} \alpha & 1 & 1 \\ 1 & \alpha & 1 \\ 1 & 1 & \alpha \end{pmatrix},$$

which gives a matrix that indeed has three non-zero mass eigenstates, $\frac{T}{3}(\alpha-1, \alpha-1, \alpha+2)$, but two of the masses are degenerate. In order to get three different mass eigenstates, more modifications are needed, e.g.

$$M = \begin{pmatrix} K & A & B \\ A & K & B \\ B & B & K \end{pmatrix},$$

where all the matrix elements A, B, K have dimension mass.
We now have a situation with three different mass eigenstates, corresponding to three families, meaning that we have both mixing and CP-violation, since mixing is a feature of non-degenerate families.
In our earlier article, the mass matrices were studied in a numerical, purely phenomenological framework. In order to find physically realistic mass matrices, we must however take into account constraints, above all from CP-violation.

14.2.3 Ansatz 3

It is pointless to study only one matrix ansatz: to be sure that our mass matrices are consistent with the Jarlskog invariant, we always have to consider both mass matrices, the up-quark matrix and the down-quark matrix.
Here we consider two simple mass matrices of the kind studied in [5],

$$M_u = \begin{pmatrix} K & A & B \\ A & K & B \\ B & B & K \end{pmatrix} \qquad \text{and} \qquad M_d = \begin{pmatrix} L & X & Y \\ X & L & Y \\ Y & Y & L \end{pmatrix} \tag{14.3}$$

where the matrix elements K, A, B, L, X, Y all have dimension mass. We immediately see that their commutator

$$M_u M_d - M_d M_u = \begin{pmatrix} 0 & 0 & AY - BX \\ 0 & 0 & AY - BX \\ BX - AY & BX - AY & 0 \end{pmatrix} \tag{14.4}$$

has determinant zero, so they clearly do not fulfil the requirements for quark mass matrices corresponding to physical particles.

14.2.4 Ansatz 4

In order to obtain more realistic mass matrices, we therefore introduce complexification,

$$M_u = \begin{pmatrix} K & A & B \\ A & K & B \\ B & B & K \end{pmatrix} \quad \text{and} \quad M_d = \begin{pmatrix} L & X+iG & Y+iF \\ X-iG & L & Y+iF \\ Y-iF & Y-iF & L \end{pmatrix} \tag{14.5}$$

where M_u and M_d are the mass matrices for the up-sector and down-sector, respectively. Now the determinant for the commutator is non-vanishing,

$$\det[M_u, M_d] = 8i\,BFG^2(A^2 - B^2),$$

thus

$$J_{CP} = -i\,\det[M_u, M_d]/2P_uP_d = 4BFG^2(A^2 - B^2)/P_uP_d \tag{14.6}$$

14.2.5 Ansatz 5

We however need to reduce the number of parameters, and therefore try different versions of complexification, ending up with this simple choice, with six parameters K, A, B, L, Y, F:

$$M_u = \begin{pmatrix} K & A & B \\ A & K & B \\ B & B & K \end{pmatrix} \quad \text{and} \quad M_d = \begin{pmatrix} L & Y & Y-iF \\ Y & L & Y \\ Y+iF & Y & L \end{pmatrix} \tag{14.7}$$

This parametrization gives a non-vanishing determinant for the commutator:

$$\det(M_uM_d - M_dM_u) = 2i\,BF^3(A^2 - B^2),$$

The matrix M_u in (12.7) is flavour symmetric in the first two families. This can be seen by spelling out the mass Lagrangian in flavour space:

$$\mathcal{L}_m = \bar{\phi}M_u\phi = (\bar{\phi}_1, \bar{\phi}_2, \bar{\phi}_3) \begin{pmatrix} K & A & B \\ A & K & B \\ B & B & K \end{pmatrix} \begin{pmatrix} \phi_1 \\ \phi_2 \\ \phi_3 \end{pmatrix} =$$

$$= K(\bar{\phi}_1\phi_1 + \bar{\phi}_2\phi_2 + \bar{\phi}_3\phi_3) + A(\bar{\phi}_1\phi_2 + \bar{\phi}_2\phi_1) + B[(\bar{\phi}_1 + \bar{\phi}_2)\phi_3 + \bar{\phi}_3(\phi_1 + \phi_2)],$$

where ϕ_j are flavour states with charge $2/3$, and the flavour symmetry in the first two families means that the mass Lagrangian is invariant under exchange of ϕ_1 and ϕ_2.
The corresponding flavour symmetry in the down-quark mass matrix M_d, is broken by the presence of complex matrix elements.

14.2.6 Solving ansatz 5

The choice of having one completely real mass matrix facilitates the calculation, since M_u has explicit, easily calculated eigenvalues

$$\begin{aligned} m_1 &= K - A \\ m_2 &= (2K + A - \sqrt{8B^2 + A^2})/2 \\ m_3 &= (2K + A + \sqrt{8B^2 + A^2})/2, \end{aligned}$$

In order to get a picture of the structure of M_u, we want to insert numerical quark mass values in m_j (for our purpose, it is not important that there is some uncertainty in the quark masses). Using these quark mass values [8], [9] at M_Z:

$$\begin{aligned} m_u(M_z) = 1.24\ MeV,\ m_c(M_z) = 624\ MeV,\ m_t(M_z) = 171550\ MeV \\ m_d(M_z) = 2.69\ MeV,\ m_s(M_z) = 53.8\ MeV,\ \ m_b(M_z) = 2850\ MeV \end{aligned} \tag{14.8}$$

we get these numerical values for the matrix elements in the up-sector

$$K = 57391.75, \quad A = 57390.5, \quad B = 56923.2,$$

and the mass matrix for the up-quarks shows a nearly democratic texture:

$$M_u(M_Z) = \begin{pmatrix} 57391.75 & 57390.5 & 56923.22 \\ 57390.5 & 57391.75 & 56923.22 \\ 56923.22 & 56923.22 & 57391.75 \end{pmatrix} = 56923.22 MeV \begin{pmatrix} 1.00823 & 1.00820 & 1 \\ 1.00820 & 1.00823 & 1 \\ 1 & 1 & 1.00823 \end{pmatrix} \tag{14.9}$$

This allows us to numerically calculate the determinant for the commutator:

$$\det(M_u M_d - M_d M_u) = 2i\,BF^3(A^2 - B^2),$$

which we insert into J_{CP} to calculate the numerical value of F,

$$J_{CP} = -i\ \det[M_u, M_d]/2P_uP_d = BF^3(A^2 - B^2)/P_uP_d = 0.00003096,$$

i.e. $F^3 = 0.00003096 \times P_uP_d/(B(A^2 - B^2))$, which gives $F = 42.295 MeV$.
To calculate the matrix elements of the mass matrix for the down-sector,

$$M_d = \begin{pmatrix} L & Y & Y - iF \\ Y & L & Y \\ Y + iF & Y & L \end{pmatrix},$$

we use matrix invariants. The cleanest way to express the matrix invariants of a 3 $\times$ 3 matrix M, is in terms of traces:

1. $trace(M) = m_1 + m_2 + m_3$
2. $C_2(M) = m_1m_2 + m_1m_3 + m_3m_2 = \frac{1}{2}[(trace(M))^2 - trace(M^2)]$
3. $det(M) = m_1m_2m_3 = \frac{1}{6}[trace(M))^3 + 2trace(M^3) - 3trace(M)trace(M^2)]$,

where $C_2(M)$ is our private notation. In the case of M_d, these invariants are

1. $trace(M_d) = 3L$
2. $C_2(M_d) = 3L^2 - 3Y^2 - F^2$

3. $\det(M_d) = L^3 + 2Y^3 - L(3Y^2 + F^2)$

From relation 2., we see that $3Y^2 + F^2 = 3L^2 - C_2(M_d)$, thus

$$\det(M_d) = L^3 + 2Y^3 - L(3L^2 - C_2(M_d)) \;\Rightarrow\; 2Y^3 = \det(M_d) + 2L^3 - LC_2(M_d)$$

and

$$Y = [\frac{\det(M_d) + 2L^3 - LC_2(M_d)}{2}]^{1/3}$$

Inserting the numerical values from (12.8) into the matrix invariants, we get

$$Y = 940.4MeV,$$

and we can write the numerical mass matrices as

$$M_u(M_Z) = 56923.22MeV \begin{pmatrix} 1.00823 & 1.00820 & 1 \\ 1.00820 & 1.00823 & 1 \\ 1 & 1 & 1.00823 \end{pmatrix}$$

and

$$M_d(M_Z) = 940.35MeV \begin{pmatrix} 1.03 & 1 & 1 - i\,0.045 \\ 1 & 1.03 & 1 \\ 1 + i\,0.045 & 1 & 1.03 \end{pmatrix}$$

which both have a democratic texture and satisfy the requirements for CP-violation. As a check, we insert the determinant of their commutator in the expression for J_{CP}, and get

$J_{CP} = 460273644675702800/2(m_u - m_c)(m_c - m_t)(m_t - m_u)(m_d - m_s).. = 0.00003097.$

Similar results are obtained for quark mass values at $2GeV$ [10].

14.3 Mass eigenvalues

The eigenvalues of the up-quarks were easily found:

$$(m_1, m_2, m_3) = (K - A, (2K + A - \sqrt{8B^2 + A^2})/2, (2K + A + \sqrt{8B^2 + A^2})/2),$$

but in order to find the eigenvalues of M_d, we must solve

$$\det \begin{pmatrix} L - \lambda & Y & Y - iF \\ Y & L - \lambda & Y \\ Y + iF & Y & L - \lambda \end{pmatrix} = 0$$

That is,

$$(L - \lambda)^3 + 2Y^3 - (L - \lambda)(3Y^2 + F^2) = 0$$

We substitute $\lambda = L + w$, which gives the cubic equation

$$w^3 - w(3Y^2 + F^2) - 2Y^3 = 0$$

We make the ansatz $w = u\cos\theta$, where

$u = 2\sqrt{\frac{3Y^2+F^2}{3}}$ and $\cos(3\theta) = Y^3(\frac{3}{3Y^2+F^2})^{3/2}$, and we get

$$m_j = L + 2\sqrt{\frac{3Y^2+F^2}{3}}\cos\left[\frac{1}{3}\arccos[Y^3(\frac{3}{3Y^2+F^2})^{3/2}] - \frac{2\pi j}{3}\right]$$

where $j = 1, 2, 3$ and m_j are the down-quark masses m_d, m_s, m_b.

14.4 The reduction of parameters

We can express the up quark matrix elements in terms of the up-quark masses:

$K = (m_u + m_c + m_t)/3$
$A = (m_c + m_t - 2m_u)/3$
$B = \frac{1}{3}\sqrt{(m_t - 2m_c + m_u)(2m_t - m_c - m_u)/2}$

Likewise, the down sector has matrix elements

$L = (m_d + m_s + m_t)/3$
$Y = [\frac{\det(M_d)+2L^3-LC_2(M_d)}{2}]^{1/3}$
$F = [0.00003096 \times P_u P_d/(B(A^2 - B^2))]^{1/3}$

We see that the last down-quark matrix element is a function of the up-quark matrix elements A and B, which allows us to reformulate A:

$$A^2 - B^2 = 0.00003096\frac{P_u P_d}{F^3 B} \quad \Rightarrow$$

$$A = \sqrt{\frac{(BF)^3 + 0.00003096 P_u P_d}{F^3 B}}$$

where $P_u = (m_u - m_c)(m_c - m_t)(m_t - m_u)$ and $P_d = (m_d - m_s)(m_s - m_b)(m_b - m_d)$. Our two mass matrices are now defined by five parameters, K, B, L, Y, F.
So the mass eigenvalues for the up-sector are expressed in terms of K, B, F, while the mass eigenvalues for the down-sector are expressed in terms of L, Y, F, i.e. the mass eigenvalues of the two sectors are not independent of each other, but intertwined.

14.5 Conclusion

We have shown that the mass matrices of the up-quarks and the down-quarks are mutually dependent, linked by the constraint of CP-violation. Taking into account this constraint, specifically the Jarlskog invariant, we found the simple ansatz (12.7) of nearly democratic mass matrices.
That the CP-violation constraint reduces the number of matrix parameters from six to five, means that the mass eigenvalues of the up-quarks and the down-quarks are intertwined. This is explicitly demonstrated in our approach, for example by expressing A, which is a matrix element in the up-sector matrix M_u, as

$$A = \sqrt{\frac{(BF)^3 + 0.00003096 P_u P_d}{F^3 B}}$$

where $P_u = (m_u - m_c)(m_c - m_t)(m_t - m_u)$, $P_d = (m_d - m_s)(m_s - m_b)(m_b - m_d)$, and B and F are matrix elements in the up-sector and down-sector matrices, respectively.
So we have explicitly shown that the constraint from the CP-violation reduces the number of parameters in the mass matrices, implying that the quark mass eigenvalues intertwined.
This is demonstrated by means of a concrete ansatz, but the interdependence of the mass eigenstates is independent of the model.

References

1. C. Jarlskog, “Commutator of the Quark Mass Matrices in the Standard Electroweak Model and a Measure of Maximal CP Nonconservation”, Phys. Rev. Lett. 55 (1985) 1039, https://doi.org/10.1103/PhysRevLett.55.1039.
2. M. Kobayashi, T. Maskawa; Maskawa (1973), “CP-Violation in the Renormalizable Theory of Weak Interaction”, Progress of Theoretical Physics 49 (2): 652–657
3. Wolfenstein, L. (1983). "Parametrization of the Kobayashi-Maskawa Matrix". Physical Review Letters. 51 (21): 1945–1947.
4. https://pdg.lbl.gov/2018/reviews/rpp2018-rev-ckm-matrix.pdf
5. A. C. Kleppe, “Quark mass matrices inspired by a numerical relation”, arXiv:2504.02104 [hep-ph], Proceedings to the 27th workshop What Comes Beyond the Standard Models, Vol.25, 2024, p. 87 - 101.
6. H. Fritzsch, Phys. Lett. B 70, 436 (1977), Phys. Lett. B 73, 317 (1978)
7. A. Kleppe, “A democratic suggestion”, arXiv:1608.08988 [hep-ph]
8. Matthias Jamin, private communication (2015), and FLAG Working Group, “Review of lattice results concerning low energy particle physics” (2014), arXiv:hep-lat/1310.8555v2
9. M. Jamin, J. Antonio Oller and A. Pich, "Light quark masses from scalar sum rules", arXiv:hep-ph/0110194v2
10. https://pdg.lbl.gov/2023/tables/rpp2023-sum-quarks.pdf

Bled Workshops
in Physics
Vol. 26, No. 1

Proceedings of the 28th Workshop
What Comes Beyond . . . *(p. 175)*
Bled, Slovenia, July 6–17, 2025

15 Spontaneous baryosynthesis with large initial phase

M.A. Krasnov[1], M.Yu. Khlopov[2], U. Aydemir[3]

[1] Research Institute of Physics Southern Federal University, Rostov-on-Don, 344090, Russia
[2]Virtual Institute of Astroparticle Physics, Paris, 75018, France
[3] Department of Physics, Middle East Technical University, Ankara, 06800, Türkiye

Abstract. We numerically investigate particle production by a pseudo-Nambu-Goldstone boson (pNGB) in spontaneous baryogenesis, focusing on large initial misalignment angles. Our analysis confirms the established cubic dependence of the baryon asymmetry on the initial phase for small angles. However, this scaling breaks down for larger angles, with particle production saturating as the initial phase approaches π in Minkowski spacetime.
Povzetek: Avtorji z numerično simulacijo preučujejo sponano bariogenezo, ki jo sproži psevdo-Nambu-Goldstonov bozon. Potrdijo kubično odvisnost barionske asimetrije za majhne kote. Vendar se pri večjih kotih ta odvisnost poruši, produkcija delcev pa se ustali, ko se začetna faza približa fazi π v Minkowskega prostoru-času.

15.1 Introduction

Observational data unequivocally confirms the existence of a universe dominated by matter, with a significant asymmetry between baryons and antibaryons. This is puzzling, as fundamental physics offers no obvious reason for such an imbalance in the production of particles and antiparticles. This baryon asymmetry is quantified by the present-day baryon-to-entropy ratio, $(\Delta n_B/s)_0 \simeq 8.6 \times 10^{-11}$ [1]. For decades, a major challenge in cosmology has been to identify a physical process that naturally explains this value, rather than simply treating it as an initial condition of the universe. The foundational framework for this, proposed by Sakharov and Kuzmin [2, 3], connects the generation of a baryon excess from an initially symmetric state to CP-violating processes that occur out of equilibrium and that do not conserve baryon number. Subsequent research has expanded this idea, leading to various proposed mechanisms that tie the origin of the baryon asymmetry to new physics beyond the Standard Model.
One such mechanism, known as spontaneous baryogenesis, was introduced in Refs. [4, 5] and further explored in Refs. [6, 7] In this scenario, the asymmetry arises from the relaxation of a (pseudo) Nambu-Goldstone boson specifically, the phase $\theta = \phi/f$ of a spontaneously broken global $U(1)$ baryonic symmetry toward the minimum of its potential. Here, $f/\sqrt{2}$ corresponds to the magnitude of the vacuum expectation value of the complex scalar field responsible for the symmetry breaking. This field acts as a spectator during inflation, coexisting with the inflaton.

An explicit symmetry-breaking term, given by the potential $V(\theta) = \Lambda^4(1-\cos\theta)$[1], tilts the potential and gives mass to the originally massless boson. The field θ is coupled derivatively to a non-conserved baryonic current via the dimension-5 operator $\mathcal{L}_B = f^{-1} J_B^\mu \partial_\mu \phi$, where $J_B^\mu = \overline{Q}\gamma^\mu Q$ and Q is a new heavy fermion carrying baryon number. As θ undergoes damped oscillations, it is converted into either baryons or antibaryons, depending on the direction in which it rolls toward the minimum of the tilted potential. The resulting asymmetry is thus determined by the initial angle θ_i.

This work investigates the consequences of large initial misalignment angles within the spontaneous baryogenesis framework. While the small-angle approximation frequently used in the literature is convenient and insightful, the phase distribution at the end of inflation does not necessarily favor such small values. It is therefore essential to explore the implications of large misalignment angles. The most intriguing starting point is $\theta_i \simeq \pi$, which corresponds to the local maximum of the potential. The phase will then roll down to a minimum at either $\theta = 0$ or $\theta = 2\pi$, depending on the direction of motion.

Consequently, $\theta_i = \pi$ represents a domain wall separating two degenerate vacuum states. In our analysis, we therefore initiate the motion from $\theta_i \simeq \pi$ to study its impact on baryon asymmetry generation.

While it is possible that inflation is driven by the Nambu-Goldstone boson itself a model known as "natural inflation" [8] recent analyses strongly disfavor this scenario [9,10] due to tensions with PLANCK data [1], particularly the constraints on the tensor-to-scalar ratio r and the scalar spectral index n_s.

In this paper, we assume the Nambu-Goldstone boson responsible for baryogenesis is a spectator field during inflation and remain neutral regarding the specific mechanism driving inflation. We posit that the Nambu-Goldstone boson emerges during inflation, but its classical dynamics are frozen, with only quantum fluctuations being active.

The structure of this paper is as follows. Section 13.2 provides a concise overview of the model that gives rise to the (pseudo) Nambu-Goldstone boson. Section 13.3 examines the probability distribution of the baryon asymmetry. In Section 13.4, we detail our numerical approach to solving the equation of motion in Minkowski space-time. Our analysis culminates in Section 13.5 with the computation of the baryon asymmetry, where we illustrate its dependence on the Nambu-Goldstone boson's initial value. We conclude with a summary and discussion. Throughout this work, we use units where $c = \hbar = k_B = 1$, unless stated otherwise.

15.2 Theoretical Framework

We begin by outlining the fundamentals of the spontaneous baryogenesis model, based on the seminal works of A. Dolgov and colleagues [6,7]. The central element is a complex scalar field Φ that experiences spontaneous symmetry breaking,

[1]This is analogous to the QCD axion potential, though here it is not generated by QCD instanton effects.

producing a Nambu-Goldstone boson which subsequently facilitates baryon number generation. The Lagrangian includes Φ along with heavy fermionic fields: a fermion Q, postulated to carry baryon charge, and a lepton field L:

$$\mathcal{L} = \partial_\mu \Phi^* \partial^\mu \Phi - V(\Phi) + i\overline{Q}\gamma^\mu \partial_\mu Q + i\overline{L}\gamma^\mu \partial_\mu L - \\ - m_Q \overline{Q} Q - m_L \overline{L} L + g(\Phi \overline{Q} L + \Phi^* \overline{L} Q). \quad (15.1)$$

The Yukawa interaction term, $g(\Phi\overline{Q}L + \Phi^*\overline{L}Q)$, is critical, as it later enables the production of the Q field and the violation of baryon number. This Lagrangian is invariant under a classical global $U(1)$ symmetry associated with baryon number, under which the fields transform as:

$$\Phi \to e^{i\alpha}\Phi, \quad Q \to e^{i\alpha}Q, \quad L \to L. \quad (15.2)$$

The scalar potential $V(\Phi)$ is designed to induce spontaneous symmetry breaking (SSB) of this $U(1)$ at the energy scale f:

$$V(\Phi) = \lambda \left(\Phi^*\Phi - f^2/2\right)^2. \quad (15.3)$$

This potential generates a nonzero vacuum expectation value (VEV), $\langle\Phi\rangle = \frac{f}{\sqrt{2}} e^{i\phi/f}$, breaking the $U(1)$ symmetry. Expanding around this VEV reveals the angular degree of freedom ϕ as the massless Nambu-Goldstone boson.
Expressing the field as $\Phi(x) = \frac{f}{\sqrt{2}} e^{i\theta(x)}$, where $\theta(x) \equiv \phi(x)/f$, and substituting into the original Lagrangian yields the effective theory below the SSB scale:

$$\mathcal{L} = \frac{f^2}{2}\partial_\mu\theta\partial^\mu\theta + i\overline{Q}\gamma^\mu\partial_\mu Q + i\overline{L}\gamma^\mu\partial_\mu L - m_Q\overline{Q}Q - m_L\overline{L}L + \\ + \frac{gf}{\sqrt{2}}\left(\overline{Q}Le^{i\theta} + \overline{L}Qe^{-i\theta}\right) - V(\theta). \quad (15.4)$$

This Lagrangian remains invariant under the shifted $U(1)$ transformation:

$$Q \to e^{i\alpha}Q, \quad L \to L, \quad \theta \to \theta + \alpha. \quad (15.5)$$

To generate a mass for the θ field and provide a potential for it to evolve, an explicit symmetry-breaking term is introduced. This potential, analogous to the axion potential from QCD instantons but treated here as a generic low-energy effect parameterized by a scale $\Lambda \ll f$, is:

$$V(\theta) = \Lambda^4(1 - \cos\theta). \quad (15.6)$$

This potential tilts the initial Mexican hat, endowing the pseudo-Nambu-Goldstone boson with a mass $m_\theta \sim \Lambda^2/f$.
The Lagrangian in Eq. (13.4) can be rewritten by applying the field redefinition $Q \to e^{-i\theta(x)}Q$. This transformation eliminates the phase from the Yukawa interaction and gives rise to a derivative coupling term:

$$\mathcal{L} = \frac{f^2}{2}\partial_\mu\theta\partial^\mu\theta + i\overline{Q}\gamma^\mu\partial_\mu Q + i\overline{L}\gamma^\mu\partial_\mu L - m_Q\overline{Q}Q - m_L\overline{L}L + \\ + \frac{gf}{\sqrt{2}}(\overline{Q}L + \overline{L}Q) + \partial_\mu\theta\overline{Q}\gamma^\mu Q - V(\theta). \quad (15.7)$$

The term $\partial_\mu\theta\overline{Q}\gamma^\mu Q$ is the distinctive feature of spontaneous baryogenesis.

15.3 Asymmetry Distribution

The initial value of the phase field θ_i at the onset of its oscillations is not fixed but is determined by quantum fluctuations during cosmological inflation. We examine the probability distribution $f(\phi, t)$ for a light scalar field ϕ (with $\theta = \phi/f$) during inflation. This distribution can be derived from the Fokker-Planck equation [11,12], which, for a massless field ($m \ll H_\star$), results in a Gaussian distribution. Starting from an initial value ϕ_u when inflation begins, the probability density of finding the field at value ϕ after time t is:

$$f(\phi, t) = \frac{1}{\sqrt{2\pi}, \sigma(t)} \exp\left(-\frac{(\phi - \phi_u)^2}{2\sigma^2(t)}\right), \tag{15.8}$$

where $\sigma(t) = \frac{H_\star}{2\pi}\sqrt{H_\star t}$. This describes the field's random walk due to quantum fluctuations superimposed on the classical slow-roll motion. The baryon asymmetry produced in spontaneous baryogenesis is highly dependent on the initial phase θ_i at the end of inflation. Converting the distribution for ϕ into one for the phase $\theta_i = \phi_i/f$, and assuming inflation lasts for $N \approx 60$ e-folds ($t \approx 60H_\star^{-1}$), we obtain the probability distribution for the initial misalignment angle after inflation:

$$f(\theta_i) = \frac{1}{\sqrt{2\pi}, \sigma'} \exp\left(-\frac{(\theta_i - \theta_u)^2}{2\sigma'^2}\right), \tag{15.9}$$

where $\sigma' = \frac{H_\star}{2\pi f}\sqrt{60}$. A key aspect of cosmological inflation is that causally disconnected regions evolve independently. The entire observable universe today originates from approximately $e^{3N} \approx e^{180}$ such independent Hubble patches at the end of inflation. Within each patch, θ_i is nearly uniform but varies randomly between patches according to the distribution (13.9). This renders spontaneous baryogenesis an *inhomogeneous* process on super-Hubble scales at this epoch; different regions will yield different baryon asymmetries. The probability that a given Hubble patch has a misalignment angle shifted by more than π from its initial value θ_u is:

$$P(|\theta_i - \theta_u| > \pi) = 1 - \mathrm{erf}\left(\frac{\pi}{\sqrt{2}\sigma'}\right). \tag{15.10}$$

Assuming the symmetry breaking scale f is similar to the Hubble scale during inflation ($f \approx H_\star$), we find $\sigma' \approx \sqrt{60}/(2\pi) \approx 1.23$, and thus:

$$P(|\theta_i - \theta_u| > \pi) \approx 1 - \mathrm{erf}(\pi) \approx 10^{-5}. \tag{15.11}$$

Although this probability for a single patch is low, the total number of patches is immense. The expected number of patches within our observable universe that have experienced such a large fluctuation is:

$$n_{\text{regions}} = e^{180} \times P(|\theta_i - \theta_u| > \pi) \approx 10^{78} \times 10^{-5} \gg 1. \tag{15.12}$$

Therefore, it is statistically certain that regions with $\theta_i \sim \pi$ exist within our current horizon. This necessitates a thorough investigation of the baryogenesis mechanism for these large initial misalignment angles, which is the principal objective of this study.

15.4 Numerical Solution in a Static Universe

This section examines the equation of motion in Minkowski space-time, with the simplification of massless fermions. For an arbitrary initial phase, the relevant semiclassical equation of motion is [6]:

$$\ddot{\theta} + \frac{\Lambda^4}{f^2}\sin\theta = -\frac{4g^2}{\pi^2}\int_0^\infty \omega^2 d\omega \times \\ \times \int_{-\infty}^0 dt' \sin(2\omega t') \sin[\theta(t+t') - \theta(t)], \quad (15.13)$$

which can be reformulated as:

$$\ddot{\theta} + \frac{\Lambda^4}{f^2}\sin\theta = -\frac{g^2}{2\pi^2}\lim_{\omega\to\infty}\int_{-\infty}^0 dt' \left[\frac{\cos 2\omega t' - 1}{t'}\right] \times \\ \times \left[\ddot{\theta}(t+t')\cos\Delta\theta - \dot{\theta}^2(t+t')\sin\Delta\theta\right], \quad (15.14)$$

where $\Delta\theta = \theta(t+t') - \theta(t)$. It is important to note that Eq. (13.14) is derived from a treatment where the scalar field θ is classical, while the fermion fields Q and L are treated quantum mechanically. This imposes limitations on the allowed initial conditions for θ. For example, the configuration $\theta_i = \pi$ with $\dot{\theta}_i = 0$ is not physically meaningful, as it would yield the static solution $\theta = \pi$.
We begin the solution process by rewriting Eq. (13.14) and denoting the integral as:

$$\ddot{\theta} + \frac{\Lambda^4}{f^2}\sin\theta = \frac{g^2}{\pi^2}\lim_{\omega\to\infty}\int_{-\infty}^0 dt' \left[\frac{\sin^2\omega t'}{t'}\right] \times \\ \times \left[\ddot{\theta}(t+t')\cos\Delta\theta - \dot{\theta}^2(t+t')\sin\Delta\theta\right] \equiv \mathcal{I}. \quad (15.15)$$

A crucial step in our approach is to treat ω as large but finite, effectively introducing a cutoff to the integration limit in (13.13). Since the pseudo-Nambu-Goldstone boson emerges at energies below f, it is physically justified to set the effective theory's cutoff energy at $\omega \sim f$. Given that the cosine potential becomes significant at scales much lower than f (as indicated before Eq. (13.6)), we also have $m = \Lambda^2/f \ll \omega \sim f$.
We now proceed without the limit operator and analyze the integral:

$$\mathcal{I}(t) = \frac{g^2}{\pi^2}\int_{-\infty}^0 dt' \left[\frac{\sin^2\omega t'}{t'}\right] \times \\ \times \left[\ddot{\theta}(t+t')\cos\Delta\theta - \dot{\theta}^2(t+t')\sin\Delta\theta\right]. \quad (15.16)$$

Integrating this expression by parts yields:

$$\mathcal{I}(t) = \frac{g^2}{\pi^2}\frac{\sin^2 \omega t'}{t'}\dot{\theta}(t+t') \cdot \cos\left[\Delta\theta\right]|_{-\infty}^{0} - \\ - \frac{g^2}{\pi^2}\int_{-\infty}^{0} dt'\dot{\theta}(t+t') \cdot \cos\left[\theta(t+t') - \theta(t)\right] \times \\ \times \left(\frac{\omega \sin\left(2\omega t'\right)}{t'} - \frac{\sin^2\left(\omega t'\right)}{t'^2}\right). \quad (15.17)$$

Recalling standard representations of the Dirac delta-function:

$$\delta(t) = \lim_{\omega\to\infty}\frac{\sin \omega t}{\pi t},\ \delta(t) = \lim_{\omega\to\infty}\frac{\sin^2 \omega t}{\pi\omega t^2}. \quad (15.18)$$

Given that $\Lambda^2/f \ll \omega \leq f$, we can approximate:

$$\frac{\omega \sin\left(2\omega t'\right)}{t'} - \frac{\sin^2\left(\omega t'\right)}{t'^2} \approx \pi\omega\delta(t'). \quad (15.19)$$

This approximation leads to the following equation of motion for the Nambu-Goldstone boson:

$$\ddot{\theta} + \frac{g^2\omega}{\pi}\dot{\theta} + \frac{\Lambda^4}{f^2}\sin\theta = 0. \quad (15.20)$$

To solve this equation, we rewrite it using dimensionless variables (where the prime denotes a derivative with respect to $\Lambda^2 t/f$):

$$\theta'' + \frac{g^2\omega f}{\Lambda^2\pi}\theta' + \sin\theta = 0. \quad (15.21)$$

Introducing the notation

$$\Gamma \equiv \frac{g^2\omega f}{\Lambda^2\pi}, \quad (15.22)$$

which we treat as a free parameter in our calculations and can be interpreted as a dimensionless decay rate. Since there is no established relation between ω and g, Γ can assume any positive value. Consequently, we explore both small ($\Gamma \leq 1$) and large ($\Gamma > 1$) values of Γ.
Figure 13.1 displays numerical solutions to Eq. (13.21) for different Γ values, starting from an initial phase near π. The results are shown in two subfigures for clarity. Unlike the case of small oscillations, we observe that larger Γ values result in a longer duration for the field to reach the potential minimum.This behavior stems from the large initial phase, which causes the potential term in the equation of motion to behave differently compared to the small oscillation regime.

15.5 Baryon Asymmetry Calculation

This section presents the calculation of the baryon asymmetry using the solutions to the equation of motion obtained previously.

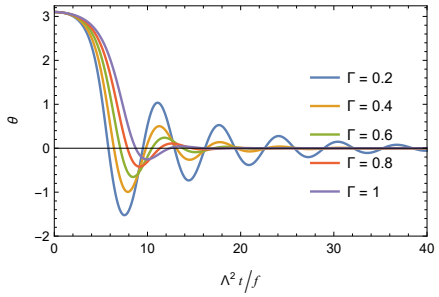

(a) Numerical solutions for sample values of $\Gamma \leqslant 1$.

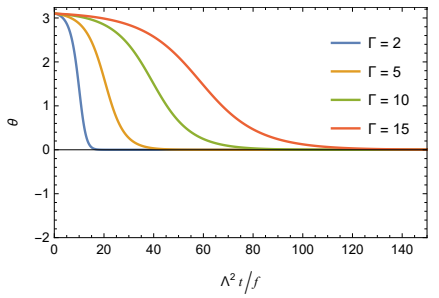

(b) Numerical solutions for sample values of $\Gamma > 1$.

Fig. 15.1: Numerical solutions of Eq. (13.21) with initial conditions $\theta_{in} = 3.1$ and $\dot{\theta}_{in} = 0$ for different values of Γ in Minkowski space.

Following [7], the baryon (B) and antibaryon ($\overline{B}$) number densities in Minkowski space are given by:

$$n_{B,\overline{B}} = \frac{g^2 f^2}{2\pi^2} \int_0^\infty \omega^2 d\omega \left| \int_{-\infty}^{+\infty} e^{2i\omega t \pm i\theta(t)} dt \right|^2 , \tag{15.23}$$

where $+\theta(t)$ corresponds to baryons and $-\theta(t)$ to antibaryons. Note that ω in these integrals is not the same variable as in the equations of motion, despite the shared notation.
Defining the time integral as:

$$\int_{-\infty}^{+\infty} e^{2i\omega t \pm i\theta(t)} dt = N_\pm(\omega) ,$$

it can be shown that:

$$N_\pm(\omega) = -\frac{i e^{\pm i\theta_i}}{2\omega} + \frac{i}{2\omega} + \int_0^{+\infty} e^{2i\omega t} (e^{\pm i\theta(t)} - 1) dt, \tag{15.24}$$

where we omit delta functions due to the ω^2 factor in the outer integral. This is further justified by the strict lower limit $\omega = m_Q + m_L > 0$. The final term in (13.24) is evaluated numerically, similar to the integral in the previous section.

We now proceed to calculate the baryon asymmetry. First, we verify that our method reproduces the results of Ref. [7], where the baryon asymmetry was found to scale as θ_{in}^3 for small oscillations. For this purpose, we consider small initial phase values and plot the results with a cubic fit, as shown in Fig. 13.2.

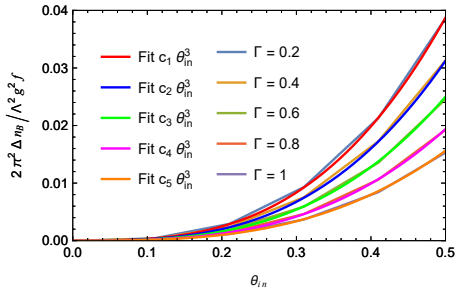

(a) Numerical solutions for sample values of $\Gamma \leqslant 1$.

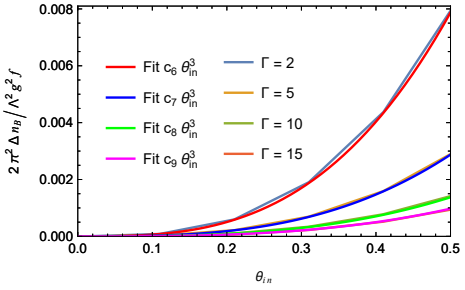

(b) Numerical solutions for sample values of $\Gamma > 1$.

Fig. 15.2: Baryon asymmetry in Minkowski space for a small initial phase and larger Γ values, with cubic fit functions. This serves to validate our methodology. The coefficients c_i are: $c_1 \approx 0.31,, c_2 \approx 0.25,, c_3 \approx 0.2,, c_4 \approx 0.155,, c_5 \approx 0.125, c_6 \approx 0.063,, c_7 \approx 0.023,, c_8 \approx 0.011,, c_9 \approx 0.0078$.

Next, we present the results for larger initial phases. The baryon asymmetry in Minkowski space is displayed in Fig. 13.3. For small oscillations, the oscillation period is $T \sim 1/m_\theta$, but this relation does not hold for a large initial phase. The apparent saturation of particle production as the initial phase approaches π is likely due to the oscillation period becoming significantly longer than the harmonic approximation would suggest. Although a deviation from the cubic dependence is evident, the calculated values remain of the same order of magnitude.

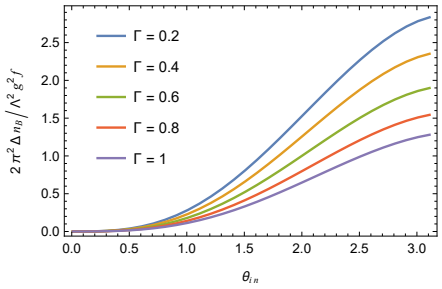

(a) Numerical solutions for sample values of $\Gamma \leqslant 1$.

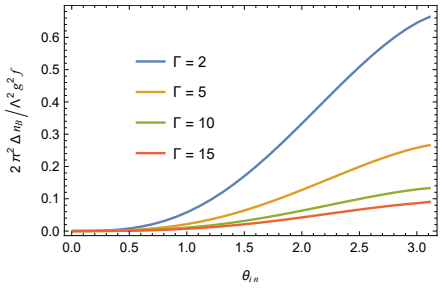

(b) Numerical solutions for sample values of $\Gamma > 1$.

Fig. 15.3: Baryon asymmetry Δn_B as a function of the initial phase in Minkowski space-time. Particle production increases rapidly until $\theta_i \approx 1$, after which the rate decelerates considerably, tending toward saturation as θ_i approaches π. The curve's behavior is not strongly influenced by the value of Γ when it is small. However, for larger Γ values (as seen in Fig. 3(b)), the effects are more pronounced.

15.6 Discussion and Conclusion

We have re-examined the spontaneous baryogenesis scenario mediated by a Nambu-Goldstone boson. The common practice in the literature has been to employ the small-angle approximation for the cosine potential. However, the phase's probability distribution, shaped by quantum fluctuations during inflation, implies a non-negligible likelihood for substantial phase variations. This calls into question the reliability of the small-angle approximation and underscores the need to study large misalignment angles.

The primary aim of this paper was to investigate the key consequences of deviating from the small-angle approximation. As a first step, we worked within Minkowski spacetime, neglecting universe expansion, which is valid when the decay rate Γ of the pNGB field oscillations is significantly greater than the Hubble expansion rate. We computed the baryon asymmetry for an initial phase near π, as this value, located at a local maximum of the cosine potential, represents the most extreme case of large misalignment. Our analysis, illustrated in Fig. 13.3, reveals that the

effects of a large misalignment angle on the generated baryon asymmetry are not substantially different from those predicted by the small-angle approximation in Minkowski space.

15.7 Acknowledgements

The work of M. K. was performed in Southern Federal University with financial support of grant of Russian Science Foundation 25-07-IF.

References

1. Y. Akrami et al: Planck2018 results: X. Constraints on inflation, A&A **641** (2020) A10.
2. A. D. Sakharov: Violation of CP Invariance, C asymmetry, and baryon asymmetry of the universe, Pisma Zh. Eksp. Teor. Fiz. **5** (1967) 32–35.
3. V.A. Kuzmin: CP-noninvariance and baryon asymmetry of the universe, JETP Letters **12** (1970) 228–230.
4. A. G. Cohen, D. B. Kaplan: Thermodynamic Generation of the Baryon Asymmetry, Phys. Lett. B **199** (1987) 251–258.
5. A. G. Cohen, D. B. Kaplan: SPONTANEOUS BARYOGENESIS, Nucl. Phys. B **308** (1988) 913–928.
6. A. Dolgov, K. Freese: Calculation of particle production by Nambu-Goldstone bosons with application to inflation reheating and baryogenesis, Phys. Rev. D **51** (1995) 2693–2702.
7. A. Dolgov, K. Freese, R. Rangarajan, M. Srednicki: Baryogenesis during reheating in natural inflation and comments on spontaneous baryogenesis, Phys. Rev. D **56** (1997) 6155–6165.
8. K. Freese, A. J. Frieman, A. V. Olinto: Natural inflation with pseudo - Nambu-Goldstone bosons, Phys. Rev. Lett. **65** (1990) 3233–3236.
9. K. Alam, K. Dutta, N. Jaman: CMB constraints on natural inflation with gauge field production, JCAP **12** (2024) 015.
10. F.B.M. dos Santos, G. Rodrigues, J.G. Rodrigues, R. de Souza,J.S. Alcaniz: Is natural inflation in agreement with CMB data?, JCAP **03** (2024) 038.
11. A.D. Linde: Scalar field fluctuations in the expanding universe and the new inflationary universe scenario, Phys. Lett. B **5** (1982) 335–339.
12. V. Vennin, A.A. Starobinsky: Correlation functions in stochastic inflation, EPJC **9** (2015).

Bled Workshops
in Physics
Vol. 26, No. 1

Proceedings of the 28th Workshop
What Comes Beyond . . . *(p. 185)*
Bled, Slovenia, July 6–17, 2025

16 Describing the internal spaces of fermion and boson fields with the superposition of odd (for fermions) and even (for bosons) products of operators γ^a, enables understanding of all the second quantised fields (fermion fields, appearing in families, and boson fields, tensor, vector, scalar) in an equivalent way

N.S. Mankoč Borštnik[†]

Department of Physics, University of Ljubljana, SI-1000 Ljubljana, Slovenia

Abstract. Using the odd and even "basis vectors", which are the superposition of odd and even products of γ^a's, to describe the internal spaces of the second quantised fermion and boson fields, respectively, offers in even-dimensional spaces, like it is $d = (13+1)$, the unique description of all the properties of the observed fermion fields (quarks and leptons and antiquarks and antileptons appearing in families) and boson fields (gravitons, photons, weak bosons, gluons and scalars) in a unique way, providing that all the fields have non zero momenta only in $d = (3+1)$ of the ordinary space-time, bosons have the space index α (which is for tensors and vectors $\mu = (0,1,2,3)$ and for scalars $\sigma \geq 5$). In any even-dimensional space, there is the same number of internal states of fermions appearing in families and their Hermitian conjugate partners as it is of the two orthogonal groups of boson fields having the Hermitian conjugate partners within the same group. A simple action for massless fermion and boson fields describes all the fields uniquely. The paper overviews the theory, presents new achievements and discusses the open problems of this theory.

Povzetek:: Avtorica predstavi svoj predlog za opis fermionskih in bozonskih polj v drugi kvantizaciji. Definira "bazne vektorje", ki so za fermione lihe in za bozone sode superpozicije operatorjev γ^a, da z njimi opiše v sodorazsežnih notranjih prostorih, kot je $d = (13+1)$, spine in naboje fermionskih polj (kvarkov in leptonov ter antikvarkov in antileptonov, ki se v tem opisu pojavljajo skupaj v družinah) in bozonskih polj (gravitonov, fotonov, šibkih bozonov, gluonov in skalarjev, med njimi je Higgsovo polje, ki se pojavijo v dveh ortogonalnih skupinah), pri privzetku, da imajo vsa polja neničelne gibalne količine samo v $d = (3+1)$ delu prostora-časa. Bozonska polja nosijo prostorski indeks α (ki je za tenzorje in vektorje $\mu = (0,1,2,3)$ in za skalarje $\sigma \geq 5$. V vseh sodorazsežnih prostorih, je število lihih "baznih vektorjev" in njihovih hermitovsko konjugiranih partnerjih enako številu sodih "baznih vektorjev". S preprosto akcijo opiše članek brezmasna fermionska in bozonska polja in interakcijo med njimi na equivalenten način. Članek predstavi teorijo, zadnje dosežke ter (še) odprte probleme.

[†]norma.mankoc@fmf.uni-lj.si

16.1 Introduction

The author, with collaborators, succeeded in demonstrating in a long series of works [1,1,2,4,5,7–9,11–18] that the model, named the *spin-charge-family* theory, offers an elegant description of the second-quantised fermion fields, appearing in families, written as the tensor products of the basis in ordinary space-time and the basis, named "basis vectors", in internal spaces, presented as superpositions of odd products of operators γ^a, arranged in nilpotents and projectors, which are eigenvectors of the (chosen) Cartan subalgebra members [1,1,2,4,5,7–9].
Three years ago [19–22] the author started to use an equivalent description for boson fields, as so far used for fermion fields, recognising the possibility from 30 years ago [1,1,2,19–22]: The internal space of boson second quantised fields can be described by the "basis vectors", presented as superpositions of even products of operators γ^a, arranged in nilpotents and projectors, which are eigenvectors of the Cartan subalgebra members. Fermions, described by an odd number of nilpotents, the rest of the projectors, and bosons described by an even number of nilpotents, the rest of projectors, fulfil the Dirac's postulates for the second quantised fields, explaining the postulates.
There are in $2(2n+1)$-dimensional spaces $2^{\frac{d}{2}-1}\times 2^{\frac{d}{2}-1}$ "basic vectors" of fermion fields and the same number of their Hermitian conjugate partners, and $2^{\frac{d}{2}-1}\times 2^{\frac{d}{2}-1}$ "basic vectors" of each of the two kinds of boson fields, as presented in Sect. 14.2.
It turned out that both types of "basic vectors" of boson fields can be expressed as the algebraic products[1] of fermion fields and their Hermitian conjugate partners 14.2.1. This means that knowing the "basic vectors" of fermion fields we know

[1]The algebraic product of any two members of the odd or even "basis vectors" can easily be calculated when taking into account the relations following from Eq.(14.4)

$$
\begin{aligned}
&\gamma^a\ {}^{ab}_{}(k) = \eta^{aa}\ {}^{ab}_{}[-k], \quad \gamma^b\ {}^{ab}_{}(k) = -ik\ {}^{ab}_{}[-k], \quad \gamma^a\ {}^{ab}_{}[k] = {}^{ab}_{}(-k), \quad \gamma^b\ {}^{ab}_{}[k] = -ik\eta^{aa}\ {}^{ab}_{}(-k),\\
&\tilde{\gamma^a}\ {}^{ab}_{}(k) = -i\eta^{aa}\ {}^{ab}_{}[k], \quad \tilde{\gamma^b}\ {}^{ab}_{}(k) = -k\ {}^{ab}_{}[k], \quad \tilde{\gamma^a}\ {}^{ab}_{}[k] = i\ {}^{ab}_{}(k), \quad \tilde{\gamma^b}\ {}^{ab}_{}[k] = -k\eta^{aa}\ {}^{ab}_{}(k),\\
&{}^{ab}_{}(k)\ {}^{ab}_{}(-k) = \eta^{aa}\ {}^{ab}_{}[k], \quad {}^{ab}_{}(-k)\ {}^{ab}_{}(k) = \eta^{aa}\ {}^{ab}_{}[-k], \quad {}^{ab}_{}(k)\ {}^{ab}_{}[k] = 0, \quad {}^{ab}_{}(k)\ {}^{ab}_{}[-k] = {}^{ab}_{}(k),\\
&{}^{ab}_{}(-k)\ {}^{ab}_{}[k] = {}^{ab}_{}(-k), \quad {}^{ab}_{}[k]\ {}^{ab}_{}(k) = {}^{ab}_{}(k), \quad {}^{ab}_{}[k]\ {}^{ab}_{}(-k) = 0, \quad {}^{ab}_{}[k]\ {}^{ab}_{}[-k] = 0,\\
&{}^{ab\,\dagger}_{}(k) = \eta^{aa}\ {}^{ab}_{}(-k), \quad ({}^{ab}_{}(k))^2 = 0, \quad {}^{ab}_{}(k)\ {}^{ab}_{}(-k) = \eta^{aa}\ {}^{ab}_{}[k],\\
&{}^{ab\,\dagger}_{}[k] = {}^{ab}_{}[k], \quad ({}^{ab}_{}[k])^2 = {}^{ab}_{}[k], \quad {}^{ab}_{}[k]\ {}^{ab}_{}[-k] = 0.
\end{aligned}
\tag{16.1}
$$

$$
\begin{aligned}
&\tilde{({}^{ab}_{}(k))}\ {}^{ab}_{}(k) = 0, \quad \tilde{({}^{ab}_{}(k))}\ {}^{ab}_{}(-k) = -i\eta^{aa}\ {}^{ab}_{}[-k], \quad \widetilde{{}^{ab}_{}(-k)}\ {}^{ab}_{}(k) = -i\eta^{aa}\ {}^{ab}_{}[k], \quad \tilde{({}^{ab}_{}(k))}\ {}^{ab}_{}[k] = i\ {}^{ab}_{}(k),\\
&\tilde{({}^{ab}_{}(k))}\ {}^{ab}_{}[-k] = 0, \quad \widetilde{{}^{ab}_{}(-k)}\ {}^{ab}_{}[k] = 0, \quad \widetilde{{}^{ab}_{}(-k)}\ {}^{ab}_{}[-k] = i\ {}^{ab}_{}(-k), \quad \tilde{({}^{ab}_{}[k])}\ {}^{ab}_{}(k) = {}^{ab}_{}(k),\\
&\tilde{({}^{ab}_{}[k])}\ {}^{ab}_{}(-k) = 0, \quad \widetilde{{}^{ab}_{}[k]}\ {}^{ab}_{}[k] = 0, \quad \widetilde{{}^{ab}_{}[-k]}\ {}^{ab}_{}[k] = {}^{ab}_{}[k], \quad \tilde{({}^{ab}_{}[k])}\ {}^{ab}_{}[-k] = {}^{ab}_{}[-k],
\end{aligned}
\tag{16.2}
$$

also the "basic vectors" of the boson fields, although the properties of fermion fields are very different from the properties of the boson fields 14.2.1.
The starting assumptions:
i. The second quantised fermion and boson fields are described as a tensor product of basis in ordinary space-time and of "basis vectors" describing the internal spaces of fermions (as a superposition of an odd product of operators γ^a) and bosons (as a superposition of even products of operators γ^a),
ii. Fermions and bosons have non-zero momentum only in $d = (3+1)$,
iii. Bosons carry the space index α,
offer an elegant and unique description of all the properties of the so far observed fermion and boson fields,
lead to:
a. Fermions appear in families, which include fermions and antifermions.
b. Bosons appear in two orthogonal groups, one group transforms family members into other family members, the second group transforms any of the family members into the same family member of the rest of the families.
c. Fermion fields obey the anti-commutation relations and boson fields obey the commutation relations, both obeying the postulates of Dirac for the second-quantised fermion and boson fields, explaining Dirac's postulates of the second quantisation of fermion and boson fields.
d. The analysis of the fermion and boson internal spaces with respect to the subgroups $SO(1,3), SU(2), SU(2), SU(3), U(1)$ of the group $SO(13,1)$, offers the description of the observed families of quarks and leptons, appearing in families, and of tensor (gravitons), vector (photons, weak bosons, gluons), and scalar (Higgs) boson fields, explaining also other observed properties of fermions and bosons (like the appearance of the dark matter [14], the matter-antimatter asymmetry in the universe [15], several predictions [**?**, **?**]). e. The Pauli matrices in any even d can easily be represented with the "basis vectors" for fermion fields, and any matrices in the adjoint representations can be written with the "basis vectors" for boson fields.
f. The vacuum is not the negative energy Dirac vacuum; it is just the quantum vacuum.
g. Although the internal spaces of fermions and bosons demonstrate so many different properties (anticommuting fermions appear in families, and have half-integer spins and charges in the fundamental representations, commuting bosons

---

$$
\begin{aligned}
S^{ac}{}^{ab}{}^{cd}(k)(k) &= -\frac{i}{2}\eta^{aa}\eta^{cc}{}^{ab}[-k]{}^{cd}[-k], \quad S^{ac}{}^{ab\,cd}[k][k] = \frac{i}{2}{}^{ab}(-k){}^{cd}(-k),\\
S^{ac}{}^{ab}{}^{cd}(k)[k] &= -\frac{i}{2}\eta^{aa}{}^{ab}[-k]{}^{cd}(-k), \quad S^{ac}{}^{ab\,cd}[k](k) = \frac{i}{2}\eta^{cc}{}^{ab}(-k){}^{cd}[-k],\\
\tilde{S}^{ac}{}^{ab}{}^{cd}(k)(k) &= \frac{i}{2}\eta^{aa}\eta^{cc}{}^{ab}[k]{}^{cd}[k], \quad \tilde{S}^{ac}{}^{ab\,cd}[k][k] = -\frac{i}{2}{}^{ab}(k){}^{cd}(k),\\
\tilde{S}^{ac}{}^{ab}{}^{cd}(k)[k] &= -\frac{i}{2}\eta^{aa}{}^{ab}[k]{}^{cd}(k), \quad \tilde{S}^{ac}{}^{ab\,cd}[k](k) = \frac{i}{2}\eta^{cc}{}^{ab}(k){}^{cd}[k]\ .
\end{aligned}
\tag{16.3}
$$

appear in two orthogonal groups, have no families, and have integer spins and charges in adjoint representations), the simple algebraic multiplication with the γ^a relates both kinds of "basis vectors".
h. In odd-dimensional spaces, $d = (2n+1)$, the fermion and boson fields have very peculiar properties: Half of the "basis vectors", $2^{\frac{2n}{2}-1} \times 2^{\frac{2n}{2}-1}$, have the properties of fields in 2n-dimensional part of space (the anticommuting "basis vectors" appear in families and have their Hermitian conjugate partners in a separate group, the commuting "basis vectors" appear in two orthogonal groups) among the rest of the "basis vectors", that is $2^{\frac{2n}{2}-1} \times 2^{\frac{2n}{2}-1}$, anticommuting appear in two orthogonal groups, and commuting appear in families and have their Hermitian conjugate partners in a separate group [20–22].

In this contribution, all fields, fermions and bosons (tensors, vectors and scalars) are massless. There are condensates [9], which make several scalar fields, as well as some of the fermion and vector boson fields, massive. We do not discuss in this contribution the breaking of symmetries and appearance of massive fermion fields, the scalar boson fields and some of the vector fields; the breaks of symmetries are expected to follow similarly to the case when we describe the boson fields with ω^{ab}_{α} and $\tilde{\omega}^{ab}_{\alpha}$ [9].

In Subsect. 14.5.1 we discuss our expectation that this new way of treating the boson fields will show what might be reasons for the appearance of the condensates. And other problems that are not yet solved.
In Sects. 14.2, 14.3, the internal spaces of fermion and boson fields are shortly presented as superposition of odd (for fermions) and even (for bosons) products of operators γ^a. The creation operators for fermion and boson second quantised fields are presented as tensor products of "basis vectors" with basis in ordinary space-time.
In Subsects. 14.2.1, 14.2.2, the " basis vectors" describing the internal spaces of fermion and boson fields, and the creation operators for fermion and bosons are presented.
In Sect. 14.3, the states active only in $d = (3+1)$ are discussed, as well as the algebraic relations among fermion and boson fields for the case that the internal space has $d = (5+1)$ and $d = (13+1)$, Subsect. 15.2.1.
In Sect. 15.17, a simple action for the fermion and all the boson fields (tensors, vectors, scalars) are presented for a flat space.
In Subsect. 14.4.1, the Lorentz invariance of the action is discussed.
In Sect. 14.5, we present shortly what we have learned in the last three years.
In Subsect. 14.5.1, the problems which remain to be solved in this theory, to find out whether the theory offers the right description of the observed fermion and boson second quantised fields which determine the history (and the future) of our universe.

16.2 Internal spaces of second quantised fermion and boson fields

This section overviews briefly (following several papers [22] and the references therein) the description of the internal spaces of the second-quantised fermion and boson fields as algebraic products of nilpotents and projectors, which are the superposition of odd and even products of γ^a's.
As explained in Sect. 14.6, Eq. 14.45, the Grassmann algebra offers two kinds of operators, γ^a's and $\tilde{\gamma}^a$'s with the properties (14.46)

$$\begin{aligned}
&\{\gamma^a, \gamma^b\}_+ = 2\eta^{ab} = \{\tilde{\gamma}^a, \tilde{\gamma}^b\}_+ \,,\\
&\{\gamma^a, \tilde{\gamma}^b\}_+ = 0 \,, \quad (a,b) = (0,1,2,3,5,\cdots,d) \,,\\
&\quad (\gamma^a)^\dagger = \eta^{aa}\gamma^a \,, \quad (\tilde{\gamma}^a)^\dagger = \eta^{aa}\tilde{\gamma}^a \,.
\end{aligned} \tag{16.4}$$

We use one of the two kinds, γ^a's, to generate the "basis vectors" describing internal spaces of fermions and bosons. They are arranged in products of nilpotents and projectors.

$$\begin{aligned}
&\overset{ab}{(k}: = \frac{1}{2}(\gamma^a + \frac{\eta^{aa}}{ik}\gamma^b) \,, \quad (\overset{ab}{(k)})^2 = 0 \,,\\
&\overset{ab}{[k}: = \frac{1}{2}(1 + \frac{i}{k}\gamma^a\gamma^b) \,, \quad (\overset{ab}{[k]})^2 = \overset{ab}{[k]} \,,
\end{aligned} \tag{16.5}$$

so that each nilpotent and each projector is the eigenstate of one of the Cartan (chosen) subalgebra members of the Lorentz algebra

$$\begin{aligned}
&S^{03}, S^{12}, S^{56}, \cdots, S^{d-1\,d} \,,\\
&\tilde{S}^{03}, \tilde{S}^{12}, \tilde{S}^{56}, \cdots, \tilde{S}^{d-1\,d} \,,\\
&\mathcal{S}^{ab} = S^{ab} + \tilde{S}^{ab} \,,
\end{aligned} \tag{16.6}$$

where $S^{ab} = \frac{i}{4}\{\gamma^a, \gamma^b\}_+$, while $\tilde{S}^{ab} = \frac{i}{4}\{\tilde{\gamma}^a, \tilde{\gamma}^b\}_+$ are used to determine additional quantum numbers, in the case of fermions are called the family quantum numbers.
Being eigenstates of both operators, of S^{ab} and $\tilde{S}^{ab}$, nilpotents and projectors carry both quantum numbers S^{ab} and $\tilde{S}^{ab}$

$$\begin{aligned}
S^{ab}\ \overset{ab}{(k)} &= \frac{k}{2}\ \overset{ab}{(k)} \,, \qquad \tilde{S}^{ab}\ \overset{ab}{(k)} = \frac{k}{2}\ \overset{ab}{(k)} \,,\\
S^{ab}\ \overset{ab}{[k]} &= \frac{k}{2}\ \overset{ab}{[k]} \,, \qquad \tilde{S}^{ab}\ \overset{ab}{[k]} = -\frac{k}{2}\ \overset{ab}{[k]} \,,
\end{aligned} \tag{16.7}$$

with $k^2 = \eta^{aa}\eta^{bb}$.

In even-dimensional spaces, the states in internal spaces are defined by the "basis vectors" which are products of $\frac{d}{2}$ nilpotents and projectors, and are the eigenstates of all the Cartan subalgebra members.
Fermions are products of an odd number of nilpotents (at least one), *the rest are projectors; Bosons are products of an even number of nilpotents* (or none), *the rest are projectors*. We

call them odd and even "basis vectors".

The odd "basis vectors" have the eigenvalues of the Cartan subalgebra members, Eq. (15.3, 15.4), either of S^{ab} or $\tilde{S}^{ab}$, equal to half integer, $\pm\frac{i}{2}$ or $\pm\frac{1}{2}$.
The even "basis vectors" have the eigenvalues of the Cartan subalgebra members, Eq. (15.3, 15.4), $\mathcal{S}^{ab} = S^{ab} + \tilde{S}^{ab}$, which is $\pm i$ or ± 1 or zero.

16.2.1 "Basis vectors" describing internal spaces of fermion and boson fields

It turns out that the odd products of nilpotents (at least one, the rest are projectors), *odd "basis vectors"*, differ essentially from the even products of nilpotents (none or at least two), *even "basis vectors"* (the rest are projectors).

The odd "basis vectors", named $\hat{b}^{m\dagger}_{f}$, m determine the family member, f determines the family, appear in $2^{\frac{d}{2}-1}$ irreducible representations, called families, all with the same properties with respect to S^{ab}, distinguishing with respect to the family quantum numbers $\tilde{S}^{ab}$. Each family has $2^{\frac{d}{2}-1}$ members. Their Hermitian conjugate partners $(\hat{b}^{m\dagger}_{f})^{\dagger} = \hat{b}^{m}_{f}$, appearing in a separate group, have $2^{\frac{d}{2}-1} \times 2^{\frac{d}{2}-1}$ members. As already written, the odd "basis vectors" have the eigenvalues of the Cartan subalgebra members, Eq. (15.3, 15.4), either of S^{ab} or $\tilde{S}^{ab}$ half integer, $\pm\frac{i}{2}$ or $\pm\frac{1}{2}$. The algebraic product of any two members of the odd "basis vectors" are equal to zero[2].

$$\hat{b}^{m\dagger}_{f} *_A \hat{b}^{m'\dagger}_{f'} = 0\,, \quad \hat{b}^{m}_{f} *_A \hat{b}^{m'}_{f'} = 0\,, \quad \forall m, m', f, f'\,. \tag{16.10}$$

The Hermitian conjugate partners $\hat{b}^{m}_{f} = (\hat{b}^{m\dagger}_{f})^{\dagger}$ of the "basis vectors" appear in a separate group with $2^{\frac{d}{2}-1} \times 2^{\frac{d}{2}-1}$ members.
Choosing the vacuum state equal to

$$|\psi_{oc}> = \sum_{f=1}^{2^{\frac{d}{2}-1}} \hat{b}^{m}_{f} *_A \hat{b}^{m\dagger}_{f} |1>\,, \tag{16.11}$$

[2]Let us present the odd "basis vectors" and their Hermitian conjugate partners for $d = (3+1)$. The odd "basis vectors" appear in two families, each family has two members.

$$\begin{array}{cc|cc} & f=1 & & f=2 \\ \tilde{S}^{03} = \frac{i}{2}, \tilde{S}^{12} = -\frac{1}{2} & & \tilde{S}^{03} = -\frac{i}{2}, \tilde{S}^{12} = \frac{1}{2} & S^{03} \quad S^{12} \\ \hat{b}^{1\dagger}_{1} = \overset{03}{(+i)}\overset{12}{[+]} & & \hat{b}^{1\dagger}_{2} = \overset{03}{[+i]}\overset{12}{(+)} & \frac{i}{2} \quad \frac{1}{2} \\ \hat{b}^{2\dagger}_{1} = \overset{03}{[-i]}\overset{12}{(-)} & & \hat{b}^{2\dagger}_{2} = \overset{03}{(-i)}\overset{12}{[-]} & -\frac{i}{2} \; -\frac{1}{2}\,. \end{array} \tag{16.8}$$

Their Hermitian conjugate partners have the properties

$$\begin{array}{cc|cc} S^{03} = -\frac{i}{2}, S^{12} = \frac{1}{2} & & S^{03} = \frac{i}{2}, S^{12} = -\frac{1}{2} & \tilde{S}^{03} \; \tilde{S}^{12} \\ \hat{b}^{1}_{1} = \overset{03}{(-i)}\overset{12}{[+]} & & \hat{b}^{1}_{2} = \overset{03}{[+i]}\overset{12}{(-)} & -\frac{i}{2} \; -\frac{1}{2} \\ \hat{b}^{2}_{1} = \overset{03}{[-i]}\overset{12}{(+)} & & \hat{b}^{2}_{2} = \overset{03}{(+i)}\overset{12}{[-]} & \frac{i}{2} \; \frac{1}{2}\,. \end{array} \tag{16.9}$$

The vacuum state $|\psi_{oc}>$, Eq. (15.6), is equal to: $|\psi_{oc}> = \frac{1}{\sqrt{2}}(\overset{03}{[-i]}\overset{12}{[+]} + \overset{03}{[+i]}\overset{12}{[-]})$.

for one of the members m, which can be anyone of the odd irreducible representations f, it follows that the odd "basis vectors" obey the relations

$$\begin{aligned}
\hat{b}^{m}_{f} *_{A} |\psi_{oc}> &= 0.|\psi_{oc}>, \\
\hat{b}^{m\dagger}_{f} *_{A} |\psi_{oc}> &= |\psi^{m}_{f}>, \\
\{\hat{b}^{m}_{f}, \hat{b}^{m'}_{f'}\}_{*_A +} |\psi_{oc}> &= 0.|\psi_{oc}>, \\
\{\hat{b}^{m\dagger}_{f}, \hat{b}^{m'\dagger}_{f'}\}_{*_A +} |\psi_{oc}> &= 0.|\psi_{oc}>, \\
\{\hat{b}^{m}_{f}, \hat{b}^{m'\dagger}_{f'}\}_{*_A +} |\psi_{oc}> &= \delta^{mm'}\delta_{ff'}|\psi_{oc}>,
\end{aligned} \tag{16.12}$$

as postulated by Dirac for the second quantised fermion fields. Here the odd "basis vectors" anti-commute, since the odd products of γ^{a}'s anti-commute.

The odd "basis vectors" $\hat{b}^{m\dagger}_{f}$, which are the superposition of odd products of γ^{a}'s, appear in the case that the internal space has $d = 2(2n+1)$, in $2^{\frac{d}{2}-1}$ families with $2^{\frac{d}{2}-1}$ members each. Their Hermitian conjugate partners appear in a separate group and have $2^{\frac{d}{2}-1} \times 2^{\frac{d}{2}-1}$ members. The odd "basis vectors" and their Hermitian conjugate partners are normalised as follows

$$< \psi_{oc}|(\hat{b}^{m\dagger}_{f})^{\dagger} *_{A} \hat{b}^{m'\dagger}_{f'}|\psi_{oc}> = \delta^{mm'}\delta_{ff'} < \psi_{oc}|\psi_{oc}>, \tag{16.13}$$

the vacuum state $< \psi_{oc}|\psi_{oc}>$ is normalised to identity.

The even "basis vectors", appear in two orthogonal groups, named ${}^{I}\hat{\mathcal{A}}^{m\dagger}_{f}$ and ${}^{II}\hat{\mathcal{A}}^{m\dagger}_{f}$

$${}^{I}\hat{\mathcal{A}}^{m\dagger}_{f} *_{A} {}^{II}\hat{\mathcal{A}}^{m\dagger}_{f} = 0 = {}^{II}\hat{\mathcal{A}}^{m\dagger}{}_{.f} *_{A} {}^{I}\hat{\mathcal{A}}^{m\dagger}_{f}\,. \tag{16.14}$$

Each group has $2^{\frac{d}{2}-1} \times 2^{\frac{d}{2}-1}$ members with the Hermitian conjugate partners within the group.
The even "basis vectors" have the eigenvalues of the Cartan subalgebra members, Eq. (15.3), $\mathcal{S}^{ab} = S^{ab} + \tilde{S}^{ab}$, equal to $\pm i$ or ± 1 or zero.
The algebraic products, $*_{A}$, of two members of each of these two groups have the property

$${}^{i}\hat{\mathcal{A}}^{m\dagger}_{f} *_{A} {}^{i}\hat{\mathcal{A}}^{m'\dagger}_{f'} \rightarrow \begin{cases} {}^{i}\hat{\mathcal{A}}^{m\dagger}_{f'}, i = (I, II) \\ \text{or zero}\,. \end{cases} \tag{16.15}$$

For a chosen (m, f, f'), there is (out of $2^{\frac{d}{2}-1}$) only one m' giving a non-zero contribution [3].

[3] Let us present the $2^{\frac{4}{2}-1} \times 2^{\frac{4}{2}-1}$ "basis vectors" for $d = (3+1)$, the members of the group ${}^{I}\mathcal{A}^{m\dagger}_{f}$,

$$\begin{array}{cccc|cccc}
 & & \mathcal{S}^{03} & \mathcal{S}^{12} & & & \mathcal{S}^{03} & \mathcal{S}^{12} \\
{}^{I}\mathcal{A}^{1\dagger}_{1} = & \overset{03}{[+i]}\overset{12}{[+]} & 0 & 0 & {}^{I}\mathcal{A}^{1\dagger}_{2} = & \overset{03}{(+i)}\overset{12}{(+)} & i & 1 \\
{}^{I}\mathcal{A}^{2\dagger}_{1} = & \overset{03}{(-i)}\overset{12}{(-)} & -i & -1 & {}^{I}\mathcal{A}^{2\dagger}_{2} = & \overset{03}{[-i]}\overset{12}{[-]} & 0 & 0,
\end{array} \tag{16.16}$$

To be able to propose the action for fermion and boson second quantized fields, we need to know the algebraic application, $*_A$, of boson fields on fermion fields and fermion fields on boson fields.

The algebraic application, $*_A$, of the even "basis vectors" ${}^{I}\hat{\mathcal{A}}^{m\dagger}_{f}$ on the odd "basis vectors" $\hat{b}^{m'\dagger}_{f'}$ gives

$$ {}^{I}\hat{\mathcal{A}}^{m\dagger}_{f} \; *_A \; \hat{b}^{m'\dagger}_{f'} \rightarrow \begin{cases} \hat{b}^{m\dagger}_{f'} , \\ \text{or zero} . \end{cases} \tag{16.18} $$

Eq. (15.10) demonstrates that ${}^{I}\hat{\mathcal{A}}^{m\dagger}_{f}$, applying on $\hat{b}^{m'\dagger}_{f'}$, transforms the odd "basis vector" into another odd "basis vector" of the same family, transferring to the odd "basis vector" integer spins or gives zero.

We find for the second group of boson fields ${}^{II}\hat{\mathcal{A}}^{m\dagger}_{f}$

$$ \hat{b}^{m\dagger}_{f} *_A \; {}^{II}\hat{\mathcal{A}}^{m'\dagger}_{f'} \rightarrow \begin{cases} \hat{b}^{m\dagger}_{f''} , \\ \text{or zero} . \end{cases} \tag{16.19} $$

demonstrating that the application of the odd "basis vector" $\hat{b}^{m\dagger}_{f}$ on ${}^{II}\hat{\mathcal{A}}^{m'\dagger}_{f'}$ leads to another odd "basis vector" $\hat{b}^{m\dagger}_{f''}$ belonging to the same family member m of a different family f''.

The rest of possibilities give zero.

$$ \hat{b}^{m\dagger}_{f} *_A \; {}^{I}\hat{\mathcal{A}}^{m'\dagger}_{f'} = 0 , \quad {}^{II}\hat{\mathcal{A}}^{m\dagger}_{f} *_A \; \hat{b}^{m'\dagger}_{f'} = 0 , \;\; \forall (m, m', f, f') . \tag{16.20} $$

Let us add that the internal spaces of boson second quantized fields can be written as the algebraic products of the odd "basis vectors" and their Hermitian conjugate partners: $\hat{b}^{m\dagger}_{f}$ *and* $(\hat{b}^{m''\dagger}_{f'})^{\dagger}$.

$$ {}^{I}\hat{\mathcal{A}}^{m\dagger}_{f} = \hat{b}^{m'\dagger}_{f'} *_A (\hat{b}^{m''\dagger}_{f'})^{\dagger} , \tag{16.21} $$

$$ {}^{II}\hat{\mathcal{A}}^{m\dagger}_{f} = (\hat{b}^{m'\dagger}_{f'})^{\dagger} *_A \hat{b}^{m'\dagger}_{f''} . \tag{16.22} $$

Family members $\hat{b}^{m'\dagger}_{f'}$ of any family f' generates in the algebraic product $\hat{b}^{m'\dagger}_{f'} *_A (\hat{b}^{m''\dagger}_{f'})^{\dagger}$ the same $2^{\frac{d}{2}-1} \times 2^{\frac{d}{2}-1}$ even "basis vectors" ${}^{I}\hat{\mathcal{A}}^{m\dagger}_{f}$, each family member m' generates in $(\hat{b}^{m'\dagger}_{f'})^{\dagger} *_A \hat{b}^{m'\dagger}_{f''}$ the same $2^{\frac{d}{2}-1} \times 2^{\frac{d}{2}-1}$ even "basis vectors" ${}^{II}\hat{\mathcal{A}}^{m\dagger}_{f}$ [4].

---

and $2^{\frac{4}{2}-1} \times 2^{\frac{4}{2}-1}$ even "basis vectors" ${}^{II}\mathcal{A}^{m\dagger}_{f}$, $m = (1,2)$, $f = (1,2)$,

$$ \begin{array}{cccc} & \mathcal{S}^{03} & \mathcal{S}^{12} & \\ {}^{II}\mathcal{A}^{1\dagger}_{1} = & [+i]^{03}[-]^{12} & 0 \quad 0 & , \\ {}^{II}\mathcal{A}^{2\dagger}_{1} = & (-i)^{03}(+)^{12} & -i \quad 1 & , \end{array} \qquad \begin{array}{cccc} & \mathcal{S}^{03} & \mathcal{S}^{12} & \\ {}^{II}\mathcal{A}^{1\dagger}_{2} = & (+i)^{03}(-)^{12} & i \quad -1 & \\ {}^{II}\mathcal{A}^{2\dagger}_{2} = & [-i]^{03}[+]^{12} & 0 \quad 0 & . \end{array} \tag{16.17} $$

One can easily check the above relations if taking into account Eq. 15.19, and the relation 15.8.

[4] It follows that ${}^{I}\hat{\mathcal{A}}^{m\dagger}_{f}$, expressed by $\hat{b}^{m'\dagger}_{f'} *_A (\hat{b}^{m''\dagger}_{f'})^{\dagger}$, applying on $\hat{b}^{m'''\dagger}_{f''}$, obey Eq. (15.10), and $\hat{b}^{m'''\dagger}_{f''}$ applying on ${}^{II}\hat{\mathcal{A}}^{m\dagger}_{f}$, expressed by $(\hat{b}^{m'\dagger}_{f'})^{\dagger} *_A \hat{b}^{m'\dagger}_{f''}$, obey Eq. (15.11).

The scalar product of a boson field ${}^{i}\hat{\mathcal{A}}^{m\dagger}_{f}$, $i = (I, II)$ with its Hermitian conjugate partner can easily be calculated, after recognising that any of the two groups of the boson "basis vectors" have their Hermitian conjugate partners within the same group. It follows for ${}^{I}\hat{\mathcal{A}}^{m\dagger}_{f}$, when we take into account Eqs. (15.12,15.13), ${}^{I}\hat{\mathcal{A}}^{m\dagger}_{f} = \hat{b}^{m'\dagger}_{f'} *_{A} (\hat{b}^{m''\dagger}_{f'})^{\dagger}$

$$({}^{I}\hat{\mathcal{A}}^{m\dagger}_{f})^{\dagger} *_{A} {}^{I}\hat{\mathcal{A}}^{m\dagger}_{f} = \hat{b}^{m''\dagger}_{f'} *_{A} (\hat{b}^{m'\dagger}_{f'})^{\dagger} *_{A} \hat{b}^{m'\dagger}_{f'} *_{A} (\hat{b}^{m''\dagger}_{f'})^{\dagger} = \\ = \hat{b}^{m''\dagger}_{f'} *_{A} (\hat{b}^{m''\dagger}_{f'})^{\dagger}. \tag{16.23}$$

For the scalar product of a boson field ${}^{II}\hat{\mathcal{A}}^{m\dagger}_{f} = (\hat{b}^{m'\dagger}_{f'})^{\dagger} *_{A} \hat{b}^{m'\dagger}_{f''}$ with its Hermitian conjugate partner we equivalently find

$$({}^{II}\hat{\mathcal{A}}^{m\dagger}_{f})^{\dagger} *_{A} {}^{II}\hat{\mathcal{A}}^{m\dagger}_{f} = (\hat{b}^{m'\dagger}_{f''})^{\dagger} *_{A} \hat{b}^{m'\dagger}_{f'} *_{A} (\hat{b}^{m'\dagger}_{f'})^{\dagger} *_{A} \hat{b}^{m'\dagger}_{f''} = \\ = (\hat{b}^{m'\dagger}_{f'})^{\dagger} *_{A}, \hat{b}^{m'\dagger}_{f'} \tag{16.24}$$

16.2.2 Fermions and bosons creation operators

The creation operators for either fermions or bosons must be defined as the tensor products, $*_{T}$, of both contributions, the "basis vectors" describing the internal space of fermions or bosons and the basis in ordinary space-time in the momentum or coordinate representation.
To the boson second quantized fields we need to add the space index α.

Let us start with the definition of the single particle states in ordinary space-time in momentum representation, briefly overviewing Refs. [22], ([9], Subsect. 3.3 and App. J).

$$|\vec{p}> = \hat{b}^{\dagger}_{\vec{p}}\,|0_{p}>, \quad <\vec{p}\,| =< 0_{p}\,|\,\hat{b}_{\vec{p}}\,, \\ <\vec{p}\,|\,\vec{p}\,'> = \delta(\vec{p}-\vec{p}\,') =< 0_{p}\,|\hat{b}_{\vec{p}}\;\hat{b}^{\dagger}_{\vec{p}\,'}|\,0_{p}>, \\ < 0_{p}\,|\hat{b}_{\vec{p}'}, \hat{b}^{\dagger}_{\vec{p}}\,|\,0_{p}> = \delta(\vec{p}\,'-\vec{p})\,, \tag{16.25}$$

with $< 0_{p}\,|\,0_{p} >= 1$. The operator $\hat{b}^{\dagger}_{\vec{p}}$ pushes a single particle state with zero momentum by an amount $\vec{p}$. Taking into account that $\{\hat{p}^{i}\,, \hat{p}^{j}\}_{-} = 0$ and $\{\hat{x}^{k}\,, \hat{x}^{l}\}_{-} = 0$, while $\{\hat{p}^{i}\,, \hat{x}^{j}\}_{-} = i\eta^{ij}$, it follows

$$< \vec{p}\,|\,\vec{x}> =< 0_{\vec{p}}\,|\,\hat{b}_{\vec{p}}\;\hat{b}^{\dagger}_{\vec{x}}|0_{\vec{x}}> = (< 0_{\vec{x}}\,|\,\hat{b}_{\vec{x}}\;\hat{b}^{\dagger}_{\vec{p}}\;|0_{\vec{p}}>)^{\dagger} \\ < 0_{\vec{p}}\,|\{\hat{b}^{\dagger}_{\vec{p}}\,, \hat{b}^{\dagger}_{\vec{p}\,'},\}_{-}|0_{\vec{p}}> = 0\,, \quad < 0_{\vec{p}}\,|\{\hat{b}_{\vec{p}}\,, \hat{b}_{\vec{p}\,'},\}_{-}|0_{\vec{p}}> = 0\,, \quad < 0_{\vec{p}}\,|\{\hat{b}_{\vec{p}}\,, \hat{b}^{\dagger}_{\vec{p}\,'},\}_{-}|0_{\vec{p}}> = 0\,, \\ < 0_{\vec{x}}\,|\{\hat{b}^{\dagger}_{\vec{x}}\,, \hat{b}^{\dagger}_{\vec{x}\,'},\}_{-}|0_{\vec{x}}> = 0\,, \quad < 0_{\vec{x}}\,|\{\hat{b}_{\vec{x}}\,, \hat{b}_{\vec{x}\,'},\}_{-}|0_{\vec{x}}> = 0\,, \quad < 0_{\vec{x}}\,|\{\hat{b}_{\vec{x}}\,, \hat{b}^{\dagger}_{\vec{x}\,'},\}_{-}|0_{\vec{x}}> = 0\,, \\ < 0_{\vec{p}}\,|\{\hat{b}_{\vec{p}}\,, \hat{b}^{\dagger}_{\vec{x}}\}_{-}|0_{\vec{x}}> = e^{i\vec{p}\cdot\vec{x}}\frac{1}{\sqrt{(2\pi)^{d-1}}}\,, \quad < 0_{\vec{x}}\,|\{\hat{b}_{\vec{x}}\,, \hat{b}^{\dagger}_{\vec{p}}\}_{-}|0_{\vec{p}}> = e^{-i\vec{p}\cdot\vec{x}}\frac{1}{\sqrt{(2\pi)^{d-1}}} \tag{16.26}$$

The momentum basis is continuously infinite, while the internal space of either fermion or boson fields has a finite number of "basis vectors", in our case twice $2^{\frac{d}{2}-1} \times 2^{\frac{d}{2}-1}$ for fermions and twice $2^{\frac{d}{2}-1} \times 2^{\frac{d}{2}-1}$ for bosons.

The creation operator for a free massless fermion field of the energy $p^{0} = |\vec{p}|$, belonging to the family f and to a superposition of family members m applying on

the vacuum state ($|\psi_{oc}> *_T |0_{\vec{p}}>$) can be written as (we follow [9], Subsect.3.3.2, and the references therein)

$$\hat{b}^{s\dagger}_f(\vec{p}) = \sum_m c^{sm}{}_f(\vec{p})\, \hat{b}^{\dagger}_{\vec{p}} *_T \hat{b}^{m\dagger}_f . \tag{16.27}$$

The vacuum state for fermions, $|\psi_{oc}> *_T |0_{\vec{p}}>$, includes both spaces, the internal part, Eq.(15.6), and the momentum part, Eq. (15.14). The creation operators in the coordinate representation can be written as $\hat{b}^{s\dagger}_f(\vec{x}, x^0) = \sum_m \hat{b}^{m\dagger}_f *_T \int_{-\infty}^{+\infty} \frac{d^{d-1}p}{(\sqrt{2\pi})^{d-1}} c^{sm}{}_f(\vec{p})\, \hat{b}^{\dagger}_{\vec{p}}\, e^{-i(p^0 x^0 - \varepsilon \vec{p}\cdot\vec{x})}$ [20], ([9], subsect. 3.3.2. and the references therein).
The creation operators, $\hat{b}^{s\dagger}_f(\vec{p})$, and their Hermitian conjugate partners annihilation operators, $(\hat{b}^{s\dagger}_f(\vec{p}))^\dagger = \hat{b}^{s}_f(\vec{p})$, creating and annihilating the single fermion states, respectively, fulfil when applying the vacuum state, ($|\psi_{oc}> *_T |0_{\vec{p}}>$), the anticommutation relations for the second quantized fermions, postulated by Dirac (Ref. [9], Subsect. 3.3.1, Sect. 5). The anticommuting properties of the creation operators for fermions are determined by the odd "basis vectors", the basis in ordinary space-time, namely, commute [5].

The creation operator for a free massless boson field of the energy $p^0 = |\vec{p}|$, with the "basis vectors" belonging to one of the two groups, ${}^i\hat{\mathcal{A}}^{m\dagger}_f$, $i = (I, II)$, applying on the vacuum state, $|1> *_T |0_{\vec{p}}>$, must carry the space index a, describing the a component of the boson field in the ordinary space [6]. We, therefore, add the space index a [7], as well as the dependence on the momentum [22]

$${}^i\hat{\mathcal{A}}^{m\dagger}_{fa}(\vec{p}) = {}^i\mathcal{C}^m{}_{fa}(\vec{p}) *_T {}^i\hat{\mathcal{A}}^{m\dagger}_f \,, i = (I, II)\,, \tag{16.29}$$

with ${}^i\mathcal{C}^m{}_{fa}(\vec{p}) = {}^i\mathcal{C}^m{}_{fa}\, \hat{b}^{\dagger}_{\vec{p}}$, with $\hat{b}^{\dagger}_{\vec{p}}$ defined in Eqs. (15.14, 14.26) [8].
The creation operators for boson fields in the coordinate representation one finds using Eqs. (15.14, 14.26),

$${}^i\hat{\mathcal{A}}^{m\dagger}_{fa}(\vec{x}, x^0) = {}^i\hat{\mathcal{A}}^{m\dagger}_f *_T \int_{-\infty}^{+\infty} \frac{d^{d-1}p}{(\sqrt{2\pi})^{d-1}}\, {}^i\mathcal{C}^m{}_{fa}\, \hat{b}^{\dagger}_{\vec{p}}\, e^{-i(p^0 x^0 - \varepsilon \vec{p}\cdot\vec{x})}|_{p^0=|\vec{p}|} \,, i = (I, II)$$

[5]

$$\begin{aligned}
< 0_{\vec{p}} |\{\hat{b}^{s'}_{f'}(\vec{p'}),\, \hat{b}^{s\dagger}_f(\vec{p})\}_+ |\psi_{oc}> |0_{\vec{p}}> &= \delta^{ss'}\delta_{ff'}\,\delta(\vec{p}' - \vec{p}) \cdot |\psi_{oc}>\,,\\
\{\hat{b}^{s'}_{f'}(\vec{p'}),\, \hat{b}^{s}_f(\vec{p})\}_+ |\psi_{oc}> |0_{\vec{p}}> &= 0 \cdot |\psi_{oc}> |0_{\vec{p}}>\,,\\
\{\hat{b}^{s'\dagger}_{f'}(\vec{p'}),\, \hat{b}^{s\dagger}_f(\vec{p})\}_+ |\psi_{oc}> |0_{\vec{p}}> &= 0 \cdot |\psi_{oc}> |0_{\vec{p}}>\,,\\
\hat{b}^{s\dagger}_f(\vec{p}) |\psi_{oc}> |0_{\vec{p}}> &= |\psi^s_f(\vec{p})>\,,\\
\hat{b}^{s}_f(\vec{p}) |\psi_{oc}> |0_{\vec{p}}> &= 0 \cdot |\psi_{oc}> |0_{\vec{p}}>\,,\\
|p^0| &= |\vec{p}|\,.
\end{aligned} \tag{16.28}$$

[6] According to the Eqs.(14.23, 14.24) the vacuum state can be chosen to be identity.)

[7] We use either α or a for the boson space index. α can be either μ or σ, while a can be n or s.

[8] In the general case, the energy eigenstates of bosons are in a superposition of ${}^i\hat{\mathcal{A}}^{m\dagger}_f$, for either $i = I$ or $i = II$.

.
Assuming that the internal space has $d = (13+1)$, while fermions and bosons have nonzero momenta only in $d = (3+1)$ of the ordinary space-time, the Clifford even boson creation operators, ${}^{I}\hat{\mathcal{A}}^{m\dagger}_{fa}$, manifest for a equal to $n = (0,1,2,3)$ all the properties, Eq. (15.9), of the fermion fields (quarks and leptons and antiquarks and antileptons, appearing in families), as assumed by the *standard model* before the electroweak phase transitions (after analysing $SO(13,1)$ with respect to the subgroups $SO(1,3)$, $SU(2)\times SU(2)$, $SU(3)$ and $U(1)$ of the Lorentz group $SO(13,1)$. For a equal to $s \geq 5$, the even "basis vectors", ${}^{II}\hat{\mathcal{A}}^{m\dagger}_{fs}$ manifest properties of the scalar Higgs, causing after the electroweak phase transitions masses of quarks and leptons and antiquarks and antileptons, appearing in families, and some of the gauge fields.
The assumption that the internal spaces of fermion and boson fields are describable by the odd and even "basis vectors", respectively, leads to the conclusion that the internal spaces of all the boson fields - gravitons (the gauge fields of the spins $SO(1,3)$), photons (the gauge fields of $U(1)$), weak bosons (the gauge fields of one of the $SU(2)$) and gluons (the gauge fields of $SU(3)$ - must also be described by the even "basis vectors", all must carry the index $a = n = (0,1,2,3)$.

Both groups of even "basis vectors" manifest as the gauge fields of the corresponding fermion fields: One concerning the family members quantum numbers, determined by S^{ab}, the other concerning the family quantum numbers, determined by $\tilde{S}^{ab}$.

Let us point out that although it looks like that this theory postulates two kinds of boson fields, not yet observed so far, this is not the case: All the theories so far postulate the families of fermions and the scalar fields giving masses to fermions and weak bosons in addition to the internal spaces of fermions and bosons. In our case, the families are present without being postulated. Our boson fields of the second kind have, in theories so far, realization in Higgs.
The proposed description of the internal spaces offers families of fermions, scalar fields and gauge fields: ${}^{I}\hat{\mathcal{A}}^{m\dagger}_{f}$, transferring the integer quantum numbers to the odd "basis vectors", $\hat{b}^{m\dagger}_{f}$, changes the family members' quantum numbers, leaving the family quantum numbers unchanged, manifesting the properties of the gauge fields; The second group, ${}^{II}\hat{\mathcal{A}}^{m\dagger}_{f}$, transferring the integer quantum numbers to the "basis vector" $\hat{b}^{m\dagger}_{f}$, changes the family quantum numbers leaving the family members quantum numbers unchanged, manifesting properties of the scalar fields, which give masses to quarks and leptons, and to the weak bosons.

16.3 States of fermions and bosons active only in $d = (3+1)$

We take the states of fermion and boson fields to have non-zero momentum only in $d = (3+1)$. This refers to the Poincaré group (with the infinitesimal generators $M^{ab}(= L^{ab} + S^{ab}), p^{c}$) applying only in $d = (3+1)$, while in the internal space, the Lorentz group (with the infinitesimal generators S^{ab}) applies to the whole internal space $d = 2(2n+1)$. We discuss in this section the algebraic relations

among fermion and boson fields (14.2, 14.2.1) in the case that the internal space has $d=(5+1)$ and $d=(13+1)$, Subsect. 15.2.1.
The odd and even "basis vectors" are presented in the case that $d=(5+1)$ in App. 14.7 in Table 14.1.
In Table 14.8 the odd "basis vectors" are presented in the case that $d=(13+1)$ for one family of fermions - quarks and leptons and antiquarks and antileptons - as products of an odd number of nilpotents (at least one, up to seven), the rest are projectors (from six to zero). The "basis vectors" are eigenstates of all the Cartan subalgebra memebers, Eq. (15.3), of the Lorentz algebra.
The creation and annihilation operators are for odd and even "basis vectors" the tensor products, $*_T$, of the basis in ordinary space-time in $d=(3+1)$, and the "basis vectors" in internal space, with $d=(5+1)$ or $d=(13+1)$: For anti-commuting creation operators we have $\hat{b}^{s\dagger}_f(\vec{p}) = \sum_m c^{sm}{}_f(\vec{p})\, \hat{b}^{\dagger}_{\vec{p}}\ *_T\ \hat{b}^{m\dagger}_f$, Eq. (15.15).
For the commuting creation operators with the "basis vectors" belonging to one of the two groups, ${}^i\hat{\mathcal{A}}^{m\dagger}_f, i=(I,II)$, carrying the space index a, we have ${}^i\hat{\mathcal{A}}^{m\dagger}_{fa}(\vec{p}) = {}^i\mathcal{C}^m{}_{fa}(\vec{p})\ *_T\ {}^i\hat{\mathcal{A}}^{m\dagger}_f\ , i=(I,II)$, Eq. (15.16).

16.3.1 Internal spaces of fermions and bosons in $d=(5+1)$ and $d=(13+1)$

a. Let us start with *the toy model for electrons, positrons, photons and gravitons in* $d=(5+1)$ *with non zero momenta in* $d=(3+1)$.
We follow here to some extent a similar part in the Ref. ([22], and the references therein). This toy model is to show the reader, in a simple model, what the new description of the internal spaces of fermion and boson fields offers.
In Table 14.1 the odd "basis vectors" $\hat{b}^{m\dagger}_f$, appearing in four ($2^{\frac{d=6}{2}-1}$) families, each family having four ($2^{\frac{d=6}{2}-1}$) family members, are presented in the first group, as products of an odd number of nilpotents (one or three) and the remaining projectors. Their Hermitian conjugate partners are presented in the second group, again with 16 members.
The even basis vectors appear in the third and the second group.
Table 14.1 presents the eigenvalues of all Cartan subalgebra members, Eq. (15.3); for S^{ab}, and $\tilde{S}^{ab}$, while $\mathcal{S}^{ab}=(S^{ab}+\tilde{S}^{ab})$, when looking for the Cartan eigenvalues of the even "basis vectors", presenting internal spaces of boson fields.
The reader can check the relations appearing in Eqs. (15.5 – 15.13) by taking into account Eqs. (14.1, 15.19, 14.3).
The corresponding creation and annihilation operators for free massless fermion, $\hat{b}^{m\dagger}_f(\vec{p}) = \hat{b}^{\dagger}_{\vec{p}}\ *_T\ \hat{b}^{m\dagger}_f$, Eq. (15.15), and for free massless boson fields, ${}^i\hat{\mathcal{A}}^{m\dagger}_{fa}, i=(I,II)$, carrying the space index a, we have ${}^i\hat{\mathcal{A}}^{m\dagger}_{fa}(\vec{p}) = {}^i\mathcal{C}^m{}_{fa}(\vec{p})\ *_T\ {}^i\hat{\mathcal{A}}^{m\dagger}_f\ , i=(I,II)$, Eq. (15.16).

Let us call the first $\hat{b}^{m\dagger}_f$ of the"basis vectors" in Table 14.1, $\hat{b}^{1\dagger}1 = \overset{03}{(+i)}\overset{12}{[+]}\overset{56}{[+]}$, the "basis vector" of the "electron", and the third "basis vector" $\hat{b}^{3\dagger}_1 = \overset{03}{[-i]}\overset{12}{[+]}\overset{56}{(-)}$ of the first family the "basis vector" of the "positron", although the quantum numbers of the "electron" are ($S^{03}=\frac{i}{2}$, $S^{12}=\frac{1}{2}$ and $S^{56}=\frac{1}{2}$), and of the "positron"

are ($S^{03} = -\frac{i}{2}$, $S^{12} = \frac{1}{2}$ and $S^{56} = \frac{1}{2}$). One can transform the "electron" to the "positron" by S^{05}

The "basis vectors" of the"positron" and "electron" have fractional charges and both appear in four families, reachable from the first one by the application of $\tilde{S}^{ab}$. For example, one generates the second family by applying $\tilde{S}^{05}$ on the first family. The corresponding "photon" field, its "basis vector" indeed, describing the internal space of "photon", must be a product of projectors only, since the photon does not change the charge of the positron or electron.

There is only one even "basis vector", when applied to the "basis vector" of the "electron" gives a non-zero contribution, the "basis vector" ${}^{I}\hat{\mathcal{A}}^{1\dagger}_{3} = \overset{03}{[+i]}\overset{12}{[+]}\overset{56}{[+]}$. There is also only one even "basis vector", which, applying to the "basis vector" of the "positron", gives a non-zero contribution. Both even "basis vectors" have the properties of photons.

$$
\begin{aligned}
{}^{I}\hat{\mathcal{A}}^{1\dagger}_{3ph}(\equiv \overset{03}{[+i]}\overset{12}{[+]}\overset{56}{[+]}) \ *_A \ \hat{b}^{1\dagger}_{f}(\equiv \overset{03}{(+i)}\overset{12}{[+]}\overset{56}{[+]}) \ &\rightarrow \hat{b}^{1\dagger}_{f}\,, \\
{}^{I}\hat{\mathcal{A}}^{3\dagger}_{2ph}(\equiv \overset{03}{[-i]}\overset{12}{[+]}\overset{56}{[-]}) \ *_A \ \hat{b}^{3\dagger}_{f}(\equiv \overset{03}{[-i]}\overset{12}{[+]}\overset{56}{(-)}) \ &\rightarrow \hat{b}^{3\dagger}_{f}\,. \qquad (16.30)
\end{aligned}
$$

The same "photon" makes the same transformations on the corresponding "electron" (or "positron") of all the families. Obviously, the Cartan subalgebra quantum numbers, Eq. (15.3), ($S^{ab} + \tilde{S}^{ab}$, applying on any member of the "photon" is equal to zero: ($S^{03} + \tilde{S}^{03} = 0$, $S^{12} + \tilde{S}^{12} = 0$ and $S^{56} + \tilde{S}^{56} = 0$) of either ${}^{I}\hat{\mathcal{A}}^{1\dagger}_{3ph}$ or ${}^{I}\hat{\mathcal{A}}^{3\dagger}_{2ph}$, are zero, since the projectors have properties that $S^{ab} = -\tilde{S}^{ab}$, Eq. (15.4).

Let us check the relation of Eq. (15.12), using Eq. (14.1).

$$
\begin{aligned}
{}^{I}\hat{\mathcal{A}}^{1\dagger}_{3}(\equiv \overset{03}{[+i]}\overset{12}{[+]}\overset{56}{[+]}) &= \hat{b}^{1\dagger}_{1}(\equiv \overset{03}{(+i)}\overset{12}{[+]}\overset{56}{[+]}) \ *_A \ (\hat{b}^{1\dagger}_{1})^{\dagger}(\equiv ((\overset{03}{(+i)}\overset{12}{[+]}\overset{56}{[+]})^{\dagger})\,. \\
{}^{I}\hat{\mathcal{A}}^{3\dagger}_{2}(\equiv \overset{03}{[-i]}\overset{12}{[+]}\overset{56}{[+]}) &= \hat{b}^{1\dagger}_{1}(\equiv \overset{03}{(+i)}\overset{12}{[+]}\overset{56}{[+]}) \ *_A \ (\hat{b}^{1\dagger}_{1})^{\dagger}(\equiv ((\overset{03}{(+i)}\overset{12}{[+]}\overset{56}{[+]})^{\dagger})\,.
\end{aligned}
$$

We demonstrated on one example, that knowing the odd "basis vectors" we can reproduce all the even "basis vectors", ${}^{I}\hat{\mathcal{A}}^{m\dagger}_{f}$. In Ref. [22] the relations among even "basis vectors", and the odd "basis vectors" are presented in Tables (2,3,4,5). Tables (2,3) relate ${}^{I}\hat{\mathcal{A}}^{m\dagger}_{f}$ and odd "basis vectors", while Tables (4,5) relate ${}^{II}\hat{\mathcal{A}}^{m\dagger}_{f}$ and odd "basis vectors".

We can repeat all the relations obtained for ${}^{I}\hat{\mathcal{A}}^{m\dagger}_{f}$ in this subsection also for ${}^{II}\hat{\mathcal{A}}^{m\dagger}_{f}$. Kipping in mind Eq. (15.13), we easily see the essential difference between ${}^{I}\hat{\mathcal{A}}^{m\dagger}_{f}$ and ${}^{II}\hat{\mathcal{A}}^{m\dagger}_{f}$. While ${}^{I}\hat{\mathcal{A}}^{m\dagger}_{f}$ transform family members of odd "basis vectors" among themselves, keeping family quantum number unchanged, transform ${}^{II}\hat{\mathcal{A}}^{m\dagger}_{f}$ a particular family member to the same family member of all the families, changing the family quantum numbers.

We can correspondingly not speak about "photons" but of a kind of Higgs if having $\alpha = (5,6)$.

Let us point out that the even "basis vectors", determining the creation and annihilation operators in a tensor product with the basis in ordinary space-time, determine spins and charges of boson fields. Having non zero momentum only in $d = (3+1)$, they carry space index $a = n = (0,1,2,3)$. They behave in the case that internal space has $(5+1)$ dimensions as a "photon", as we just discussed. Our "photon" can exchange the momentum in ordinary space-time with "electron" or "positron", but can not influence any internal property, like there are the spins, S^{03} and S^{12}, or the charge S^{56}.

Let us see what represents the even "basis vectors", ${}^{I}\hat{\mathcal{A}}^{1\dagger}_{4}$, with two nilpotents in the $SO(1,3)$ subgroup of the group $SO(5,1)$. The two spins, S^{03} and S^{12}, enables the creation operators, which are the tensor product of the basis in ordinary space-time and the even "basis vectors" with two nilpotents, Eq. (15.16), to form "gravitons".

$$
\begin{aligned}
{}^{I}\hat{\mathcal{A}}^{1\dagger}_{4n}(\vec{p}) &= {}^{I}\mathcal{C}^{1}{}_{4n}(\vec{p}) \ast_{T} {}^{I}\hat{\mathcal{A}}^{1\dagger}_{4}(\equiv \hat{b}^{1\dagger}_{1} \ast_{A} (\hat{b}^{1\dagger}_{1})^{\dagger}) \,, \\
{}^{I}\hat{\mathcal{A}}^{2\dagger}_{3n}(\vec{p}) &= {}^{I}\mathcal{C}^{2}{}_{3n}(\vec{p}) \ast_{T} {}^{I}\hat{\mathcal{A}}^{2\dagger}_{3}(\equiv \overset{03}{(-i)}\overset{12}{(-)}\overset{56}{[+]} = (\hat{b}^{2\dagger}_{1} \ast_{A} (\hat{b}^{1\dagger}_{1})^{\dagger}) \,.
\end{aligned}
$$

When a boson ${}^{I}\hat{\mathcal{A}}^{1\dagger}_{4n}(\vec{p})$ scatters on a "electron" with the spin down, $\hat{b}^{2\dagger}_{1}(\vec{p})(\equiv \hat{b}^{\dagger}_{\vec{p}} \ast_{T} \hat{b}^{2\dagger}_{1}$, Eq. (15.15), changes its spin from $\downarrow$ to $\uparrow$, and transfers the momentum to the "electron". This boson ${}^{I}\hat{\mathcal{A}}^{1\dagger}_{4n}(\vec{p})$, transferring the integer spin to the "electron" in addition to momentum of the space-time, is obviously "graviton" with $\mathcal{S}^{03} = i$ and $\mathcal{S}^{12} = 1$, changing the quantum numbers $S^{03} = -\frac{i}{2}$ and $S^{12} = -\frac{1}{2}$ of $\hat{b}^{2\dagger}_{1}(\vec{p})$ to $S^{03} = \frac{i}{2}$ and $S^{12} = \frac{1}{2}$ of $\hat{b}^{1\dagger}_{1}(\vec{p})$.

Let us check for two cases, how do the "basis vectors" of "gravitons" behave when "gravitons" scatter.

$$
\begin{aligned}
&{}^{I}\hat{\mathcal{A}}^{2\dagger}_{3gr}(\equiv \overset{03}{(-i)}\overset{12}{(-)}\overset{56}{[+]}) \ast_{A} {}^{I}\hat{\mathcal{A}}^{1\dagger}_{4gr}(\equiv \overset{03}{(+i)}\overset{12}{(+)}\overset{56}{[+]}) \rightarrow {}^{I}\hat{\mathcal{A}}^{2\dagger}_{4ph}(\equiv \overset{03}{[-i]}\overset{12}{[-]}\overset{56}{[+]}) \,, \\
&{}^{I}\hat{\mathcal{A}}^{1\dagger}_{4gr}(\equiv \overset{03}{(+i)}\overset{12}{(+)}\overset{56}{[+]}) \ast_{A} {}^{I}\hat{\mathcal{A}}^{2\dagger}_{3gr}(\equiv \overset{03}{(-i)}\overset{12}{(-)}\overset{56}{[+]}) \rightarrow {}^{I}\hat{\mathcal{A}}^{1\dagger}_{3ph}(\equiv \overset{03}{[+i]}\overset{12}{[+]}\overset{56}{[+]}) \,. \qquad (16.31)
\end{aligned}
$$

There are also even "basis vectors" of the kind ${}^{I}\hat{\mathcal{A}}^{m\dagger}_{f}$ which change spin and charges, changing for example "electrons" into "positrons" [9].

Not to be observed at observable energies, the breaking of symmetries must make such bosons very heavy. Looking at the even "basis vector" in this toy model, there are one fourth of ${}^{I}\hat{\mathcal{A}}^{m\dagger}_{f}$, which are "photons" (two of them, ${}^{I}\hat{\mathcal{A}}^{1\dagger}_{3}$ and ${}^{I}\hat{\mathcal{A}}^{2\dagger}_{4}$, not able to change the quantum numbers of the "electrons", Table 14.1) or "gravitons" (${}^{I}\hat{\mathcal{A}}^{2\dagger}_{3}$ and ${}^{I}\hat{\mathcal{A}}^{1\dagger}_{4}$, which change the spin of "electrons").

There are four of ${}^{I}\hat{\mathcal{A}}^{m\dagger}_{f}$, which are "photons" (two of them, ${}^{I}\hat{\mathcal{A}}^{3\dagger}_{2}$ and ${}^{I}\hat{\mathcal{A}}^{4\dagger}_{1}$, not able to change the quantum numbers of the "positron", Table 14.1) or "gravitons" (${}^{I}\hat{\mathcal{A}}^{3\dagger}_{1}$ and ${}^{I}\hat{\mathcal{A}}^{4\dagger}_{2}$, which change the spin of "positrons", Table 14.1).

The rest eight ${}^{I}\hat{\mathcal{A}}^{m\dagger}_{f}$ relate "electrons" and "positrons".

As we already said, repeating the relations for ${}^{I}\hat{\mathcal{A}}^{m\dagger}_{f}$, Eq. (14.30, 14.31), also for ${}^{II}\hat{\mathcal{A}}^{m\dagger}_{f}$, we shall not get "photons" or "gravitons", which both transform family members of odd "basis

[9] The corresponding bosons transform "electrons" into "positrons", ${}^{I}\hat{\mathcal{A}}^{2\dagger}_{1}(\equiv \overset{03}{(-i)}\overset{12}{[-]}\overset{56}{(+)}) \ast_{A} \hat{b}^{4\dagger}_{1}(\equiv \overset{03}{(+i)}\overset{12}{(-)}\overset{56}{(-)}) \rightarrow \hat{b}^{2\dagger}_{1}(\equiv \overset{03}{[-i]}\overset{12}{(-)}\overset{56}{[+]})$.

vectors" among themselves, keeping the family quantum number unchanged. Carrying the space index equal to $(5,6)$, the scalar bosons ${}^{II}\hat{\mathcal{A}}^{m\dagger}_{f}$ ("photons" and "gravitons") cause, as a kind of "Higgs", the masses of fermion fields.

b. *The case, which offers the "basis vectors" for all the so far observed fermion and boson fields, requires for internal space* $d=(13+1)$*, and for the space-time, in which fermions and bosons have non zero momenta,* $d=(3+1)$, at least at observable energies.
In Table 14.2, App. 14.8, the $2^{\frac{14}{2}-1}$ odd "basis vectors" present one irreducible representation, one family, of quarks and leptons and antiquarks and antileptons, analysed with respect to the subgroups $SO(3,1), SU(2)_{I}, SU(2)_{II}, SU(3), U(1)$ of the group $SO(13,1)$. One can notice that the content of the subgroup $SO(7,1)$ (including subgroups $SO(3,1), SU(2)_{I}, SU(2)_{II}$) are identical for quarks and leptons, as well as for antiquarks and antileptons; due to two $SU(2)$ subgroups $SU(2)_{I}, SU(2)_{II}$, first representing the weak charge, postulated by the *standard model*, the second $SU(2)_{II}$ group members are not observed at low energies. Quarks and leptons, and antiquarks and antileptons distinguish only in the $SU(3)\times U(1)$ part of the group $SO(13,1)$.
From the first member, the odd "basis vector" u^{c1}_{R} in Table 14.2, follow the rest odd "basis vectors" by the application of the infinitesimal generators of the Lorentz group S^{ab} (as well as by the application of ${}^{I}\hat{\mathcal{A}}^{m\dagger}_{f}$). All the first members of the other families follow from the one presented in Table 14.2 by applying on u^{c1}_{R} by $\tilde{S}^{ab}$ (as well as by the application of ${}^{II}\hat{\mathcal{A}}^{m\dagger}_{f}$).

The corresponding creation and annihilation operators are tensor products of a "basis vector" and the basis in ordinary space-time, for example, $u^{c1}_{R}(\vec{p}) = u^{c1}_{R} \ast_{T} \hat{b}_{\vec{p}}$.

The even "basis vectors" can be obtained, according to Eqs. (15.12, 15.13), as the algebraic products of the odd "basis vectors" and their Hermitian conjugate partners. In a tensor product with the basis in ordinary space-time, and with the space index $a=n(=0,1,2,3)$ added, ${}^{I}\hat{\mathcal{A}}^{m\dagger}_{fa}(\vec{p}) = {}^{I}\mathcal{C}^{m}{}_{fa}(\vec{p}) \ast_{T} {}^{I}\hat{\mathcal{A}}^{m\dagger}_{f}$.
${}^{I}\hat{\mathcal{A}}^{m\dagger}_{f\alpha}(\vec{p})$ manifest the properties of the tensors $(a=n)$, vectors $(a=n)$ and scalar $(a=s\geq 5)$ gauge fields, observed so far.
In a tensor product with the basis in ordinary space-time, and with the space index $a=s\geq 5$ added, ${}^{I}\hat{\mathcal{A}}^{m\dagger}_{f\alpha}(\vec{p})$ manifest the properties of the scalar fields, like the Higgs and other scalar fields, bringing masses to quarks and leptons and antiquarks and antileptons and to weak bosons, for example.
Let us look in Table 14.2 for $e^{-\dagger}_{L}$, 29^{th} line. The photon ${}^{I}\hat{\mathcal{A}}^{\dagger}_{ph\, e^{-\dagger}_{L}\rightarrow e^{-\dagger}_{L}}$ interacts with $e^{-\dagger}_{L}$ as follows

$$
{}^{I}\hat{\mathcal{A}}^{\dagger}_{ph\, e^{-\dagger}_{L}\rightarrow e^{-\dagger}_{L}}(\equiv\overset{03\ \ 12\ \ 56\ \ 78\ 9\,10\,11\,12\,13\,14}{[-i][+][-][+][+]\ [+]\ \ [+]\ }) \ast_{A} e^{-\dagger}_{L}, (\equiv\overset{03\ \ 12\ \ 56\ \ 78\ \ 9\,10\,11\,12\,13\,14}{[-i][+](-)(+)(+)\,(+)\,(+)}) \rightarrow
$$

$$
e^{-\dagger}_{L}(\equiv\overset{03\ \ 12\ \ 56\ \ 78\ 9\,10\,11\,12\,13\,14}{[-i][+](-)(+)(+)\,(+)\,(+)f}), \qquad {}^{I}\hat{\mathcal{A}}^{\dagger}_{ph\, e^{-\dagger}_{L}\rightarrow e^{-\dagger}_{L}} = e^{-\dagger}_{L}, \ast_{A}(e^{-\dagger}_{L})^{\dagger}, \tag{16.32}
$$

Let us look for the weak boson, transforming $e^{-\dagger}_{L}$ from the 29^{th} line into $\nu^{\dagger}_{L}$ from the 31^{st} line.

It follows

$$ {}^{\mathrm{I}}\hat{\mathcal{A}}^{\dagger}_{w1\, e_{\mathrm{L}}\to\nu_{\mathrm{L}}}(\equiv[-\mathrm{i}]^{03}[+]^{12}(+)^{56}(-)^{78}[+]^{9\,10\,11\,12\,13\,14}[+]\ [+]\ ) \ast_{\mathrm{A}}\ e_{\mathrm{L}}^{-\dagger}(\equiv[-\mathrm{i}]^{03}[+]^{12}(-)^{56}(+)^{78}(+)^{9\,10\,11\,12\,13\,14}(+)\ (+)\ ) \to $$
$$ \nu_{\mathrm{L}}^{\dagger}, (\equiv[-\mathrm{i}]^{03}[+]^{12}[+]^{56}[-]^{78}(+)^{9\,10\,11\,12\,13\,14}(+)\ (+)\ ), \qquad {}^{\mathrm{I}}\hat{\mathcal{A}}^{\dagger}_{w1\, e_{\mathrm{L}}\to\nu_{\mathrm{L}}} = \nu_{\mathrm{L}}^{\dagger} \ast_{\mathrm{A}}\ (e_{\mathrm{L}}^{-\dagger})^{\dagger}\,. \tag{16.33} $$

Knowing the "basis vectors" of the fermions, we can find all the internal spaces, the "basis vectors", of bosons fields. Not all of the products of nilpotents and projectors, chosen to be the eigenvectors of all the Cartan subalgebra members, Eq. (15.3), are needed at observable fields, as we learned from the toy model with the dimension of the internal space $(5+1)$. The breaks of symmetries also make that the observed fermions and antifermions properties do not manifest as belonging to the one family.

However, studying all the boson fields might help to recognise why and how the properties of fermions and bosons change with breaking symmetries, if this theory describing the internal spaces of fermion and boson fields with odd and even "basis vectors" is what our universe obeys. Demonstrating so many simple and elegant descriptions of the second quantized fields, explaining the assumptions of other theories, makes us hop that the theory might be what the universe obeys.

Since the graviton in this theory is understood in an equivalent way as all the gauge fields observed so far, let us at the end of this section, try to analyse the "basis vectors" of the gravitons if the internal space has $\mathrm{d} = (13+1)$.
We must take into account that the "gravitons" do have the spin and handedness (non-zero $\mathcal{S}^{03}$ and $\mathcal{S}^{12}$, which means that this part must be presented by two nilpotents, $(\pm\mathrm{i})^{03}(\pm)^{12}$) in $\mathrm{d} = (3+1)$, and do not have weak, colour and $\mathrm{U}(1)$ charges (all the rest must be projectors), and have, as all the vector gauge fields, the space index n.
We can then easily find the "basis vector" of the graviton, ${}^{\mathrm{I}}\hat{\mathcal{A}}^{\dagger}_{\mathrm{gr}\, u_{\mathrm{R}}^{c1\dagger}\to u_{\mathrm{R}}^{c1\dagger}}$, which applying on $u_{\mathrm{R}}^{c1\dagger}$ with spin up, appearing in the first line of the table 14.2, transforms it into $u_{\mathrm{R}}^{c1\dagger}$ with spin down, appearing in the second line of the table 14.2.

$$ {}^{\mathrm{I}}\hat{\mathcal{A}}^{\dagger}_{\mathrm{gr}\, u^{c1\dagger}_{\mathrm{R}\uparrow}\to u^{c1\dagger}_{\mathrm{R}\downarrow}}(\equiv(-\mathrm{i})^{03}(-)^{12}[+]^{56}[+]^{78}[+]^{9\,10\,11\,12\,13\,14}[-]\ [-]\ ) \ast_{\mathrm{A}}\ u^{c1\dagger}_{\mathrm{R}\uparrow}(\equiv(+\mathrm{i})^{03}[+]^{12}[+]^{56}(+)^{78}(+)^{9\,10\,11\,12\,13\,14}[-]\ [-]\ ) \to $$
$$ u^{c1\dagger}_{\mathrm{R}\downarrow}, (\equiv[-\mathrm{i}]^{03}(-)^{12}[+]^{56}(+)^{78}(+)^{9\,10\,11\,12\,13\,14}[-]\ [-]\ ), \qquad {}^{\mathrm{I}}\hat{\mathcal{A}}^{\dagger}_{\mathrm{gr}\, u^{c1\dagger}_{\mathrm{R}\uparrow}\to u^{c1\dagger}_{\mathrm{R}\downarrow}} = u^{c1\dagger}_{\mathrm{R}\downarrow} \ast_{\mathrm{A}}\ (u^{c1\dagger}_{\mathrm{R}\uparrow})^{\dagger}\,. \tag{16.34} $$

Let us look at the "scattering" (algebraic application, $\ast_{\mathrm{A}}$) of the graviton with the "basis vector" ${}^{\mathrm{I}}\hat{\mathcal{A}}^{\dagger}_{\mathrm{gr}\, u^{c1\dagger}_{\mathrm{R}\uparrow}\to u^{c1\dagger}_{\mathrm{R}\downarrow}}$ with the graviton with the "basis vector"

$$ {}^{\mathrm{I}}\hat{\mathcal{A}}^{\dagger}_{\mathrm{gr}\, u^{c1\dagger}_{\mathrm{R}\downarrow}\to u^{c1\dagger}_{\mathrm{R}\uparrow}}(\equiv(+\mathrm{i})^{03}(+)^{12}[+]^{56}[+]^{78}[+]^{9\,10\,11\,12\,13\,14}[-]\ [-]\ ) $$

,

$$ {}^{\mathrm{I}}\hat{\mathcal{A}}^{\dagger}_{\mathrm{gr}\, u^{c1\dagger}_{\mathrm{R}\uparrow}\to u^{c1\dagger}_{\mathrm{R}\downarrow}}(\equiv(-\mathrm{i})^{03}(-)^{12}[+]^{56}[+]^{78}[+]^{9\,10\,11\,12\,13\,14}[-]\ [-]\ ) \ast_{\mathrm{A}}\ {}^{\mathrm{I}}\hat{\mathcal{A}}^{\dagger}_{\mathrm{gr}\, u^{c1\dagger}_{\mathrm{R}\downarrow}\to u^{c1\dagger}_{\mathrm{R}\uparrow}}(\equiv(+\mathrm{i})^{03}(+)^{12}[+]^{56}[+]^{78}[+]^{9\,10\,11\,12\,13\,14}[-]\ [-]\ ) \to $$

$$(\overset{03\ \ 12\ 56\ 78\ 9\,10\,11\,12\,13\,14}{\equiv[-i][-][+][+][+]\ [-]\ \ [-]}) = u^{c1\dagger}_{R\downarrow}\ *_A\ (u^{c1\dagger}_{R\downarrow})^\dagger = {}^{I}\hat{\mathcal{A}}^\dagger_{ph\,u^{c1\dagger}_{R\downarrow}\to u^{c1\dagger}_{R\downarrow}}\,,$$

to recognize how easily one finds the internal space of bosons.

The creation operators for gravitons must carry the space index n, like: ${}^{I}\hat{\mathcal{A}}^\dagger_{gr\,u^{c1\dagger}_{R\uparrow}\to u^{c1\dagger}_{R\downarrow}n}(\vec{p})$.

16.4 Action for fermion and boson fields

In this section, a simple action for massless fermion and boson (tensors, vectors, scalars) fields are presented for a flat space, taking into account that the internal spaces of fermions and bosons are determined in $d = (13+1)$ by the odd "basis vectors" (for fermions) and by the even "basis vectors" for bosons, taking into account the relations among "basis vectors" of fermions and bosons as presented in Eqs. (15.5 - 15.9) and Eqs. (15.10 - 15.13).
We present the fermion and boson fields as tensor products of the "basis vectors" and basis in ordinary space-time as in Eqs. (15.15, 15.16). Boson fields carry in addition the space index a, which is for tensor and vector gauge fields equal to $n = (0,1,2,3)$ and for scalars $s \geq 5$.
There are several articles ([9] and the references therein), in which the vector boson fields, operating on fermion and boson fields, are described by $\omega^{ab}{}_n\, S^{ab}$; in this paper the vector boson fields are described by ${}^{I}\hat{\mathcal{A}}^{m\dagger}_{f\,n} = {}^{I}\hat{\mathcal{A}}^{m\dagger}_{f}\ {}^{I}\mathcal{C}^{m}{}_{f\,n}(x)$; and $\tilde{\omega}^{ab}_n\, \tilde{S}^{ab}$; in this paper the scalar boson fields are described by ${}^{II}\hat{\mathcal{A}}^{m\dagger}_{f\,n} =. {}^{II}\hat{\mathcal{A}}^{m\dagger}_{f}\ {}^{II}\mathcal{C}^{m}{}_{f\,n}$; $(a, b...,$ and (m, f) denote the internal spaces of fermion and boson fields, (n, s) denote space-time index.

Let us present the action, in which the internal spaces of the fermion and boson fields are described by odd and even "basis vectors", respectively. Let it be repeated that the even "basis vectors" for bosons can be represented by the algebraic products of the odd "basis vectors" and their Hermitian conjugate partners, as presented in Eqs. (15.12,15.13). The fermion fields, ψ represents several fermion fields, each of which is the tensor product of the odd "basis vector" and basis in ordinary space-time, Eq. (15.15). The boson fields, ${}^{i}\hat{\mathcal{A}}^{m\dagger}_{f\,a}(x) = {}^{I}\hat{\mathcal{A}}^{m\dagger}_{f}\ {}^{i}\mathcal{C}^{m}{}_{f\,a}(x), i = (I, II)$ are the tensor products of the even "basis vectors", ${}^{i}\hat{\mathcal{A}}^{m\dagger}_{f}$ and basis in ordinary space-time, with ${}^{i}\mathcal{C}^{m}{}_{f\,a}(x)$, carrying the space index a, Eq. (15.16).

$$\begin{aligned}
\mathcal{A} &= \int d^4x\, \frac{1}{2}\,(\bar{\psi}\,\gamma^a p_{0a}\psi) + h.c. + \\
&\quad \int d^4x \sum_{i=(I,II)} {}^{i}\hat{F}^{m\,f}_{ab}\ {}^{i}\hat{F}^{mfab}\,, \\
p_{0a} &= p_a - \sum_{mf} {}^{I}\hat{\mathcal{A}}^{m\dagger}_{fa}(x) - \sum_{mf} {}^{II}\hat{\mathcal{A}}^{m\dagger}_{fa}(x)\,, \\
{}^{i}\hat{F}^{m\,f}_{ab} &= \partial_a\, {}^{i}\hat{\mathcal{A}}^{m\dagger}_{fb}(x) - \partial_b\, {}^{i}\hat{\mathcal{A}}^{m\dagger}_{fa}(x) + \varepsilon f^{mfm''f''m'f'}\, {}^{i}\hat{\mathcal{A}}^{m''\dagger}_{f''a}(x)\, {}^{i}\hat{\mathcal{A}}^{m'\dagger}_{f'b}(x)\,, \\
&\quad i = (I, II)\,. \qquad (16.35)
\end{aligned}$$

Vector boson fields, ${}^{i}\hat{\mathcal{A}}^{m\dagger}_{fa}$ and ${}^{i}\hat{F}^{mf}_{ab}$, must have index (a,b) equal to $(n,p) = (0,1,2,3)$; ${}^{i}\hat{\mathcal{A}}^{m\dagger}_{fn}$ and ${}^{i}\hat{F}^{mf}_{np}$, $i = (I, II)$.

For scalar boson fields, ${}^{i}\hat{\mathcal{A}}^{m\dagger}_{fa}$ and ${}^{i}\hat{F}^{mf}_{ab}$, must have index $a = s \geq 5$, and ${}^{i}\hat{F}^{mf}_{ab}$, must have index a or $b = s$, $s \geq 5$ and the rest $n = (0,1,2,3)$.

$$
\begin{aligned}
{}^{i}\hat{F}^{mf}_{ns} &= \partial_n \, {}^{i}\hat{\mathcal{A}}^{m\dagger}_{fs}(x) - \partial_s \, {}^{i}\hat{\mathcal{A}}^{m\dagger}_{fn} + \varepsilon f^{mfm''f''m'f'} \, {}^{i}\hat{\mathcal{A}}^{m''\dagger}_{f''n}(x) \, {}^{i}\hat{\mathcal{A}}^{m'\dagger}_{f's}(x)\,, \\
& \qquad i = (I, II)\,. \qquad (16.36)
\end{aligned}
$$

Since ${}^{ii}\hat{\mathcal{A}}^{m''\dagger}_{f''n}(x)$ does not dependent on the space index s, the term with the derivative ∂_s is zero, $\partial_s \, {}^{ii}\hat{\mathcal{A}}^{m\dagger}_{fn}(x) = 0$.
The part of the action corresponding to the scalar fields is equal to

$$
\int d^4x \sum_{i=(I,II)} {}^{i}\hat{F}^{mf}_{ns} \; {}^{i}\hat{F}^{mfns}\,. \qquad (16.37)
$$

Moreover, needs further study.

16.4.1 Lorentz invariance

Let us look for the general Lorentz transformations $\Lambda = e^{i\omega_{ab}M^{ab}}$, where ω_{ab} do not depend on the space-time coordinates, $\omega_{ab} \neq \omega_{ab}(x)$, of a fermion field $\psi(x) = \Lambda\psi'(x')$ while checking the properties of the expectation values of the operators $\mathcal{O}$, where $\mathcal{O} = I$ (the identity) or $\mathcal{O} = \gamma^0\gamma^a p_a$, in the context

$$
\begin{aligned}
(\Lambda\psi(x))^\dagger \, \mathcal{O} \, \Lambda\psi(x) &= \psi(x)^\dagger \, \mathcal{O} \, \psi(x)\,, \\
\Lambda &= e^{i\omega_{ij}M^{ij} + i\omega_{0i}M^{0i}}\,. \qquad (16.38)
\end{aligned}
$$

It is not difficult to see the validity of Eq. (14.38) in the lowest order, $(\Lambda\psi'(x'))^\dagger = ((1 + i\omega_{ij}S^{ij} + i\omega_{0i}S^{0i})\psi'(x'))^\dagger$, provided that $\omega^*_{ij} = \omega_{ij}$, while $\omega^*_{0i} = -\omega_{0i}$, $(i,j) = (1,2,..,d)$, for either $\mathcal{O} = I$ or for $\mathcal{O} = \gamma^0\gamma^a p_a$.
The case $\mathcal{O} = \gamma^0\gamma^a p_a$ concerns the Dirac (Weyl indeed) Lagrange density for the kinetic term for massless fermion fields.
Looking at transformations in the first order in the way

$$
\begin{aligned}
&\frac{1}{2}\{(\gamma^0\gamma^a p_a \, (1 + i\omega_{ij}S^{ij} + i\omega_{0i}S^{0i})\psi')^\dagger)(1 + i\omega_{ij}S^{ij} + i\omega_{0i}S^{0i})\psi' + \\
&\quad \varepsilon((1 + i\omega_{ij}S^{ij} + i\omega_{0i}S^{0i})\psi')^\dagger \gamma^0\gamma^a p_a \, (1 + i\omega_{ij}S^{ij} + i\omega_{0i}S^{0i})\psi'\}, \\
&\qquad = \frac{1}{2}\{(p_a\psi')^\dagger\gamma^0\gamma^a\psi' + (\psi')^\dagger\gamma^0\gamma^a p_a\psi'\}, \qquad (16.39)
\end{aligned}
$$

after taking into account that $\omega^*_{ij} = \omega_{ij}$, while $\omega^*_{0i} = -\omega_{0i}$, and that $(S^{ij})^\dagger = S^{ij}$, $(S^{0i})^\dagger = -S^{0i}$.
We know the relations among fermion and boson fields, Eqs. (15.10, 15.11, 15.12, 15.13), correspondingly we know the covariant derivative applying to the fermion fields.

We can learn from Eqs. (15.12,15.13) how do even"basis vectors", ${}^{i}\hat{\mathcal{A}}^{m\dagger}_{fa}$, behave if we transform $\psi(x) \rightarrow \Lambda\psi'(x')$. Following relations in Eq. (14.39), we find

$$ {}^{I}\hat{\mathcal{A}}^{m\dagger}_{f} \rightarrow \Lambda \hat{b}^{m\dagger}_{f'} \ *_{A} \ (\Lambda \hat{b}^{m'\dagger}_{f'})^{\dagger} = {}^{I}\hat{\mathcal{A}}^{m\dagger}_{f} \,. \tag{16.40} $$

Repeating the equivalent procedure for ${}^{II}\hat{\mathcal{A}}^{m\dagger}_{f}$, ${}^{II}\hat{\mathcal{A}}^{m\dagger}_{f} \rightarrow (\Lambda \hat{b}^{m\dagger}_{f'})^{\dagger} \ *_{A} \ \Lambda \hat{b}^{m'\dagger}_{f'} = {}^{II}\hat{\mathcal{A}}^{m\dagger}_{f}$, we learn about the covariant derivative

$$ p_{0a} = p_a - \sum_{m,f} {}^{I}\hat{\mathcal{A}}^{m\dagger}_{fa}(x) - \sum_{m,f} {}^{II}\hat{\mathcal{A}}^{m\dagger}_{fa}(x) \,, $$

if we take into account Eq. (15.16), ${}^{i}\hat{\mathcal{A}}^{m\dagger}_{fa}(x) = {}^{i}\hat{\mathcal{A}}^{m\dagger}_{f} \, {}^{i}\mathcal{C}^{m\dagger}_{fa}(x)$.

It remains to see what happens with the covariant derivative on $\Lambda\psi'$ for $\Lambda = \Lambda(x)$. We must repeat Eq. (14.39) for $\Lambda(x)$, where we must take into account only $p_a\Lambda x$, which is really $p_n\Lambda(x)$, $x^n = (x^0, x^1, x^2, x^3)$.

$$ \begin{aligned} &(\gamma^0\gamma^a p_{0a}\Lambda(x)\psi')^{\dagger}(\Lambda(x)\psi') + \varepsilon(\Lambda(x)\psi')^{\dagger}\gamma^0\gamma^a p_{0a}\Lambda(x)\psi' \,, \\ &p_{0a} = p_a - \sum_{mf} {}^{I}\hat{\mathcal{A}}^{m\dagger}_{fa} - \sum_{mf} {}^{II}\hat{\mathcal{A}}^{m\dagger}_{fa} \,. \end{aligned} \tag{16.41} $$

Eq. (14.41) offers besides the kinetic term for massless fermions, also the interaction with the massless boson fields of two kinds, $\sum_{mf} {}^{I}\hat{\mathcal{A}}^{m\dagger}_{fa}$ and $\sum_{mf} {}^{II}\hat{\mathcal{A}}^{m\dagger}_{fa}$, leading to

$$ \begin{aligned} &\frac{1}{2}\{ [(p_a\psi')^{\dagger}\gamma^0\gamma^a\psi' + \psi'^{\dagger}\gamma^0\gamma^a p_a\psi'] + \\ &\psi'^{\dagger}[(p_a\Lambda)^{\dagger} - \sum_{mf}({}^{I}\hat{\mathcal{A}}^{m\dagger}_{fa})^{\dagger}\Lambda^{\dagger} - \sum_{mf}({}^{II}\hat{\mathcal{A}}^{m\dagger}_{fa})^{\dagger}\Lambda^{\dagger}]\gamma^0\gamma^a\Lambda\psi' + \\ &\psi'^{\dagger}\Lambda^{\dagger}\gamma^0\gamma^a[(p_a\Lambda) - \sum_{mf} {}^{I}\hat{\mathcal{A}}^{m\dagger}_{fa}\Lambda - \sum_{mf} {}^{II}\hat{\mathcal{A}}^{m\dagger}_{fa}\Lambda]\psi'\}. \end{aligned} \tag{16.42} $$

16.5 Conclusion

The proposed theory, built on the assumption that the internal spaces of fermion and boson fields are described by odd (for fermions) and even (for bosons) products of operators γ^a, offers the unique description of spins and charges of fermion and boson second quantised field, as well as the unique description of the action for all fermion and boson fields. Both fields, fermions and bosons, are assumed to be massless and appear in a flat space-time. The breaking of symmetries is not yet discussed in this contribution [10].

We arrange in any $d = 2(2n+1)$ dimensional internal space, the fermion and boson states to be eigenvectors of all the members of the Cartan subalgebra, Eq. (15.3), we call these eigenstates the "basis vectors". The "basis vectors" for fermion fields

[10] We expect that the break of symmetries follow to some extent the breaking of symmetries, as already discussed in Ref. [9], but we hope that we can learn more from this new way of describing internal spaces of fermions and bosons.

have an odd number of nilpotents, and for the boson fields, an even number of nilpotents, the rest are projectors, Eq.(15.4).
The fermion "basis vectors" appear in $2^{\frac{d}{2}-1}$ families, each family having $2^{\frac{d}{2}-1}$ members; and there are $2^{\frac{d}{2}-1}2^{\frac{d}{2}-1}$ of their Hermitian conjugate partners, appearing in a separate group.
The boson "basis vectors" appear in two orthogonal groups, each with $2^{\frac{d}{2}-1}2^{\frac{d}{2}-1}$ members and have their Hermitian conjugate partners within the same group.
The "basis vectors" for bosons are expressible as the algebraic products of fermion "basis vectors" and their Hermitian conjugate partners, Eqs. (15.12, 15.13).
The second quantised fermion fields are tensor products of the "basis vectors" and basis in ordinary space time, Eq. (15.15).
The second quantised boson fields are tensor products of the "basis vectors" and basis in ordinary space time, and carry the space-time index, Eq. (15.16).
Both fields obey the postulates of Dirac of the second quantised fields, determined with the properties of the "basis vectors".
In the case that internal space has $d = (13+1)$, while the fermion and boson fields have non zero momenta only in $d = (3+1)$ of ordinary space-time, the fermion and boson (tensor, vector, scalar) fields (with the space index (0,1,2,3) for tensors and vectors, and ≥ 5 for scalars) manifest at observable energies, the quarks and leptons and antiquarks and antileptons, Table 14.2, with spins and charges in fundamental representations, appearing in families; and gravitons, weak bosons of two kinds, gluons and photons, as well as the scalar fields, have spins and charges determined by "basis vectors" in adjoint representations.

We have treated so far massless fermion and boson fields, assumed to be valid before any break of symmetry. Looking in Table 14.2, we see that quarks differ from leptons and antiquarks from antileptons only in the $SU(3) \times U(1)$ part of $SO(13,1)$ (what means that right-handed neutrinos and left-handed antineutrinos are included, and are predicted to be observed). The breaking of symmetries is supposed to lead at the observable energies to the *standard model* prediction [11].
Taking into account the algebraic multiplication among fermion "basis vectors", Eq. (14.1) and among boson "basis vectors", Eqs. (15.8, 15.9), and among fermion and boson "basis vectors", Eqs. (15.10, 15.11, 15.12, 15.13), it is not difficult to choose the action which includes all fermion and boson fields equivalently, manifesting the Lorentz invariance, Eq. (15.17).

The covariant derivatives in the fermion part of the action, $\int d^4x \, \frac{1}{2}(\bar{\psi}\gamma^a p_{0a}\psi) + h.c.$, include interaction with the graviton (boson) field (for example, ${}^{I}\hat{\mathcal{A}}^{\dagger}_{gr\, u^{c\,1\,\dagger}_{R,1st} \to u^{c\,1\,\dagger}_{R,2nd}}$, with the "basis vector" $\overset{03}{(-i)}\overset{12}{(-)}\overset{56}{[+]}\overset{78}{[+]}\overset{9\,10}{[+]}\overset{11\,12}{[-]}\overset{13\,14}{[-]}$, which transforms the quark with spin $\uparrow$ to the quark with spin $\downarrow$), the two $SU(2)$ weak fields, the colour $SU(3)$ fields, and the photon $U(1)$ fields. Gravitons have two nilpotents in the part

[11] The breaks of symmetries were studied when the boson fields were described by $S^{ab}\omega_{ab\alpha}$ and $\tilde{S}^{ab}\tilde{\omega}_{ab\alpha}$, ([9], Subsect. 6.2 and references therein), instead of by ${}^{I}\hat{\mathcal{A}}^{m\dagger}_{f}$ and ${}^{II}\hat{\mathcal{A}}^{m\dagger}_{f}$.

$SO(3,1)$, weak bosons have two nilpotents in the part $SO(4)$, gluons have two nilpotents in the part $SO(6)$, while photons have only projectors, since they do not carry any charge.

There is no negative energy Dirac sea for fermions. Fermions have only ordinary quantum vacuum.
Without breaking symmetries, there would also exist boson fields carrying more than one charge at the same time, like the weak and colour charge, or the spin, weak charge and colour charge, which we have not yet observed.

Although we understand better and better what the theory offers, giving more and more hope that we can learn from this theory the history of the universe, the origin of the dark energy, the dynamics insight into the black holes, and many other answers, yet there remain a lot of open questions awaiting answers.

16.5.1 What should we understand

If this contribution offers an acceptable description of the internal degrees of freedom of fermion and boson fields - what would mean that nature does use the proposed "basis vectors" in the flat space-time, and when all the second quantised fields are massless, and correspondingly, nature uses also the simple action 15.17 - we should be able to reproduce the *standard model* action before the electroweak break (which assumes the action for the massive scalar fields, Higgs fields and Yukawa couplings, and a kind of coupling to the gravity).
The proposed theory can treat all the fermion fields (appearing in families) and boson fields (gravitons, photons, weak bosons and gluons) in an equivalent way. Knowing the "basis vectors" describing the internal space of fermions (and the Hermitian conjugate partners of the "basis vectors"), we know also the "basis vectors" of all boson fields.
There are $2^{\frac{d}{2}-1}$ families of fermion fields with $2^{\frac{d}{2}-1}$ members each. And there are $2^{\frac{d}{2}-1} \times 2^{\frac{d}{2}-1}$ their Hermitian conjugate partners.
The two orthogonal boson "basis vectors" have together twice $2^{\frac{d}{2}-1} \times 2^{\frac{d}{2}-1}$ members. (The "basis vectors" of the scalar Higgs fields have the properties of the second kind of these two kinds of "basis vectors " **[?]**.)
If we start with $d = (13+1)$ for the internal space and with $d = (3+1)$ for the space-time, there are many more families in this theory than the observed three. The theory predicts that the three observed families are the members of the group of four families **[?]**. The theory predicts the second group of four families, contributing to the dark matter [**?**, 14].
Moreover, there are also many more boson fields of the two kinds than the observed vector gauge fields and the scalar fields. (There are boson fields which carry several charges.)
To be able to explain why "nature has decided" to break symmetries, we should know the properties this theory has with respect to:
a. The renormalisability and anomalies in even and odd dimensional spaces.
b. How does the second kind of the boson "basis vectors" contribute to the

breaking of symmetries, while the first kind of the boson "basis vectors" seems to mainly determine the properties of all the observed boson fields, with the gravity included. (Although the boson "basis vectors" with the non-zero spins and charges, in tensor products with the basis in ordinary space-time and with scalar indices $\alpha \geq 5$, might contribute to the breaking of symmetries.)
c. The differences in odd, $d = (2n+1)$, and even, $d = (2(2n+1))$, dimensional spaces. While in even dimensional spaces, $d = 2(2n+1)$, the odd "basis vectors" anticommute and have their Hermitian conjugated "basis vectors" in a separate group, and the even "basis vectors" commute and appear in two orthogonal groups, have the "basis vectors" in $d = 2(2n+1)+1$ strange properties; half of the odd and even "basis vectors" behave like in $d = 2(2n+1)$, in the second half, the anticommutng odd "basis vectors" appear in two orthogonal groups, while the commuting even "basis vectors" appear in families and have the Hermitian conjugate partners in a separate group.
d. The differences in even dimensional internal spaces, when $d = 2(2n+1)$ and $d = 4n$. While in $d = 2(2n+1)$ the "basis vectors" for fermions and antifermions appear in the same family, in $d = 4n$ the "basis vectors" of a family do not include antifermions. Correspondingly, the vacuum in $d = 2(2n+1)$ is just the quantum vacuum, while in $d = 4n$ the Dirac sea with the negative energies must be invented.
e. How to present and interpret the Feynman diagrams in this theory in comparison with the Feynman diagrams so far presented and interpreted. (This will hopefully be done in collaboration in this proceedings.)
f. It might be useful to extend the second quantised fermion and boson fields to strings, with the first step already done in Ref. nh2023Bled.

16.6 Grassmann and Clifford algebras

This part is taken from Ref. [22–24], following Refs. [1,1,9,16].
The author started to describe internal spaces of anti-commuting or commuting second quantized fields by using the Grassmann algebra.
In Grassmann d-dimensional space there are d anti-commuting (operators) θ^a, and d anti-commuting operators which are derivatives with respect to θ^a, $\frac{\partial}{\partial\theta_a}$.

$$\{\theta^a, \theta^b\}_+ = 0\,, \qquad \{\frac{\partial}{\partial\theta_a}, \frac{\partial}{\partial\theta_b}\}_+ = 0\,,$$
$$\{\theta_a, \frac{\partial}{\partial\theta_b}\}_+ = \delta^b_a\,,\ (a,b) = (0,1,2,3,5,\cdots,d)\,. \tag{16.43}$$

The choice

$$(\theta^a)^\dagger = \eta^{aa}\frac{\partial}{\partial\theta_a}\,, \quad \text{leads to} \quad (\frac{\partial}{\partial\theta_a})^\dagger = \eta^{aa}\theta^a\,, \tag{16.44}$$

with $\eta^{ab} = diag\{1,-1,-1,\cdots,-1\}$.
θ^a and $\frac{\partial}{\partial\theta_a}$ are, up to the sign, Hermitian conjugate to each other. The identity is a self-adjoint member of the algebra.

In d-dimensional space, there are 2^d superposition of products of θ^a, the Hermitian conjugated partners of which are the corresponding superposition of products of $\frac{\partial}{\partial\theta_a}$ [9,29].
We can make from θ^a's and their conjugate momenta $p^{\theta a} = i\,\frac{\partial}{\partial\theta_a}$ two kinds of the operators, γ^a and $\tilde{\gamma}^a$ [1],

$$\begin{aligned}
&\gamma^a = (\theta^a + \frac{\partial}{\partial\theta_a})\,, \quad \tilde{\gamma}^a = i\,(\theta^a - \frac{\partial}{\partial\theta_a})\,,\\
&\theta^a = \frac{1}{2}\,(\gamma^a - i\tilde{\gamma}^a)\,, \quad \frac{\partial}{\partial\theta_a} = \frac{1}{2}\,(\gamma^a + i\tilde{\gamma}^a)\,,
\end{aligned} \tag{16.45}$$

each offers 2^d superposition of products of γ^a or $\tilde{\gamma}^a$ ([9] and references therein)

$$\begin{aligned}
&\{\gamma^a,\gamma^b\}_+ = 2\eta^{ab} = \{\tilde{\gamma}^a,\tilde{\gamma}^b\}_+\,,\\
&\{\gamma^a,\tilde{\gamma}^b\}_+ = 0\,, \quad (a,b) = (0,1,2,3,5,\cdots,d)\,,\\
&\quad (\gamma^a)^\dagger = \eta^{aa}\,\gamma^a\,, \quad (\tilde{\gamma}^a)^\dagger = \eta^{aa}\,\tilde{\gamma}^a\,.
\end{aligned} \tag{16.46}$$

The Grassmann algebra offers the description of the internal space of *anti-commuting integer spin second quantized fields* and of the *commuting integer spin second quantized fields* [9]. Both algebras, the superposition of odd products of γ^a's or of $\tilde{\gamma}^a$'s, offer the description of the second quantized half integer spins and charges in the fundamental representations of the group [9], Table 14.2 represents one family of quarks and leptons and antiquarks and antileptons.
The superposition of even products of either γ^a's or $\tilde{\gamma}^a$'s offer the description of the commuting second uantized boson fields with integer spins [20,21,24]), manifesting from the point of the subgroups of the $SO(d-1,1)$ group, spins and charges in the adjoint representations.

There is so far observed only one kind of the anti-commuting half-integer spin second quantized fields.

The *postulate*, which determines how does $\tilde{\gamma}^a$ operate on γ^a, reduces the presentations of the two Clifford subalgebras, γ^a and $\tilde{\gamma}^a$, to the one described by γ^a [1,5,16]

$$\{\tilde{\gamma}^a B = (-)^B\, i\, B\gamma^a\}|\psi_{oc}>\,, \tag{16.47}$$

with $(-)^B = -1$, if B is (a function of) odd products of γ^a's, otherwise $(-)^B = 1$ [5], the vacuum state $|\psi_{oc}>$ is defined in Eq. (15.6) of Subsect. 14.2.1.

After the postulate of Eq. (14.47) the vector space of γ^a's are chosen to describe the internal space of fermions, while $\tilde{\gamma}^a$'s are used to determine the family quantum numbers of the fermion fields.

16.7 Odd and even "basis vectors" in $(5+1)$-dimensional space

In this appendix, the even and odd "basis vectors" are presented for the choice $d = (5+1)$, needed in Sect. (14.3). The presentation follows the paper [20].

Table 14.1 presents $2^{d=6}$ "eigenvectors" of the Cartan subalgebra members, Eq. (15.3), of the odd and even "basis vectors" which are the superposition of odd ($\hat{b}^{m\dagger}_f$, 16), and their Hermitian conjugate partners $(\hat{b}^{m\dagger}_f)^\dagger$, 16), and of even (${}^I\mathcal{A}^m_f$, 16), and (${}^{II}\mathcal{A}^m_f$, 16), products of γ^a's, helpful in Sect. (14.3). Table 14.1 is presented in several papers ([9,20], and references therein).
Odd and even "basis vectors" are presented as products of nilpotents and projectors, Eqs. (15.4,14.1). The odd "basis vectors" are products of odd number of nilpotents, one or three, the rest are projectors, two or zero; the even "basis vectors" are products of even number of nilpotents, zero or two, the rest are projectors, three or one.

16.8 One family representation of odd "basis vectors" in $d = (13+1)$

This appendix, is following similar appendices in Refs. [9,20,21]
One irreducible representation, one family, of the odd "basis vectors" describing the internal spaces of fermions in $d = (13+1)$, analysed with respect to the subgroups $SO(3,1) \times SU(2) \times SU(2) \times SU(3) \times U(1)$, is presented. One family contains the "basis vectors" of quarks and leptons and antiquarks and antileptons with the quantum numbers assumed by the *standard model* before the electroweak break, with right handed neutrinos and left handed antineutrinos included, due to two $SU(2)$ subgroups, $SU(2)_I$ and $SU(2)_{II}$, with the hypercharge of the *standard model* $Y = \tau^{23} + \tau^4$, Eqs. (14.49 - 14.51).
The generators S^{ab} of the Lorentz transformations in the internal space of fermions with $d = (13+1)$, analysed with respect to the subgroups $SO(3,1) \times SU(2) \times SU(2) \times SU(3) \times U(1)$, are presented as

$$\vec{N}_\pm (= \vec{N}_{(L,R)}) := \frac{1}{2}(S^{23} \pm iS^{01}, S^{31} \pm iS^{02}, S^{12} \pm iS^{03}), \tag{16.48}$$

$$\vec{\tau}^1 := \frac{1}{2}(S^{58} - S^{67}, S^{57} + S^{68}, S^{56} - S^{78}),$$
$$\vec{\tau}^2 := \frac{1}{2}(S^{58} + S^{67}, S^{57} - S^{68}, S^{56} + S^{78}), \tag{16.49}$$

$$\begin{aligned}\vec{\tau}^3 :=& \frac{1}{2}\{S^{9\,12} - S^{10\,11}, S^{9\,11} + S^{10\,12}, S^{9\,10} - S^{11\,12}, S^{9\,14} - S^{10\,13},\\ & S^{9\,13} + S^{10\,14}, S^{11\,14} - S^{12\,13}, S^{11\,13} + S^{12\,14}, \frac{1}{\sqrt{3}}(S^{9\,10} + S^{11\,12} - 2S^{13\,14})\},\\ \tau^4 :=& -\frac{1}{3}(S^{9\,10} + S^{11\,12} + S^{13\,14}),\end{aligned} \tag{16.50}$$

$$Y := \tau^4 + \tau^{23}, \quad Q := \tau^{13} + Y, \tag{16.51}$$

The (chosen) Cartan subalgebra operators, determining the commuting operators in the above equations, is presented in Eq. (15.3).

Table 16.1: This table, taken from [20], represents for the internal space $d = (5+1)\ 2^d = 64$ "eigenvectors" of the Cartan subalgebra, Eq. (15.3), members of the odd and even "basis vectors" which are the superposition of odd and even products of γ^a's in $d = (5+1)$-dimensional internal space. Table is divided into four groups. The first group, odd I, is (chosen) to represent "basis vectors", $\hat{b}_f^{m\dagger}$, appearing in $2^{\frac{d}{2}-1} = 4$ "families" ($f = 1,2,3,4$), each "family" having $2^{\frac{d}{2}-1} = 4$ "family" members ($m = 1,2,3,4$). The second group, odd II, contains Hermitian conjugate partners of the first group for each "family" separately, $\hat{b}_f^{m} = (\hat{b}_f^{m\dagger})^\dagger$. The odd I or odd II are products of an odd number of nilpotents (one or three) and projectors (two or none). The "family" quantum numbers of $\hat{b}_f^{m\dagger}$, that is the eigenvalues of $(\tilde{S}^{03}, \tilde{S}^{12}, \tilde{S}^{56})$, appear for the first *odd I* group, and the two last *even I* and *even II* groups above each "family", the quantum numbers of the "family" members (S^{03}, S^{12}, S^{56}) are written in the last three columns. For the Hermitian conjugated partners of *odd I*, presented in the group *odd II*, the quantum numbers (S^{03}, S^{12}, S^{56}) are presented above each group of the Hermitian conjugate partners, the last three columns tell eigenvalues of $(\tilde{S}^{03}, \tilde{S}^{12}, \tilde{S}^{56})$. Each of the two groups with the even number of γ^a's, *even I* and *even II*, has their Hermitian conjugated partners within its group. The quantum numbers f, that is the eigenvalues of $(\tilde{S}^{03}, \tilde{S}^{12}, \tilde{S}^{56})$, are written above each column of four members, the quantum numbers of the members, (S^{03}, S^{12}, S^{56}), are written in the last three columns. To find the quantum numbers of $(\mathcal{S}^{03}, \mathcal{S}^{12}, \mathcal{S}^{56})$ one has to take into account that $\mathcal{S}^{ab} = S^{ab} + \tilde{S}^{ab}$.

"basis vectors" $(\tilde{S}^{03}, \tilde{S}^{12}, \tilde{S}^{56})$	m $\rightarrow$	f = 1 $(\frac{i}{2}, -\frac{1}{2}, -\frac{1}{2})$	f = 2 $(-\frac{i}{2}, -\frac{1}{2}, \frac{1}{2})$	f = 3 $(-\frac{i}{2}, \frac{1}{2}, -\frac{1}{2})$	f = 4 $(\frac{i}{2}, \frac{1}{2}, \frac{1}{2})$	S^{03}	S^{12}	S^{56}
odd I $\hat{b}_f^{m\dagger}$	1	03 12 56 (+i)[+][+]	03 12 56 [+i](+)[+]	03 12 56 [+i](+)(+)	03 12 56 (+i)(+)(+)	$\frac{i}{2}$	$\frac{1}{2}$	$\frac{1}{2}$
	2	[−i](−)[+]	(−i)(−)(+)	(−i)[−][+]	[−i][−](+)	$-\frac{i}{2}$	$-\frac{1}{2}$	$\frac{1}{2}$
	3	[−i][+](−)	(−i)[+][−]	(−i)(+)(−)	[−i](+)[−]	$-\frac{i}{2}$	$\frac{1}{2}$	$-\frac{1}{2}$
	4	(+i)(−)(−)	[+i](−)[−]	[+i][−](−)	(+i)[−][−]	$\frac{i}{2}$	$-\frac{1}{2}$	$-\frac{1}{2}$
(S^{03}, S^{12}, S^{56})	$\rightarrow$	$(-\frac{i}{2}, \frac{1}{2}, \frac{1}{2})$ 03 12 56	$(\frac{i}{2}, \frac{1}{2}, -\frac{1}{2})$ 03 12 56	$(\frac{i}{2}, -\frac{1}{2}, \frac{1}{2})$ 03 12 56	$(-\frac{i}{2}, -\frac{1}{2}, -\frac{1}{2})$ 03 12 56	$\tilde{s}^{03}$	$\tilde{s}^{12}$	$\tilde{s}^{56}$
odd II $\hat{b}_f^{m}$	1	(−i)[+][+]	[+i][+](−)	[+i](−)[+]	(−i)(−)(−)	$-\frac{i}{2}$	$-\frac{1}{2}$	$-\frac{1}{2}$
	2	[−i](+)[+]	(+i)(+)(−)	(+i)[−][+]	[−i][−](−)	$\frac{i}{2}$	$\frac{1}{2}$	$-\frac{1}{2}$
	3	[−i][+](+)	(+i)[+][−]	(+i)(−)(+)	[−i](−)[−]	$\frac{i}{2}$	$-\frac{1}{2}$	$\frac{1}{2}$
	4	(−i)(+)(+)	[+i](+)[−]	[+i][−](+)	(−i)[−][−]	$-\frac{i}{2}$	$\frac{1}{2}$	$\frac{1}{2}$
$(\tilde{S}^{03}, \tilde{S}^{12}, \tilde{S}^{56})$	$\rightarrow$	$(-\frac{i}{2}, \frac{1}{2}, \frac{1}{2})$ 03 12 56	$(\frac{i}{2}, -\frac{1}{2}, \frac{1}{2})$ 03 12 56	$(-\frac{i}{2}, -\frac{1}{2}, -\frac{1}{2})$ 03 12 56	$(\frac{i}{2}, \frac{1}{2}, -\frac{1}{2})$ 03 12 56	S^{03}	S^{12}	S^{56}
even I ${}^{I}\mathcal{A}_f^m$	1	[+i](+)(+)	(+i)[+](+)	[+i][+][+]	(+i)(+)[+]	$\frac{i}{2}$	$\frac{1}{2}$	$\frac{1}{2}$
	2	(−i)[−](+)	[−i](−)(+)	(−i)(−)[+]	[−i][−][+]	$-\frac{i}{2}$	$-\frac{1}{2}$	$\frac{1}{2}$
	3	(−i)(+)[−]	[−i][+][−]	(−i)[+](−)	[−i](+)(−)	$-\frac{i}{2}$	$\frac{1}{2}$	$-\frac{1}{2}$
	4	[+i][−][−]	(+i)(−)[−]	[+i](−)(−)	(+i)[−](−)	$\frac{i}{2}$	$-\frac{1}{2}$	$-\frac{1}{2}$
$(\tilde{S}^{03}, \tilde{S}^{12}, \tilde{S}^{56})$	$\rightarrow$	$(\frac{i}{2}, \frac{1}{2}, \frac{1}{2})$ 03 12 56	$(-\frac{i}{2}, -\frac{1}{2}, \frac{1}{2})$ 03 12 56	$(\frac{i}{2}, -\frac{1}{2}, -\frac{1}{2})$ 03 12 56	$(-\frac{i}{2}, \frac{1}{2}, -\frac{1}{2})$ 03 12 56	S^{03}	S^{12}	S^{56}
even II ${}^{II}\mathcal{A}_f^m$	1	[−i](+)(+)	(−i)[+](+)	[−i][+][+]	(−i)(+)[+]	$-\frac{i}{2}$	$\frac{1}{2}$	$\frac{1}{2}$
	2	(+i)[−](+)	[+i](−)(+)	(+i)(−)[+]	[+i][−][+]	$\frac{i}{2}$	$-\frac{1}{2}$	$\frac{1}{2}$
	3	(+i)(+)[−]	[+i][+][−]	(+i)[+](−)	[+i](+)(−)	$\frac{i}{2}$	$\frac{1}{2}$	$-\frac{1}{2}$
	4	[−i][−][−]	(−i)(−)[−]	[−i](−)(−)	(−i)[−](−)	$-\frac{i}{2}$	$-\frac{1}{2}$	$-\frac{1}{2}$

The corresponding relations for $\tilde{S}^{ab}$, determining the family quantum numbers, follow if we replace in above equations S^{ab} by $\tilde{S}^{ab}$.

The hypercharge Y and the electromagnetic charge Q relate to the *standard model* quantum numbers.

For fermions, the operator of handedness Γ^d is determined as follows:

$$\Gamma^{(d)} = \prod_a (\sqrt{\eta^{aa}}\gamma^a) \cdot \begin{cases} (i)^{\frac{d}{2}}, & \text{for d even}, \\ (i)^{\frac{d-1}{2}}, & \text{for d odd}. \end{cases} \tag{16.52}$$

All the families (all the irreducible representations) follow from this one by applying, let say, on the first member, u^{c1}_R, all possible $\tilde{S}^{ab}$, Eq. (14.3). Let us start with $\tilde{S}^{01}$ which transforms $u^{c1}_{R,f=1}(\equiv \overset{03}{(+i)}\ \overset{12}{[+]} \mid \overset{56}{[+]}\ \overset{78}{(+)} \parallel \overset{9\,10}{(+)}\ \overset{11\,12}{[-]}\ \overset{13\,14}{[-]})$ of this first family to $u^{c1}_{R,f=2}(\equiv \overset{03}{[+i]}\ \overset{12}{(+)} \mid \overset{56}{[+]}\ \overset{78}{(+)} \parallel \overset{9\,10}{(+)}\ \overset{11\,12}{[-]}\ \overset{13\,14}{[-]})$. From the first family member of the second family all the members of the second family follow by the application of S^{ab}. There are obviously, the same number of families as there is the number of the family members.

The even "basis vectors", analysed with respect to the same subgroups, $(SO(3,1) \times SU(2) \times SU(2) \times SU(3) \times U(1))$ of the $SO(13,1)$ group, offer the description of the internal spaces of the corresponding tensor, vector and scalar gauge fields, appearing in the *standard model* before the electroweak break [24,28,30]; as explained in Sect. 15.2.1. There are breaks of symmetries which make the very limited number of families observed at observable energies.
The even "basis vectors" are be expressible as products of the odd "basis vectors" and their Hermitian conjugate partners, as presented in Eqs. (15.12, 15.13).

i		$\mid^a\psi_i>$	$\Gamma^{(3,1)}$	S^{12}	τ^{13}	τ^{23}	τ^{33}	τ^{38}	τ^4	Y	Q
		(Anti)octet, $\Gamma^{(7,1)} = (-1)\,1$, $\Gamma^{(6)} = (1)\,-1$ of (anti)quarks and (anti)leptons									
	u^{c1}_R	$\overset{03}{(+i)}\ \overset{12}{[+]} \mid \overset{56}{[+]}\ \overset{78}{(+)} \parallel \overset{9\,10}{(+)}\ \overset{11\,12}{[-]}\ \overset{13\,14}{[-]}$	1	$\frac{1}{2}$	0	$\frac{1}{2}$	$\frac{1}{2}$	$\frac{1}{2\sqrt{3}}$	$\frac{1}{6}$	$\frac{2}{3}$	$\frac{2}{3}$
2	u^{c1}_R	$\overset{03}{[-i]}\ \overset{12}{(-)} \mid \overset{56}{[+]}\ \overset{78}{(+)} \parallel \overset{9\,10}{(+)}\ \overset{11\,12}{[-]}\ \overset{13\,14}{[-]}$	1	$-\frac{1}{2}$	0	$\frac{1}{2}$	$\frac{1}{2}$	$\frac{1}{2\sqrt{3}}$	$\frac{1}{6}$	$\frac{2}{3}$	$\frac{2}{3}$
3	d^{c1}_R	$\overset{03}{(+i)}\ \overset{12}{[+]} \mid \overset{56}{(-)}\ \overset{78}{[-]} \parallel \overset{9\,10}{(+)}\ \overset{11\,12}{[-]}\ \overset{13\,14}{[-]}$	1	$\frac{1}{2}$	0	$-\frac{1}{2}$	$\frac{1}{2}$	$\frac{1}{2\sqrt{3}}$	$\frac{1}{6}$	$-\frac{1}{3}$	$-\frac{1}{3}$
4	d^{c1}_R	$\overset{03}{[-i]}\ \overset{12}{(-)} \mid \overset{56}{(-)}\ \overset{78}{[-]} \parallel \overset{9\,10}{(+)}\ \overset{11\,12}{[-]}\ \overset{13\,14}{[-]}$	1	$-\frac{1}{2}$	0	$-\frac{1}{2}$	$\frac{1}{2}$	$\frac{1}{2\sqrt{3}}$	$\frac{1}{6}$	$-\frac{1}{3}$	$-\frac{1}{3}$
5	d^{c1}_L	$\overset{03}{[-i]}\ \overset{12}{[+]} \mid \overset{56}{(-)}\ \overset{78}{(+)} \parallel \overset{9\,10}{(+)}\ \overset{11\,12}{[-]}\ \overset{13\,14}{[-]}$	-1	$\frac{1}{2}$	$-\frac{1}{2}$	0	$\frac{1}{2}$	$\frac{1}{2\sqrt{3}}$	$\frac{1}{6}$	$\frac{1}{6}$	$-\frac{1}{3}$
6	d^{c1}_L	$\overset{03}{-(+i)}\ \overset{12}{(-)} \mid \overset{56}{(-)}\ \overset{78}{(+)} \parallel \overset{9\,10}{(+)}\ \overset{11\,12}{[-]}\ \overset{13\,14}{[-]}$	-1	$-\frac{1}{2}$	$-\frac{1}{2}$	0	$\frac{1}{2}$	$\frac{1}{2\sqrt{3}}$	$\frac{1}{6}$	$\frac{1}{6}$	$-\frac{1}{3}$
7	u^{c1}_L	$\overset{03}{-[-i]}\ \overset{12}{[+]} \mid \overset{56}{[+]}\ \overset{78}{[-]} \parallel \overset{9\,10}{(+)}\ \overset{11\,12}{[-]}\ \overset{13\,14}{[-]}$	-1	$\frac{1}{2}$	$\frac{1}{2}$	0	$\frac{1}{2}$	$\frac{1}{2\sqrt{3}}$	$\frac{1}{6}$	$\frac{1}{6}$	$\frac{2}{3}$
8	u^{c1}_L	$\overset{03}{(+i)}\ \overset{12}{(-)} \mid \overset{56}{[+]}\ \overset{78}{[-]} \parallel \overset{9\,10}{(+)}\ \overset{11\,12}{[-]}\ \overset{13\,14}{[-]}$	-1	$-\frac{1}{2}$	$\frac{1}{2}$	0	$\frac{1}{2}$	$\frac{1}{2\sqrt{3}}$	$\frac{1}{6}$	$\frac{1}{6}$	$\frac{2}{3}$
9	u^{c2}_R	$\overset{03}{(+i)}\ \overset{12}{[+]} \mid \overset{56}{[+]}\ \overset{78}{(+)} \parallel \overset{9\,10}{[-]}\ \overset{11\,12}{(+)}\ \overset{13\,14}{[-]}$	1	$\frac{1}{2}$	0	$\frac{1}{2}$	$-\frac{1}{2}$	$\frac{1}{2\sqrt{3}}$	$\frac{1}{6}$	$\frac{2}{3}$	$\frac{2}{3}$

Continued on next page

i		$\vert^{a}\psi_{i}>$ (Anti)octet, $\Gamma^{(7,1)}=(-1)\,1$, $\Gamma^{(6)}=(1)\,-1$ of (anti)quarks and (anti)leptons	$\Gamma^{(3,1)}$	S^{12}	τ^{13}	τ^{23}	τ^{33}	τ^{38}	τ^{4}	Y	Q
10	$u_{R}^{c\,2}$	03 12 56 78 9 10 11 12 13 14 [−i] (−) | [+] (+) || [−] (+) [−]	1	$-\frac{1}{2}$	0	$\frac{1}{2}$	$-\frac{1}{2}$	$\frac{1}{2\sqrt{3}}$	$\frac{1}{6}$	$\frac{2}{3}$	$\frac{2}{3}$
11	$d_{R}^{c\,2}$	03 12 56 78 9 10 11 12 13 14 (+i) [+] | (−) [−] || [−] (+) [−]	1	$\frac{1}{2}$	0	$-\frac{1}{2}$	$-\frac{1}{2}$	$\frac{1}{2\sqrt{3}}$	$\frac{1}{6}$	$-\frac{1}{3}$	$-\frac{1}{3}$
12	$d_{R}^{c\,2}$	03 12 56 78 9 10 11 12 13 14 [−i] (−) | (−) [−] || [−] (+) [−]	1	$-\frac{1}{2}$	0	$-\frac{1}{2}$	$-\frac{1}{2}$	$\frac{1}{2\sqrt{3}}$	$\frac{1}{6}$	$-\frac{1}{3}$	$-\frac{1}{3}$
13	$d_{L}^{c\,2}$	03 12 56 78 9 10 11 12 13 14 [−i] [+] | (−) (+) || [−] (+) [−]	-1	$\frac{1}{2}$	$-\frac{1}{2}$	0	$-\frac{1}{2}$	$\frac{1}{2\sqrt{3}}$	$\frac{1}{6}$	$\frac{1}{6}$	$-\frac{1}{3}$
14	$d_{L}^{c\,2}$	03 12 56 78 9 10 11 12 13 14 − (+i) (−) | (−) (+) || [−] (+) [−]	-1	$-\frac{1}{2}$	$-\frac{1}{2}$	0	$-\frac{1}{2}$	$\frac{1}{2\sqrt{3}}$	$\frac{1}{6}$	$\frac{1}{6}$	$-\frac{1}{3}$
15	$u_{L}^{c\,2}$	03 12 56 78 9 10 11 12 13 14 − [−i] [+] | [+] [−] || [−] (+) [−]	-1	$\frac{1}{2}$	$\frac{1}{2}$	0	$-\frac{1}{2}$	$\frac{1}{2\sqrt{3}}$	$\frac{1}{6}$	$\frac{1}{6}$	$\frac{2}{3}$
16	$u_{L}^{c\,2}$	03 12 56 78 9 10 11 12 13 14 (+i) (−) | [+] [−] || [−] (+) [−]	-1	$-\frac{1}{2}$	$\frac{1}{2}$	0	$-\frac{1}{2}$	$\frac{1}{2\sqrt{3}}$	$\frac{1}{6}$	$\frac{1}{6}$	$\frac{2}{3}$
17	$u_{R}^{c\,3}$	03 12 56 78 9 10 11 12 13 14 (+i) [+] | [+] (+) || [−] [−] (+)	1	$\frac{1}{2}$	0	$\frac{1}{2}$	0	$-\frac{1}{\sqrt{3}}$	$\frac{1}{6}$	$\frac{2}{3}$	$\frac{2}{3}$
18	$u_{R}^{c\,3}$	03 12 56 78 9 10 11 12 13 14 [−i] (−) | [+] (+) || [−] [−] (+)	1	$-\frac{1}{2}$	0	$\frac{1}{2}$	0	$-\frac{1}{\sqrt{3}}$	$\frac{1}{6}$	$\frac{2}{3}$	$\frac{2}{3}$
19	$d_{R}^{c\,3}$	03 12 56 78 9 10 11 12 13 14 (+i) [+] | (−) [−] || [−] [−] (+)	1	$\frac{1}{2}$	0	$-\frac{1}{2}$	0	$-\frac{1}{\sqrt{3}}$	$\frac{1}{6}$	$-\frac{1}{3}$	$-\frac{1}{3}$
20	$d_{R}^{c\,3}$	03 12 56 78 9 10 11 12 13 14 [−i] (−) | (−) [−] || [−] [−] (+)	1	$-\frac{1}{2}$	0	$-\frac{1}{2}$	0	$-\frac{1}{\sqrt{3}}$	$\frac{1}{6}$	$-\frac{1}{3}$	$-\frac{1}{3}$
21	$d_{L}^{c\,3}$	03 12 56 78 9 10 11 12 13 14 [−i] [+] | (−) (+) || [−] [−] (+)	-1	$\frac{1}{2}$	$-\frac{1}{2}$	0	0	$-\frac{1}{\sqrt{3}}$	$\frac{1}{6}$	$\frac{1}{6}$	$-\frac{1}{3}$
22	$d_{L}^{c\,3}$	03 12 56 78 9 10 11 12 13 14 − (+i) (−) | (−) (+) || [−] [−] (+)	-1	$-\frac{1}{2}$	$-\frac{1}{2}$	0	0	$-\frac{1}{\sqrt{3}}$	$\frac{1}{6}$	$\frac{1}{6}$	$-\frac{1}{3}$
23	$u_{L}^{c\,3}$	03 12 56 78 9 10 11 12 13 14 − [−i] [+] | [+] [−] || [−] [−] (+)	-1	$\frac{1}{2}$	$\frac{1}{2}$	0	0	$-\frac{1}{\sqrt{3}}$	$\frac{1}{6}$	$\frac{1}{6}$	$\frac{2}{3}$
24	$u_{L}^{c\,3}$	03 12 56 78 9 10 11 12 13 14 (+i) (−) | [+] [−] || [−] [−] (+)	-1	$-\frac{1}{2}$	$\frac{1}{2}$	0	0	$-\frac{1}{\sqrt{3}}$	$\frac{1}{6}$	$\frac{1}{6}$	$\frac{2}{3}$
25	ν_{R}	03 12 56 78 9 10 11 12 13 14 (+i) [+] | [+] (+) || (+) (+) (+)	1	$\frac{1}{2}$	0	$\frac{1}{2}$	0	0	$-\frac{1}{2}$	0	0
26	ν_{R}	03 12 56 78 9 10 11 12 13 14 [−i] (−) | [+] (+) || (+) (+) (+)	1	$-\frac{1}{2}$	0	$\frac{1}{2}$	0	0	$-\frac{1}{2}$	0	0
27	e_{R}	03 12 56 78 9 10 11 12 13 14 (+i) [+] | (−) [−] || (+) (+) (+)	1	$\frac{1}{2}$	0	$-\frac{1}{2}$	0	0	$-\frac{1}{2}$	−1	−1
28	e_{R}	03 12 56 78 9 10 11 12 13 14 [−i] (−) | (−) [−] || (+) (+) (+)	1	$-\frac{1}{2}$	0	$-\frac{1}{2}$	0	0	$-\frac{1}{2}$	−1	−1
29	e_{L}	03 12 56 78 9 10 11 12 13 14 [−i] [+] | (−) (+) || (+) (+) (+)	-1	$\frac{1}{2}$	$-\frac{1}{2}$	0	0	0	$-\frac{1}{2}$	$-\frac{1}{2}$	−1
30	e_{L}	03 12 56 78 9 10 11 12 13 14 − (+i) (−) | (−) (+) || (+) (+) (+)	-1	$-\frac{1}{2}$	$-\frac{1}{2}$	0	0	0	$-\frac{1}{2}$	$-\frac{1}{2}$	−1
31	ν_{L}	03 12 56 78 9 10 11 12 13 14 − [−i] [+] | [+] [−] || (+) (+) (+)	-1	$\frac{1}{2}$	$\frac{1}{2}$	0	0	0	$-\frac{1}{2}$	$-\frac{1}{2}$	0
32	ν_{L}	03 12 56 78 9 10 11 12 13 14 (+i) (−) | [+] [−] || (+) (+) (+)	-1	$-\frac{1}{2}$	$\frac{1}{2}$	0	0	0	$-\frac{1}{2}$	$-\frac{1}{2}$	0
33	$\bar{u}_{L}^{c\,1}$	03 12 56 78 9 10 11 12 13 14 [−i] [+] | [+] (+) || [−] (+) (+)	-1	$\frac{1}{2}$	0	$\frac{1}{2}$	$-\frac{1}{2}$	$-\frac{1}{2\sqrt{3}}$	$-\frac{1}{6}$	$\frac{1}{3}$	$\frac{1}{3}$
34	$\bar{d}_{L}^{c\,1}$	03 12 56 78 9 10 11 12 13 14 (+i) (−) | [+] (+) || [−] (+) (+)	-1	$-\frac{1}{2}$	0	$\frac{1}{2}$	$-\frac{1}{2}$	$-\frac{1}{2\sqrt{3}}$	$-\frac{1}{6}$	$\frac{1}{3}$	$\frac{1}{3}$
35	$\bar{u}_{L}^{c\,1}$	03 12 56 78 9 10 11 12 13 14 − [−i] [+] | (−) [−] || [−] (+) (+)	-1	$\frac{1}{2}$	0	$-\frac{1}{2}$	$-\frac{1}{2}$	$-\frac{1}{2\sqrt{3}}$	$-\frac{1}{6}$	$-\frac{2}{3}$	$-\frac{2}{3}$
36	$\bar{u}_{L}^{c\,1}$	03 12 56 78 9 10 11 12 13 14 − (+i) (−) | (−) [−] || [−] (+) (+)	-1	$-\frac{1}{2}$	0	$-\frac{1}{2}$	$-\frac{1}{2}$	$-\frac{1}{2\sqrt{3}}$	$-\frac{1}{6}$	$-\frac{2}{3}$	$-\frac{2}{3}$
37	$\bar{d}_{R}^{c\,1}$	03 12 56 78 9 10 11 12 13 14 (+i) [+] | [+] [−] || [−] (+) (+)	1	$\frac{1}{2}$	$\frac{1}{2}$	0	$-\frac{1}{2}$	$-\frac{1}{2\sqrt{3}}$	$-\frac{1}{6}$	$-\frac{1}{6}$	$\frac{1}{3}$
38	$\bar{d}_{R}^{c\,1}$	03 12 56 78 9 10 11 12 13 14 − [−i] (−) | [+] [−] || [−] (+) (+)	1	$-\frac{1}{2}$	$\frac{1}{2}$	0	$-\frac{1}{2}$	$-\frac{1}{2\sqrt{3}}$	$-\frac{1}{6}$	$-\frac{1}{6}$	$\frac{1}{3}$
39	$\bar{u}_{R}^{c\,1}$	03 12 56 78 9 10 11 12 13 14 (+i) [+] | (−) (+) || [−] (+) (+)	1	$\frac{1}{2}$	$-\frac{1}{2}$	0	$-\frac{1}{2}$	$-\frac{1}{2\sqrt{3}}$	$-\frac{1}{6}$	$-\frac{1}{6}$	$-\frac{2}{3}$
40	$\bar{u}_{R}^{c\,1}$	03 12 56 78 9 10 11 12 13 14 [−i] (−) | (−) (+) || [−] (+) (+)	1	$-\frac{1}{2}$	$-\frac{1}{2}$	0	$-\frac{1}{2}$	$-\frac{1}{2\sqrt{3}}$	$-\frac{1}{6}$	$-\frac{1}{6}$	$-\frac{2}{3}$
41	$\bar{d}_{L}^{c\,2}$	03 12 56 78 9 10 11 12 13 14 [−i] [+] | [+] (+) || (+) [−] (+)	-1	$\frac{1}{2}$	0	$\frac{1}{2}$	$\frac{1}{2}$	$-\frac{1}{2\sqrt{3}}$	$-\frac{1}{6}$	$\frac{1}{3}$	$\frac{1}{3}$
42	$\bar{d}_{L}^{c\,2}$	03 12 56 78 9 10 11 12 13 14 (+i) (−) | [+] (+) || (+) [−] (+)	-1	$-\frac{1}{2}$	0	$\frac{1}{2}$	$\frac{1}{2}$	$-\frac{1}{2\sqrt{3}}$	$-\frac{1}{6}$	$\frac{1}{3}$	$\frac{1}{3}$
43	$\bar{u}_{L}^{c\,2}$	03 12 56 78 9 10 11 12 13 14 − [−i] [+] | (−) [−] || (+) [−] (+)	-1	$\frac{1}{2}$	0	$-\frac{1}{2}$	$\frac{1}{2}$	$-\frac{1}{2\sqrt{3}}$	$-\frac{1}{6}$	$-\frac{2}{3}$	$-\frac{2}{3}$
44	$\bar{u}_{L}^{c\,2}$	03 12 56 78 9 10 11 12 13 14 − (+i) (−) | (−) [−] || (+) [−] (+)	-1	$-\frac{1}{2}$	0	$-\frac{1}{2}$	$\frac{1}{2}$	$-\frac{1}{2\sqrt{3}}$	$-\frac{1}{6}$	$-\frac{2}{3}$	$-\frac{2}{3}$
45	$\bar{d}_{R}^{c\,2}$	03 12 56 78 9 10 11 12 13 14 (+i) [+] | [+] [−] || (+) [−] (+)	1	$\frac{1}{2}$	$\frac{1}{2}$	0	$\frac{1}{2}$	$-\frac{1}{2\sqrt{3}}$	$-\frac{1}{6}$	$-\frac{1}{6}$	$\frac{1}{3}$
46	$\bar{d}_{R}^{c\,2}$	03 12 56 78 9 10 11 12 13 14 − [−i] (−) | [+] [−] || (+) [−] (+)	1	$-\frac{1}{2}$	$\frac{1}{2}$	0	$\frac{1}{2}$	$-\frac{1}{2\sqrt{3}}$	$-\frac{1}{6}$	$-\frac{1}{6}$	$\frac{1}{3}$
47	$\bar{u}_{R}^{c\,2}$	03 12 56 78 9 10 11 12 13 14 (+i) [+] | (−) (+) || (+) [−] (+)	1	$\frac{1}{2}$	$-\frac{1}{2}$	0	$\frac{1}{2}$	$-\frac{1}{2\sqrt{3}}$	$-\frac{1}{6}$	$-\frac{1}{6}$	$-\frac{2}{3}$
48	$\bar{u}_{R}^{c\,2}$	03 12 56 78 9 10 11 12 13 14 [−i] (−) | (−) (+) || (+) [−] (+)	1	$-\frac{1}{2}$	$-\frac{1}{2}$	0	$\frac{1}{2}$	$-\frac{1}{2\sqrt{3}}$	$-\frac{1}{6}$	$-\frac{1}{6}$	$-\frac{2}{3}$
49	$\bar{d}_{L}^{c\,3}$	03 12 56 78 9 10 11 12 13 14 [−i] [+] | [+] (+) || (+) (+) [−]	-1	$\frac{1}{2}$	0	$\frac{1}{2}$	0	$\frac{1}{\sqrt{3}}$	$-\frac{1}{6}$	$\frac{1}{3}$	$\frac{1}{3}$
50	$\bar{d}_{L}^{c\,3}$	03 12 56 78 9 10 11 12 13 14 (+i) (−) | [+] (+) || (+) (+) [−]	-1	$-\frac{1}{2}$	0	$\frac{1}{2}$	0	$\frac{1}{\sqrt{3}}$	$-\frac{1}{6}$	$\frac{1}{3}$	$\frac{1}{3}$
51	$\bar{u}_{L}^{c\,3}$	03 12 56 78 9 10 11 12 13 14 − [−i] [+] | (−) [−] || (+) (+) [−]	-1	$\frac{1}{2}$	0	$-\frac{1}{2}$	0	$\frac{1}{\sqrt{3}}$	$-\frac{1}{6}$	$-\frac{2}{3}$	$-\frac{2}{3}$

i		$\vert^{a}\psi_{i}>$	$\Gamma^{(3,1)}$	S^{12}	τ^{13}	τ^{23}	τ^{33}	τ^{38}	τ^{4}	Y	Q
		(Anti)octet, $\Gamma^{(7,1)} = (-1)\,1$, $\Gamma^{(6)} = (1) - 1$ of (anti)quarks and (anti)leptons									
52	$\tilde{u}^{c^3}_{L}$	03 12 56 78 9 10 11 12 13 14 $-(+i)(-)\vert(-)[-]\vert\vert(+)\quad(+)\quad[-]$	-1	$-\frac{1}{2}$	0	$-\frac{1}{2}$	0	$\frac{1}{\sqrt{3}}$	$-\frac{1}{6}$	$-\frac{2}{3}$	$-\frac{2}{3}$
53	$\tilde{d}^{c^3}_{R}$	03 12 56 78 9 10 11 12 13 14 $(+i)[+]\vert[+][-]\vert\vert(+)\quad(+)\quad[-]$	1	$\frac{1}{2}$	$\frac{1}{2}$	0	0	$\frac{1}{\sqrt{3}}$	$-\frac{1}{6}$	$-\frac{1}{6}$	$\frac{1}{3}$
54	$\tilde{d}^{c^3}_{R}$	03 12 56 78 9 10 11 12 13 14 $-[-i](-)\vert[+][-]\vert\vert(+)\quad(+)\quad[-]$	1	$-\frac{1}{2}$	$\frac{1}{2}$	0	0	$\frac{1}{\sqrt{3}}$	$-\frac{1}{6}$	$-\frac{1}{6}$	$\frac{1}{3}$
55	$\tilde{u}^{c^3}_{R}$	03 12 56 78 9 10 11 12 13 14 $(+i)[+]\vert(-)(+)\vert\vert(+)\quad(+)\quad[-]$	1	$\frac{1}{2}$	$-\frac{1}{2}$	0	0	$\frac{1}{\sqrt{3}}$	$-\frac{1}{6}$	$-\frac{1}{6}$	$-\frac{2}{3}$
56	$\tilde{u}^{c^3}_{R}$	03 12 56 78 9 10 11 12 13 14 $[-i](-)\vert(-)(+)\vert\vert(+)\quad(+)\quad[-]$	1	$-\frac{1}{2}$	$-\frac{1}{2}$	0	0	$\frac{1}{\sqrt{3}}$	$-\frac{1}{6}$	$-\frac{1}{6}$	$-\frac{2}{3}$
57	$\tilde{e}_{L}$	03 12 56 78 9 10 11 12 13 14 $[-i][+]\vert[+](+)\vert\vert[-]\quad[-]\quad[-]$	-1	$\frac{1}{2}$	0	$\frac{1}{2}$	0	0	$\frac{1}{2}$	1	1
58	$\tilde{e}_{L}$	03 12 56 78 9 10 11 12 13 14 $(+i)(-)\vert[+](+)\vert\vert[-]\quad[-]\quad[-]$	-1	$-\frac{1}{2}$	0	$\frac{1}{2}$	0	0	$\frac{1}{2}$	1	1
59	$\tilde{\nu}_{L}$	03 12 56 78 9 10 11 12 13 14 $-[-i][+]\vert(-)[-]\vert\vert[-]\quad[-]\quad[-]$	-1	$\frac{1}{2}$	0	$-\frac{1}{2}$	0	0	$\frac{1}{2}$	0	0
60	$\tilde{\nu}_{L}$	03 12 56 78 9 10 11 12 13 14 $-(+i)(-)\vert(-)[-]\vert\vert[-]\quad[-]\quad[-]$	-1	$-\frac{1}{2}$	0	$-\frac{1}{2}$	0	0	$\frac{1}{2}$	0	0
61	$\tilde{\nu}_{R}$	03 12 56 78 9 10 11 12 13 14 $(+i)[+]\vert(-)(+)\vert\vert[-]\quad[-]\quad[-]$	1	$\frac{1}{2}$	$-\frac{1}{2}$	0	0	0	$\frac{1}{2}$	$\frac{1}{2}$	0
62	$\tilde{\nu}_{R}$	03 12 56 78 9 10 11 12 13 14 $-[-i](-)\vert(-)(+)\vert\vert[-]\quad[-]\quad[-]$	1	$-\frac{1}{2}$	$-\frac{1}{2}$	0	0	0	$\frac{1}{2}$	$\frac{1}{2}$	0
63	$\tilde{e}_{R}$	03 12 56 78 9 10 11 12 13 14 $(+i)[+]\vert[+][-]\vert\vert[-]\quad[-]\quad[-]$	1	$\frac{1}{2}$	$\frac{1}{2}$	0	0	0	$\frac{1}{2}$	$\frac{1}{2}$	1
64	$\tilde{e}_{R}$	03 12 56 78 9 10 11 12 13 14 $[-i](-)\vert[+][-]\vert\vert[-]\quad[-]\quad[-]$	1	$-\frac{1}{2}$	$\frac{1}{2}$	0	0	0	$\frac{1}{2}$	$\frac{1}{2}$	1

Table 16.2: The left-handed ($\Gamma^{(13,1)} = -1$, Eq. (14.52)) irreducible representation representing one family of spinors — the product of the odd number of nilpotents and of projectors, both are eigenvectors of the Cartan subalgebra of the $SO(13,1)$ group [5, 15], manifesting the subgroup $SO(7,1)$ of the colour charged quarks and antiquarks and the colourless leptons and antileptons — is presented. It contains the left-handed ($\Gamma^{(3,1)} = -1$) weak ($SU(2)_{I}$) charged ($\tau^{13} = \pm\frac{1}{2}$), and $SU(2)_{II}$ chargeless ($\tau^{23} = 0$) quarks and leptons, and the right-handed ($\Gamma^{(3,1)} = 1$) weak ($SU(2)_{I}$) chargeless and $SU(2)_{II}$ charged ($\tau^{23} = \pm\frac{1}{2}$) quarks and leptons, both with the spin S^{12} up and down ($\pm\frac{1}{2}$, respectively). Quarks distinguish from leptons only in the $SU(3) \times U(1)$ part: Quarks are triplets of three colours ($c^{i} = (\tau^{33}, \tau^{38}) = [(\frac{1}{2}, \frac{1}{2\sqrt{3}}), (-\frac{1}{2}, \frac{1}{2\sqrt{3}}), (0, -\frac{1}{\sqrt{3}})$, carrying the "fermion charge" ($\tau^{4} = \frac{1}{6}$). The colourless leptons carry the "fermion charge" ($\tau^{4} = -\frac{1}{2}$). The same multiplet contains also the left handed weak ($SU(2)_{I}$) chargeless and $SU(2)_{II}$ charged antiquarks and antileptons and the right handed weak ($SU(2)_{I}$) charged and $SU(2)_{II}$ chargeless antiquarks and antileptons. Antiquarks distinguish from antileptons again only in the $SU(3) \times U(1)$ part: Antiquarks are anti-triplets carrying the "fermion charge" ($\tau^{4} = -\frac{1}{6}$). The anti-colourless antileptons carry the "fermion charge" ($\tau^{4} = \frac{1}{2}$). $Y = (\tau^{23} + \tau^{4})$ is the hyper charge, the electromagnetic charge is $Q = (\tau^{13} + Y)$. One can calculate, taking into account Eq. (14.3), also the family quantum numbers of the presented family: $\tilde{S}^{03} = \frac{i}{2}, \tilde{S}^{12} = -\frac{1}{2}, \tilde{S}^{56} = -\frac{1}{2}, \tilde{S}^{78} = \frac{1}{2}, \tilde{S}^{9\,10} = \frac{1}{2}, \tilde{S}^{11\,12} = \frac{1}{2}, \tilde{S}^{13\,14} = \frac{1}{2}$.

16.9 Acknowledgement

The author thanks Department of Physics, FMF, University of Ljubljana, Society of Mathematicians, Physicists and Astronomers of Slovenia for supporting the research on the *spin-charge-family* theory, and Matjaž Breskvar of Beyond Semiconductor for donations, in particular for sponsoring the annual workshops entitled "What comes beyond the standard models" at Bled, in which the ideas and realizations, presented in this paper, were discussed. The author thanks Holger Beck Nielsen for fruitful discussions.

References

1. N. Mankoč Borštnik, "Spin connection as a superpartner of a vielbein", *Phys. Lett.* **B 292** (1992) 25-29.
2. N. Mankoč Borštnik, "Spinor and vector representations in four dimensional Grassmann space", *J. of Math. Phys.* **34** (1993) 3731-3745.
3. N. Mankoč Borštnik, "Unification of spin and charges in Grassmann space?", hep-th 9408002, IJS.TP.94/22, Mod. Phys. Lett.**A (10)** No.7 (1995) 587-595.
4. A. Borštnik Bračič, N. S. Mankoč Borštnik, "On the origin of families of fermions and their mass matrices", hep-ph/0512062, Phys. Rev. **D 74** 073013-28 (2006).
5. N.S. Mankoč Borštnik, H.B.F. Nielsen, *J. of Math. Phys.* **43**, 5782 (2002) [arXiv:hep-th/0111257]. "How to generate families of spinors", *J. of Math. Phys.* **44** 4817 (2003) [arXiv:hep-th/0303224].
6. N.S. Mankoč Borštnik, D. Lukman, "Vector and scalar gauge fields with respect to $d = (3+1)$ in Kaluza-Klein theories and in the *spin-charge-family theory*", *Eur. Phys. J. C* **77** (2017) 231.
7. N.S. Mankoč Borštnik, H.B.F. Nielsen, "Understanding the second quantization of fermions in Clifford and in Grassmann space", *New way of second quantization of fermions — Part I and Part II*, [arXiv:2007.03517, arXiv:2007.03516].
8. N. S. Mankoč Borštnik, H. B. Nielsen, "How does Clifford algebra show the way to the second quantized fermions with unified spins, charges and families, and with vector and scalar gauge fields beyond the *standard model*", Progress in Particle and Nuclear Physics, http://doi.org/10.1016.j.ppnp.2021.103890 .
9. N.S. Mankoč Borštnik, H.B.F. Nielsen, "The spin-charge-family theory offers understanding of the triangle anomalies cancellation in the standard model", *Fortschritte der Physik, Progress of Physics* (2017) 1700046, www.fp-journal.org, DOI: 10.1002/prop.201700046 http://arxiv.org/abs/1607.01618.
10. N. S. Mankoč Borštnik, "Do we understand the internal spaces of second quantized fermion and boson fields, with gravity included? The relation with strings theories", N.S. Mankoč Borštnik, H.B. Nielsen, "A trial to understand the supersymmetry relations through extension of the second quantized fermionand boson fields, either to strings or to odd dimensional spaces", Proceedings to the 27^{th} Workshop "What comes beyond the standard models", 8 - 17 July, 2024, Ed. N.S. Mankoč Borštnik, H.B. Nielsen, A. Kleppe, Založba Univerze v Ljubljani, December 24, DOI: 10.51746/9789612974848, [arxiv: 2312.07548]]
11. G. Bregar, M. Breskvar, D. Lukman, N.S. Mankoč Borštnik, "Predictions for four families by the Approach unifying spins and charges" *New J. of Phys.* **10** (2008) 093002, G. Bregar, M. Breskvar, D. Lukman, N.S. Mankoč Borštnik, "Families of Quarks and Leptons and Their Mass Matrices", Proceedings to the 10^{th} international workshop "What Comes Beyond the Standard Model", 17 -27 of July, 2007, Ed. Norma Mankoč Borštnik, Holger Bech Nielsen, Colin Froggatt, Dragan Lukman, DMFA Založništvo, Ljubljana December 2007, p.53-70,[hep-ph/0711.4681, hep-ph/0606159, hep/ph-07082846].
12. G. Bregar, N.S. Mankoč Borštnik, "Does dark matter consist of baryons of new stable family quarks?", *Phys. Rev. D* **80**, 083534 (2009), 1-16. of new stable family quarks?", *Phys. Rev. D* **80**, 083534 (2009), 1-16.
13. N.S. Mankoč Borštnik, "Matter-antimatter asymmetry in the *spin-charge-family* theory", *Phys. Rev.* **D 91** (2015) 065004 [arXiv:1409.7791].
14. N.S. Mankoč Borštnik N S, "The spin-charge-family theory is explaining the origin of families, of the Higgs and the Yukawa couplings", *J. of Modern Phys.* **4** (2013) 823 [arXiv:1312.1542].

15. G. Bregar, N.S. Mankoč Borštnik, "The new experimental data for the quarks mixing matrix are in better agreement with the *spin-charge-family* theory predictions", Proceedings to the 17^{t}h Workshop "What comes beyond the standard models", Bled, 20-28 of July, 2014, Ed. N.S. Mankoč Borštnik, H.B. Nielsen, D. Lukman, DMFA Založništvo, Ljubljana December 2014, p.20-45 [arXiv:1502.06786v1] [arxiv:1412.5866].
16. N.S. Mankoč Borštnik, M. Rosina, "Are superheavy stable quark clusters viable candidates for the dark matter?", International Journal of Modern Physics D (IJMPD) **24** (No. 13) (2015) 1545003.
17. N. S. Mankoč Borštnik, "Clifford odd and even objects offer description of internal space of fermions and bosons, respectively, opening new insight into the second quantization of fields", The 13^{th} Bienal Conference on Classical and Quantum Relativistic Dynamics of Particles and Fields IARD 2022, Prague, $6-9$ June [http://arxiv.org/abs/2210.07004], Journal of Physics: Conference Series, Volume 2482/2023, Proceedings https://iopscience.iop.org/issue/1742-6596/2482/012012.
18. N. S. Mankoč Borštnik, "How Clifford algebra helps understand second quantized quarks and leptons and corresponding vector and scalar boson fields, opening a new step beyond the standard model", Reference: [arXiv: 2210.06256, physics.gen-ph V2]. Nuclear Physics B 994 (2023) 116326 NUPHB 994 (2023) 116326 .
19. N. S. Mankoč Borštnik, "Clifford odd and even objects in even and odd dimensional spaces", Symmetry 2023,15,818-12-V2 94818, https:doi.org/10.3390/sym15040818, [arxiv.org/abs/2301.04466] , https://www.mdpi.com/2073-8994/15/4/818 Manuscript ID: symmetry-2179313.
20. N. S. Mankoč Borštnik, "Can the "basis vectors", describing the internal spaces of fermion and boson fields with the Clifford odd (for fermion) and Clifford even (for boson) objects, explain interactions among fields, with gravitons included?" [arxiv: 2407.09482].
21. N.S. Mankoč Borštnik, H.B. Nielsen, "Can the "basis vectors", describing the internal space of point fermion and boson fields with the Clifford odd (for fermions) and Clifford even (for bosons) objects, be meaningfully extended to strings?", Proceedings to the 26^{rd} Workshop "What comes beyond the standard models", 10 - 19 July, 2023, Ed. N.S. Mankoč Borštnik, H.B. Nielsen, M.Yu. Khlopov, A. Kleppe, Založba Univerze v Ljubljani, DOI: 10.51746/9789612972097, December 23, [arxiv:2312.07548].
22. N. S. Mankoč Borštnik, "How Clifford algebra can help understand second quantization of fermion and boson fields", [arXiv: 2210.06256. physics.gen-ph V1].
23. N.S. Mankoč Borštnik, H.B. Nielsen, "Discrete symmetries in the Kaluza-Klein-like theories", doi:10.1007/ *Jour. of High Energy Phys.* **04** (2014)165, [http://arxiv.org/abs/1212.2362v3].
24. D. Lukman, N. S. Mankoč Borštnik, "Properties of fermions with integer spin described in Grassmann", Proceedings to the 21^{st} Workshop "What comes beyond the standard models", 23 of June - 1 of July, 2018, Ed. N.S. Mankoč Borštnik, H.B. Nielsen, D. Lukman, DMFA Založništvo, Ljubljana, December 2018 [arxiv:1805.06318, arXiv:1902.10628]
25. T. Troha, D. Lukman and N.S. Mankoč Borštnik, "Massless and massive representations in the *spinor technique*", *Int. J Mod. Phys.* **A 29**, 1450124 (2014) [21 pages] DOI: 10.1142/S0217751X14501243.
26. N.S. Mankoč Borštnik, "How far has so far the Spin-Charge-Family theory succeeded to offer the explanation for the observed phenomena in elementary particle physics and cosmology", Proceedings to the 26^{rd} Workshop "What comes beyond the standard models", 10 - 19 July, 2023, Ed. N.S. Mankoč Borštnik, H.B. Nielsen, M.Yu. Khlopov, A. Kleppe, Založba Univerze v Ljubljani, DOI: 10.51746/9789612972097, December 23, [http://arxiv.org/abs/2312.14946].

27. N.S. Mankoč Borštnik, "New way of second quantized theory of fermions with either Clifford or Grassmann coordinates and *spin-charge-family* theory " [arXiv: 2210.06256. physics.gen-ph V1, arXiv:1802.05554v4, arXiv:1902.10628],
28. N.S. Mankoč Borštnik, "How do Clifford algebras show the way to the second quantized fermions with unified spins, charges and families, and to the corresponding second quantized vector and scalar gauge field ", Proceedings to the 24rd Workshop "What comes beyond the standard models", 5 - 11 of July, 2021, Ed. N.S. Mankoč Borštnik, H.B. Nielsen, D. Lukman, A. Kleppe, DMFA Založništvo, Ljubljana, December 2021, [arXiv:2112.04378].
29. G. Bregar, N.S. Mankoč Borštnik, "Can we predict the fourth family masses for quarks and leptons?", Proceedings (arxiv:1403.4441) to the 16 th Workshop "What comes beyond the standard models", Bled, 14-21 of July, 2013, Ed. N.S. Mankoč Borštnik, H.B. Nielsen, D. Lukman, DMFA Založništvo, Ljubljana December 2013, p. 31-51, [http://arxiv.org/abs/1212.4055].

BLED WORKSHOPS
IN PHYSICS
VOL. 26, NO. 1

Proceedings of the 28th Workshop
What Comes Beyond . . . *(p. 216)*
Bled, Slovenia, July 6–17, 2025

17 How to present and interpret the Feynman diagrams in this theory describing fermion and boson fields in a unique way, in comparison with the Feynman diagrams so far presented and interpreted?

N.S. Mankoč Borštnik[1], H.B. Nielsen[2]

[1]Department of Physics, University of Ljubljana, SI-1000 Ljubljana, Slovenia
[2]Niels Bohr Institute, University of Copenhagen, Denmark

Abstract. Abstract: Although the internal spaces describing spins and charges of fermions' and bosons' second-quantised fields have such different properties, yet we can all describe them equivalently with the "basis vectors" which are a superposition of odd (for fermions) and even (for bosons) products of γ^a's. In an even-dimensional internal space, as it is $d = (13+1)$, odd "basis vectors" appear in $2^{\frac{d}{2}-1}$ families with $2^{\frac{d}{2}-1}$ members each, and have their Hermitian conjugate partners in a separate group, while even "basis vectors" appear in two orthogonal groups. Algebraic multiplication of boson and fermion "basis vectors" determine the interactions between fermions and bosons, and among bosons themselves, and correspondingly also their action. Tensor products of the "basis vectors" and basis in ordinary space-time determine states for fermions and bosons, if bosons obtain in addition the space index α. We study properties of massless fermions and bosons with the internal spaces determined by the "basis vectors" while assuming that fermions and bosons are active only in $d = (3+1)$ of the ordinary space-time. We discuss the Feynman diagrams in this theory, describing internal spaces of fermion and boson fields with odd and even "basis vectors", respectively, in comparison with the Feynman diagrams of the theories so far presented and interpreted.

Povzetek: Četudi imajo notranji prostori, ki opisujejo spine in naboje fermionskih in bozonskih polj v drugi kvantizaciji, tako različne lastnosti, jih lahko opišemo z "baznimi vektorji", ki so superpozicija lihih (za fermione) in sodih (za bozone) produktov operatorjev γ^a. V sodorazsežnih notranjih prostorih, kot je $d = (13+1)$, se lihi "bazni vektorji" pojavljajo v $2^{\frac{d}{2}-1}$ družinah, ki imajo po $2^{\frac{d}{2}-1}$ članov. Njihovi hermitsko konjugiranani partnerji tvorijo ločeno skupino. Sodi "bazni vektorji" pa se pojavljajo v dveh ortogonalnih skupinah. Algebraično množenje "baznih vektorjev" bozonov in fermionov določa način interakcije med fermioni in bozoni ter med samimi bozoni in s tem tudi njihovo akcijo. Tenzorski produkti "baznih vektorjev" in baze v navadnem prostoru in času določajo fermionska in bozonska stanja, če bozonom pripišemo tudi prostorski indeks α in dovolimo fermionom in bozonom, da so aktivni samo v $d = (3+1)$. Avtorja analizirata lastnosti brezmasnih fermionov in bozonov, ki jim spine in naboje določajo lihi (fermionom) in sodi (bozonom) "bazni vektorji". V tej teoriji obravnavata Feynmanove diagrame in jih primerjata s Feynmanovimi diagrami do sedaj predstavljenih teorij.

17.1 Introduction

Authors studied (together, and with the collaborators) in a series of papers the properties of the second quantized fermion and boson fields [1–5,7,9,10,13–18, 20–22], trying to understand what are the elementary laws of nature for massless fermion and boson fields, and whether all the second quantized fields, fermions' and bosons', can be described in an unique and simple way.
Accepting the idea of the papers [10,20–22] that internal spaces of fermions and bosons are described by "basis vectors" which are the superposition of odd (for fermions) and even (for bosons) products of the operators γ^a's, the authors continue to find out whether and to what extent "nature manifests" the proposed idea.
As presented in one contribution of this proceedings ([6], the talk of one of the two authors), the idea that the internal spaces of fermion and boson fields are described by the odd and even "basis vectors" which are products of nilpotents and projectors, all of which are the eigenvectors of the Cartan subalgebra members of the Lorentz algebra in the internal space of the fermion and boson fields, enabling to explain the second quantisation postulates of Dirac determines uniquely in even-dimensional spaces with $d = 2(2n+1)$ also the action for interacting massless fermion, antifermion and boson fields.
In Sect. 15.2, we present and comment on the Feynman diagrams for interacting fermions and bosons when describing internal spaces with our proposal, paying attention to massless fermions and bosons, and for fermions and bosons in ordinary theories.
In Sect. 15.3 we comment on the results of our presentation.
In the introduction, we overview:
a. The construction of the odd and even "basis vectors" describing the internal spaces of fermions and bosons.
b. The algebraic products among fermion and boson "basis vectors" which determine the action for both fields and interactions among them.
c. The tensor products of "basis vectors" and the basis in ordinary space-time, determining the massless anticommuting fermion and commuting boson second quantised fields, in which bosons gain the vector index α, while fermions and bosons are active (have non-zero momentum) only in $d = (3+1)$, while the internal spaces have $d = (13+1)$. Bosons can gain a vector index $\mu = (0,1,2,3)$, representing gravitons of spin ± 2, vectors of spin ± 1 (photons, weak bosons, gluons) or a scalar index $\sigma = (5,6,...,13)$, representing scalars (Higgs and others).
In Sect. 15.2, we present and comment on the Feynman diagrams for interacting fermions and bosons when describing internal spaces with our proposal, paying attention to massless fermions and bosons, and for fermions and bosons in ordinary theories.
In Sect. 15.3 we comment on the results of our presentation.

17.1.1 States of the second quantized fermion and boson fields

This Subsect. 15.1.1 is a short overview of several similar sections, presented in Refs. [6,9,20,22], the last one, Ref. [6], appears in this Proceedings.

In this contribution, all the second quantised fermion and boson states are assumed to be massless. They are constructed as tensor products of "basis vectors", which determine the anti-commutation properties of fermions and commutation properties of bosons, also in the tensor product with basis in ordinary space-time. We present the "basis vectors" as products of nilpotents and projectors, so that they are eigenstates of all the Cartan subalgebra members of the Lorentz algebra in the $d = (13+1)$-dimensional internal space, while the space-time has only $d = (3+1)$.
The Grassmann algebra offers two kinds of operators γ^a's [6, 9, 20, 22], we call them γ^a's and $\tilde{\gamma}^a$'s with the properties

$$\begin{aligned}
&\{\gamma^a, \gamma^b\}_+ = 2\eta^{ab} = \{\tilde{\gamma}^a, \tilde{\gamma}^b\}_+ \,, \\
&\{\gamma^a, \tilde{\gamma}^b\}_+ = 0 \,, \quad (a, b) = (0, 1, 2, 3, 5, \cdots, d) \,, \\
&\quad (\gamma^a)^\dagger = \eta^{aa}\gamma^a \,, \quad (\tilde{\gamma}^a)^\dagger = \eta^{aa}\tilde{\gamma}^a \,.
\end{aligned} \tag{17.1}$$

We use γ^a's, to generate the "basis vectors" describing internal spaces of fermions and bosons, arranging them to be products of nilpotents and projectors

$$\begin{aligned}
&\overset{ab}{(k)}: = \frac{1}{2}(\gamma^a + \frac{\eta^{aa}}{ik}\gamma^b) \,, \quad (\overset{ab}{(k)})^2 = 0 \,, \\
&\overset{ab}{[k]}: = \frac{1}{2}(1 + \frac{i}{k}\gamma^a\gamma^b) \,, \quad (\overset{ab}{[k]})^2 = \overset{ab}{[k]} \,.
\end{aligned} \tag{17.2}$$

Nilpotents are a superposition of an odd number of γ^a's, projectors of an even number of γ^a's, both are chosen to be the eigenstate of one of the (chosen) Cartan subalgebra members of the Lorentz algebra of $S^{ab} = \frac{i}{4}\{\gamma^a, \gamma^b\}_+$, and $\tilde{S}^{ab} = \frac{i}{4}\{\tilde{\gamma}^a, \tilde{\gamma}^b\}_+$ in the internal space of fermions and bosons.

$$\begin{aligned}
&S^{03}, S^{12}, S^{56}, \cdots, S^{d-1\,d} \,, \\
&\tilde{S}^{03}, \tilde{S}^{12}, \tilde{S}^{56}, \cdots, \tilde{S}^{d-1\,d} \,, \\
&\mathcal{S}^{ab} = S^{ab} + \tilde{S}^{ab} \,.
\end{aligned} \tag{17.3}$$

$$\begin{aligned}
S^{ab}\ \overset{ab}{(k)} &= \frac{k}{2}\ \overset{ab}{(k)} \,, \qquad \tilde{S}^{ab}\ \overset{ab}{(k)} = \frac{k}{2}\ \overset{ab}{(k)} \,, \\
S^{ab}\ \overset{ab}{[k]} &= \frac{k}{2}\ \overset{ab}{[k]} \,, \qquad \tilde{S}^{ab}\ \overset{ab}{[k]} = -\frac{k}{2}\ \overset{ab}{[k]} \,,
\end{aligned} \tag{17.4}$$

with $k^2 = \eta^{aa}\eta^{bb}$.
In even-dimensional spaces, the states in internal spaces are defined by the "basis vectors" which are products of $\frac{d}{2}$ nilpotents and projectors, and are the eigenstates of all the Cartan subalgebra members.

a. "Basis vectors" including an odd number of nilpotents (at least one, the rest are projectors) anti-commute, since the odd products of γ^a's anti-commute. The odd "basis vectors" are used to describe fermions. The odd "basis vectors" appear in internal spaces with $d = 2(2n+1)$ in $2^{\frac{d}{2}-1}$ irreducible representations, called families, with the quantum numbers determined by $\frac{d}{2}$ members of Eq. (15.3). Each

family has $2^{\frac{d}{2}-1}$ members. S^{ab} transform family members within each family. $\tilde{S}^{ab}$ transform a family member of one family to the same family member of the rest of family. The Hermitian conjugated partners of the odd "basis vectors" have $2^{\frac{d}{2}-1} \times 2^{\frac{d}{2}-1}$ members and appear in a different group. The odd "basis vectors" and their Hermitian conjugated partners have together 2^{d-1} members.

We call the odd "basis vectors" $\hat{b}_f^{m\dagger}$, and their Hermitian conjugated partners $\hat{b}_f^{m} = (\hat{b}_f^{m\dagger})^{\dagger}$. m denotes the membership and f the family quantum number of the odd "basis vectors".

The algebraic product, $*_A$, of any two members of the odd "basis vectors" are equal to zero. And any two members of their Hermitian conjugated partners have the algebraic product, $*_A$, equal to zero.

$$\hat{b}_f^{m\dagger} *_A \hat{b}_{f'}^{m'\dagger} = 0\,, \quad \hat{b}_f^{m} *_A \hat{b}_{f'}^{m'} = 0\,, \quad \forall m, m', f, f'\,. \tag{17.5}$$

Choosing the vacuum state equal to

$$|\psi_{oc}> = \sum_{f=1}^{2^{\frac{d}{2}-1}} \hat{b}_f^{m} {}_{*_A} \hat{b}_f^{m\dagger}\,|1>\,, \tag{17.6}$$

for one of the members m, anyone of the odd irreducible representations f, it follows that the odd "basis vectors" obey the relations

$$\begin{aligned}
\hat{b}_f^{m} {}_{*_A} |\psi_{oc}> &= 0.|\psi_{oc}>\,,\\
\hat{b}_f^{m\dagger} {}_{*_A} |\psi_{oc}> &= |\psi_f^{m}>\,,\\
\{\hat{b}_f^{m}, \hat{b}_{f'}^{m'}\}_{*_A+}|\psi_{oc}> &= 0.|\psi_{oc}>\,,\\
\{\hat{b}_f^{m\dagger}, \hat{b}_{f'}^{m'\dagger}\}_{*_A+}|\psi_{oc}> &= 0.|\psi_{oc}>\,,\\
\{\hat{b}_f^{m}, \hat{b}_{f'}^{m'\dagger}\}_{*_A+}|\psi_{oc}> &= \delta^{mm'}\delta_{ff'}|\psi_{oc}>\,,
\end{aligned} \tag{17.7}$$

as postulated by Dirac for the second quantised fermion fields. In Eq. (15.7) odd "basis vectors" anti-commute, since γ^a's obey Eq. (15.1).
Being eigenstates of operators S^{ab} and $\tilde{S}^{ab}$, when (a, b) belong to Eq. (15.3), nilpotents and projectors carry both quantum numbers S^{ab} and $\tilde{S}^{ab}$, Eq. (15.3). S^{ab} transform the odd "basis vectors" of family f to all the members of the same family, $\tilde{S}^{ab}$ transform a particular family member to the same family member of all the families.

b. The even "basis vectors" commute, since the even products of γ^a's commute, Eq. (15.1). In internal spaces with $d = 2(2n+1)$, the even "basis vectors" appear in two orthogonal groups. We name them ${}^{I}\hat{\mathcal{A}}_f^{m\dagger}$ and ${}^{II}\hat{\mathcal{A}}_f^{m\dagger}$.

$${}^{I}\hat{\mathcal{A}}_f^{m\dagger} *_A {}^{II}\hat{\mathcal{A}}_f^{m\dagger} = 0 = {}^{II}\hat{\mathcal{A}}^{m\dagger}{}_{.f} *_A {}^{I}\hat{\mathcal{A}}_f^{m\dagger}\,. \tag{17.8}$$

Each group has $2^{\frac{d}{2}-1} \times 2^{\frac{d}{2}-1}$ members with the Hermitian conjugate partners within the group.
The even "basis vectors" have the eigenvalues of the Cartan subalgebra members, Eq. (15.3), equal to $\mathcal{S}^{ab} = (S^{ab} + \tilde{S}^{ab})$, their eigenvalues are $\pm i$ or ± 1 or zero. According to Eq. (15.4), the eigenvalues of $\mathcal{S}^{ab}$ are for projectors equal zero; $\mathcal{S}^{ab} (= S^{ab} + \tilde{S}^{ab}) \overset{ab}{[\pm]} = 0$.
The algebraic products, $*_A$, of two members of each of these two groups have the property

$$ {}^{i}\hat{\mathcal{A}}^{m\dagger}_{f} *_A {}^{i}\hat{\mathcal{A}}^{m'\dagger}_{f'} \rightarrow \begin{cases} {}^{i}\hat{\mathcal{A}}^{m\dagger}_{f'}, i = (I, II) \\ \text{or zero}. \end{cases} \tag{17.9} $$

i is either I or II. For a chosen (m, f, f'), there is (out of $2^{\frac{d}{2}-1}$) only one m' giving a non-zero contribution.
We further find

$$ {}^{I}\hat{\mathcal{A}}^{m\dagger}_{f} *_A \hat{b}^{m'\dagger}_{f'} \rightarrow \begin{cases} \hat{b}^{m\dagger}_{f'}, \\ \text{or zero}. \end{cases} \tag{17.10} $$

Eq. (15.10) demonstrates that ${}^{I}\hat{\mathcal{A}}^{m\dagger}_{f}$, applying on $\hat{b}^{m'\dagger}_{f'}$, transforms the odd "basis vector" into another odd "basis vector" of the same family, transferring to the odd "basis vector" integer spins or gives zero.
For the second group of boson fields, ${}^{II}\hat{\mathcal{A}}^{m\dagger}_{f}$, it follows

$$ \hat{b}^{m\dagger}_{f} *_A {}^{II}\hat{\mathcal{A}}^{m'\dagger}_{f'} \rightarrow \begin{cases} \hat{b}^{m\dagger}_{f''}, \\ \text{or zero}. \end{cases} \tag{17.11} $$

The application of the odd "basis vector" $\hat{b}^{m\dagger}_{f}$ on ${}^{II}\hat{\mathcal{A}}^{m'\dagger}_{f'}$ leads to another odd "basis vector" $\hat{b}^{m\dagger}_{f''}$ belonging to the same family member m of a different family f''.
The rest of possibilities give zero.
Knowing the odd "basic vectors", we can generate all the even "basic vectors"

$$ {}^{I}\hat{\mathcal{A}}^{m\dagger}_{f} = \hat{b}^{m'\dagger}_{f'} *_A (\hat{b}^{m''\dagger}_{f'})^{\dagger}, \tag{17.12} $$

$$ {}^{II}\hat{\mathcal{A}}^{m\dagger}_{f} = (\hat{b}^{m'\dagger}_{f'})^{\dagger} *_A \hat{b}^{m'\dagger}_{f''}. \tag{17.13} $$

c. To define the fermion and boson second quantized fields we must write the tensor product, $*_T$ of the "basis vectors" in internal space with $d = (13 + 1)$ and the ordinary space-time in the case fermions and bosons have non-zero momentum only in $d = (3 + 1)$. For boson fields, we need to postulate the space index α, which is for vectors (representing gravitons, photons, weak bosons, gluons) equal to $\mu = (0, 1, 2, 3)$ and for scalars equal to $\sigma \geq 5$.

Let us start with basis in ordinary space-time, following Refs. [6,9,20,22].

$$
\begin{aligned}
|\vec{p}> = \hat{b}^{\dagger}_{\vec{p}}\,|0_p>\,, \quad <\vec{p}\,| =< 0_p\,|\hat{b}_{\vec{p}}\,,\\
<\vec{p}\,|\vec{p}\,'> = \delta(\vec{p}-\vec{p}\,') =< 0_p\,|\hat{b}_{\vec{p}}\;\hat{b}^{\dagger}_{\vec{p}\,'}|\,0_p>\,,\\
< 0_p\,|\hat{b}_{\vec{p}\,'},\,\hat{b}^{\dagger}_{\vec{p}}\,|\,0_p> = \delta(\vec{p}\,'-\vec{p})\,,
\end{aligned}
\tag{17.14}
$$

with $< 0_p\,|\,0_p> = 1$. The operator $\hat{b}^{\dagger}_{\vec{p}}$ pushes a single particle state with zero momentum by an amount $\vec{p}$.

The creation operator for a free massless fermion field of the energy $p^0 = |\vec{p}|$, belonging to the family f and to a superposition of family members m applying on the vacuum state ($|\psi_{oc}> *_T |0_{\vec{p}}>$) can be written as

$$
\hat{b}^{m\dagger}_{f}(\vec{p}) \;=\; \hat{b}^{\dagger}_{\vec{p}} *_T \hat{b}^{m\dagger}_{f}\,. \tag{17.15}
$$

The creation operator for a free massless boson field of the energy $p^0 = |\vec{p}|$, with the "basis vectors" belonging to one of the two groups, ${}^{i}\hat{\mathcal{A}}^{m\dagger}_{f}$, $i = (I, II)$, applying on the vacuum state, $|1> *_T |0_{\vec{p}}>$, carrying the space index α, we have

$$
{}^{i}\hat{\mathcal{A}}^{m\dagger}_{f\alpha}(\vec{p}) \;= {}^{i}\mathcal{C}^{m}{}_{f\alpha}(\vec{p}) *_T {}^{i}\hat{\mathcal{A}}^{m\dagger}_{f}\;, i = (I, II)\,, (f, m) \tag{17.16}
$$

with ${}^{i}\mathcal{C}^{m}{}_{f\alpha}(\vec{p}) = {}^{i}\mathcal{C}^{m}{}_{f\alpha}\,\hat{b}^{\dagger}_{\vec{p}}$, and (f, m) are fixed values, the same on both sides.

Le us add that the Lorentz rotations work on both spaces only in $\doteq(3+1)$.

d. Knowing the application among fermion and boson "basis vectors", from Eq. (15.8) to Eq. (15.13), we can write down the action

$$
\begin{aligned}
\mathcal{A} &= \int d^4x\,\frac{1}{2}\,(\bar{\psi}\,\gamma^{a}p_{0a}\psi) + h.c. + \\
&\quad \int d^4x \sum_{i=(I,II)} {}^{i}\hat{F}^{m\,f}_{ab}\;{}^{i}\hat{F}^{mfab}\,,\\
p_{0a} &= p_a - \sum_{mf} {}^{I}\hat{\mathcal{A}}^{m\dagger}_{fa}(x) - \sum_{mf} {}^{II}\hat{\mathcal{A}}^{m\dagger}_{fa}(x)\;,\\
{}^{i}\hat{F}^{m\,f}_{ab} &= \partial_a\,{}^{i}\hat{\mathcal{A}}^{m\dagger}_{fb}(x) - \partial_b\,{}^{i}\hat{\mathcal{A}}^{m\dagger}_{fa}(x) + \varepsilon f^{mfm''f''m'f'}\,{}^{i}\hat{\mathcal{A}}^{m''\dagger}_{f''a}(x)\,{}^{i}\hat{\mathcal{A}}^{m'\dagger}_{f'b}(x)\,,\\
&\quad i = (I, II)\,.
\end{aligned}
\tag{17.17}
$$

Vector boson fields, ${}^{i}\hat{\mathcal{A}}^{m\dagger}_{fa}$ (and in ${}^{i}\hat{F}^{m\,f}_{ab}$), must have index (a, b) equal to $(n, p) = (0, 1, 2, 3)$; ${}^{i}\hat{\mathcal{A}}^{m\dagger}_{fn}$ (and in ${}^{i}\hat{F}^{m\,f}_{np}$), $i = (I, II)$.

17.2 Feynman diagrams in our way and in the way with ordinary theories

This section studies the Feynman diagrams in the case when the "basis vectors" describe the internal spaces of fermion and boson fields; the "basis vectors" of

fermions have an odd number of nilpotents, and those of bosons have an even number of nilpotents, with the rest being projectors. We compare these Feynman diagrams with those in which the internal spaces of fermions and bosons are described by matrices, while the fermion families must be postulated, as is the case in most theories.

Let it be repeated: We study the scattering of fermion in boson fields, which are tensor products of the "basis vectors" and basis in ordinary space-time. "Basis vectors" determine spins and charges of fermions and bosons, families of fermion fields and two kinds of boson fields, as well as anti-commutativity and commutativity of fields.

In $d = 2(2n+1)$, each family of "basis vectors" of fermion fields includes fermions and anti-fermions: $d = (13+1)$ includes quarks and leptons and anti-quarks and anti-leptons. Quarks have identical $d = (7+1)$ part of $d = (13+1)$ as leptons; anti-quarks have identical $d = (7+1)$ part of $d = (13+1)$ as anti-leptons. Quarks are distinguished from leptons and anti-quarks from anti-leptons only in the $SO(6)$ part of $SO(13,1)$.

"Basis vectors" in $d = 4n$ include fermions and do not include anti-fermions; there are no anti-fermions in $d = 4n$ [1]. To have fermions and anti-fermions, the internal space must be $d = 2(2n+1)$.

Since we assume that fermions and bosons have non-zero momenta only in $d = (3+1)$ of ordinary space-time, the Lorentz rotations, $M^{ab} = L^{ab} + S^{ab} + \tilde{S}^{ab}$, connecting both spaces are possible only in $d = (3+1)$. For $d \geq 5$ the Lorentz

[1] Let us look at one family of the fermion "basis vectors" in $d = (7+1)$, to notice that we do not have members who could represent antiparticles with opposite charge and opposite handedness. On the left-hand side, the "basis vectors" are presented, on the right-hand side, their Hermitian conjugate partners. In the case of $d = (7+1)$ and when taking care of only the internal spaces of fermions and bosons, the discrete symmetry operator $\mathbb{C}_{\mathcal{N}}\mathcal{P}_{\mathcal{N}}^{(d-1)}$, Eq. (24) in [22], simplifies to $\gamma^0\gamma^5\gamma^7$. Having odd numbers of operators γ^a's, it would transform a fermion into a boson. We easily notice that there are no pairs, which would have opposite handedness and opposite charges.

$$
\begin{aligned}
&d = 4n\,,\\
&\hat{b}_1^{1\dagger} = {}^{03\ \ 12\ \ 56\ \ 78}(+i)[+][+][+]\,, \qquad \hat{b}_1^{1} = {}^{03\ \ 12\ \ 56\ \ 78}(-i)[+][+][+]\\
&\hat{b}_1^{2\dagger} = {}^{03\ \ 12\ \ 56\ \ 78}[-i](-)[+][+]\,, \qquad \hat{b}_1^{2} = {}^{03\ \ 12\ \ 56\ \ 78}[-i](+)[+][+]\,,\\
&\hat{b}_1^{3\dagger} = {}^{03\ \ 12\ \ 56\ \ 78}(+i)[+](-)(-)\,, \qquad \hat{b}_1^{3} = {}^{03\ \ 12\ \ 56\ \ 78}(-i)[+](+)(+)\,,\\
&\hat{b}_1^{4\dagger} = {}^{03\ \ 12\ \ 56\ \ 78}[-i](-)(-)(-)\,, \qquad \hat{b}_1^{4} = {}^{03\ \ 12\ \ 56\ \ 78}[-i](+)(+)(+)\,,\\
&\hat{b}_1^{5\dagger} = {}^{03\ \ 12\ \ 56\ \ 78}[-i][+](-)[+]\,, \qquad \hat{b}_1^{5} = {}^{03\ \ 12\ \ 56\ \ 78}[-i][+](+)[+]\\
&\hat{b}_1^{6\dagger} = {}^{03\ \ 12\ \ 56\ \ 78}(+i)(-)(-)[+]\,, \qquad \hat{b}_1^{6} = {}^{03\ \ 12\ \ 56\ \ 78}(-i)(+)(+)[+]\,,\\
&\hat{b}_1^{7\dagger} = {}^{03\ \ 12\ \ 56\ \ 78}[-i][+][+](-)\,, \qquad \hat{b}_1^{7} = {}^{03\ \ 12\ \ 56\ \ 78}[-i][+][+](+)\,,\\
&\hat{b}_1^{8\dagger} = {}^{03\ \ 12\ \ 56\ \ 78}(+i)(-)[+](-)\,, \qquad \hat{b}_1^{8} = {}^{03\ \ 12\ \ 56\ \ 78}(-i)(+)[+](+)\,,
\end{aligned}
\tag{17.18}
$$

rotations concern only S^{ab} and $\tilde{S}^{ab}$, that is only the internal space.

Let us also point out that since each family in this presentation of the internal spaces of fermions and bosons includes fermions and anti-fermions, no negative energy Dirac sea of fermions is needed. The vacuum state is only the quantum vacuum. Correspondingly, our Feynman diagrams can differ from the usual ones with the Dirac sea whenever in the diagram both the fermion and the anti-fermion appear. [2] Eq. (15.5) reminds us that all fermion "basis vectors" are orthogonal, and also their Hermitian conjugate partners are among themselves orthogonal.

17.2.1 "Basis vectors" in $d = (5+1)$ and in $d = (13+1)$

Let us present fermion and boson "basis vectors" for some cases, $d = (5+1)$ and $d = (13+1)$, to understand better the difference between the Feynman diagrams in our case and in most of theories.
In Table 14.1 all odd "basis vectors" and their Hermitian conjugated partners, and all even "basis vectors" of two kinds are presented. Let us check their properties with respect to Eqs. (15.5 - 15.13) to easier follow the discussions on Feynman diagrams.

In Eq. (15.4) we read that either the nilpotents or projectors carry both quantum numbers S^{ab} and S^{ab}. While for fermions the first, S^{ab}, determines the family member quantum number (presented in Table 14.1 for $\hat{b}_f^{m\dagger}$ in the last three columns), and $\tilde{S}^{ab}$ the family quantum number (presented in Table 14.1 for $\hat{b}_f^{m\dagger}$ above each family), are for bosons the quantum numbers, expressed as $\mathcal{S}^{ab} = (S^{ab} + \tilde{S}^{ab})$, for nilpotents of integer values and for projectors zero.

Let us check that the boson "basis vector" ${}^{I}\hat{\mathcal{A}}_1^{4\dagger}(\equiv \overset{03}{(+i)}\overset{12}{(+)}\overset{56}{[+]})$ is expressible by $\hat{b}_1^{1\dagger}(\equiv \overset{03}{(+i)}\overset{12}{[+]}\overset{56}{[+]}) *_A (\hat{b}_1^{2\dagger})^{\dagger}(\equiv \overset{03}{[-i]}\overset{12}{(+)}\overset{56}{[+]})$. One can check this by recognizing that, $\overset{03}{(+i)} *_A \overset{03}{[-i]} = \overset{03}{(+i)}$, $\overset{12}{[+]} *_A \overset{12}{(+)} = \overset{12}{(+)}$ and $\overset{56}{[+]} *_A \overset{56}{[+]} = \overset{56}{[+]}$, which can be calculated using Eq. (15.2), or read in Eq. (15.19) of the footnote [3]. Using this footnote one easily finds that all odd "basis vectors" are orthogonal, as well are orthogonal among themselves all Hermitian conjugated partners.

---

[2] We should also not forget that our second quantised fields, when they have an odd number of nilpotents, anti-commute; when they have an even number of nilpotents, they commute: They are second quantised fields needing no postulates.

[3]

$$
\begin{aligned}
&\overset{ab}{(k)}\overset{ab}{(-k)} = \eta^{aa}\overset{ab}{[k]}\,, \quad \overset{ab}{(-k)}\overset{ab}{(k)} = \eta^{aa}\overset{ab}{[-k]}\,, \quad \overset{ab}{(k)}\overset{ab}{[k]} = 0\,, \quad \overset{ab}{(k)}\overset{ab}{[-k]} = \overset{ab}{(k)}\,,\\
&\overset{ab}{(-k)}\overset{ab}{[k]} = \overset{ab}{(-k)}\,, \quad \overset{ab}{[k]}\overset{ab}{(k)} = \overset{ab}{(k)}\,, \quad \overset{ab}{[k]}\overset{ab}{(-k)} = 0\,, \quad \overset{ab}{[k]}\overset{ab}{[-k]} = 0\,.
\end{aligned}
\tag{17.19}
$$

If we call $\hat{b}^{1\dagger}_1(\equiv(\overset{03}{+i})\overset{12}{[+]}\overset{56}{[+]})$ the fermion with the spin $\uparrow$ having the charge $\frac{1}{2}$ ($S^{56}\ \overset{56}{[+]} = \frac{1}{2}\ \overset{56}{[+]}$) and the right handedness, then we can call $\hat{b}^{3\dagger}_1(\equiv\overset{03}{[-i]}\overset{12}{[+]}\overset{56}{(-)})$ its anti-fermion with the spin $\uparrow$ having the charge $-\frac{1}{2}$ and the left handedness.

Table 14.1, made for $d = (5+1)$, contains four families with four odd "basis vectors" for fermions. Each family contains two fermions with the positive charge, $S^{56} = \frac{1}{2}$, one with the spin up, $\uparrow$, and the other with spin down, $\downarrow$; and two anti-fermions, again one with the spin up, $\uparrow$, and one with the spin down, $\downarrow$. The tensor product with the basis in ordinary space, Eq. (15.15), represent fermions and anti-fermions - a kind of electrons and positrons, in this model.
Moreover, we have 16 corresponding Hermitian conjugate partners.
From these 16 odd "basis vectors", $\hat{b}^{m\dagger}_f$, and their 16 Hermitian conjugated partners, $\hat{b}^{m}_f$, we construct two groups of 16 even "basis vectors", representing the internal spaces of bosons, presented in Table 14.1 as ${}^{I}\hat{\mathcal{A}}^{m\dagger}_f$ and ${}^{II}\hat{\mathcal{A}}^{m\dagger}_f$. The tensor products of even "basis vectors" with the basis in the ordinary space-time, and with the space index $\alpha = \mu \leq 3$ or $\alpha = \sigma \geq 5$, Eq. (15.15), represent two kinds of boson fields, describing besides gravitons and photons also additional vector boson fields and scalars.

Let us study some of the even "basis vectors", representing ${}^{I}\hat{\mathcal{A}}^{m\dagger}_f$ and ${}^{II}\hat{\mathcal{A}}^{m\dagger}_f$, looking for them either as algebraic products of fermions and their Hermitian conjugated partners, or by using Eqs. (15.10, 15.11).
One can find ${}^{I}\hat{\mathcal{A}}^{2\dagger}_3$ by the algebraic product of $\hat{b}^{2\dagger}_1\ *_A\ (\hat{b}^{1\dagger}_1)^\dagger$:

$$\hat{b}^{2\dagger}_1(\equiv\overset{03}{[-i]}\overset{12}{(-)}\overset{56}{[+]})\ *_A\ (\hat{b}^{1\dagger}_1)^\dagger(\equiv(\overset{03}{+i})\overset{12}{[+]}\overset{56}{[+]})^\dagger \rightarrow {}^{I}\hat{\mathcal{A}}^{2\dagger}_3(\equiv\overset{03}{(-i)}\overset{12}{(-)}\overset{56}{[+]},$$

or by looking for ${}^{I}\hat{\mathcal{A}}^{m\dagger}_f$, which applying on $\hat{b}^{1\dagger}_1$ transforms it to $\hat{b}^{2\dagger}_1$:

$${}^{I}\hat{\mathcal{A}}^{m\dagger}_f(\equiv\overset{03}{(-i)}\overset{12}{(-)}\overset{56}{[+]})\ *_A\ \hat{b}^{1\dagger}_1(\equiv(\overset{03}{+i})\overset{12}{[+]}\overset{56}{[+]}) \rightarrow \hat{b}^{2\dagger}_1(\equiv\overset{03}{[-i]}\overset{12}{(-)}\overset{56}{[+]}).$$

This ${}^{I}\hat{\mathcal{A}}^{m\dagger}_f(\equiv\overset{03}{(-i)}\overset{12}{(-)}\overset{56}{[+]}) = {}^{I}\hat{\mathcal{A}}^{2\dagger}_3$, transforms the fermion of right-handedness with spin up to the fermion of right-handedness with spin down. **We recognise it as the even "basis vector" of graviton** (which in tensor product with the basis in ordinary space-time and carrying the space index μ presents the graviton). In Table 14.1 is placed on the second line of the third column.

The even "basis vector" of the graviton which transforms $\hat{b}^{2\dagger}_1$ into $\hat{b}^{1\dagger}_1$ is ${}^{I}\hat{\mathcal{A}}^{1\dagger}_4(\equiv(\overset{03}{+i})\overset{12}{(+)}\overset{56}{[+]}$), appearing in the first line of the fourth column.
The even "basis vector" of the **graviton in** $d = (13+1)$, which would transform the right-handed electron with spin up into the right-handed electron with spin down, presented in Table 6 of the Ref. [6] on the 27 and 28 lines, would have a similar construction as ${}^{I}\hat{\mathcal{A}}^{2\dagger}_3$, namely ${}^{I}\hat{\mathcal{A}}^{\dagger}_{e^-_{R\uparrow}\rightarrow e^-_{R\downarrow}}(\equiv\overset{03}{(-i)}\overset{12}{(-)}\overset{56}{[-]}\overset{78}{[-]}\overset{9\,10}{[+]}\ \overset{11\,12}{[+]}\overset{13\,14}{[+]}$; all the eigenvalues of the Cartan subalgebra members except $\overset{03}{(-i)}\overset{12}{(-)}$ must be zero, that means that the only nilpotents must appear in the first two columns, all the

rest must be projectors.

The even "basis vectors" representing the internal space of photons, having no charges, must be constructed from only projectors, either in the internal space of $d=(5+1)$, or in the internal space of $d=(13+1)$.

Let us generate some of the even "basis vectors" of the second group ${}^{II}\hat{\mathcal{A}}^{m\dagger}_{f}$, presented at Table 14.1 in the last four columns. We can do this with the algebraic products of Hermitian conjugated partners of the even "basis vectors" and the even "basis vectors", Eq. (15.13), or by using Eq. (15.11).

$$ {}^{II}\hat{\mathcal{A}}^{1\dagger}_{3}(\equiv \overset{03}{[-i]}\overset{12}{[+]}\overset{56}{[+]}) = (\hat{b}^{1\dagger}_{1})^{\dagger} *_{A} \hat{b}^{1\dagger}_{1}$$

.
Eq. (15.11) requires:

$$ \hat{b}^{1\dagger}_{1}(\equiv \overset{03}{(+i)}\overset{12}{[+]}\overset{56}{[+]}) *_{A} {}^{II}\hat{\mathcal{A}}^{1\dagger}_{3}(\equiv \overset{03}{[-i]}\overset{12}{[+]}\overset{56}{[+]}) \rightarrow \hat{b}^{1\dagger}_{1}$$

.
Let be added that ${}^{II}\hat{\mathcal{A}}^{1\dagger}_{3} = (\hat{b}^{2\dagger}_{1})^{\dagger} *_{A} \hat{b}^{2\dagger}_{1} = (\hat{b}^{m\dagger}_{1})^{\dagger} *_{A} \hat{b}^{m\dagger}_{1}$, for all $m=(1,2,3,4)$ of the first family.

One can check that the same is true also for all the members of Table 6 of Ref. [6]; Any of the 64 members, either quarks or leptons, as well as antiquarks and antileptons of this family generates the same ${}^{II}\hat{\mathcal{A}}^{\dagger}_{e^{-}_{R\uparrow}\rightarrow e^{-}_{R\uparrow}}$

$$ {}^{II}\hat{\mathcal{A}}^{\dagger}_{e^{-}_{R\uparrow}\rightarrow e^{-}_{R\uparrow}}(\equiv \overset{03}{[-]}\overset{12}{[+]} \mid \overset{56}{[+]}\overset{78}{[-]} \parallel \overset{9}{[-]}\overset{10}{[-]}\overset{11}{[-]}\overset{12}{[-]}\overset{13}{[-]}\overset{14}{[-]} = (e^{-}_{R\uparrow})^{\dagger}(\equiv \overset{03}{(+i)}\overset{12}{[+]} \mid \overset{56}{(-)}\overset{78}{[-]} \parallel \overset{9}{(+)}\overset{10}{(+)}\overset{11}{(+)}\overset{12}{(+)}\overset{13}{(+)}\overset{14}{(+)})^{\dagger} *_{A} e^{-}_{R\uparrow}$$

.

17.2.2 Feynman diagrams in our way and questions to be answered

The action for fermion and boson second quantised fields, Eq. (15.17), demonstrating the relations among fermion and boson "basis vectors", presented in Eqs. (15.8 - 15.13), determines Feynman diagrams for our description of internal spaces.

Let us shortly repeat the differences between our way of describing the internal spaces of fermion and boson fields, and the usual way - the most noticeable differences:
a. The odd (anti-commuting) "basis vectors", describing the internal spaces of fermion fields appear in families ($2^{\frac{d}{2}-1}$); In ordinary theories, the families are postulated, and the anti-commutativity is postulated; the internal spaces of fermions are described by matrices in fundamental representations;
b. Each family (with $2^{\frac{d}{2}-1}$ members) contains in $d=2(2n+1)$ "basis vectors" of fermions and anti-fermions, the Hermitian conjugate partner of the odd "basis vectors" of fermions appear in a separate group, no Dirac sea is correspondingly

needed, as we see in Table 14.1 for $d=(5+1)$, and in Table 2 in the reference [6] for $d=(13+1)$; In ordinary theories, the antifermions are postulated as the holes in the Dirac sea; The interpretation of a particle-antiparticle pair as the particle taken out of the Dirac sea, while a missing particle in the Dirac sea is interpreted as an antiparticle, requires that a particle-antiparticle annihilation is interpreted as the particle going back to the Dirac sea;

c. The algebraic products of odd "basis vectors", independently to which family they belong, are mutually orthogonal, Eq. (15.5), and so are mutually orthogonal also their Hermitian conjugate partners; The algebraic products of the odd "basis vectors" with their Hermitian conjugate partners are non-zero;

$$\begin{aligned} \hat{b}^{m\dagger}_{f} *_A \hat{b}^{m'\dagger}_{f} = 0\,, \quad \hat{b}^{m}_{f} *_A \hat{b}^{m'}_{f} = 0\,, \\ \forall\,(m,m',f)\,, \\ \hat{b}^{m}_{f} *_A \hat{b}^{m'\dagger}_{f} \neq 0\,; \end{aligned} \tag{17.20}$$

However, in the case $d=4n$, the families include only fermions, no antifermions. In this case the Dirac sea might help. Namely, if we choose the appropriate families, the Hermitian conjugate values of charges of the odd "basis vectors" can have the opposite values for charges as the "basis vectors". Let us treat the case SO(7,1), choosing the families, so that the Hermitian conjugate partners carry the opposite charge. It is not difficult to continue this Eq. (15.21) with the choices of appropriate families for the remaining four cases. However, this construction, jumping among different families, is unacceptable. A better advice is to enlarge the internal space to $d=2(2n+1)$.

$$\begin{aligned} & d=4n\,, \\ \hat{b}^{1\dagger}_{2} =& (+i)[+](+)(+)^{03\;12\;56\;78}\,, \qquad \hat{b}^{1}_{2} = (-i)[+](-)(-)^{03\;12\;56\;78} \\ \hat{b}^{2\dagger}_{2} =& [-i](-)(+)(+)^{03\;12\;56\;78}\,, \qquad \hat{b}^{2}_{2} = [-i](+)(-)(-)^{03\;12\;56\;78}\,, \\ \hat{b}^{3\dagger}_{1} =& (+i)[+](-)(-)^{03\;12\;56\;78}\,, \qquad \hat{b}^{3}_{1} = (-i)[+](+)(+)^{03\;12\;56\;78}\,, \\ \hat{b}^{4\dagger}_{1} =& [-i](-)(-)(-)^{03\;12\;56\;78}\,, \qquad \hat{b}^{4}_{1} = [-i](+)(+)(+)^{03\;12\;56\;78}\,, \end{aligned} \tag{17.21}$$

(In addition, this construction limits the number of families to only one family. Correspondingly, the families must be postulated "by hand".)

d. The commuting "basis vectors", describing the internal spaces of boson fields appear in two orthogonal groups, having their Hermitian conjugated partners within each group; The ordinary theories recognise only one kind of fields (although the scalar fields might be recognised as the second kind), the commutativity is postulated;

e. Both commuting "basis vectors" are expressible by algebraic products of odd "basis vectors" and their Hermitian conjugated partners, Eqs. (15.12, 15.13); Ordinary theories describe internal spaces of bosons with matrices in the adjoint representations;

The differences in the description of the internal spaces of fermion and boson fields in our case, and in usual cases, cause the differences in presenting Feynman diagrams.

The most noticeable difference is that our description of the internal spaces of fermion fields tells us that all the odd "basis vectors" are mutually orthogonal, Eq. (15.5), and so are mutually orthogonal also their Hermitian conjugate partners. We expect that our Feynman diagrams will differ from the usual ones when fermions and antifermion meet.
In our case, the two odd "basis vectors" can interact only by exchanging a boson represented with the even "basis vectors", as demonstrated in Eqs.(15.10, 15.11). The particle in ordinary theories (leaving the hole in the Dirac sea) resembles our particle (except that our particles are massless, and have their internal space presented by odd "basis vectors", and not by matrices), while the antiparticle (in ordinary theories, its hole in the Dirac sea), does not really resemble our antiparticle (of opposite charges to the particles, belonging to the same family [6], unless the break of symmetry mixes families, bringing them masses. Our antiparticles move in the same way as particles; this is not the case with the hole in the Dirac sea.
Let us start with drawing the Feynman diagram for a fermion, representing an electron, with the internal space described by the odd "basis vector" $\hat{b}^{1\dagger}_1(\equiv(\overset{03}{+}\overset{12}{i})\overset{56}{[+][+]})$, Table 14.1, with the momentum $\vec{p}_1$, radiating the photon with the even "basis vector" ${}^{II}\hat{\mathcal{A}}^{1\dagger}_3(\equiv[\overset{03}{-}\overset{12}{i}\overset{56}{][+][+]}\equiv (\hat{b}^{1\dagger}_1)^\dagger *_A \hat{b}^{1\dagger}_1)$ with the momentum $\vec{p}_3$, while the electron with the odd "basis vector" $\hat{b}^{1\dagger}_1$; $\hat{b}^{1\dagger}_1(\equiv(\overset{03}{+}\overset{12}{i})\overset{56}{[+][+]}) *_A {}^{II}\hat{\mathcal{A}}^{1\dagger}_3(\equiv[\overset{03}{-}\overset{12}{i}\overset{56}{][+][+]}) \rightarrow \hat{b}^{1\dagger}_1$; continues its way with smaller momentum $\vec{p}_2$. This event, when an electron radiates a photon, is presented in Fig. 15.1. The equivalent diagram is valid also for the electron in the ordinary theories, only the photon will not be described in our way.

The equivalent Feynman diagram represents, in the case that the odd "basis vectors" describe the internal space of fermions, also the event that a positron, with the internal space described by $\hat{b}^{3\dagger}_1(\equiv[\overset{03}{-}\overset{12}{i}\overset{56}{][+](-)})$, Table 14.1, and with the momentum $\vec{p}_1$ in ordinary space, radiates a photon with the internal space represented by the even "basis vector" ${}^{II}\hat{\mathcal{A}}^{1\dagger}_3(\equiv[\overset{03}{-}\overset{12}{i}\overset{56}{][+][+]}\equiv (\hat{b}^{3\dagger}_1)^\dagger *_A \hat{b}^{3\dagger}_1)$. Either the electron or the positron belongs to the same family. (Their algebraic products are zero.) However, the corresponding Feynman diagram in the usual theories, representing the positron, should have the arrows for the positron turned back, $\uparrow$ should be turned into $\downarrow$.

The event, when a positron $\hat{b}^{3\dagger}_1$ radiates a photon ${}^{II}\hat{\mathcal{A}}^{1\dagger}_3$, is presented in Fig. 15.2.

Since the fermions in our case differ from fermions in the usual theory - our fermions and antifermions belong to the same family, while the families distinguish among themselves only in the family quantum numbers - let us see how we can draw the Feynman rule for the annihilation of an electron and positron in the case that the internal space has $d = 2(2n + 1)$, the most promising is $d = (13 + 1)$ dimensions, this choice offers all the quarks and leptons and antiquarks and antileptons, observed at low energies in an elegant way, treating all the boson fields in an equivalent way, with gravitons included. We take Figure 2 from

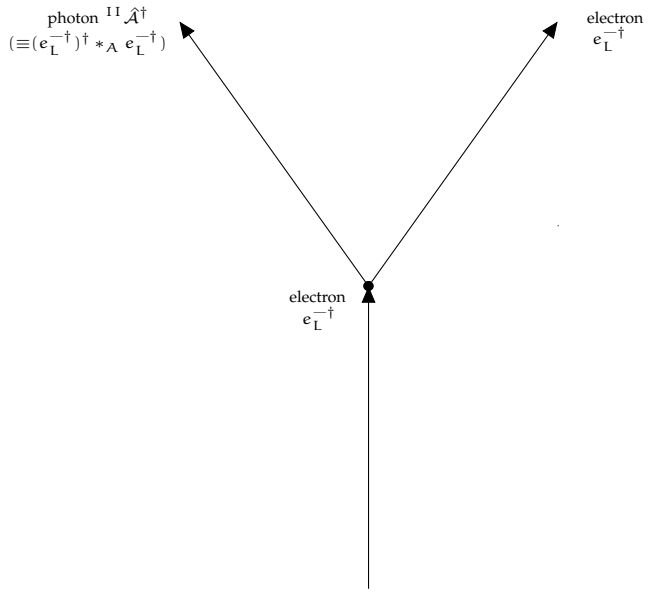

Fig. 17.1: An electron, with the internal space described by $\hat{b}_1^{1\dagger}$ and with the momentum $\vec{p}_1$ in ordinary space, Table 14.1, radiates the photon with the "basis vector" ${}^{II}\hat{\mathcal{A}}_3^{1\dagger}(\equiv[-i][+][+]\equiv (\hat{b}_1^{1\dagger})^{\dagger} *_A \hat{b}_1^{1\dagger})$, with the momentum $\vec{p}_3$, while the electron, $\hat{b}_1^{1\dagger}$, continues its way with a smaller momentum $\vec{p}_2$, Fig. 15.1. This diagram is representing also the electron in the usual theories, except that photons are not presented in our way. For the electron with the "basis vector", $e_L^{-\dagger}(\equiv[-i][+](-)(+)(+)\,(+)\,(+)\,)$, from Table 2 in Ref. [6], the photon with the "basis vector" ${}^{II}\hat{\mathcal{A}}^{\dagger}(\equiv\,(e_L^{-\dagger})^{\dagger} *_A e_L^{-\dagger} \equiv[-i][+]\,[+][-][-]\,[-]\,\,[-]\,)$ takes away the momentum.

.

Ref. [22]. Looking at the figure 15.3, we see that they differ from the corresponding Feynman diagram for the electron-positron annihilation in usual theories: The photon ${}^{II}\hat{\mathcal{A}}^{\dagger}_{phe^{\dagger}e}$ going from electron to positron and back, is, in usual theories, replaced by a straight line representing the electron, which, after radiating a photon, continues its way up to the positron, which is going down instead of going up in our case - $\uparrow$ should be turned into $\downarrow$.
We can use figures 15.1 and 15.2 to try to make the diagram as close to the usual diagrams as possible. Let us try this.
Taking into account figures 15.1 and 15.2, to try to make the diagram as close to the usual diagrams as possible, lead to Fig. 15.4.
Although the Feynman diagram for the electron-positron annihilation, presented in Fig. 15.4, seems quite close to what we are looking for, it leaves open the question whether the electron and positron transfer all the momentum to the two

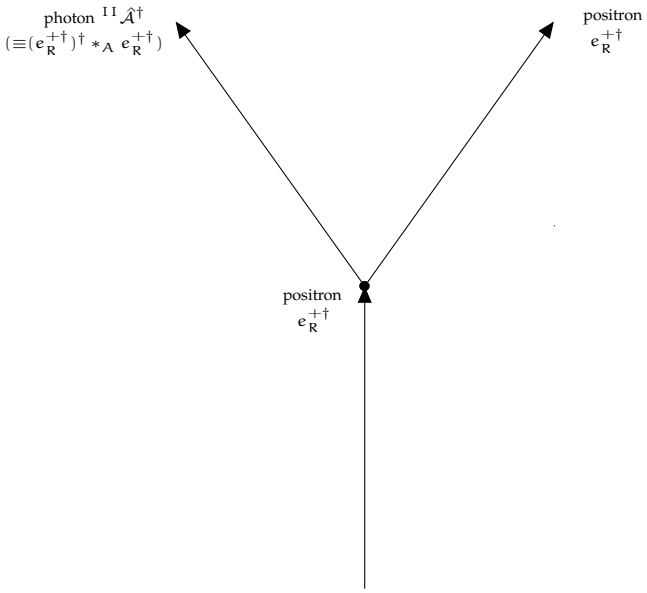

Fig. 17.2: A positron, with the internal space described by $\hat{b}_1^{3\dagger}$ and with the momentum $\vec{p}_1$ in ordinary space, Table 14.1, radiates the photon with the "basis vector" ${}^{II}\hat{\mathcal{A}}_3^{1\dagger}(\equiv[-i]^{03}[+]^{12}[+]^{56}\equiv (\hat{b}_1^{3\dagger})^{\dagger} *_A \hat{b}_1^{3\dagger} = (\hat{b}_1^{1\dagger})^{\dagger} *_A \hat{b}_1^{1\dagger})$, with the momentum $\vec{p}_3$, while the positron, $\hat{b}_1^{3\dagger}$, continues its way with smaller momentum $\vec{p}_2$, Fig. 15.2. For the positron with the "basis vector", $e_R^{+\dagger}(\equiv(+i)^{03}[+]^{12}[+]^{56}[-]^{78}[-]^{9\,10}\ [-]^{11\,12}\ [-]^{13\,14})$, from Table 2 in Ref. [6], the photon with the "basis vector" ${}^{II}\hat{\mathcal{A}}^{\dagger}(\equiv (e_R^{+\dagger})^{\dagger} *_A e_R^{+\dagger} \equiv[-i]^{03}[+]^{12}$ $[+]^{56}[-]^{78}[-]^{9\,10}\ [-]^{11\,12}\ [-]^{13\,14})$ takes away the momentum. The corresponding Feynman diagram in the usual theories, representing the positron should have the arrows for the positron turned back, $\uparrow$ should be turned into $\downarrow$.

.

photons.

Let us try with a slightly different interpretation. The electron $e_L^{-\dagger}$ radiates a photon $(e_L^{-\dagger})^{\dagger} *_A e_L^{-\dagger}$, turns to the right and meets a positron $e_R^{+\dagger}$ who already emitted a photon $(e_R^{+\dagger})^{\dagger} *_A e_R^{+\dagger}$, and has turned to the left. They go together into the quantum vacuum without the momenta in ordinary space-time, as presented in Fig. 15.5.
The symbolic diagram with the electron and the positron going into the vacuum "simultaneously" is of course expected to be/become the usual propagator for a fermion.
We might argue for that by writing down the properties which this propagator-like operator must have with respect to symmetries (the vacuum must remain

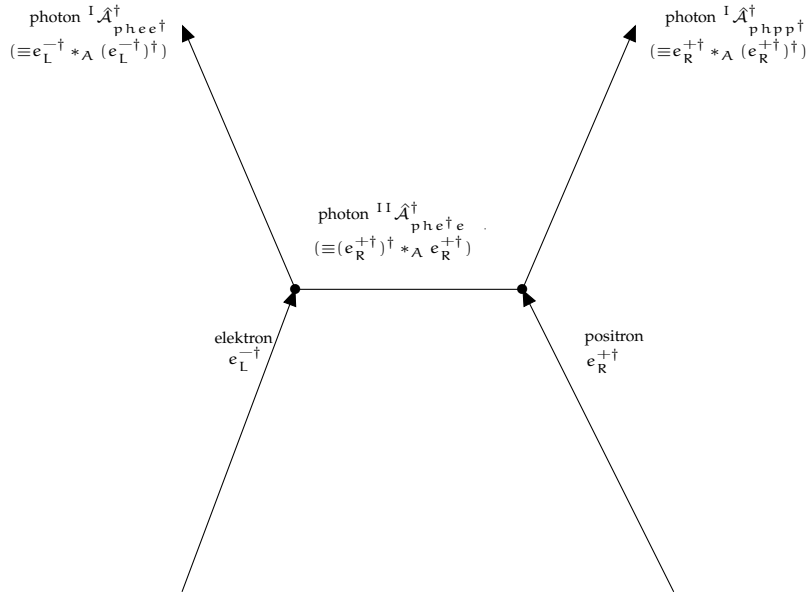

Fig. 17.3: The figure is taken from Fig. 2 in Ref. [22]. Annihilation of an electron, $e^{-\dagger}_{\mathrm{L}}$, and positron, $e^{+\dagger}_{\mathrm{R}}$, into two photons, is studied for the case that the internal space has $(13+1)$ dimensions; the internal spaces of $e^{-\dagger}_{\mathrm{L}}$ and $e^{+\dagger}_{\mathrm{R}}$ are taken from Table 2 Ref. [6], from the line 29^{th} and 63^{rd}, respectively, and the "photons" are generated following the procedure for the case that the internal space has $(5+1)$ dimensions. The "basis vector" of an electron carries the charge $Q=-1$ (in the ordinary space the electron has the momentum $\vec{p}_1$), the "basis vector" of its anti-particle positron carries $Q=+1$ (in ordinary space positron has momentum $\vec{p}_2$). The "basis vectors" of two photons taking away the momenta $\vec{p}_1$ and $\vec{p}_2$, named ${}^{\mathrm{I}}\hat{\mathcal{A}}^{\dagger}_{\mathrm{phee}^{\dagger}}$ and ${}^{\mathrm{I}}\hat{\mathcal{A}}^{\dagger}_{\mathrm{phpp}^{\dagger}}$, respectively, are represented by $e^{-\dagger}_{\mathrm{L}} *_{\mathcal{A}} (e^{-\dagger}_{\mathrm{L}})^{\dagger}$ and $e^{+\dagger}_{\mathrm{R}} *_{\mathcal{A}} (e^{+\dagger}_{\mathrm{R}})^{\dagger}$, respectively. The "basis vector" of a photon, ${}^{\mathrm{II}}\hat{\mathcal{A}}^{\dagger}_{\mathrm{phe}^{\dagger}\mathrm{e}} = {}^{\mathrm{II}}\hat{\mathcal{A}}^{\dagger}_{\mathrm{php}^{\dagger}\mathrm{p}}$, exchanged by $e^{-\dagger}_{\mathrm{L}}$ and $e^{+\dagger}_{\mathrm{R}}$, is equal to $(e^{-\dagger}_{\mathrm{L}})^{\dagger} *_{\mathcal{A}} e^{-\dagger}_{\mathrm{L}} = (e^{+\dagger}_{\mathrm{R}})^{\dagger} *_{\mathcal{A}} e^{+\dagger}_{\mathrm{R}}$ (due to the fact that $e^{-\dagger}_{\mathrm{L}}$ and $e^{+\dagger}_{\mathrm{R}}$ belong to the same family). This exchange results in transferring the momenta $\vec{p}_1$ and $\vec{p}_2$ from $e^{-\dagger}_{\mathrm{L}}$ and $e^{+\dagger}_{\mathrm{R}}$, to the two photons ${}^{\mathrm{I}}\hat{\mathcal{A}}^{\dagger}_{\mathrm{phee}^{\dagger}}$ and ${}^{\mathrm{I}}\hat{\mathcal{A}}^{\dagger}_{\mathrm{phpp}^{\dagger}}$, respectively, leaving the "basis vectors" $e^{-\dagger}_{\mathrm{L}}$ and $e^{+\dagger}_{\mathrm{R}}$ without momenta in ordinary space, in the quantum vacuum.

.

symmetric under the symmetries of the theory) and the properties of causality as to which particle is to propagate only forward in time.
In the present article, we shall postpone these arguments for getting the usual propagator, but it is, of course, logically needed to argue for it. If one assumes the usual Dirac sea vacuum, it should be rather obvious what our line with the vacuum blob in the middle must be.

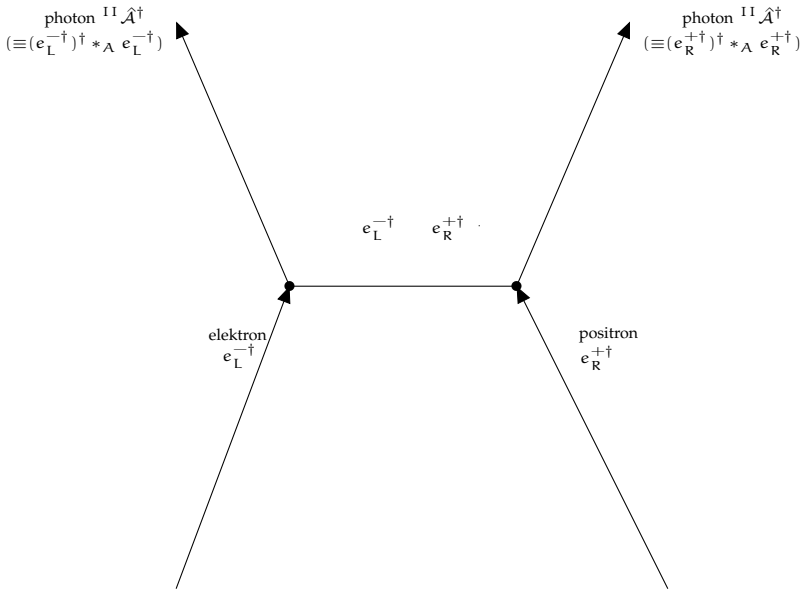

Fig. 17.4: The left-hand side represents the path of the electron, $e_L^{-\dagger}$, which radiates a photon $(e_L^{-\dagger})^{\dagger} *_A e_L^{-\dagger}$, and continues its way straight to the right, up to a positron, $e_R^{+\dagger}$ coming up. They both radiate a photon $(e_L^{-\dagger})^{\dagger} *_A e_L^{-\dagger}$ and $(e_R^{+\dagger})^{\dagger} *_A e_R^{+\dagger}$ (both are of the same kind) and remain without momenta in the quantum vacuum. It can also happen the opposite: The positron, $e_R^{+\dagger}$, radiates a photon $(e_R^{+\dagger})^{\dagger} *_A e_R^{+\dagger}$, and continues its way straight to the left, up to an electron, $e_L^{-\dagger}$ coming up from the left hand side. Both radiate a photon $(e_L^{-\dagger})^{\dagger} *_A e_L^{-\dagger}$ of the same kind. Both remain without momentum in the quantum vacuum.

.

We need in the next step to present all the measured Feynman diagrams in our way; that is, with fermions (quarks and leptons and antiquarks and antileptons), whose internal space is described by the odd “basis vectors”, the “basis vectors” with the odd number of nilpotents, which are all mutually orthogonal, and with bosons (gravitons, weak bosons, photons, gluons, scalars), whose internal spaces are described by the even "basis vectors ” the “basis vectors” with the even number of nilpotents, which appear in two orthogonal groups. We must see whether we can agree with the experiments and find a way to represent them that we will agree on.

17.3 Presenting open problems concerning Feynman diagrams

Accepting the idea of the papers [10, 20–22] that *the internal spaces (spins and charges) of fermions and bosons are described by “basis vectors” which are the odd* (for fermions [9]) *and even* (for bosons) *products of nilpotents*, Eq. (15.2), the authors are trying to find out whether and up to what extent “nature manifests” the proposed

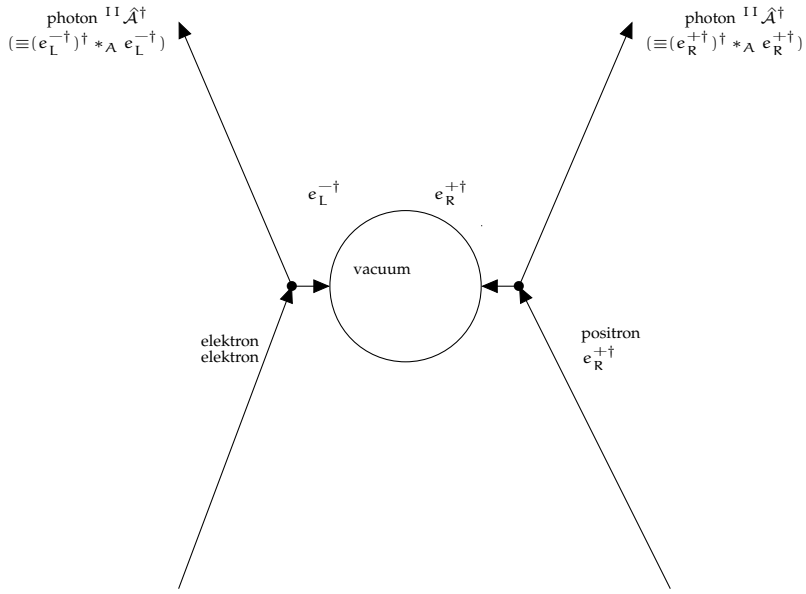

Fig. 17.5: The electron $e_L^{-\dagger}$ radiates a photon ${}^{I}\hat{\mathcal{A}}^{\dagger}_{phee^{\dagger}}(\equiv e_L^{-\dagger} *_A (e_L^{-\dagger})^{\dagger})$, and goes to the right to the vacuum. The positron $e_L^{+\dagger}$, radiates a photon ${}^{I}\hat{\mathcal{A}}^{\dagger}_{phpp^{\dagger}}(\equiv e_R^{+\dagger} *_A (e_R^{+\dagger})^{\dagger}$, and turning to the left remains with electron in the vacuum.

idea, offering hopefully the unifying theory of gravity, all the gauge fields, the scalar fields, and the fermion and antifermion fields.

In this contribution, we study *massless fermion and boson fields under the condition that they have non-zero momentum only in* $d = (3+1)$, *while internal spaces have* $d = 2(2n+1)$, the choice of $d = (13+1)$ offers the description of the second quantised quarks, leptons and antiquarks and antileptons and of all the second quantised vector (gravitons, weak bosons, photons, gluons) and scalar fields.

Let us mention again that if we choose the internal space with $d = 4n$, that is $d = (4n-1)+1$, the families include only fermions, no antifermions; Eq. (15.18) manifests the properties of the corresponding "basis vectors" in the case that $4n = 7+1$. (In such cases, the Dirac sea would be needed. The more elegant choice is to enlarge the internal space to $d = 4n+2$, as it is $d = (13+1)$, which offer the description that quarks and leptons distinguish only in the $SO(6)$ part of $SO(13+1)$, and antiquarks and antileptons distinguish only in the $SO(6)$ part of $SO(13+1)$.)

All the fields are tensor products of the odd (fermion fields) and even (boson fields) "basis vectors" and basis in ordinary space-time, while the boson fields have in addition the space index α ($\alpha = \mu = (0,1,2,3)$ for vectors, and $\alpha = \sigma \geq 5$) for scalars). We correspondingly have the Poincaré symmetry only in $d = (3+1)$.

The algebraic products of "basis vectors" of boson and fermion fields determine the action for fermions and bosons, Eqs. (15.5- 15.16).

The odd (anti-commuting) "basis vectors", appear in families, including in $d = 2(2n+1)$ fermions and antifermions (all odd "basis vectors" are mutually orthogonal, Hermitian conjugate partner of the odd "basis vectors" appear in a separate group, no Dirac sea is correspondingly needed); In ordinary theories, the families are postulated, and the anti-commutativity is postulated; matrices describe the internal spaces of fermions in fundamental representations; The antifermions are postulated as the holes in the Dirac sea.
The even (commuting) "basis vectors", appear in the proposed theory in two orthogonal groups; and all even "basis vectors" are expressible by algebraic products of odd "basis vectors" and their Hermitian conjugate partners. In ordinary theories, instead of our even "basis vectors" the matrices in adjoint representations are used.
The difference in properties of the second-quantised fields in the proposed theory and the ordinary theories require, among many other things, studying also the Feynman diagrams and compare them to the experimentally confirmed the Feynman diagrams of the ordinary theories.
The Feynman diagram for electron-positron annihilation, presented in Fig. 15.3, looks unacceptable in comparison with the Feynman diagram for electron-positron annihilation in ordinary theories. Figs. 15.4 and 15.5 seems quite close to what we are looking for. The symbolic diagram with the electron and the positron going into the vacuum "simultaneously" is expected to become the usual propagator for a fermion.
In the present article, we postponed the arguments about the properties which the propagator-like operator must have with respect to symmetries of the theory and the properties of causality.
We need to present all the measured Feynman diagrams in our way; that is, with fermions (quarks and leptons, antiquarks and antileptons), whose internal space is described by the odd "basis vectors", which are all mutually orthogonal, and with bosons (gravitons, weak bosons, photons, gluons, scalars), whose internal space is described by the even "basis vectors" which appear in two orthogonal groups. We expect that we can agree with the experiments and find a way to represent them that we will agree on.
Let us conclude by saying that if we describe the internal spaces of fermions and bosons with the "basis vectors" in $d = (13+1)$, and assume that fermion and boson fields have non-zero momentum only in $d = (3+1)$ of the ordinary space-time, then we unify gravity and all the gauge fields: $SO(3,1)$ determines spins and handedness of gravitons, fermions, and antifermions, $SU(2) \times SU(2)$ determine weak charges of fermions and bosons, $SU(3) \times U(1)$ determine the colour charges of quarks and antiquarks and gluons. Photons' "basis vectors" are products of only projectors, with all spins and charges equal to zero, gravitons' "basis vectors" have two nilpotents only in $SO(3,1)$ part of $SO(13,1)$, weak bosons' "basis vectors" have two nilpotents in $SU(2)$ part of $SO(13,1)$, gluons' "basis vectors" have two nilpotents in $SO(6)$ part of $SO(13,1)$. Fermions' "basis vectors" have odd number of nilpotents spread over $SO(13,1)$. They appear in families.

17.4 Appendix: A useful table

Table 1: This table, taken from [20], represents $2^d = 64$ "eigenvectors" of the Cartan subalgebra, Eq. (3), members of odd and even "basis vectors" which are the superposition of odd and even products of γ^a's in $d = (5+1)$-dimensional internal space, divided into four groups. The first group, *odd I*, is chosen to represent "basis vectors", named $\hat{b}^{m\dagger}_f$, appearing in $2^{\frac{d}{2}-1} = 4$ "families" ($f = 1,2,3,4$), each "family" having $2^{\frac{d}{2}-1} = 4$ "family" members ($m = 1,2,3,4$). The second group, *odd II*, contains Hermitian conjugated partners of the first group for each "family" separately, $\hat{b}^m_f = (\hat{b}^{m\dagger}_f)^\dagger$. Either *odd I* or *odd II* are products of an odd number of nilpotents (one or three) and projectors (two or none). The "family" quantum numbers of $\hat{b}^{m\dagger}_f$, that is the eigenvalues of $(\tilde{S}^{03}, \tilde{S}^{12}, \tilde{S}^{56})$, appear for the first *odd I* group above each "family", the quantum numbers of the "family" members (S^{03}, S^{12}, S^{56}) are written in the last three columns. For the Hermitian conjugated partners of *odd I*, presented in the group *odd II*, the quantum numbers (S^{03}, S^{12}, S^{56}) are presented above each group of the Hermitian conjugated partners, the last three columns tell eigenvalues of $(\tilde{S}^{03}, \tilde{S}^{12}, \tilde{S}^{56})$. Each of the two groups with the even number of γ^a's, *even I* and *even II*, has their Hermitian conjugated partners within its group. The quantum numbers f, that is the eigenvalues of $(\tilde{S}^{03}, \tilde{S}^{12}, \tilde{S}^{56})$, are written above column of four members, the quantum numbers of the members, (S^{03}, S^{12}, S^{56}), are written in the last three columns. To find the quantum numbers of $(\mathbf{S}^{03}, \mathbf{S}^{12}, \mathbf{S}^{56})$ one has to take into account that $\mathbf{S}^{ab} = S^{ab} + \tilde{S}^{ab}$.

"basis vectors" $(\tilde{S}^{03}, \tilde{S}^{12}, \tilde{S}^{56})$	m $\rightarrow$	$f=1$ $(\frac{i}{2}, -\frac{1}{2}, -\frac{1}{2})$	$f=2$ $(-\frac{i}{2}, -\frac{1}{2}, \frac{1}{2})$	$f=3$ $(-\frac{i}{2}, \frac{1}{2}, -\frac{1}{2})$	$f=4$ $(\frac{i}{2}, \frac{1}{2}, \frac{1}{2})$	S^{03}	S^{12}	S^{56}
odd I $\hat{b}^{m\dagger}_f$	1	$^{03\ \ 12\ \ 56}_{(+i)[+][+]}$	$^{03\ \ 12\ \ 56}_{[+i][+](+)}$	$^{03\ \ 12\ \ 56}_{[+i](+)[+]}$	$^{03\ \ 12\ \ 56}_{(+i)(+)(+)}$	$\frac{i}{2}$	$\frac{1}{2}$	$\frac{1}{2}$
	2	$[-i](-)[+]$	$(-i)(-)(+)$	$(-i)[-][+]$	$[-i][-](+)$	$-\frac{i}{2}$	$-\frac{1}{2}$	$\frac{1}{2}$
	3	$[-i][+](-)$	$(-i)[+][-]$	$(-i)(+)(-)$	$[-i](+)[-]$	$-\frac{i}{2}$	$\frac{1}{2}$	$-\frac{1}{2}$
	4	$(+i)(-)(-)$	$[+i](-)[-]$	$[+i][-](-)$	$(+i)[-][-]$	$\frac{i}{2}$	$-\frac{1}{2}$	$-\frac{1}{2}$
$(\tilde{S}^{03}, \tilde{S}^{12}, \tilde{S}^{56})$	$\rightarrow$	$(-\frac{i}{2}, \frac{1}{2}, \frac{1}{2})$ $^{03\ \ 12\ \ 56}$	$(\frac{i}{2}, \frac{1}{2}, -\frac{1}{2})$ $^{03\ \ 12\ \ 56}$	$(\frac{i}{2}, -\frac{1}{2}, \frac{1}{2})$ $^{03\ \ 12\ \ 56}$	$(-\frac{i}{2}, -\frac{1}{2}, -\frac{1}{2})$ $^{03\ \ 12\ \ 56}$	$\tilde{S}^{03}$	$\tilde{S}^{12}$	$\tilde{S}^{56}$
odd II $\hat{b}^m_f$	1	$(-i)[+][+]$	$[+i][+](-)$	$[+i](-)[+]$	$(-i)(-)(-)$	$-\frac{i}{2}$	$-\frac{1}{2}$	$-\frac{1}{2}$
	2	$[-i](+)[+]$	$(+i)(+)(-)$	$(+i)[-][+]$	$[-i][-](-)$	$\frac{i}{2}$	$\frac{1}{2}$	$-\frac{1}{2}$
	3	$[-i][+](+)$	$(+i)[+][-]$	$(+i)(-)(+)$	$[-i](-)[-]$	$\frac{i}{2}$	$-\frac{1}{2}$	$\frac{1}{2}$
	4	$(-i)(+)(+)$	$[+i](+)[-]$	$[+i][-](+)$	$(-i)[-][-]$	$-\frac{i}{2}$	$\frac{1}{2}$	$\frac{1}{2}$
$(\tilde{S}^{03}, \tilde{S}^{12}, \tilde{S}^{56})$	$\rightarrow$	$(-\frac{i}{2}, \frac{1}{2}, \frac{1}{2})$ $^{03\ \ 12\ \ 56}$	$(\frac{i}{2}, -\frac{1}{2}, \frac{1}{2})$ $^{03\ \ 12\ \ 56}$	$(-\frac{i}{2}, -\frac{1}{2}, -\frac{1}{2})$ $^{03\ \ 12\ \ 56}$	$(\frac{i}{2}, \frac{1}{2}, -\frac{1}{2})$ $^{03\ \ 12\ \ 56}$	S^{03}	S^{12}	S^{56}
even I ${}^{I}\mathcal{A}^m_f$	1	$[+i](+)(+)$	$(+i)[+](+)$	$[+i][+][+]$	$(+i)(+)[+]$	$\frac{i}{2}$	$\frac{1}{2}$	$\frac{1}{2}$
	2	$(-i)[-](+)$	$[-i](-)(+)$	$(-i)(-)[+]$	$[-i][-][+]$	$-\frac{i}{2}$	$-\frac{1}{2}$	$\frac{1}{2}$
	3	$(-i)(+)[-]$	$[-i][+][-]$	$(-i)[+](-)$	$[-i](+)(-)$	$-\frac{i}{2}$	$\frac{1}{2}$	$-\frac{1}{2}$
	4	$[+i][-][-]$	$(+i)(-)[-]$	$[+i](-)(-)$	$(+i)[-](-)$	$\frac{i}{2}$	$-\frac{1}{2}$	$-\frac{1}{2}$
$(\tilde{S}^{03}, \tilde{S}^{12}, \tilde{S}^{56})$	$\rightarrow$	$(\frac{i}{2}, \frac{1}{2}, \frac{1}{2})$ $^{03\ \ 12\ \ 56}$	$(-\frac{i}{2}, -\frac{1}{2}, \frac{1}{2})$ $^{03\ \ 12\ \ 56}$	$(\frac{i}{2}, -\frac{1}{2}, -\frac{1}{2})$ $^{03\ \ 12\ \ 56}$	$(-\frac{i}{2}, \frac{1}{2}, -\frac{1}{2})$ $^{03\ \ 12\ \ 56}$	S^{03}	S^{12}	S^{56}
even II ${}^{II}\mathcal{A}^m_f$	1	$[-i](+)(+)$	$(-i)[+](+)$	$[-i][+][+]$	$(-i)(+)[+]$	$-\frac{i}{2}$	$\frac{1}{2}$	$\frac{1}{2}$
	2	$(+i)[-](+)$	$[+i](-)(+)$	$(+i)(-)[+]$	$[+i][-][+]$	$\frac{i}{2}$	$-\frac{1}{2}$	$\frac{1}{2}$
	3	$(+i)(+)[-]$	$[+i][+][-]$	$(+i)[+](-)$	$[+i](+)(-)$	$\frac{i}{2}$	$\frac{1}{2}$	$-\frac{1}{2}$
	4	$[-i][-][-]$	$(-i)(-)[-]$	$[-i](-)(-)$	$(-i)[-](-)$	$-\frac{i}{2}$	$-\frac{1}{2}$	$-\frac{1}{2}$

References

1. N. Mankoč Borštnik, "Spinor and vector representations in four dimensional Grassmann space", *J. of Math. Phys.* **34** (1993) 3731-3745.
2. N. Mankoč Borštnik, "Unification of spin and charges in Grassmann space?", hep-th 9408002, IJS.TP.94/22, Mod. Phys. Lett.**A (10)** No.7 (1995) 587-595.
3. N. Mankoč Borštnik, H. Nielsen, "Why odd space and odd time dimensions in even dimensional spaces?", *Phys. Lett.* **B 486** (2000) 25-29, 314-321, [arXiv: hep-ph/0005327/v3]
4. A. Borštnik Bračič, N. S. Mankoč Borštnik, "On the origin of families of fermions and their mass matrices", hep-ph/0512062, Phys. Rev. **D 74** 073013-28 (2006).
5. N.S. Mankoč Borštnik, H.B.F. Nielsen, "How to generate spinor representations in any dimension in terms of projection operators", *J. of Math. Phys.* **43**, 5782 (2002) [arXiv:hep-th/0111257], "How to generate families of spinors", *J. of Math. Phys.* **44** 4817 (2003) [arXiv:hep-th/0303224].
6. N.S. Mankoč Borštnik, "Describing the internal spaces of fermion and boson fields with the superposition of odd (for fermions) and even (for bosons) products of operators γ^a, enables understanding of all the second quantised fields (fermion fields, appearing in families, and boson (fields, tensor, vector, scalar) in an equivalent way" , Proceedings to the 28^{th} Workshop "What comes beyond the standard models", Bled, 4 - 16 July, 2025, Ed. N.S. Mankoč Borštnik, H.B. Nielsen, Maxim Yu. Khlopov, A. Kleppe, Založba Univerze v Ljubljani, December 2025.
7. N.S. Mankoč Borštnik, D. Lukman, "Vector and scalar gauge fields with respect to $d = (3+1)$ in Kaluza-Klein theories and in the *spin-charge-family theory*", *Eur. Phys. J. C* **77** (2017) 231.
8. N.S. Mankoč Borštnik, H.B.F. Nielsen, "Understanding the second quantization of fermions in Clifford and in Grassmann space", *New way of second quantization of fermions — Part I and Part II*, [arXiv:2007.03517, arXiv:2007.03516].
9. N. S. Mankoč Borštnik, H. B. Nielsen, "How does Clifford algebra show the way to the second quantized fermions with unified spins, charges and families, and with vector and scalar gauge fields beyond the *standard model*", Progress in Particle and Nuclear Physics, http://doi.org/10.1016.j.ppnp.2021.103890 .
10. N.S. Mankoč Borštnik, "Do we understand the internal spaces of second quantized fermion and boson fields (with gravity included)?", Journal of Physics: Conference Series, Volume 2987, The 14th Biennial Conference on Classical and Quantum Relativistic Dynamics of Particles and Fields (IARD 2024) 03/06/2024 - 06/06/2024 Espoo, Finland J. Phys.: Conf. Ser. 2987 012008 DOI 10.1088/1742-6596/2987/1/012008 Published under licence by IOP Publishing Ltd
11. N.S. Mankoč Borštnik, H.B.F. Nielsen, "The spin-charge-family theory offers understanding of the triangle anomalies cancellation in the standard model", *Fortschritte der Physik, Progress of Physics* (2017) 1700046, www.fp-journal.org, DOI: 10.1002/prop.201700046 http://arxiv.org/abs/1607.01618.
12. N. S. Mankoč Borštnik, "Do we understand the internal spaces of second quantized fermion and boson fields, with gravity included? The relation with strings theories", N.S. Mankoč Borštnik, H.B. Nielsen, "A trial to understand the supersymmetry relations through extension of the second quantized fermionand boson fields, either to strings or to odd dimensional spaces", Proceedings to the 27^{th} Workshop "What comes beyond the standard models", 8 - 17 July, 2024, Ed. N.S. Mankoč Borštnik, H.B. Nielsen, A. Kleppe, Založba Univerze v Ljubljani, December 24, DOI: 10.51746/9789612974848, [arxiv: 2312.07548]]
13. G. Bregar, M. Breskvar, D. Lukman, N.S. Mankoč Borštnik, "Predictions for four families by the Approach unifying spins and charges" *New J. of Phys.* **10** (2008) 093002, G. Bregar,

M. Breskvar, D. Lukman, N.S. Mankoč Borštnik, "Families of Quarks and Leptons and Their Mass Matrices", Proceedings to the 10^{th} international workshop "What Comes Beyond the Standard Model", 17 -27 of July, 2007, Ed. Norma Mankoč Borštnik, Holger Bech Nielsen, Colin Froggatt, Dragan Lukman, DMFA Založništvo, Ljubljana December 2007, p.53-70,[hep-ph/0711.4681, hep-ph/0606159, hep/ph-07082846].

14. G. Bregar, N.S. Mankoč Borštnik, "Does dark matter consist of baryons of new stable family quarks?", *Phys. Rev. D* **80**, 083534 (2009), 1-16. of new stable family quarks?", *Phys. Rev. D* **80**, 083534 (2009), 1-16.
15. N.S. Mankoč Borštnik, "Matter-antimatter asymmetry in the *spin-charge-family* theory", *Phys. Rev.* **D 91** (2015) 065004 [arXiv:1409.7791].
16. N.S. Mankoč Borštnik N S, "The spin-charge-family theory is explaining the origin of families, of the Higgs and the Yukawa couplings", *J. of Modern Phys.* **4** (2013) 823 [arXiv:1312.1542].
17. G. Bregar, N.S. Mankoč Borštnik, "The new experimental data for the quarks mixing matrix are in better agreement with the *spin-charge-family* theory predictions", Proceedings to the 17^{t}h Workshop "What comes beyond the standard models", Bled, 20-28 of July, 2014, Ed. N.S. Mankoč Borštnik, H.B. Nielsen, D. Lukman, DMFA Založništvo, Ljubljana December 2014, p.20-45 [arXiv:1502.06786v1] [arxiv:1412.5866].
18. N.S. Mankoč Borštnik, M. Rosina, "Are superheavy stable quark clusters viable candidates for the dark matter?", International Journal of Modern Physics D (IJMPD) **24** (No. 13) (2015) 1545003.
19. N. S. Mankoč Borštnik, "Clifford odd and even objects offer description of internal space of fermions and bosons, respectively, opening new insight into the second quantization of fields", The 13^{th} Bienal Conference on Classical and Quantum Relativistic Dynamics of Particles and Fields IARD 2022, Prague, $6-9$ June [http://arxiv.org/abs/2210.07004], Journal of Physics: Conference Series, Volume 2482/2023, Proceedings https://iopscience.iop.org/issue/1742-6596/2482/012012.
20. N. S. Mankoč Borštnik, "How Clifford algebra helps understand second quantized quarks and leptons and corresponding vector and scalar boson fields, opening a new step beyond the standard model", Reference: [arXiv: 2210.06256, physics.gen-ph V2]. Nuclear Physics B 994 (2023) 116326 NUPHB 994 (2023) 116326 .
21. N. S. Mankoč Borštnik, "Clifford odd and even objects in even and odd dimensional spaces", Symmetry 2023,15,818-12-V2 94818, https:doi.org/10.3390/sym15040818, [arxiv.org/abs/2301.04466] , https://www.mdpi.com/2073-8994/15/4/818 Manuscript ID: symmetry-2179313.
22. N. S. Mankoč Borštnik, "Can the "basis vectors", describing the internal spaces of fermion and boson fields with the Clifford odd (for fermion) and Clifford even (for boson) objects, explain interactions among fields, with gravitons included?" [arxiv: 2407.09482].
23. N.S. Mankoč Borštnik, H.B. Nielsen, "Can the "basis vectors", describing the internal space of point fermion and boson fields with the Clifford odd (for fermions) and Clifford even (for bosons) objects, be meaningfully extended to strings?", Proceedings to the 26^{rd} Workshop "What comes beyond the standard models", 10 - 19 July, 2023, Ed. N.S. Mankoč Borštnik, H.B. Nielsen, M.Yu. Khlopov, A. Kleppe, Založba Univerze v Ljubljani, DOI: 10.51746/9789612972097, December 23, [arxiv:2312.07548].
24. N. S. Mankoč Borštnik, "How Clifford algebra can help understand second quantization of fermion and boson fields", [arXiv: 2210.06256. physics.gen-ph V1].
25. N.S. Mankoč Borštnik, H.B. Nielsen, "Discrete symmetries in the Kaluza-Klein-like theories", doi:10.1007/ *Jour. of High Energy Phys.* **04** (2014)165, [http://arxiv.org/abs/1212.2362v3].
26. D. Lukman, N. S. Mankoč Borštnik, "Properties of fermions with integer spin described in Grassmann", Proceedings to the 21^{st} Workshop "What comes beyond the standard

models", 23 of June - 1 of July, 2018, Ed. N.S. Mankoč Borštnik, H.B. Nielsen, D. Lukman, DMFA Založništvo, Ljubljana, December 2018 [arxiv:1805.06318, arXiv:1902.10628]

27. T. Troha, D. Lukman and N.S. Mankoč Borštnik, "Massless and massive representations in the *spinor technique*", *Int. J Mod. Phys.* **A 29**, 1450124 (2014) [21 pages] DOI: 10.1142/S0217751X14501243.
28. N.S. Mankoč Borštnik, "How far has so far the Spin-Charge-Family theory succeeded to offer the explanation for the observed phenomena in elementary particle physics and cosmology", Proceedings to the 26rd Workshop "What comes beyond the standard models", 10 - 19 July, 2023, Ed. N.S. Mankoč Borštnik, H.B. Nielsen, M.Yu. Khlopov, A. Kleppe, Založba Univerze v Ljubljani, DOI: 10.51746/9789612972097, December 23, [http://arxiv.org/abs/2312.14946].
29. N.S. Mankoč Borštnik, "New way of second quantized theory of fermions with either Clifford or Grassmann coordinates and *spin-charge-family* theory " [arXiv: 2210.06256. physics.gen-ph V1, arXiv:1802.05554v4, arXiv:1902.10628],
30. N.S. Mankoč Borštnik, "How do Clifford algebras show the way to the second quantized fermions with unified spins, charges and families, and to the corresponding second quantized vector and scalar gauge field ", Proceedings to the 24rd Workshop "What comes beyond the standard models", 5 - 11 of July, 2021, Ed. N.S. Mankoč Borštnik, H.B. Nielsen, D. Lukman, A. Kleppe, DMFA Založništvo, Ljubljana, December 2021, [arXiv:2112.04378].
31. G. Bregar, N.S. Mankoč Borštnik, "Can we predict the fourth family masses for quarks and leptons?", Proceedings (arxiv:1403.4441) to the 16 th Workshop "What comes beyond the standard models", Bled, 14-21 of July, 2013, Ed. N.S. Mankoč Borštnik, H.B. Nielsen, D. Lukman, DMFA Založništvo, Ljubljana December 2013, p. 31-51, [http://arxiv.org/abs/1212.4055].

BLED WORKSHOPS
IN PHYSICS
VOL. 26, NO. 1

Proceedings of the 28th Workshop
What Comes Beyond . . . *(p. 238)*
Bled, Slovenia, July 6–17, 2025

18 How Should We Interpret Space Dimension? – Trial for a Mathematical Foundation in Higher Dimensional Physics

Euich Miztani[†]

JEin Institute for Fundamental Science (JIFS) 5-14, Yoshida-honmachi, Sakyo-ku, Kyoto, Japan. 606-8317
Keimei Gakkan High School, 1-23-15, Shinmichi, Nishi-ku, Nagoya, Japan. 451-0043

In memory of the late Prof. Ichiro Yokota of Shinshu University, known for his research of cellular decompositions of classical Lie groups and realizations of exceptional Lie groups.

Abstract. In modern physics we could say that space dimension is derived from physical conditions. Kaluza-Klein theory and D-brane are typical examples. However, not only by such conditions, we should also think about space dimension with insights from known facts without any physical conditions. In this talk we rethink space dimensionality from scratch.
Povzetek: V tem prispevku razpravlja avtor o posebni teoriji relativnosti in njeni novi Liejevi grupi v realnem prostoru. Posebna teorija relativnosti Alberta Einsteina temelji na geometrijskem opisu. Elektromagnetna teorija pa je algebrska in zapletena. Delo Minkowskega je razširilo opis na štirirazsežni prostor-čas, ki je prav tako popolnoma algebrski. Avtor pokaže, kako lahko razumemo Einsteinove ideje enostavneje in bolj fenomenološko. Obravnava posebno ortogonalno grupo v realnem prostoru, ki ni ortogonalna grupa SO(1,3).

18.1 Examples of Physical Conditions

Let us think about these physical conditions:

1. The standard model requires 19 numerical constants whose values are determined by experimental results. That is one of the motivations for particle physicists to establish a unified theory beyond the standard model.
2. Hendrik Lorentz and George FitzGerald introduced a strange idea that space is contracted to explain the results of the Michelson-Morley experiment: the Lorentz-FitzGerald contraction.
3. Epicycles given on the orbits of planets to support geocentric theory. Epicycles made more accurate the geocentric theory than Copernicus in the 16th century.
4. Astronomers before Isaac Newton believed that the orbits of planets were on the celestial spheres.

[†]euichi@jein.jp, keimeigakkan80@icloud.com

5. Universe models based on 3-sphere or 3-hyperboloid. The problem needs to be explained in detail. Let us think of an easy example. There is a ball rolling on the table as shown in Figure 1 (Fig. 1). This could be considered a motion only on the plane if it does not bounce. So, we could say it is a motion in 2-dimensional space. On the other hand, could we really say that this is motion in 2-dimensional space? This way of thinking is based on the concept of binding condition by analytical dynamics. It ignores the vertical degree of freedom because the gravity of the ball is kept in balance with the normal force by the table. Therefore, it is a fake 2-dimensional motion.

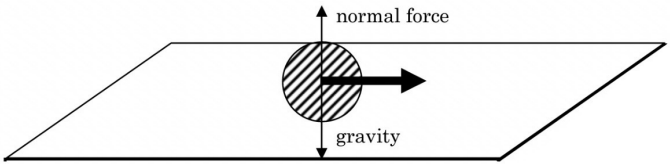

Fig. 1

We can think of ourselves on Earth in this way, which means we are living in a closed 2-dimensional space or sphere. Furthermore, what about the thinking in cosmology that we are in a Universe which is a '3-dimensional' sphere or 3-sphere in topology? It will be true that this is also based on the concept of 'binding condition'. If so, as shown in Fig. 2, the centrifugal force given to our galaxy moving in the Universe is perfectly balanced with a 'centripetal one'.

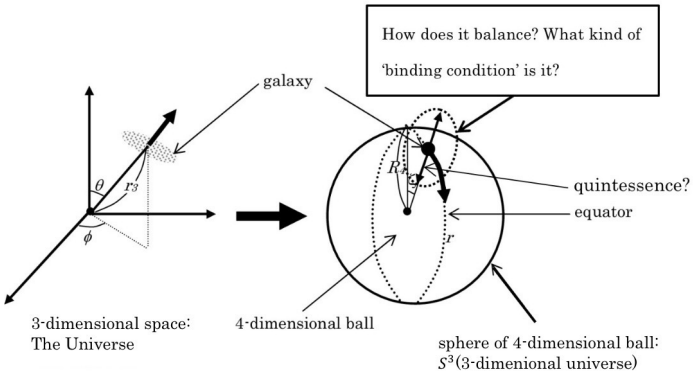

Fig. 2

Does this give a 'binding condition' to our galaxy just like a ball on the table and therefore we cannot perceive the 4^{th}-dimensional degree of freedom? Especially, what is this kind of 'centripetal force'? Does that hint at a 5^{th} force (quintessence) following gravity, electro-magnetic force, weak force and strong force in nature? Otherwise, as shown in Fig. 3, our galaxy will be thrown into '4^{th}-dimensional

space'. Or is there something special to support the galaxy like the 'celestial sphere'?

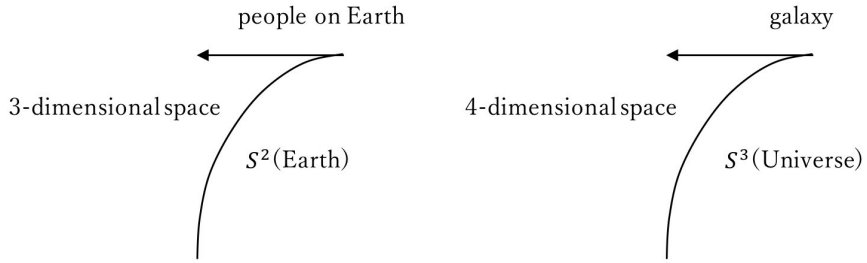

Fig. 3

As well as that, we would be spun off into space if not keeping the balance between the centrifugal force of the Earth's rotation and gravity.

Thus, we are sure that it is preferable to introduce fewer physical conditions.
There are two types of modern celestial spheres.

One is 'macroscopic' celestial sphere: cosmology based on hyper-surface like that of de Sitter space, anti-de Sitter space and brane.
Another type is 'microscopic' celestial sphere: which is for particles in higher dimensional space. That is, compactified higher dimensional space based on Kaluza-Klein theory like Calabi-Yau manifolds in string theory and the ADD model.
Astronomers before Isaac Newton assumed that celestial spheres formed with 'undetectable' force(s) were the reasons why heavenly bodies did not fall to the Earth. Nowadays, physicists likewise assume that there are modern celestial spheres: 'hyper-surface' in cosmology and 'compactified' higher dimensional space in higher dimensional physics that are formed with 'undetectable' force(s). So that, cosmologists say that we are confined in such a strange hyper-surface, which is nothing more though 'imagination' in mathematics. Particle physicists proclaim that particles need wound-up higher dimensional space in order to get many more degrees of freedom in higher dimensional physics.

18.2 Concrete Insights

By giving physical conditions, we know that even incorrect ideas were justified in the past, like the examples above. Especially for higher dimensional space, we had to assume an unknown force (see example 5 above). Kaluza-Klein theory also needs an unknown force to compactify extra-dimensional space, as well as the 3-manifold universe model mentioned above. Therefore, it is important what the spatial dimension is. Firstly, let us delve deeper into this matter.

18.2.1 Facts

Fact 1. We have never detected any particles travelling or confined forever in 2-dimensional space or a plane in our Universe. The case will be also about D2-brane in our 3-dimensional Universe.

Fact 2. Suppose for example, that we are living in 5-dimensional space but we only have 3 variables of x, y and z. That is why we cannot see extra-dimensional space. However, this thought is incorrect. This is clear from Fact 1.

Fact 3. Suppose that as we are on Earth, we are living on a 2-dimensional sphere. However, who amongst us believes that we are living in a 2-dimensional space?

Now, let us consider those Facts above as an axiom.

Axiom 1. Lower dimensional spaces are not subspaces of higher dimensional ones. They are disjoint of each other as shown in Fig. 4.

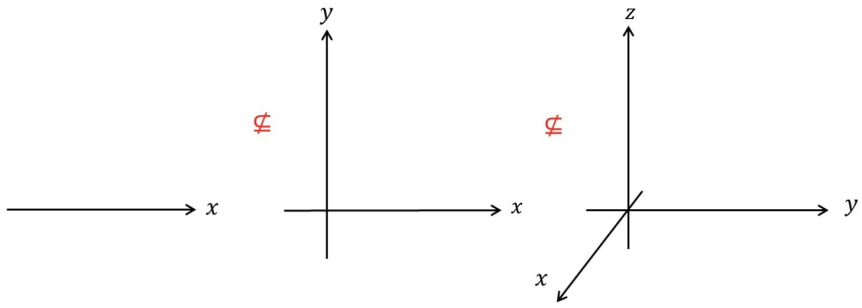

Fig. 4

These dimensional spaces are different worlds from each other. Now, let us imagine a situation like that of Alice in Wonderland. She starts from our 3-dimensional world, where the point has 'theoretically' the 3 variables of x, y and z; or in other words the 3 degrees of freedom of x, y and z. She, in our 3-dimensional space is transferred to a 1-dimensional tunnel. In the tunnel, will she have only one degree of freedom?
When Alice returns from the tunnel to the usual 3-dimensional world, what will become of the variables or the degrees of freedom that she has? The answer is that Alice has 3 variables of x, y and z even in 1-dimensional space. Even if she goes to a much higher dimensional world like 10-dimensional space, she has only the 3 variables or co-ordinates of x, y and z; though that does NOT mean (x, y, z, 0, 0, 0, 0, 0, 0, 0). Then, when she comes back to our world, it is the same as before she travelled into 1-dimensional space. Let us consider these matters.

18.2.2 A Point Mapping from Lower to Higher Dimensional Space

An equation $x = a$ is a point in 1-dimensional space, a line in 2-dimensional space and a plane in 3-dimensional space. Though the equation is always the same, the graph is different among different dimensional spaces as shown in Fig. 5. We should discuss them from a unified viewpoint.

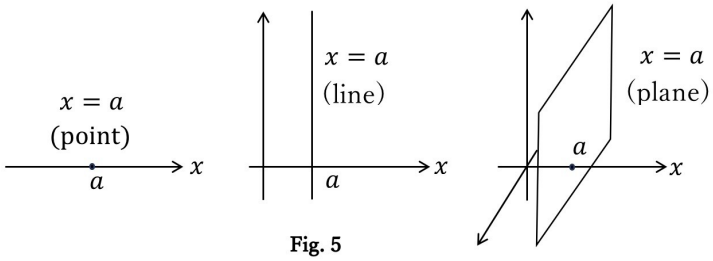

Fig. 5

Definition 1. If point $x = a$ in 1-dimensional space is mapped to any higher dimensional spaces, y and z co-ordinates or variables for the point are never given.

For example, if $x = a$ in 1-dimensional space is mapped into 2-dimensional space, the co-ordinate keeps $x = a$, NOT $(x, y) = (a, 0)$. If $x = a$ in 1-dimensional space is mapped into 3-dimensional space, the co-ordinate keeps $x = a$, NOT $(x, y, z) = (a, 0, 0)$. See also Fig. 6.

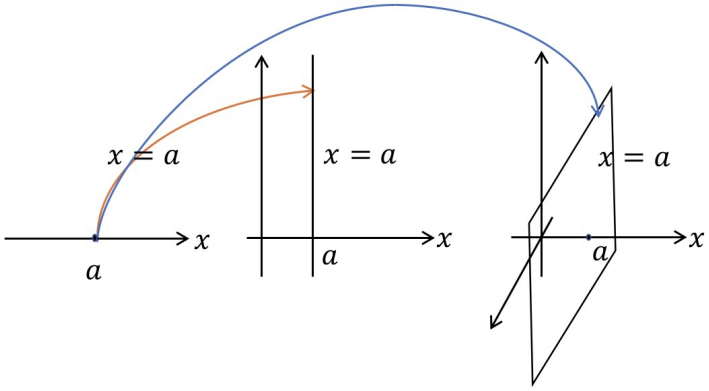

Fig. 6

Considering the practical case of projection into higher dimension, we should reconsider our thoughts about the system of equations from a graphical viewpoint. For example, let us consider a system of equations $f(x, y, z) = x^2 + y^2 + z^2 - 1 = 0$ and $g(x, y) = x - y = 0$. This produces two simultaneous equations $h_1(x, z) = 2x^2 + z^2 - 1 = 0$ and $h_2(y, z) = 2y^2 + z^2 - 1 = 0$. That appears inconsistent because these equations of ellipse seem not to be solutions indicating intersections of the sphere $f(x, y, z)$ and the line $g(x, y)$. However, considering $g(x, y)$ as a plane projected into 3-dimensional space, it makes sense that $h_1(x, z)$ and $h_2(y, z)$ are equations which are projected into $x - z$ plane or $y - z$ plane, as shown in Fig. 7.

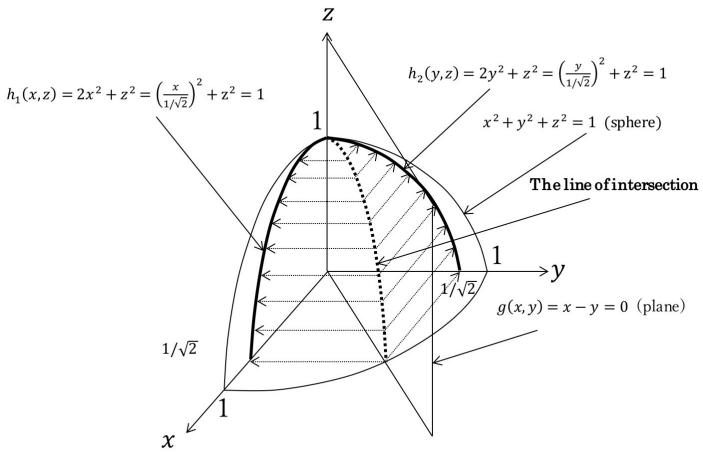

Fig. 7

Since the curve of intersection is indicated by $(x, y, z) = (h_1(x, z), h_2(y, z), z)$ as a plane projected into 3-dimensional space, Therefore,
$(x, y, z) = \left(\pm\sqrt{\frac{1-z^2}{2}}, \pm\sqrt{\frac{1-z^2}{2}}, z\right), \because -1 \leq z \leq 1.$

Remark. From the viewpoint of quantum theory, it might suggest a wave function collapse.

Only if $z = 0$ (plane), then $(x, y, z) = \left(\pm\sqrt{1/2}, \pm\sqrt{1/2}, 0\right)$. It shows that the sphere $f(x, y, z) = x^2 + y^2 + z^2 - 1 = 0$ intersects the planes $x - y = 0$ and $z = 0$. Based on the result above, the system of arbitrary equations below makes sense:

$$\begin{cases} f_1(x_1, x_2, x_3, \ldots\ldots, x_l) = 0 \\ f_2(x_1, x_2, x_3, \ldots\ldots, x_m) = 0 \\ \vdots \\ f_k(x_1, x_2, x_3, \ldots\ldots\ldots\ldots, x_r) = 0 \end{cases}$$

18.2.3 A Point mapping from Higher to Lower Dimensional Space

As well as mapping a point from lower to higher dimensional space, we would like to define the map of a point from higher to lower dimensional space.

Definition 2. If a point is mapped to lower dimensional space, the original number of co-ordinates never changes. In other words, if a point is mapped from higher to any lower dimensional space, the degrees of freedom or the number of its co-ordinates is never decreased.

Example 1. Let us consider a transformation of homogeneous co-ordinates. As shown in Fig. 8, the number of variables is 3: (x, y, z). On the other hand, as shown in Fig. 9, let us transform the co-ordinates via scaling or mapping f: $(x, y, z) \mapsto$

$(x/z, y/z)$ and the inverse $\varphi : (x/z, y/z) \mapsto (x, y, z)$. Then the equation $x^2+y^2 = z^2$ changes to $\left(\frac{x}{z}\right)^2 + \left(\frac{y}{z}\right)^2 = X^2 + Y^2 = 1$.

The relationship between $x^2 + y^2 = z^2$ in 3-dimensional space and $\left(\frac{x}{z}\right)^2 + \left(\frac{y}{z}\right)^2 = X^2+Y^2 = 1$ in 2-dimensional space is that the hyperboloid $x^2+y^2 = z^2$ is projected on to the circle $\left(\frac{x}{z}\right)^2 + \left(\frac{y}{z}\right)^2 = X^2 + Y^2 = 1$. However, $\left(\frac{x}{z}\right)^2 + \left(\frac{y}{z}\right)^2 = 1$'keeps the number of variables '3" in '2'-dimensional space. These two true variables of x, y and the parameter z control the radius of the circle. It is shown as a unit circle in Fig. 8.

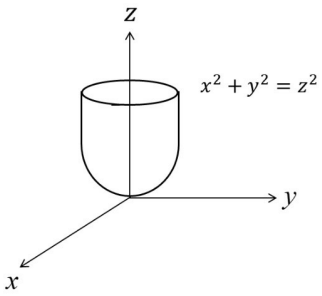

Fig. 8

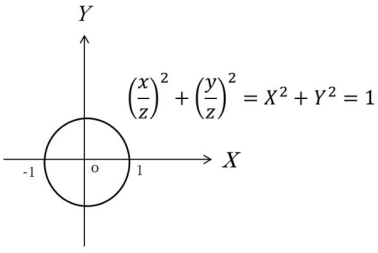

Fig. 9

Example 2. The case below is in a series of mappings from higher to lower dimensional space. As shown in Fig.10, a co-ordinate in $B^3 = (r_3, \alpha, \beta)$ is projected in $B^2 = (r_3 cos\alpha, \beta) = (r_2, \beta)$, B^2 in $B^1 = r_3 cos\alpha cos\beta = r_2 cos\beta = r_1$, B^3 in B^1. Therefore,

$$\begin{array}{cccccc} B^3 & \to & B^2 & B^2 & \to B^1 & B^3 \quad \to B^1 \\ \cup & & \cup & \cup & \cup & \cup \\ (r_3, \alpha, \beta) & \mapsto & (r_2, \beta) & (r_2, \beta) & \mapsto r_1 & (r_3, \alpha, \beta) \mapsto r_1 \end{array}$$

The commutative diagram with morphisms ($f \circ g = E_{32}E_{21} = E_{31}$) is shown in Fig. 11.

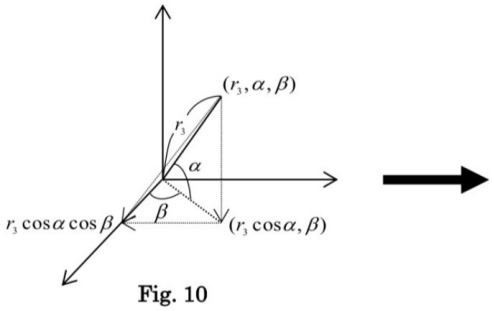

Fig. 10

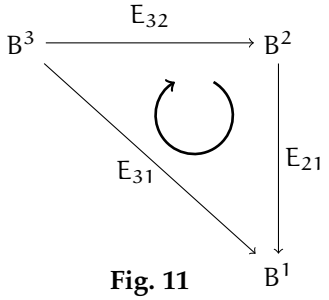

Fig. 11

Likewise, mapping into lower dimensional space by this method, the commutative diagram with morphisms (Fig.11) can be changed to any other combinations by:

$(r_n, \theta_1, \ldots, \theta_{n-1}) \in B^n$,

$(r_{n-1}(= r_n \cos\theta_n), \theta_1, \ldots, \theta_{n-1}) \in B^{n-1}$,

$(r_{n-2}(= r_n \cos\theta_n \cos\theta_{n-1}), \theta_1, \ldots, \theta_{n-2}) \in B^{n-2}$,

.....,

....,
....,
$(r_2(= r_n \cos\theta_n \cos\theta_{n-1} \ldots \cos\theta_2), \theta_1) \in B^2$,
$(r_1\ (= r_n \cos\theta_n \cos\theta_{n-1} \ldots \cos\theta_1)) \in B^1$.

Example 3. We utilize the fundamental theorem on homomorphisms for linear algebra. Let V and W be vector spaces, f be a linear mapping from V to W, then we have:

$$V/\mathrm{Ker}(f) \simeq \mathrm{Img}(f).$$

f: $R^3 \ni \begin{pmatrix} x \\ y \\ z \end{pmatrix} \mapsto x + y + z \in R$ is a homomorphism.

$$\because f(g_1 + g_2) = f\left(\begin{pmatrix} x_1 \\ y_1 \\ z_1 \end{pmatrix} + \begin{pmatrix} x_2 \\ y_2 \\ z_2 \end{pmatrix}\right) = f\begin{pmatrix} x_1 + x_2 \\ y_1 + y_2 \\ z_1 + z_2 \end{pmatrix}$$
$$= (x_1 + x_2) + (y_1 + y_2) + (z_1 + z_2)$$
$$= f\begin{pmatrix} x_1 \\ y_1 \\ z_1 \end{pmatrix} + f\begin{pmatrix} x_2 \\ y_2 \\ z_2 \end{pmatrix} = f(g_1) + f(g_2).$$

Here, $g_i \in (x_i, y_i, z_i, \ldots)$. However, since the bijection of f is not verified, we cannot refer to the inverse. Instead, we consider $\bar{f}$: $G/\mathrm{Ker}(f) \to G'$.

Paying attention to $\begin{pmatrix} x \\ y \\ z \end{pmatrix} = x\begin{pmatrix} 1 \\ 0 \\ -1 \end{pmatrix} + y\begin{pmatrix} 0 \\ 1 \\ -1 \end{pmatrix} + \begin{pmatrix} 0 \\ 0 \\ x+y+z \end{pmatrix}$,

$$\begin{pmatrix} 0 \\ 0 \\ x+y+z \end{pmatrix} + R\begin{pmatrix} 1 \\ 0 \\ -1 \end{pmatrix} + R\begin{pmatrix} 0 \\ 1 \\ -1 \end{pmatrix} = \begin{pmatrix} x \\ y \\ z \end{pmatrix} + R\begin{pmatrix} 1 \\ 0 \\ -1 \end{pmatrix} + R\begin{pmatrix} 0 \\ 1 \\ -1 \end{pmatrix}.$$

Since $\mathrm{Ker}(f) = \left\{\begin{pmatrix} x \\ y \\ z \end{pmatrix}, f\begin{pmatrix} x \\ y \\ z \end{pmatrix} = 0\right\} = \left\{\begin{pmatrix} x \\ y \\ z \end{pmatrix}, x + y + z = 0\right\}$,

$$\bar{f}: R^3/\mathrm{Ker}(f) = R^3/\left(R\begin{pmatrix} 1 \\ 0 \\ -1 \end{pmatrix} + R\begin{pmatrix} 0 \\ 1 \\ -1 \end{pmatrix}\right)$$
$$= \left\{\begin{pmatrix} x \\ y \\ z \end{pmatrix} + R\begin{pmatrix} 1 \\ 0 \\ -1 \end{pmatrix} + R\begin{pmatrix} 0 \\ 1 \\ -1 \end{pmatrix} : \begin{pmatrix} x \\ y \\ z \end{pmatrix} \in R^3\right\}$$
$$\mapsto x + y + z \in R.$$

See also Fig.12. Since $x + y + z$ has 3 degrees of freedom or 3 variables in R, the invariant is 3.

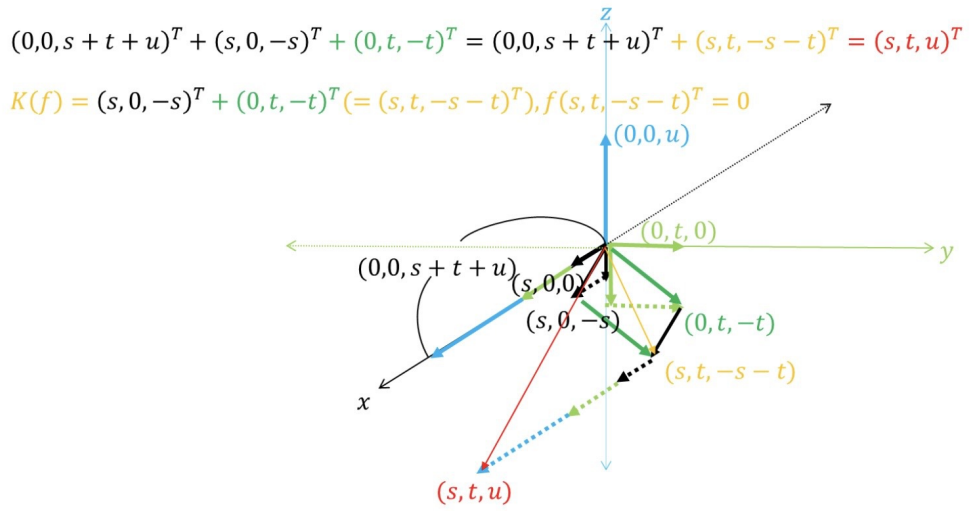

Fig. 12

Remark. $\begin{pmatrix}1\\0\\-1\end{pmatrix}$ and $\begin{pmatrix}0\\1\\-1\end{pmatrix}$ are perpendicular to $\begin{pmatrix}1\\1\\1\end{pmatrix}$,
$\because (1,0,-1)\,(1,1,1) = (0,1,-1)\,(1,1,1) = 0$. The orthogonality is significant in this discussion.

The inverse φ is as follows. Since φ: $\mathrm{Im}gf \ni h = f(g) \to gKer(f) \in G/Ker(f)$,

$$R \ni \bar{f}(g) = x+y+z \mapsto R^3/\left(R\begin{pmatrix}1\\0\\-1\end{pmatrix} + R\begin{pmatrix}0\\1\\-1\end{pmatrix}\right)$$
$$= \left\{\begin{pmatrix}x\\y\\z\end{pmatrix} + R\begin{pmatrix}1\\0\\-1\end{pmatrix} + R\begin{pmatrix}0\\1\\-1\end{pmatrix} : \begin{pmatrix}x\\y\\z\end{pmatrix} \in R^3\right\}.$$

Now, let us pay attention to the invariant throughout a series of the mappings above. For example, let us think of f: $R^4 \ni \begin{pmatrix}x_1\\x_2\\x_3\\x_4\end{pmatrix} \mapsto \begin{pmatrix}x_1+x_3\\x_2+x_4\end{pmatrix} \in R^2$. Or another case $\mapsto \begin{pmatrix}x_1+x_3+x_4\\x_2\end{pmatrix}$ is also fine.

Then, $Ker(f) = \left\{\begin{pmatrix}x_1\\x_2\\x_3\\x_4\end{pmatrix}; f\begin{pmatrix}x_1\\x_2\\x_3\\x_4\end{pmatrix} = 0\right\} = \left\{\begin{pmatrix}x_1\\x_2\\x_3\\x_4\end{pmatrix}; \begin{pmatrix}x_1+x_3\\x_2+x_4\end{pmatrix} = 0\right\}$

$$= \left\{s\begin{pmatrix}1\\0\\-1\\0\end{pmatrix} + t\begin{pmatrix}0\\1\\0\\-1\end{pmatrix}; s,t \in R\right\} = \left\{R\begin{pmatrix}1\\0\\-1\\0\end{pmatrix} + R\begin{pmatrix}0\\1\\0\\-1\end{pmatrix}\right\}.$$

$$\text{Since } R^4/\mathrm{Ker}(f) = R^4/\left\{ R\begin{pmatrix}1\\0\\-1\\0\end{pmatrix} + R\begin{pmatrix}0\\1\\0\\-1\end{pmatrix}\right\}$$

$$= \left\{ \begin{pmatrix}x_1\\x_2\\x_3\\x_4\end{pmatrix} + R\begin{pmatrix}1\\0\\-1\\0\end{pmatrix} + R\begin{pmatrix}0\\1\\0\\-1\end{pmatrix};\ \begin{pmatrix}x_1\\x_2\\x_3\\x_4\end{pmatrix} \in R^4 \right\},$$

$$\bar{f}(g) = E_{42}x = R^4/\mathrm{Ker}(f) \mapsto \begin{pmatrix}x_1+x_3\\x_2+x_4\end{pmatrix}.$$

Remark. For $\begin{pmatrix}1\\1\\1\\1\end{pmatrix} \in R^4$, $\begin{pmatrix}1\\0\\-1\\0\end{pmatrix}$ and $\begin{pmatrix}0\\1\\0\\-1\end{pmatrix}$ are orthogonal. Thinking of another mapping based on the orthogonality we are naturally able to think of the case

$$f\colon R^5 \ni \begin{pmatrix}x_1\\x_2\\x_3\\x_4\\x_5\end{pmatrix} \mapsto \begin{pmatrix}x_1+x_3+x_5\\x_2+x_4\end{pmatrix} \in R^2.$$

$$\text{Then, } \mathrm{Ker}(f) = \left\{ \begin{pmatrix}x_1\\x_2\\x_3\\x_4\\x_5\end{pmatrix};\ f\begin{pmatrix}x_1\\x_2\\x_3\\x_4\\x_5\end{pmatrix} = 0 \right\} = \left\{ \begin{pmatrix}x_1\\x_2\\x_3\\x_4\\x_5\end{pmatrix};\ \begin{pmatrix}x_1+x_3+x_5\\x_2+x_4\end{pmatrix} = 0 \right\}$$

$$= \left\{ s\begin{pmatrix}1\\0\\-1\\0\\0\end{pmatrix} + t\begin{pmatrix}0\\1\\0\\-1\\0\end{pmatrix} + u\begin{pmatrix}1\\0\\0\\0\\-1\end{pmatrix};\ s,t,u \in R \right\}$$

$$= \left\{ R\begin{pmatrix}1\\0\\-1\\0\\0\end{pmatrix} + R\begin{pmatrix}0\\1\\0\\-1\\0\end{pmatrix} + R\begin{pmatrix}1\\0\\0\\0\\-1\end{pmatrix} \right\}.$$

$$\text{Since } R^5/\mathrm{Ker}(f) = R^5/\left\{ R\begin{pmatrix}1\\0\\-1\\0\\0\end{pmatrix} + R\begin{pmatrix}0\\1\\0\\-1\\0\end{pmatrix} + R\begin{pmatrix}1\\0\\0\\0\\-1\end{pmatrix} \right\}$$

$$= \left\{ \begin{pmatrix}x_1\\x_2\\x_3\\x_4\\x_5\end{pmatrix} + R\begin{pmatrix}1\\0\\-1\\0\\0\end{pmatrix} + R\begin{pmatrix}0\\1\\0\\-1\\0\end{pmatrix} + R\begin{pmatrix}1\\0\\0\\0\\-1\end{pmatrix};\ \begin{pmatrix}x_1\\x_2\\x_3\\x_4\\x_5\end{pmatrix} \in R^5 \right\},$$

$$\bar{f}(g) = E_{52}x = R^5/Ker(f) \mapsto \begin{pmatrix} x_1 + x_3 + x_5 \\ x_2 + x_4 \end{pmatrix}.$$

Thus, we can see the lawlike composition for $R^n/Ker(f)$.
On the other hand, let us think of mapping from lower to higher dimensional space. For example, for $E_{13} : R^1 \to R^3/Ker(f)$,
$x \mapsto \begin{pmatrix} x \\ 0 \\ 0 \end{pmatrix} + R\begin{pmatrix} 0 \\ 1 \\ 0 \end{pmatrix} + R\begin{pmatrix} 0 \\ 0 \\ 1 \end{pmatrix} = \begin{pmatrix} x \\ * \\ * \end{pmatrix}$. See also Fig. 13.
In this case, the unit vector $\begin{pmatrix} 1 \\ 0 \\ 0 \end{pmatrix}$ of $\begin{pmatrix} x \\ 0 \\ 0 \end{pmatrix}$ is also orthogonal to $\begin{pmatrix} 0 \\ 1 \\ 0 \end{pmatrix}$ and $\begin{pmatrix} 0 \\ 0 \\ 1 \end{pmatrix}$. Thus, the orthogonality is essential for E_{lm}. We will define E_{lm} in Section 3 (**Description with Matrices**).
Therefore, $x = a \mapsto \begin{pmatrix} a \\ 0 \\ 0 \end{pmatrix} + R\begin{pmatrix} 0 \\ 1 \\ 0 \end{pmatrix} + R\begin{pmatrix} 0 \\ 0 \\ 1 \end{pmatrix} = \begin{pmatrix} x \\ * \\ * \end{pmatrix}$.

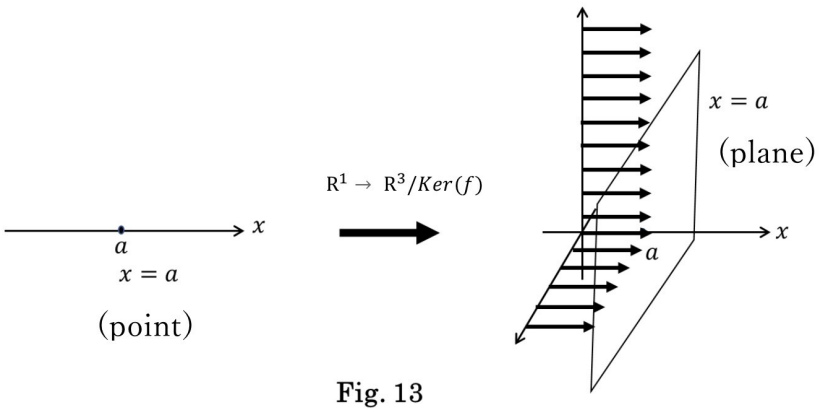

Fig. 13

Example 4. In the context of dimensional reduction, we could think of differentiation for some polynomial equations. For example, $\frac{f(x,y)}{\partial x \partial y} = z_{xy}$ is also considered a mapping from 3 to 1-dimensional space. It is natural that we can consider integration as the inverse.

Remark. In transferring any point among different dimensional spaces, the original number of variables of any point remains the same. Those four examples above can be summarized in another axiom:

Axiom 2. The number of variables of any point in the original n-dimensional space remains the same, even though the point transfers into any other dimensional space. It is equivalent to an invariant of topology (see also **Open Problems** below).

18.3 Description with Matrices

Let us introduce a specific matrix operator to project a point between mutual dimensions. This matrix is different from a conventional one. It includes a special operator needing a temporary variable for operation. This is because the number of variables of a point before and after this operation is the same. Demonstrating this, for example, operating by an operator E_{12} to map a point A_1 from 1 to 2-dimensional space (A_2), the equation is $A_2 = E_{12}A_1$. Therefore:

$$\begin{pmatrix} x \\ y \end{pmatrix} = \begin{pmatrix} 1 & 0 \\ 0 & D \end{pmatrix} \begin{pmatrix} a \\ T \end{pmatrix} = \begin{pmatrix} a \\ DT \end{pmatrix}. \tag{3.1}$$

D denotes a matrix element making the dimension higher and T a temporary variable to correspond to the 2-dimensional space after operation. Therefore, DT are all real numbers of y. This process of Eq. 3.1 is shown in Fig. 14.

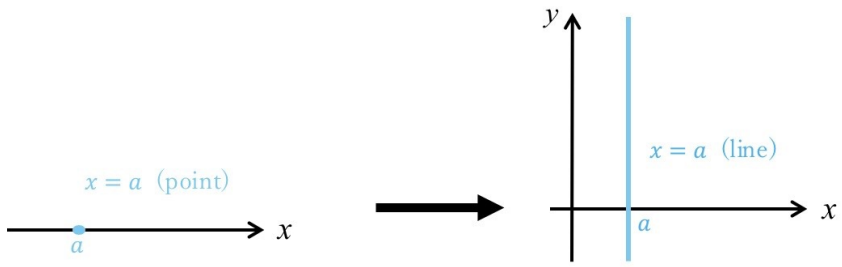

Fig. 14

Operating another case from 1 to 3-dimensional space, then:

$$\begin{pmatrix} x \\ y \\ z \end{pmatrix} = \begin{pmatrix} 1 & 0 & 0 \\ 0 & D & 0 \\ 0 & 0 & D \end{pmatrix} \begin{pmatrix} a \\ T \\ T \end{pmatrix} = \begin{pmatrix} a \\ DT \\ DT \end{pmatrix}. \tag{3.2}$$

Similarly, mapping from 3 to 2-dimensional space is operated as:

$$\begin{pmatrix} x \\ y \\ z \end{pmatrix} = \begin{pmatrix} 1 & 0 & 0 \\ 0 & 1 & 0 \\ 0 & 0 & D^{-1} \end{pmatrix} \begin{pmatrix} a \\ b \\ c \end{pmatrix} = \begin{pmatrix} a \\ b \\ D^{-1}c \end{pmatrix}. \tag{3.3}$$

D^{-1} denotes an element making the dimension lower and inverse of D. Eq. 3.3 is shown in Fig. 15. Then, if returning the point mapped from 3 into 2-dimensional space by Eq. 3.3 to the original dimensional space, the operation is as follows:

$$\begin{pmatrix} x \\ y \\ z \end{pmatrix} = \begin{pmatrix} 1 & 0 & 0 \\ 0 & 1 & 0 \\ 0 & 0 & D \end{pmatrix} \begin{pmatrix} a \\ b \\ D^{-1}c \end{pmatrix} = \begin{pmatrix} 1 & 0 & 0 \\ 0 & 1 & 0 \\ 0 & 0 & D \end{pmatrix} \begin{pmatrix} 1 & 0 & 0 \\ 0 & 1 & 0 \\ 0 & 0 & D^{-1} \end{pmatrix} \begin{pmatrix} a \\ b \\ c \end{pmatrix} = \begin{pmatrix} a \\ b \\ c \end{pmatrix}. \tag{3.4}$$

Therefore, $E_{32}E_{23}(= (E_{23})^{-1}E_{23}) = E_{33} \equiv 1.$ (3.5)

Remark. The operators E_{32} and E_{23} of Eq.3.5 are ordered from left to right for convenience. The matrices of Eq.3.4 are contrarily ordered for the operators and obviously calculated from right to left.

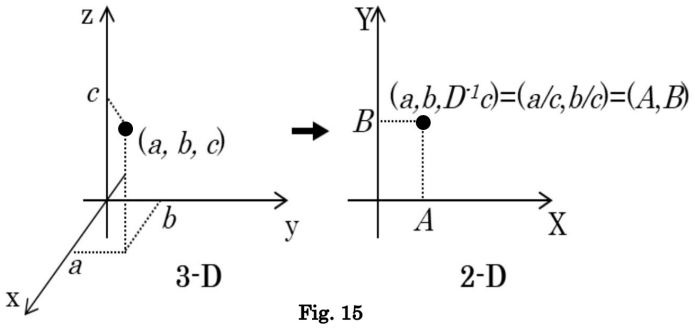

Fig. 15

The general operator, which is dimensional unit matrix E_{lm}, is:
If $l < m$,

$$E_{lm} = \mathrm{diag}(\overbrace{1,1,1,\ldots,1,1,1}^{l},\overbrace{D,D,D,\ldots,D,D,D}^{m-l}).$$

If $m < l$,

$$E_{lm} = (E_{ml})^{-1} = \mathrm{diag}(\overbrace{1,1,1,\ldots,1,1,1}^{m},\overbrace{D^{-1},D^{-1},D^{-1},\ldots,D^{-1},D^{-1},D^{-1}}^{l-m}).$$

Therefore, $E_{jk}E_{kj} = E_{jj} \equiv 1 \equiv E_{kj}E_{jk} = E_{kk}$. (3.6)
Furthermore,

$$E_{0n} = \mathrm{diag}(\overbrace{D,D,D,\ldots,D,D,D}^{n}),$$

$$E_{n0} = (E_{0n})^{-1} = \mathrm{diag}(\overbrace{D^{-1},D^{-1},D^{-1},\ldots,D^{-1},D^{-1},D^{-1}}^{n}).$$

18.4 The Groupoid

The unchangeable number of variables can be considered as a 'symmetry' in physics or 'invariant' in mathematics. To make this point absolutely clear we would like to discuss it in an algebraic way.

Proposition. *In the former section, matrices in a series of partially functional operations make the groupoid action. They are indicated by equations as follows:*
(i) $E_{lm}E_{mn} = E_{ln}$ (automorphism, proven in Section 5 below), (4.1)
(ii) $(E_{kl}E_{lm})E_{mn} = E_{kl}(E_{lm}E_{mn})$ (associative), (4.2)
(iii) $E_{jk}E_{kj} = E_{jj} \equiv 1 \equiv E_{kj}E_{jk} = E_{kk}$ (inverse), (4.3)
or $E_{lm}E_{ml} = E_{lm}(E_{lm})^{-1} = (E_{ml})^{-1}E_{ml} \equiv 1$, (4.4)
(iv) $E_{kl}E_{lm}E_{ml} = E_{kl}E_{lm}(E_{lm})^{-1} = E_{kl}$ (right identity), (4.5)
and $E_{lk}E_{kl}E_{lm} = (E_{kl})^{-1}E_{kl}E_{lm} = E_{lm}$ (left identity), (4.6)
(v) $(E_{lm}E_{mn})^{-1} = (E_{mn})^{-1}(E_{lm})^{-1}$, (4.7)

(vi) $E_{jj} \equiv 1$ (identity equivalent to the scalar value). (4.8)
(i) and (vi) are peculiar to the groupoid.
The operators in Section 3 above explicitly showed the groupoid. However, we have never calculated such matrices. Therefore, we need to check and verify that they really work.

Proof. At first, formula (i) is as follows:
a1) If $0 < l < m < n$ (mapping into higher dimensions),

$$x' = E_{lm}x = diag(\overbrace{1,1,\ldots,1}^{l},\overbrace{D,D,\ldots,D}^{m-l})(x_1,x_2,\ldots,x_l,\overbrace{T,T,\ldots,T}^{m-l})^T$$
$$= (x_1,x_2,\ldots,x_l,\overbrace{DT,DT,\ldots,T}^{m-l})^T.$$

Therefore,

$$E_{mn}x' = diag(\overbrace{1,1,\ldots,1}^{m},\overbrace{D,D,\ldots,D}^{n-m})(x_1,x_2,\ldots,x_l,\overbrace{DT,DT,\ldots,DT}^{m-l}\overbrace{T,T,\ldots,T}^{n-m})^T$$
$$= (x_1,x_2,\ldots,x_l,\overbrace{DT,DT,\ldots,T}^{n-l})^T$$
$$= diag(\overbrace{1,1,\ldots,1}^{l},\overbrace{D,D,\ldots,D}^{n-l})(x_1,x_2,\ldots,x_l,\overbrace{T,T,\ldots,T}^{n-l})^T$$
$$= E_{ln}x.$$

a2) If $0 < l < n < m$ (mapping into higher dimensions),

$$x' = E_{lm}x = diag(\overbrace{1,1,\ldots,1}^{l},\overbrace{D,D,\ldots,D}^{m-l})(x_1,x_2,\ldots,x_l,\overbrace{T,T,\ldots,T}^{m-l})^T$$
$$= (x_1,x_2,\ldots,x_l,\overbrace{DT,DT,\ldots,T}^{m-l})^T.$$

Therefore, $E_{mn}x' = (E_{nm})^{-1}x'$

$$= diag(\overbrace{1,1,\ldots,1}^{n},\overbrace{D^{-1},D^{-1},\ldots,D^{-1}}^{m-n})(x_1,x_2,\ldots,x_l,\overbrace{DT,DT,\ldots,DT}^{m-l})^T$$
$$= (x_1,x_2,\ldots,x_l,\overbrace{DT,DT,\ldots,DT}^{n-l}\overbrace{T,T,\ldots,T}^{m-n})^T.$$

Remark. T is temporary. For example,

$$\begin{pmatrix}1 & 0 & 0\\ 0 & D^{-1} & 0\\ 0 & 0 & D^{-1}\end{pmatrix}\begin{pmatrix}a\\ DT\\ DT\end{pmatrix} = \begin{pmatrix}1 & 0 & 0\\ 0 & D^{-1} & 0\\ 0 & 0 & D^{-1}\end{pmatrix}\begin{pmatrix}1 & 0 & 0\\ 0 & D & 0\\ 0 & 0 & D\end{pmatrix}\begin{pmatrix}a\\ T\\ T\end{pmatrix}$$
$$= \begin{pmatrix}1 & 0 & 0\\ 0 & 1 & 0\\ 0 & 0 & 1\end{pmatrix}\begin{pmatrix}a\\ T\\ T\end{pmatrix} = \begin{pmatrix}a\\ T\\ T\end{pmatrix} = a.$$

Therefore :

$$= (x_1,x_2,\ldots,x_l,\overbrace{DT,DT,\ldots,DT}^{n-l})^T$$
$$= diag(\overbrace{1,1,\ldots,1}^{l},\overbrace{D,D,\ldots,D}^{n-l})(x_1,x_2,\ldots,x_l,\overbrace{T,T,\ldots,T}^{n-l})^T = E_{ln}x.$$

a3) If $0 < m < l < n$ (mapping into higher dimensions),

$$x' = E_{lm}x = (E_{ml})^{-1}\,x = diag(\overbrace{1,1,\ldots,1}^{m},\overbrace{D^{-1},D^{-1},\ldots,D^{-1}}^{l-m})(x_1,x_2,\ldots,x_l)^T$$
$$= (x_1,x_2,\ldots,x_m,D^{-1}x_{m+1},D^{-1}x_{m+2},\ldots,D^{-1}x_l)^T.$$

Therefore :

$$E_{mn}x' = diag(\overbrace{1,1,\ldots,1}^{m},\overbrace{D,D,\ldots,D}^{n-m})\times$$
$$\times\,(x_1,x_2,\ldots,x_m,\overbrace{D^{-1}x_{m+1},D^{-1}x_{m+2},\ldots,D^{-1}x_l}^{l-m},\overbrace{T,T,\ldots,T}^{n-l})^T$$
$$= (x_1,x_2,\ldots,x_l,\overbrace{DT,DT,\ldots,DT}^{n-l})^T$$
$$= diag(\overbrace{1,1,\ldots,1}^{l},\overbrace{D,D,\ldots,D}^{n-l})(x_1,x_2,\ldots,x_l,\overbrace{T,T,\ldots,T}^{n-l})^T$$
$$= E_{ln}x.$$

b1) If $0 < n < m < l$ (mapping into lower dimensions),

$$x' = E_{lm}x = (E_{ml})^{-1}\,x = diag(\overbrace{1,1,\ldots,1}^{m},\overbrace{D^{-1},D^{-1},\ldots,D^{-1}}^{l-m})(x_1,x_2,\ldots,x_l)^T$$
$$= (x_1,x_2,\ldots,x_m,D^{-1}x_{m+1},D^{-1}x_{m+2},\ldots,D^{-1}x_l)^T.$$

Therefore :

$$E_{mn}x^{'} = (E_{nm})^{-1}\,x^{'}$$
$$= diag(\overbrace{1,1,\ldots,1}^{n},\overbrace{D^{-1}D^{-1},\ldots,D^{-1}}^{m-n}\overbrace{1,1,\ldots,1}^{l-m})\times$$
$$\times\,(x_1,x_2,\ldots,x_m,D^{-1}x_{m+1},D^{-1}x_{m+2},\ldots,D^{-1}x_l)^T$$
$$= (x_1,x_2,\ldots,x_n,D^{-1}x_{n+1},D^{-1}x_{n+2},\ldots,D^{-1}x_l)^T$$
$$= diag(\overbrace{1,1,\ldots,1}^{n},\overbrace{D^{-1}D^{-1},\ldots,D^{-1}}^{l-n})(x_1,x_2,\ldots,x_l)^T$$
$$= (E_{nl})^{-1}\,x = E_{ln}x.$$

b2) If $0 < n < l < m$ (mapping into lower dimensions),

$$x' = E_{lm}x = diag(\overbrace{1,1,\ldots,1}^{l},\overbrace{D,D,\ldots,D}^{m-l})(x_1,x_2,\ldots,x_l,\overbrace{T,T,\ldots,T}^{m-l})^T$$
$$= (x_1,x_2,\ldots,x_l,\overbrace{DT,DT,\ldots,DT}^{m-l})^T.$$

Therefore:

$$E_{mn}x' = (E_{nm})^{-1}\,x' = diag(\overbrace{1,1,\ldots,1}^{n},\overbrace{D^{-1}D^{-1},\ldots,D^{-1}}^{m-n})(x_1,x_2,\ldots,x_l,\overbrace{DT,DT,\ldots,DT}^{m-l})^T$$
$$= (x_1,x_2,\ldots,x_n,D^{-1}x_{n+1},D^{-1}x_{n+2},\ldots,D^{-1}x_l,\overbrace{T,T,\ldots,T}^{m-l})^T$$
$$= diag(\overbrace{1,1,\ldots,1}^{n},\overbrace{D^{-1}D^{-1},\ldots,D^{-1}}^{l-n})(x_1,x_2,\ldots,x_l)^T$$
$$= (E_{nl})^{-1}x = E_{ln}x.$$

b3) If $0 < m < n < l$ (mapping into lower dimensions),

$$x' = E_{lm}x = (E_{ml})^{-1}x = diag(\overbrace{1,1,\ldots,1}^{m},\overbrace{D^{-1},D^{-1},\ldots,D^{-1}}^{l-m})(x_1,x_2,\ldots,x_l)^T$$
$$= (x_1,x_2,\ldots,x_m,D^{-1}x_{m+1},D^{-1}x_{m+2},\ldots,D^{-1}x_l)^T.$$

Therefore :

$$E_{mn}x' = diag(\overbrace{1,1,\ldots,1}^{m},\overbrace{D,D,\ldots,D}^{n-m}\overbrace{1,1,\ldots,1}^{l-n})\times$$
$$\times (x_1,x_2,\ldots,x_m,D^{-1}x_{m+1},D^{-1}x_{m+2},\ldots,D^{-1}x_l)^T$$
$$= (x_1,x_2,\ldots,x_n,D^{-1}x_{n+1},D^{-1}x_{n+2},\ldots,D^{-1}x_l)^T$$
$$= diag(\overbrace{1,1,\ldots,1}^{n},\overbrace{D^{-1}D^{-1},\ldots,D^{-1}}^{l-n})(x_1,x_2,\ldots,x_l)^T$$
$$= (E_{nl})^{-1}x = E_{ln}x.$$

Proof of (ii), the associative law is as follows: since $(E_{kl}E_{lm})E_{mn} = E_{km}E_{mn} = E_{kn}$ and $E_{kl}(E_{lm}E_{mn}) = E_{kl}E_{ln} = E_{kn}$ from (i), $(E_{kl}E_{lm})E_{mn} = E_{kl}(E_{lm}E_{mn})$.
Proof of (iii) follows the rule of Eq. 3.6. Another proof is from formula (i): $f\left(AA^{-1}\right) = I = f(A)\,f(A^{-1})$. Therefore, $f(A^{-1}) = f(A)^{-1}$, where $f\left(A^{-1}\right) = E_{ml}$ and $f(A)^{-1} = (E_{lm})^{-1}$.
Proof of (iv) is trivial from (ii).
Proof of (v), $E_{lm}E_{mn}\,(E_{lm}E_{mn})^{-1} = E_{lm}E_{mn}\,(E_{mn})^{-1}\,(E_{lm})^{-1} = E_{ll} \equiv 1$.
Finally, proof of (vi) is as follows. For $G = \{E_{lm}\}$, the scalar multiplication by 1 in field k holds as $s\colon 1 \times G = G \times 1 \to G$. It is compatible with the matrix multiplications in G. Then,
$E_{mn} = I_m E_{mn} \equiv 1E_{mn} = E_{mn}1 \equiv E_{mn}I_n = E_{mn}$. Since it is 'mapping to itself' in the narrow sense of the word, it is equivalent to conventional unit matrices. □
Since this groupoid is homomorphism from (i), it can be considered as a representation of groupoid. Strictly speaking, it is automorphism. This will be proven later.

From Another Viewpoint. For E_{lm}, the binary operation is partially defined but not for any two elements arbitrarily taken from G. That is a groupoid. However, we must note that group axioms do not claim that such a whole process ought to be done. To confirm that, let us try to give the following five conditions as group axioms:
(1) We randomly take any two elements in a set G.
(2) For any two elements taken from G, the operation is closed in G,
s.t. $\forall a, b, c \in G$, $ab = c$.
(3) For any a, b, c in G, $(ab)\,c = a(bc)$: associative law holds.
(4) There exists unique identity e.
(5) For each a in G, its inverse b exists, s.t. $ab = ba = e$.
What we must pay attention to is whether or not the first condition should be included as an axiom of a group. If accepting that to be a fact, we should introduce a concept of axioms in probability theory. That is, in group theory, we assume the whole event for any two elements arbitrarily taken from G in the manner of probability theory. Then, define binary operation as such for any elements taken from G at random. It means we should consider so-called 'sample space' in measure theory for probability in group theory. Group axioms naturally do not take such

another axiomatic system in probability theory.

Remark. There are $N \times N \times N \times N$ combinations of operations by E_{lm}. Even when the operations are valid there are $N \times N \times N$ combinations. This obviously means that there are far more combinations than the ordinary algebraic operations in **N, Z, Q, R, C** and square matrices. Nevertheless, $N \times N \times N \times N$ operations for all those elements create a 'sample space'. That is the 'axiom of probability theory', not an 'axiom of a group'.
Textbooks of algebra often write that the definition of a group is closed by $G \times G \to G$. That will be fine if the algebra you are dealing with is in **N, Z, Q, R, C** or square matrices. However, it violates the 'axioms of a group' and strengthens them on their own.
If we interpret the axioms of a group correctly, it will be enough to say that $E_{ij}E_{jk}$ hold for any E_{lm} in G, which have already $N \times N \times N$ combinations more than $N \times N$ combinations. This is the same as the logic of the associative law in linear algebra. That is, if $M_{jk} = A$, $M_{kl} = B$ and $M_{lm} = C$, then $M_{jk}M_{kl}M_{lm} = ABC = (AB)C = A(BC)$. In this case there are $N \times N \times N \times N$ combinations that are more than $N \times N \times N$ combinations in the algebraic case of ABC. Therefore, there is no problem.
However, considering E_{lm} to be a groupoid, more people will recognize and discuss it further. So, we also need to discuss it as a groupoid.

18.5 The Groupoid Representation

Proposition. *Equation of the groupoid* $E_{lm}E_{mn} = E_{ln}$ *is automorphism.*

Proof. Firstly, the automorphism is proven as follows. Let $f(A)$ be E_{lm}, $f(B)$ be E_{mn}.
a1) If $0 < l < m < n$ (mapping into higher dimensions),
for $f(A)(B)$,

$$(f(A))(x) = x' = E_{lm}x = \mathrm{diag}(\overbrace{1,1,\ldots,1}^{l},\overbrace{D,D,\ldots,D}^{m-l})(x_1,x_2,\ldots,x_l,\overbrace{T,T,\ldots,T}^{m-l})^T$$
$$= (x_1,x_2,\ldots,x_l,\overbrace{DT,DT,\ldots,T}^{m-l})^T.$$

Then,

$$(f(B))(x') = E_{mn}x'$$
$$= \mathrm{diag}(\overbrace{1,1,\ldots,1}^{m},\overbrace{D,D,\ldots,D}^{n-m})(x_1,x_2,\ldots,x_l,\overbrace{DT,DT,\ldots,DT}^{m-l}\overbrace{T,T,\ldots,T}^{n-m})^T$$
$$= (x_1,x_2,\ldots,x_l,\overbrace{DT,DT,\ldots,T}^{n-l})^T$$
$$= \mathrm{diag}(\overbrace{1,1,\ldots,1}^{l},\overbrace{D,D,\ldots,D}^{n-l})(x_1,x_2,\ldots,x_l,\overbrace{T,T,\ldots,T}^{n-l})^T = E_{ln}x.$$

For $f(AB)$,
$(f(AB))(x) = E_{lm}E_{mn}x$

$$= \mathrm{diag}(\overbrace{1,1,\ldots,1}^{l},\overbrace{D,D,\ldots,D}^{m-l}\overbrace{1,1,\ldots,1}^{n-m})\mathrm{diag}(\overbrace{1,1,\ldots,1}^{m},\overbrace{D,D,\ldots,D}^{n-m})\times$$
$$\times\,(x_1,x_2,\ldots,x_l,\overbrace{T,T,\ldots,T}^{n-l})^T$$
$$= (x_1,x_2,\ldots,x_l,\overbrace{DT,DT,\ldots,T}^{n-l})^T$$
$$= \mathrm{diag}(\overbrace{1,1,\ldots,1}^{l},\overbrace{D,D,\ldots,D}^{n-l})(x_1,x_2,\ldots,x_l,\overbrace{T,T,\ldots,T}^{n-l})^T = E_{ln}x.$$

Therefore, $f(AB) = f(A)(B)$.

a2) If $0 < l < n < m$ (mapping into higher dimensions),
for $f(A)\,f(B)$,

$$(f(A))(x) = x' = E_{lm}x = \mathrm{diag}(\overbrace{1,1,\ldots,1}^{l},\overbrace{D,D,\ldots,D}^{m-l})(x_1,x_2,\ldots,x_l,\overbrace{T,T,\ldots,T}^{m-l})^T$$
$$= (x_1,x_2,\ldots,x_l,\overbrace{DT,DT,\ldots,T}^{m-l})^T.$$

Then,

$$(f(B))(x') = E_{mn}x' = (E_{nm})^{-1}x'$$
$$= \mathrm{diag}(\overbrace{1,1,\ldots,1}^{n},\overbrace{D^{-1},D^{-1},\ldots,D^{-1}}^{m-n})(x_1,x_2,\ldots,x_l,\overbrace{DT,DT,\ldots,DT}^{m-l})^T$$
$$= (x_1,x_2,\ldots,x_l,\overbrace{DT,DT,\ldots,DT}^{n-l}\overbrace{T,T,\ldots,T}^{m-n})^T = (x_1,x_2,\ldots,x_l,\overbrace{DT,DT,\ldots,DT}^{n-l})^T$$
$$= \mathrm{diag}(\overbrace{1,1,\ldots,1}^{l},\overbrace{D,D,\ldots,D}^{n-l})(x_1,x_2,\ldots,x_l,\overbrace{T,T,\ldots,T}^{n-l})^T = E_{ln}x.$$

For $f(AB)$,

$$(f(AB))(x) = (E_{lm}E_{mn})x = \mathrm{diag}(\overbrace{1,1,\ldots,1}^{l},\overbrace{D,D,\ldots,D}^{m-l})\times$$
$$\times\mathrm{diag}(\overbrace{1,1,\ldots,1}^{n},\overbrace{D^{-1},D^{-1},\ldots,D^{-1}}^{m-n})(x_1,x_2,\ldots,x_l,\overbrace{T,T,\ldots,T}^{m-l})^T$$
$$= (x_1,x_2,\ldots,x_l,\overbrace{DT,DT,\ldots,DT}^{n-l}\overbrace{T,T,\ldots,T}^{m-n})^T = (x_1,x_2,\ldots,x_l,\overbrace{DT,DT,\ldots,DT}^{n-l})^T$$
$$= \mathrm{diag}(\overbrace{1,1,\ldots,1}^{l},\overbrace{D,D,\ldots,D}^{n-l})(x_1,x_2,\ldots,x_l,\overbrace{T,T,\ldots,T}^{n-l})^T = E_{ln}x.$$

Therefore, $f(AB) = f(A)(B)$.

a3) If $0 < m < l < n$ (mapping into higher dimensions),
for $f(A)\,f(B)$,

$$(f(A))(x) = x' = E_{lm}x = (E_{ml})^{-1}x = \mathrm{diag}(\overbrace{1,1,\ldots,1}^{m},\overbrace{D^{-1},D^{-1},\ldots,D^{-1}}^{l-m})(x_1,x_2,\ldots,x_l)^T$$
$$= (x_1,x_2,\ldots,x_m,D^{-1}x_{m+1},D^{-1}x_{m+2},\ldots,D^{-1}x_l)^T.$$

Then,

$$(f(B))(x') = E_{mn}x'$$
$$= \mathrm{diag}(\overbrace{1,1,\ldots,1}^{m},\overbrace{D,D,\ldots,D}^{n-m})(x_1,x_2,\ldots,x_m,\overbrace{D^{-1}x_{m+1},D^{-1}x_{m+2},\ldots,D^{-1}x_l}^{l-m},\overbrace{T,T,\ldots,T}^{n-l})^T$$

$$= (x_1, x_2, \ldots, x_l, \overbrace{DT, DT, \ldots, DT}^{n-l})^T$$
$$= diag(\overbrace{1, 1, \ldots, 1}^{l}, \overbrace{D, D, \ldots, D}^{n-l})(x_1, x_2, \ldots, x_l, \overbrace{T, T, \ldots, T}^{n-l})^T = E_{ln}x.$$

For $f(AB)$,

$$(f(AB))(x) = (E_{lm}E_{mn})x$$
$$= diag(\overbrace{1, 1, \ldots, 1}^{m}, \overbrace{D^{-1}, D^{-1}, \ldots, D^{-1}}^{l-m}, \overbrace{1, 1, \ldots, 1}^{n-l}) \times$$
$$\times diag(\overbrace{1, 1, \ldots, 1}^{l}, \overbrace{D, D, \ldots, D}^{n-m})(x_1, x_2, \ldots, x_l \overbrace{T, T, \ldots, T}^{n-l})^T$$
$$= (x_1, x_2, \ldots, x_l, \overbrace{DT, DT, \ldots, DT}^{n-l})^T$$
$$= diag(\overbrace{1, 1, \ldots, 1}^{l}, \overbrace{D, D, \ldots, D}^{n-l})(x_1, x_2, \ldots, x_l, \overbrace{T, T, \ldots, T}^{n-l})^T = E_{ln}x.$$

Therefore, $f(AB) = f(A)(B)$.

b1) If $0 < n < m < l$ (mapping into lower dimensions),
for $f(A)f(B)$,

$$(f(A))(x) = E_{lm}x = (E_{ml})^{-1}x = diag(\overbrace{1, 1, \ldots, 1}^{m}, \overbrace{D^{-1}, D^{-1}, \ldots, D^{-1}}^{l-m})(x_1, x_2, \ldots, x_l)^T$$
$$= (x_1, x_2, \ldots, x_m, D^{-1}x_{m+1}, D^{-1}x_{m+2}, \ldots, D^{-1}x_l)^T.$$

Then,

$$(f(B))(x) = E_{mn}x' = (E_{nm})^{-1}x'$$
$$= diag(\overbrace{1, 1, \ldots, 1}^{n}, \overbrace{D^{-1}D^{-1}, \ldots, D^{-1}}^{m-n}, \overbrace{1, 1, \ldots, 1}^{l-m}) \times$$
$$\times (x_1, x_2, \ldots, x_m, D^{-1}x_{m+1}, D^{-1}x_{m+2}, \ldots, D^{-1}x_l)^T$$
$$= (x_1, x_2, \ldots, x_n, D^{-1}x_{n+1}, D^{-1}x_{n+2}, \ldots, D^{-1}x_l)^T$$
$$= diag(\overbrace{1, 1, \ldots, 1}^{n}, \overbrace{D^{-1}D^{-1}, \ldots, D^{-1}}^{l-n})(x_1, x_2, \ldots, x_l)^T$$
$$= (E_{nl})^{-1}x = E_{ln}x.$$

For $f(AB)$,

$$(f(AB))(x) = (E_{lm}E_{mn})x = diag(\overbrace{1, 1, \ldots, 1}^{m}, \overbrace{D^{-1}, D^{-1}, \ldots, D^{-1}}^{l-m}) \times$$
$$\times diag(\overbrace{1, 1, \ldots, 1}^{n}, \overbrace{D^{-1}D^{-1}, \ldots, D^{-1}}^{m-n}, \overbrace{1, 1, \ldots, 1}^{l-m})(x_1, x_2, \ldots, x_l)^T$$
$$= (x_1, x_2, \ldots, x_n, D^{-1}x_{n+1}, D^{-1}x_{n+2}, \ldots, D^{-1}x_l)^T$$
$$= diag(\overbrace{1, 1, \ldots, 1}^{n}, \overbrace{D^{-1}D^{-1}, \ldots, D^{-1}}^{l-n})(x_1, x_2, \ldots, x_l)^T$$
$$= (E_{nl})^{-1}x = E_{ln}x.$$

Therefore, $f(AB) = f(A)(B)$.

b2) If $0 < n < l < m$ (mapping into lower dimensions),
for $f(A)f(B)$,

$$(f(A))(x) = x' = E_{lm}x = \mathrm{diag}(\overbrace{1,1,\ldots,1}^{l},\overbrace{D,D,\ldots,D}^{m-l})(x_1,x_2,\ldots,x_l,\overbrace{T,T,\ldots,T}^{m-l})^T$$
$$= (x_1,x_2,\ldots,x_l,\overbrace{DT,DT,\ldots,DT}^{m-l})^T.$$

Then,

$$(f(B))(x') = E_{mn}x' = (E_{nm})^{-1}x'$$
$$= \mathrm{diag}(\overbrace{1,1,\ldots,1}^{n},\overbrace{D^{-1}D^{-1},\ldots,D^{-1}}^{m-n})(x_1,x_2,\ldots,x_l,\overbrace{DT,DT,\ldots,DT}^{m-l})^T$$
$$= (x_1,x_2,\ldots,x_n,D^{-1}x_{n+1},D^{-1}x_{n+2},\ldots,D^{-1}x_l,\overbrace{T,T,\ldots,T}^{m-l})^T$$
$$= (x_1,x_2,\ldots,x_n,D^{-1}x_{n+1},D^{-1}x_{n+2},\ldots,D^{-1}x_l)^T$$
$$= \mathrm{diag}(\overbrace{1,1,\ldots,1}^{n},\overbrace{D^{-1}D^{-1},\ldots,D^{-1}}^{l-n})(x_1,x_2,\ldots,x_l)^T$$
$$= (E_{nl})^{-1}x = E_{ln}x.$$

For $f(AB)$,

$$(f(AB))(x) = (E_{lm}E_{mn})x = \mathrm{diag}(\overbrace{1,1,\ldots,1}^{l},\overbrace{D,D,\ldots,D}^{m-l})\times$$
$$\times\ \mathrm{diag}(\overbrace{1,1,\ldots,1}^{n},\overbrace{D^{-1}D^{-1},\ldots,D^{-1}}^{m-n})(x_1,x_2,\ldots,x_l,\overbrace{T,T,\ldots,T}^{m-l})^T$$
$$= (x_1,x_2,\ldots,x_n,D^{-1}x_{n+1},D^{-1}x_{n+2},\ldots,D^{-1}x_l,\overbrace{T,T,\ldots,T}^{m-l})^T$$
$$= (x_1,x_2,\ldots,x_n,D^{-1}x_{n+1},D^{-1}x_{n+2},\ldots,D^{-1}x_l)^T$$
$$= \mathrm{diag}(\overbrace{1,1,\ldots,1}^{n},\overbrace{D^{-1}D^{-1},\ldots,D^{-1}}^{l-n})(x_1,x_2,\ldots,x_l)^T$$
$$= (E_{nl})^{-1}x = E_{ln}x.$$

Therefore, $f(AB) = f(A)(B)$.

b3) If $0 < m < n < l$ (mapping into lower dimensions),
for $f(A)\,f(B)$,

$$(f(A))(x) = x' = E_{lm}x = (E_{ml})^{-1}x = \mathrm{diag}(\overbrace{1,1,\ldots,1}^{m},\overbrace{D^{-1},D^{-1},\ldots,D^{-1}}^{l-m})(x_1,x_2,\ldots,x_l)^T$$
$$= (x_1,x_2,\ldots,x_m,D^{-1}x_{m+1},D^{-1}x_{m+2},\ldots,D^{-1}x_l)^T.$$

Then,

$$(f(B))(x') = E_{mn}x'$$
$$= \mathrm{diag}(\overbrace{1,1,\ldots,1}^{m},\overbrace{D,D,\ldots,D}^{n-m}\overbrace{1,1,\ldots,1}^{l-n})(x_1,x_2,\ldots,x_m,D^{-1}x_{m+1},D^{-1}x_{m+2},\ldots,D^{-1}x_l)^T$$
$$= (x_1,x_2,\ldots,x_n,D^{-1}x_{n+1},D^{-1}x_{n+2},\ldots,D^{-1}x_l)^T$$
$$= \mathrm{diag}(\overbrace{1,1,\ldots,1}^{n},\overbrace{D^{-1}D^{-1},\ldots,D^{-1}}^{l-n})(x_1,x_2,\ldots,x_l)^T$$
$$= (E_{nl})^{-1}x = E_{ln}x.$$

For $f(AB)$,

$$(f(AB))(x) = (E_{lm}E_{mn})x$$

$$= diag(\overbrace{1,1,\ldots,1}^{m},\overbrace{D^{-1},D^{-1},\ldots,D^{-1}}^{l-m})diag(\overbrace{1,1,\ldots,1}^{m},\overbrace{D,D,\ldots,D}^{n-m}\overbrace{1,1,\ldots,1}^{l-n})(x_1,x_2,\ldots,x_l)^T$$
$$= (x_1,x_2,\ldots,x_n,D^{-1}x_{n+1},D^{-1}x_{n+2},\ldots,D^{-1}x_l)^T$$
$$= diag(\overbrace{1,1,\ldots,1}^{n},\overbrace{D^{-1}D^{-1},\ldots,D^{-1}}^{l-n})(x_1,x_2,\ldots,x_l)^T$$
$$= (E_{nl})^{-1}x = E_{ln}x.$$

Therefore, $f(AB) = f(A)(B)$.

18.6 The Finite Simple Groupoid

18.6.1 A modelling of the Transformation Groupoid

We discuss a movement as follows. There is a point on the whole number line. We move it as an integer m to another one n on that line. We denote it as ${}_iT_j$. We think of the whole elements $G = \{{}_iT_j \,|i,j\in Z\}$. Then, we discuss the partial operation ${}_iT_k = {}_iT_{jj}T_k$. It expresses repetition of the movement. G makes a groupoid. This is a modelling of the groupoid on the line as mentioned in former sections. In this section, we think of the subgroupoids.

18.6.2 Introduction

Thinking of a point on the whole number line, we move the point at the integer m to another one n on the same line, as shown in Fig. 16. We denote the movement ${}_mT_n$.

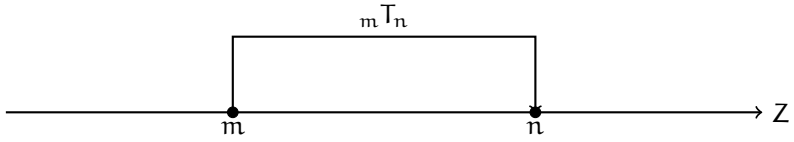

Fig.16

We think of all the elements $G = \{{}_mT_n \,|m,n\in Z\}$. Now, let us think of the partial function for the repetition of the movement ${}_lT_n = {}_lT_{mm}T_n$. It means a series of movements of a point at the integer l to m, then m to n on the whole number line. There are 6 types of procedures for ${}_lT_n = {}_lT_{mm}T_n$ as shown in Fig. 17.

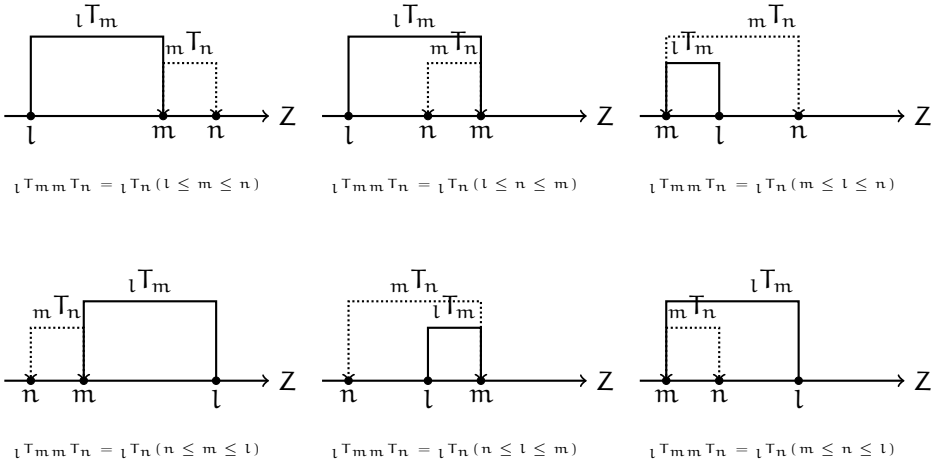

Fig.17

Theorem. *Laws under the rule of partial operations in G are as follows:*

I. $_i T_{jj} T_k = {}_i T_k$, (6.1)

II. $(_i T_{jj} T_k)_k T_l = {}_i T_j (_j T_{kk} T_l)$, (6.2)

III. $(_i T_j)^{-1} = {}_j T_i$, (6.3)

IV. $_i T_{jj} T_{kk} T_j = {}_i T_{jj} T_k (_j T_k)^{-1} = {}_i T_j$ (right identity) (6.4)

and $_j T_{ii} T_{jj} T_k = (_i T_j)^{-1} {}_i T_{jj} T_k = {}_j T_k$ (left identity), (6.5)

V. $_i T_{jj} T_i = {}_i T_i \equiv 1 \equiv {}_j T_{ii} T_j = {}_j T_j$. (6.6)

Proof. (I) is trivial by the definition (see also Eq. 4.1).
The proof of (II) is as follows. From (I), $(_i T_{jj} T_k)_k T_l = {}_i T_{kk} T_l = {}_i T_l$ and $_i T_j (_j T_{kk} T_l) = {}_i T_{jj} T_l = {}_i T_l$.
(III) is clear under the operation on the whole number line.
(IV) is trivial from (I).
The proof of (V) is as follows. Since $_m T_m$ is 'mapping to itself' on the number line, it is an identity. Furthermore, the identity is unique because $_m T_m$ is equivalent to 1. □

18.6.3 The Subgroupoids

Let us think of the subgroupoids.They mainly consist of two subgroupoids:

$H = \{_{2m-1} T_{2n-1} \,|m, n \in Z\}$, (6.7)

$H' = \{_{2m} T_{2n} \,|m, n \in Z\}$. (6.8)

The rest $G - (H \cup H') = \{_{2i-1} T_{2j,2k} \, T_{2l-1} \,|i, j, k, l \in Z\}$ (6.9)

are not subgroupoids but subsets.

Remark. If $\{_{2m-1} T_{2n}\}\{_{2n} T_{2m-1}\} = \{_{2m-1} T_{2m-1}\} = 1$, then they are not in $G - (H \cup H')$.

We need to pay attention to such an operation. If we take an element like $_4 T_{33} T_2 = {}_4 T_2$, it is not in $G - (H \cup H')$ but H'. Such an operation is equivalent to operations

in G. Eventually, H, $H^{'}$ and $G-(H\cup H')$ are disjoint. Therefore, the direct sum decomposition is:

$$G=\{{}_{2m-1}T_{2n-1}\}\sqcup\{{}_{2m}T_{2n}\}\sqcup\{{}_{2i-1}T_{2j}\}\sqcup\{{}_{2k}T_{2l-1}\}\sqcup\{{}_{u}T_{u}\}. \tag{6.10}$$

Proposition 1. H and $H^{'}$ are not normal subgroupoids of G.

Proof. Let us assume that H is a normal subgroupoid. Let g, for example, be any element in ${}_{2m-1}T_{2n}$. Operating gH is impossible unless any element in H is ${}_{2n}T_{2l-1}$ or ${}_{2n}T_{2l}$ under the rule of the partial function. Therefore, gH cannot be left coset. $gH\notin G$ in this case. Then, let us operate Hg. As $H=\{{}_{2k-1}T_{2m-1}\}$, it holds and the right coset $Hg={}_{2k-1}T_{2n}$. Therefore, $gH\neq Hg$.
Likewise, let us assume that $H^{'}$ is a normal subgroupoid. Let, for example, $\forall g'\in{}_{2m}T_{2n-1}$. Operating $g'H'$, it cannot be operated unless any elements in H' are ${}_{2n-1}T_{2l}$ or ${}_{2n-1}T_{2l-1}$. They are not in $H^{'}$ either. Therefore, $g'H'\notin G$. Operating $H'g$, it holds since any elements in $H^{'}$ are ${}_{2k}T_{2m}$. Then, $H'g'={}_{2k}T_{2n-1}$. Therefore, $g'H'\neq H'g'$. □
As another way of creating subgroupoids from the groupoid, let us think of $H''=\{{}_{m}T_{n}\,|k<m<l, k<n<l, k, l, m, n\in Z\}$. However, none of them are normal subgroupoids other than the identity: for H'', only if $m=n$ ($\because H''=\{{}_{l}T_{l}\}\equiv 1$), then $gH''=H''g$. It is trivial ($g_{kl}1=1g_{kl}=g_{kl}$).

Proposition 2. *The maximal proper subgroupoid H''' is a set of extracting elements whose index number i or j of ${}_{i}T_{j}$ is fixed and all the inverses are from G. In other words, any element should have inverse also in subgroupoid by the two-step 'subgroupoid' test. For example, $H'''=G-(\{{}_{m}T_{0}\}\cup\{{}_{0}T_{m}\})$. It graphically means that only the point '0' is skipped in a series of operations on the number line. Likewise, it is also not the normal subgroupoid.*

Proof. ${}_{m}T_{0}H'''$ does not hold but $H'''{}_{m}T_{0}$ does. Therefore, ${}_{m}T_{0}H^{'''}\neq H'''_{m}T_{0}$. □
From this proof, it is clear that any other smaller subgroupoids extracting any other subsets or families of sets will not be normal. The simplest example is a case of $G=\{{}_{m}T_{n}\,|m,n=0,1,2\}$ and the smallest subgroupoid (except for the identity as subgroupoid) is $\{{}_{m}T_{n}\,|m,n=0,1\}$, $\{{}_{m}T_{n}\,|m,n=1,2\}$ and $\{{}_{m}T_{n}\,|m,n=0,2\}$. Based on the proof above, it is trivial that none of these subgroupoids are normal. Contrarily, what will happen if we sum up those extracted families of sets? What we get interested in will be if such a summed-up subset makes a subgroupoid of G. To confirm it, let us think of such a total subset s_k as follows:

$$s_k=(\{{}_{m}T_{-m}\}\cup\{{}_{-m}T_{m}\})\cup\ldots\cup(\{{}_{m}T_{-1}\}\cup\{{}_{-1}T_{m}\})\cup(\{{}_{m}T_{0}\}\cup\{{}_{0}T_{m}\})\cup(\{{}_{m}T_{1}\}\cup\{{}_{1}T_{m}\})\cup\ldots$$
$$\ldots\cup(\{{}_{m}T_{k}\}\cup\{{}_{k}T_{m}\}) \tag{6.11}$$

where $0<k\leq m$. If $k=m$, $s_k=s_m=G$.
If corresponding this model on the line to the groupoid that we have discussed, then:

$$s_k=(\{{}_{m}T_{0}\}\cup\{{}_{0}T_{m}\})\cup(\{{}_{m}T_{1}\}\cup\{{}_{1}T_{m}\})\cup\ldots\cup(\{{}_{m}T_{k}\}\cup\{{}_{k}T_{m}\}). \tag{6.12}$$

If thinking of the partial operation ${}_{k+1}T_{kk}T_{k+2}$, then ${}_{k+1}T_{kk}T_{k+2}={}_{k+1}T_{k+2}\notin s_k$. Besides, if ${}_{m}T_{m-1}\ {}_{m-1}T_{m}$, then ${}_{m}T_{m-1}\ {}_{m-1}T_{m}={}_{m}T_{m}\notin s_{m-1}$. Thus, any such total subsets do not make the subgroupoid. If adding ${}_{m}T_{m}$ on to s_{m-1}, $s_{m-1}\sqcup{}_{m}T_{m}$

results in G. Verifying them on the number line will be clearer.

Therefore, we resulted in proving that ${}_{\mathfrak{l}}\mathrm{T}_{\mathfrak{m}}$ is a finite simple 'group', not only a finite simple groupoid. See also **From Another Viewpoint** and **Remark** in Section 4 above about **the Groupoid**. That is the so-called 'Conway's nightmare' among group theorists researching the classification of finite simple groups. Most of those theorists believe that any new finite simple groups do not exist. However, some are apprehensive about the possible existence of such groups. John Horton Conway of 'Conway's nightmare' is known as one of the contributors of finite simple groups.

18.7 The Invariant or Symmetry Towards Noether's Theorem

- Invariant: In theoretical physics, an invariant means a physical system unchanged under mathematical operation. This is also called symmetry.
- Noether's theorem: this states that every differential symmetry of the action of a physical system with conservative forces has a corresponding law of conservation.
- Noether's theorem holds that there are not only differential symmetries but also discrete ones.Parity and selection rule in quantum theory are such examples.

Then, what is the invariant in the groupoid that we have discussed?

- The invariant is the conservation of the degrees of freedom. Wherever a point is mapped, its degrees of freedom are conserved.
- It suggests that if higher dimensional physics were described by the groupoid, we might find an unknown physical law of conservation.

Furthermore, what is the preferable unification of string theories? See below:

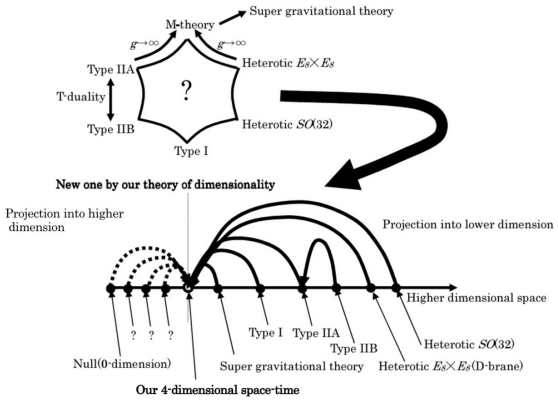

- The upper model is by M-theory.
- The lower one is by our theory of dimensionality.

18.8 The Set Theoretical Approach

Remark. Metric space, that is the concept of distance, is NOT defined in set theory. There is no concept of neighbourhood. A, B and C are not Hausdorff space.

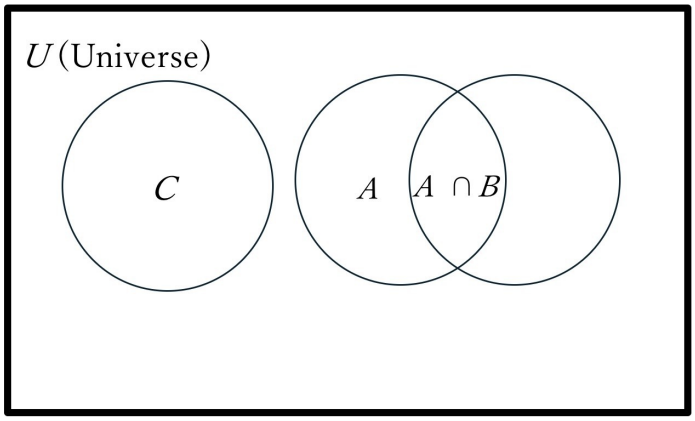

18.8.1 Empirical Thought of Dimensionality

We have never detected higher dimensional space, much less infinite dimensional space.

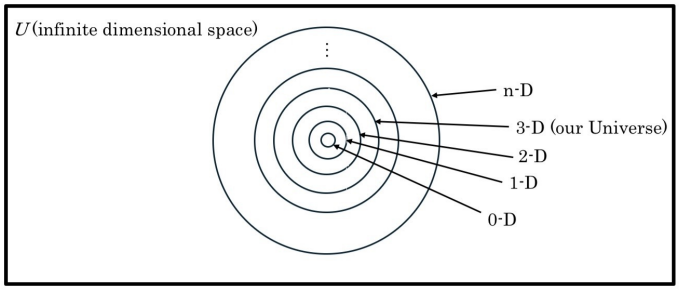

18.8.2 M-theory

M-theory states that our Universe (3-brane) drifts on the 'bulk'. However, we have neither detected Calabi-Yau manifold nor'bulk'.

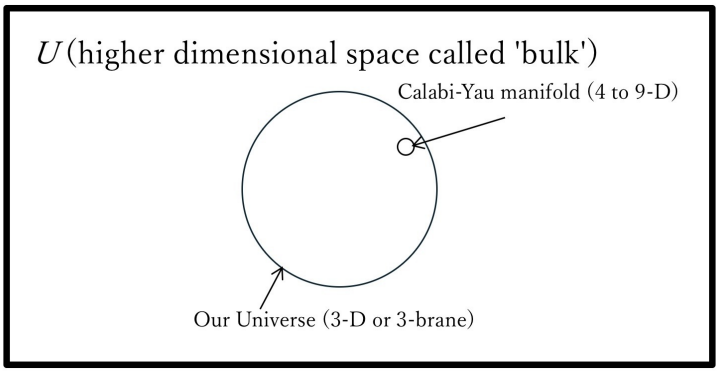

18.8.3 Still Empirical but Rational Thought of Dimensionality

This model is far simpler and more reasonable than M-theory. However, we have never detected infinite dimensional space.

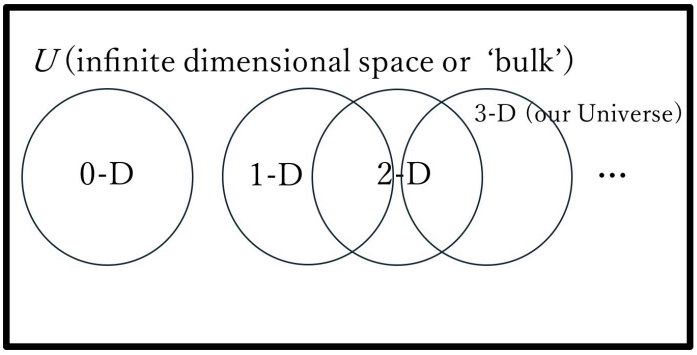

18.8.4 Non-empirical Thought of Dimensionality

We should not empirically think of dimensionality. We should not introduce U (universe in set theory), including $\mathcal{U}_n$. Each dimensional space $\mathcal{U}_n$ is independent from others as shown in the Venn diagrams below. There is neither interaction nor union. They are disjoint from each other. Therefore:

$$\mathcal{U}_0 \cap \mathcal{U}_1 \cap \mathcal{U}_2 \cap \ldots \cap \mathcal{U}_n = (\mathcal{U}_0 \cup \mathcal{U}_1 \cup \mathcal{U}_2 \cup \ldots \cup \mathcal{U}_n)^c = \emptyset$$

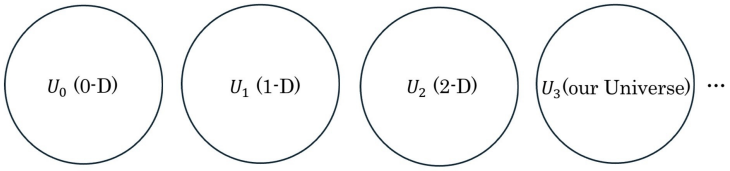

In our theory of dimensionality, we think of a point mapped into another universe, U_n. However, for example, any point in U_1 cannot be a point in U_3 even after mapping $f(f: S \rightarrow S')$ because the point after the mapping should keep the character in U. Any point in U_n keeps its original n-degrees of freedom before and after mapping. Therefore, the changelessness of the degrees of freedom has symmetry, as the degrees of freedom are changeless after a series of operations.

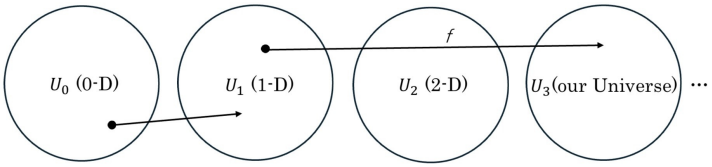

Furthermore, Georg Cantor pointed out that since 1-dimensional set and 2-dimensional set have the same cardinality, dimensionality is nonsense. Giuseppe Peano was inspired by that idea and showed it graphically. It is known as the Peano curvé However, those ideas are wrong because they overlook the degrees of freedom that any point has in our discussion of dimensionality.
You may think that since vector has magnitude and direction, it solves the problem of dimensionality that the Peano curve produces. However, that is also wrong.
As shown in the graphs below, those vectors on the left-hand side are identified as a vector on the right-hand side.The vectors shown in the left-hand graph are obviously in 2-dimensional space. Nevertheless, they are identifiable as a vector in the 1-dimensional graph as shown on the right-hand side.

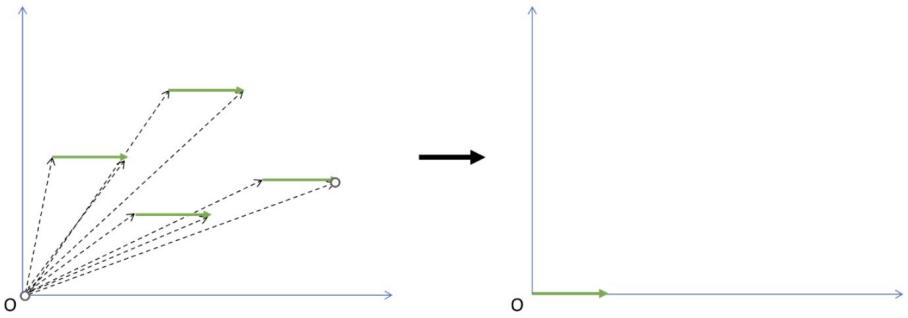

Conclusions
We are going to reconstruct geometry itself through our discussion of dimensionality, it is inevitable. It is therefore important also for mathematics, not only for physics.
We mainly reconstruct three classical geometries.
1. Euclidean geometry
2. Co-ordinate geometry by René Descartes and Pierre de Fermat

3. Erlangen Programme by Felix Klein

For 1, any point could be a line and a plane in the orthogonal co-ordinates; as well as a circle and a sphere in the polar co-ordinates. There is also mapping from lower into higher dimensional space. It contradicts the first to third postulates of 'Elements'.
For 2, any point keeps its original degrees of freedom mapping into any other dimensional space. Descartes's point is nothing more than a label in the co-ordinates. He got the idea of co-ordinate geometry when he saw a fly on a military tent. However, he overlooked the degrees of freedom that the fly had.
For 3, all geometries by mapping between different dimensional spaces are operated by a groupoid. Erlangen Programme is only about mapping in the same dimensional space. We could call it 'mapping to itself' because $E_{mm} = 1 = I$.
It is important for both higher and lower dimensional physics.

Furthermore, the differences between classical dimensionality and our discussion of dimensionality are like between geocentric and heliocentric theories. Kaluza-Klein theory is based on a 3-dimensional centric idea, so that the extra dimensional space should be compactified. However, no-one knows why only higher dimensional space is compactified. Besides, there are some other problems:

- It is a background dependent theory. Correct theories tend to be background 'independent'like Lee Smolin points out.
- The internal space is 'ineffectual' against relativistic effects. Actually, from the Dirac and the Pauli equations any spin of electrons stays unchanged against relativistic effects. If such a compactified space were embedded into our space, why and how is the compactified internal space NOT ineffectual against relativistic effects? Remember Calabi-Yau manifold is a higher dimensional 'internal (complex)' space.

We could also state that the difference is like between absolute and relative space. Brane or braneworld belongs to 'absolute' higher or infinite dimensional space. In other words, any dimensional space belongs to a higher one. However, our dimensionality is not like that. Any different dimensional space is NOT a subspace of others. They are independent from each other.

Open Problems
Viewing topology from our theoretical viewpoint of dimensionality, we will need to redefine various concepts in topology.
For example, in topology, S^1 is equivalent to $\mathbf{R}\cup\{\infty\}$. However, in the context of our theory of dimensionality, S^1 has two degrees of freedom in 2-dimensional space.Mapping S^1 to 1-dimensional space, it is $\mathbf{R}\cup\{\infty\}$ having two degrees of freedom.Therefore, degrees of freedom for $\mathbf{R}\cup\{\infty\}$ is invariant from our viewpoint.
If mapping S^1 to R^3, S^1 becomes a cylinder. If S^1 to S^3, S^1 becomes T^2.
Pullback should be redefined. For example, a point $(x, y) = (a, b)$ is mapped into 1-dimensional space, then pulled back. It loses the information of y-co-ordinate, so that it is $x = a$, a line in 2-dimensional space. However, in the context of our

theory of dimensionality, it never loses the information because the two degrees of freedom are conserved in terms of its 'invariant'. Therefore, by our notation, $E_{21}E_{12} = E_{22} = I$. On the other hand, $x = a$ is a point in 1-dimensional space and a line in 2-dimensional space in terms of invariant. Therefore, $E_{12}E_{21} = E_{11} = I$. It is similar to pullback but it is based on quite a different concept from our theory of dimensionality.
Since merely introducing degrees of freedom as invariant in topology, the redefinition will not be a complicated issue.

Acknowledgements

The author appreciates Prof. Susan Hansen, who voluntarily and patiently listened to explanations of this research; proofread to correct grammatical errors; and offered significant suggestions and opinions for English expression. The author also appreciates Prof. Louis Kauffman, who gave the opportunity to think of **Open Problems**.
The author further appreciates Dr. Astri Kleppe and Rei Takaba for their support for this paper's TeX format.

References

1. Felix Klein (1872), Vergleichende Betrachtungen über neuere geometrische Forschungen. *Mathematische Annalen* 43, 1893,
   pp. 63-100. (Also: Gesammelte Abh., Springer 1921, Vol. 1,
   pp. 460-497). Also known as 'Erlangen Programme', about English translation:
   https://doi.org/10.48550/arXiv.0807.3161
2. Euich Miztani, Projections and Dimensions, *Communications in Applied Geometry*, Research India Publications, ISSN 2249-4286, 2011, Vol. 1, pp. 7-18.
   https://dx.doi.org/10.37622/CAG/1.1.2011.7-16
3. Euich Miztani, A Transportation Group and Its Subgroups, *Advances in Algebra*, Research India Publications, ISSN 0973-6964, 2015, Vol. 8, no. 1, pp. 25-31.
   https://dx.doi.org/10.37622/AA/8.1.2015.25-31
4. Euich Miztani, A Group Representation — Notations for "Projections and Dimensions", *Communications in Applied Geometry*, Research India Publications, ISSN 2249-4286, 2016, Vol. 3,
   no. 1, pp. 21-27.
   https://dx.doi.org/10.37622/CAG/3.1.2016.21-27
5. Euich Miztani, Transformation Groupoid and Its Representation, presentation slides for 'Knots and Representation Theory Seminar', organized in Moscow, Russia, on 19th December, 2022.
   http://dx.doi.org/10.13140/RG.2.2.31717.27369
   https://www.ktrt-seminars.com/
6. Euich Miztani, Transformation Groupoid and Its Representation — A Theory of Dimensionality, presented at the proceedings of the 26th Workshop in 2023, held at Bled in Slovenia: What Comes Beyond the Standard Models? pp.173-191.
   https://doi.org/10.51746/9789612972097
   http://bsm.fmf.uni-lj.si/

7. Euich Miztani, Transformation Groupoid Based on Quotient Vector Spaces — A Mathematical Definition for Theory of Dimensionality, presentation slides for 'Knots and Representation Theory Seminar', organized in Moscow, Russia, on 30th December, 2023.
http://dx.doi.org/10.13140/RG.2.2.16133.73444
https://www.ktrt-seminars.com/
8. Euich Miztani, supplementary slides for the 28th Workshop in 2025, held online at Bled in Slovenia: What Comes Beyond the Standard Models, Correspondence Relationship or Internal Space?
http://dx.doi.org/10.13140/RG.2.2.10950.69448

BLED WORKSHOPS
IN PHYSICS
VOL. 26, NO. 1

Proceedings of the 28th Workshop
What Comes Beyond . . . *(p. 268)*
Bled, Slovenia, July 6–17, 2025

19 Erratum to the Proceedings of 27th Workshop What Comes Beyond the Standard Models (2024), pp. 156-175

Euich Miztani†

JEIN Institute for Fundamental Science (JIFS) VBL Kyoto University, Yoshida honmachi, Sakyo-ku, Kyoto, 600-8813. Japan

1. E_q. 1.13 on page 159 should be corrected as

$$B_z = B_z^{'} \sin\theta + B_y^{'} \cos\theta.$$

The subscripts of B were wrong.

2. E_q. 1.14a on page 159 should be corrected as

$$B_z = \sqrt{1-(v/c)^2} B_z^{'} + \frac{v}{c} B_y^{'}.$$

It is not squared to $B_z^{'}$ on the right-hand side.

3. E_q. 1.19 on page 160 should be corrected as

$$B_y = \sqrt{1-(v/c)^2} B_y^{'} + \frac{v}{c} B_z^{'} = \frac{1}{\beta} B_y^{'} + \frac{v}{c} B_z^{'}.$$

It is not squared to $B_y^{'}$ in the equations.

4. The equation on line 6 in the second paragraph in the subsection 12.2.1 on page 165 should be corrected as RHS $= B_z - \frac{c}{c}\left(\frac{1}{c}E_y\right) = B_z - \frac{1}{c}E_y$. Therefore, $B_z = \frac{1}{c}E_y$. RHS was mistakenly replaced by RHS of E_q. 1.8 on page 158. Any letters c are not capitalized in the equation.

5. The equation in Figure 25 on page 174 should be corrected as

$$r'\omega' dt' = \sqrt{1-\left(\frac{v}{c}\right)^2}\omega' dt' = \sqrt{1-\left(\frac{v}{c}\right)^2} c dt'.$$

All the results of the paper are unchanged.

†euichi@jein.jp

BLED WORKSHOPS
IN PHYSICS
VOL. 26, NO. 1

Proceedings of the 28th Workshop
What Comes Beyond . . . *(p. 269)*
Bled, Slovenia, July 6–17, 2025

20 Ontological Fluctuating Lattice Cut Off

Holger Bech Nielsen†

Niels Bohr Institute, Jagtvej 155a Copenhagen N, Denmark

Abstract. Remarkably accurate fine structure constants are calculated from assumptions further developped from two earlier publications on "Approximate SU(5)..." [4] and "Remarkable scale relation,..." [1]. In "Remarkable scale relation,..." we have put together a series of energy scales related to various physical phenomena such as the Planck scale , a scale, which we call fermion tip being a certain extrapolation related to the heaviest fermions in the Standard model, an approximate $SU(5)$ unification scale (without susy); and then we found, that as function of the power of an imagined lattice link length supposedly relavant for the scale in question, these powers are rather well linearly related to the logarithms of the associated energy scales [1]. The coincidence of these scales fitting a straight line is remarkable and in some cases quite intriguing. It may in fact be taken as an evidence for Nature truly/ontologically having a *fluctuating* lattice, meaning, that the size of the links say fluctuate quantum mechanically and from place to place and time to time. We review a self-reference obtaining the three fine structure constants via three theoretically predictable quantities, among which is a scale on our straight line plot, namely for an *approximate* SU(5)-like unification (SU(5) coupling relations are only true in a classical approximation). Concentrating on the four energy scales, for which most precise numbers make sense (this is new in the present article), we interpolate to the approximate unification scale to such an accuracy, that it combined with the quantum corrections making the deviation from genuine SU(5) delivers the differences between the three inverse fine structure constants agreeing within errors being a few units on the second place after the comma! E.g. we predict the difference between the non-abelian inverse fine structure constants at the Z^0-mass M_Z to be $(1/\alpha_2 - 1/\alpha_3)(M_Z)|_{predict} = 29.62 - 8.42 = 21.20$, while the experimental difference is $29.57 - 8.44 = 21.13$ both with uncertainties of order ± 0.05.

Povzetek: Avtor predstavi zelo natančen izračun konstant fine strukture, ki sloni na predpostavkah, argumentiranih v člankih [1, 4]. Predstavi Ref. [1], v kateri je avtor upeljal vrsto energijskih mrež, povezanih z različnimi fizikalnimi pojavi, kot je Planckova skala, skala najtežjih fermionov v *standardnem modelu*, približna skala poenotenja z uporabo grupe $SU(5)$ (brez susy). Ko poveže logaritme ustreznih energijskih skal z namišljeno mrežo, najde linearno zvezo, ki mu v limiti poenotenja ponudi zelo natančne vrednosti vseh energijskih skal. Zdi se, da Narava uporablja nihajočo mrežo, ki ponazarja kvantno mehansko nihanja povezav in se spreminja s krajem in časom. Avtor od tu izračuna tri konstante fine strukture. Predvideva, denimo, da je razlika med neabelovimi inverznimi vrednostmi konstant fine strukture pri masi Z^0 M_Z $(1/\alpha_2 - 1/\alpha_3)(M_Z)|_{predict} = 29,62 - 8,42 = 21,20$, medtem ko je eksperimentalna razlika $29,57 - 8,44 = 21,13$, obe z negotovostmi reda velikosti $\pm 0,05$.

†Speaker at the Workshop "What comes beyond the Standard Models" in Bled.
email: hbech@nbi.dk

"When I die my first question to the Devil will be: What is the meaning of the fine structure constant?"

Wolfgang Pauli [66]

20.1 Introduction

We have found a rather surprising phenomenological relation between a series of about 9 energy scales [1–3]. For each energy scale in the series we speculate to what power the link length a of a lattice quantum field theory - we actually in this article as the word "ontological" in the title suggests that a lattice truly exist in Nature - should be raised in order to be relevant for the scale in question, say a^n. Then we plot the logarithm of the energy scales versus this power n as argued for. And then the scales come on a straight line crudely at least. Some of the scales are our own inventions for the purpose of the present work, but at least e.g. a scale for the string tension for strings approximately making up the hadrons [60, 65, 67–69], or the Planck scale associated to the Newton gravitational constant G are wellknown energy scales since long.
That the different scales all give points on an approximate straight line, is a remarkable result, even if we do not quite know, what is behind this remarkable observation. As examples of scales we have "inflation energy density" and "inflection rate" [52–54],the scale of see-saw neutrinos, "see-saw" [39,48–51], the domaine walls tension [62], and the scale of mass of a dimuon resonance, which we want to identify as a monopole related, say bound state of monopoles, particle [57, 58]. .
We have, however, a very suggestive explanation being, that there truly exist a lattice, but that this lattice is far from a regular lattice with the same lattice constant all over. On the contrary it is crucial for our idea, that the length of the links (= the lattice constant roughly) varies dramatically from place to place and we would also assume from time to time, and really we would even like the lattice-like structure to be in superposition of states with various link sizes, if that makes sense. The crucial point is, that looking at some place at some moment, one can by accident find the lattice-like structure there very tight or very rough as it can happen. Especially the link size a will statistically fluctuate wildly. On the figure you can see, how such a "lattice" which has different tightness in different places may look in an accidental moment.

20.2 Ontological Fluctuating Lattice Cut Off

An irregular lattice with big density differences

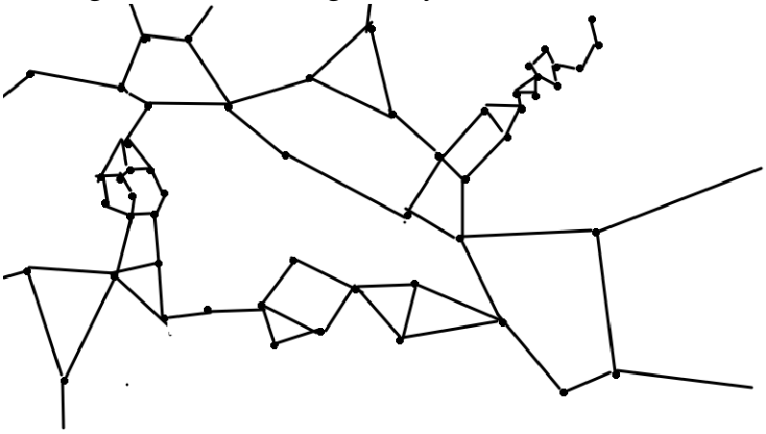

The present work may be considered a work on our project Random Dynamics [11,12,27] and for instance some works on why just the Standard Model group [30–32] and thoughts upon the possibilities [38] for using numerology. Old reviews of our Random Dynamics are [3,72,73] and the original part of an article see [70] coming up with the idea. The present work began by the finestructure constant calculations discussed in section 18.8 below, which really has the philosophy, that the approximate SU(5) relations between the (running) couplings at some scale - which call in our model μ_u - is an accident occurring because the classical lattice action happens to be SU(5) invariant, because it is a representation of the Standard Model group, that happens to be a unitary 5×5 matrix. So we predict quantum corrections to SU(5), and thus true SU(5) GUT is only **approximate**. But even though we thus do not have genuine SU(5), the GUT SU(5) earlier works are used by us [6–8], but we actually in our model as a further specialty rather have a cross product of three (approximate) SU(5)'s [21,25,26]. Well, we should rather say we assume that there truly is a cross product of three copies of the Standard Model group with their Yang Mills fields, while the remaining Yang Mills components of the SU(5)'s do not exist.

Especially the finestructure project in Random Dynamics may be found in [13–19, 22,23]. The idea that the gauge groups we see should be diagonal subgroups of say a cross product of three of the same group, was favoured by, that we invented a mechanism "confusion" [28,29] that tended to make diagonal subgroups only survive, when possible. So whatever the gauge group behind, we should only see the diagonal subgroup, and thus we claimed it likely, that we have several isomorphous cross predict factors in the true group behind. We called this anti-GUT. In any case we assume in the present article, that the Standard Model group is repeated three times in this way in the present article. This assumption is most relevant for our fine structure constants calculation.

20.2.1 Our model

Finestructure Constants Let us resume shortly, what our model, especially for the finestructure constant part, is: There exists a fundamental gauge theory lattice, which is fluctuating in the sense of being somewhere and sometime very tight and somewhere and sometimes very rough. It is for a gauge group Standard model group cross producted with itself to third power. So each family of Fermions can have its own out of the three cross product factors to couple to. One could equivalently take it, that there were three lattices on top of each other, three layers so to speak with only the Standard model group each. Such an Anti-gut is supposed to break down to only the Standard model group (diagonal breaking) presumably at the scale of the local lattice size. It is this breaking we told in the old papers were due to "confusion" [28,29].
A crucial point for the approximate SU(5) is, that we think of the link objects as 5×5 unitary matrices, that though are restricted to only take such values that they occur in the five dimensional representation of the Standard model group. But thinking on the link-variables this way makes it natural, that the plaquette actions should be the trace of such a 5×5 matrix. But this is exactly the same as the most natural SU(5) theory action. Since the finestructure constants at the scale in question, the scale of the link length say, is given by the form of the action we have in first approximation SU(5) related couplings even though we only have the gauge group being the Standard model one. However, now there are quantum corrections, which are essentially the effect of quantum fluctuations of say the plaquette variables, and they can in our model only be in the directions of the really existing Standard model group, while there can be no fluctuations in the non-existing 12 only SU(5) dimensions of fluctuations. But now when there in our model is one Standard model group for each family of fermions (i.e. 3) we get the quantum correction multiplied by 3.
The most remarkable progress of the present article is, that we use the straight line with the energy scales versus the power to which the link length a is raised in connection with the energy scale in question to predict the replacement for the unification scale for the approximate minimal(i.e. without susy) SU(5) to predict the differences between the three inverse fine structure constants with the fantastic accuracy of having the deviation from the experimental differences only of the order 0.05 for differences that can be of order 20. I.e. less than a percent deviation! We also do predict the genuine fine structure constants themselves, but by an uncertainty rather only 3 units in the inverse fine structure constants.
It should be mentioned that Senjanovic and Zantedeschi [45] have sought to rescue SU(5) GUT by means of higher dimensional operators, and get to a very similar replacement for unification as we do $10^{14} GeV$. In principle our approach is very similar, since having a lattice at least in principle could induce higher dimensional operators.

Diagonal Subgroup Fine structure constant formula To understand the factors 3 occurring in our formulas one should have in mind that when we have breaking of the symmetry from a group to some cross product power, say $G \times G \times G$

(this is a thrid power of G), then if the fine structure constants for the here three groups isomorphic to G are say $\alpha_{Peter}, \alpha_{Paul}$, and α_{Maria}, then the finestructure constant for the diagonal subgroup G_{diag} of the cross product

$$G_{diag} \subset G \times G \times G \tag{20.1}$$

$$\text{i.e. } G_{diag} = \{(g, g, g) | g \in G\} \tag{20.2}$$

we have the fine structure constant relation

$$\frac{1}{\alpha_{diag}} \approx \frac{1}{\alpha_{Peter}} + \frac{1}{\alpha_{Paul}} + \frac{1}{\alpha_{Maria}} \tag{20.3}$$

$$\text{or } \approx \frac{3}{\alpha_{Peter}}, \text{ if } \alpha_{Peter} = \alpha_{Paul} = \alpha_{Maria}. \tag{20.4}$$

The Series of Scales The assumptions needed to make the lattice constant associated with the energy scales, is that the coupling parameters in the lattice action are of order unity, and in addition the assumption about Log Normal distribution of the link variable in the fluctuating lattice, as to be described in next section 18.3. The idea of a strongly fluctuating lattice may be supported by the idea, that the metric of general relativity fluctuates corresponding to diffeomorphism transformations. Such fluctuations of the metric would be suggested, if we believe as Ninomiya Førster and myself and Shenker suggested that gauge symmetries come about due to strong quantum fluctuations in the gauge [59–61]; the idea is that it is the lattice that is part of the gauge variable, which are taken to exist. Thus we would see it as the lattice fluctuating relative to us, although it might really rather be the metric giving space-time, that fluctuate relative to the lattice..

20.2.2 Plan of article

The introduction was section 20.1.
In the following section 18.3 we introduce the statistical distribution to desribe the probability distribution, if one takes out a random link and looks fro it geometrical size a.
In section 18.4 we use the three lowest energy scales as an example to give an idea of how we estimate the relevant power n to which the link gets raised concerning the scale in question.
The presentation of the main plot with the points, that should by our model have about 9 points for nine scales lie on a straight line in section 18.5.
One of our energy scales, which we invented ourselves as so many of them, is the energy scale for masses of monopoles, as we want to predict (although these monopoles are not very strongly tied to our model, we would prefer them to be there, but really our model could still survive even if there did not exist monopoles), and we assign a short section 18.6 to such monopole related particles, and we seek to identify a particle that is not itself a monopole but rather some by gluons confined set of monopole like particles, presumably with no genuine monopole field around in the outside. But it could be bound from particles with genuine monopolic magnetic charge. We seek to identify this monopole related

particle with what is presumably a statistical fluctuation peak in $\mu uon^+ + \mu uon^-$ at a mass 27 GeV at LHC, but also seen at LEP.
A last section 18.8 before the conclusion is assigned to our prediction of the finestructure constants for the three simple Lie algebras of the Standard Model.
In section 18.9 we conclude and make a tiny outlook.

20.3 Log Normal Distribution

The Log Normal distribution [74] (sometimes called after Galton, McAlister, Gibrat, or Cobb-Douglas) means a statistical distribution of a quantity, such that the logarithm of this quantity becomes distributed as a normal distribution around some mean, but with the Gaussian distribution being for the logarithm. Such a Log Normal will, in analogy to the central limit theorem for summing a lot of (only weakly dependent) random variable, result, if one multiplies a lot of random variables. E. g. imagine a human being playing with his fortune on the bourse or making speculations some way or another, then typically the gain or loss will be proportional to the amount of money, with which he has been able to speculate, and thus to his fortune. After many such speculations we should be able to trust that the probability distribution for his fortune - at the late time - should have a Log Normal distribution. Indeed the distributions of fortunes of different people on the Earth is rather well a Log Normal one. If the lattice, Nature has given us (remember in this article we believe there truly exist a lattice, ontological lattice),has it so that, if we go around in it the link size will locally vary by some not too big factor up or down, with about the same probability, independently of whether the lattice locally is tight or rough, then the lattice link distribution will end up roughly a Log Normal distribution also.
We like to think of the Log Normal distribution as a distribution, which under very mild assumptions comes by itself. It is really like it should be in Random Dynamics, that even say if the truth were not a lattice but some other type of cut off- a cut off momentum-energy scale Λ say - then we should still guess a Log Normal distribution for this other type of cut off parameter, Λ say.

20.3.1 Main Philosophy

The main point of our work is to assume, that we have a lattice - this shall then be fluctuating in tightness, being somewhere tight, somewhere rough with big links and net holes - and then the various physical energy scales are calculated each of them from some power of the length a of a link. While for a rather narrow distrbution of a variable a say it is so that whatever the power of the variable a you need for your purpose you get about the same value for the effective typical a

size,

$$\sqrt[n]{< a^n >} \approx \text{ n-independent (for narrow distributions.}$$

However, Galton distribution:

$$P(\ln a)\,d\ln(a) = \frac{1}{\sqrt{2\pi\sigma}} \exp(-\frac{(\ln a - \ln a_0)^2}{2\sigma})\,d\ln a$$

$$\text{gives rather } \sqrt[n]{< a^n >} = a_0 \exp(\frac{n}{2} * \sigma). \tag{20.5}$$

Exceptional case $n = 0$:

The expression $\sqrt[0]{< a^0 >}$ is not good but we reasonably replace it

$$\sqrt[0]{< a^0 >} \to \exp(< \ln(a) >) = a_0 \tag{20.6}$$

$$\text{for our Log Normal.} P(\ln a)\,d\ln(a) = \frac{1}{\sqrt{2\pi\sigma}} \exp(-\frac{(\ln a - \ln a_0)^2}{2\sigma})\,d\ln a \tag{20.7}$$

$$\text{so again } \sqrt[n]{< a^n >} = a_0 \exp(\frac{n}{2} * \sigma) \tag{20.8}$$

20.3.2 Fluctuating Lattice stressed

Comparing Our fluctuating lattice with usual Wilson one

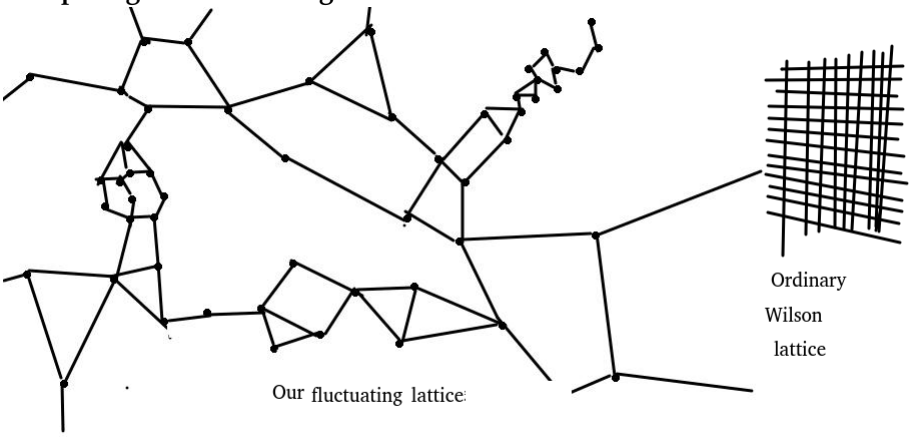

Ontological lattice mean really in Nature existing lattice

Usual non-fluctuating lattice→ Fundamental scale.
Our fluctuating lattice → Several different fundamental scales.

20.4 Example of Three Scales

Introductory Examples of Powers of the Link Size to Average
To get an idea of how we may derive the relevant average of a power $< a^n >$ let us for example think of a particle, a string, or a domaine wall being described by

action of the Nambu-Goto types

$$\text{Particle action} S_{particle} = C_{particle} \int \sqrt{\frac{dX^\mu}{d\tau} g_{\mu\nu} \frac{dX^\nu}{d\tau}} d\tau \tag{20.9}$$

$$= C_{particle} \int \sqrt{\dot{X}^2} d\tau \tag{20.10}$$

$$\text{String action } S_{string} = C_{string} \int d^2\Sigma \sqrt{(\dot{X} \cdot X')^2 - (\dot{X})^2 (X')^2} \tag{20.11}$$

$$= -\frac{1}{2\pi\alpha'} \int d^2\Sigma \sqrt{(\dot{X} \cdot X')^2 - (\dot{X})^2 (X')^2} \tag{20.12}$$

Domain wall action

$$\text{Domain wall action } S_{wall} = C_{wall} \int d^3\Sigma \tag{20.13}$$

$$\det \begin{bmatrix} (\dot{X})^2 & \dot{X} \cdot X' & \dot{X} \cdot X^{(2)} \\ X' \cdot \dot{X} & (X')^2 & X' \cdot X^{(2)} \\ X^{(2)} \cdot \dot{X} & X^{(2)} \cdot X' & (X^{(2)})^2 \end{bmatrix} \tag{20.14}$$

Here of course these three extended structures are described by repectively 1, 2, and 3 of the parameters say τ, σ, β, the derivatives with respect to which are denoted by respectively $\dot{}, ', \text{and} ^{(2)}$. So e.g. $d^3\Sigma = d\tau d\sigma d\beta$ and

$$X^{(2)} = \frac{\partial X^\mu}{\partial \beta} \tag{20.15}$$

$$X' = \frac{\partial X^\mu}{\partial \sigma} \tag{20.16}$$

$$\dot{X} = \frac{\partial X^\mu}{\partial \tau} \tag{20.17}$$

$$\tag{20.18}$$

Finally of course $\cdot$ is the Minkowski space inner product.
Now imagine, that in the world with the ontological lattice, which we even like to take fluctuating, these tracks of objects, the particle track, the string track or the wall-track, should be identified with selections of in the practicle case a series of links, in the string case a surface of plaquettes, and in the wall-case a three dimensional structure of cubes, say. One must imagine that there is some dynamical marking of the lattice objects - plaquettes in the string case e.g.- being in an extended object. Now the idea is that we assume the action for the lattice to have parameters of order unity. In that case the order of magnitude of the effective tensions meaning the coefficients $C_{particle}, C_{string}, C_{wall}$ can be estimated in terms of the statistical distribution of the link length - for which we can then as the ansatz in the model take the Galton distribution (18.5) - by using respectively the averages of the powers 1, 2, 3, for our three types of extended objects. I.e. indeed we say that by order of magnitude, the mass of the particle, the square root of the string energy density or the string tension, and the cubic root of the domain wall

tension are given as the inverses of averages of a like:

$$\text{Particle mass } m \sim < a >^{-1} \tag{20.19}$$

$$\text{Square root of string tension } \sqrt{\frac{1}{2\pi\alpha'}} \sim \sqrt{< a^2 >}^{-1} \tag{20.20}$$

$$\text{String tension itself } \frac{1}{2\pi\alpha'} \sim < a^2 >^{-1} \tag{20.21}$$

$$\text{Cubic root of wall tension } S^{1/3} \sim \sqrt[3]{< a^3 >}^{-1} \tag{20.22}$$

$$\text{wall tension itself } S \sim < a^3 >^{-1} . \tag{20.23}$$

Here the $\sim$ approximate equalities are supposed to hold order of magnitudewise under the assumption that no very small or very big numbers are present in the coupling parameters of the lattice, so that it is the somehow averaged lattice that gives the order of magnitude for these energy densities or tensions.

20.4.1 Illustration of the idea

Although our speculations for the three energy scales - meaning numbers with dimension of energy - which we in my speculation attach to these three objects, the particle, the string, and the wall, are indeed very speculative only, and that we shall give a bit better set of such scales in next subsection, let us nevertheless as a pedagogical example consider these three first:

20.5 Main Plot

Our Phantastic Plot: Agreeing Order-of-magnitudewise for 9 Energy scales

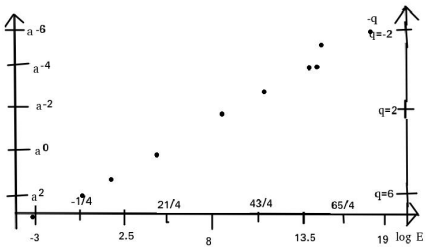

Fig. 20.1: Plot of the (inverse) power n, into which comes the lattice link length a, when forming the physical energy scale of energy E, versus its logarithm of this energy with basis 10 $\log E$ using GeV as energy unit

.

Main Plot a bit bigger and with names

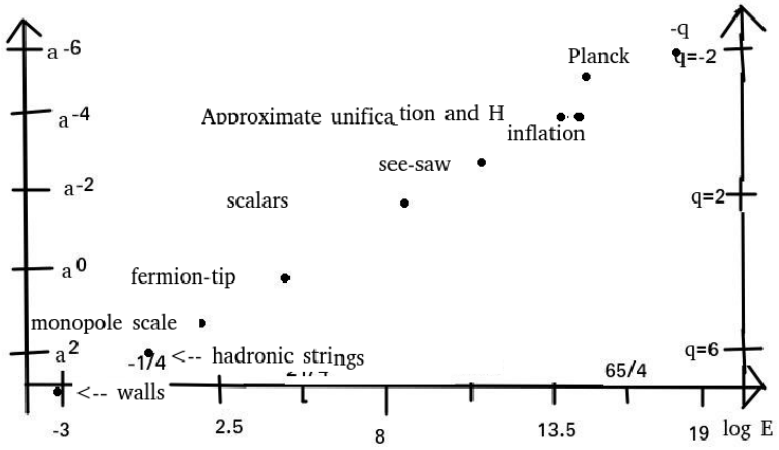

Comments on the Main Plot

- Two cosmological points "$H_{inflation}$" and one related to the energy density in the inflation time (which I did not give a name, but call it $\sqrt[4]{V_{inflation}}$), do not fit quite perfect on the straight line, but not so badly either.
- For Planckscale I used the reduced planck scale with an 8π divided out of the gravitational constant G. But this theoretically best suggested.
- Some energy scales are wellknown: "Planck", the cosmological ones, an only approximate SU(5) "unification" scale, The "see-saw" mass scale, the energy scale of hadron physics taken as an approximate "string" theory i.e. α' defining a scale.

- But the rest is my own inventions/speculations:
  "scalars" meaning I speculate that a lot of scalars have their mass and possible vacuum expectation values of this energy order of magnitude;
  "fermion tip" which is the tip or top of an extrapolation of the density of the numbers of standard model fermion masses on a logarith of the mass abscissa;
  "monopoles" a certain dimuon resonance barely observed of mass 27 GeV is speculatively taken as being somehow to monopoles, which though are presumably cofined because of their QCD features;
  "walls" are the domain walls around dark matter in my own and Colin Froggatts darkmatter model, their energy scale is the third root of the wall tension.

20.5.1 Remarks on Higgs Etc.

In the second paragraph of the introduction, section 20.1, we mentioned several of the energy scales, which we consider, but did not mention that very speculatively we predict an energy scale given by $\sqrt{< a^{-2} >}$, at which there should be "a lot" of scalar particles having their mass - analogous to that the see-saw scale is a scale at which "a lot"(at least there must be one or two) fermions have their mass -. Now it would have been very nice for our model, if the Higgs mass had been

at this scale, but that is not at all the case. It is wellknown that the small Higgs mass is a mystery, and that there is even the hierarchy problem that the bare Higgs mass must be surprisingly much finetuned. The author actually has a very different story about why the Higgs mass should be so small, based on the idea that there is a complex action and a selection principle of the initial conditions (the details of the cosmological start) so as to arrange many things, the future and probably even the parameters like the Higgs mass, so as to minimize the Higgs field square [34–36]. But this is quite different story than the present article [43,44], but it means that the present article had no luck with the Higgs mass.
However, this energy scale with the lot of scalar masses, would expectedly also lead to some non-zero expectation values in vacuum for these scalar fields and thus break symmetries spontaneously. This we claimed in the previous article as a good candidate for the breaking of the symmetries leading to the rather big mass ratios of the quarks and the charged leptons. The order of magnitudes for this "little hierarchy" [40–42] mass ratio problem is actually fitting with the ratio of the see-saw scale to our invented and predicted many scalars scale [1].

20.6 "Monopole Energy Scale

When we have gauge group $SMG = S(U(2)\times U(3))$ suggested in the O'Raifeartaigh-way [33] [1] on a lattice one gets monopoles unless it is the covering **group** (i.e. a simply connected group). We thus do expect monopoles, if we take the lattice seriously, in fact monopoles corresponding the the three copies of the Standard Model group SMG assumed in our model in the cross product. Because of subgroup of the center of the covering group divided out involving all the three groups U(1), SU(2), and SU(3), the monopoles will have magnetic fields from all the three groups. Especially they would have gluon fields around them, and it is easy to imagine them getting clumped together by the confining vacuum(of QCD).
If we really shall associate the dimuon resonance perhaps observed [57,58](see figure 18.2) with monopoles, of course it must be a combination of monopoles with zero monopolic charge. A true monopole would be stable of course. But a bound state living long enough to be seen as a resonance is not excluded.
Indeed a dimuon decaying has been seen in events selected with some b-activity in LHC [57]; but most remarkably Heister could dig a similar resonance out of the data of already stopped LEP [58].

20.7 The four best points on our line

Many on the points on our straight line, being our great success, are only definable order of magnitudewise, because they involve thoertical models not yet well

[1] O'Raifeartaigh propose to assign a **group** and not only a Lie algebra to a phenomenologically found model, such as the Standard Model, by using the information about the representations found to exist physically and choose that Lie **group** which allows as few as possible representations, but nevertheless the physically realized ones. On a lattice then the link variables and thus also the plaquette variables should run on/take values in this chosen **group**.

Fig. 20.2: **Can this Peak in $\mu\bar{\mu}$ be Monopole Related?**

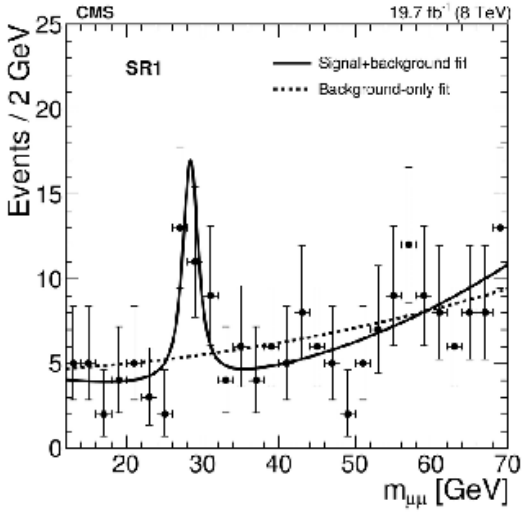

established. Such lack of even more than order of magnitude numbers due to there being no established theory is the trouble for the energy scales, such as the "see-saw", the inflation connected scales $H_{inflation}$,...,and the "monopole scale". For our "domaine wall" scale [75] the uncertainties in the parameters are so big, that even trusting our theory of dark matter, the energy scale would be ill defined, and known to of order of magnitude at best. But for **four of our scales** it is at least possible to write down some more accurate numbers, and if we postulate, that we shall use the appropriate root of the quantity occurring as a coefficient in the Lagrangian, we can argue, that we shall chose the reduced planck scale and we make at least formally a welldefined number for the Planck scale. Similarly the quantity $\frac{1}{4\pi\alpha'}$ occurring in the string action could give a welldefined number for the "string-" scale. When looking for an approximate unification or replacement for the unification scale,the value of the energy scale μ_u is of course renormalisation scheme dependent, but that we can hope is not causing too much uncertainty in practice. The fermion tip scale is in priciple an extrapolation from masses which are well measured.

20.7.1 String scale

In the string theory for hadrons [67–69], which never became perfectly working, the coefficient in the action for the string is given by $\frac{1}{2\pi\alpha'}$, where $\alpha(m^2)$ is the Regge trajectory as function of mass square. S. S. Afonin and I. V. Pusenkov [64] find in their fit I, that $1/\alpha' = 1.10 GeV^2$, while Sonnenshein et al. [65] find $\alpha' = 0.95 GeV^{-2}$ and looking at various Chew Frautschi plots [76] you see e.g. the ρ and a pair slope of m^2 versus spin J means $1/\alpha' = 1.16 GeV^2$, for ω and f almost the same, and for ϕ f' a slope $1/\alpha' = 1.2 GeV^2$. As a midle between the large $1/\alpha'$ from Chew Frautischi plots by eye and the small $1/\alpha' = 1.05 GeV^2$ from Sonnenshein et

al [65] we may choose the Afonin et all $1/\alpha' = 1.10 GeV^2$:

$$\text{Slope } a = 1.10 GeV^2 (\text{Afonin et al.}) \tag{20.24}$$

$$\text{Thus } \alpha' = 1/a = 0.909 GeV^{-2} (a \text{ is here not the link length})$$

$$\text{and } \frac{1}{2\pi\alpha'} = \frac{a}{2\pi} = 0.175 GeV^2 \tag{20.25}$$

$$\text{so that“string scale”} = \sqrt{0.175 GeV^2} = 0.418 GeV \tag{20.26}$$

$$\text{and } \log(\text{“string scale”}) = -.3784 (\text{in GeV}) \tag{20.27}$$

20.7.2 Fermion tip scale

A few estimates, 5 fermion masses are combined with the top-mass to give a value for the extrapolation to the “fermion tip” below here (the combinations not involving the top mass are not used in our averaging to get a most accurate “tip” value):

From b to t

$$\frac{(2.2374 - 0.6212)\sqrt{3.5}}{\sqrt{9.5} - \sqrt{3.5}} + 2.2374 = 4.7334 \tag{20.28}$$

$$10^{4.7334} = 5.4129 * 10^4 GeV \tag{20.29}$$

From τ to t

$$\frac{(2.2374 - 0.2496)\sqrt{3.5}}{\sqrt{13.5} - \sqrt{3.5}} + 2.2374 = 4.2995 \tag{20.30}$$

$$10^{4.2995} = 1.9930 * 10^4 GeV \tag{20.31}$$

From τ to b

$$\frac{(0.6212 - 0.2496)\sqrt{9.5}}{\sqrt{13.5} - \sqrt{9.5}} + 0.6212 = 2.5558 \tag{20.32}$$

$$10^{2.5558} = 3.5959 * 10^2 GeV \tag{20.33}$$

From c to t

$$\frac{(2.2374 - 0.1038)\sqrt{3.5}}{\sqrt{17.5} - \sqrt{3.5}} + 2.2374 = 3.9635 \tag{20.34}$$

$$10^{3.9635} = 9.1942 * 10^3 GeV \tag{20.35}$$

From μ to t

$$\frac{(2.2374 - (-0.9761))\sqrt{3.5}}{\sqrt{21.5} - \sqrt{3.5}} + 2.2374 = 4.4109 \tag{20.36}$$

$$10^{4.4109} = 2.5758 * 10^4 GeV \tag{20.37}$$

From s to t

$$\frac{(2.2374 - (-1.0292))\sqrt{3.5}}{\sqrt{25.5} - \sqrt{3.5}} + 2.2374 = 4.1598 \tag{20.38}$$

$$10^{4.1598} = 1.4448 * 10^4 GeV \tag{20.39}$$

$$\tag{20.40}$$

20.7.3 Some averaging

The average of the fermion tip scale calculated "from the uppermost 5 fermions (except for t) to t" gives

$$\log(\text{" fermion tip"}_{\,\text{first 5}}) = \frac{4.7334 + 4.2995 + 3.9635 + 4.4109 + 4.1598}{5}$$
$$= 4.31342 \tag{20.41}$$
$$10^{4.31342} = 2.0578 * 10^4 GeV \tag{20.42}$$

20.7.4 Resume the Four Scales with Precise Numbers

The numbers obtained for the four scales, for which we can meaningfully write more than order of magnitude numbers are

$$\text{"string scale"} = 0.418 \pm 3\% GeV \rightarrow \log = -0.3788 \pm 0.013$$
$$\text{"fermion tip"} = 2.0578 * 10^4 GeV \pm 60\% \rightarrow \log = 4.3134 \pm 0.2$$
$$\text{"unification scale"(R)} = \mu_u = (5.116 \pm 0.1) * 10^{13} GeV \rightarrow \log = 13.7090 \pm 0.01$$
$$\text{"unification scale"(D)} = \mu_u = (4.383 \pm 0.1) * 10^{13} GeV \rightarrow \log = 13.6419 \pm 0.01$$
$$\text{"Reduced Planck scale"} = 2.434 * 10^{18} GeV \pm 2.2 * 10^{-3}\% \rightarrow \log = 18.3862 \pm 0.000001$$

(The two by 14% different scales given for the unification μ_u are obtained from our model, in which the deviation from true minimal $SU(5)$ GUT can be considered a quantum correction, by requiring respectively

- **R:** that the ratio of the differences among the three $1/\alpha_i(\mu_u)$ be the right one;
- **D:** that the outermost of the three $1/\alpha_i(\mu_u)$'s have the right difference q)

The power of the link variable n in the relevant $\sqrt[n]{< a^n >}$ for the string scale and the Reduced Planck scale are respectively $n = 2$ and $n = -6$. Thus the difference is 8, and the increase in the energy scale per decrease in the value of n is a factor

$$\text{"factor"} = \exp(\sigma/2) = \sqrt[8]{\frac{2.343 * 10^{18} GeV}{0.418 GeV}} = 220.584 \tag{20.43}$$
$$\text{or } \log(\text{"factor"}) = \log(e) * \sigma/2 = \frac{18.3862 - (0.3788)}{8} \tag{20.44}$$
$$= 18.7650/8 = 2.345625 \tag{20.45}$$
$$\sigma/2 = \ln(220.584) = 5.3963 \tag{20.46}$$
$$\text{Width in ln: } \sqrt{\sigma} = 3.285 \tag{20.47}$$

(Our notation in the present article is so, that we used σ for what is usually called σ^2, so that one standard deviation in the logarithm is actually given by our $\sqrt{\sigma} = 3.285$ meaning, that since the average is at the logarithm of the "fermion tip" scale at $2.06 * 10^4 GeV$, the one standard deviation scales are $2.06 * 10^4 GeV * \exp(\pm 3.285)$ and becomes increase and decrease by 26.71. One standard deviation under the average reaches down to 771.3 GeV)

The slope "factor" obtained using 'fermion tip" together with the Planck scale instead of the string-scale is (accidentally ?) very close to the already obtained slope. The value for the unification scale predicted by our straight line is

$$\mu_u = 10^{18.3862-2*2.345625} = 10^{13.6949} \tag{20.48}$$

$$= 4.9534 * 10^{13} GeV. \tag{20.49}$$

$$\text{this means } \ln(\frac{\mu_u}{M_Z}) = \ln(\frac{4.9534 * 10^{13} GeV}{91.1876 GeV}) \tag{20.50}$$

$$= \ln(0.05432) + 13 * \ln(10) = 27.0208. \tag{20.51}$$

It falls between the two by different requirements methods (**R** and **D** above) of using finestructure constant data and our quantum correction to SU(5) model. So we must consider the agreement of the straight line story very good.

20.8 Fine structure constants

We shall now review [4] an article, in which I got the three fine structure constants in the Standard Model written in terms of three parameters, which all can be given a physical meaning and be calculated from theory. This work is reminiscent of an SU(5) unified theory, but this SU(5) symmetry is not a true symmetry of the theory of this work, which rather only has gauge symmetry under the Standard Model Group $S(U(2) \times U(3))$ or even more correct the third power of this group $(S(U(2) \times U(3))^3 = S(U(2) \times U(3)) \times S(U(2) \times U(3)) \times S(U(2) \times U(3))$. The $SU(5)$ like symmetry approximately for the fine structure constants only comes in, because the action taken for the standard model group happens in the first classical approximation to give the SU(5) relations between the fine structure constants. Then the quantum correction is given as one of our three parameters due the three separate standard model groups it should be multiplied by three compared to what it would be with only one standard model group, but it can be calculated; using the breaking to the diagonal subgroup of the three standard model groups leads to that the corrections for the inverse fine structure constants for the diagonal subgroups becomes three times this first calculated.
The parameter μ_u giving energy scale for the approximate SU(5) like symmetry is one of the energy scales in the series of energy scales treated as the main point of the present article, and can as such be determined from the other scales on our straight line, and that is what we mean by, that this parameter is theoretically calculable.
Let us, however, start by telling a tiny progress concerning the third of our theoretically calculable parameters, namely the replacement for the unified coupling of SU(5), for which we have postulated the inverse fine structure constant to be just three times the - on a lattice written Standard Model group gauge theory - critical coupling for some expected phase transition (or potentially instead a strong cross over).

20.8.1 Critial coupling for Standard Model Group

In our previous work [4] we calculated from the experimentally known fine structure constants (at say the Z-mass scale) and our form of the expressions for the quantum corrections providing the deviations from usual GUT-SU(5) fine structure constant relations the so to speak experimental fine structure constants at the approximate unified scale:
Using the ratios of the deviations between the inverse finestrucuture constants for the three standard model subgroups, U(1), SU(2), and SU(3) predicted by our quantum correction model we found from the experimentally known fine structure constants at say the Z^0-mass scale, the three inverse running finestructure constants at the scale μ_u at which they could meet in the sense of fitting our deviation ratios;

$$1/\alpha_3(\mu_u)|_{\text{“data”}} = 38.59 \tag{20.52}$$

$$1/\alpha_{1\ SU(5)}(\mu_u)|_{\text{“data”}} = 41.43 \tag{20.53}$$

$$1/\alpha_2(\mu_u)|_{\text{“data”}} = 43.21 \tag{20.54}$$

We suppose that the best way to extract from these due to the quantum fluctuation effects from genuine SU(5) GUT deviating fine structure constants at the approximate unifying scale $\mu_u = 5.12 * 10^{13} GeV$ an average to be compared with our prediction of it being a critical value (separating phases) just multiplied by three (for the 3 one makes use of (18.3)), is to use the with dimension of the group logarithmically weighted average.
The concept of seperate critical finestructure constant for the three subgroups $U(1)$, SU(2) and SU(3) is not quite good, because one shall really think of an a priori complicated phase diagram (see the figure from Don Bennetts thesis [63]), in which one for any combination of three fine structure constants have one phase or the other realized. Indeed there are several different phases at least in our mean field approximation used for getting an overview of the phases. Among the different phase borders appearing according to this mean field approximation we find in the thesis by Don Bennett [63], that there is one border separating one phase with confinement for all three simple subgroups and one where they are approximately realized in an approximate perturbative Yang Mills, although they or some of them might after all confine at lower energy scales. This phase border corresponds to a transition at a fixed value of the simple subgroup dimension weighted average of the logarithms of the three (inverse) finestructure constants. Thus we believe that it is for this dimension of groups weighted average that our - from old time suggested [14–16, 18, 19] - assumption that the “fundamental” fine structure constants should be critical can be applied.
In fact we already said, that we shall find in Don Bennetts thesis [63], that there is a phase transition surface in the space of (inverse) finestrucutre constants, which precisely lies along a surface, where the dimensionally weighted logarithms of the fine structure constant takes a specific value.

This dimension of group weighted average is for the experimental values of the finestructure at the scale μ_u,

Just dimension weighted:

$$1/\alpha_{SMG}(\mu_u)|_{d-av.} = \frac{8}{12} * 38.59 + \frac{1}{12}41.43 + \frac{3}{12} * 43.21 \tag{20.55}$$

$$= 25.73 + 3.45 + 10.80 \tag{20.56}$$

$$= 39.98; \tag{20.57}$$

Logarithmic averaging:

$$\log(1/\alpha_{SMG}(\mu_u))|_{l-d-av.} = \frac{8}{12} * \log(38.59) + \frac{1}{12}\log(41.43) + \frac{3}{12} * \log(43.21)$$

$$= 1.6013 \tag{20.58}$$

$$\text{giving } 1/\alpha_{SMG}(\mu_u)|_{l-d-av.} = 39.93. \tag{20.59}$$

Now we shall compare this 39.98, which is kind of from data determined unifed inverted finestructure constant with the critical coupling first for $SU(5)$, which we got in the old work [10,23] to be

$$3/\alpha_{5\ crit} = 45.93 \tag{20.60}$$

$$\tag{20.61}$$

and below with our now believed to be better estimate of the SMG critical coupling we shall get 38.2965 ± 3 (see equation (18.113)).

20.8.2 The Way from Don Bennetts Thesis

Actually using a crude mean field approximation for estimating the phase diagrams for non-simple groups such as the Standard Model group Don Bennett in his thesis [63] (see also [18]) found the phase diagram for e.g. the standard model *group* as a function of what on the figure is denoted as the logarithms of the various simple groups, which together form the standard model group. Since the group volume is measured in the Cartan-Killing metric [77], and the normalization of the latter is given by the fine structure constant for the simple group in question, you can in drawing phase diagrams use e.g. the logarithms of the group volumes to represent the fine structure constants. In the mean field approximation used in this thesis by Don Bennett it is so simple that the phase transition for a simple group occurs just, when the volume $Vol(G)$ (normalized by the fine structure constant variable in terms of which we ask for a critical coupling) equals to $\sqrt{6\pi}$ rised to the power of the group dimension:

$$Vol(G)_{crit} = \sqrt{6\pi}^{dimG} \tag{20.62}$$

For a cross product of just some simple groups such as $U(1) \times SU(2) \times SU(3)$ the phase diagram would just be a trivial cross product of the phase diagrams of the groups in the cross product with no interaction so to speak between the factors, because the volume of the cross product group is simply a product of that of the factors in the cross product.

However, for e.g. the standard model group

$$SMG = S(U(2) \times U(3)) = U(1) \times SU(2) \times SU(3)/\{(2\pi, -1, \exp(i\frac{2\pi}{3})1)^n | n \in Z\}$$

fluctuation in one simple group factor can influence the other factors and the phases of the system thus become more complicated. But we shall still assume, that it is group volume being on one or the other side of a certain value (not necessarily exactly $(6\pi)^{dim(G)/2}$) that matters for the phase. The complication/"interaction" that one has divided out a subgroup $\{(2\pi, -1, \exp(i\frac{2\pi}{3})1)^n | n \in Z\}$ of the center of the cross product makes fluctuations in the fields for one simple group enhance the fluctuations of the by the division related simple group. We think of that as an "interaction" between the simple subgroups. For this kind of combining the simple groups with their centers getting "mixed up" it is crucial that these simple groups have non-trivial centers, so let us remind the reader, that an $SU(N)$ group has a center consisting of the matrices

$$Center(SU(N)) = \{\exp(\frac{ik2\pi}{N}) * 1_{N\times N} | k \in Z\}. \tag{20.63}$$

One can thus corresponding to each $SU(N)$ form one with its center divided out

$$SU(N)_{\text{with center divided out}} = SU(N)/\{\exp(\frac{ik2\pi}{N}) * 1_{N\times N} | k \in \} \tag{20.64}$$

To divide out the center of course diminishes the volume by a factor N, and thus according to the rule (in mean field approximation) that the critical coupling correspond to the volume being $\sqrt{6\pi}^{dimG}$ one would have to adjust the fine structure constant to again bring the volume with the new critical coupling to be again $\sqrt{6\pi}^{dimG}$. So

$$\frac{1}{\alpha_{N\ crit}}|_{\text{with center divided out}} = N^{\frac{1}{dim(SU(N))/2}} \frac{1}{\alpha_{N\ crit}}. \tag{20.65}$$

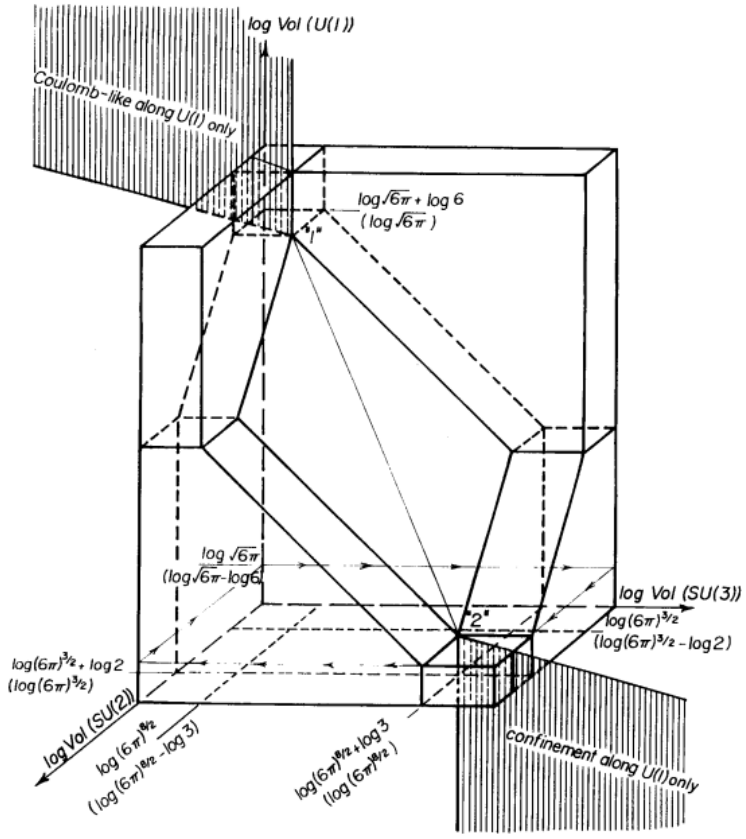

Figure 16: Construction of the phase diagram for the Standard Model Group to lowest order.

20.8.3 Critical Fine structure constant for the Standard Model Group

The mean field approximation used by Don Bennett suggests, that for a group that is a simple Cartesian product of some groups, as e.g. the Standard Model Group without the division out of the part of the center otherwise being in the definition of this group, the phase transition border or just transition point determined for the product

$$1/\alpha_{1\ SU(5)} * (1/\alpha_2)^3 * (1/\alpha_3)^8 \text{ having "special value"} \tag{20.66}$$

$$\approx \quad \text{"related to"} (6\pi)^{12}. \tag{20.67}$$

When we in the same approximation want the critical finestructure constants at the phase transition between the confinement phase with total "confinement" for the full group with some subset of the center divided out, as e.g. the true Standard model group $G_{SMG} = S(U(2) \times U(3))$, we shall just calculate the factor $Cd(Z_{do})$ = "the cardinal number of the subgroup of the center being divided out", by which the volume of the group is being reduced by this division out, and then the dimension weighted product of the inverse fine structure constants 18.66 shall get its for criticality required value increased by this factor. So e.g. this product is for the Standard Model Group $G_{SMG} = (U(1) \times SU(2) \times SU(3))/Z_6$ a factor 6 larger than for the simple Cartesian product of the three groups from which the Standard Model one is composed. I.e.

$$\begin{aligned}
[1/\alpha_{1\ SU(5)} * (1/\alpha_2)^3 * (1/\alpha_3)^8]_{crit\ for\ G_{smg}} = \\
= 6 * [1/\alpha_{1\ SU(5)} * (1/\alpha_2)^3 * (1/\alpha_3)^8]_{crit\ cross\ product} = \\
= 6 * [1/\alpha_{1\ SU(5)} * (1/\alpha_2)^3 * (1/\alpha_3)^8]_{crit\ U(1)\times SU(2)\times SU(3)}.
\end{aligned}$$

This form is the reason, why the combination of the three fine structure constants, which can be postulated to have a critical value - or as we shall assume in our model just 3 times the critical value - is the logarithmically dimension weighted average of the inverse fine structure constants, as explained more in subsection 18.8.5.

20.8.4 Calculation of the Critical (Inverse) Finestructure constant average

For estimating the critical coupling for the Standard Model **group** SMG we shall make use of our formula by Laperashvili et al. developed by use of renorm group and monopoles being assumed and used for the critical inverse coupling squares (~ inverse fine structure constants)

$$\alpha^{-1}_{N\,crit} = \frac{N}{2}\sqrt{\frac{N+1}{N-1}}\alpha^{-1}_{u(1)\ crit} \tag{20.68}$$

$$\text{where } \alpha^{lat}_{U(1)\ crit} \approx 0.20 \pm 0.015 \tag{20.69}$$

$$\text{or } \alpha^{-1}_{U(1)\ crit} \approx 5 \pm 7.5\% = 5 \pm 0.4 \tag{20.70}$$

20.8.5 The Average, that can be Calculated as Critical

In [4] we find, that insisting on the ratios of the differences of the inverse finestructure constants at the "approximate unification " should be as required from our quantum correction model - i.e. the $1/\alpha_{1\ SU(5)}$ shall divide the interval from $1/\alpha_3$ to $1/\alpha_2$ into pieces in the ratio 3:2 - the " unification scale inverse finestructure constant" would have to have the inverse fine structure constants

$$1/\alpha_{1\ SU(5)}(\mu_u) = 41.355 \pm 0.017 \tag{20.71}$$
$$1/\alpha_2(\mu_u) = 43.203 \pm 0.02 \tag{20.72}$$
$$1/\alpha_3(\mu_u) = 38.585 \pm 0.05. \tag{20.73}$$

when using the experimental fine structure constants (we have reproduced these "experimental" fine structure constants below in (18.126, 18.129, 18.132) in this article) at say the M_Z mass.
Because it is supposed to be the total group volume that matters it is expected, that it is the logarithmic average of these quantities weighted by the dimensions of the simple groups that we shall expect to be obtainable as critical value:
The basis 10 logarithms for these inverse fine structure constants at our replacement for unification scale μ_u are

$$\log(1/\alpha_{1\ SU(5)}(\mu_u)) = 1.6165 \tag{20.74}$$
$$\log(1/\alpha_2(\mu_u)) = 1.6355 \tag{20.75}$$
$$\log(1/\alpha_3(\mu_u)) = 1.5864 \tag{20.76}$$
$$\text{Average } \log(1/\alpha_{av}(\mu_u)) = \frac{1 * 1.6165 + 3 * 1.6355 + 8 * 1.5864}{12} \tag{20.77}$$
$$= \frac{19.2143}{12} \tag{20.78}$$
$$= 1.6012 \tag{20.79}$$
$$\text{giving } 1/\alpha_{av}(\mu_u) = 39.920. \tag{20.80}$$

20.8.6 Calculation of Critical Coupling

Using these formulas we get

$$SU(2)(/Z_2) \tag{20.81}$$
$$1/\alpha_{crit\,SU(2)} = 1/\alpha_{1\,crit} * \frac{2}{2} * \sqrt{\frac{2+1}{2-1}} \tag{20.82}$$
$$= 1/\alpha_{U(1)\,crit} * \sqrt{3} = 8.660 \tag{20.83}$$
$$\text{while } 1/\alpha_{SU(2)/z_{2\,crit}} = 1/\alpha_{SO(3)\,crit} = 1/\alpha_{U(1)\,crit}\sqrt{3} * \sqrt[3]{4} = 13.747$$
$$\text{to compare with "old" } 1/\alpha_{2\,crit} = 15.7 \pm 1 \text{(unexponentiated)}$$
$$= 16.5 \pm 1 \text{(exponentiated)} \tag{20.84}$$
$$\tag{20.85}$$

$$SU(3)(/Z_3)$$

$$\text{"old" } 1/\alpha_{SU(3)\ crit} = 1/\alpha_{U(1)\ crit} * \frac{3}{2}\sqrt{\frac{3+1}{3-1}} \quad (20.86)$$

$$= 5 * \frac{3}{\sqrt{2}} = 5 * 2.1213 \quad (20.87)$$

$$= 10.6066 \quad (20.88)$$

$$\text{while } 1/\alpha_{SU(3)/Z_3\ crit} = 1/\alpha_{U(1)\ crit} * \frac{3}{\sqrt{2}} * 3^{2/8} \quad (20.89)$$

$$= 13.9591 \quad (20.90)$$

$$\text{to compare with "old" } 1/\alpha_{3\ crit} = 17.7 \pm 1(\text{unexponentiated})$$

$$= 18.9 \pm 1(\text{exponentiated}) \quad (20.91)$$

We here compared with our old estimates, see e.g. Don Bennett's thesis [63], from which we have included as figures the most critical formulas, and find that our expressions using the

$$1/\alpha_{SU(N)\ crit} = \frac{N}{2} * \sqrt{\frac{N+1}{N-1}} 1001[9]$$

tend to give a bit lower inverse critical fine structure constants than the "old" estimates. These "old" critical inverse fine structure constant estimates were truly lattice artifact calculations made for a meeting of three phases - a confining one, an approximate one with $SU(N)/Z_N$ surviving as approximately perturbative Yang Mills, and finally one where it is SU(N), that survives -, and so the monopoles in these "old" estimates were lattice-artifact monopoles. Contrary our presently used calculation [9,10,23] rather has a monopole in the continuum - which is better in agreement with the very speculative story in the present work, that a resonance decaying into a pair of muons of mass 27 GeV should be related to monopoles -
The reason we suggest, that it is the critical couplings for the SU(2) and SU(3) with their center divided out, so really the critical couplings for $SU(2)/Z_2$ and $SU(3)/Z_3$, that should be compared to the "old" numbers, is that the dominant term in the lattice theory for these critical couplings are the ones corresponding to these groups with the center divided out.
The distinction "unexponentiated" versus "exponentiated" is just a tiny variation in the corrections in the "old" calculation, see Don Bennetts thesis [63].

Table 4:

Table 4: SU(2) Gauge Coupling	
Prediction for continuum limit coupling estimate, $1/\alpha_{2,\,triple\,point,\,cont.}$, using 1. not exponentiated: 2. exponentiated:	$\overbrace{0.71 \cdot 20}^{14.2} + \overbrace{0.89 \cdot 1.7}^{1.5} = 15._7 \pm 1$ $\overbrace{0.75 \cdot 20}^{15._0} + \overbrace{0.89 \cdot 1.7}^{1.5} = 16._5 \pm 1$
Experimental value [24, 25] for $1/\alpha_2$ reduced by a factor 3: "desert extrapolation [24, 25]" to Planck scale with one Higgs:	$\frac{1}{3} \cdot \alpha_2^{-1}(M_Z) = \frac{1}{3} \cdot (29.7 \pm 0.2) = 9.9 \pm 0.07$ $\overset{desert}{\longrightarrow} \frac{1}{3} \cdot \alpha_2^{-1}(\mu_{Pl.}) = \frac{1}{3} \cdot 49._5 = 16.5$
$\beta_{adj.,\,triple\,point}$ (i.e., at triple point)	2.4 (ca. 5% uncertainty from MC)
$\beta_{f\,triple\,point}$ (i.e., at triple point)	0.54 (ca. 10% uncertainty from MC)
$\beta_{adj.}$-contribution to $1/\alpha_{2,\,triple\,point}$ (without continuum correction)	$4\pi \frac{C^{(2)}_{adj.}}{(2^2-1)} \beta_{adj,\,triple\,point} = 4\pi \cdot (2/3) \cdot 2.4 = 20$
β_f-contribution to $1/\alpha_{2,\,triple\,point}$ (without continuum correction):	$4\pi \frac{C^{(2)}_{f}}{(2^2-1)} \beta_{f\,triple\,point} = 4\pi \cdot (\frac{3}{4}/3) \cdot 0.54 = 1.7$
Full $1/\alpha_{2,\,triple\,point}$ (without continuum correction):	$1/\alpha_{2,\,triple\,point,\,full,\,no\,cont.} = 20 + 1.7 = 21.7$
Continuum correction factor for $\beta_{adj.}$-contribution: 1. not exponentiated (using (220)): 2. exponentiated:	$1 - C^{(2)}_{adj.} \pi \alpha_{2,\,triple\,point,\,full,\,no.\,cont.} =$ $1 - 2\pi/21.7 = 1 - 0.290 = 0.71$ $\exp(-C^{(2)}_{adj.} \pi \alpha_{2,\,triple\,point,\,full,\,no.\,cont.}) =$ $\exp(-2\pi/21.7) = \exp(-0.290) = 0.75$
Continuum correction factor for β_f-contribution: 1. not exponentiated (using (220)): 2. exponentiated:	$1 - C^{(2)}_{f} \pi \alpha_{2,\,triple\,point,\,full,\,no.\,cont.} =$ $1 - (\frac{3}{4})\pi/21.7 = 1 - 0.109 = 0.89$ $\exp(-C^{(2)}_{f} \pi \alpha_{2,\,triple\,point,\,full,\,no.\,cont.}) =$ $\exp(-(\frac{3}{4})\pi/21.7) = \exp(-0.109) = 0.90$

Table 5:

Table 3: SU(3) Gauge Coupling	
Prediction for continuum limit coupling estimate, $1/\alpha_{3,\,triple\ point,\,cont.}$, using	
1. not exponentiated:	$\overbrace{0.65\cdot 25}^{16._3}+\overbrace{0.84\cdot 1.7}^{1.4}=17._7\pm 1$
2. exponentiated:	$\overbrace{0.70\cdot 25}^{17._5}+\overbrace{0.85\cdot 1.7}^{1.4}=18._9\pm 1$
Experimental value [24, 25] for $1/\alpha_3$ reduced by a factor 3:	$\frac{1}{3}\cdot\alpha_3^{-1}(M_Z)=\frac{1}{3}\cdot(8.47\pm 0.5)=2.8\pm 0.2$
"desert extrapolation [24, 25]" to Planck scale with one Higgs:	$\overset{desert}{\longrightarrow}\frac{1}{3}\cdot\alpha_3^{-1}(\mu_{_{PL}})=\frac{1}{3}\cdot 53\pm 0.7=17.7\pm 0.3$
$\beta_{adj.,\,triple\ point}$ (i.e., at triple point)	5.4 (ca. 5% uncertainty)
$\beta_{f\ triple\ point}$ (i.e., at triple point)	0.8 (ca. 20% uncertainty)
$\beta_{adj.}$-contribution to $1/\alpha_{3,\,triple\ point}$ (without continuum correction)	$4\pi\frac{C^{(2)}_{adj.}}{(3^2-1)}\beta_{adj,\,triple\ point}=4\pi\cdot(3/8)\cdot 5.4=25$
β_f-contribution to $1/\alpha_{3,\,triple\ point}$ (without continuum correction):	$4\pi\frac{C^{(2)}_{f}}{(3^2-1)}\beta_{f\ triple\ point}=4\pi\cdot(\frac{4}{3}/8)\cdot 0.8=1.7$
Full $1/\alpha_{3,\,triple\ point}$ (without continuum correction):	$1/\alpha_{3,\,triple\ point,\,full,\,no\ cont.}=25+1.7=26._7$
Continuum correction factor for $\beta_{adj.}$-contribution:	
1. not exponentiated (using (220)):	$1-C^{(2)}_{adj.}\pi\alpha_{3,\,triple\ point,\,full,\,no.\ cont.}=$ $1-3\pi/26.7=1-0.35=0.65$
2. exponentiated:	$\exp(-C^{(2)}_{adj.}\pi\alpha_{3,\,triple\ point,\,full,\,no.\ cont.})=$ $\exp(-3\pi/26.7)=\exp(-0.35)=0.70$
Continuum correction factor for β_f-contribution:	
1. not exponentiated (using (220)):	$1-C^{(2)}_{f}\pi\alpha_{3,\,triple\ point,\,full,\,no.\ cont.}=$ $1-(\frac{4}{3})\pi/26.7=1-0.16=0.84$
2. exponentiated:	$\exp(-C^{(2)}_{f}\pi\alpha_{3,\,triple\ point,\,full,\,no.\ cont.})=$ $\exp(-(\frac{4}{3})\pi/26.7)=\exp(-0.16)=0.85$

Our Expression for the SMG critical Inverse Fine structure constant Let us now use our formulas to get first a critical couplig relation for the simple cross product group $U(1) \times SU(2) \times SU(3)$ and then for the Standard odel **group** $SMG = S(U(2) \times U(3))$ for the logarithmically dimension weighted (inverse) fine structure constant:

$$U(1) \times SU(2) \times SU(3) \tag{20.92}$$

$$1/\alpha_{av\ U(1)\times SU(2)\times SU(3)\ crit} = \sqrt[12]{1/\alpha_{U(1)\ crit} * (1/\alpha_{SU(2)\ crit})^3 * (1/\alpha_{SU(3)\ crit})^8}$$

$$= \sqrt[12]{(1/\alpha_{U(1)\ crit})^{12} * (\sqrt{3})^3 * (\frac{3}{2} * \sqrt{2})^8} \tag{20.93}$$

$$= 1/\alpha_{U(1)\ crit} * \sqrt[12]{3^{3/2} * 3^8 * 2^{-4}} \tag{20.94}$$

$$= 1/\alpha_{U(1)\ crit} * 3^{19/24} * 2^{-1/3} \tag{20.95}$$

$$= 5 * 2.3863/1.2599 \tag{20.96}$$

$$= 9.4699 \tag{20.97}$$

$$SMG = S(U(2) \times U(3))$$

$$1/\alpha_{av\ SMG\ crit} = \sqrt[12]{6 * 1/\alpha_{U(1)\ crit} * (1/\alpha_{SU(2)\ crit})^3 * (1/\alpha_{SU(3)\ crit})^8}$$

$$= \sqrt[12]{6^2 * 1/(\alpha_{U(1)\ crit})^{12} * (\sqrt{3})^3 * (\frac{3}{2} * \sqrt{2})^8} \tag{20.98}$$

$$= 1/\alpha_{U(1)\ crit} 6^{2/12} * 3^{19/24} * 2^{-1/3} \tag{20.99}$$

$$= 1/\alpha_{U(1)\ crit} * 3^{23/24} * 2^{-1/6} \tag{20.100}$$

$$= 5 * 2.86577 * 0.890899 \tag{20.101}$$

$$= 5 * 2.55311 \tag{20.102}$$

$$= 12.76550 \tag{20.103}$$

$$3/\alpha_{av\ SMG\ crit} = 38.2968 \tag{20.104}$$

This last number (18.104) and the experimental averaged number $\frac{3}{\alpha_{av}(\mu_u)}$, (18.80), agrees with a deviation of only 1.6 (meaning only 4%) which is even agreement with minimal estimate of the uncertainty of the theoretical number of 7.5 %, which would mean one standard deviation being 2.9.

20.8.7 Resume of the Fine structure calculation

We can resume our model for the fine structure constants by writting the values of the inverse fine structure constants for the three subgroups U(1), Su(2), amd SU(3) in SU(5)-adjusted notation (it just means we use $1/\alpha_{1\ SU(5)} = \frac{3}{5} * 1/\alpha_1$ instead of the $1/\alpha_1$ itself for the Standard Model U(1)) in terms of the three parameters $\ln(\frac{\mu_u}{M_Z})$, q, and $3/\alpha_{av\ SMG\ crit}$, which we claim, we have calculated, under our

assumptions of course:

$$1/\alpha_{1\ SU(5)}(M_Z) = \frac{\frac{41}{10}}{2\pi} * \ln(\frac{\mu_u}{M_Z}) + \frac{3}{10} * q + \frac{3}{\alpha_{av\ SMG\ crit}} \quad (20.105)$$

$$1/\alpha_2(M_Z) = \frac{-\frac{19}{6}}{2\pi} * \ln(\frac{\mu_u}{M_Z}) + \frac{7}{10} * q + + \frac{3}{\alpha_{av\ SMG\ crit}} \quad (20.106)$$

$$1/\alpha_3(M_Z) = \frac{-7}{2\pi} * \ln(\frac{\mu_u}{M_Z}) - \frac{3}{10} * q + \frac{3}{\alpha_{av\ SMG\ crit}} \quad (20.107)$$

$$(20.108)$$

The terms with q give the deviation from genuine SU(5) GUT and represent the quantum correction in the lattice theory to an action, which in the classical approximation happens to give the SU(5) invariance relation between the three standard model fine strucutre constants. The action we imagine in our model is namely expressed in terms of a 5×5 matrix representation of the only true gauge theory in our model - that of the Standard Model group -, and the simplest trace happens to be identical to an SU(5) action. The coefficients to q, i.e. 3/10, 7/10, and -3/10, have been arranged, so that the correction to the difference $1/\alpha_2 - 1/\alpha_{1\ SU(5)}$ becomes 2/3 of that of the difference $1/\alpha_{1\ SU(5)} - 1/\alpha_3$ as estimated in our article [4]. Further they are arranged to make contribution to the dimension weighted average zero, i.e.

$$1 * \frac{3}{10} + 3 * \frac{7}{10} + 8 * \frac{-3}{10} = 0. \quad (20.109)$$

The parameter q would, if there was only a simple Wilson lattice (in one layer) be $q = \pi/2$, but it is an important physical assumption in our model, that we do not truly have only the Standard Model gauge group, but rather a **cross product of three** Standard Model groups with each other together. This makes the quantum correction three times as big (see (18.3)), and we thus have

$$q = 3 * \pi/2 = 4.7124. \quad (20.110)$$

The same factor 3 signaling, that the genuine gauge group should be $SMG \times SMG \times SMG$ rather than just SMG, comes in and makes averaged inverse finestructure constant at the essential unification scale μ_u become $3/\alpha_{av\ SMG\ crit}$ rather than just the critical inverse finestructure constant itself. It is supposed that this factor 3 is the number of families. So to speak: Each family has its own SMG gauge group.
Let us collect the **Theoretical Parameter Values**:
Let us first assign uncertainties which are minimal needed, i.e. it would be hard to avoid these uncertainties, but there might be further ones (e.g. our formula for critical coupling [10,23] could have similar or further uncertainties):

$$\ln \mu_u M_Z = \ln(\frac{4.9534 * 10^{13} GeV}{91.1876 GeV}) = 27.0204 \pm 0.01 (\text{see (18.51)}) \quad (20.111)$$

$$q = 3 * \pi/2 = 4.7124 \pm 0.05 \quad (20.112)$$

$$\frac{3}{\alpha_{av\ SMG\ crit}} = 3 * 12.76550 = 38.2965 \pm 3 \quad (20.113)$$

(The error on q we propose to take as a higher order correction and thus percentwise of the order of α.)
We can now simply calculate the predictions for the inverse fine structure constants at the M_Z scale and compare with the experimentally determined values:

$$\begin{aligned} 1/\alpha_{1\ SU(5)}(M_Z)|_{predicted} &= \frac{\frac{41}{10}}{2\pi} * 27.0204 + \frac{3}{10} * 4.7124 + 38.2965 \\ &= 17.6318 + 1.4137 + 38.2965 \quad (20.114) \\ &= 57.3420 \pm 3 \quad (20.115) \\ \text{to compare with } 1/\alpha_{1\ SU(U)}(M_Z)|_{exp} &= 59.008 \pm 0.013. \quad (20.116) \\ 1/\alpha_2(M_Z) &= \frac{-\frac{19}{6}}{2\pi} * 27.0204 + \frac{7}{10} * 4.7124 + 38.2965 \\ &= -13.6180 + 3.2987 + 38.2965 \quad (20.117) \\ &= 27.9772 \pm 3 \quad (20.118) \\ \text{to compare with } 1/\alpha_2(M_Z)|_{exp} &= 29.569 \pm 0.017 \quad (20.119) \\ 1/\alpha_3(M_Z) &= \frac{-7}{2\pi} * 27.0204 - \frac{3}{10} * 4.7124 + 38.2965 \\ &= -30.1030 - 1.4137 + 38.2965 \quad (20.120) \\ &= 6.7798 \pm 3 \quad (20.121) \\ \text{to compare with } 1/\alpha_3(M_Z)|_{exp} &= 8.446 \pm 0.05 \quad (20.122) \end{aligned}$$

Our predictions agree wonderfully within the by the critical coupling parameter $\frac{3}{\alpha_{av\ SMG\ crit}}$ dominated uncertainty, which we had put to ± 3. However the deviation is very systematic, all the three inverse fine structure constants being just 1.6414 bigger experimentally than our prediction. So if we gave up trusting accurately our critical coupling parameter $\frac{3}{\alpha_{av\ SMG\ crit}}$, and instead just fitted it to the experimental data, while still keeping our two other theoretically predicted parameters, q and $\ln(\frac{\mu_u}{M_Z})$, we could hope for a higher accuracy predition. In fact let us change our critical coupling parameter to a to data fitted value by replacing it like:

$$\frac{3}{\alpha_{av\ SMG\ crit}} = 38.2965 \rightarrow 38.2965 + 1.6414 = 39.9379 \quad (20.123)$$

Then we would get rather:

$$\begin{aligned} 1/\alpha_{1\ SU(5)}(M_Z)|_{predicted} &= \frac{\frac{41}{10}}{2\pi} * 27.0204 + \frac{3}{10} * 4.7124 + 39.9379 \\ &= 17.6318 + 1.4137 + 39.9379 \quad (20.124) \\ &= 58.9834 \pm 0.02 \quad (20.125) \\ \text{to compare with } 1/\alpha_{1\ SU(U)}(M_Z)|_{exp} &= 59.008 \pm 0.013., \quad (20.126) \end{aligned}$$

and

$$1/\alpha_2(M_Z) = \frac{-\frac{19}{6}}{2\pi} * 27.0204 + \frac{7}{10} * 4.7124 + 39.9379$$
$$= -13.6180 + 3.2987 + 39.9379 \quad (20.127)$$
$$= 29.6186 \pm 0.04 \quad (20.128)$$
$$\text{to compare with } 1/\alpha_2(M_Z)|_{exp} = 29.569 \pm 0.017 \quad (20.129)$$
$$1/\alpha_3(M_Z) = \frac{-7}{2\pi} * 27.0204 - \frac{3}{10} * 4.7124 + 39.9379$$
$$= -30.1030 - 1.4137 + 39.9379 \quad (20.130)$$
$$= 8.4212 \pm 0.02 \quad (20.131)$$
$$\text{to compare with } 1/\alpha_3(M_Z)|_{exp} = 8.446 \pm 0.05 \quad (20.132)$$

The agreement is still within our a bit arbitrarily estimated uncertainties in spite of, that we now have the uncertainty on the second decimal in the inverse fine structure constants, and we only fitted **one** of our **three** theoretically predicted parameters! The q being the quantum correction breaking SU(5), and the replacement for unification scale μ_u used in our parameter $\ln(\frac{\mu_u}{M_Z})$ seemingly are so accurate as to admit for only deviations on the second decimal after the "."! The difference $1/\alpha_{1\ SU(5)}(M_Z) - 1/\alpha_2(M_Z)$ predicted to 29.365 with one promille accuracy was experimentally 29.439 deviating by only 0.074 meaning 2.5 .

20.9 Conclusion

We have found a phenomenologically surprisingly well agreeing relation involving about 9 different energy scales in physics and the supposed power n of the link variable a which should be relvant for these different scales a^n. In fact the logarithms of the energies of the different scales versus the power n of the link variable associated turned out to be a linear relation described by a straight line. It must be admitted that most of these energy scales are only meaningful order of magnitudewise. But at the end we considered four of the scales, which at least had the chance of giving more than only order of magnitude numbers for the energies. It turned out, that taking it, that we should use the energy occurring in the Lagrangian (as a coefficient being this energy to some power) these four points fall very well on the straight line with the accuracy achievable with them. In fact we used three of the points among these four to make a prediction for the one being the unification scale for an approximate SU(5) unification of the fine structure constants. Using this unification scale from the straight line μ_u together with our earlier model for a quantum effect breaking the SU(5), which was in our picture only an accidental classical approximation being SU(5) invariant, we obtained values for the differences between the three inverse fine structure constants in the Standard Model deviating only from the experimentally determined numbers corresponding to an error ± 0.05 for the these differences, which are e.g. 21.20. So our model agrees for these differences to **a quarter of a percent!**
We also did obtain predictions for the fine structure constants proper, but because of the dependence on the at least so far not so well calculated critical fine structure

constant for the Standard Model group (even the concept might be not well enough defined) we only get the inverse fine structure constants with error estimates of the order ± 3, but even that is very good!
Our story of the straight line for the logarithms of the energy scales versus the power to which the link size a should be raised to relate to the scale in question, is indeed very intriguing. For some of the energy scales we can easily imagine, that under the assumption of, the parameters of the lattice theory being of order unity compared to the local lattice links, we get the energy scale given by some power of the link, averaged of course appropriately. This is for instance the case for the scales as the approximate unification scale μ_u and the Planck scale, and scales for masses of a lot of bosons, or of a lot of fermions (taken to be the see-saw scale). But when we come to the hadron-string scale, then one would say, that properties of hadron physics should be given by QCD alone and not depend much on the lattice, since the lattice should function only as a cut off and when expressed in terms of the renormalized couplings, the cut off should drop out. Nevertheless it was most accurately the hadron string scale, we used in our so successful prediction of the inverse fine structure constant differences. So one would say, that it is physically absurd, that this hadron string scale should fall on the same line as the scales, which are easy to conceive of as lattice link size connected. Either one would need to say, that something more than just QCD is involved in making confinement and some effective hadronic strings, or one would have to take it that some mysterious - yet to be understood - principle in the lattice physics just arrange this lattice to produces its string action to just agree with that of the effective hadron strings. Both ways to explain the strange coincidence sounds physically very strange.
The domain wall scale, which we expect would be due to some phase border in a mainly QCD and quark physics grounded physics, would be in the same way intriguing and mysterious. It would again require either something else than just QCD-physics, or some mysterious adjustment of the lattice knowledgeable about QCD, or may be opposite some QCD parameter should be adjusted to make our straight line coincidence work.
The scale of monopole or related particle mass, could better without too much mystery be an effect of an ontological lattice.

20.9.1 Outlook

As an optimistic outlook we imagine the possibility, that our high accuracy success with the inverse fine structure constant differences could open the way for a numerological study of higher energies than what is directly reachable by the accelerators of the day.
A point, that came out of the present works, is that the cut off scale in our model is much closer, i.e. much lower in energy, than for instance, what many of us would have believed before, the Planck scale. Thus cut off effects are potentially to be seen in very accurately measured quantities, such as the anomalous magnetic moments, or the finestrucure constants themselves. In our Corfu 2024 proceedings [3] we gave an example of how to estimate such cut off effects in our model. The cut off effects seem to be on the borderline of being observable with the present experimental accuracy.

Acknowledgements

The author thanks the Niels Bohr Institute for status as emeritus. This work was discussed in both Bled Workshop 2024 and 2025 and the Corfu Institute last year 2024.

References

1. Holger Bech Nielsen(Bohr Inst.) "Remarkable Scale Relation, Approximate SU(5), Fluctuating Lattice"
   Universe 11 (2025) 7, 211 • e-Print: 2411.03552 • DOI: 10.3390/universe11070211
2. H. B. Nielsen, "Fluctuating Lattice, Several Energy Scales" Bled virtually, July 2024 arXiv:2502.16369v1 [hep-ph] 22 Feb 2025
3. Holger Bech Nielsen, "Approximate Minimal SU(5), Several Fundamental Scales, Fluctuating Lattice", arXiv:2505.06716v1 [hep-ph] 10 May 2025
4. Holger Bech Nielsen, " Approximate SU(5), Fine structure constants", arXiv:2403.14034 (hep-ph) (not yet published, but hopefully)
5. P. Minkowski, Phys. Lett. B 67, 421 (1977). R. N. Mohapatra and G. Senjanovic, Phys. Rev. Lett. 44, 912 (1980).
6. Georgi, Howard; Glashow, Sheldon (1974). "Unity of All Elementary-Particle Forces". Physical Review Letters. 32 (8): 438. Bibcode:1974PhRvL..32..438G. doi:10.1103/PhysRevLett.32.438. S2CID 9063239.
7. Masiero, A.; Nanopoulos, A.; Tamvakis, K.; Yanagida, T. (1982). "Naturally Massless Higgs Doublets in Supersymmetric SU(5)". Physics Letters B. 115 (5): 380–384. Bibcode:1982PhLB..115..380M. doi:10.1016/0370-2693(82)90522-6.
8. Georgi, Howard; Glashow, Sheldon (1974). "Unity of all elementary-particle forces". Physical Review Letters. 32 (8): 438. Bibcode:1974PhRvL..32..438G. doi:10.1103/PhysRevLett.32.438. S2CID 9063239
9. L. V. Laperashvili (ITEP, Moscow, Russia), H. B. Nielsen, D.A. Ryzhikh "Phase Transition in Gauge Theories and Multiple Point Model" arXiv:hep-th/0109023 Phys.Atom.Nucl.65:353-364,2002; Yad.Fiz.65:377-389,2002
10. Larisa Laperashvili, Dmitri Ryzhikh " [SU(5)]3 SUSY unification" Larisa Laperashvili, Dmitri Ryzhikh arXiv:hep-th/0112142v1 17 Dec 2001 [SU(5)]3 SUSY unification
11. Grigory E. Volovik Introduction: Gut and Anti-Gut
    https://doi.org/10.1093/acprof:oso/9780199564842.003.0001
    Journal: The Universe in a Helium Droplet, 2009, p. 1-8
    Publisher: Oxford University PressOxford
    Author: VOLOVIK GRIGORY E.
12. CRITICAL COUPLINGS AND THREE GENERATIONS IN A RANDOM-DYNAMICS INSPIRED MODEL IVICA PICEK FIZIKA B (1992) 1, 99-110
13. D.L.Bennett, L.V. Laperashvili, H.B. Nielsen, Fine structure Constants at the Planck scale from Multiple Point Prinicple. Bled workshop Vol 8, No. 2 (2007) Proceedings of the Tenth workshop " What comes beyond the standard models Bled Slovenia July 17-27-2007.
14. D. Bennett, H.B. Nielsen, and I Picek. Phys. Lett. B208 275 (1988).
15. H. B. Nielsen, "Random Dynamics and relations between the number of fermion generations and the fine structure constants", Acta Physica Polonica Series B(1), 1989. Crakow School of Theoretical Physics, Zakopane, Poland.

16. H.B. Nielsen and N. Brene, Gauge Glass, Proc. of the XVIII International Symposium on the Theory of Elementary Particles, Ahrenshoop, 1985 (Institut fur Hochenergiphysik, Akad. der Wissenschaften der DDR, Berlin-Zeuthen, 1985); D.L. Bennett, N. Brene, L. Mizrachi
17. H.B. Nielsen, Phys. Lett. B178 (1986) 179.
18. arXiv:hep-ph/9311321v1 19 Nov 1993 November 19, 1993 D.L. Bennett, H.B. Nielsen "Predictions for Nonabelian Fine Structure Constants from Multicriticality" arXiv:hep-ph/9311321v1 19 Nov 1993 November 19, 1993
19. Bennett, D. L. ; Nielsen, H. B. "Gauge Couplings Calculated from Multiple Point Criticality Yield $\alpha^{-1} = 137 \pm 9$: at Last, the Elusive Case of U(1)" arXiv:hep-ph/9607278, Int.J.Mod.Phys. A14 (1999) 3313-3385
20. H.B.Nielsen, Y.Takanishi "Baryogenesis via lepton number violation in Anti-GUT model" arXiv:hep-ph/0101307 Phys.Lett. B507 (2001) 241-251
21. L.V.Laperashvili and C. Das, Corpus ID: 119330911 "$[SU(5)]^3$ SUSY unification" (2001) arXiv: High Energy Physics - Theory
22. Paolo Cea, Leonardo Cosmai "Deconfinement phase transitions in external fields" XXIIIrd International Symposium on Lattice Field Theory 25-30 July 2005 Trinity College, Dublin, Ireland
23. L. V. Laperashvili, D. A. Ryzhikh, H. B. Nielsen, "Phase transition couplings in U(1) and SU(N) regularized gauge theories"
January 2012International Journal of Modern Physics A 16(24)
DOI:10.1142/S0217751X01005067
24. L.V.Laperashvili, H.B.Nielsen and D.A.Ryzhikh, Int.J.Mod.Phys. A16 , 3989 (2001); L.V.Laperashvili, H.B.Nielsen and D.A.Ryzhikh, Yad.Fiz. 65 (2002).
25. C.R. Das, C.D. Froggatt, L.V. Laperashvili, H.B. Nielsen "Flipped SU(5), see-saw scale physics and degenerate vacua" arXiv:hep-ph/0507182, Mod.Phys.Lett. A21 (2006) 1151-1160
26. Larisa Laperashvili, Dmitri Ryzhikh "$[SU(5)]^3$ SUSY unification" arXiv:hep-th/0112142v1 17 Dec 2001
27. Holger Bech Nielsen "Random Dynamics and Relations Between the Number of Fermion Generations and the Fine Structure Constants" Jan, 1989, Acta Phys.Polon.B 20 (1989) 427
Contribution to:
XXVIII Cracow School of Theoretical Physics
Report number:
NBI-HE-89-01
28. H. B. Nielsen, Astri Kleppe et al., http://bsm.fmf.uni-lj.si/bled2019bsm/talks/HolgerTransparencesconfusion2.pdf Bled Workshop July 2019, "What comes Beyand the Standard Models".
29. D.L. Bennett, , Holger Bech Nielsen, , N. Brene, , L. Mizrachi "THE CONFUSION MECHANISM AND THE HETEROTIC STRING" Jan, 1987, 20th International Symposium on the Theory of Elementary Particles, 361 (exists KEK-scanned version)
30. Holger Bech Nielsen, and Don Bennett, "Seeking a Game in which the standard model Group shall Win" (2011) 33 pages Part of Proceedings, 14th Workshop on What comes beyond the standard models? : Bled, Slovenia, July 11-21, 2011 Published in: Bled Workshops Phys. 12 (2011) 2, 149
Contribution to: Mini-Workshop Bled 2011, 14th Workshop on What Comes Beyond the Standard Models?, 149
31. Holger Bech Nielsen Niels Bohr Institutet, Blegdamsvej 15 -21 DK 2100Copenhagen E-mail: hbech at nbi.dk, hbechnbi at gmail.com "Small Representations Explaining, Why standard model group?" PoS(CORFU2014)045. Proceedings of the Corfu Summer

Institute 2014 "School and Workshops on Elementary Particle Physics and Gravity", 3-21 September 2014 Corfu, Greece
32. H. Nielsen Published 22 April 2013 Physics Physical Review D DOI:10.1103/PhysRevD.88.096001Corpus ID: 119245261
"Dimension Four Wins the Same Game as the Standard Model Group"
33. L. O'Raifeartaigh, "The Dawning of Gauge Theory", Princeton University Press (1997)
34. SEMINAR ZAVODA ZA TEORIJSKU FIZIKU (Zajedni˘cki seminari Zavoda za teorijsku fiziku, Zavoda za eksperimentalnu fiziku i Zavoda za teorijsku fiziku PMF-a) Relations derived from minimizing the Higgs field squared (integrated over space-time) Holger Bech Nielsen The Niels Bohr Institute, Copenhagen, Denmark
35. H.B. Nielsen "Complex Action Support from Coincidences of Couplings" arXiv:1103.3812v2 [hep-ph] 26 Mar 2011
36. H.B. Nielsen,arXiv:1006.2455v2 "Remarkable Relation from Minimal Imaginary Action Model " arXiv:1006.2455v2 [physics.gen-ph] 2 Mar 2011
37. U.-J. Wiese "Ultracold Quantum Gases and Lattice Systems: Quantum Simulation of Lattice Gauge Theories ", arXiv:1305.1602v1 [quant-ph] 7 May 2013
38. H.B. Nielsen, S.E. Rugh and C. Surlykke, Seeking Inspiration from the Standard Model in Order to Go Beyond It, Proc. of Conference held on Korfu (1992)
39. C.D. Froggatt, H.B. Nielsen and Y. Takanishi, Nucl. Phys. B 631, 285 (2002) [arXiv:hep-ph/0201152];
H.B. Nielsen and Y. Takanishi, Phys. Lett. B 543, 249 (2002) [arXiv:hep-ph/0205180].
40. H.B. Nielsen and C.D. Froggatt, Masses and mixing angles and going be- yond thye Standard Model, Proceedings of the 1st International Workshop on What comes beyond the Standard Model, Bled, July 1998, p. 29, ed. N. Mankoc Borstnik, C.D. Froggatt and H.B. Nielsen DMFA - zaloznistvo, Ljubljana, 1999; hep-ph/9905455
C.D. Froggatt and H.B. Nielsen, Hierarchy of quark masses, Cabibbo angles and CP violation, Nucl. Phys. B147 (1979) 277.
H.B. Nielsen and Y. Takanishi, Neutrino mass matrix in Anti-GUT with see-saw mechanism, Nucl. Phys. B604 (2001) 405.
C.D. Froggatt, M. Gibson and H.B. Nielsen, Neutrino masses and mixing from the AGUT model
41. Ferruccio Feruglio "Fermion masses, critical behavior and universality" JHEP03(2023)236Published for SISSA by Springer Received: March 1, 2023 Accepted: March 13, 2023 Published: March 29, 2023 JHEP03(2023)236
42. H.B. Nielsen* and C.D. Froggatt, "Connecting Insights in Fundamental Physics: Standard Model and Beyond Several degenerate vacua and a model for DarkMatter in the pure Standard Model" Volume 376 - Corfu Summer Institute 2019 "School and Workshops on Elementary Particle Physics and Gravity" (CORFU2019)
43. Keiichi Nagao and Holger Bech Nielsen "Formulation of Complex Action Theory" arXiv:1104.3381v5 [quant-ph] 23 Apr 2012
44. 1) H. B. Nielsen and M. Ninomiya, Int. J. Mod. Phys. A 21 (2006) 5151; arXiv:hep-th/0601048; arXiv:hep-th/0602186; Int. J. Mod. Phys. A 22 (2008) 6227.
2) D. L. Bennett, C. D. Froggatt and H. B. Nielsen, the proceedings of Wendisch-Rietz 1994 -Theory of elementary particles- , p.394-412; the proceedings of Adriatic Meeting on Particle Physics: Perspectives in Particle Physics '94, p.255-279. Talk given by D. L. Bennett, "Who is Afraid of the Past" (A resume of discussions with H. B. Nielsen) at the meeting of the Cross-disciplinary Initiative at NBI on Sep. 8, 1995. D. L. Bennett, arXiv:hep-ph/9607341.
3) H. B. Nielsen and M. Ninomiya, the proceedings of Bled 2006 -What Comes Beyond the Standard Models-, p.87-124, arXiv:hep-ph/0612250.

4) H. B. Nielsen and M. Ninomiya, arXiv:0802.2991 [physics.gen-ph]; Int. J. Mod. Phys. A 23 (2008) 919; Prog. Theor. Phys. 116 (2007) 851.
5) H. B. Nielsen and M. Ninomiya, the proceedings of Bled 2007 -What Comes Beyond the Standard Models- , p.144-185.
6) H. B. Nielsen and M. Ninomiya, arXiv:0910.0359 [hep-ph]; the proceedings of Bled 2010 -What Comes Beyond the Standard Models-, p.138-157.
7) H. B. Nielsen, arXiv:1006.2455 [physic.gen-ph].
8) H. B. Nielsen and M. Ninomiya, arXiv:hep-th/0701018.
9) H. B. Nielsen, arXiv:0911.3859 [gr-qc].
10) H. B. Nielsen, M. S. Mankoc Borstnik, K. Nagao and G. Moultaka, the proceedings of Bled 2010 -What Comes Beyond the Standard Models-, p.211-216.
11) K. Nagao and H. B. Nielsen, Prog. Theor. Phys. 125 No. 3, 633 (2011) -

45. Goran Senjanovic and Michael Zantedeschi, "Minimal SU(5) theory on the edge: the importance of being effective" Goran Senjanovic arXiv:2402.19224v1 [hep-ph] 29 Feb 2024
46. Johan Thoren, Lund University Bachelor Thesis "Grand Unified Theories: SU (5), SO(10) and supersymmetric SU (5)"
47. A.A. Migdal "Phase transitions in gauge and spin-lattice systems" L. D. Landau Theoretical Physics Institute. USSR Academy of Sciences (Submitted June II, 1975) Zh. Eksp. Teor. Fiz. 69, 1457-1465 (October 1975)
48. Stephen F. King "Neutrino mass and mixing in the seesaw playground" Available online at www.sciencedirect.com ScienceDirect Nuclear Physics B 908 (2016) 456–466 www.elsevier.com/locate/nuclphysb
49. Rabindra N. Mohapatra "Physics of Neutrino Mass" SLAC Summer Institute on Particle Physics (SSI04), Aug. 2-13, 2004
50. W. Grimus, L. Lavoura, "A neutrino mass matrix with seesaw mechanism and two-loop mass splitting" arXiv:hep-ph/0007011v1 3 Jul 2000 UWThPh-2000-26
51. Sacha Davidson and Alejandro Ibarra "A lower bound on the right-handed neutrino mass from leptogenesis" arXiv:hep-ph/0202239v2 23 Apr 2002 OUTP-02-10P IPPP/02/16 DCPT/02/32
52. K. Enquist, "Cosmologicaæ Infaltion", arXiv:1201.6164v1 [gr-qc] 30 Jan 2012
53. Andrew Liddle, An Introduction to Cosmological Inflation",arXiv:astro-ph/9901124v1 11 Jan 1999
54. Nicola Bellomo, Nicola Bartolo, Raul Jimenez, Sabino Matarrese,c,d,e,g Licia Verde "Measuring the Energy Scale of Inflation with Large Scale Structures" arXiv:1809.07113v2 [astro-ph.CO] 26 Nov 2018
55. C. D. Froggatt and H. B. Nielsen, Nucl. Phys. B 147, 277-298 (1979)
56. Roberto AUZZI, Stefano BOLOGNESI, Jarah EVSLIN, Kenichi KONISHI, Hitoshi MURAYAMA, "NONABELIAN MONOPOLES" arXiv:hep-th/0405070v3 23 Jun 2004 ULB-TH-04/11, IFUP-TH/2004-5
57. The CMS collaboration EUROPEAN ORGANIZATION FOR NUCLEAR RESEARCH (CERN) CERN-EP-2018-204 2018/12/18 CMS-HIG-16-017 "Search for resonances in the mass spectrum of muon pairs produced in association with b quark jets in proton-proton collisions at $\sqrt{s}$ = 8 and 13 TeV" arXiv:1808.01890v2 [hep-ex] 17 Dec 2018
58. Arno Heister, "Observation of an excess at 30 GeV in the opposite sign di-muon spectra of $Z \rightarrow bb + X$ events recorded by the ALEPH experiment at LEP" E-mail: Arno.Heister@cern.ch arXiv:1610.06536v1 [hep-ex] 20 Oct 2016 Prepaired for submission to JHEP.
59. D. Foerster, H.B. Nielsen a b, M. Ninomiya, "Dynamical stability of local gauge symmetry Creation of light from chaos" Physics Letters B Volume 94, Issue 2, 28 July 1980, Pages 135-140

60. H.B.Nielsen "Field theories without fundamental gauge symmetries" Published:20 December 1983: https://doi.org/10.1098/rsta.1983.0088, Philosophical Transactions of the Royal Society of London. Series A, Mathematical and Physical Sciences
61. M. Lehto, H.B. Nielsen, Masao Ninomiya "Time translational symmetry" Physics Letters B Volume 219, Issue 1, 9 March 1989, Pages 87-91 Physics Letters B
62. C. D. Froggatt and H.B. Nielsen, "Domain Walls and Hubble Constant Tension" arXiv:2406.07740 [astro-ph.CO] (or arXiv:2406.07740v1 [astro-ph.CO] for this version) https://doi.org/10.48550/arXiv.2406.07740
63. Don Bennett, " Multiple Point Criticality, Nonlocality and Finetuning in Fundamental Physics: Predictions for Gauge Coupling Constants gives $\alpha^{-1} = 136.8 \pm 9$" D.L. Bennett Ph.D. Thesis The Niels Bohr Institute Blegdamsvej 17, DK-2100 Copenhagen Ø, Denmark, arXiv:hep-ph/9607341 (or arXiv:hep-ph/9607341v1 for this version) https://doi.org/10.48550/arXiv.hep-ph/9607341
64. S. S. Afonin and I. V. Pusenkov "Linear radial Regge trajectories for mesons with any quark flavor1" arXiv:1606.05218v1 [hep-ph] 16 Jun 2016
65. Jacob Sonnenschein and Dorin Weissman "A rotating string model versus baryon spectra Jacob Sonnenschein and Dorin Weissman" arXiv:1408.0763v3 [hep-ph] 1 Jan 2015
66. "137 | The Fine Structure Constant, Physics - ArsMagine.com". Ars Magine - Umetnost promišljanja i uobrazilje (in Serbian). Retrieved 28 June 2024.
67. H. B. Nielsen, "An almost physical interpretation of the dual N point function", Nordita preprint (1969); unpublished
68. Y. Nambu, Duality and Hadrodynamics, notes prepared for Copenhagen High Energy Symposium, August 1970 (unpublished).
69. L. Susskind, Phys. Rev. Lett. 23, 545 (1969). L. Susskind, Nuovo Cim. A 69, 457–496 (1970
70. As for the initiation of Random Dynamics, See "Fundamentals of Quark Models". Proceedings: 17th Scottish Universities Summer School in Physics, St. Andrews, Aug 1976, I.M. Barbour, A.T. Davies (Glasgow U.);1977 - 588 pages; Edinburgh: SUSSP Publ. (1977); Conference: C76-08-01; Contributions: Dual Strings, Holger Bech Nielsen (Bohr Inst.). Aug 1974, 71 pp.;NBI-HE-74-15 In the last section the idea of "Random Dynamics " is introduced based on finding Weyl equation in "whatever"
71. Origin of Symmetries https://doi.org/10.1142/0090 | August 1991 Pages: 596 Edited by: C D Froggatt (Univ. Glasgow) and H B Nielsen (Niels Bohr Inst.)
72. D L Bennett, N Brene and H B Nielsen "Random Dynamics" Published under licence by IOP Publishing Ltd Physica Scripta, Volume 1987, Number T15Citation D L Bennett et al 1987 Phys. Scr. 1987 158DOI 10.1088/0031-8949/1987/T15/022 Physica Scripta
73. Nielsen, H.B. (1992). "Random Dynamics, Three Generations, and Skewness." In: Teitelboim, C., Zanelli, J. (eds) Quantum Mechanics of Fundamental Systems 3. Series of the Centro de Estudios Científicos de Santiago. Springer, Boston, MA. https://doi.org/10.1007/978-1-4615-3374-0_9
74. Johnson, Norman L.; Kotz, Samuel; Balakrishnan, N. (1994), " 14: Lognormal Distributions", Continuous univariate distributions. Vol. 1, Wiley Series in Probability and Mathematical Statistics: Applied Probability and Statistics (2nd ed.), New York: John Wiley & Sons, ISBN 978-0-471-58495-7, MR 1299979
75. Holger Bech Nielsen, and Colin D. Froggatt "Domain Walls and Hubble Constant Tension" arXiv:2406.07740v1 [astro-ph.CO] 11 Jun 2024
76. https://sites.google.com/view/nolan-fitzpatrick-physics/chew-frautschi-plots
77. "Killing form", Encyclopedia of Mathematics, EMS Press, 2001 [1994]

BLED WORKSHOPS
IN PHYSICS
VOL. 26, NO. 1

Proceedings of the 28th Workshop
What Comes Beyond . . . *(p. 303)*
Bled, Slovenia, July 6–17, 2025

21 Multimessenger probes of fundamental physics: Gravitational Waves, Dark Matter and Quantum Gravity

S. Ray[1‡‡], T. E. Bikbaev[2,3§§], M. Yu. Khlopov[4¶¶], V. I. Korchagin[3***], T. P. Shestakova[5†††], D. O. Sopin[2,3], M. A. Krasnov[2,3], R. V. Tkachenko[3], A. Chaudhuri[3], A.Kharakhashyan[3], O. A. Maltseva[3], R. I. Ayala Oña[5], V. A. Opara[5], M. F. Uspenskaia[5], S. Roy Chowdhury[6‡‡‡], A. Sanyal[7§§§] and D. Santra[8¶¶¶]

[1] Centre for Cosmology, Astrophysics and Space Science (CCASS), GLA University, Mathura 281406, Uttar Pradesh, India
[2] National Research Nuclear University MEPhI, 115409 Moscow, Russia;
[3] Research Institute of Physics, Southern Federal University, Stachki 194 Rostov on Don 344090, Russia
[4] Virtual Institute of Astroparticle physics, 75018 Paris, France
[5] Department of Theoretical and Computational Physics, Southern Federal University Sorge 5 Rostov on Don 344090, Russia
[6] Department of Physics, Vidyasagar College, Kolkata 700006, West Bengal, India
[7] Department of Mathematics, Jadavpur University, Kolkata 700032, West Bengal, India
[8] Institute of Engineering and Management, Kolkata 700091, West Bengal, India

Abstract. In the present article we provide a synoptic review of the contents – physical, astrophysical, and cosmological manifestations of the theory of fundamental interactions within and beyond standard models. Our particular emphasis is on the development and identification of modified and quantum gravity effects, dark matter physics, and their verification schemes based on the theoretical, experimental and observational methods. However, the present review does not intent to provide a holistic and panoramic scenario of the theme rather highlights some features on the theory of fundamental interactions: within and beyond standard models, so that interested readers can get a trailers of the entire topic and enthrall to reach at the oceanic beach to look at the wholesome.

Keywords: compact stars; gravitational waves; composite dark matter; quantum gravity

‡‡saibal.ray@gla.ac.in
§§bikbaev.98@bk.ru
¶¶khlopov@apc.univ-paris7.fr
***vkorchagin@sfedu.ru
†††shestakova@sfedu.ru
‡‡‡souravrc79@gmail.com
§§§aritrasanyal1@gmail.com
¶¶¶deeptendu.santra@gmail.com

21.1 Introduction

Scientific (technical as well as technological) problem that the present review aims to include the development of models for the physics of composite and axion-like dark matter (DM), and their manifestations in cosmological scenarios, the structure and evolution of astrophysical objects, the distribution and possible forms of DM objects, the development of an approach to the quantization of gravity based on the extended phase space formalism, and the possibilities of testing such manifestations using multichannel astronomy methods, highlighting the special role of gravitational waves (GWs) astronomy, as well as in the Earth's ionosphere and magnetosphere.
However, under the theory of fundamental interactions one should not only stick to the general themes within the arena rather beyond standard models also, specifically, the following issues which are expected to be considered:

- due to the manifestation of the effects of modified gravity:
  1. to study the possibility of the occurrence of stochastic GWs during the first-order electroweak phase transition;
  2. to consider the observed properties of compact stars and primordial black holes (PBH);
  3. to explore various inflationary models;
  4. to compare the predicted effects with multi-channel observational data using Bayesian estimation.
- in connection with the study of dark matter :
  1. examine the physics of axion-like particles;
  2. develop a quantum-mechanical numerical model of the interaction of a composite DM particle, the X-helium dark atom, with the nucleus of ordinary matter at different stages of the evolution of the Universe;
  3. elucidate the forms and density distribution of DM in the Milky Way halo and near-Earth space;
  4. search for manifestations of DM in the ionosphere, stratosphere, and near-Earth space.
- in connection with the quantization of gravity:
  1. study of cosmological models with supersymmetry and supergravity;
  2. investigation of alternative formulations of general relativity, for example, in Ashtekar variables used in loop quantum gravity (LQG), from the point of view of the proposed approach;
  3. obtaining corrections describing small quantum-gravitational effects, the consequences of which one could hope to detect in the near future in observational data.

The problem of the physical foundations of modern inflationary cosmology with baryosynthesis, DM, and dark energy inevitably turns to extensions of the standard models (ESMs) of fundamental interactions, including modified gravity. The solution to this crucial problem of fundamental science should lead to the identification and exploration of new forms of matter and energy, the importance of which cannot be overestimated [1]. Research into the possible manifestations of modified and quantum gravity (QG), the physical nature of DM, and its manifestations is significantly complemented.
In recent years, the discovery of GWs and the rapid development of GWs astronomy have transformed modern astrophysics and cosmology. Since the first detection of GW150914 [2], the Advanced LIGO, Virgo, and KAGRA collaborations have reported more than two hundred compact-binary coalescences [3], enabling detailed studies of black-hole and NS

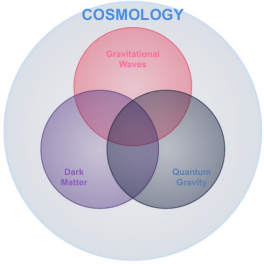

Fig. 21.1: A Venn diagram illustration of the gravitational waves, dark matter and quantum gravity based cosmological scenario of the present review

populations [4,5]. Meanwhile, several promising GW sources – such as white-dwarf binaries, magnetars, core-collapse supernovae, and PBHs, remain undetected [6–13], offering exciting prospects for the coming era. At nanohertz frequencies, pulsar timing arrays (PTA) including PPTA, NANOGrav, EPTA/InPTA, and CPTA have recently reported evidence for an isotropic stochastic background [14–17], triggering active investigation into its astrophysical and possible beyond-standard-model origins. With next-generation detectors such as ET, CE, LISA, and LGWA expanding coverage from sub-Hz to multi-kHz bands [18–22], GW astronomy is poised to probe early-Universe phase transitions, exotic compact objects, and hidden sectors of DM and modified gravity [23–25].

The search for a consistent quantum theory of gravity remains one of the most fundamental open problems in physics. General relativity (GR) successfully describes gravity as a property of spacetime geometry, but it is inherently classical. It exhibits breakdowns near singularities in connections to the Big Bang and black-hole interiors, and hence becomes incompatible with the quantum field theories governing the other fundamental forces [26–28]. Furthermore, coupling classical spacetime to quantum matter leads to conceptual inconsistencies involving quantum superposition and entanglement. These shortcomings strongly suggest that spacetime must possess a quantum structure at the Planck scale.

GWs now provide a unique observational pathway into the quantum aspects of gravity [29–32]. Their propagation is sensitive to the nature of spacetime, and their generation in compact-object mergers probes the strongest dynamical gravity accessible to observation. QG frameworks, including string theory, LQG, asymptotic safety, group field theory, and nonlocal gravity predict measurable GW signatures [33–35]. These include (i) corrections to black-hole ringdown spectra near the horizon, (ii) modified dispersion during propagation, and (iii) characteristic imprints in the primordial SGWB [2,36–39]. While current observations remain consistent with GR predictions, forthcoming experiments promise order-of-magnitude improvements in sensitivity, enabling the first genuine empirical constraints on QG [40–43].

Dark matter, comprising the majority of the Universe's matter content, remains one of the greatest unresolved problems in physics. Strong-gravity astrophysical environments provide natural laboratories where DM can accumulate into dense spikes, gravitational atoms, or other compact substructures [44,45]. Capture and thermalization of DM inside neutron stars (NSs) may trigger collapse into low-mass black holes, altering the compact-object mass function [46]. Advances in quantum-sensing–based GW detection also open the possibility of precision, gravitational-only searches for DM through accelerations induced by passing particles or micro-halos [47]. DM substructure can further leave observable imprints on binary dynamics: over-dense halos surrounding black-hole binaries can induce

dynamical friction driven phase shifts, enabling inference of halo profiles with multi-band GW observations [44,48]. It is to be mentioned that absence of sub-Chandrasekhar-mass black-hole mergers already constrains non-annihilating DM models motivated by NS implosion [46, 49]. Therefore, diffractive GW lensing by low-mass halos can create frequency-dependent interference signatures, providing a baryon-independent probe of small-scale DM structure [50].

In parallel, PBHs, formed from the platform of early-universe density fluctuations, remain compelling DM candidates [51–53]. This is because they interact purely through gravity and can naturally reside in dense DM spikes around supermassive BHs, generating distinctive GW signatures [54]. Essentially, GW observations allow direct tests of this scenario, as PBH mergers are predicted to exhibit characteristic mass and spin distributions that differ from those of astrophysical BHs [55]. Additionally, a population of unresolved PBH mergers would contribute to a SGWB, providing further constraints on the PBH-DM fraction with both currently available and futuristic detector networks [13,56,57].

Under these auspicious arenas, we aim to provide a glimpse of the theory of fundamental interactions, within and beyond standard models in a highlighted manner as much as possible. Therefore, the outline of the article is planned as follows: in Section 2, we provide the current state of research on the issue of beyond standard models, specifically in the three specific avenues, such as compact stars and gravitational waves (in subsection 2.1), dark matter (in subsection 2.2), and quantum gravity (in subsection 2.3). In Section 3, there are a few comments on the present status and future pathways of the topics.

21.2 An overview of the status of research on the standard models: within and beyond

The topics proposed for consideration in this review are widely discussed in modern world scientific literature and can be represented in a coherent manner as follows:

21.2.1 Gravitational waves

The observation of GWs from binary NS (BNS) mergers – most prominently GW170817, GW190425, and the more recent GW230529, has opened a decisive new window into the micro-physical composition of ultra-dense matter. In GW170817, the component masses are $1.46^{+0.12}_{-0.10}\,M_\odot$ and $1.27^{+0.09}_{-0.09}\,M_\odot$, yielding a total system mass of $\sim 2.74\,M_\odot$ under low-spin priors [58]. GW190425 is inferred to host significantly heavier components, with masses $2.1^{+0.5}_{-0.4}\,M_\odot$ and $1.3^{+0.3}_{-0.2}\,M_\odot$ and a total mass of $3.4^{+0.3}_{-0.1}\,M_\odot$ [59]. More recently, GW230529 has been associated with a highly asymmetric system, with component masses $3.6^{+0.8}_{-1.2}\,M_\odot$ and $1.4^{+0.6}_{-0.2}\,M_\odot$ (90% credible intervals) [60].

These multi-messenger events provide unprecedented access to dynamical information encoded in the tidal response, mass–radius relations, and possible post-merger oscillation spectra, enabling precision tests of the equation of state (EOS) at supra-nuclear densities far beyond the reach of terrestrial experiments [61–63]. Because the inspiral waveform is particularly sensitive to the tidal deformability Λ [64–69], and the post-merger remnant probes still higher densities [71,72], BNS mergers offer a unique opportunity to explore the phase structure of dense QCD matter.

Understanding of the EOS in this regime is crucial for mapping the QCD phase diagram and exploring how strongly interacting matter behaves under extreme compression. A transition to deconfined quark matter – whether through a first-order phase change or a smooth crossover – would alter macroscopic observables such as the maximum mass,

radius and tidal deformability of compact stars [73,74]. GWs measurements, therefore, provide a promising platform to test for such exotic phases, complementing constraints from nuclear theory [75–78] and observations of massive compact stars.
To investigate this physics, one may employ a thermodynamically consistent quark-matter EOS implemented through a custom `BagModelEOS` framework, which includes perturbative QCD corrections, an effective bag constant and colour-flavour-locked (CFL) pairing contributions [79–81]. This enables consistent modeling of both hybrid stars and self-bound SQSs. The resulting stellar sequences exhibit modified mass-radius relations and tidal deformabilities, which can be confronted with the current GW constraints to assess whether present observations allow or even favor the presence of quark stars [74,82].

Quark-matter EOS and stellar structure Quark matter in NS interiors is often modeled not as self-bound, but as a high-density phase that emerges only beyond a hadron-quark phase transition in the core, leading to hybrid stars composed of a hadronic envelope surrounding a quark core [83]. In such stars, the pressure vanishes at the stellar surface, where the composition remains purely hadronic. Therefore, the global mass-radius and tidal deformability properties are predominantly governed by the nuclear EOS, with quark matter affecting only the innermost region. This behavior is qualitatively different from that of self-bound SQSs, whose EOSs yield a finite surface density and a sharp density discontinuity at a nonzero surface pressure [84]. As a consequence, standard parameterized NS EOS frameworks, typically formulated for hadronic or hybrid star compositions, cannot faithfully reproduce the self-bound nature and sharp surface of SQSs [85].
The EOS of ultra-dense matter remains one of the central unresolved challenges in compact-star physics. While hadronic matter dominates near nuclear saturation density, ($n_0 \simeq 0.16\,\mathrm{fm}^{-3}$), theoretical and phenomenological arguments suggest that at the asymptotically high densities, strongly interacting matter may transition to a CFL phase of three-flavor quark matter [86,87]. However, the phase structure of cold QCD in the intermediate density regime, ($\sim 1-10\,n_0$), remains poorly constrained, and thus it is still unknown whether compact stars observed in nature are gravity bound NSs or self-bound QSs [75,88,89].
To rigorously explore this uncertainty, it is essential to employ multiple complementary representations of the quark matter EOS. These range from phenomenological models, such as MIT bag type frameworks and their extensions, including perturbative QCD corrections and color superconducting pairing to high density effective theories constructed to ensure thermodynamic consistency and causality while enabling robust relativistic stellar structure modeling [79,81,91].
For analytic studies and anisotropic configurations, a simplified MIT-bag-like EOS [89–91] and parametrized by the thermodynamic potential, can be employed as follows:

$$\Omega(\mu) = \sum_{u,d,s,e} \Omega_0 + \frac{3(1-a_4)}{4\pi^2}\mu^4 + B_{\mathrm{eff}} + \frac{3m_s^4 - 48\delta^2\mu^2}{16\pi^2}, \tag{21.1}$$

$$\epsilon(\mu) = -P_r(\mu) + \mu\, n_{\mathrm{tot}}(\mu), \tag{21.2}$$

where μ is the quark chemical potential, m_s the strange quark mass, a_4 a perturbative QCD correction parameter, δ a pairing parameter, and B_{eff} the effective bag constant. Here, P_r and ϵ denote the radial pressure and energy density, respectively.
In connection to Stellar Structure and Tidal Deformability, let us now discuss about the equilibrium configuration which is governed by the Tolman-Oppenheimer-Volkoff (TOV)

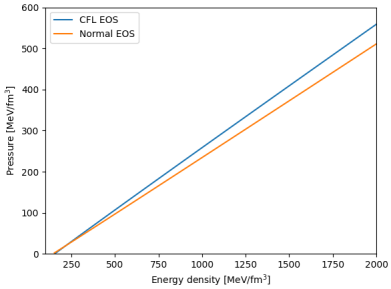

Fig. 21.2: Variation of the pressure vs. density (the EOS) for CFL (non CFL) quark strange stars

equations as

$$\frac{dP_r}{dr} = -\frac{G(\epsilon + P_r/c^2)(m + 4\pi r^3 P_r/c^2)}{r(r - 2Gm/c^2)}, \tag{21.3}$$

$$\frac{dm}{dr} = 4\pi r^2 \frac{\epsilon}{c^2}, \tag{21.4}$$

with the boundary conditions $P_r(0) = P_c$, $m(0) = 0$, and $P_r(R) = 0$ defining the stellar radius R.
To confront the models with GW observations, the tidal deformability can be computed by using the formula [64–69]

$$\Lambda = \frac{2}{3} k_2 \left(\frac{c^2 R}{GM}\right)^5, \tag{21.5}$$

where M and R denote the gravitational mass and radius, and k_2 is the quadrupolar Love number. However, the latter depends on the compactness

$$C = \frac{GM}{Rc^2},$$

and on the solutions to the perturbation equations.
Introducing perturbation functions $H(r)$ and $\beta(r)$, the relevant system is

$$\frac{dH}{dr} = \beta, \tag{21.6}$$

$$\frac{d\beta}{dr} = 2\left(1 - \frac{2Gm}{rc^2}\right)^{-1}\left[-\frac{\beta}{r} - \frac{4\pi G}{c^4}\left(\epsilon + \frac{P_r}{c^2}\right)e^{\lambda}H - \frac{6e^{\lambda}}{r^2}H + \frac{4\pi G}{c^4}\left(5\epsilon + 9\frac{P_r}{c^2} + \frac{\epsilon + P_r/c^2}{dP_r/d\epsilon}\right)H - \left(\frac{d\lambda}{dr}\right)\beta\right], \tag{21.7}$$

where $\lambda(r)$ is defined through the metric function in the standard TOV spacetime.
Current constraints on binary tidal deformabilities and NS masses from GW170817, GW190425, and subsequent detections do not exclude self-bound SQSs as viable alternatives to ordinary hadronic NSs, particularly for equations of state capable of supporting high maximum masses and moderate tidal responses [92–97]. As GW sensitivity improves and more events are catalogued, precision constraints on the tidal signatures, radii, and maximum masses of compact objects will play a decisive role in probing the existence of absolutely stable quark

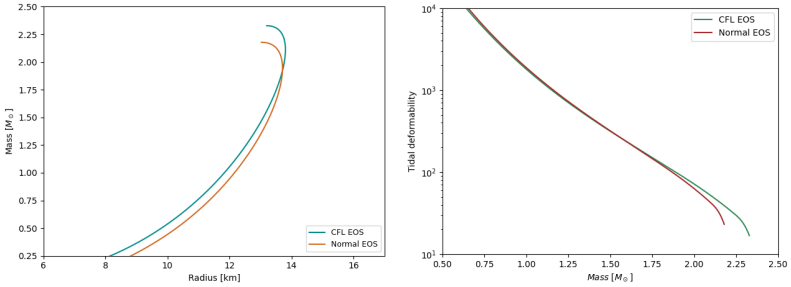

Fig. 21.3: The variation of the mass–radius relation (left), the tidal deformability as a function of mass for CFL (non CFL) SQSs

matter. Future multimessenger observations, especially those combining next-generation GW detectors with X-ray radius measurements, may thus offer the first definitive test of the strange-matter hypothesis [98–100].

21.2.2 Dark Matter

Dark Matter distribution in the Milky Way galaxy Determining mass distribution of the Milky Way's DM halo is currently one of the most important tasks in galactic astronomy. Two approaches based on observational data were used to study the shape of the DM halo in our Galaxy. The first approach is based on kinematics and spatial distribution of stellar streams in the halo. The approach assumes that stellar streams are the remnants of the dwarf galaxies or star clusters disrupted by tidal forces, and motion of stars in space and the spatial distribution approximately corresponds to the orbit at the progenitor galaxy. Information on the orbit of stars in the stellar stream, combined with kinematic data of the stars included in the stream under assumption of quasi-stationarity of a stellar stream, allows determination the density distribution and the shape of the DM halo. A detailed review of this approach and the results obtained are given in the recent review [101]. As noticed by authors [101], there are several factors that can influence the formation and the structure of a stellar stream. Such factors include the equilibrium properties of the progenitor system determining ejection velocity of the stars from a progenitor galaxy, the phase-space distribution of the stream stars, the gravitational field of the Milky Way determining the orbit of the progenitor system and the overall shape of the stream, influence of the non-stationary processes such as time- dependence bar and spiral arms potentials, and possible presence of the DM substructures in the DM halo, which can create density variations in the stream. The Milky Way bar is the main driver of the dynamics of stellar streams in the inner regions of the Milky Way galaxy. With a bar mass of 10^{10} solar masses and a semi-major axis of 3 kpc, the influence of resonances with the galactic bar has a significant and observable effect on the kinematics of stars. Stellar streams passing through the plane of the disk with peri-centers about a few kpc can be significantly influenced by the bar. The time-varying dipole asymmetry of the bar enhances the chaotic diffusion of orbits in the central regions of the Galaxy and causes a truncation of its length [102], as well as leads to a spread of the stellar flux over a large region [103].
The second method to study DM halo of the Milky Way is based on the kinematics of halo objects, such as globular clusters or field stars. This approach assumes that the selected objects are in dynamical equilibrium with the Milky Way potential, so the problem is to determine the galactic potential such that the observed positions and velocities of the halo

object sample are consistent with the equilibrium assumption. A few previous studies have attempted to determine the Milky Way potential this way using axisymmetric form of the Jeans equations to calculate the density distribution in the Galactic halo [104–108]. The authors of [104] selected a sample of halo stars from the SDSS catalog and found that the halo has the shape of an oblate spheroid with a semi-axis ratio of 0.7 ± 0.1. The authors of [105] determined that the inner DM halo within 5–10 kpc from the galactic center and found on the contrary that halo has the shape of an elongated spheroid with a semi-axis ratio of 1.5–2.0. The authors of [107], based their study on a sample of RR Lyrae stars from the GAIA DR2 catalog, and found that the shape of the hidden halo is close to spherical with a semi-axis ratio of 1.01 ± 0.06.

Several attempts have been made to model the positions and velocities of halo objects using the phase-space distribution function [109–112]. The authors of [109] determined the three-dimensional distribution of the DM density in the Galactic halo by simultaneously modeling the distribution function of halo stars and the Galactic potential. An important improvement in the implementation of the method in [109] is that the authors explicitly considered the errors in distances, which were ignored in previous studies. Modeling the distribution function of halo objects authors [109] used McMillan model [113], from which most of the parameters for the distribution of the baryonic component in the bulge, stellar and gaseous disks were taken, and assumed unlike the McMillan's model [113], that the DM halo in the Milky Way can be flattened. Based on a sample of 16197 RR Lyrae stars distributed in the halo of the Milky Way at distances from 5 to 27.5 kpc from the galactic center, authors [109] showed that the distribution of DM in the halo of Milky Way galaxy is close to spherical with a semi-axial ratio $\rightarrow 0.963$. The ambiguity of the conclusions about the shape of the hidden mass halo, as well as of new and refined data on the distribution of baryonic matter in the thick disk of the Galaxy, with its mass comparable to the mass of the thin disk, as well as the new data on the local density of baryonic matter in the solar neighborhood, make possible to more accurately determine both the shape of the Milky Way DM halo and for a number of models the concentration of the DM particles in the solar neighborhood.

There is progress in the development of new methods in studying the distribution of DM in the Milky Way halo. The long-standing enigma of the Galactic disk's large-scale warp and flare has been addressed through a novel mechanism: a misaligned DM halo. Authors [114], analyzing TNG50 cosmological magneto-hydrodynamic simulations, found that the DM halo tilted to the stellar one can quantitatively reproduce the observed amplitude and orientation of the warp structure in the Milky Way disk. The model successfully explains warp across a broad range of observational tracers, including stars of all ages and the gaseous components. Comparative analysis confirms that the warp and flare induced by the tilted halo model better explain observational data compared to the alternative explanations such as the tidal influence of the Large Magellanic Cloud. The persistence of such halo-disk misalignment is supported by cosmological simulations, which indicate that tilted dark halos are common and long-lived. A plausible origin for this configuration is a major merger event in the Galaxy's early history. Consequently, the tilted DM halo model establishes a new paradigm for probing galactic DM. The observed warp and flare in the Milky Way disk are put as constraints on shape and density distribution in the DM halo.

The existence of a tilted Milky Way halo is supported also by a growing body of independent studies. Authors [115] use Schwarzschild orbit-superposition model to study the Gaia-Sausage/Enceladus stellar orbits and constrained the parameters of the Milky Way's DM halo. The key result of authors is that the observed distribution of stars in the Gaia-Sausage/Enceladus stream can be supported in equilibrium if the DM halo is non-spherical and tilted relative to the galactic disk. Authors of [115] find that the best-fitting model is a

prolate halo with its long axis inclined at 43 degrees to the disk plane. This result provides evidence that the Galaxy's DM halo is substantially tilted, being, probably, an imprint of Milky Way accretion history. Authors of [116] came to a similar conclusion using data from H3 Survey to map the 3D structure of the Milky Way's stellar halo, dominated by the Gaia-Sausage/Enceladus (GSE) merger. They showed that the GSE stellar component forms a tilted, triaxial ellipsoid with density described by a double-broken power law with break radii at approximately 12 and 28 kpc, interpreted this result as successive apo-centers of a merging galaxy. The best-fit model of [116] is a near-prolate spheroid (axis ratios 10:8:7) with its major axis tilted 25° above the Galactic plane providing evidence that the underlying Milky Way DM halo must be tilted and non-spherical.

Dark atom model During the last three decades, the mainstream in studies of cosmological dark matter has been concentrated on theoretical analysis and experimental searches for Weakly Interacting Massive Particles (WIMPs). This trend was strongly motivated by the WIMP miracle (natural explanation of the observed dark matter density by frozen out primordial particles with weak annihilation cross section and masses in the range of tens-hundreds GeV) and possible description of WIMPs as Lightest Supersymmetric Particles (LSP). It stimulated a direct search for WIMPs in underground detectors by recoiling nuclei from their scattering in detectors. This search was strongly aligned with the expectation of discovery of supersymmetric partners of ordinary particles at the Large Hadron Collider (LHC). The latter was related with the possibility of supersymmetric solution for the problem of Higgs boson mass divergence and for the origin of the electroweak symmetry breaking and implied the existence of SUSY particles in the energy range, accessible for the LHC.

The results of underground dark matter searches look controversial. Although the positive result of more than three decades of DAMA/NaI and DAMA/LIBRA experiments is claimed to have a very high level of significance (at 13.5 standard deviations), negative results of other groups in their WIMPs searches make it hardly possible to interpret these positive results in terms of WIMPs.

The dark atom model proposed a non-WIMP interpretation of the positive results of DAMA experiments (see [1] for review and references). Its only element of new physics is the existence of $-2n$ charged stable particles. If such particles possess electroweak charges, sphaleron transitions maintain balance between the excess of baryons over antibaryons and the excess of charged $-2n$ particles over their antiparticles. This possibility may be related to the composite nature of Higgs boson, which provides non-SUSY solution for the problems of the Standard model. If Higgs boson constituents are charged, their bound states can be multi-charged stable particles. Since such constituents possess electroweak charges, they participate in electroweak sphaleron transitions, which maintain balance of baryon asymmetry with excess of charged $-2n$ particles over their antiparticles. Such an excess leads to formation of dark atoms, in which excessive $-2n$ particles are bound with n helium nuclei, formed in Big Bang Nucleosynthesis. At $n > 1$ dark atoms are Thomson-like. They are α-particle nuclei, in which $+2n$ electric charge is compensated by $-2n$ charged lepton inside them.

Due to strong (nuclear) interaction of dark atoms with baryons with $\sigma_o = \pi {r_o}^2 \sim 10^{-252}, where r_o \sim 2 \cdot 10^{-132}$ is the geometric size of dark atoms, their gas is in thermal equilibrium with baryonic plasma and experiences radiation pressure, which converts density fluctuations in sound waves. It leads to suppression of shortwave density fluctuations, but at $t > 10^6$, corresponding to $T < 1$, when $n_b \frac{\Delta E}{E} \sigma v t < 1 baryonic number density n_b$ decreases and dark atoms decouple from plasma and radiation, playing the role of warmer than cold dark matter in successive large scale structure formation.

In spite of their strong (nuclear) interaction dark atoms behave like collisionless gas at the scale of galaxy and the averaged baryonic matter of galaxy is transparent for it, while the nonhomogeneities of baryonic matter with number density n_b and size R, satisfying the condition $n_b \sigma_o R > 1$ are opaque for dark atoms. At $n_b(m_p/m_o)\sigma_o R > 1$ dark atoms can be captured by a matter object.
Terrestrial matter is opaque for dark atoms and their concentration in it is determined by the balance of the incoming cosmic flux and diffusion of the slowed down dark atoms to the center of Earth. Since the incoming flux possess annual modulation and the local concentration of dark atoms is adjusted to the incoming flux at the timescale less than hour, dark atom concentration in underground detectors experiences annual modulation, while low energy binding of dark atoms with nuclei explains positive result of DAMA experiments. We address various aspects of dark atom hypothesis and stipulate its open problems, which are

- Formation of neutral dark atoms in the period of Big Bang Nucleosynthesis can be accompanied by capture of additional helium nuclei and/or protons and anomalous isotope production
- Multiple helium capture by dark atoms should take into account Bose-Einstein statistics of α-particles
- Annual modulation of low energy binding of dark atoms with nuclei should be accompanied by high energy release in MeV-tens MeV range due to their full merging.

21.2.3 Quantum gravity

Approaches to quantum gravity and unresolved issues Constructing a quantum theory of gravity is a fundamental problem in modern theoretical physics. Following the creation of general relativity and quantum mechanics in the first third of the 20th century, the question arose how to unify Einstein's theory of gravity and quantum principles. The question became even more pressing after S. W. Hawking and R. Penrose having proved their singularity theorems, when it became clear that classical general relativity was insufficient to explain processes in the Early Universe, and quantum concepts were needed. Theorists such as M. P. Bronstein, P. Bergman, P. A. M. Dirac, J. A. Wheeler, B. DeWitt, S. W. Hawking and many others have worked on constructing a quantum theory of gravity. Currently, numerous approaches exist, ranging from the first attempt to construct a quantum theory of gravity the Wheeler-DeWitt quantum geometrodynamics, to LQG.
Most approaches to constructing a quantum theory of gravity are based on Dirac's approach to quantizing gauge fields [117] and the Wheeler-DeWitt equation [118], which is a direct consequence of applying Dirac's approach to gravity. However, in our opinion, the Dirac-Wheeler-DeWitt approach does not take into account features of gravity. Wheeler, Hawking, and other physicists have argued that all possible spacetime topologies should be considered in QG. This means that a gravitating system may not possess asymptotic states that are typically assumed in the quantum theory of non-gravitational fields and ensure gauge invariance of the theory, when using path integrals with asymptotic boundary conditions. If asymptotic states are absent, the proofs of gauge invariance, applicable to non-gravitational field theories, are not valid, and the Wheeler-DeWitt equation loses its meaning. However, the alternative approach, so-called extended phase space approach [119–121], has been proposed. In this approach, Hamiltonian dynamics in extended phase space, as an alternative to Dirac's generalized Hamiltonian dynamics, is constructed, and the theory is quantized using the path integral method. From the path integral, a Schrödinger equation for the wave function of the Universe can be obtained by generalizing the standard Feynman procedure.

In the framework of the extended phase space formalism, we consider the ideas underlying other approaches – supersymmetry and supergravity, as well as LQG. The concept of supersymmetry originates from the works of Golfand and Likhtman [122], Akulov and Volkov [123], Arnowitt, Nath and Zumino [124], and others. Despite the fact that the theory of supersymmetry has not been confirmed experimentally, and it has not been proven that it is possible to construct a theory of supergravity without divergences, several hundred papers devoted supersymmetry and supergravity are published annually. Supersymmetric cosmological models have never been studied in the framework of the extended phase space approach. It is expected that study of supersymmetric cosmological models may shed light on the questions: What is the role of gauge degrees of freedom, previously considered as redundant, in QG? What is the geometric structure of superspace, whose coordinates include anticommuting (or Grassmannian) coordinates corresponding to fermion and ghost fields?

LQG began with Ashtekar's idea to reformulate general relativity as a theory similar to the Yang-Mills theories and introducing special variables [125]. Those who work within this approach touch upon various aspects of cosmology, BH physics, and other fields [126, 127]. As in the case of supersymmetry, we would like to answer the questions: Is Ashtekar's formulation equivalent to the standard formulation of general relativity? Is the extended phase space approach applicable to Ashtekar's formulation?

In the absence of experimental (observational) data for a quantum theory of gravity, the search for small quantum-gravitational effects in the Early Universe is particularly important. It is supposed that the effects are described by quantum-gravitational corrections and their consequences could be detected in the anisotropy of the cosmic microwave background radiation (CMB). If such effects are discovered, comparing theoretical predictions with observational data would help identify a correct approach to constructing QG. Therefore, our another goal is finding the spectrum of cosmological perturbations and comparing it with the spectrum of CMB. A great contribution to the theory of cosmological perturbations at the classical and quantum levels was made by Mukhanov [128]. Currently, several groups are working in this field. Let us mention, for example, the group of Kiefer that makes use of the Born-Oppenheimer approximation for gravity, when the gravitational field is considered to be a classical slowly changing field, while quantized matter fields being rapidly changing. It results in the Schrödinger equation for matter fields on the background of gravitational field with quantum-gravitational corrections [129, 130].

The features of the extended phase space approach The central place in the extended phase space formalism is given to the Schrödinger equation for the wave function of the Universe. We use the path integral approach, since it contains a special procedure of derivation of the Schrödinger equation proposed by Feynman [131]. Feynman applied this procedure to a simple case of a particle in an external field. The procedure was later generalized in [132] for Lagrangians quadratic in velocities. However, to apply the method to cosmological models, which are systems with constraints, the method required further generalization, which was made in the papers [119, 120]. In accordance with the general principles of quantization of gauge theories, we use a path integral with an effective action in Lagrangian form, including gauge-fixing and ghost terms.

As was said above, gravitating systems may not possess asymptotic states, the existence of which is assumed in particle physics. For example, a closed isotropic universe has no asymptotic states. If a system possesses asymptotic states, asymptotic boundary conditions are imposed on the path integral, ensuring the gauge invariance of the theory. In the case of gravity, imposing these conditions seems unjustified, and in our approach, we refuse them [121]. As a consequence, the resulting Schrödinger equation is gauge-noninvariant

(dependent on the choice of reference frame). Its solution is interpreted as describing the geometry of the Universe and the distribution of matter fields from the viewpoint of the observer in a certain reference frame.
For example, for a simple model of a closed isotropic universe the following Schrödinger equation was obtained:

$$\left[-\frac{1}{2}\sqrt{\frac{N}{a}}\frac{d}{da}\left(\sqrt{\frac{N}{a}}\frac{d\Psi}{da}\right)+\frac{1}{2}Na\Psi-Na^3\varepsilon(a)\Psi\right]\Bigg|_{N=f(a)}=E\Psi, \tag{21.8}$$

where a is a scale factor, N is the lapse function fixed by the gauge condition $N=f(a)$, and matter fields are described phenomenologically, by the function $\varepsilon(a)=\frac{\varepsilon_0}{a^n}$, ε_0 is a constant whose dimensionality in the Plank units is $\rho_{Pl}l_{Pl}^n$ [133]. Depending on a choice of the gauge condition, one obtains equations with different potentials presented at Fig. 19.4.

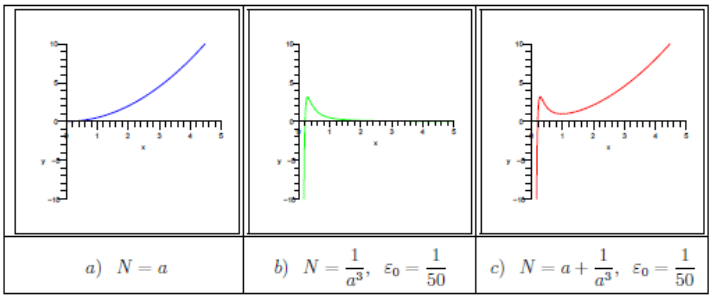

Fig. 21.4: Potentials in the Schrödinger equation for different gauge conditions

The equations with different gauge conditions and potentials were solved numerically to find the spectra of E in the right-hand side of Eq. (19.8) and corresponding probability distributions. Some results are presented at Figs. 19.5 and 19.6.

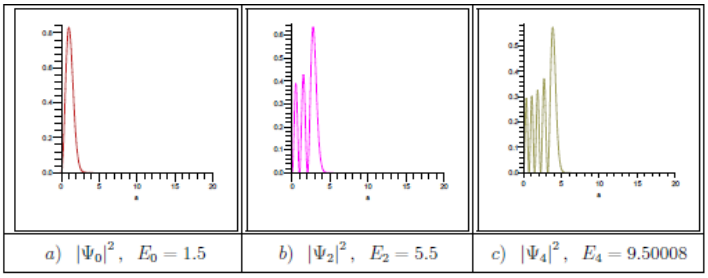

Fig. 21.5: The probability distributions for solutions to Eq. (19.8), $N=a$

In the course of the previous research, the algorithm has been developed that enables one to obtain the Schrödinger equation for any cosmological model. Different models may be chosen for different problems, and it gives a perspective to explore a wide range of issues.

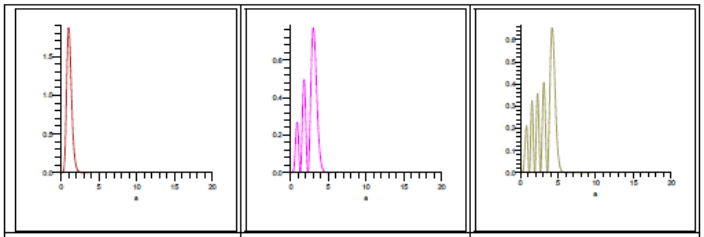

Fig. 21.6: The probability distributions for solutions to Eq. (19.8), $N = a + \frac{1}{a^3}$, $\varepsilon_0 = 7$

21.3 Conclusion

Some of the salient features of the presented review work can be provided as follows:

• **Gravitational waves**:
(i) Recent Bayesian analyses that incorporate the tidal deformability constraints from GW170817, GW190425, and GW230529 have begun to narrow the viable parameter space of strange quark matter EOSs, particularly within phenomenological `Bag Model-like` frameworks. Current studies indicate that for CFL (non CFL) quark matter models favored by observational data tend to be relatively stiff, with effective bag constants of order $B_{\rm eff}^{1/4} \sim 145\ (137)$ MeV, perturbative QCD correction parameters a_4 around $0.70\ (66)$ and CFL pairing parameter $\Delta \sim 67.88$ [134]. The CFL pairing parameter remains only weakly constrained, reflecting the limited sensitivity of global stellar properties such as the masses, radii, and tidal deformabilities to the microscopic details of color superconductivity. Nonetheless, future high-precision measurements of the tidal signatures of massive compact objects could provide a decisive probe of the color superconducting gap.
(ii) Assuming that the binary components in observed mergers can be modelled as SQSs, EOSs with CFL pairing are found to naturally support large maximum gravitational masses. Within the `Bag Model-like EOS` framework, one can explicitly evaluate the macroscopic stellar properties. For CFL (non CFL) SQSs, a nonrotating maximum mass $M_{\rm TOV} \simeq 2.33\ (2.18)\, M_\odot$, with a corresponding radius $R \simeq 13.20\ (13.02)$ km, and tidal deformability $\Lambda \simeq 16.01\ (21.84)$. These values, corresponding to maximum masses around $2.4\ M_\odot$ [135,136], are consistent with earlier theoretical estimates for self-bound SQSs based on similar EOS assumptions. The behavior of the EOS parameters, as well as the resulting mass-radius and mass-tidal deformability relations, is illustrated in Figs. 19.2 and 19.3.
(iii) An intriguing implication of these results is that some of the unusually heavy secondary components identified in systems such as GW190814 and GW230529 may be interpreted as SQS candidates. In particular, compact objects residing in the putative mass gap between standard NSs and BHs can be naturally accommodated within the CFL quark-matter scenario for sufficiently large effective bag constants and pairing gaps. Improved precision in future GW observations, especially for high mass binaries, will therefore be crucial for distinguishing gravity-bound hadronic NSs from self-bound SQSs, and may ultimately provide the first robust astrophysical evidence of deconfined quark matter in nature.

• **Dark matter**:

(i) Galaxies and their clusters are the objects that manifest a presence of the DM in the Universe. Study of the DM halos of the galaxies is therefore one of the important tasks in the galactic astronomy. In particular, determination of the shape and of the density distribution in the DM halo of the Milky Way galaxy allows to estimate quantitatively the density and concentration of DM particles in the solar neighborhood. Important steps have been done recently in this direction thanks to the flow of data provided by GAIA mission. GAIA data allowed to measure in detail the density distribution in the Milky Way thin and thick disks as well as the shape and the density distribution in the Milky Way's central bar/bulge. This, in combination with the new data on radial and vertical scales of the Milky Way disks, and new data on the density of the stellar disks in the solar neighborhood allowed to measure the DM density in the solar neighborhood. Estimates of the flux of the DM particle on the Earth's surface are crucial for the ongoing and planned DM particle detection experiments. A detection of yearly and diurnal modulations of flux of the DM particles caused by the motion of the Earth could test predictions of the Standard Model extensions and characterize the nature of the DM particles.
(ii) The search for evidence of DM in experimental studies of ionospheric processes is relevant because in recent years, there has been an increase in the number of articles linking anomalous effects in the ionosphere to the possible influence of DM, with these effects being quite diverse. Analysis of anomalies in the ionosphere and near-Earth space is of significant practical interest in the field of space object detection using telescopes. Because the ionosphere scatters low-frequency signals, telescope images can be blurred and their resolution reduced. Therefore, identifying and eliminating such anomalies helps improve the efficiency of various technological systems in space and on the ground.
(iii) The relevance of developing a quantum-mechanical numerical model of the interaction of a X-helium dark atom (a DM atom, which is a coupled quantum-mechanical system consisting of an X particle and n primordial helium nuclei) with the nucleus of ordinary matter is caused by the problem of DM, which, according to measurements by the Planck and WMAP experiments, accounts for the majority of the energy density of non-relativistic matter in the Universe, and its contribution to the total matter density in the modern Universe is about 26%, while it is unknown which particles constitute DM particles. Theory predicts that DM consists of new massive particles that go beyond the Standard Model of physics. Therefore, the use of a quantum-mechanical numerical model of the interaction of a X-helium dark atom with the nucleus of ordinary matter to explain the paradoxes of direct searches for DM particles and to justify physical experiments testing the dark atom hypothesis is a highly important, fundamental, and pressing task in modern physics.

• **Quantum gravity**:
(i) An investigation of supersymmetric models on the background of gravity gives the opportunity to clarify the role of fermionic and ghost degrees of freedom, their influence on geometric structure of configurational space and regularization of vacuum energy.
(ii) The study of alternative formulations of general relativity, particularly in Ashtekar's variables used in loop QG, from the perspective of the proposed approach, aims to answer the following questions: Is Ashtekar's formulation equivalent to the standard formulation of general relativity? Is the extended phase space formalism applicable to Ashtekar's formulation?
(iii) To obtain quantum-gravitational corrections, many authors use expansion in powers of some parameter in accordance with the Born-Oppenheimer approximation. The question about the choice of expansion parameter has not been sufficiently addressed in previous works on this topic. It is important to answer, what physically corresponds to the limiting value of the parameter? As a result of the expansion, one would obtain the Schrödinger

equation for matter fields against the background of a classical gravitational field with quantum-gravitational corrections.

Acknowledgments

We all are thankful to the authority of the Bled Workshop-2025 for providing us a platform to disseminate our ideas, which were partly there in the Presentations as well as Discussions sessions altogether and thus eventually got a definite shape in the form of this Review article. The work of T.E.B., D.O.S. and M.K.A. was performed in Southern Federal University with financial support of grant of Russian Science Foundation № 25-07-IF. The research of V.I.K., R.V.K., A.K. and O.A.M. was carried out in the Southern Federal University with financial support from the Ministry of Science and Higher Education of the Russian Federation (State contract GZ0110/23-10-IF).

References

1. M. Khlopov: What comes after the Standard Model? Prog. Part. Nucl. Phys. **116** (2020), 103824.
2. B. P. Abbott et al.: Observation of Gravitational Waves from a Binary Black Hole Merger, Phys. Rev. Lett. **116** (2016) 061102.
3. https://gwosc.org/eventapi/html/GWTC/
4. K. S. Thorne: Gravitational waves, arXiv preprint gr-qc/9506086 (1995).
5. S. Perkins, N. Yune, E. Berti: Probing fundamental physics with gravitational waves: The next generation, Phys. Rev. **103** (2021) 044024.
6. A. Maselli, S. Marassi, M. Branchesi: Binary white dwarfs and decihertz gravitational wave observations: From the Hubble constant to supernova astrophysics, Astron. Astrophys **635** (2020) A120.
7. R. Ciolfi, L. Rezzolla: Twisted-torus configurations with large toroidal magnetic fields in relativistic stars, Mon. Not. R. Astron. Soc. Lett. **435** (2013) L43–L47.
8. S. R. Chowdhury, M. Khlopov: The Stochastic Gravitational Wave Background from Magnetars, Universe **7** (2021) 10.
9. S. R. Chowdhury, M. Khlopov: Stochastic gravitational wave background due to core collapse resulting in neutron stars, Phys. Rev. D **110** (2024) 063037.
10. E. Abdikamalov, G. Pagliaroli, D. Radice: *Gravitational Waves from Core-Collapse Supernovae, in Handbook of Gravitational Wave Astronomy*, Springer (2021) 1–37.
11. M. Sasaki, T. Suyama, T. Tanaka, S. Yokoyama: Primordial Black Hole Scenario for the Gravitational-Wave Event GW150914, Phys. Rev. Lett. **117** (2016) 061101.
12. S. Mukherjee, J. Silk: Can we distinguish astrophysical from primordial black holes via the stochastic gravitational wave background?, Mon. Not. Roy. Astron. Soc. **506** (2021) 3977.
13. S. R. Chowdhury, A. Basak, M. Khlopov, M. Krasnov: Inferring the Merger History of Primordial Black Holes from Gravitational-Wave data and the Stochastic Signatures, arXiv:2507.21332 (2025).
14. D. J. Reardon et al. (PPTA Collaboration): Search for an Isotropic Gravitational-wave Background with the Parkes Pulsar Timing Array, Astrophys. J. Lett. **951** (2023) L6.
15. G. Agazie et al. (NANOGrav Collaboration): The NANOGrav 15 yr Data Set: Evidence for a Gravitational-wave Background, Astrophys. J. Lett. **951** (2023) L8.
16. J. Antoniadis et al. (EPTA & InPTA Collaborations): The second data release from the European Pulsar Timing Array – III. Search for gravitational wave signals, Astron. Astrophys **678** (2023) A50.

17. H. Xu et al. (CPTA Collaboration): Searching for the Nano-Hertz Stochastic Gravitational Wave Background with the Chinese Pulsar Timing Array Data Release I, Res. Astron. Astrophys. **23** (2023) 075024.
18. M. Punturo, et al.: The Einstein Telescope: a third-generation gravitational wave observatory, Class. Quant. Grav. **27** (2010) 194002.
19. B. P. Abbott, et al.: Exploring the sensitivity of next generation gravitational wave detectors. Class. Quant. Grav. **34** (2017) 18.
20. C. Caprini et al.: Reconstructing the spectral shape of a stochastic gravitational wave background with LISA, JCAP **11** (2019) 017.
21. P. Ajith et al.: The Lunar Gravitational-wave Antenna: Mission Studies and Science Case, JCAP **01** (2025) 108.
22. M. Bailes, et al.: Gravitational-wave physics and astronomy in the 2020s and 2030s, Nat. Rev. Phys. **3** (2021) 344–366.
23. P. Schwaller: Gravitational Waves from a Dark Phase Transition, Phys. Rev. Lett. **115** (2015) 181101.
24. G. Bertone et al.: Gravitational wave probes of dark matter: challenges and opportunities, SciPost Phys. Core **3** (2020) 007.
25. C. Gowling, M. Hindmarsh, D. Hooper, J. Torrado: Reconstructing physical parameters from template gravitational wave spectra at LISA: first order phase transitions, JCAP **04** (2023) 061.
26. S. W. Hawking, G. F. R. Ellis: *The Large Scale Structure of Space-Time*, Cambridge University Press (1973).
27. S. Weinberg: Ultraviolet divergences in quantum theories of gravitation, (1980).
28. C. Kiefer: Quantum gravity - an unfinished revolution, arXiv:2302.13047 (2023).
29. S. M. Carroll: The cosmological constant. Living reviews in relativity **4** (2001): 1-56.
30. A. Addazi, et al.: Quantum gravity phenomenology at the dawn of the multimessenger era-a review. Prog. Part. Nuc. Phys. **125** (2022) 103948.
31. J. P. Uzan: Fundamental constants: from measurement to the universe, a window on gravitation and cosmology, Living Rev. Rel. **28** (2025) 1–330.
32. T. Callister, L. Jenks, D. E. Holz, N. Yunes: New probe of gravitational parity violation through nonobservation of the stochastic gravitational wave background, Phys. Rev. D **111** (2025) 044041.
33. G. Calcagni: *Quantum Gravity and Gravitational Wave Astronomy, in Handbook of Gravitational Wave Astronomy*, Springer (2021).
34. J. Polchinski: *String theory, volume 1: An introduction to the bosonic string (Vol. 1)*. Cambridge: Cambridge university press (2005).
35. A. Ashtekar, J. Lewandowski: Background independent quantum gravity: a status report, Class. Quantum Grav. **21** (2004) R53.
36. M. Arzano, A. J. M. Medved, E. C. Vagenas: Hawking radiation as tunnelling through the quantum horizon, JHEP **09** (2005) 037.
37. G. Amelino-Camelia: Quantum-spacetime phenomenology, Living Rev. Rel. **16** (2013) 5.
38. S. R. Chowdhury, D. Deb, F. Rahaman, S. Ray, B. K. Guha: Noncommutative black hole in the Finslerian spacetime, Class. Quantum Grav. **38** (2021) 145019.
39. M. D. C. Torri et al.,: Testing Quantum Gravity with Gravitational Waves from the ringdown of binary Black Holes coalescences: A New Frontier in Fundamental Physics, arXiv:2511.02056 (2025).
40. N. Yunes, L. S. Finn: Constraining effective quantum gravity with LISA, J. Phys. Conf. Ser. **154** (2009) 012041.
41. V. Cardoso, P. Pani: Testing the nature of dark compact objects: a status report, Living Rev. Rel. **22** (2019) 4.

42. G. Calcagni et al.,: Quantum gravity and gravitational-wave astronomy, JCAP **10** (2019) 012.
43. M. Evans et al.,: A Horizon Study for Cosmic Explorer: Science, Observatories, and Community, arXiv:2109.09882 (2021).
44. G. Bertone: Dark matter, black holes, and gravitational waves, Nucl. Phys. B **1003** (2024) 116487.
45. M. Baryakhtar et al.: Dark Matter in Extreme Astrophysical Environments, arXiv:2203.07984 (2022).
46. S. Bhattacharya, B. Dasgupta, R. Laha, A. Ray: Can LIGO Detect Nonannihilating Dark Matter?, Phys. Rev. Lett. **131** (2023) 091401.
47. D. Carney, S. Ghosh, G. Krnjaic, J. M. Taylor: Proposal for gravitational direct detection of dark matter, Phys. Rev. D **102** (2020) 072003.
48. S. Robles: Improved treatment of dark matter capture in compact stars, SciPost Phys. Proc. **12** (2023) 057.
49. D. Tahelyani, A. Bhattacharyya, A. S. Sengupta: Probing dark matter halo profiles with multiband observations of gravitational waves, Phys. Rev. D **111** (2025) 083041.
50. X. Guo, Y. Lu: Probing the nature of dark matter via gravitational waves lensed by small dark matter halos, Phys. Rev. D **106** (2022) 023018.
51. A. M. Green, B. J. Kavanagh: Primordial black holes as a dark matter candidate, J. Phys. G **48** (2021) 043001.
52. B. Carr, F. Kühnel: Primordial black holes as dark matter candidates, SciPost Phys. Lect. Notes **48** (2022).
53. A. M. Green: Primordial black holes as a dark matter candidate — a brief overview, Nucl. Phys. B **1003** (2024) 116494.
54. W.-X. Feng, S. Bird, H.-B. Yu: Gravitational Waves from Primordial Black Hole Dark Matter Spikes, Astrophys. J. **986** (2025) 151.
55. E. Bagui, S. Clesse, V. De Luca et al.: Primordial black holes and their gravitational-wave signatures, Living Rev. Rel. **28** (2025) 1.
56. A. Romero-Rodríguez, S. Kuroyanagi: LVK constraints on PBHs from stochastic gravitational wave background searches, arXiv:2407.00205 (2024).
57. W. Cui, F. Huang, J. Shu, Y. Zhao: Stochastic gravitational wave background from PBH–ABH mergers, Chin. Phys. C **46** (2022) 055103.
58. B. P. Abbott et al. (LIGO/Virgo): GW170817: Observation of Gravitational Waves from a Binary Neutron Star Inspiral, Phys. Rev. Lett. **119** (2017) 161101.
59. B. P. Abbott et al.: GW190425: Observation of a Compact Binary Coalescence with Total Mass $\sim 3.4\ M_\odot$, Astrophys. J. Lett. **892** (2020) L3.
60. B. P. Abbott et al.: Observation of Gravitational Waves from the Coalescence of a 2.5-4.5 $M_\odot$ Compact Object and a Neutron Star, Astrophys. J. Lett. **970** (2024) L34.
61. A. Bauswein, H.-T. Janka: Measuring Neutron Star Properties via Gravitational Waves from Neutron Star Mergers, Phys. Rev. Lett. **108** (2012) 011101.
62. M. Shibata, K. Hotokezaka: Merger and Mass Ejection of Neutron Star Binaries, Annu. Rev. Nucl. Part. Sci. **69** (2019) 41.
63. L. Baiotti: Gravitational waves from neutron star mergers and their relation to the nuclear equation of state, Prog. Part. Nucl. Phys. **109** (2019) 103714.
64. T. Hinderer: Tidal Love Numbers of Neutron Stars, Phys. Rev. D **677** (2008) 1216.
65. T. Hinderer, B. Lackey, R. Lang, J. Read: Tidal deformability of neutron stars with realistic equations of state and their gravitational wave signatures in binary inspiral, Phys. Rev. D **81** (2010) 123016.
66. K. Chatziioannou: Neutron Star tidal deformability and equation-of-state constraints, Gen. Relativ. Gravit. **52** (2020) 109.

67. S. Das, S. Ray, M. Khlopov, K.K. Nandi and B.K. Parida, Anisotropic compact stars: Constraining model parameters to account for physical features of tidal Love numbers, Ann. Phys. **433** (2021) 168597.
68. S. Das, B.K. Parida, S. Ray and S.K. Paul, Role of anisotropy on the tidal deformability of compact stellar objects, Phys. Sci. Forum **1** (2021) 1.
69. S. Ray, S. Das, K.K. Ghosh, B.K. Parida, S.K. Pal and M. Indra, Study of anisotropic compact stars by exploring tidal deformability, New Astron. **104** (2023) 102069.
70. S. Ray, R. Bhattacharya, S. K. Sahay, A. Aziz, A. Das, Gravitational wave: generation and detection techniques, Int. J. Mod. Phys. D **33** (2024) 2340006.
71. A. Bauswein, O. Just, H. Janka, N. Stergioulas: Neutron Star Radius Constraints from GW170817 and Future Detections, Astrophys. J. Lett. **850** (2017) L34.
72. K. Takami, L. Rezzolla, L. Baiotti: Spectral properties of the post-merger gravitational-wave signal from binary neutron stars, Phys. Rev. D **91** (2015) 064001.
73. M. Alford, S. Han, M. Prakash: Generic conditions for stable hybrid stars, Phys. Rev. D **88** (2013) 083013.
74. I. Bombaci, A. Drago, D. Logoteta, G. Pagliara, I. Vidaña: Was GW190814 a Black Hole–Strange Quark Star System? Phys. Rev. Lett. **126** (2021) 162702.
75. F. Özel, P. Freire: Masses, Radii, and the Equation of State of Neutron Stars, Annu. Rev. Astron. Astrophys. **54** (2016) 401.
76. I. Tews, J. Carlson, S. Gandolfi, S. Reddy: Constraining the Speed of Sound inside Neutron Stars with Chiral Effective Field Theory Interactions and Observations, Astrophys. J. **860** (2018) 149.
77. P.T.H. Pang et al.: An updated nuclear-physics and multi-messenger astrophysics framework for binary neutron star mergers, Nat. Commun. **14** (2023) 8352.
78. R. Somasundaram et al.: Inferring three-nucleon couplings from multimessenger neutron star observations, Nat. Commun. **16** (2025) 9819.
79. E. Farhi and R. Jaffe: Strange matter, Phys. Rev. D **30** (1984) 2379.
80. M. Alford, K. Rajagopal, S. Reddy, F. Wilczek: Minimal color-flavor-locked–nuclear interface, Phys. Rev. D **64** (2001) 074017.
81. A. Kurkela, E. S. Fraga, J. Schaffner-Bielich, A. Vuorinen: Constraining neutron star matter with QCD, Astrophys. J. **789** (2014) 127.
82. Z. Cao, L. Chen, P. Chu, Y. Zhou: GW190814: Circumstantial evidence for up-down quark star, Phys. Rev. D **106** (2022) 083007.
83. C. Xia, Z. Zhu, X. Zhou, A. Li: Sound velocity in dense stellar matter with strangeness and compact stars, Chin. Phys. C **45** (2021) 055104.
84. A. Li, Z. Miao, S. Han, B. Zhang: Constraints on the Maximum Mass of Neutron Stars with a Quark Core from GW170817 and NICER PSR J0030+0451 Data, Astrophys. J. **913** (2021) 27.
85. C. Zhang: Probing up-down quark matter via gravitational waves, Phys. Rev. D **101** (2020) 043003.
86. G. Baym et al.: From hadrons to quarks in neutron stars: a review, Rept. Prog. Phys. **81** (2018) 056902.
87. E. Annala et al.: Evidence for quark-matter cores in massive neutron stars, Nat. Phys. **16** (2020) 907.
88. A. R. Bodmer: Collapsed nuclei, Phys. Rev. D **4** (1971) 1601.
89. E Witten: Cosmic separation of phases, Phys. Rev. D **30** (1984) 272.
90. C. Alcock, E. Farhi, A. Olinto: Strange stars, Astrophys. J. **310** (1986) 261.
91. M. Alford, M. Braby, M. Paris, S. Y. Reddy: Hybrid Stars that Masquerade as Neutron Stars, Astrophys. J. **629** (2005) 969.
92. B. A. Li et al.: GW170817 constraints on the equation of state of quark stars, Phys. Rev. D **98** (2018) 083013.

93. J. E. Christian, J. Schaffner-Bielich: GW170817 and the maximum mass of quark stars, Phys. Rev. D **98** (2018) 063009.
94. A. Bauswein et al.: Identifying strange stars from compact binary mergers, Phys. Rev. Lett. **122** (2019) 061102.
95. D. Blaschke, M. Cierniak: Strange quark matter after GW170817, Astron. Nachr. **341** (2020) 845.
96. R. Nandi, P. Char: Strange star equation of state constraints from GW170817 and GW190425, Astrophys. J. **921** (2021) 149.
97. M. G. Alford, A. Sedrakian: Constraints on quark matter in neutron stars from GW170817, Phys. Rev. Lett. **127** (2021) 132701.
98. O. Lourenço et al.: Tidal deformability of strange stars and the GW170817 event, Phys. Rev. D **103** (2021) 103010.
99. B.-L. Li, Y. Yan, J.-L. Ping: Tidal deformabilities and radii of strange quark stars, Phys. Rev. D **104** (2021) 043002.
100. J. V. Zastrow, J. P. Pereira, R. C. R. de Lima, J. E. Horvath: Constraints on QCD-based equation of state of quark stars from neutron star maximum mass, radius, and tidal deformability observations, arXiv:2504.08926 (2025).
101. A. Bonaca, A. M. Price-Whelan: Stellar streams in the Gaia era. New Astron. Rev. **100** (2024) 101713.
102. K. Hattori, M. Valluri, E. Vasiliev: Action-based distribution function modeling for constraining the shape of the Galactic dark matter halo, Mon. Not. Roy. Astron. Soc. **508** (2021) 5468–5492.
103. S. Pearson, A. M. Price-Whelan, K. V. Johnston: Tops and length asymmetry in the stellar stream Palomar 5 as effects of Galactic bar rotation. Nat. Astro., **1** (2017) 633–639.
104. S. R. Loebman et al.,: The Milky Way tomography with Sloan digital sky survey. V. Mapping the dark matter halo, Astrophys. J. **794** (2014) 151.
105. A. Bowden, N. W. Evans, A. A. Williams: Is the dark halo of the Milky Way prolate? Mon. Not. Roy. Astron. Soc. **460** (2016) 329–337.
106. G. Eadie, M. Juric: The cumulative mass profile of the Milky Way as determined by globular cluster kinematics from Gaia DR2. Astrophys. J., **875** (2019) 159.
107. C. Wegg, O. Gerhard, M. Bieth: The gravitational force field of the Galaxy measured from the kinematics of RR Lyrae in Gaia. Mon. Not. Roy. Astron. Soc. **485** (2019) 3296–3316.
108. M. S. Nitschai, M. Cappellari, N. Neumayer: First Gaia dynamical model of the Milky Way disc with six phase space coordinates. Mon. Not. Roy. Astron. Soc. **494** (2020) 6001–6011.
109. P. J. McMillan, J. Binney: Analyzing surveys of our Galaxy I. Basic astrometric data. Mon. Not. Roy. Astron. Soc. **419** (2012) 2251–2263.
110. P. J. McMillan, J. J. Binney: Analyzing surveys of our Galaxy II. Determining the potential. Mon. Not. Roy. Astron. Soc. **433** (2014) 1411-1424.
111. J. Binney, T. Piffi: A distribution function of the Galaxy's dark halo, Monthly Mon. Not. Roy. Astron. Soc. **454** (2015) 3653-3663.
112. D. R. Cole, J. Binney: A centrally heated dark halo for our Galaxy, Mon. Not. R. Astron. Soc. **465** (2016) 798-810.
113. P.J. McMillan: The mass distribution and gravitational potential of the Milky Way. Mon. Not. Roy. Astron. Soc. **465** (2016) 76–94.
114. J. J. Han, C. Conroy, L. Hernquist: A tilted dark halo origin of the Galactic disk warp and flare, Nat. Astron. **7** (2023): 1481–1485.
115. A. M. Dillamore, J. L. Sanders: Geometry of the Milky Way's dark matter from dynamical models of the tilted stellar halo, arXiv e-prints (2025): arXiv-2510.

116. J. J. Han et al.: The stellar halo of the Galaxy is tilted and doubly broken, Astron. J. **164** (2022) 249.
117. P. A. M. Dirac: *Lectures on quantum mechanics*, Yeshiva University Press, New York, 1964.
118. B. S. DeWitt: Quantum Theory of Gravity. I. The Canonical Theory, Phys. Rev. **160** (1967) 1113–1148.
119. V. A. Savchenko, T. P. Shestakova, G. M. Vereshkov: Quantum geometrodynamics in extended phase space – I. Physical problems of interpretation and mathematical problems of gauge invariance, Gravit. Cosmol. **7** (2001) 18–28.
120. V. A. Savchenko, T. P. Shestakova, G. M. Vereshkov: Quantum geometrodynamics in extended phase space – II. The Bianchi IX model, Gravit. Cosmol. **7** (2001) 102–116.
121. T. P. Shestakova: Is the Wheeler - DeWitt equation more fundamental than the Schrödinger equation? Int. J. Mod. Phys. D **27** (2018) 1841004.
122. Yu. A. Golfand, E. P. Likhtman: Extension of the Algebra of Poincare Group Generators and violation of P Invariance, JETP Lett. **13** (1971) 323–326.
123. D. V. Volkov, V. P. Akulov: Possible Universal Neutrino Interaction, JEPT Lett. **16** (1972) 438–440.
124. R. Arnowitt, P. Nath, B. Zumino: Superfield densities and action principle in curved superspace, Phys. Lett. **56** (1975) 81–84.
125. A. Ashtekar: New Variables for Classical and Quantum Gravity, Phys. Rev. Lett. **57** (1986) 2244–2247.
126. R. Gambini, J. Pullin: *A first course in loop quantum gravity*, Oxford University Press, Oxford, 2011.
127. C. Rovelli, F. Vidotto: *Covariant loop quantum gravity. An elementary introduction to quantum gravity and spinfoam theory*, Cambridge University Press, Cambridge, 2015.
128. V. Mukhanov, H. Feldman, R. Brandenberger: Theory of cosmological perturbations, Phys. Rep. **215** (1992) 203–333.
129. C. Kiefer, T. P. Singh: Quantum gravitational corrections to the functional Schrödinger equation, Phys. Rev. D **44** (1991) 1067–1076.
130. C. Kiefer, M. Kramer: Quantum gravitational contributions to the cosmic microwave background anisotropy spectrum, Phys. Rev. Lett. **108** (2012) 021301.
131. R. P. Feynman: Space-time approach to non-relativistic quantum mechanics, Rev. Mod. Phys. **20** (1948) 367–387.
132. K. S. Cheng: Quantization of a general dynamical system by Feynman's path integration formulation, J. Math. Phys. **13** (1972) 1723–1726.
133. T. P. Shestakova: Quantum cosmological solutions: its dependence on gauge conditions and physical interpretation, in: M. C. Duffy, V. O. Gladyshev, A. N. Morozov, P. Rowlands, *Physical Interpretation of Relativity Theory: Proceedings of International Scientific Meeting*, Bauman Moscow State Technical University Press, Moscow, 2007.
134. Z. Miao, J. Jiang, A. Li, L. Chen: Bayesian Inference of Strange Star Equation of State Using the GW170817 and GW190425 Data, Astrophys. J. Lett. **917** (2021) L22.
135. E. Zhou, X. Zhou, A. Li: Constraints on interquark interaction parameters with GW170817 in a binary strange star scenario, Phys. Rev. D **97** (2018) 083015.
136. R. O. Gomes, V. Dexheimer, S. Han, S. Schramm: Constraining Strangeness in Dense Matter with GW170817, Mon. Not. Roy. Astron. Soc. **485** (2019) 4873.

BLED WORKSHOPS
IN PHYSICS
VOL. 26, NO. 1

Proceedings of the 28th Workshop
What Comes Beyond . . . *(p. 323)*
Bled, Slovenia, July 6–17, 2025

22 The extended phase space approach to quantization of gravity and its perspective

T. P. Shestakova[†]

Department of Theoretical and Computational Physics, Southern Federal University, Sorge St. 5, Rostov-on-Don 344090, Russia

Abstract. The prerequisites of the extended phase space approach to quantization of gravity, which is alternative to the Wheeler – DeWitt one and other existing approaches, are presented. The features of the proposed approach and conclusions from its underlying ideas are discussed.
Povzetek: Avtorica predstavi predpogoje za razširitev faznega prostora, ki naj omogoči kvantizacijo gravitacije, ki je alternativa Wheeler-DeWittovemu in drugim obstoječim pristopom. Obravnava značilnosti predlaganega pristopa, povzame zaključke in diskutira odprte probleme, ki so povezani s kvantizacijo gravitacije.

22.1 Introduction

I shall present the extended phase space approach to quantization of gravity [1–5]. The approach is alternative to existing approaches to quantization of gravity. The main idea, which it is based upon, is:
The quantization of gravity implies consideration of spacetimes with a nontrivial topology. In this case, the gravitating system has no asymptotic states, and this fact distinguishes gravity from other gauge fields.
The founders of quantum geometrodynamics, the first approach to quantization of gravity, like Wheeler, Hawking and others, spoke that the Universe may have a nontrivial topology. However, this conjecture on a nontrivial topology appears to be in contradiction with the assumption on asymptotic states that is used in the path integral quantization of gauge theories.
To understand this contradiction, let us start with a brief review of quantization methods. The most of approaches to quantization of gravity have been elaborated to be consistent with the Dirac quantization scheme for constrained theories. Dirac remembered that he had been excited by the role that the Hamiltonian formalism had played when quantum mechanics had been created. He wrote in his "Lectures on quantum mechanics" [6] that

> "...if we can put the classical theory into the Hamiltonian form, then we can always apply certain standard rules so as to get a first approximation to a quantum theory."

[†]shestakova@sfedu.ru

As it is known, Dirac faced the problem, how to construct the Hamiltonian formalism for a constrained system, since in this case, the Hamilton function cannot be constructed by the usual rule,

$$H = p_a \dot{q}^a + \pi_\alpha \dot{\lambda}^\alpha - L. \tag{22.1}$$

Here, all generalized coordinates are divided into two groups: $\{q^a\}$ are the so-called physical variables, while $\{\lambda^\alpha\}$ are gauge, or non-physical degrees of freedom, the velocities of which cannot be expressed from the momenta equations,

$$\pi_\alpha = \frac{\partial L}{\partial \dot{\lambda}^\alpha} = 0 \tag{22.2}$$

It is worth noting that, in the beginning, Dirac included gauge variables into phase space together with physical ones, otherwise he would not get the secondary constraints by means of the Poisson brackets,

$$\dot{\pi}_\alpha = \{\pi_\alpha, H\} = \varphi_\alpha, \tag{22.3}$$

but afterwards he declared that they are not of physical interest, redundant degrees of freedom.
Dirac is believed to find the solution to the problem by introducing the two postulates:

- One should add a linear combination of constraints $\{\varphi_\alpha\}$ to the Hamiltonian:

$$H = H_0 + \lambda^\alpha \varphi_\alpha. \tag{22.4}$$

- When quantizing, the constraints in the operator form become conditions imposed on the state vector:

$$\varphi_\alpha |\Psi\rangle = 0. \tag{22.5}$$

Why these rules are postulates? They cannot be derived from other fundamental physical statements, also, they cannot be justified by a reference to the correspondence principle. Moreover, these postulates have never been verified by any physical experiments, while very successful theories, confirmed experimentally, are based on different methods.
For example, quantum electrodynamics is based on the Lagrangian formalism and perturbation theory. Ironically, the Dirac approach is used only in various attempts to quantize gravity, in other words, in the sphere where, until now, we have not got any experimental data.
Meanwhile, the development of quantization methods gave a hint how Hamiltonian dynamics can be constructed differently. In the path integral quantization of gauge theories, the gauge-invariant action of an original theory is replaced by an effective action which includes gauge fixing and ghost terms. A gauge condition can be chosen in such a way that it would introduce missing velocities into the effective Lagrangian. An example is given by the Lorentz gauge in electrodynamics,

$$S_{ED} \to S_{eff} = \int d^4x \left(\mathcal{L}_{ED} + \mathcal{L}_{gf} + \mathcal{L}_{ghost}\right); \tag{22.6}$$

$$\mathcal{L}_{gf} = \pi \partial_\mu A^\mu = \pi \left(\dot{A}^0 + \partial_i A^i\right). \tag{22.7}$$

Here, π is a Lagrange multiplier and, at the same time, a momentum conjugate to A_0. It is easy to see that, using the effective Lagrangian, the Hamilton function can be constructed according to the usual rule because the terms with derivatives of A_0 with respect to time vanish:

$$\mathcal{H} = \pi \dot{A}_0 + p_i \dot{A}^i - \mathcal{L}. \tag{22.8}$$

We have two basic approaches to quantization: the canonical approach relying on the Hamiltonian formalism, and the path integral approach. In the canonical approach, the spacetime topology is restricted by a product of the real line with some three-dimensional manifold. In quantum field theory, the path integral approach was originally used for construction of the S-matrix, that implies that particles in initial and final (asymptotic) states are outside the interaction region. In its turn, it means that the path integral is considered under asymptotic boundary conditions which exclude nonphysical degrees of freedom in initial and final states. The asymptotic boundary conditions ensure gauge invariance of the path integral and, therefore, gauge invariance of the whole theory. However, in the case of gravity, the assumption on asymptotic states is valid only in asymptotically flat spacetimes. Returning to the question about non-trivial topology, we come to the conclusion that both canonical and path integral approaches do not admit an arbitrary topology of spacetime.
Further, we refuse the assumption about asymptotic states, and we shall work in extended phase space that includes, on equal footing, physical, gauge and ghost degrees of freedom. So, we shall come to the formulation of Hamiltonian dynamics in extended phase space, which will be considered in the next Section. It is a prerequisite of quantization, and it explains why the proposed approach has been called the extended phase space approach to quantization of gravity.

22.2 The formulation of Hamiltonian dynamics in extended phase space

This new formulation of Hamiltonian dynamics is based on introducing missing velocities into an effective Lagrangian by means of gauge conditions in a differential form. Thanks to it, the Hamiltonian can be constructed by the same rule as for unconstrained systems.
Varying the effective action, one obtains modified Einstein equations that include additional terms resulting from the gauge fixing and ghost parts of the action. One should add gauge conditions and ghost equations to the modified Einstein equations, so one gets the extended set of Lagrangian equations.
The Hamiltonian set of equations in extended phase space is completely equivalent to the extended set of Lagrangian equations. The equivalence implies that the constraints, gauge conditions and ghost equations are Hamilton equations. Thus, the description of the dynamics appears to be as close as possible to the description of a system without constraints, while the constraints are preserved. They are modified just like other Einstein equations.
The extended phase space approach enables us to solve some problems we face in the Dirac formalism. For example, we know that, in the theory of gravity, different parameterizations of variables are used. The gravitational field can be represented by components of the metric tensor as well as by the Arnowitt – Deser – Misner variables. From the viewpoint of the Lagrangian formalism, it is just a change of variables.

$$g_{00} = \gamma_{ij}N^iN^j - N^2; \quad g_{0i} = \gamma_{ij}N^j; \quad g_{ij} = \gamma_{ij}. \tag{22.9}$$

In theories without constraints, any change of variables in the Lagrangian formalism corresponds to a canonical transformation in the Hamiltonian formalism. However, in the Dirac approach, this change of variables, which touches upon gauge variables, is not canonical.
This change of variables, which is absolutely legal in the Lagrangian formalism, leads to a contradiction from the viewpoint of the Dirac approach. One can check that the Poisson

bracket between the lapse function and the momenta conjugate to the spatial component of the metric tensor in not zero [7, 8]:

$$\{N, \Pi^{ij}\}\Big|_{g_{\mu\nu}, p^{\lambda\rho}} \neq 0. \tag{22.10}$$

At least, it means that the Dirac Hamiltonian dynamics is not completely equivalent to the original (Lagrangian) formulation of the Einstein theory.
However, when we deal with the effective action and introduce the gauge fixing term, the momenta are modified, which results in correct values of the Poisson brackets.
It has been demonstrated in the full gravitational theory that a transformation of field variables in the Lagrangian formalism touching upon gauge degrees of freedom is a canonical transformation in extended phase space if one chooses a differential form of gauge conditions [8].
In the Dirac formalism, constraints are generators of transformations in phase space,

$$\delta B = \{B, \phi_\alpha\}\varepsilon^\alpha(x). \tag{22.11}$$

For example, in the case of electrodynamics, we have

$$\delta A^0 = \varepsilon(x), \quad \delta A^i = \partial^i \xi(x). \tag{22.12}$$

In the theory of gravity, one cannot obtain correct transformations for all degrees of freedom, including gauge ones, using constraints as generators.
In the Batalin – Fradkin – Vilkovisky approach the generator (the BRST charge) can be constructed as a series in Grassmannian (ghost) variables with coefficients given by generalized structure functions of constraints' algebra [9, 10].

$$\Omega_{BFV} = \int d^3x \left(c^\alpha U_\alpha^{(0)} + c^\beta c^\gamma U_{\gamma\beta}^{(1)\alpha} \rho_\alpha + \cdots \right). \tag{22.13}$$

Since the idea of construction of the BRST charge (20.13) is based on the constraints' algebra, one also cannot get correct transformations for all degrees of freedom, including gauge ones, by means of this generator.
There exist another way to construct the BRST charge making use of global BRST symmetry and the Noether theorem. The BRST charge for the Yang – Mills fields constructing according to the Noether theorem coincides exactly with the one obtained by the Batalin – Fradkin – Vilkovisky prescription.
However, in the case of gravity, the BRST charge constructed according to the method of Batalin, Fradkin and Vilkovisky, differs from the BRST charge constructed by the Noether theorem. The latter (Noether) charge generates the correct transformations for all degrees of freedom, including gauge ones.
This means that the group of transformations generated by gravitational constraints differs from the group of gauge transformations of general relativity in the Lagrangian formalism.

22.3 Quantization

Now I shall turn to quantization. I prefer path integral quantization, since this approach enables us to explore systems without asymptotic states and problems related to gauge invariance. If we consider a gravitating system without asymptotic states, gauge invariance of the theory cannot be proved. It means that the Wheeler – DeWitt equation, that expresses this gauge invariance, loses its sense. But one can derive a Schrödinger equation from the path integral instead, which is believed to maintain a fundamental meaning.

As it is known, for the first time the Schrödinger equation was derived from the path integral by Feynman in his seminal paper of 1948 [11]. Then, it was generalized by Cheng [12] for quadratic Lagrangians,

$$L(x,\dot{x}) = \frac{1}{2} g_{ij}(x)\dot{x}^i\dot{x}^j. \tag{22.14}$$

The Schrödinger equation for the Lagrangian (20.14) is as following:

$$i\hbar\frac{\partial\psi}{\partial t} = -\frac{\hbar^2}{2}\frac{1}{\sqrt{g}}\frac{\partial}{\partial x^i}\left(\sqrt{g}g^{ij}\frac{\partial\psi}{\partial x^j}\right) + \frac{\hbar^2}{6}R\psi. \tag{22.15}$$

Here $g_{ij}(x)$ is a metric of configurational space. g is its determinant, and the quantum correction appears that is proportional to $\hbar^2$ and the curvature R of the configurational space.
We shall consider the effective action for a model with a finite number of degrees of freedom which includes gauge fixing and ghost terms.

$$S = \int dt\left[\frac{1}{2}g_{ab}(N,q)\dot{q}^a\dot{q}^b - U(N,q) + \pi\left(\dot{N} - \frac{\partial f}{\partial q^a}\dot{q}^a\right) + N\dot{\bar{\theta}}\dot{\theta}\right]. \tag{22.16}$$

Again, g_{ab} is a metric of configurational space, $\{q^a\}$ denote physical degrees of freedom and N is a gauge variable, it may be the lapse function or not, depending on the model, $U(N,q)$ is a potential. We introduces the gauge condition $N = f(q)$ in a differential form (like in electrodynamics) and ghost fields θ, $\bar{\theta}$.
The Hamilton function in extended phase space is:

$$\begin{aligned} H &= \frac{1}{2}g^{ab}p_a p_b + \pi p_a\frac{\partial f}{\partial q_a} + \frac{1}{2}\pi^2\frac{\partial f}{\partial q^a}\frac{\partial f}{\partial q_a} - U(N,q) + \frac{1}{N}\bar{\mathcal{P}}\mathcal{P} \\ &= \frac{1}{2}G^{\alpha\beta}P_\alpha P_\beta + U(N,q) + \frac{1}{N}\bar{\mathcal{P}}\mathcal{P}; \end{aligned} \tag{22.17}$$

where

$$G = \begin{pmatrix} \frac{\partial f}{\partial q^a}\frac{\partial f}{\partial q_a} & \frac{\partial f}{\partial q_a} \\ \frac{\partial f}{\partial q_a} & g^{ab} \end{pmatrix}, \tag{22.18}$$

$Q^\alpha = \{N, q^a\}$; $P_\alpha = \{\pi, p_a\}$.
Now, we need to generalize the Feynman method for constrained systems. As a result, we come to the Schrödinger equation,

$$i\frac{\partial\Psi(N,q,\theta,\bar{\theta};t)}{\partial t} = H\Psi(N,q,\theta,\bar{\theta};t). \tag{22.19}$$

This equation is a direct mathematical consequence of the path integral with the effective action without asymptotic boundary conditions. I shall refer to it as the mathematical Schrödinger equation.
The Hamilton operator H corresponds (up to operator ordering) to the Hamilton function in extended phase space (20.17),

$$H = -\frac{1}{2M}\frac{\partial}{\partial Q^\alpha}\left(MG^{\alpha\beta}\frac{\partial}{\partial Q^\beta}\right) + U(N,q) + V[f] - \frac{1}{N}\frac{\partial}{\partial\theta}\frac{\partial}{\partial\bar{\theta}}, \tag{22.20}$$

Here M is the measure in the path integral, $V[f]$ is a quantum correction which is proportional to $\hbar^2$ and the curvature of configurational space.

The wave function, that is a solution to this equation, defined on extended configurational space. The extended configurational space includes physical and gauge degrees of freedom and ghosts.

$$\Psi(N, q, \theta, \bar{\theta}; t) = \int \Psi_k(q, t)\delta(N - f(q) - k)(\bar{\theta} + i\theta)dk. \tag{22.21}$$

The δ-function fixes the gauge condition (up to a constant k). The function $\Psi_k(q, t)$, which depends only on the physical variables, contains information about the physical system. Substituting this general solution into the mathematical Schrödinger equation, we come to the physical Schrödinger equation, and the "physical" Hamilton operator $H_{(phys)}[f]$ depends on the chosen gauge conditions.

$$i\frac{\partial\Psi_k(q, t)}{\partial t} = H_{(phys)}[f]\Psi_k(q, t), \tag{22.22}$$

$$H_{(phys)}[f] = \left[-\frac{1}{2M}\frac{\partial}{\partial q^a}\left(Mg^{ab}\frac{\partial}{\partial q^b}\right) + U(N, q) + V[f]\right]\Bigg|_{N=f(q)+k}, \tag{22.23}$$

The wave function of the Universe satisfying this equation will describe geometry of the Universe from the point of view of an observer in some fixed reference frame.

22.4 Where the extended phase space approach leads

Now I shall turn to the consequences of this approach. First, I would like to address the question of non-trivial topology which I have already mentioned.

From a theoretical point of view, the path integral enables one to consider spacetimes with non-trivial topology using various coordinates in different regions. Indeed, let us consider a spacetime manifold that includes regions with different gauge conditions. Imagine that the spacetime manifold consists of several regions $\mathcal{R}_1, \mathcal{R}_2, \mathcal{R}_3, \ldots$, in each of them different gauge conditions $C_1, C_2, C_3, \ldots$, being imposed. The regions are separated by boundaries $\mathcal{S}_1, \mathcal{S}_2, \ldots$. For example, if $\mathcal{S}_1$ is the boundary between the regions $\mathcal{R}_1$ and $\mathcal{R}_2$, one has

$$\begin{aligned}
&\int \exp\left(iS\left[g_{\mu\nu}\right]\right) \prod_{x\in\mathcal{M}} M\left[g_{\mu\nu}\right] \prod_{\mu,\,\nu} dg_{\mu\nu}(x) \\
&\quad = \int \exp\left(iS_{(eff)}\left[g_{\mu\nu},\, C_1,\, \mathcal{R}_1\right]\right) \prod_{x\in\mathcal{R}_1} M\left[g_{\mu\nu},\, \mathcal{R}_1\right] \prod_{\mu,\,\nu} dg_{\mu\nu}(x) \\
&\qquad \times \exp\left(iS_{(eff)}\left[g_{\mu\nu},\, C_2,\, \mathcal{R}_2\right]\right) \prod_{x\in\mathcal{R}_2} M\left[g_{\mu\nu},\, \mathcal{R}_2\right] \prod_{\mu,\,\nu} dg_{\mu\nu}(x) \\
&\qquad \times \prod_{x\in\mathcal{S}_1} M\left[g_{\mu\nu},\, \mathcal{S}_1\right] \prod_{\mu,\,\nu} dg_{\mu\nu}(x) \times \ldots
\end{aligned} \tag{22.24}$$

There exists a problem if the boundaries between regions are not spacelike hypersurfaces of equal time. The assumption on an arbitrary topology prevents us from introducing a global time in the whole spacetime, one should rather consider different clocks in every region. However, now we consider a simple case when the hypersurfaces $\mathcal{S}_1, \mathcal{S}_2, \ldots$, correspond to some time instants $t_0, t_1, \ldots$.

As we can see from (20.23), the Hamilton operator in the Schrödinger equation in each region will depend on the chosen reference frame (gauge conditions). This Hamilton operator governs time evolution of the gravitational system within the region, and, as in ordinary quantum mechanics, the evolution will be unitary. For example, if $|g^{(0)}_{\mu\nu}, \mathcal{S}_0\rangle$ is an initial state in the region $\mathcal{R}_1$, the final state in this region is

$$|g^{(1)}_{\mu\nu}, \mathcal{S}_1\rangle = \exp\left[-iH_{1(phys)}(t_1 - t_0)\right] |g^{(0)}_{\mu\nu}, \mathcal{S}_0\rangle. \tag{22.25}$$

Then the evolution continues in the region $\mathcal{R}_2$, but state vectors in $\mathcal{R}_2$ belong to another Hilbert space. Therefore, we should expand the final state in $\mathcal{R}_1$ in a new basis, that means a transformation of this state as

$$\mathcal{P}(\mathcal{S}_1,\, t_1)\exp\left[-iH_{1(phys)}(t_1-t_0)\right]|g^{(0)}_{\mu\nu},\, \mathcal{S}_0\rangle. \tag{22.26}$$

where the operator $\mathcal{P}(\mathcal{S}_1,\, t_1)$ is a projection operator and it is not unitary in general. In this way, we shall obtain,

$$\begin{aligned}|g^{(3)}_{\mu\nu}, \mathcal{S}_3\rangle &= \exp\left[-iH_{3(phys)}(t_3-t_2)\right]\mathcal{P}(\mathcal{S}_2,\, t_2)\\ &\times \exp\left[-iH_{2(phys)}(t_2-t_1)\right]\mathcal{P}(\mathcal{S}_1,\, t_1)\\ &\times \exp\left[-iH_{1(phys)}(t_1-t_0)\right]|g^{(0)}_{\mu\nu},\, \mathcal{S}_0\rangle.\end{aligned} \tag{22.27}$$

From this consideration, we come to the following conclusion:
At any boundary between the regions with different gauge conditions unitary evolution may be broken down. The operators $\mathcal{P}(\mathcal{S}_i,\, t_i)$ project the states obtained as a result of unitary evolution in the region $\mathcal{R}_i$ onto a basis in the Hilbert space in the neighboring region $\mathcal{R}_{i+1}$.
Now we shall consider a small variation of the gauge condition. Let $H_{(phys)}[f]$ is a physical Hamilton operator in the region with the gauge condition $N = f(q) + k$ (20.23), while $H_{(phys)}[f+\delta f]$ is a physical Hamilton operator in the region with a modified gauge condition $N = f(q) + \delta f(q) + k$,

$$\begin{aligned}H_{(phys)}[f+\delta f] = \Bigg[&-\frac{1}{2M}\frac{\partial}{\partial q^a}\left(Mg^{ab}\frac{\partial}{\partial q^b}\right)\\ &+\ U(N,q) + V[f+\delta f]\Bigg]\Bigg|_{N=f(q)+\delta f+k}.\end{aligned} \tag{22.28}$$

Bearing in mind that the variation of the gauge condition is small, one can present $H_{(phys)}[f+\delta f]$ in the form:

$$H_{(phys)}[f+\delta f] = H_{(phys)}[f] + W[\delta f] + \delta U[\delta f] + V_1[\delta f], \tag{22.29}$$

where $W[\delta f]$ is not Hermitian operator with respect to the basis in the region with a gauge condition $N = f(q) + k$.
Moreover, one can generalize these results for the case of time-dependent gauge conditions. The path integral approach implies that one should approximate the effective action, including the gauge condition, at each small time interval $[t_i, t_{i+1}]$. Let us suppose that changing the gauge condition at the time interval is

$$\delta f_i(q) = \alpha f_i(q), \tag{22.30}$$

and α is a small parameter, so that

$$N(t) = f(q) + \sum_{i=0}^{n}\alpha f_i(q)\theta(t-t_i) + k. \tag{22.31}$$

Let us note that, at each time interval, the gauge condition does not depend on time. For example, at the interval $[t_n.t_{n+1}]$ the gauge condition is

$$N = f(q) + \sum_{i=0}^{n-1}\alpha f_i(q) + \delta f_n(q) + k. \tag{22.32}$$

and we come to the case considered above. **In the case of time-dependent gauge conditions, it means that at every moment of time we have a Hamilton operator acting in its own "instantaneous" Hilbert space. The "instantaneous" Hamilton operator is a Hermitian operator at every moment of time, but it is non-Hermitian with respect to the Hilbert space that we had at the previous moment.**

22.5 Final remarks

In conclusion, let us compare the equation (20.27) with the one describing the evolution of a quantum system according to von Neumann [13],

$$|\Psi(t_N)\rangle = U(t_N, t_{N-1})\mathcal{P}(t_{N-1})U(t_{N-1}, t_{N-2}) \times \ldots U(t_3, t_2)\mathcal{P}(t_2)U(t_2, t_1)\mathcal{P}(t_1)U(t_1, t_0)|\Psi(t_0)\rangle. \quad (22.33)$$

As is well known, von Neumann wrote that there exist two ways of changing a quantum state of a physical system, namely, unitary evolution and changes as results of measurements over the physical system. In (20.33), the projection operators $\mathcal{P}(t_i)$ correspond to measurements made at $t_0, t_1, \ldots, t_{N-1}$. The analogy between (20.27) and (20.33) could be understood if we accept the interpretation of the reference frame as a measuring instrument representing the observer in quantum gravity. At the moments $t_0, t_1, \ldots, t_{N-1}$, transitions from one reference frame to another take place, and interaction between the measuring instrument (reference frame) and the physical subsystem changes. It makes us go to another Hilbert space.

However, we have already mentioned that, in general, the projection operators are not Hermitian. It leads to the following question:

Can quantum gravity be the origin of nonunitarity?

This question remains open and requires further investigations. Many physicists believe that unitarity is an inseparable property of any physical theory that cannot be broken down. On the other hand, in the framework of unitary evolution, it is not possible to describe irreversible processes we face all around. When one needs to describe such processes, one has to introduce some non-unitary operators artificially, so to say, "by hands". In contrast, in the extended phase space approach to quantization of gravity, the emergence of projection operators follows from the logical development of the accepted prerequisites.

It is important to remember that all the conclusions above are consequences of the assumption on a non-trivial topology and the absence of asymptotic states.

These conclusions cannot be obtained in approaches based on the Wheeler – DeWitt equation or using the assumption on asymptotic states.

The extended phase space approach leads to qualitatively new results which were outlined briefly in this talk.

Now, some words about the perspectives.

The next step in our investigation is to compare the extended phase space approach with other approaches to quantization of gravity. For example, in loop quantum gravity, the so called Ashtekar's variables are used instead of components of the metric tensor. Using these variables, one can explore cosmological models. It is planned to compare the results of loop quantum cosmology with those obtained in the extended phase space approach.

A very important question, in my opinion, is the question about the role of gauge degrees of freedom. Dirac considered them as redundant, but, especially in the theory of gravity, they have a clear geometrical meaning. If we drop them out of the theory, we destroy spacetime continuum that was a great achievement of the relativistic theory. The work with the effective action tell us that ghost fields are also not just auxiliary variables. They are not

equal identically to zero. In non-gravitational gauge theories they appeared in inner loops of Feynman diagrams, but in gravity, where there may not be asymptotic states, they may play some additional role. We do not know now what this role is.
In the mathematical Schrödinger equation, the wave function is defined on extended configurational space, its coordinates are physical, gauge and ghost degrees of freedom. Ghost degrees of freedom give a contribution to curvature of configurational space, which, as I mentioned, is included to quantum correction to the Schrödinger equation. In a fact, extended configurational space is a superspace in the sense that it contains anticommuting coordinates. But it is not a superspace of supersymmetric theories. We have questions: Is it possible to reformulate supersymmetric theories in a way to be compatible with the extended phase space approach? Could it reveal us something new about the role of non-physical degrees of freedom?
At last, we would like to have theoretical predictions that could be verified by observational data. The hope is related with quantum gravitational corrections to the Wheeler – DeWitt equation, or, in our case, to the Schrödinger equation. Unfortunately, the observational data is not exact enough to be compared with the theoretical predictions made in the framework of various approaches to quantization of gravity. Nevertheless, our technical capabilities are quickly developing, as well as our understanding of physical laws.
Let me finish with the quote of John Tyndall [14], a British physicist of XIXth century.

> "...Believing, as I do, in the continuity of nature, I cannot stop abruptly where our microscopes cease to be of use. Here the vision of the mind authoritatively supplements the vision of the eye. By a necessity engendered and justified by science I cross the boundary of the experimental evidence..."

Acknowledgements

I am grateful to the Organizers for the opportunity to present the extended phase space approach to quantization of gravity at this workshop.

References

1. V. A. Savchenko, T. P. Shestakova and G. M. Vereshkov: Quantum geometrodynamics of the Bianchi IX model in extended phase space, Int. J. Mod. Phys. **A14** (1999) 4473–4490.
2. V. A. Savchenko, T. P. Shestakova and G. M. Vereshkov: The exact cosmological solution to the dynamical equations for the Bianchi IX model, Int. J. Mod. Phys. **A15** (2000) 3207–3220.
3. V. A. Savchenko, T. P. Shestakova and G. M. Vereshkov: Quantum geometrodynamics in extended phase space – I. Physical problems of interpretation and mathematical problems of gauge invariance, Gravitation & Cosmology **7** (2001) 18–28.
4. V. A. Savchenko, T. P. Shestakova and G. M. Vereshkov: Quantum geometrodynamics in extended phase space – II. The Bianchi IX model, Gravitation & Cosmology **7** (2001) 102–116.
5. T. P. Shestakova: Is the Wheeler - DeWitt equation more fundamental than the Schrödinger equation? Int. J. Mod. Phys. **D27** (2018) 1841004.
6. P. A. M. Dirac: *Lectures on quantum mechanics*, Yeshiva University Press, New York, 1964.
7. N. Kiriushcheva, S. V. Kuzmin: The Hamiltonian formulation of general relativity: myth and reality, Central Eur. J. Phys. **9** (2011) 576-615.
8. T. P. Shestakova: Hamiltonian formulation for the theory of gravity and canonical transformations in extended phase space, Class. Quantum Grav. **28** (2011) 055009.

9. M. Hennaux: Hamilton form of the path integral for theories with a gauge freedom, Phys. Rep. **126** (1985) 1-66.
10. T. P. Shestakova: The role of BRST charge as a generator of gauge transformations in quantization of gauge theories and gravity, in: Proceedings of "Frontiers of Fundamental Physics 14", PoS(FFP14)175, DOI: 10.22323/1.224.0175.
11. R. P. Feynman: Space-time approach to non-relativistic quantum mechanics, Rev. Mod. Phys. **20** (1948) 367-387.
12. K. S. Cheng: Quantization of a general dynamical system by Feynman's path integration formulation, J. Math. Phys. **13** (1972) 1723-1726.
13. I. von Neumann, *Mathematical Foundations of Quantum Mechanics*, Princeton University Press, Princeton, 1955.
14. J. Tyndall: *Fragments of Science: A Series of Detached Essays, Lectures, and Reviews*, Vol. II, Longmans, Green, and Co, London, 1892, p. 191.

BLED WORKSHOPS
IN PHYSICS
VOL. 26, NO. 1

Proceedings of the 28th Workshop
What Comes Beyond . . . *(p. 333)*
Bled, Slovenia, July 6–17, 2025

23 The renormalization group invariants and exact results for various supersymmetric theories

K.V. Stepanyantz[†]

Moscow State University, 119991, Moscow, Russia

Abstract. Some recent all-loop results on the renormalization of supersymmetric theories are summarized and reviewed. In particular, we discuss how it is possible to construct expressions which do not receive quantum corrections in all orders for certain $\mathcal{N} = 1$ supersymmetric theories. For instance, in $\mathcal{N} = 1$ SQED+SQCD there is a renormalization group invariant combination of two gauge couplings. For the Minimal Supersymmetric Standard Model there are two such independent combinations of the gauge and Yukawa couplings. We investigate the scheme-dependence of these results and verify them by explicit three-loop calculations. We also argue that the all-loop exact β-function and the corresponding renormalization group invariant can exist in the 6D, $\mathcal{N} = (1,0)$ supersymmetric higher derivative gauge theory interacting with a hypermultiplet in the adjoint representation.
Povzetek: Avtor predstavi nedavne rezultate renormalizacije z vsemi zankami za supersimetrične teorije. Za nekatere supersimetrične teorije $\mathcal{N} = 1$ pokaže, kako skonstruirati izraze, ki so v vseh redih brez kvantnih popravkov. Na primer, supersimetrična teorija $\mathcal{N} = 1$ SQED+SQCD ponudi primer, pri katerem sta dve od sklopitvenih konstant povezani in je renormalizacijska grupa invariantna glede na obe sklopitveni konstanti. Za minimalno supersimetrično razširitev *standardnega modela* obstajata dve taki neodvisni kombinaciji umeritvenih polj in Yukawinih sklopitev. Avtor preverja odvisnost rezultatov od izbrane sheme z uporabo treh zank. Pokaže, da imamo v modelu 6D, $\mathcal{N} = (1,0)$, s supersymmetrično umeritveno teorijo višjih redov in s hipermultipletom v adjungirani upodobitvi funkcijo β, izračunano z vsemi zankami in skupaj z njo invariantno renormalizacijsko grupo.

23.1 Introduction

Quantum corrections can tell a lot about the structure of the surrounding world. For instance, comparing the theoretical predictions for the electron anomalous magnetic moment with the experimental data we conclude that it is necessary to describe nature by quantum field theory [1]. Analyzing the unification of the running gauge couplings in the Standard model and its supersymmetric extensions [2–4] and comparing the results with the predictions of the Grand Unified theories we obtain a strong indirect indication for the existence of supersymmetry [5,6]. One more evidence in favour of supersymmetry in the high energy

[†]stepan@m9com.ru

physics is provided by the absence of divergent quantum corrections to the Higgs boson mass in this case. Moreover, the detailed analysis of quantum corrections to the (lightest) Higgs boson mass, to the anomalous magnetic moment of muon, etc. can provide some important information about new physics beyond the Standard model, see the reviews in [7] and references therein. Some important information can also be obtained by investigating the renormalization group invariants (RGIs), which, by definition, are the scale independent values. Some of them can be approximate (see, e.g., [6,8]), but sometimes it is even possible to construct the expressions that are scale independent in all orders (see, e.g. [9,10]).

In this paper we describe how one can construct all-order exact RGIs in certain supersymmetric theories. Namely, we consider $\mathcal{N}=1$ supersymmetric chromodynamics interacting with supersymmetric electrodynamics (SQCD+SQED), the Mininmal Supersymmetric Standard Model (MSSM), and the higher derivative 6D, $\mathcal{N}=(1,0)$ supersymmetric Yang–Mills theory theory interacting with the hypermultiplet in the adjoint representation. For all these theories we will construct such combinations of couplings that do not depend on scale in all orders of the perturbation theory.

The paper is organized as follows. In Sect. 21.2 some basic information about the superfield formulation of the supersymetric theories is recalled. Some features of quantum corrections in supersymmetric theories that are revealed by the higher covariant regularization are discussed in Sect. 21.3. After that, in Sect. 21.4 the RGI composed from two gauge couplings is constructed for $\mathcal{N}=1$ SQCD+SQED. Analogous RGIs for MSSM are presented in Sect. 21.5. A possibility of constructing an RGI for a certain 6D, $\mathcal{N}=(1,0)$ higher derivative supersymmetric theory is analyzed in Sect. 21.6. A brief summary of the results is given in Conclusion.

23.2 Superfield formultion of supersymmetric theories and some aspects of their renormalization

In $\mathcal{N}=1$ superspace renormalizable supersymmetric gauge theories (with a single gauge coupling) are described by the manifestly supersymmetric action

$$S = \frac{1}{2e_0^2}\,\mathrm{Re}\,\mathrm{tr}\int d^4x\,d^2\theta\,W^a W_a + \frac{1}{4}\int d^4x\,d^4\theta\,\phi^{*i}(e^{2V})_i{}^j\phi_j$$
$$+\Big\{\int d^4x\,d^2\theta\,\Big(\frac{1}{4}m_0^{ij}\phi_i\phi_j + \frac{1}{6}\lambda_0^{ijk}\phi_i\phi_j\phi_k\Big) + \mathrm{c.c.}\Big\}. \qquad (23.1)$$

Here ϕ_i are the chiral matter superfields in the representation R of the gauge group G, which, by definition, satisfy the constraint $\bar{D}_{\dot a}\phi_i = 0$. (In our notation $\bar{D}_{\dot a}$ and D_a denote the left and right components of the supersymmetric covariant derivative, respectively.) The gauge superfield V is Hermitian, $V^+ = V$. Its gauge field strength is the chiral superfield

$$W_a = \frac{1}{8}\bar{D}^2\Big(e^{-2V}D_a e^{2V}\Big). \qquad (23.2)$$

The renormalizability requires that the superpotential should be no more than cubic in chiral superfields. According to the well-known theorem [11], in this case it does not receive divergent quantum corrections. However, nonrenormalization of the superpotential does not imply that masses and Yukawa couplings in the supersymmetric case are not renormalized. In fact, their renormalization appears to be related to the renormalization of the chiral matter superfields. Namely, if $\phi_i = (\sqrt{Z})_i{}^j\phi_{R,j}$, then

$$m^{ij} = m_0^{kl}(\sqrt{Z})_k{}^i(\sqrt{Z})_l{}^j; \qquad \lambda^{ijk} = \lambda_0^{mnp}(\sqrt{Z})_m{}^i(\sqrt{Z})_n{}^j(\sqrt{Z})_p{}^k. \qquad (23.3)$$

Unexpectedly, the renormalization of the gauge couplings in the supersymmetric case is also related to the renormalization of chiral matter superfields by the exact Novikov, Shifman, Vainshtein, and Zakharov (NSVZ) β-function [9,12–14]. For theories with a single gauge coupling it can be written in the form

$$\beta(\alpha,\lambda) = -\frac{\alpha^2\Big(3C_2 - T(R) + C(R)_i{}^j(\gamma_\phi)_j{}^i(\alpha,\lambda)/r\Big)}{2\pi(1 - C_2\alpha/2\pi)}, \tag{23.4}$$

where $\alpha = e^2/4\pi$ and λ are the gauge and Yukawa coupling constants, respectively, and $r \equiv \dim G$. For the pure $\mathcal{N} = 1$ SYM theory (which does not contain chiral matter superfields) the NSVZ equation produces the all-order exact formula for the β-function, which can equivalently be reformulated as the statement that in all orders of the perturbation theory the expression

$$\Big(\frac{\mu^3}{\alpha}\Big)^{C_2}\exp\Big(-\frac{2\pi}{\alpha}\Big) = \mathrm{RGI} \tag{23.5}$$

does not receive quantum corrections [13].

Nevertheless, it is necessary to remember that the all-loop equations describing the renormalization of supersymmetric theories are valid only for certain renormalization prescriptions. For instance, in the $\overline{\mathrm{DR}}$-scheme the NSVZ equation does not hold starting from the order $O(\alpha^4)$ (the three-loop approximation for the β-function and the two-loop approximation for the anomalous dimension) [15–18]. However, the all-loop NSVZ renormalization prescription can be constructed with the help of the higher covariant derivative regularization [19–21] in the superfield formulation [22,23] considered in the next section.

23.3 Quantum properties of supersymmetric theories regularized by higher covariant derivatives

For supersymmetric theories the higher covaraint derivative regularization allows revealing some nontrivial feature of quantum corrections which are not seen in the case of using the dimensional reduction, see, e.g., [24,25]. It is introduced by adding to the action (21.1) terms with higher gauge and supersymmetric covariant derivatives (denoted by $\bar\nabla_{\dot\alpha}$ and ∇_α). After that, the regularized action takes the form

$$\begin{aligned} S_{\mathrm{reg}} &= \frac{1}{2e_0^2}\,\mathrm{Re}\,\mathrm{tr}\int d^4x\,d^2\theta\,W^\alpha\Big[e^{-2V}R\Big(-\frac{\bar\nabla^2\nabla^2}{16\Lambda^2}\Big)e^{2V}\Big]_{A\,dj}W_\alpha \\ &+\frac{1}{4}\int d^4x\,d^4\theta\,\phi^{*i}\Big[F\Big(-\frac{\bar\nabla^2\nabla^2}{16\Lambda^2}\Big)e^{2V}\Big]_i{}^j\phi_j \\ &+\Big[\int d^4x\,d^2\theta\,\Big(\frac{1}{4}m_0^{ij}\phi_i\phi_j + \frac{1}{6}\lambda_0^{ijk}\phi_i\phi_j\phi_k\Big) + \mathrm{c.c.}\Big], \end{aligned} \tag{23.6}$$

where the functions $R(x)$ and $F(x)$ should rapidly increase at infinity and satisfy the condition $R(0) = F(0) = 1$. Due to the former property of these functions, divergences remain only in the one-loop approximation. For regularizing these residual divergences, one can insert into the generating functional some special Pauli–Villars determinants [21]. The details of the corresponding construction can be found in [26,27].

As was noted in numerous calculations made in supersymmetric theories in the lowest (up to four loops) orders of the perturbation theory with the higher derivative regularization [28–35], the NSVZ equation appears in this case because the integrals giving the β-function defined in terms of the bare couplings are integrals of double total derivatives with respect

to the loop momenta. For instance, in the one-loop approximation the β-function for the theory (21.1) is written in the form [26]

$$\frac{\beta(\alpha_0,\lambda_0)}{\alpha_0^2} = \int \frac{d^4q}{(2\pi)^4}\frac{d}{d\ln\Lambda}\frac{\partial}{\partial q^\mu}\frac{\partial}{\partial q_\mu}\Big\{ -\frac{\pi C_2}{q^2}\Big[\ln\Big(1+\frac{M_\varphi^2}{q^2R^2(q^2/\Lambda^2)}\Big) +2\ln\Big(1+\frac{M_\varphi^2}{q^2}\Big)\Big] + \frac{\pi T(R)}{q^2}\ln\Big(1+\frac{M^2}{q^2F^2(q^2/\Lambda^2)}\Big)\Big\} + O(\alpha_0,\lambda_0^2), \tag{23.7}$$

where M and M_φ are masses of the Pauli–Villars superfields, and a small vicinity of the singular point $q^\mu = 0$ should be excluded from the integration region. In all orders the factorization of integrals giving the β-function into integrals of double total derivatives has been proved in [36] in the Abelian case and in [37] for general non-Abelian gauge theories. The double total derivatives effectively cut internal lines in (vacuum) supergraphs thus reducing a number of loop integrations by 1 and giving superdiagrams contributing to the anomalous dimensions of various quantum superfields. After that, (for $\mathcal{N}=1$ supersymmetric theories regularized by higher covarant derivatives) the NSVZ β-function is obtained in all orders for the renormalization group functions (RGFs) defined in terms of the bare couplings by summing singular contributions [38] and taking into account the nonrenormalization of the triple gauge-ghost vertices [39].

For the standard RGFs defined in terms of the renormalized couplings the NSVZ equation holds in all orders in the HD+MSL scheme [40], when a theory is regularized by Higher Derivatives, and divergences are removed by Minimal Subtractions of Logarithms [24,32]. This in particular implies that for the pure $\mathcal{N}=1$ SYM theory the RGI (21.5) is valid in the HD+MSL scheme and is not valid in the $\overline{DR}$ scheme.

Involving the statement that the HD+MSL is an all-loop NSVZ scheme, it is possible to use the NSVZ equation for obtaining the β-function(s) in higher orders on the base of the anomalous dimension(s) in the previous loops, see, e.g., [41–44].

23.4 Renormalization of $\mathcal{N}=1$ SQCD+SQED

Following [45], we argue that in $\mathcal{N}=1$ SQCD+SQED one can construct an all-loop RGI from two gauge couplings $\alpha_s \equiv g^2/4\pi$ and $\alpha = e^2/4\pi$. In the massless limit this theory is described by the superfield action

$$S = \frac{1}{2g^2}\,\mathrm{Re}\,\mathrm{tr}\int d^4x\,d^2\theta\,W^a W_a + \frac{1}{4e^2}\,\mathrm{Re}\int d^4x\,d^2\theta\,\boldsymbol{W}^a\boldsymbol{W}_a + \sum_{a=1}^{N_f}\frac{1}{4}\int d^4x\,d^4\theta\,\Big(\phi_a^+ e^{2V+2q_a\boldsymbol{V}}\phi_a + \widetilde{\phi}_a^+ e^{-2V^T-2q_a\boldsymbol{V}}\widetilde{\phi}_a\Big), \tag{23.8}$$

where the subscript a numerates flavors. It is invariant under the transformations of the group $G\times U(1)$, V and $\boldsymbol{V}$ being the gauge superfields corresponding to the subgroups G and $U(1)$, respectively. The chiral matter superfields ϕ_a and $\widetilde{\phi}_a$ belong to the (conjugated) representations R and $\bar{R}$, respectively, and have opposite $U(1)$ charges $\pm q_a e$.

For the theory (21.8) the renormalization of the gauge couplings is described by the NSVZ β-functions, which are also valid for theories with multiple gauge couplings, see [46,47]. For an irreducible representation R and $q_a = 1$ they are written as

$$\frac{\beta_s(\alpha_s,\alpha)}{\alpha_s^2} = -\frac{1}{2\pi(1-C_2\alpha_s/2\pi)}\Big[3C_2 - 2T(R)N_f\Big(1-\gamma(\alpha_s,\alpha)\Big)\Big];$$
$$\frac{\beta(\alpha,\alpha_s)}{\alpha^2} = \frac{1}{\pi}\dim R\,N_f\Big(1-\gamma(\alpha_s,\alpha)\Big), \tag{23.9}$$

where we took into account that all anomalous dimensions coincide in the particular case under consideration. Comparing two expressions in Eq. (21.9), we see that the anomalous dimension of the matter superfeilds can be eliminated, and the gauge β-functions satisfy the all-order exact equation

$$\Big(1 - \frac{C_2\alpha_s}{2\pi}\Big)\frac{\beta_s(\alpha_s,\alpha)}{\alpha_s^2} = -\frac{3C_2}{2\pi} + \frac{T(R)}{\dim R}\cdot\frac{\beta(\alpha,\alpha_s)}{\alpha^2}, \tag{23.10}$$

which relates running of the strong and electromagnetic couplings in the theory under consideration. Evidently, Eq. (21.10) should be valid in the HD+MSL scheme, because the original NSVZ equations are also satisfied for this renormalization prescription. Integrating Eq. (21.10) we easily obtain that the expression

$$\Big(\frac{\alpha_s}{\mu^3}\Big)^{C_2}\exp\Big(\frac{2\pi}{\alpha_s} - \frac{T(R)}{\dim R}\cdot\frac{2\pi}{\alpha}\Big) = \mathrm{RGI} \tag{23.11}$$

vanishes after differentiating with respect to $\ln\mu$. This implies that it does not depend on scale and, therefore, is an RGI.

For the theory (21.8) with different $U(1)$ charges q_a Eq. (21.10) does not hold. However, in this case it is possible to relate the $\mathcal{N}=1$ SQCD β-function and the Adler D-function [48] in all orders by the equation [45],

$$\beta_s(\alpha_s) = -\frac{\alpha_s^2}{2\pi(1 - C_2\alpha_s/2\pi)}\left[3C_2 - \frac{4\,T(R)N_f D(\alpha_s)}{3\,\mathbf{q}^2\dim R}\right], \tag{23.12}$$

where $\mathbf{q^2} \equiv \sum\limits_{a=1}^{N_f}(q_a)^2$.

In the the three-loop approximation (where the scheme dependence becomes essential) Eqs. (21.10) and (21.12) have been verified by explicit calculations in [44], where the three-loop β-functions for the $\mathcal{N}=1$ SQCD+SQED have been calculated for a general renormalization prescription supplementing the higher covariant derivative regularization. In particular, it has been demonstrated that in the HD+MSL scheme these equations are satisfied this approximation and are not valid in the $\overline{\mathrm{DR}}$ scheme. This in particular implies that the expression (21.11) is not an RGI in the $\overline{\mathrm{DR}}$ scheme starting from three loops, where the scheme dependence manifests itself.

23.5 The Minimal Supersymmetric Standard Model

The MSSM is the simplest supersymmetric extension of the Standard Model. It is a gauge theory with the group $SU(3)\times SU(2)\times U(1)$ and softly broken supersymmetry, where quarks, leptons, and Higgs fields are components of the chiral matter superfields. Evidently, in the MSSM there are 3 gauge couplings

$$\alpha_3 = \frac{e_3^2}{4\pi}; \qquad \alpha_2 = \frac{e_2^2}{4\pi}; \qquad \alpha_1 = \frac{5}{3}\cdot\frac{e_1^2}{4\pi} \tag{23.13}$$

corresponding to the subgroups $SU(3)$, $SU(2)$, and $U(1)$, respectively. The MSSM action also contains dimensionless Yukawa couplings $(Y_U)_{IJ}$, $(Y_D)_{IJ}$, and $(Y_E)_{IJ}$ (which are 3×3

matrices) and the parameter μ with the dimension of mass inside the superpotential

$$W = (Y_U)_{IJ}\left(\widetilde{U}\,\widetilde{D}\right)^a_I \begin{pmatrix} 0 & 1 \\ -1 & 0 \end{pmatrix} \begin{pmatrix} H_{u1} \\ H_{u2} \end{pmatrix} U_{aJ} + (Y_D)_{IJ}\left(\widetilde{U}\,\widetilde{D}\right)^a_I$$
$$\times \begin{pmatrix} 0 & 1 \\ -1 & 0 \end{pmatrix} \begin{pmatrix} H_{d1} \\ H_{d2} \end{pmatrix} D_{aJ} + (Y_E)_{IJ}\left(\widetilde{N}\,\widetilde{E}\right)_I \begin{pmatrix} 0 & 1 \\ -1 & 0 \end{pmatrix} \begin{pmatrix} H_{d1} \\ H_{d2} \end{pmatrix}$$
$$\times E_J + \mu\,(H_{u1}\ H_{u2}) \begin{pmatrix} 0 & 1 \\ -1 & 0 \end{pmatrix} \begin{pmatrix} H_{d1} \\ H_{d2} \end{pmatrix}. \tag{23.14}$$

The renormalization group running of the gauge couplings in the MSSM ia described exactly in all loops by three NSVZ equations [46], which relate three gauge β-functions of the theory to the anomalous dimensions of the chiral matter superfields. Similarly, RGFs describing the renormalization of the Yukawa couplings and of the parameter μ are also related to the anomalous dimensions of the matter superfields due to the nonrenormalization of the superpotential [11].

According to [49], after eliminating the anomalous dimensions of the chiral matter superfields and μ from the resulting system of (all-order exact in the HD+MSL scheme) equations we obtain

$$0 = \Big(\frac{1}{\alpha_2} - \frac{\pi}{\alpha_2^2}\Big)\beta_2 - \frac{5\pi}{3\alpha_1^2}\beta_1 + 6 + 3\gamma_\mu - \gamma_{\det Y_E} - \frac{4}{3}\gamma_{\det Y_U} - \frac{1}{3}\gamma_{\det Y_D};$$
$$0 = \Big(\frac{3}{\alpha_3} - \frac{2\pi}{\alpha_3^2}\Big)\beta_3 - 3 + 3\gamma_\mu - \gamma_{\det Y_U} - \gamma_{\det Y_D}. \tag{23.15}$$

Integrating these equations we obtain that the expressions

$$\mathrm{RGI}_1 \equiv \frac{\mu^3\,\mu^6\,\alpha_2}{(\det Y_E)\,(\det Y_U)^{4/3}\,(\det Y_D)^{1/3}}\,\exp\Big(\frac{\pi}{\alpha_2} + \frac{5\pi}{3\alpha_1}\Big);$$
$$\mathrm{RGI}_2 \equiv \frac{\mu^3\,(\alpha_3)^3}{\mu^3\det Y_U \det Y_D}\,\exp\Big(\frac{2\pi}{\alpha_3}\Big) \tag{23.16}$$

do not depend on the renormalization scale *in all orders*. However, this renormalization group invariance is valid only for some special renormalization prescriptions. In fact, the scheme dependence of the equations becomes essential starting from the order $O(\alpha^2, \alpha Y^2, Y^4)$ corresponding to the three-loop approximation for the β-functions and to the two-loop approximation for the anomalous dimensions. In the HD+MSL scheme these RGFs have been calculated in [42]. After substituting them into Eq. (21.15) it was demonstrated that in the HD+MSL scheme these equation are really satisfied independently of the values of regularization parameters. However, in the $\overline{\mathrm{DR}}$ scheme the expressions in the right hand sides of Eq. (21.15) do not vanish in that orders where the scheme dependence becomes essential. (The corresponding RGFs needed for making this verification were taken from [50].) Therefore, in this scheme the expressions (21.16) are scale independent only in the two first orders of the perturbation theory.

23.6 6D, $\mathcal{N} = (1,0)$ higher derivative theory in the harmonic superspace

It would be interesting to reveal if quantum corrections in supersymmetric theories may remain their attractive features in higher dimensions. Usual supersymmetric theories in

higher dimensions are not renormalizable, because the degree of divergence increases with the number of loops. However, in this case it is possible to consider theories with higher derivatives. It is convenient to describe them using 6D, $\mathcal{N} = (1,0)$ harmonic superspace [51–55] analogous to the usual 4D, $\mathcal{N} = 2$ harmonic superspace [56,57], because in this case $\mathcal{N} = (1,0)$ supersymmetry is manifest.

Following Ref. [58], we consider the 6D, $\mathcal{N} = (1,0)$ supersymmetric theory similar to the one presented in [59], which in the harmonic superspace is described by the action

$$S = \pm\frac{1}{2e_0^2}\,\mathrm{tr}\int d\zeta^{(-4)}(F^{++})^2 - \frac{2}{e_0^2}\,\mathrm{tr}\int d\zeta^{(-4)}\widetilde{q^+}\nabla^{++}q^+. \tag{23.17}$$

Here the gauge superfield V^{++} and the hypermultiplet q^+ in the adjoint representation of the gauge group satisfy the analyticity conditions, and F^{++} is the harmonic superspace analog of the gauge field strength.

In components the action (21.17) (among others) contains the term with higher derivatives of the gauge field

$$S = \mathrm{tr}\int d^6x\left\{\pm\frac{1}{e_0^2}(\mathcal{D}_\mu F^{\mu\nu})^2 + \dots\right\}. \tag{23.18}$$

Due to the presence of higher derivatives, the degree of divergence for the theory (21.17) does not increase with a number of loops. The possible divergences are either quadratic or logarithmical, but the quadratic divergences cancel each other in the one-loop approximation (and presumably in all loops). The theory (21.17) is not anomalous [60] and seems to be renormalizable. Moreover, the hypermultiplet and ghosts do not receive divergent quantum corrections [58].

To reveal possible features of the quantum correction structure, we regularize the theory (21.17) by higher covariant derivatives. The higher derivative term is constructed with the help of the operator

$$\Box \equiv \frac{1}{2}(D^+)^4(\nabla^{--})^2, \tag{23.19}$$

which is analogous to the Laplace operator when acting on analytic superfields. Then the regularized action can be written in the form

$$S_{\mathrm{reg}} = \pm\frac{1}{2e_0^2}\,\mathrm{tr}\int d\zeta^{(-4)}F^{++}R\Big(\frac{\Box}{\Lambda^2}\Big)F^{++} - \frac{2}{e_0^2}\,\mathrm{tr}\int d\zeta^{(-4)}\widetilde{q^+}\nabla^{++}q^+, \tag{23.20}$$

where $R(0) = 1$ and $R(x) \to \infty$ at $x \to \infty$. For regularizing the residual one-loop divergences it is also necessary to add the Pauli–Villars superfields with the mass $M = a\Lambda$ as discussed in detail in [58].

After calculating one-loop divergent superdiagrams, it was obtained that the quadratic divergences cancel each other, while the sum of the logarithmical ones gives the β-function $\beta(\alpha_0)$ of the form

$$\frac{\beta(\alpha_0)}{\alpha_0^2} = \mp 2\pi C_2\int\frac{d^6q}{(2\pi)^6}\frac{d}{d\ln\Lambda}\frac{\partial}{\partial q_\mu}\frac{\partial}{\partial q^\mu}\left[\frac{1}{q^4}\ln\left(1+\frac{M^4}{q^4R(q^2/\Lambda^2)}\right)\right] + O(\alpha_0). \tag{23.21}$$

Therefore, exactly as in the 4D case, the β-function is given by integrals of double total derivatives with respect to the loop momentum. Note that, due to the presence of an arbitrary regulator function $R(x)$, this fact is highly nontrivial. After calculating the loop integral we obtain the one-loop result

$$\beta(\alpha_0) = \mp\frac{\alpha_0^2 C_2}{2\pi^2} + O(\alpha_0^3). \tag{23.22}$$

This expression agrees with the results of the calculations made in [59, 61–63] by various methods after taking into account the contribution of the hypermultiplet q^+ in the adjoint representation.

The resemblance in the structure of the one-loop results for 4D, $\mathcal{N}=1$ supersymmetric Yang–Mills theory and for the 6D, $\mathcal{N}=(1,0)$ higher derivative theory under consideration allows suggesting that it may be possible to construct an all-loop exact expression for the β-function. In [58] it was suggested that in the 6D case the result has the form

$$\beta(\alpha_0) = \mp \frac{\alpha_0^2 C_2}{2\pi^2\Big(1 \mp \alpha_0 C_2/8\pi^2\Big)}. \tag{23.23}$$

Certainly, this guess should be verified by explicit multiloop calculations and (if possible) rigorously proved in all orders. If the expression (21.23) is really true, then after integrating the renormalization group equation we obtain that the expression

$$\Big(\frac{\alpha}{\mu^4}\Big)^{C_2} \exp\Big(\pm\frac{8\pi^2}{\alpha}\Big) = \mathrm{RGI} \tag{23.24}$$

does not receive quantum corrections in any order of the perturbation theory and is a 6D analog of Eq. (21.5).

Conclusion

For certain $\mathcal{N}=1$ supersymmetric theories with multiple gauge couplings it is possible to construct such combinations of various couplings that do not depend on scale in all orders or, in other words, RGIs. In particular, in $\mathcal{N}=1$ SQCD interacting with $\mathcal{N}=1$ SQED such an RGI can be constructed from the strong and electromagnetic coupling constants (if the matter superfields have the same absolute values of the electromagnetic charges). This in particular implies that in this theory two gauge couplings do not run independently. For the MSSM (and also for NMMSM) one can construct two independent RGIs from the gauge couplings, Yukawa couplings and the μ parameter. They are scale independent in all orders in the HD+MSL scheme, when a theory is regularized by Slavnov's higher covariant derivative method, and divergences are removed by minimal subtractions of logarithms. This fact has been confirmed by explicit calculations in the three-loop approximation, where the dependence on the renormalization prescription is already essential. However, in the $\overline{\mathrm{DR}}$ scheme the above mentioned RGIs start to depend on scale from the three-loop order due to the scheme dependence.

We also argued that the behaviour of quantum corrections in a certain 6D, $\mathcal{N}=(1,0)$ supersymmetric theory with higher derivatives is very similar to the one in the pure 4D, $\mathcal{N}=1$ SYM theory. In particular, this theory presumably possesses an exact NSVZ-like β-function, which leads to the all-loop renormalization group invariance of the expression (21.24).

References

1. M. E. Peskin, D. V. Schroeder: *An Introduction to quantum field theory*, Addison-Wesley, 1995.
2. J. R. Ellis, S. Kelley, D. V. Nanopoulos: Probing the desert using gauge coupling unification, Phys. Lett. B **260** (1991) 131–137.

3. U. Amaldi, W. de Boer, H. Furstenau: Comparison of grand unified theories with electroweak and strong coupling constants measured at LEP, Phys. Lett. B **260** (1991) 447–455.
4. P. Langacker, M. X. Luo: Implications of precision electroweak experiments for M_t, ρ_0, $\sin^2\theta_W$ and grand unification, Phys. Rev. D **44** (1991) 817–822.
5. R. N. Mohapatra: *Unification and Supersymmetry. The Frontiers of Quark - Lepton Physics: The Frontiers of Quark-Lepton Physics*, Springer, 2002.
6. S. Raby: Supersymmetric Grand Unified Theories: From Quarks to Strings via SUSY GUTs, Lect. Notes Phys. **939** (2017), 1–308.
7. S. Navas *et al.* [Particle Data Group]: Phys. Rev. D **110** (2024) no.3, 030001.
8. I. Jack, D. R. T. Jones, C. G. North: N=1 supersymmetry and the three loop anomalous dimension for the chiral superfield, Nucl. Phys. B **473** (1996), 308–322.
9. V. A. Novikov, M. A. Shifman, A. I. Vainshtein, V. I. Zakharov: Exact Gell-Mann-Low Function of Supersymmetric Yang-Mills Theories from Instanton Calculus, Nucl. Phys. B **229** (1983) 381–393.
10. J. Hisano, M. A. Shifman: Exact results for soft supersymmetry breaking parameters in supersymmetric gauge theories, Phys. Rev. D **56** (1997), 5475–5482.
11. M. T. Grisaru, W. Siegel, M. Rocek: Improved Methods for Supergraphs, Nucl. Phys. B **159** (1979), 429.
12. D. R. T. Jones: More on the Axial Anomaly in Supersymmetric Yang-Mills Theory, Phys. Lett. **123B** (1983) 45–46.
13. V. A. Novikov, M. A. Shifman, A. I. Vainshtein, V. I. Zakharov: Beta Function in Supersymmetric Gauge Theories: Instantons Versus Traditional Approach, Phys. Lett. **166B** (1986), 329–333.
14. M. A. Shifman, A. I. Vainshtein: Solution of the Anomaly Puzzle in SUSY Gauge Theories and the Wilson Operator Expansion, Nucl. Phys. B **277** (1986) 456–486.
15. I. Jack, D. R. T. Jones, C. G. North: N=1 supersymmetry and the three loop gauge Beta function, Phys. Lett. B **386** (1996) 138–140.
16. I. Jack, D. R. T. Jones, C. G. North: Scheme dependence and the NSVZ Beta function, Nucl. Phys. B **486** (1997) 479–499.
17. I. Jack, D. R. T. Jones, A. Pickering: The Connection between DRED and NSVZ, Phys. Lett. B **435** (1998) 61–66.
18. R. V. Harlander, D. R. T. Jones, P. Kant, L. Mihaila, M. Steinhauser: Four-loop beta function and mass anomalous dimension in dimensional reduction, JHEP **12** (2006), 024.
19. A. A. Slavnov: Invariant regularization of nonlinear chiral theories, Nucl. Phys. B **31** (1971) 301–315.
20. A. A. Slavnov: Invariant regularization of gauge theories, Theor. Math. Phys. **13** (1972) 1064–1066.
21. A. A. Slavnov: The Pauli-Villars Regularization for Nonabelian Gauge Theories, Theor. Math. Phys. **33** (1977) 977–981.
22. V. K. Krivoshchekov: Invariant Regularizations for Supersymmetric Gauge Theories, Theor. Math. Phys. **36** (1978) 745–752.
23. P. C. West: Higher Derivative Regulation Of Supersymmetric Theories, Nucl. Phys. B **268** (1986) 113–124.
24. K. V. Stepanyantz: Structure of Quantum Corrections in $\mathcal{N} = 1$ Supersymmetric Gauge Theories, Bled Workshops Phys. **18** (2017) no.2, 197–213.
25. K. Stepanyantz: The higher covariant derivative regularization as a tool for revealing the structure of quantum corrections in supersymmetric gauge theories, Proceedings of the Steklov Institute of Mathematics **309** (2020) 284–298.

26. S. S. Aleshin, A. E. Kazantsev, M. B. Skoptsov, K. V. Stepanyantz: One-loop divergences in non-Abelian supersymmetric theories regularized by BRST-invariant version of the higher derivative regularization, JHEP **05** (2016), 014.
27. A. E. Kazantsev, M. B. Skoptsov, K. V. Stepanyantz: One-loop polarization operator of the quantum gauge superfield for $\mathcal{N} = 1$ SYM regularized by higher derivatives, Mod. Phys. Lett. A **32** (2017) no.36, 1750194.
28. A. V. Smilga, A. Vainshtein: Background field calculations and nonrenormalization theorems in 4-D supersymmetric gauge theories and their low-dimensional descendants, Nucl. Phys. B **704** (2005), 445–474.
29. A. B. Pimenov, E. S. Shevtsova, K. V. Stepanyantz: Calculation of two-loop beta-function for general N=1 supersymmetric Yang–Mills theory with the higher covariant derivative regularization, Phys. Lett. B **686** (2010), 293–297.
30. I. L. Buchbinder, K. V. Stepanyantz: The higher derivative regularization and quantum corrections in N=2 supersymmetric theories, Nucl. Phys. B **883** (2014), 20–44.
31. I. L. Buchbinder, N. G. Pletnev, K. V. Stepanyantz: Manifestly N=2 supersymmetric regularization for N=2 supersymmetric field theories, Phys. Lett. B **751** (2015), 434–441.
32. V. Y. Shakhmanov, K. V. Stepanyantz: New form of the NSVZ relation at the two-loop level, Phys. Lett. B **776** (2018), 417.
33. A. E. Kazantsev, V. Y. Shakhmanov, K. V. Stepanyantz: New form of the exact NSVZ β-function: the three-loop verification for terms containing Yukawa couplings, JHEP **04** (2018), 130.
34. M. D. Kuzmichev, N. P. Meshcheriakov, S. V. Novgorodtsev, I. E. Shirokov, K. V. Stepanyantz: Three-loop contribution of the Faddeev–Popov ghosts to the β -function of $\mathcal{N} = 1$ supersymmetric gauge theories and the NSVZ relation, Eur. Phys. J. C **79** (2019) no.9, 809.
35. I. Shirokov, V. Shirokova: The four-loop β-function from vacuum supergraphs and the NSVZ relation for $\mathcal{N} = 1$ SQED regularized by higher derivatives, Eur. Phys. J. C **84** (2024) no.3, 249.
36. K. V. Stepanyantz: Derivation of the exact NSVZ β-function in N=1 SQED, regularized by higher derivatives, by direct summation of Feynman diagrams, Nucl. Phys. B **852** (2011) 71–107.
37. K. V. Stepanyantz: The β-function of $\mathcal{N} = 1$ supersymmetric gauge theories regularized by higher covariant derivatives as an integral of double total derivatives, JHEP **1910** (2019) 011.
38. K. Stepanyantz: The all-loop perturbative derivation of the NSVZ β-function and the NSVZ scheme in the non-Abelian case by summing singular contributions, Eur. Phys. J. C **80** (2020) 911.
39. K. V. Stepanyantz: Non-renormalization of the $V\bar{c}c$-vertices in $\mathcal{N} = 1$ supersymmetric theories, Nucl. Phys. B **909** (2016) 316–335.
40. A. L. Kataev, K. V. Stepanyantz: NSVZ scheme with the higher derivative regularization for $\mathcal{N} = 1$ SQED, Nucl. Phys. B **875** (2013), 459–482.
41. A. Kazantsev, K. Stepanyantz: Two-loop renormalization of the matter superfields and finiteness of $\mathcal{N} = 1$ supersymmetric gauge theories regularized by higher derivatives, JHEP **06** (2020), 108.
42. O. Haneychuk, V. Shirokova, K. Stepanyantz: Three-loop β-functions and two-loop anomalous dimensions for MSSM regularized by higher covariant derivatives in an arbitrary supersymmetric subtraction scheme, JHEP **09** (2022), 189.
43. I. Shirokov, K. Stepanyantz: The three-loop anomalous dimension and the four-loop β-function for $\mathcal{N}$ = 1 SQED regularized by higher derivatives, JHEP **04** (2022), 108.
44. O. Haneychuk, K. Stepanyantz: Three-loop verification of the equations relating running of the gauge couplings in $\mathcal{N} = 1$ SQCD + SQED, Eur. Phys. J. C **85** (2025) no.5, 540.

45. A. L. Kataev, K. V. Stepanyantz: Exact Relations between Running of α_s and α in $\mathcal{N}=1$ SQCD + SQED, JETP Lett. **121** (2025) no.5, 315–319.
46. M. A. Shifman: Little miracles of supersymmetric evolution of gauge couplings, Int. J. Mod. Phys. A **11** (1996), 5761–5784.
47. D. Korneev, D. Plotnikov, K. Stepanyantz, N. Tereshina: The NSVZ relations for $\mathcal{N}$ = 1 supersymmetric theories with multiple gauge couplings, JHEP **10** (2021), 046.
48. S. L. Adler: Some Simple Vacuum Polarization Phenomenology: $e^+e^- \to$ Hadrons: The μ - Mesic Atom x-Ray Discrepancy and g_μ^{-2}, Phys. Rev. D **10** (1974), 3714–3728.
49. D. Rystsov, K. Stepanyantz: All-loop renormalization group invariants for the MSSM, Phys. Rev. D **111** (2025) no.1, 016012.
50. I. Jack, D. R. T. Jones, A. F. Kord: Snowmass benchmark points and three-loop running, Annals Phys. **316** (2005), 213–233.
51. P. S. Howe, G. Sierra, P. K. Townsend: Supersymmetry in Six-Dimensions, Nucl. Phys. B **221** (1983), 331–348.
52. P. S. Howe, K. S. Stelle, P. C. West: N=1 d = 6 harmonic superspace, Class. Quant. Grav. **2** (1985), 815.
53. B. M. Zupnik: Six-dimensional Supergauge Theories in the Harmonic Superspace, Sov. J. Nucl. Phys. **44** (1986), 512.
54. E. A. Ivanov, A. V. Smilga: Conformal properties of hypermultiplet actions in six dimensions, Phys. Lett. B **637** (2006), 374–381.
55. I. L. Buchbinder, N. G. Pletnev: Construction of 6D supersymmetric field models in N=(1,0) harmonic superspace, Nucl. Phys. B **892** (2015), 21–48.
56. A. Galperin, E. Ivanov, S. Kalitzin, V. Ogievetsky, E. Sokatchev: Unconstrained N=2 Matter, Yang-Mills and Supergravity Theories in Harmonic Superspace, Class. Quant. Grav. **1** (1984), 469–498.
57. A. S. Galperin, E. A. Ivanov, V. I. Ogievetsky, E. S. Sokatchev: *Harmonic superspace*, Cambridge Univ. Pr., UK, (2001).
58. I. L. Buchbinder, A. S. Budekhina, E. A. Ivanov, K. V. Stepanyantz: Structure of divergences in the higher-derivative supersymmetric 6D gauge theory, Phys. Rev. D **111** (2025) no.12, 125014.
59. E. A. Ivanov, A. V. Smilga, B. M. Zupnik: Renormalizable supersymmetric gauge theory in six dimensions, Nucl. Phys. B **726** (2005), 131–148.
60. A. V. Smilga: Chiral anomalies in higher-derivative supersymmetric 6D theories, Phys. Lett. B **647** (2007), 298–304.
61. L. Casarin, A. A. Tseytlin: One-loop β-functions in 4-derivative gauge theory in 6 dimensions, JHEP **08** (2019), 159.
62. I. L. Buchbinder, E. A. Ivanov, B. S. Merzlikin, K. V. Stepanyantz: Supergraph calculation of one-loop divergences in higher-derivative 6D SYM theory, JHEP **08** (2020), 169.
63. I. L. Buchbinder, E. A. Ivanov, B. S. Merzlikin, K. V. Stepanyantz: The renormalization structure of 6D, $\mathcal{N} = (1, 0)$ supersymmetric higher-derivative gauge theory, Nucl. Phys. B **961** (2020), 115249.

Bled Workshops
in Physics
Vol. 26, No. 1

Proceedings of the 28th Workshop
What Comes Beyond . . . *(p. 344)*
Bled, Slovenia, July 6–17, 2025

24 Formation and Evolution of Antimatter Objects

Sattvik Yadav[†]

National Institute of Science Education and Research, India

Abstract. The fundamental question of baryogenesis and the problem of matter-antimatter asymmetry motivates this study into the formation and evolution of antimatter objects in the early universe. We hypothesize the existence of isolated antimatter domains in a baryon-asymmetric universe that survive until the era of first star formation ($Z \approx 20$). By assuming CPT-symmetry, the thermodynamics, mechanics, and energy dynamics of an antimatter gas cloud (composed of antihydrogen and antihelium) are treated symmetrically to their primordial matter counterparts. Analysis demonstrates the physical feasibility of the gravitational collapse process for a conservatively estimated antimatter domain ($\approx 5 \times 10^3 M_\odot$). The initial conditions easily satisfy the Jeans and Bonnor-Ebert mass criteria, indicating a high propensity for instability and run-away collapse. The subsequent dynamical evolution, driven by $\bar{H}_2$ cooling, is predicted to proceed identically to that of Population III star formation, leading to the formation of a dense, adiabatic anti-protostellar core. The theoretical viability of a true antistar hinges upon a critical assumption: the physical possibility of anti-nuclear fusion (e.g., anti-proton cycle) under the extreme core conditions. Assuming this symmetry holds, the collapse is predicted to yield massive Antistars ($\gtrsim 22 M_\odot$). This suggests that if antimatter domains formed in the early universe, they likely underwent stellar formation. Observational constraints on the existence of these objects must rely on the detection of characteristic high-energy γ-ray or X-ray signals resulting from matter-antimatter annihilation at the domain boundaries or during mass accretion.

Povzetek: Avtor študira vzrok za asimetrijo snovi in antisnovi v vesolju. Pri predpostavki, da so v zgodnjem vesolju, vse do nastanka prvih zvezd ($Z \approx 20$), obstojale izolirane domene antisnovi in da je simetrija CPT simetrija vesolja, so termodinamika, mehanika in energijska dinamika v domeni antisnovi (sestavljene iz antivodika in antihelija) veljale tako kot v domeni snovi. Avtor obravnava gravitacijski kolaps za domeno antimaterije velikosti, $\approx 5 \times 10^3 M_\odot$, ki ustreza Jeansovemu in Bonnor-Ebertovemu pogoju, ki kaže na veliko nagnjenost snovi k nestabilnosti in nekontroliranemu kolapsu. Evolucija antisnovi je tedaj podobna evoluciji zvezd, vse do nastanka masivnih anti-zvezd. Anihilacija snovi in anti-snovi povzroči visokoenergijske žarke γ in rentgenskih žarkov.

24.1 Introduction

The problem of baryon-asymmetry in the present universe is a prominent field study today. Theories developing upon the universe having equal amount of matter and antimatter

[†]sattvik.yadav@niser.ac.in

from the in early stages of universe fail to reach the present observed number density of matter in the universe. Modern cosmology now has shown that there indeed exist a baryon asymmetry in the universe.

The study presented in this report finds its basis by considering existence of regions of antimatter in a baryon-asymmetric universe called the antimatter domains. These are proposed to form in early stages of universe (at age of universe $\leq 10^{-6}$) through a phase transition which separate out matter and antimatter. Key features of these regions is the annihilation happening only at the boundary of these region. Thus as these regions evolve in time, particles at the boundary interact and annihilate. These are proposed to be of size upto $\sim 10^{12} M_{\odot}$ taking into account that there is continuous coalescing of different antimatter domains and these domains survive till the period of hydrogen recombination (or antihydrogen in this case) [1].

Thus if existence of such regions are possible, whether there is possibility of structure formation inside these regions is probed in this study. It covers the gas clouds and move to viability of star formation. Primary focus is upon such structures in the era of early universe at an age $\sim 10^{13}$sec (Redshift $Z \approx 20$), because this period has pressure and temperature considered viable for formation of first stars and possibly antistars. Note that the thermodynamics of antimatter is considered symmetric to the matter. This means that for a macroscopic region of antimatter, the laws of thermodynamics hold for them. In other words Equations 22.1 and 22.2 hold for antimatter regions.

$$dU = \delta Q - \delta W \tag{24.1}$$

$$S = \frac{Q_{rev}}{T} \tag{24.2}$$

Antimatter is currently considered to be CP invariant though theories also exist classifying the matter-antimatter thermodynamics and giving us the temperature measure for anti-matter by a observer in matter universe to be negative. This would affect the second law of thermodynamics (Equation 22.2), though the first law (Equation 22.1) would remain unaffected as it concerns itself with energy of the system which is positive for both matter and antimatter alike. Proceeding with the CP-invariant thermodynamics, the sections in the report are structured by first a physical description in terms of matter and the viability of that physics in the antimatter.

24.2 Initial Condition for Star Formation

The process of star formation greatly depends upon initial conditions the cloud of matter has from which the star is born. For analysis of antimatter, instead of considering the amount of antimatter possible in the domains as mentioned before, pessimistically consider this region to have a total mass of $\approx 10^5 M_{\odot}$. This include the mass of antimatter and dark matter. Assuming Λ-CDM universe, the matter to dark matter ratio in these domains (or gas clouds) is extend this to antimatter as well. This implies that for such antimatter domains present in a Λ-CDM universe, the percentage by mass of the antimatter present is 5% and the rest is filled by the dark matter. Thus, net antimatter available for the star formation is $\approx 5 \times 10^3 M_{\odot}$. The antimatter domain is assumed to have no matter domains surrounding it, thus no interaction occurs at the boundaries.

Now consider the evolution of matter counterpart of antimatter. In the early universe

at $Z \approx 20$, condensed regions of matter has already formed with an average number density of domains is $\sim 10^5 cm^{-3}$ and a temperature of 1000K [2]. These condense regions are stabilized by to primary opposing forces, the gravitational force acting inwards and the pressure exerted by the particles acting outwards. These regions at start primarily contained species such as e^-, H, H^-, H^+, He, He^+, He^{++}, H_2, H_2^+. Other molecular species are present but in trace quantities.

A gas under hydrostatic equilibrium requires it to follow the condition in Equation 22.3. These domains have the density low enough so that the gas present in the domain can be approximated to be ideal gas. These domains thus will also be referred as gas clouds of matter or (antimatter when specified). Here we assume spherical symmetry of the gas cloud which at start is isothermal. P is the local pressure, ρ is the local density, ϕ is the gravitational potential energy and r is the radial distance from center of gas cloud. This combined with the Poisson's equation (Equation 22.4) gives a description of the relation between different mechanical and thermodynamic quantities for a gas cloud in hydrostatic equilibrium.

$$\frac{dP}{dr} = -\frac{d\phi}{dr}\rho \tag{24.3}$$

$$\frac{1}{r^2}\frac{d}{dr}\left(r^2\frac{d\phi}{dr}\right) = 4\pi G\rho \tag{24.4}$$

To fully solve this system to find P, ϕ and ρ we require another equation. This a model function which describes the relation between P and ρ.

$$P = K\rho^{\gamma} \equiv K\rho^{1+\frac{1}{n}} \tag{24.5}$$

This is called the polytropic relation. K, γ and n are constants. Note that for properly chosen values of γ and K, it gives us the ideal gas equation. Assuming the gaseous constituents form a mixture of ideal gas and region encompassed is very large, this gives us the choice of $n \to \infty$. Thus solving equations 22.3, 22.4 and 22.5, we get the Lane-Emden Equation (22.6)

$$\frac{d^2w}{dz^2} + \frac{2}{z}\frac{dw}{dz} = e^{-w} \tag{24.6}$$

Where,

$$z = Ar \ , \ A^2 = \frac{4\pi G\rho_c}{K} \ , \ \phi = Kw \tag{24.7}$$

ρ_c is the central density. This differential equation is solved using the boundary condition by setting the central potential and central force 0. This equation was numerically solved, the results to which are shown in the Figure 22.1.

At a macroscopic level, the thermodynamic quantity most relevant to us is the mean molecular mass (μ) of the particles in gas cloud which is given by Equation 22.8. This applies for the period of universe considered as the temperatures were high enough for most of the atoms to be ionized. Z_i are the atomic number of the species, which corresponds to the free electrons for a neutral but ionised gas cloud and the μ_i is its molecular mass. For present universe, where in such gas clouds neutral atoms are present thereby Z_i factor is absent.

$$\mu = \left(\sum_i \frac{X_i(1+Z_i)}{\mu_i}\right)^{-1} \tag{24.8}$$

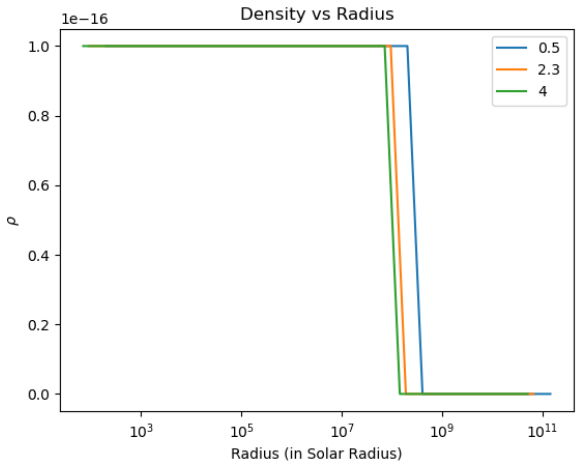

Fig. 24.1: The figure show the variation of density of a cloud with ideal gas (for ideal gas, $n \to \infty$). The gas in the primordial clouds can be approximately considered as an ideal gas, since a low density gas occupy a large volume. The figure is obtained through plotting the Lane-Emden equation. Here diffenently coloured lines corresponds to different value of the mean molecular mass μ. Blue line with $\mu = 0.5$ models the early universe, orange line with $\mu = 2.3$ models an average cloud in current universe and green line with $\mu = 4$ shows clouds with high metallicity. For a stable gas cloud with same boundary ccondition, we see that the clouds were significatly bigger in the early universe.

24.3 Process of Star Formation

24.3.1 Onset of Collapse

The initialization of collapse process happens when there are perturbation in the gas cloud. This perturbation may or may not lead to collapse depending upon the nature of perturbation or equivalently, the mass of matter upon which this perturbation is acting on. These perturbations in the gas cloud travel as sound wave, and have a finite time of propagation. In our current universe, these are produced by the shock waves emitted in supernovas and other highly energetic events. But in the early universe, such disturbances can be produced due to high energy particles or annihilation events, thus paving way for star formation. In terms of mass, the minimum mass of gas required such that a perturbation of sufficient energy is enough to start a run collapse (keeping the assumptions used before) is given by the Jeans' condition

$$M_J = 1.1 M_\odot \left(\frac{T}{10K}\right)^{\frac{3}{2}} \left(\frac{\rho}{10^{-19} g cm^{-3}}\right)^{-\frac{1}{2}} \left(\frac{\mu}{2.3}\right)^{-\frac{3}{2}} \tag{24.9}$$

A more detailed calculation through a better boundary condition encompassing the finite gas cloud gives us the Bonnor-Ebert condition [8]

$$M_B E = 1.18 \frac{R_H^2}{\mu^2 G^{\frac{3}{2}}} T^2 (P^*)^{-\frac{1}{2}} M_\odot \tag{24.10}$$

For gas with lesser mass than this limit, the perturbation form a stable wave and propagate without causing a collapse. Upon calculation using the initial conditions mentioned in the previous section we get the following mass values

μ	**Jeans Mass (in $M_\odot$)**	**Bonnor-Ebert Mass (in $M_\odot$)**
0.5	5581.491579	5689.938953
2.3	565.735623	1236.943251
4.0	246.669409	711.242369

Table 24.1: Calculated values for the Jeans Mass (JM) and Bonnor Ebert Mass (BEM) for different values of the mean molecular mass μ. We note that the collapse mass required is approximately equal to the JM and BEM of the initial gas cloud of antimatter taken. The $\mu = 0.5$ value is the mean molecular mass calculated for antimatter based upon the chemical abundance of the species mentioned earlier and by considering atomic hydrogen in majority.

Once the process of collapse starts, the gas cloud radiates energy. Due to extremely low opacity gas in the cloud in the early universe, as it primarily consisted of species of hydrogen and helium, the rate of cooling is very high. This cools the gas cloud from an initial temperature of 1000K till 200K. The energy radiated is primarily provided by highly exothermic reaction forming H_2 from H^-. It goes as follows:

$$H + e^- \rightarrow H^- + h\nu$$
$$H^- + H \rightarrow H_2 + e$$

This reaction also becomes the primary source of formation of large amount of H_2 in the early universe and for the sharp reduction of the temperature of clouds.

24.3.2 Collapse of Gas Cloud

Once the collapse start, the system is no longer in an equilibrium. Note that even though cooling of gas is occuring along its collapse, the process can still be considered quasi-isothermal. This is so because the net time required for the gas to free fall to the central point is 10^7 years, which is even greater considering the pressure acting from the gas. On the other hand, the time taken for the gas to reach thermal equilibrium is 10 years which is much less that it. Thus the isothermal assumption is safe to assume for long timescales of collapse. For describing this dynamical system, we have the following equations. From the conservation of mass in a volume element in the cloud, we have the continuity equation

$$\frac{\partial m}{\partial t} + 4\pi r^2 v \rho = 0 \tag{24.11}$$

Second, we have from the Newton's Laws of motion for element of mass m. Since the equilibrium is broken, the forces acting will be unbalanced and thus a net acceleration given by

$$m\frac{d\vec{v}}{dt} = \vec{F}_{Gravitational} + \vec{F}_{Pressure} \tag{24.12}$$

Third, conservation of angular momentum,

$$\vec{N} = \sum_{\text{over all elements}} \vec{r_i} \times (\vec{F}_{Gravitational} + \vec{F}_{Pressure}) \tag{24.13}$$

Fourth, is the local change in the energy,

$$\frac{du}{dt} + P\frac{d}{dt}\left(\frac{1}{\rho}\right) + \frac{1}{4\pi\rho r^2}\frac{\partial \Lambda}{\partial r} \tag{24.14}$$

Here Λ is the rate of cooling of the gas. This quantity is very hard to construct analytically as the it depend upon the opacity, density and chemical nature of various species present in the cloud. Some theoretical calculation and numerical fitting corrections over experimental data obtained in the laboratory gives us the estimate of this cooling as follows [4]

$$\Lambda_{LTE} = \Lambda_{rot} + \Lambda_{vib} \tag{24.15}$$

$$\Lambda_{rot} = \frac{9.5 \times 10^{-22}(T_3)^{3.76}}{1 + 0.12(T_3)^{2.1}} e^{-\left(\frac{0.13}{T_3}\right)^3} + 3 \times 10^{-24} e^{-\left(\frac{0.51}{T_3}\right)} \tag{24.16}$$

$$\Lambda_{rot} = 6.7 \times 10^{-19} e^{-\left(\frac{5.86}{T_3}\right)} + 1.6 \times 10^{-18} e^{-\left(\frac{11.7}{T_3}\right)} \tag{24.17}$$

Here $T_3 = \frac{T}{1000K}$. Λ_{LTE} is the Local Thermodynamic Cooling which is due to the de-excitation of different species from a higher energy state to a lower state. Along with this, we also have contribution by Emission due to Collision of atoms. It depends upon the temperature and pressure of gas. Approximate numerically modeled function is given as follows [5]

$$\Lambda_{CIE} = 10^{-116.6+96.34logT-47.153(logT)^2+10.744(logT)^3-0.916(logT)^4} \tag{24.18}$$

Using there functions, the process of gas cloud made up of matter has been simulated by studies [2].

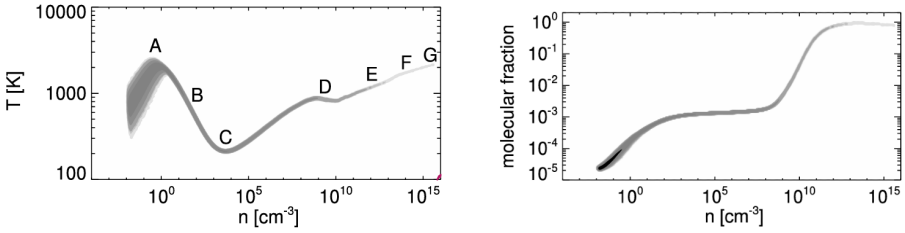

Fig. 24.2: Variation of the temperature and molecular fraction with the increase in number density as simulated for primordial matter stars.

As the process of collapse goes on, when the number density of about $10^9 cm^{-3}$ is reached, the rate of H_2 formation is further enhanced. This is due conditions being right for the 3-body reaction of H to start.

$$H + H + H \rightarrow H_2 + H$$

$$H_2 + H \rightarrow 2H_2$$

While at this stage in the current universe, the gas is opaque enough to trap the heat thereby reducing the rate of cooling, since the clouds in early universe were still lacked opacity, the cooling and the rate of collapse was still very high. When the number density reach $10^{12} cm^{-3}$ the gas finally starts becoming opaque to the outgoing radiation and thus the temperature of the gas cloud also starts increasing as seen in the figure [ref]. The inner regions of this cloud are shielded the most by increased opacity of the outer layers of the collapsing cloud. These regions later form the core of the star, now follows an adiabatic process instead of an quasi-isothermal one. The core temperature also becomes high enough to ionise the molecular species to the atomic ones.

24.3.3 Protostar Formation and Main Sequence

Once this reionisation occurs of molecular species, in the adiabatic conditions of the core has the tendancy to have nuclear fusion. Presence of two cycles are key for the nuclear burning which are shown in the Figure 22.3.

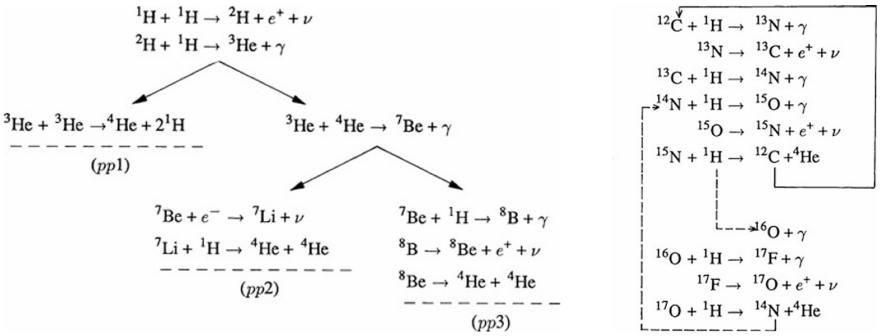

Fig. 24.3: The following figure shows the major nuclear reactions that start to occur in the core during the nuclear burning. The set of reactions on the left is the ones that start first. The set of reactions on the right is the one that becomes dominant after an increase in metallicity due to fusion reactions.

In this stage of cycle, nuclear burning is starting in certain areas of the core while in-falling of matter still occurs. This is called the protostellar stage and the adiabatic core with radiating surrounding gas is enveloped by a region (or more precisely a disc) matter. Now for this protostar to develop in an actual star, the temperature and pressure should be right. The phenomenon of a protostar core becoming degenerate and failing to ignite is the defining characteristic of brown dwarf formation. During the early stages of evolution, a protostar contracts and must release gravitational energy, leading to heating of its central core, following the typical behavior of an ideal gas sphere. If the central material consists of an ideal gas, further contraction leads to higher temperatures. the equation governing this is

$$\frac{dT_c}{T_c} = \frac{4\alpha - 3}{3\delta} \frac{d\rho_c}{\rho_c} \tag{24.19}$$

For the core which remains ideal and thus transition to have nuclear fusion have $\alpha = \delta = 1$. However, if the protostar's mass is too low, the central density increases rapidly enough that the electron gas becomes degenerate before the core can reach the necessary temperature for stable hydrogen burning (approximately 10^7 K). When degeneracy dominates the equation of state, the pressure support becomes effectively independent of the core temperature. This transition to degenerate matter removes the core's ability to self-regulate. Without this mechanism, the contraction ceases to cause the necessary continuous heating, effectively halting the evolutionary track at a maximum temperature that is too low for fusion. The object, unable to achieve the thermal equilibrium characteristic of true stars, is supported purely by the non-thermal pressure of the degenerate electrons and begins to cool, settling as a brown dwarf. Based upon this density and temperature, the calculation done gives us the minimum mass of the protostar to be $0.08M_\odot$.

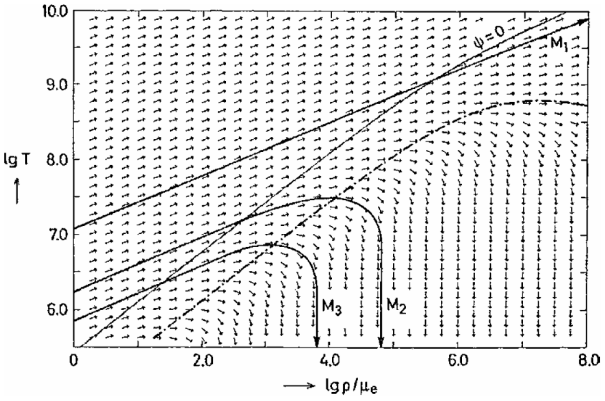

Fig. 24.4: Graph showing the region determining whether the core becomes degenerate or not. The graph plots the Equation 22.19. There is existence of two regions. One in the bottom right is due to the creation of electron degeneracy and thus represents a region where if the curve of stellar evolution enters, the star forms a brown dwarf [3].

Note that for stars in early universe, due to high infalling matter the mass of the protostars results from the initial conditions to be approximately $1M_\odot$ which is larger than what is required for protostar to go to main sequence [6]. One the star reaches this stage high amount of nuclear burning starts which creates a strong radiation feedback. This stops and blows away further infall of the matter. Various studies using similar initial condition but with much more refined physics have given approximation or bounds over the value of the star formed after the end of star formation process in the early universe. Yoshida et. al. [2] gives $\approx 100M_\odot$, Yoshida et. al. [6] gives $\approx 42M_\odot$ and Stacy et. al [7] gives a lower bound $\geq 22M_\odot$.

24.4 Case of Antimatter

Shifting the focus back to antimatter. Due to the symmetric nature with matter in terms of thermodynamics, mechanics and energy dynamics, since all the processes before the protostar formation and the main sequence depends on these quantities, for domains of

antimatter, such process is feasible. Note that the possibility of atomic antihydrogen reaction similiar to that of hydrogen is assumed here. The major hurdle occurs when we consider the start of nuclear burning in the protostar. For its antimatter counterpart, existence of such reactions is still under study. Thus if such reactions are possible, even though the initial conditions were pessimistic value, such antistars may be possible. Note that this study considers a lot of assumptions, relaxing those is still under study. Nevertheless initial values are promising for search of such stars in the universe.

24.5 Feasibility

24.5.1 Detection of Antistars

For detection of such structure in the universe, we can again look at the stages and properties of antistars. The existence of possible antistellar depends upon their detection from the data we obtain. Search for matter-antimatter annihilation products include high energy gamma ray radiation or possible transitions of certain species such as $\mathrm{p\bar{p}}$, $\mathrm{p\bar{H}e}$ or $\mathrm{He\bar{H}e}$ in X-Ray regime [9] [11].

24.5.2 Possibility of Such Stars

Feasibility of such antistars also depend upon whether there is a possibility of such stars in matter regime. There is no direct observational data for these first stars as due to the age of the universe and their large size, they would have had a short lifespan. At the same time, second generation of stars have been observed with very low metallicity and very high mass, hinting to the possibility of such massive stars .

24.6 Conclusion

The study systematically explored the viability of antistar formation within hypothesized antimatter domains in a baryon-asymmetric universe. By assuming CP-invariant thermodynamics, the physics of antihydrogen and antihelium gas clouds was treated symmetrically to their well-studied matter counterparts.

The analysis shows that the initial conditions for star formation in the early universe, specifically at $Z \approx 20$, are highly conducive to the collapse of antimatter gas clouds. Using the properties of primordial matter clouds ($\mu \approx 0.5$, $T \approx 1000$ K, $\rho \sim 10^5$ cm^{-3}), the calculated Jeans Mass ($M_J \approx 5581 M_\odot$) and Bonnor-Ebert Mass ($M_{BE} \approx 5690 M_\odot$) for $\mu = 0.5$ are remarkably close to the conservatively estimated total antimatter mass available for collapse ($\approx 5 \times 10^3 M_\odot$). This suggests that if antimatter domains of the size and density described exist, they satisfy the mass requirement for gravitational instability and subsequent collapse.

Furthermore, the processes driving collapse—cooling via $\bar{H}_2$ formation, the transition to three-body reactions, and the eventual onset of opacity at high densities—are governed by fundamental laws of thermodynamics and gravity that are assumed to hold true for antimatter. This symmetry strongly suggests that the dynamical evolution would proceed identically to that of primordial matter protostars, leading to the formation of massive antistars with predicted masses in the range of $\gtrsim 22 M_\odot$ [7]. Crucially, these massive objects would successfully overcome the electron degeneracy pressure to ignite nuclear fusion.

The entire collapse, from the onset of instability through the quasi-isothermal phase driven by $\bar{H}_2$ cooling to the formation of an opaque, adiabatic protostar core, is robustly feasible due to the symmetry in thermodynamics and mechanics. The formation of a stable, long-lived antistar, however, hinges critically on one key assumption: the feasibility of anti-nuclear fusion (e.g., anti-proton-anti-proton cycle) occurring under the high-temperature and high-pressure conditions of the anti-protostellar core.

While the feasibility of detecting antistars remains highly challenging, future searches for high-energy gamma-ray and X-ray annihilation signatures, particularly at the boundaries of gas clouds and during phases of mass accretion onto antistars, represent the only immediate avenue for observational proof. The confirmation of such massive stellar-sized antimatter objects would not only validate models of early-universe phase transitions but would also provide a crucial empirical constraint on the symmetry of the laws governing nuclear energy generation.

Acknowledgments

I would like to thank Prof. Dr. Maxim Yu. Khlopov and the entire organising committee for giving me an opportunity to present in the Bled Workshop 2025. This has been a wonderful opportunity for me to get more insight to this work as well as to know more about various fields of research by amazing speakers from across the world.

References

1. Chechetkin, V. M., Khlopov, M. Yu., & Sapozhnikov, M. G. (1982). Antiproton interactions with light elements as a test of GUT cosmology. La Rivista Del Nuovo Cimento, 5(10), 1–79.
2. Yoshida, N., Omukai, K., Hernquist, L., & Abel, T. (2006). Formation of Primordial Stars in a ΛCDM Universe. The Astrophysical Journal, 652(1), 6–25.
3. Kippenhahn, R., & Weigert, A. (2013). Stellar structure and evolution. Springer International Publishing.
4. Hollenbach, D.,& McKee, C. F. (1979). Molecule formation and infrared emission in fast interstellar shocks. I. Physical processes. The Astrophysical Journal Supplement Series, 41(3), 555–592.
5. Omukai, K. (2001). Primordial Star Formation under Far-Ultraviolet Radiation. The Astrophysical Journal, 546(2), 635–651.
6. Yoshida, N., Hosokawa, T., & Omukai, K. (2012). Formation of the first stars in the universe. Progress of Theoretical and Experimental Physics, 2012(1), 01A305.
7. Stacy, A., Greif, T. H., & Bromm, V. (2012). The first stars: Mass growth under protostellar feedback. Monthly Notices of the Royal Astronomical Society, 422(1), 290–309.
8. Larson, R. B. (1969). Numerical Calculations of the Dynamics of a Collapsing Proto-Star. Monthly Notices of the Royal Astronomical Society, 145(3), 271–295.
9. Blinnikov, S. I., Dolgov, A. D., & Postnov, K. A. (2015). Antimatter and antistars in the Universe and in the Galaxy. Phys. Rev. D, 92(2), 023516.
10. Khlopov, M. Y., Rubin, S. G., & Sakharov, A. S. (2000). Possible origin of antimatter regions in the baryon dominated universe. Phys. Rev. D, 62(8), 083505.
11. Dupourqué, S., Tibaldo, L., & von Ballmoos, P. (2021). Constraints on the antistar fraction in the Solar System neighborhood from the 10-year Fermi Large Area Telescope gamma-ray source catalog. Physical Review D, 103(8), 083016.

Bled Workshops
in Physics
Vol. 26, No. 1

Proceedings of the 28th Workshop
What Comes Beyond . . . *(p. 354)*
Bled, Slovenia, July 6–17, 2025

25 PBH-Catalyzed Phase Transitions and Gravitational Waves: Insights from PTA Data

Jiahang Zhong[†]

Department of Astronomy, School of Physical Sciences, University of Science and Technology of China, Hefei 230026, China;
CAS Key Laboratory for Research in Galaxies and Cosmology,School of Astronomy and Space Science, University of Science and Technology of China, Hefei 230026, China

Abstract. We investigate how primordial black holes (PBHs) can catalyze first-order phase transitions (FOPTs) in the early universe, thereby modifying the resulting gravitational wave (GW) signals. Through analysis of pulsar timing array (PTA) data, particularly the NANOGrav 15-year dataset, we examine the compatibility of asteroid-mass PBH dark matter with phase transition interpretations of the observed stochastic gravitational wave background (SGWB). Our results demonstrate that high PBH number densities can significantly suppress GW signals, posing challenges for the PBH dark matter hypothesis in specific mass ranges.
Povzetek: Avtor raziskuje, kako prvobitne črne luknje (PBH) katalizirajo fazne prehode prvega reda (FOPT) v zgodnjem vesolju in vplivajo na signale gravitacijskih valov (GW). Z analizo podatkov časovnega niza pulsarjev (PTA), zlasti 15-letnega nabora podatkov NANOGrav, preučuje ali lahko stohastično izmerjeno gravitacijsko valovnje ozadja (SGWB) pojasni obstoj temne snovi PBH z maso asteroida. Rezultati kažejo, da lahko visoka gostota prvobitnih črnih lukenj (PBH) znatno zavira signale gravitacijskih valov.

25.1 Introduction

Cosmological phase transitions [1–4] represent crucial events in the early universe's evolution, with first-order phase transitions (FOPTs) being particularly significant due to their potential to generate detectable gravitational wave (GW) signatures [5–7]. These transitions may be driven by new physics beyond the Standard Model, including dark sector theories or baryogenesis mechanisms [8]. Recent observations from pulsar timing arrays (PTAs) have revealed evidence for a stochastic gravitational wave background (SGWB) [9–13], which could potentially originate from cosmological sources such as FOPTs.
Beyond standard FOPT scenarios, the presence of primordial black holes (PBHs) [14–16] in the early universe before phase transitions occur can dramatically enhance nucleation rates for bubbles containing PBHs at their centers [17–27]. As illustrated in Fig. 23.1, this catalytic effect produces a bubble distribution distinct from conventional scenarios, consequently influencing the resulting GW spectrum. Recent studies have explored PBH-catalyzed FOPTs from various phenomenological

[†]jiahangzhong@mail.ustc.edu.cn

perspectives [28–30]. Our work focuses specifically on the PBH-dominated case, exploring the GW signatures generated by such catalyzed transitions and their ability to explain recent NANOGrav observations [9,31–33].

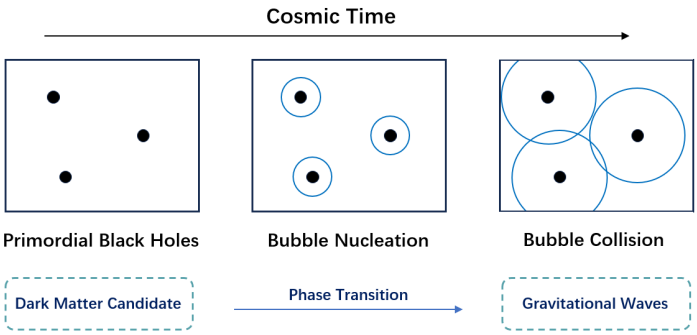

Fig. 25.1: Schematic representation of PBH-catalyzed FOPTs. PBHs serve as nucleation sites, leading to an inhomogeneous spatial distribution of vacuum bubbles.

This article is organized as follows: Section 23.2 reviews the standard formalism of FOPTs and their associated GW production mechanisms. Section 23.3 examines how PBHs catalyze phase transitions and modify GW signals. Finally, Section 23.4 assesses the compatibility of our model with NANOGrav data and discusses implications for PBH dark matter scenarios.

25.2 Cosmological Phase Transitions

First-order phase transitions occur when the universe transitions from a metastable false vacuum to a stable true vacuum state through quantum tunneling processes. This mechanism leads to the nucleation of true vacuum bubbles that subsequently expand and collide. The tunneling rate per unit volume and time is described by [34,35]:

$$\Gamma(T) \approx T^4 \left(\frac{S_3}{2\pi T}\right)^{\frac{3}{2}} \exp\left(-\frac{S_3}{T}\right), \tag{25.1}$$

where $S_3(T)$ represents the three-dimensional Euclidean action characterizing the bubble profile. The nucleation temperature T_n is defined as the temperature at which approximately one bubble nucleates per Hubble volume, satisfying $\Gamma(T_n) = H^4(T_n)$. The parameter β quantifies the inverse duration of the phase transition, while ρ_V denotes the vacuum energy density driving the transition.
Near the nucleation temperature T_n, the nucleation rate can be parameterized as:

$$\Gamma(t) = H^4(t_n) \exp(\beta(t - t_n)), \tag{25.2}$$

where t_n represents the cosmic time corresponding to T_n. Following nucleation, bubbles expand due to the pressure differential between true and false vacuum phases. In strong FOPTs, bubble wall velocities approach luminal values ($v_{wall} \sim c$), resulting in a mean bubble separation of $R_* \sim 1/\beta H$.
Gravitational wave production during FOPTs primarily arises from three mechanisms: bubble collisions, sound waves in the primordial plasma, and magnetohydrodynamic turbulence. For strong phase transitions, bubble collisions typically dominate the GW spectrum. The GW energy density can be estimated dimensionally as [7,36]:

$$\Omega_{GW} \sim \kappa^2 \left(\frac{\alpha}{1+\alpha}\right)^2 \left(\frac{\beta}{H}\right)^{-2}, \tag{25.3}$$

where $\alpha = \rho_V/\rho_{rad}$ characterizes the transition strength, and κ represents the efficiency factor for vacuum energy conversion into GWs. For strong transitions ($\alpha \gg 1$), $\kappa \sim 1$. The peak frequency of the GW spectrum scales with β.
Within the envelope approximation [37,38], the GW spectrum follows:

$$\Omega_{GW} \propto \begin{cases} k^3 & k/\beta < 1 \\ k^{-1} & k/\beta > 1 \end{cases} \tag{25.4}$$

with peak amplitude and frequency given by:

$$\Omega_{GW,peak} = 0.043 \left(\frac{\beta}{H}\right)^{-2}, \tag{25.5}$$

$$f_{GW,peak} = \frac{1.2}{2\pi}\beta. \tag{25.6}$$

25.3 PBH Catalytic Effects on Phase Transitions

Primordial black holes, potential remnants from the early universe [39,40] and candidate dark matter constituents [41–43], can significantly catalyze FOPTs by serving as preferential nucleation sites. When PBHs form before phase transitions occur, they initiate localized bubble nucleation earlier than homogeneous background processes, thereby accelerating the transition. The catalytic efficiency depends on multiple factors including PBH mass M_{PBH}, vacuum energy density ρ_V, and bubble wall tension σ_w.
We focus on the regime where PBHs strongly catalyze phase transitions, leading to bubble nucleation around PBHs near the critical temperature T_c (corresponding to cosmic time t_c). The total nucleation rate incorporates both background and PBH-induced contributions [30]:

$$\Gamma(t) = \Gamma_b(t) + \Gamma_{PBH}(t), \tag{25.7}$$

where $\Gamma_b(t) = H^4(T_n)e^{\beta(t-t_n)}$ represents the standard background rate, and $\Gamma_{PBH}(t) = n_{pbh}H^3\delta(t-t_c)$ denotes the PBH-induced component. The normalized PBH number density per Hubble volume, n_{pbh}, is given by:

$$n_{pbh}(t)H^3 = \left(\frac{a(t)}{a_0}\right)^{-3} \rho_{c,0}\Omega_{DM,0}\frac{f_{pbh}}{M_{pbh}}, \tag{25.8}$$

where f_{pbh} represents the present PBH mass fraction, $\rho_{c,0} = 3H_0^2/(8\pi G)$ is the current critical density, and $\Omega_{DM,0}$ is the current normalized dark matter density. The PBH catalytic term modifies the bubble nucleation-time distribution, promoting earlier nucleation and larger bubble formation around PBHs. This alteration affects GW signals by changing the effective transition timescale. Assuming the bubble wall velocity $v_w = 1$, the effective inverse timescale is then related to mean bubble separation:

$$\frac{\beta_e}{\beta} = \frac{R_{sep}(n_{pbh} = 0)}{R_{sep}(n_{pbh})}. \tag{25.9}$$

The mean bubble separation R_{sep} is determined by:

$$R_{sep} = (n_{bubble})^{-1/3} = \left(\int_{t_c}^{t_p} dt\, \Gamma(t) F(t)\right)^{-1/3},$$

where $F(t)$ represents the false vacuum fraction, indicating the probability that a spatial point remains in the false vacuum at time t:

$$F(t) = \exp\left(-\int_{t_c}^{t} dt' \frac{4\pi}{3} \Gamma(t') r^3(t', t)\right). \tag{25.10}$$

In the PBH-dominated regime where nucleation is primarily driven by the PBH: $\Gamma(t) \approx \Gamma_{PBH}$, we obtain:

$$\beta_e/\beta \approx 4.37 \times n_{pbh}^{1/3} \times \left(\frac{\beta}{H}\right)^{-1}. \tag{25.11}$$

The GW signal modification becomes apparent from Equation (23.3):

$$\Omega_{GW} \sim \kappa^2 \left(\frac{\alpha}{1+\alpha}\right)^2 \left(\frac{\beta}{H}\right)^{-2} \left(\frac{\beta_e}{\beta}\right)^{-2}, \tag{25.12}$$

demonstrating that the ratio β_e/β governs the overall GW amplitude modification. Consequently, in PBH-dominated scenarios, low PBH densities amplify GW signals while high densities suppress them. Within the envelope approximation, the peak GW amplitude and frequency become:

$$\Omega_{GW,peak} = 0.043 \left(\frac{\beta_e}{H}\right)^{-2}, \tag{25.13}$$

$$f_{GW,peak} = \frac{1.2}{2\pi} \beta_e. \tag{25.14}$$

25.4 Implications from PTA Stochastic Gravitational Wave Background

Recent pulsar timing array observations have provided evidence for a stochastic gravitational wave background (SGWB) [9–13]. While this signal is broadly consistent with gravitational waves from supermassive black hole binary mergers [44,45],

reconciling its amplitude with theoretical predictions remains challenging [46–49], leaving the astrophysical origin an open question. An intriguing alternative suggests the SGWB may originate from cosmological sources [32], particularly from FOPTs [50–54].

The substantial amplitude of the observed SGWB necessitates strong phase transitions to explain the signal naturally. A strong FOPT occurring near $T \sim 0.1$ GeV could potentially account for PTA observations [55]. Accounting for cosmic evolution, the present-day GW energy density redshifts to:

$$\Omega_{GW,0}h^2 \approx 1.6 \times 10^{-5} \left(\frac{g_*}{100}\right)^{-1/3} \Omega_{GW}, \tag{25.15}$$

while the peak frequency redshifts to:

$$f_{GW,0} = 1.65 \times 10^{-8} \left(\frac{f_{GW}}{H}\right) \left(\frac{T}{0.1\text{GeV}}\right). \tag{25.16}$$

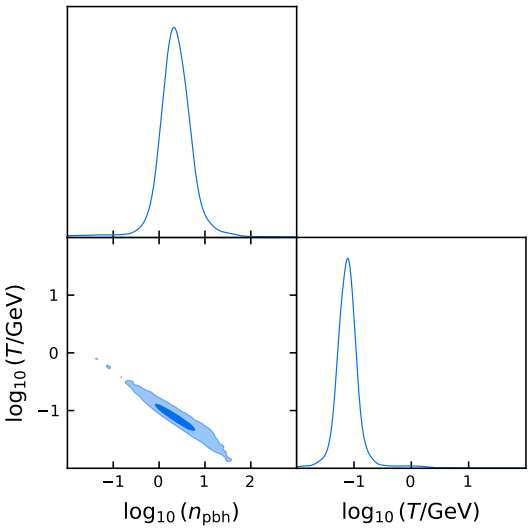

Fig. 25.2: Posterior probability distribution for PBH-catalyzed PT model fit to the NANOGrav 15-year dataset. The 1σ and 2σ confidence regions are shown in progressively lighter blue shades.

In the previous analysis, we have quantified the catalytic effects of PBHs on PT GWs. Next, we will perform data fitting with the NANOGrav 15-year dataset [9, 31–33]. For our data analysis, we employ the PT parameters T and PBH parameter n_{pbh}. We apply the Bayesian inference method to determine the best fit of bubble collision GW spectrum in catalyzed PTs. We adopt the **ptarcade** [56] to sample the posterior probability. The priors of the PT temperature T and PBH density parameter n_{pbh} follow log-uniform distributions within $\log_{10}(T/\text{GeV}) \in [-2, 2]$

and $\log_{10}(n_{pbh}) \in [-2, 3]$, respectively. Bayesian inference using NANOGrav data yields best-fit parameters and 1σ uncertainties for the PBH-catalyzed model:

$$\log_{10} n_{pbh} = 0.349^{+0.322}_{-0.303}, \quad \log_{10}(T/\text{GeV}) = -1.116^{+0.165}_{-0.163}. \tag{25.17}$$

Figure 23.2 displays the posterior distribution for parameters n_{pbh} and T. We can see that the PT temperature aligns with the standard PT case $T \sim 0.1$GeV. The best-fit PBH number per Hubble volume $n_{pbh} \sim 2$ seems very high for PBH formation, where the probability for one hubble patch to form a PBH is usually below 10^{-5}. However, for those PBH formed long before $T \sim 0.1$GeV, the probability to find a PBH in the hubble patch increases due to cosmic expansion.
The normalized PBH number density at $T \sim 0.1$ GeV is:

$$n_{pbh}(T) \approx 1.3 \times 10^{-8} \left(\frac{M_\odot}{M_{PBH}}\right) \left(\frac{f_{PBH}}{1.0}\right) \left(\frac{0.1\text{ GeV}}{T}\right)^3 \left(\frac{g_*}{100}\right)^{-1/2}. \tag{25.18}$$

For asteroid-mass PBHs ($10^{-16} - 10^{-12} M_\odot$) comprising all dark matter, n_{pbh} reaches high values, leading to suppressed GW signals. Figure 23.3 illustrates the best-fit n_{pbh} value within the M_{PBH}-f_{PBH} parameter space.

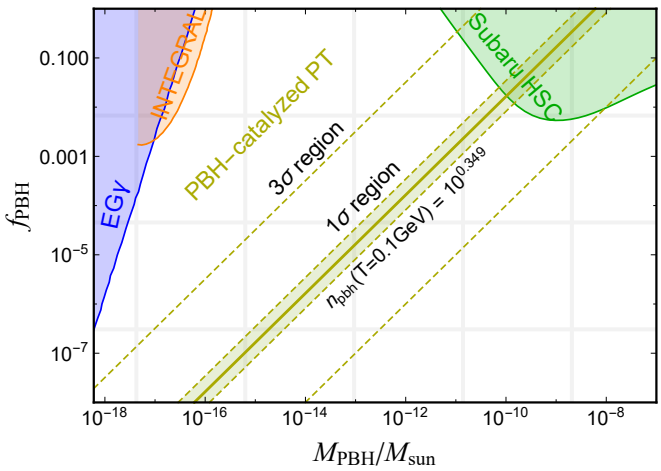

Fig. 25.3: Best-fit n_{pbh} values in the M_{PBH}-f_{PBH} parameter space, assuming $T = 0.1$ GeV. Current constraints from SUBARUHSC [57,58], extragalactic gamma-rays from Hawking evaporation (EG γ) [59], and INTEGRAL gamma-ray observations (INT) [60] are included for comparison.

Our analysis reveals that the best-fit n_{pbh} corresponds to low PBH mass fractions f_{PBH} in the asteroid-mass range. This implies that if the PTA signal originates from PBH-catalyzed phase transitions, PBHs cannot constitute all dark matter within the asteroid-mass window. Instead, only a small fraction of dark matter can exist as asteroid-mass PBHs. This conclusion aligns with previous analyzes incorporating both background and PBH contributions to catalyzed phase transitions [30].

25.5 Conclusions and Discussion

The catalytic influence of PBHs on FOPTs substantially modifies resulting GW signals, with significant implications for dark matter scenarios and early universe cosmology. In this work, we focus on PBH dominated case, where the FOPT is mainly driven by PBHs. We found that the relationship between PBH number density and the GWs amplitude is quite simple (Eq. (23.11) and Eq. (23.13)). After fit to NANOGrav data, our analysis demonstrates that asteroid-mass PBHs comprising all dark matter are largely incompatible with phase transition interpretations of PTA data. This result agrees with previous work, but the method develope in this study is simpler and more direct. In this work, we only consider PBHs as catalysts, and it is straightforward to apply our formalism to other cases of impurity-catalyzed FOPTs.
We conclude by emphasizing that, while the consequences of standard FOPTs have been extensively studied, compact objects in the early universe (like PBHs) present new opportunities to significantly change the PT scenarios.

25.6 Acknowledgements

We acknowledge Maxim Khlopov and the organizers of the 28th Workshop 'What Comes Beyond the Standard Models?' for the chance to deliver a presentation, and we are grateful to all participants for the stimulating discussions. This work was supported by the National Natural Science Foundation of China (125B1023).

References

1. J. M. Cline and P.-A. Lemieux, *Electroweak phase transition in two higgs doublet models*, *Phys. Rev. D* **55** (Mar, 1997) 3873–3881.
2. M. Losada, *High temperature dimensional reduction of the mssm and other multiscalar models in the* $\sin^2\theta_W = 0$ *limit*, *Phys. Rev. D* **56** (Sep, 1997) 2893–2913.
3. D. Bodeker, P. John, M. Laine and M. G. Schmidt, *The Two loop MSSM finite temperature effective potential with stop condensation*, *Nucl. Phys. B* **497** (1997) 387–414, [hep-ph/9612364].
4. M. Laine, *Effective theories of MSSM at high temperature*, *Nucl. Phys. B* **481** (1996) 43–84, [hep-ph/9605283].
5. E. Witten, *Cosmic Separation of Phases*, *Phys. Rev. D* **30** (1984) 272–285.
6. C. J. Hogan, *Gravitational radiation from cosmological phase transitions*, *Mon. Not. Roy. Astron. Soc.* **218** (1986) 629–636.
7. P. Athron, C. Balázs, A. Fowlie, L. Morris and L. Wu, *Cosmological phase transitions: From perturbative particle physics to gravitational waves*, *Prog. Part. Nucl. Phys.* **135** (2024) 104094, [2305.02357].
8. D. E. Morrissey and M. J. Ramsey-Musolf, *Electroweak baryogenesis*, *New J. Phys.* **14** (2012) 125003, [1206.2942].
9. NANOGrav collaboration, G. Agazie et al., *The NANOGrav 15 yr Data Set: Evidence for a Gravitational-wave Background*, *Astrophys. J. Lett.* **951** (2023) L8, [2306.16213].
10. International Pulsar Timing Array collaboration, G. Agazie et al., *Comparing Recent Pulsar Timing Array Results on the Nanohertz Stochastic Gravitational-wave Background*, *Astrophys. J.* **966** (2024) 105, [2309.00693].

11. EPTA, InPTA: collaboration, J. Antoniadis et al., *The second data release from the European Pulsar Timing Array - III. Search for gravitational wave signals*, *Astron. Astrophys.* **678** (2023) A50, [2306.16214].
12. H. Xu et al., *Searching for the Nano-Hertz Stochastic Gravitational Wave Background with the Chinese Pulsar Timing Array Data Release I*, *Res. Astron. Astrophys.* **23** (2023) 075024, [2306.16216].
13. D. J. Reardon et al., *Search for an Isotropic Gravitational-wave Background with the Parkes Pulsar Timing Array*, *Astrophys. J. Lett.* **951** (2023) L6, [2306.16215].
14. Y. B. Zel'dovich and I. D. Novikov, *The Hypothesis of Cores Retarded during Expansion and the Hot Cosmological Model*, *Sov. Astron.* **10** (1967) 602.
15. S. Hawking, *Gravitationally collapsed objects of very low mass*, *Mon. Not. Roy. Astron. Soc.* **152** (1971) 75.
16. B. J. Carr and S. W. Hawking, *Black holes in the early Universe*, *Mon. Not. Roy. Astron. Soc.* **168** (1974) 399–415.
17. P. Burda, R. Gregory and I. G. Moss, *Vacuum metastability with black holes*, *Journal of High Energy Physics* **2015** (Aug., 2015) , [1503.07331].
18. D. Canko, I. Gialamas, G. Jelic-Cizmek, A. Riotto and N. Tetradis, *On the Catalysis of the Electroweak Vacuum Decay by Black Holes at High Temperature*, *Eur. Phys. J. C* **78** (2018) 328, [1706.01364].
19. R. Gregory, I. G. Moss and B. Withers, *Black holes as bubble nucleation sites*, *JHEP* **03** (2014) 081, [1401.0017].
20. R. Gregory and I. G. Moss, *The Fate of the Higgs Vacuum*, *PoS* **ICHEP2016** (2016) 344, [1611.04935].
21. R. Gregory, I. G. Moss and N. Oshita, *Black Holes, Oscillating Instantons, and the Hawking-Moss transition*, *JHEP* **07** (2020) 024, [2003.04927].
22. W. A. Hiscock, *CAN BLACK HOLES NUCLEATE VACUUM PHASE TRANSITIONS?*, *Phys. Rev. D* **35** (1987) 1161–1170.
23. K. Kohri and H. Matsui, *Electroweak Vacuum Collapse induced by Vacuum Fluctuations of the Higgs Field around Evaporating Black Holes*, *Phys. Rev. D* **98** (2018) 123509, [1708.02138].
24. I. G. Moss, *BLACK HOLE BUBBLES*, *Phys. Rev. D* **32** (1985) 1333.
25. K. Mukaida and M. Yamada, *False Vacuum Decay Catalyzed by Black Holes*, *Phys. Rev. D* **96** (2017) 103514, [1706.04523].
26. A. Strumia, *Black holes don't source fast Higgs vacuum decay*, *JHEP* **03** (2023) 039, [2209.05504].
27. N. Oshita, M. Yamada and M. Yamaguchi, *Compact objects as the catalysts for vacuum decays*, *Physics Letters B* **791** (Apr., 2019) 149–155, [1808.01382].
28. R. Jinno, J. Kume and M. Yamada, *Super-slow phase transition catalyzed by bhs and the birth of baby bhs*, *Physics Letters B* **849** (Feb., 2024) 138465, [2310.06901].
29. Z.-M. Zeng and Z.-K. Guo, *Phase transition catalyzed by primordial black holes*, *Physical Review D* **110** (Aug., 2024) L041301, [2402.09310].
30. J. Zhong, C. Chen and Y.-F. Cai, *Can asteroid-mass PBHDM be compatible with catalyzed phase transition interpretation of PTA?*, *JCAP* **10** (2025) 033, [2504.12105].
31. NANOGrav collaboration, G. Agazie et al., *The NANOGrav 15 yr Data Set: Observations and Timing of 68 Millisecond Pulsars*, *Astrophys. J. Lett.* **951** (2023) L9, [2306.16217].
32. NANOGrav collaboration, A. Afzal et al., *The NANOGrav 15 yr Data Set: Search for Signals from New Physics*, *Astrophys. J. Lett.* **951** (2023) L11, [2306.16219].
33. N. Collaboration, *Kde representations of the gravitational wave background free spectra present in the nanograv 15-year dataset*, 2023. 10.5281/zenodo.7967584.

34. A. D. Linde, *Decay of the false vacuum at finite temperature*, *Nuclear Physics B* **216** (1983) 421.
35. S. R. Coleman, *The Fate of the False Vacuum. 1. Semiclassical Theory*, *Phys. Rev. D* **15** (1977) 2929–2936.
36. A. Kosowsky, M. S. Turner and R. Watkins, *Gravitational radiation from colliding vacuum bubbles*, *Phys. Rev. D* **45** (1992) 4514–4535.
37. R. Jinno and M. Takimoto, *Gravitational waves from bubble collisions: An analytic derivation*, *Physical Review D* **95** (Jan., 2017) .
38. R. Jinno and M. Takimoto, *Gravitational waves from bubble dynamics: Beyond the envelope*, *Journal of Cosmology and Astroparticle Physics* **2019** (Jan., 2019) 060–060.
39. M. Sasaki, T. Suyama, T. Tanaka and S. Yokoyama, *Primordial black holes - perspectives in gravitational wave astronomy -*, *Classical and Quantum Gravity* **35** (Mar., 2018) 063001, [1801.05235].
40. R.-G. Cai, Y.-S. Hao and S.-J. Wang, *Primordial black holes and curvature perturbations from false vacuum islands*, *Sci. China Phys. Mech. Astron.* **67** (2024) 290411, [2404.06506].
41. B. Carr, K. Kohri, Y. Sendouda and J. Yokoyama, *Constraints on primordial black holes*, *Rept. Prog. Phys.* **84** (2021) 116902, [2002.12778].
42. B. Carr and F. Kuhnel, *Primordial Black Holes as Dark Matter: Recent Developments*, *Ann. Rev. Nucl. Part. Sci.* **70** (2020) 355–394, [2006.02838].
43. M. Y. Khlopov, *Primordial Black Holes*, *Res. Astron. Astrophys.* **10** (2010) 495–528, [0801.0116].
44. NANOGrav collaboration, G. Agazie et al., *The NANOGrav 15 yr Data Set: Constraints on Supermassive Black Hole Binaries from the Gravitational-wave Background*, *Astrophys. J. Lett.* **952** (2023) L37, [2306.16220].
45. J. Ellis, M. Fairbairn, G. Hütsi, J. Raidal, J. Urrutia, V. Vaskonen et al., *Gravitational waves from supermassive black hole binaries in light of the NANOGrav 15-year data*, *Phys. Rev. D* **109** (2024) L021302, [2306.17021].
46. J. A. Casey-Clyde, C. M. F. Mingarelli, J. E. Greene, K. Pardo, M. Nañez and A. D. Goulding, *A Quasar-based Supermassive Black Hole Binary Population Model: Implications for the Gravitational Wave Background*, *Astrophys. J.* **924** (2022) 93, [2107.11390].
47. L. Z. Kelley, L. Blecha and L. Hernquist, *Massive Black Hole Binary Mergers in Dynamical Galactic Environments*, *Mon. Not. Roy. Astron. Soc.* **464** (2017) 3131–3157, [1606.01900].
48. L. Z. Kelley, L. Blecha, L. Hernquist, A. Sesana and S. R. Taylor, *The Gravitational Wave Background from Massive Black Hole Binaries in Illustris: spectral features and time to detection with pulsar timing arrays*, *Mon. Not. Roy. Astron. Soc.* **471** (2017) 4508–4526, [1702.02180].
49. Z.-Q. Shen, G.-W. Yuan, Y.-Y. Wang, Y.-Z. Wang, Y.-J. Li and Y.-Z. Fan, *Dark Matter Spike surrounding Supermassive Black Holes Binary and the Nanohertz Stochastic Gravitational Wave Background*, 2306.17143.
50. Y. Nakai, M. Suzuki, F. Takahashi and M. Yamada, *Gravitational Waves and Dark Radiation from Dark Phase Transition: Connecting NANOGrav Pulsar Timing Data and Hubble Tension*, *Phys. Lett. B* **816** (2021) 136238, [2009.09754].
51. W. Ratzinger and P. Schwaller, *Whispers from the dark side: Confronting light new physics with NANOGrav data*, *SciPost Phys.* **10** (2021) 047, [2009.11875].
52. X. Xue et al., *Constraining Cosmological Phase Transitions with the Parkes Pulsar Timing Array*, *Phys. Rev. Lett.* **127** (2021) 251303, [2110.03096].
53. S. Deng and L. Bian, *Constraints on new physics around the MeV scale with cosmological observations*, *Phys. Rev. D* **108** (2023) 063516, [2304.06576].
54. E. Megias, G. Nardini and M. Quiros, *Pulsar timing array stochastic background from light Kaluza-Klein resonances*, *Phys. Rev. D* **108** (2023) 095017, [2306.17071].

55. J. Ellis, M. Fairbairn, G. Franciolini, G. Hütsi, A. Iovino, M. Lewicki et al., *What is the source of the PTA GW signal?*, *Phys. Rev. D* **109** (2024) 023522, [2308.08546].
56. A. Mitridate, D. Wright, R. von Eckardstein, T. Schröder, J. Nay, K. Olum et al., *PTArcade*, 2306.16377.
57. H. Niikura et al., *Microlensing constraints on primordial black holes with Subaru/HSC Andromeda observations*, *Nature Astron.* **3** (2019) 524–534, [1701.02151].
58. N. Smyth, S. Profumo, S. English, T. Jeltema, K. McKinnon and P. Guhathakurta, *Updated Constraints on Asteroid-Mass Primordial Black Holes as Dark Matter*, *Phys. Rev. D* **101** (2020) 063005, [1910.01285].
59. A. Arbey, J. Auffinger and J. Silk, *Constraining primordial black hole masses with the isotropic gamma ray background*, *Phys. Rev. D* **101** (2020) 023010, [1906.04750].
60. R. Laha, J. B. Muñoz and T. R. Slatyer, *INTEGRAL constraints on primordial black holes and particle dark matter*, *Phys. Rev. D* **101** (2020) 123514, [2004.00627].

26 DISCUSSIONS

Elia Dmitrieff, Euich Mitzani, ..

Bled workshop "What Comes Beyond the Standard Models"

26.1 The Workshop

Our Workshop is really a *workshop*, with endless and intense discussions. Some people barely reach the end of their talk, because of the many questions and comments that come up during the presentation. The topics are many and varied, everything from dark matter to the number of families, to the number of spacetime dimensions.

26.2 Elia Dmitrieff: On compactification of higher dimensions

Dear colleagues,
In my opinion, there is a reasonable explanation we can take for the compactification.
It is the same one as we use for crystallization and, generally, for self-assembling other bound systems like atoms and galaxies.
Presumably, the compactified vacuum has the minimal value of some conservative property, and therefore it is trapped in this form.
More specifically, if we assume that the vacuum is near its second-order phase transition point (under some macroscopic external conditions), but has no strong dimensional restrictions (as usual crystals have), we can ask a question, which geometry of domain walls in such a wall-dominated vacuum would be stable because of some kind of energy minimization.
This assumption motivates us to search for the appropriate geometry among minimal hyper-surfaces for domain walls, or, equivalently, for effective close-packaging of domain bodies.
As I have shown before in my papers, the 4-dimensional packaging of specific 26-cell bodies with 78 vertices is likely the best candidate for this role, as far as I know.
Under no dimensional restrictions this 26-cell tessellation, as a primary structure, can form a secondary structure, being free to get curved and folded.
We have some analogy in proteins study, where 1D amino acid chains are folded into 3D structures stable in some range of external thermodynamic conditions, directed by Gibbs energy minimization.
The vacuum built of 26-cell-shaped domains seems to be much less complicated system rather than proteins because proteins are built of numerous different amino acids but there is only one suitable 26-cell body as a vacuum building

block. However there are 8 different orientation of these blocks and they can hold vacuum of different phases that offer some degrees of freedom.
Therefore, the problem of optimal vacuum compactification, formulated as finding an optimal secondary folding, might be solvable by just brute force checking.
Among possible folding schemes of the 26-cell tessellation, the quadruple folding along four main diagonals of its hyper cubic crystallographic unit cell is one of the most promising.
This kind of folding leads to the specific effect of coupling each even domain together with one odd domain with exactly the same orientation but residing in other layer. (In protein analogy, some amino acids in the chain are coupled together with others remote amino acids in the same chain by hydrogen or other bonds that make the folded structure stable)
Such a coupling might be an answer to the question, why the compactification occurs.
Being coupled this way, the vacuum loses its granulated domain structure because coupled domains of different kinds cancel each other in sense of zeroing the effective order parameter everywhere, excepting sites of structure defects that we see as particles.
As result, we get something looking like almost empty, flat, and isotropic space.
The metric signature likely depends on size of folding: the long folding size correspondents to the spatial dimension with translation degree of freedom, while the short-sized folding causes this dimension to be temporal, i. e. constrained by size, in which no travel is available because of immediate getting back by the loop. However, the short-sized folding cannot be of infinitesimal length since it is limited below by the minimal translation unit length of the tessellation.
I suppose that one of four folding sizes actually equals to this minimal length (maybe, also caused by some minimization) that, in turn, prevents other three dimensions to be short-sized by some seesaw mechanism, and causes the actual experimental space metric to be $3 + 1$.
Note that since this folding is quadruple, there are $2^4 = 16$ disconnected layers. Each domain is coupled with its counterpart in another layer, so there are 8 uncoupled disconnected logical layers that share the same grid geometry. It means that in case the overall tessellation is slightly curved (that should be taken as gravity, caused by geometry defects distribution), this gravity should be also shared among disconnected logical layers.
This causes emergent hidden mass effect since defects in different logical layers cannot interact with defects in other layers since they have no geometrical connections (they are not neighbors) but they influence each other through the shared tessellation and its tensor curvature.
All what I wrote above is supported by calculations of corresponding geometrical structures but no experiments are still conducted.
Experiments with the folded 4D stuff generally require 8D space but in this case they seem to be possible, and results look feasible in our $3 + 1$D world, due some tricks. Namely, convex 4D 26-cell polytopes can be mimicked by non-convex 3D shapes (looking like natural neurons) maintaining the same count

and symmetry of their interconnections. These 3D shapes can be modeled by appropriate semiconductor chips connected by copper or fiber optic wires.
This is more construction work rather than theoretical one, and I need a strong support and intensive collaboration to perform experiments of this kind.

26.3 A Question of Euich Mitzani:

Well, it'll be technically possible. However, the point in our discussion is why our space should be (3+1) dimensional. Besides, why should higher dimensional space be undetectably compactified if it exists? Isn't it unnatural? We don't get any reason for it so far.

26.4 Reply by Elia: The 4D 26-cell may be the most optimal polytope packing, dictating the dimension count to be 4

As far as I know, the most effective packaging of domains could be achieved by arrangement having exactly four orthogonal crystallographic axis. It is not proved but I have checked several candidates. Whoever could provide a better packaging or a counterexample for this hypothesis but by now it is not rejected.
Another good option is E8 having eight orthogonal axis. But it can be less effective if one takes to account also the effectiveness of packaging of its 7D facets, and 6D facets of 7D facets and so on.
That's why we probably can consider the domain tessellation using the mathematical abstraction tool known as 4-dimensional space, as a suitable language without significant losses. Someone can rephrase this claiming the physical 4-dimensional space in fact exists. But we can also use other suitable mathematical construction, say weighted graphs that have nothing to do with dimensions.
There are probably no significant dimensions in this flat tessellation besides these four, but more four dimensions appear due to its folding. So, we should consider at least 8-dimensional Cartesian reference frame to embed such a model in it.
However, the folding scheme that I am talking about puts all the domain centroids in different points of the same 3D layer. Since domains (belonging to different connected layers) are coupled in this 3D layer pairwise, they cannot leave this layer without being decoupled or leaving the tessellation. These events also could happen under some extreme, non-minimizing conditions, therefore we can look for such multidimensional effects in black holes, big bangs and so on - but not in the almost empty vacuum with just a few particles in it that is a subject in our case.
The question now is, why we in fact have $3 + 1$D but neither $2 + 2$D nor $1 + 3$D, nor $4 + 0$D.
I do not have final solution for this question but I see some analogy in folding a 2D paper sheet into a tube: after short-sized folding in one direction we get the tube that is rigid along other two dimensions. One short-sized folding establishes frustrations preventing from short-sized folding in other dimensions. It is a kind of seesaw mechanism.

If this analogy is correct, the 4D tessellation should possess short-sized folding in only one direction getting straight and rigid in three others. The three other dimensions are probably also folded but with comparatively large size, say on the cosmological scale.

We can think of long-sized compactifications as performed along not circles but ellipses with eccentricity close to 1 that are just doubled segments. The short half-axis that directs into extra $(5-8)$ dimension is negligible since the domains can reside in the same 3D grid without frustration. This is an option only when one direction is short-sized folded, so instead of spatial frustration we have just coupling and effective cancellation of two domains with the opposite parity. This effect can be the main cause to have just one dimension short compactified.

We as observers of this scheme look on it not from outside but we are also bounded inside one of its 8 doubled 3D logical layers. We are just bounded states of defects as well as everything around us, interacting EM, weak, and strong only inside our layer of connectivity.

I think that in addition to computational experiments, some natural experiments could be aimed to find some ("dark") condensed matter samples in other logical layers through their gravitational effects.

Remember, in this scheme we have two kinds of "dark matter" - both interacting and condensable (in the same connectivity layer), and non-interacting and non-condensable (residing in different layers). The overall fraction of hidden/dark mass is estimated to be $\frac{7}{8}$ of the whole mass. It must have a tendency of rising its fluctuations due to the interaction and condensation inside layers (like we observe in our part of Universe).

However, the loci corresponding to our vicinity in other layers are likely to be interstellar or even intergalactic voids holding almost no compact objects having detectable masses. In favor of this option I take results of experiments estimating the dark matter density in our vicinity in the Solar system.

So, the higher dimensions $(5-8)$ are a bit speculative, non-physical ones in this scheme. We need them only to work within the more simple Cartesian reference frame instead of intrinsic (physical) curved 4D geometry.

Discussing dimensions, I should mention another kind of degree of freedom that can be confused with dimensions. Namely, the 4D 26-cell tessellation has a degree of freedom because its bodies can be of 8 different orientations. Since the phase transition is supposed to result in appearing of domains of two kinds, the distribution of the domain kind among orientations in each translation unit can be different. The list of options is finite and we map it onto the spectrum of possible fundamental particles with quantum numbers characterizing the distribution.

These discrete (spin-like) degrees of freedom can also be considered mathematically as local discrete dimensions, which are of course different from the dimensions discussed above (but they originate from the same minimization condition). So, these two sorts of dimensions shouldn't be mixed and confused.

BLED WORKSHOPS
IN PHYSICS
VOL. 26, NO. 1

Proceedings of the 28th Workshop
What Comes Beyond . . . *(p. 368)*
Bled, Slovenia, July 6–17, 2025

27 VIA: *Discussion of BSM research on the platform of Virtual Institute of Astroparticle physics*

Maxim Yu. Khlopov

Virtual Institute of Astroparticle physics, 75018, Paris, France

Abstract. We review the experience of the unique complex of Virtual Institute of Astroparticle Physics (VIA) in presentation online for the most interesting theoretical and experimental results, participation online in conferences and meetings, various forms of collaborative scientific work as well as programs of education at distance, combining online videoconferences with extensive library of records of previous meetings and Discussions on Forum. Since 2014 VIA online lectures combined with individual work on Forum acquired the form of Open Online Courses. Aimed to individual work with students the Course is not Massive, but the account for the number of visits to VIA site can convert VIA in a supplementary tool for MOOC activity. VIA sessions, being a traditional part of Bled Workshops' program, became the platform for the XXVIII Bled Workshop "What comes beyond the Standard models?". Their interactive format preserved the traditional creative nonformal atmosphere of Bled Workshop meetings, while regular updating of the Workshop diary made possible to involve in the discussions participants from all the time zones. We openly discuss the state of art of VIA platform.

Keywords: astroparticle physics, physics beyond the Standard model, e-learning, e-science, MOOC

27.1 Introduction

Studies in astroparticle physics link astrophysics, cosmology, particle and nuclear physics and involve hundreds of scientific groups linked by regional networks (like ASPERA/ApPEC [1,2]) and national centers. The exciting progress in these studies will have impact on the knowledge on the structure of microworld and Universe in their fundamental relationship and on the basic, still unknown, physical laws of Nature (see e.g. [3,4] for review). The progress of precision cosmology and experimental probes of the new physics at the LHC and in nonaccelerator experiments, as well as the extension of various indirect studies of physics beyond the Standard model involve with necessity their nontrivial links. Virtual Institute of Astroparticle Physics (VIA) [5] was organized with the aim to play the role of an unifying and coordinating platform for such studies.
Starting from the January of 2008 the activity of the Institute took place on its website [6] in a form of regular weekly videoconferences with VIA lectures, covering all the theoretical and experimental activities in astroparticle physics and related topics. The library of records of these lectures, talks and their presentations was

accomplished by multi-lingual Forum. Since 2008 there were **220 VIA online lectures**, VIA has supported distant presentations of **192 speakers at 32 Conferences** and provided transmission of talks at **78 APC Colloquiums**.
In 2008 VIA complex was effectively used for the first time for participation at distance in XI Bled Workshop [7]. Since then VIA videoconferences became a natural part of Bled Workshops' programs, opening the virtual room of discussions to the world-wide audience. Its progress was presented in [8–23].
Here the current state-of-art of VIA complex is presented in order to clarify the way in which discussion of open questions beyond the standard models of both particle physics and cosmology were supported by the platform of VIA facility at the XXVIII Bled Workshop. Even without pandemia, there appear other obstacles, preventing participants to attend offline meeting and in this situation VIA videoconferencing supported in 2025 traditions of open discussions at Bled meetings at distant talks, while updating their records in the workshop diary on the Workshop website made possible to involve distant participants from all the time zones in these discussions.

27.2 VIA structure and activity

27.2.1 The problem of VIA site

The structure of the VIA site was initially based on Flash and is virtually ruined now in the lack of Flash support. The original structure is illustrated by the Fig. 27.1. The home page, presented on this figure, contained the information on the coming and records of the latest VIA events. The upper line of menu included links to directories (from left to right): with general information on VIA (About VIA); entrance to VIA virtual rooms (Rooms); the library of records and presentations (Previous), which contained records of VIA Lectures (Previous → Lectures), records of online transmissions of Conferences (Previous → Conferences), APC Colloquiums (Previous → APC Colloquiums), APC Seminars (Previous → APC Seminars) and Events (Previous → Events); Calendar of the past and future VIA events (All events) and VIA Forum (Forum). In the upper right angle there were links to Google search engine (Search in site) and to contact information (Contacts). The announcement of the next VIA lecture and VIA online transmission of APC Colloquium occupied the main part of the homepage with the record of the most recent VIA events below. In the announced time of the event (VIA lecture or transmitted APC Colloquium) it was sufficient to click on "to participate" on the announcement and to Enter as Guest (printing your name) in the corresponding Virtual room. The Calendar showed the program of future VIA lectures and events. The right column on the VIA homepage listed the announcements of the regularly up-dated hot news of Astroparticle physics and related areas.
In the lack of Flash support this system of links is ruined, but fortunately, they continue to operate separately and it makes possible to use VIA Forum, by direct link to it, as well as direct inks to virtual Zoom room for regular Laboratory and Seminar meetings (see Fig 27.2). The necessity to revive the VIA website and to restore all the links within VIA complex is a very important task to recreate the full scale of VIA activity.

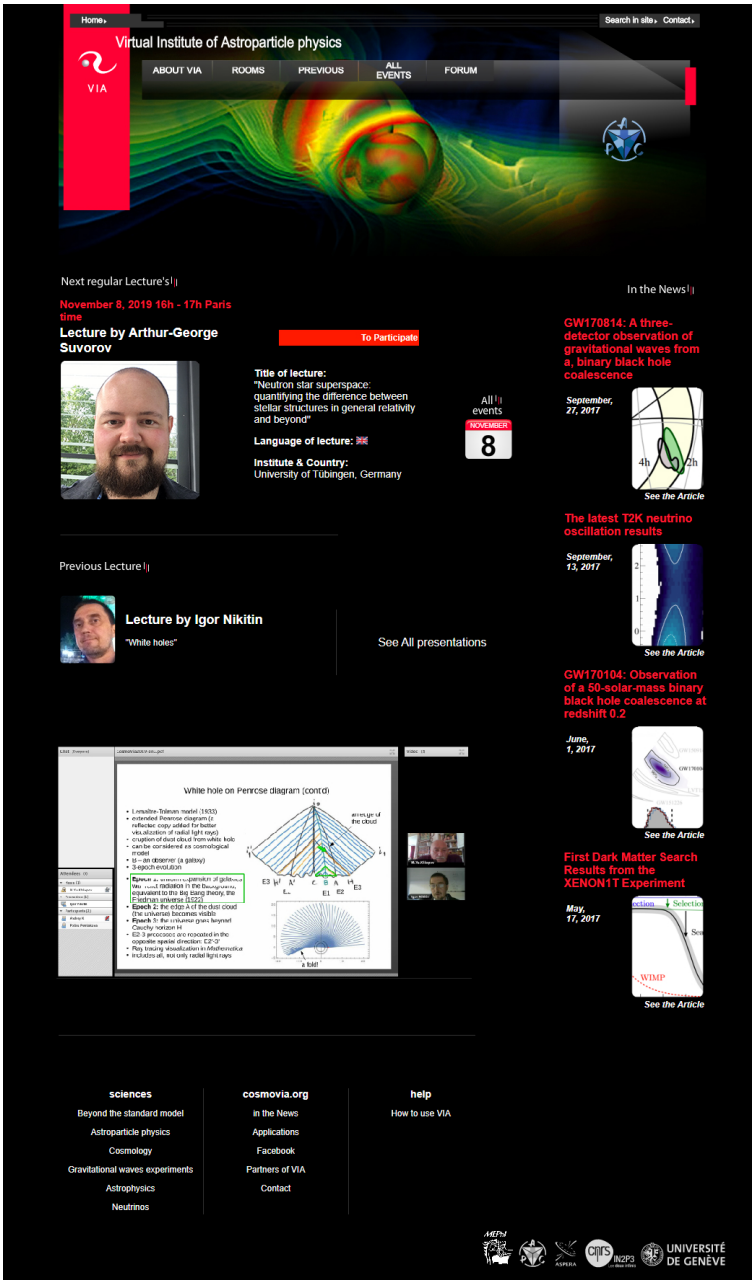

Fig. 27.1: The original home page of VIA site

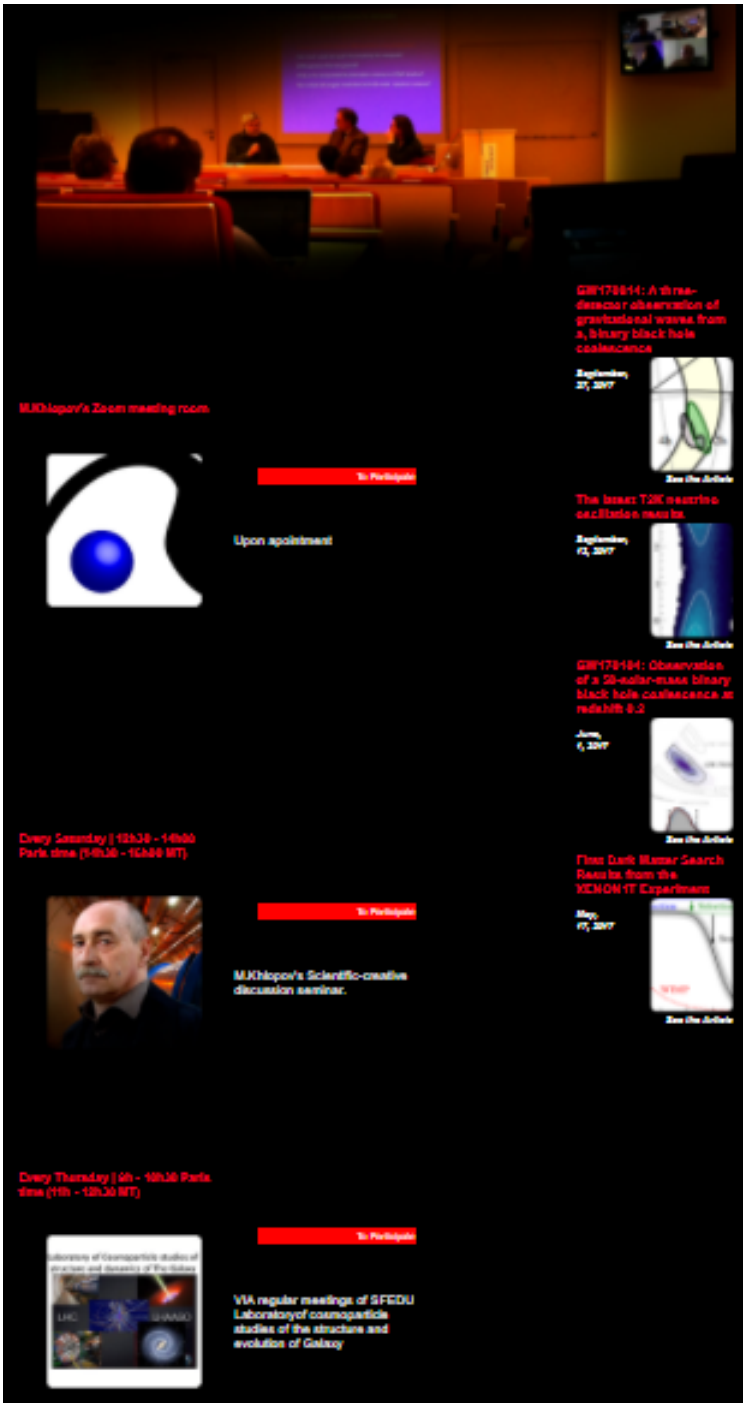

Fig. 27.2: The current home page of VIA site

27.2.2 VIA activity

In 2010 special COSMOVIA tours were undertaken in Switzerland (Geneva), Belgium (Brussels, Liege) and Italy (Turin, Pisa, Bari, Lecce) in order to test stability of VIA online transmissions from different parts of Europe. Positive results of these tests have proved the stability of VIA system and stimulated this practice at XIII Bled Workshop. The records of the videoconferences at the XIII Bled Workshop were put on VIA site [24].
Since 2011 VIA facility was used for the tasks of the Paris Center of Cosmological Physics (PCCP), chaired by G. Smoot, for the public program "The two infinities" conveyed by J.L.Robert and for effective support a participation at distance at meetings of the Double Chooz collaboration. In the latter case, the experimentalists, being at shift, took part in the collaboration meeting in such a virtual way.
The simplicity of VIA facility for ordinary users was demonstrated at XIV Bled Workshop in 2011. Videoconferences at this Workshop had no special technical support except for WiFi Internet connection and ordinary laptops with their internal webcams and microphones. This test has proved the ability to use VIA facility at any place with at least decent Internet connection. Of course the quality of records is not as good in this case as with the use of special equipment, but still it is sufficient to support fruitful scientific discussion as can be illustrated by the record of VIA presentation "New physics and its experimental probes" given by John Ellis from his office in CERN (see the records in [25]).
In 2012 VIA facility, regularly used for programs of VIA lectures and transmission of APC Colloquiums, has extended its applications to support M.Khlopov's talk at distance at Astrophysics seminar in Moscow, videoconference in PCCP, participation at distance in APC-Hamburg-Oxford network meeting as well as to provide online transmissions from the lectures at Science Festival 2012 in University Paris7. VIA communication has effectively resolved the problem of referee's attendance at the defence of PhD thesis by Mariana Vargas in APC. The referees made their reports and participated in discussion in the regime of VIA videoconference. In 2012 VIA facility was first used for online transmissions from the Science Festival in the University Paris 7. This tradition was continued in 2013, when the transmissions of meetings at Journées nationales du Développement Logiciel (JDEV2013) at Ecole Politechnique (Paris) were organized [27].
In 2013 VIA lecture by Prof. Martin Pohl was one of the first places at which the first hand information on the first results of AMS02 experiment was presented [26].
In 2014 the 100th anniversary of one of the foundators of Cosmoparticle physics, Ya. B. Zeldovich, was celebrated. With the use of VIA M.Khlopov could contribute the programme of the "Subatomic particles, Nucleons, Atoms, Universe: Processes and Structure International conference in honor of Ya. B. Zeldovich 100th Anniversary" (Minsk, Belarus) by his talk "Cosmoparticle physics: the Universe as a laboratory of elementary particles" [28] and the programme of "Conference YaB-100, dedicated to 100 Anniversary of Yakov Borisovich Zeldovich" (Moscow, Russia) by his talk "Cosmology and particle physics".
In 2015 VIA facility supported the talk at distance at All Moscow Astrophysical seminar "Cosmoparticle physics of dark matter and structures in the Universe"

by Maxim Yu. Khlopov and the work of the Section "Dark matter" of the International Conference on Particle Physics and Astrophysics (Moscow, 5-10 October 2015). Though the conference room was situated in Milan Hotel in Moscow all the presentations at this Section were given at distance (by Rita Bernabei from Rome, Italy; by Juan Jose Gomez-Cadenas, Paterna, University of Valencia, Spain and by Dmitri Semikoz, Martin Bucher and Maxim Khlopov from Paris) and its proceeding was chaired by M.Khlopov from Paris. In the end of 2015 M. Khlopov gave his distant talk "Dark atoms of dark matter" at the Conference "Progress of Russian Astronomy in 2015", held in Sternberg Astronomical Institute of Moscow State University.
In 2016 distant online talks at St. Petersburg Workshop "Dark Ages and White Nights (Spectroscopy of the CMB)" by Khatri Rishi (TIFR, India) "The information hidden in the CMB spectral distortions in Planck data and beyond", E. Kholupenko (Ioffe Institute, Russia) "On recombination dynamics of hydrogen and helium", Jens Chluba (Jodrell Bank Centre for Astrophysics, UK) "Primordial recombination lines of hydrogen and helium", M. Yu. Khlopov (APC and MEPHI, France and Russia)"Nonstandard cosmological scenarios" and P. de Bernardis (La Sapiensa University, Italy) "Balloon techniques for CMB spectrum research" were given with the use of VIA system. At the defense of PhD thesis by F. Gregis VIA facility made possible for his referee in California not only to attend at distance at the presentation of the thesis but also to take part in its successive jury evaluation.
Since 2018 VIA facility is used for collaborative work on studies of various forms of dark matter in the framework of the project of Russian Science Foundation based on Southern Federal University (Rostov on Don). In September 2018 VIA supported online transmission of **17 presentations** at the Commemoration day for Patrick Fleury, held in APC.
The discussion of questions that were put forward in the interactive VIA events is continued and extended on VIA Forum. Presently activated in English,French and Russian with trivial extension to other languages, the Forum represents a first step on the way to multi-lingual character of VIA complex and its activity. Discussions in English on Forum are arranged along the following directions: beyond the standard model, astroparticle physics, cosmology, gravitational wave experiments, astrophysics, neutrinos. After each VIA lecture its pdf presentation together with link to its record and information on the discussion during it are put in the corresponding post, which offers a platform to continue discussion in replies to this post.

27.2.3 VIA e-learning, OOC and MOOC

One of the interesting forms of VIA activity is the educational work at distance. For the last eleven years M.Khlopov's course "Introduction to cosmoparticle physics" is given in the form of VIA videoconferences and the records of these lectures and their ppt presentations are put in the corresponding directory of the Forum [29]. Having attended the VIA course of lectures in order to be admitted to exam students should put on Forum a post with their small thesis. In this thesis students are proposed to chose some BSM model and to study the cosmological scenario

based on this chosen model. The list of possible topics for such thesis is proposed to students, but they are also invited to chose themselves any topic of their own on possible links between cosmology and particle physics. Professor's comments and proposed corrections are put in a Post reply so that students should continuously present on Forum improved versions of work until it is accepted as admission for student to pass exam. The record of videoconference with the oral exam is also put in the corresponding directory of Forum. Such procedure provides completely transparent way of evaluation of students' knowledge at distance.

In 2018 the test has started for possible application of VIA facility to remote supervision of student's scientific practice. The formulation of task and discussion of progress on work are recorded and put in the corresponding directory on Forum together with the versions of student's report on the work progress.

Since 2014 the second semester of the course on Cosmoparticle physics is given in English and converted in an Open Online Course. It was aimed to develop VIA system as a possible accomplishment for Massive Online Open Courses (MOOC) activity [30]. In 2016 not only students from Moscow, but also from France and Sri Lanka attended this course. In 2017 students from Moscow were accompanied by participants from France, Italy, Sri Lanka and India [31]. The students pretending to evaluation of their knowledge must write their small thesis, present it and, being admitted to exam, pass it in English. The restricted number of online connections to videoconferences with VIA lectures is compensated by the wide-world access to their records on VIA Forum and in the context of MOOC VIA Forum and videoconferencing system can be used for individual online work with advanced participants. Indeed Google Analytics shows that since 2008 VIA site was visited by more than **250 thousand** visitors from **155** countries, covering all the continents by its geography (Fig. 27.3). According to this statistics more than half of these visitors continued to enter VIA site after the first visit. Still the form of individual

Fig. 27.3: Geography of VIA site visits according to Google Analytics

educational work makes VIA facility most appropriate for PhD courses and it could be involved in the International PhD program on Fundamental Physics, which was planned to be started on the basis of Russian-French collaborative

agreement. In 2017 the test for the ability of VIA to support fully distant education and evaluation of students (as well as for work on PhD thesis and its distant defense) was undertaken. Steve Branchu from France, who attended the Open Online Course and presented on Forum his small thesis has passed exam at distance. The whole procedure, starting from a stochastic choice of number of examination ticket, answers to ticket questions, discussion by professors in the absence of student and announcement of result of exam to him was recorded and put on VIA Forum [32].
In 2019 in addition to individual supervisory work with students the regular scientific and creative VIA seminar is in operation aimed to discuss the progress and strategy of students scientific work in the field of cosmoparticle physics.
In 2020 the regular course now for M2 students continued, but the problems of adobe Connect, related with the lack of its support for Flash in 2021 made necessary to use the platform of Zoom, This platform is rather easy to use and provides records, as well as whiteboard tools for discussions online can be solved by accomplishments of laptops by graphic tabloids. In 2022 the Open Online Course for M2 students was accompanied by special course "Cosmoparticle physics", given in English for English speaking M1 students. In 2023, 2024 and 2025 the practice of Open Online Course for M2 students was continued.

27.2.4 Organisation of VIA events and meetings

First tests of VIA system, described in [5,7–9], involved various systems of videoconferencing. They included skype, VRVS, EVO, WEBEX, marratech and adobe Connect. In the result of these tests the adobe Connect system was chosen and properly acquired. Its advantages were: relatively easy use for participants, a possibility to make presentation in a video contact between presenter and audience, a possibility to make high quality records, to use a whiteboard tools for discussions, the option to open desktop and to work online with texts in any format. The lack of support for Flash, on which VIA site was originally based, made necessary to use Zoom, which shares all the above mentioned advantages.
Regular activity of VIA as a part of APC included online transmissions of all the APC Colloquiums and of some topical APC Seminars, which may be of interest for a wide audience. Online transmissions were arranged in the manner, most convenient for presenters, prepared to give their talk in the conference room in a normal way, projecting slides from their laptop on the screen. Having uploaded in advance these slides in the VIA system, VIA operator, sitting in the conference room, changed them following presenter, directing simultaneously webcam on the presenter and the audience. If the advanced uploading was not possible, VIA streaming was used - external webcam and microphone are directed to presenter and screen and support online streaming. This experience has found proper place in the current weakening of the pandemic conditions and regular meetings in real can be streamed. Moreover, such streaming can be made without involvement of VIA operator, by direction of webcam towards the conference screen and speaker.

27.2.5 VIA activity in the conditions of pandemia and after

The lack of usual offline connections and meetings in the conditions of pandemia made the use of VIA facility especially timely and important. This facility supports regular weekly meetings of the Laboratory of cosmoparticle studies of the structure and dynamics of Galaxy in Institute of Physics of Southern Federal University (Rostov on Don, Russia) and M.Khlopov's scientific - creative seminar and their announcements occupied their permanent position on VIA homepage (Fig. 27.2), while their records were put in respective place of VIA forum, like [34] for Laboratory meetings.
The platform of VIA facility was used for regular Khlopov's course "Introduction to Cosmoparticle physics" for M2 students of MEPHI (in Russian) and in 2020 supported regular seminars of Theory group of APC.
The programme of VIA lectures continued to present hot news of astroparticle physics and cosmology, like talk by Zhen Cao from China on the progress of LHAASO experiment or lecture by Sunny Vagnozzi from UK on the problem of consistency of different measurements of the Hubble constant.
The results of this activity inspired the decision to hold in 2020 XXIII Bled Workshop online on the platform of VIA [19].
The conditions of pandemia continued in 2021 and VIA facility was successfully used to provide the platform for various online meetings. 2021 was announced by UNESCO as A.D.Sakharov year in the occasion of his 100th anniversary VIA offered its platform for various events commemorating A.D.Sakharov's legacy in cosmoparticle physics. In the framework of 1 Electronic Conference on Universe ECU2021), organized by the MDPI journal "Universe" VIA provided the platform for online satellite Workshop "Developing A.D.Sakharov legacy in cosmoparticle physics" [35].

27.3 VIA platform at the XXVIII Bled Workshop

VIA sessions at Bled Workshops continued the tradition coming back to the first experience at XI Bled Workshop [7] and developed at XII, XIII, XIV, XV, XVI, XVII, XVIII, XIX, XX, XXI and XXII Bled Workshops [8–18]. They became a regular but supplementary part of the Bled Workshop's program. In the conditions of pandemia it became the only form of Workshop activity in 2020 [19] and in 2021 [20], as well as substantial part of the hybrid Memorial XXV Bled Workshop in 2022 [21] XXVI Bled Workshop in 2023 [22] and XXVII Bled Workshop in 2024 [23].
During the XXVIII Bled Workshop the announcement of VIA sessions was put on the Workshop webpage, giving an open access to the videoconferences at the Workshop sessions. The preliminary program as well as the corrected program for each day were continuously put on Forum with the slides and records of all the talks and discussions [36].
Starting from its official opening (Fig. 27.5)
VIA facility tried to preserve the creative atmosphere of Bled discussions in the format videoconferences as at the talk " How do the "basis vectors", describing the internal spaces of fermion and boson fields with the odd (for fermion) and even

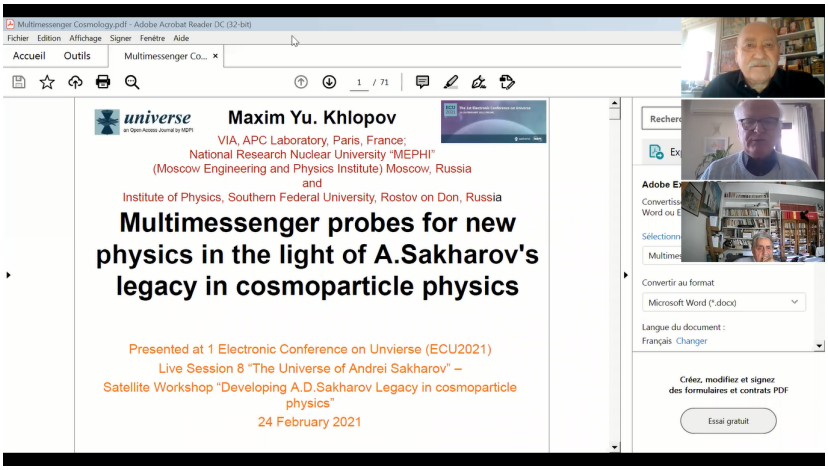

Fig. 27.4: M.Khlopov's talk "Multimessenger probes for new physics in the light of A.D.Sakharov legacy in cosmoparticle physics" at the satellite Workshop "Developing A.D.Sakharov legacy in cosmoparticle physics" of ECU2021.

(for boson) products of γ^a's, explain all the observed second-quantized fermion and boson fields and the interactions among fields" by Norma Mankoc-Borstnik or talk "Main investigation on rare processes with DAMA experimental setups" given by R.Bernabei, from Rome University, Italy (see records in [36]).
During the Workshop the VIA virtual room was open, inviting distant participants to join the discussion and extending the creative atmosphere of these discussions to the world-wide audience. The participants joined these discussions from different parts of world. The talk "Emergent Gravity from Topological Quantum Field Theory: Stochastic Gradient Flow Perspective away from the Quantum Gravity Problem" was given by A. Addazi from China, "Primordial Black Holes under Memory Burden Effect" by A. Chaudhuri from Japan, by V. Dvoeglazov from Mexico, by Saibal Ray and S. Roy Chowdhury - from India, by A.Farag from USA, by D.Fargion from Italy. M.Y. Khlopov gave his talk "Peculiar footprints of BSM physics and Cosmology" from France, while H.B. Nielsen gave his talks "Ontological Fluctuating Lattice Cut Off", "Dark Matter As Screened Ordinary Matter" and "Graph Model For Geometry" from Denmark.
VIA talks highly enriched the Workshop program and involved distant participants in fruitful discussions. The use of VIA facility has provided remote presentation of students' scientific debuts in BSM physics and cosmology. The records of all the talks and discussions can be found in VIA diary [36].
VIA facility has managed to join scientists from Japan, Mexico, USA, Denmark, Norge, France, Italy, Russia, Slovenia, India, China and many other countries in discussion of open problems of physics and cosmology beyond the Standard models. In the current situation, hindering visits of Russian scientists to Europe, it made possible Russian students to present their results and participate in these discussions

Post-festum of the twenty-eighth workshop "What Comes Beyond the Standard Models?"

Organizing Committee:
Norma Susana Mankoč Borštnik, Holger Bech Nielsen, Maxim Yu. Khlopov, Astri Kleppe

Scientific Committee:
Ignatios Antoniadis
John Ellis
Gian Francesco Giudice
Rabindra N. Mohapatra
Masao Ninomiya (二宮 正夫)

Home Workshop Diary About Bled

Workshop Diary

▼ Sunday, July 6th

Morning session:
Chair person: H. B. Nielsen
Bled/Ljubljana 9:00 Moscow/Tel Aviv 10:00 New Delhi 12:30 Beijing/Irkutsk 15:00 Tokyo 16:00 New York 03:00 San Francisco 00:00

9:00 – 9:15: N.S. Mankoč Borštnik: Opening the 28th International workshop 'What comes beyond the standard models

9:15 – 9:30: M.Yu. Khlopov: Presentation of ZOOM and informational support

9:30 – 11:30: N.S. Mankoč Borštnik: How do the "basis vectors", describing the internal spaces of fermion and boson fields with the odd (for fermion) and even (for boson) products of γ^{a}'s, explain all the observed second-quantised fermion and boson fields and the interactions among fields? Ia

11:30 – 12:30: M.Yu. Khlopov: Peculiar footprints of BSM physics and Cosmology

12:30 – 13:30: Lunch (Discussions)

Afternoon session:
Chair person: L. Bonora
Bled/Ljubljana 13:30 Moscow/Tel Aviv 14:30 New Delhi 17:00 Beijing/Irkutsk 19:30 Tokyo 20:30 New York 7:30 San Francisco 4:30

13:30 – 15:00: H.B. Nielsen: Ontological Fluctuating Lattice Cut Off Ia

15:00 – 16:30: V. Dvoeglazov: Negative-energy and tachyonic solutions

16:30 – 17:00: Coffee break

Fig. 27.5: Diary of XXVIII Bled Workshop

27.4 Conclusions

The Scientific-Educational complex of Virtual Institute of Astroparticle physics provides regular communication between different groups and scientists, working in different scientific fields and parts of the world, the first-hand information on the newest scientific results, as well as support for various educational programs at distance. This activity would easily allow finding mutual interest and organizing task forces for different scientific topics of cosmology, particle physics, astroparticle physics and related topics. It can help in the elaboration of strategy of experimental particle, nuclear, astrophysical and cosmological studies as well as in proper analysis of experimental data. It can provide young talented people from all over the world to get the highest level education, come in direct interactive contact with the world known scientists and to find their place in the fundamental research. These educational aspects of VIA activity can evolve in a specific tool for International PhD program for Fundamental physics. Involvement of young scientists in creative discussions was an important aspect of VIA activity at XXVIII Bled Workshop. VIA applications can go far beyond the particular tasks of astroparticle physics and give rise to an interactive system of mass media communications.
VIA sessions, which became a natural part of a program of Bled Workshops, maintained in 2025 the platform for online discussions of physics beyond the Standard Model involving distant participants from all the world in the fruitful atmosphere of Bled offline meeting. The experience of VIA applications at Bled Workshops plays important role in the development of VIA facility as an effective tool of e-science and e-learning.
One can summarize the advantages and flaws of online format of Bled Workshop. It makes possible to involve in the discussions scientists from all the world (young scientists, especially) free of the expenses related with meetings in real (voyage, accommodation, ...), but loses the advantage of nonformal discussions at walks along the beautiful surrounding of the Bled lake and other places of interest. The improvement of VIA technical support by involvement of Zoom provided better platform for nonformal online discussions, but in no case can be the substitute for offline Bled meetings and its creative atmosphere in real, which as we hope will be revived at the future Bled Workshops. One can summarize that VIA facility provides the online platform of Bled Workshop, involving world-wide participants in its creative and open discussions of BSM physics and cosmology.

Acknowledgements

The initial step of creation of VIA was supported by ASPERA. I express my tribute to memory of P.Binetruy and S.Katsanevas and express my gratitude to J.Ellis for permanent stimulating support, to J.C. Hamilton for early support in VIA integration in the structure of APC laboratory, to K.Belotsky, A.Kirillov, M.Laletin and K.Shibaev for assistance in educational VIA program, to A.Mayorov, A.Romaniouk and E.Soldatov for fruitful collaboration, to K.Ganga and D.Semikoz for collaboration in development of VIA activity in APC, to M.Pohl, C. Kouvaris, J.-R.Cudell, C. Giunti, G. Cella, G. Fogli and F. DePaolis for cooperation in the tests of

VIA online transmissions in Switzerland, Belgium and Italy and to D.Rouable for help in technical realization and support of VIA complex. I express my gratitude to the Organizers of Bled Workshop N.S. Mankoč Borštnik, A.Kleppe, E.Dmitrieff and H.Nielsen for cooperation in the organization of VIA online Sessions at XXVIII Bled Workshop. I am grateful to T.E.Bikbaev for technical assistance and help. I am grateful to Sandi Ogrizek for creation of the Workshop diary and effective help in its updating by presentations and records of VIA talks. .

References

1. http://www.aspera-eu.org/
2. http://www.appec.org/
3. M.Yu. Khlopov: *Cosmoparticle physics*, World Scientific, New York -London-Hong Kong - Singapore, 1999.
4. M.Yu. Khlopov: *Fundamentals of Cosmic Particle Physics*, CISP-Springer, Cambridge, 2012.
5. M. Y. Khlopov, Project of Virtual Institute of Astroparticle Physics, arXiv:0801.0376 [astro-ph].
6. http://viavca.in2p3.fr/site.html
7. M. Y. Khlopov, Scientific-educational complex - virtual institute of astroparticle physics, 981–862008.
8. M. Y. Khlopov, Virtual Institute of Astroparticle Physics at Bled Workshop, 10177–1812009.
9. M. Y. Khlopov, VIA Presentation, 11225–2322010.
10. M. Y. Khlopov, VIA Discussions at XIV Bled Workshop, 12233–2392011.
11. M. Y. .Khlopov, Virtual Institute of astroparticle physics: Science and education online, 13183–1892012.
12. M. Y. .Khlopov, Virtual Institute of Astroparticle physics in online discussion of physics beyond the Standard model, 14223–2312013.
13. M. Y. .Khlopov, Virtual Institute of Astroparticle physics and "What comes beyond the Standard model?" in Bled, 15285-2932014.
14. M. Y. .Khlopov, Virtual Institute of Astroparticle physics and discussions at XVIII Bled Workshop, 16177-1882015.
15. M. Y. .Khlopov, Virtual Institute of Astroparticle Physics — Scientific-Educational Platform for Physics Beyond the Standard Model, 17221-2312016.
16. M. Y. .Khlopov: Scientific-Educational Platform of Virtual Institute of Astroparticle Physics and Studies of Physics Beyond the Standard Model, 18273-2832017.
17. M. Y. .Khlopov: The platform of Virtual Institute of Astroparticle physics in studies of physics beyond the Standard model, 19383-3942018.
18. M. Y. .Khlopov: The Platform of Virtual Institute of Astroparticle Physics for Studies of BSM Physics and Cosmology, 20249-2612019.
19. M. Y. .Khlopov: Virtual Institute of Astroparticle Physics as the Online Platform for Studies of BSM Physics and Cosmology, 21249-2632020.
20. M. Y. .Khlopov: Challenging BSM physics and cosmology on the online platform of Virtual Institute of Astroparticle physics, 22160-1752021.
21. M. Y. .Khlopov: Virtual Institute of Astroparticle physics as the online platform for studies of BSM physics and cosmology, 23334-3472022.
22. M. Y. .Khlopov: Virtual Institute of Astroparticle physics as the online support for studies of BSM physics and cosmology. 24279-2932023.

23. M. Y. .Khlopov: Virtual Institute of Astroparticle physics as the platform for the BSM research 25238-2532024.
24. http : //viavca.in2p3.fr/whatcomesbeyondthestandardmodelsxiii.html
25. http : //viavca.in2p3.fr/whatcomesbeyondthestandardmodelsxiv.html
26. http : //viavca.in2p3.fr/pohlmartin.html
27. In http://viavca.in2p3.fr/ Previous - Events - JDEV 2013
28. http : //viavca.in2p3.fr/zeldovich100meeting.html
29. In http://bsm.fmf.uni-lj.si/bled2023bsm/ Cosmovia - Forum- Discussion in Russian - Courses on Cosmoparticle physics
30. In http://bsm.fmf.uni-lj.si/bled2023bsm/ Cosmovia - Forum - Education - From VIA to MOOC
31. In http://bsm.fmf.uni-lj.si/bled2023bsm/ Cosmovia - Forum - Education - Lectures of Open Online VIA Course 2017
32. In http://bsm.fmf.uni-lj.si/bled2023bsm/ Cosmovia - Forum - Education - Small thesis and exam of Steve Branchu
33. http : //viavca.in2p3.fr/johnellis.html
34. In http://bsm.fmf.uni-lj.si/bled2023bsm/ Cosmovia - Forum - LABORATORY OF COSMOPARTICLE STUDIES OF STRUCTURE AND EVOLUTION OF GALAXY
35. In http://bsm.fmf.uni-lj.si/bled2023bsm/ Cosmovia - Forum - CONFERENCES - CONFERENCES ASTROPARTICLE PHYSICS - The Universe of A.D. Sakharov at ECU2021
36. In http://bsm.fmf.uni-lj.si/bled2025bsm/presentations.php

BLED WORKSHOPS
IN PHYSICS
VOL. 26, NO. 1

Proceedings of the 28th Workshop
What Comes Beyond . . . *(p. 382)*
Bled, Slovenia, July 6–17, 2025

28 A poem

Astri Kleppe

Oslo

Helium

In those days, along with helium, the words
and sounds were born, the threads
that run between
all nodes.

It took some seconds, and at last
some processes inside the sun,
the world
was filled with cracks, oblivion,

and a grandmother who reads aloud
to help the children fall asleep.

BLEJSKE DELAVNICE IZ FIZIKE, LETNIK 26, ŠT. 1, ISSN 1580-4992
BLED WORKSHOPS IN PHYSICS, VOL. 26, NO. 1, ISSN 1580-4992

Zbornik 28. delavnice 'What Comes Beyond the Standard Models',
Bled, 6.–17. julij 2025
Proceedings to the 28th workshop 'What Comes Beyond the Standard Models',
Bled, July 6.–17., 2025

Uredili: Norma Susana Mankoč Borštnik, Holger Bech Nielsen, Maxim Yu. Khlopov in Astri Kleppe
Edited by Norma Susana Mankoč Borštnik, Holger Bech Nielsen, Maxim Yu. Khlopov in Astri Kleppe

Recenzenti / Reviewers:
Člani organizacijskega odbora mednarodne delavnice "What Comes Beyond the Standard Models", Bled, Slovenija, izjavljajo, da so poglobljene razprave in kritična vprašanja poskrbela za recenzijo vseh člankov, ki so objavljeni v zborniku 28. delavnice "What Comes Beyond the Standardni models", Bled, Slovenija.

The Members of the Organizing Committee of the International Workshop "What Comes Beyond the Standard Models", Bled, Slovenia, state that the articles published in the Proceedings to the 28th Workshop "What Comes Beyond the Standard Models", Bled, Slovenia are refereed at the Workshop in intense in-depth discussions.

Tehnični urednik / Technical Editor: Matjaž Zaveršnik

Založila / Published by: Založba Univerze v Ljubljani / University of Ljubljana Press

Za založbo / For the Publisher: Gregor Majdič, rektor Univerze v Ljubljani / Gregor Majdič, rector of University of Ljubljana

Izdala/Issued by: Fakulteta za matematiko in fiziko Univerze v Ljubljani / Faculty of Mathematics and Physics, University of Ljubljana.

Za izdajatelja / For the issuer: Emil Žagar dekan Fakultete za matematiko in fiziko UL / dean of the Faculty of Mathematics and Physics, University of Ljubljana.

Tisk / Printed by: Itagraf

Naklada / Print run: 100

Prva izdaja / First edition Ljubljana, 2025

Publikacija je brezplačna / Publication is free of charge

DOI: 10.51746/9789612977351To delo je ponujeno pod licenco Creative Commons

Digital copy of the book is available on: https://ebooks.uni-lj.si/

Prva e-izdaja. Knjiga je v digitalni obliki dostopna na: https://ebooks.uni-lj.si/

DOI: 10.51746/9789612977351

Kataložna zapisa o publikaciji (CIP) pripravili
v Narodni in univerzitetni knjižnici v Ljubljani

Tiskana knjiga
COBISS.SI-ID 260631043
ISBN 978-961-297-737-5

E-knjiga
COBISS.SI-ID 260529155
ISBN 978-961-297-735-1 (PDF)